A FLUOROGENIC HYPOXIA-ACTIVATED PRODRUG STRATEGY FOR TARGETED COMPOUND DELIVERY AND IMAGING OF TUMOURS

Liam O'Connor

Keble College

Thesis submitted to the University of Oxford in accordance with the requirements for the degree of Doctor of Philosophy

Trinity Term, 2016

University of Oxford

Supervisors

Prof. Stuart J. Conway

Dr Ester M. Hammond

Thesis Assessment Committee

Dr Michael R. L. Stratford

Prof. Boris Vojnovic

The studies detailed in this dissertation were performed at the Chemistry Research Laboratory, University of Oxford and the Cancer Research UK/Medical Research Council Oxford Institute for Radiation Oncology, University of Oxford, and was funded by a Medical Research Council scholarship, and Cancer Research UK.

Word count: 42,000 (exclusive of appendices, figures, schemes, tables and references).

ABSTRACT

Hypoxia, a common feature in solid tumours, is associated with aggressive phenotypes, decreased genomic stability, and with increased resistance to all forms of cancer therapy. The significant differences between the hypoxic microenvironment, and normal tissues, present a therapeutic opportunity through the design of bioreductive hypoxia-activated prodrugs (HAPs). This strategy aids the selective delivery of chemotherapeutics to hypoxic regions, reducing their effects in non-hypoxic tissue. A variety of chemical functionalities that undergo oxygen-dependent enzyme-mediated reduction have been utilised in the development of HAPs. Despite some clinical successes of HAPs, compound delivery to hypoxia remains a key challenge, and the biodistribution of any HAP is currently unclear. Therefore, we sought to develop HAPs, which become fluorescent upon reduction, and subsequently fragment to release a biologically active cargo molecule.

A proof-of-concept fluorogenic bioreductive group was initially designed and synthesised, based on a 6-nitroquinoline scaffold. A BET bromodomain inhibitor was installed as the cargo molecule of therapeutic interest for delivery to hypoxic conditions, affording a novel fluorogenic HAP for biological evaluation. We demonstrated that following reduction of the nitro group to the corresponding amine, fragmentation is induced to release the cargo BET bromodomain inhibitor. When treated with reductase enzymes under hypoxic

conditions, reduction and fragmentation occurred as desired. Under normoxic conditions, however, the novel fluorogenic HAP remained hydrolytically stable. Furthermore, following reduction to the corresponding amine and fragmentation products, a significant increase in fluorescence intensity was observed. This work represents the first example of a fluorogenic bioreductive group, and is the subject of a patent application.

Following the initial demonstration of fluorogenic bioreductive groups, we sought to improve the group's spectrophotometric properties, by focusing on achieving fluorescence in the near-infrared (NIR) region of the electromagnetic spectrum. This window represents a favourable range of wavelengths for surgical fluorescence imaging and *in vivo* interrogation. By exploiting an aminostyryl-chromenone-based NIR fluorophore, introduction of oxygen-sensitive functionalities was considered, including the nitro group. This work led to the investigation of azides as hypoxia-responsive moieties, which undergo bioreduction. This dissertation demonstrates, for the first time, the use of azides as fluorogenic molecules for the detection of hypoxia in a range of *in vitro* assays and in 3D tumour models. The oxygen-dependent enzymatic reduction of azides, a functionality traditionally considered as biologically inert, has implications for their use in other areas of chemical biology, such as click chemistry.

Further studies focused on exploiting NIR fluorophore scaffolds already employed in surgical fluorescence imaging to develop fluorogenic HAPs. We were able to show for the first time, in a cancer cell line that a single bioreductive core is capable of fragmenting to release two distinct molecules, following intracellular reduction.

Recommended studies to follow this work are discussed, which may improve the efficiency of the fragmentation process of HAPs, and also considers alternative technologies that might be used in the design of bioreductive groups for imaging. An efficient protocol for the design, synthesis and evaluation of molecularly targeted HAPs, comprising experiments of increasing biological evaluation, is also disclosed. In addition, an improved synthesis of the widely used 2-nitroimidazole bioreductive group is also reported.

ACKNOWLEDGEMENTS

First and foremost, I would like to thank my fantastic supervisors; Professor Stuart Conway, and Dr Ester Hammond, without whose guidance, patience and time invested over the past four years, this project would not have been possible. Stuart has been instrumental in directing me through my University life, at both undergraduate and postgraduate level, and provided support and advice at every turn. I thank him greatly for all the time he took to talk things through when I was unsure or required advice. I am extremely grateful to Ester for training me in the art of biological research, and being patient throughout the transition periods between chemistry and biology. Her door was always open, and she never ceased to do everything in her power to make my DPhil studies as successful as possible. I have learnt so much in both laboratories, and such a cross-disciplinary project has been a privilege I shall never forget.

Huge thanks goes to my wonderful girlfriend, Dr Natalie Theodoulou, whom has been my bedrock of encouragement and positivity, over the last four years. She never ceased to see the light in any situation and made me a better person for it. She has been a cornerstone of love, support, and continual laughs throughout my studies. Thanks to my parents; John and Joanne, and siblings; Sarah and Jack, who have always supported me in any endeavour and encouraged me to persevere and achieve the best I can.

Naturally, I would like to thank all members, past and present, of the Hammond and Conway laboratories, for making my DPhil such a great experience. Particular mention goes to Dr Cindy Cazares-Körner, who initially trained me up in the lab, and Dr David Hewings who provided early chemistry guidance. Further special mention goes to Dr Sam Grayer, Dr Angelina Sekirnik and (Dr) Iosifina Foskolou, whom all started their DPhil at the same time as me, are fantastic friends, and provided great support throughout my time in the lab. I would also like to thank Dr Michael Stratford, and Dr Lisa Folkes, for all their time, help and patience in assisting me using HPLC, and training me in its use.

Thanks to all members of staff at the Chemistry Research Laboratory, and Oxford Institute for Radiation Oncology for keeping the research wheel constantly rolling. Thanks to Medical Research Council and Cancer Research UK for funding.

TABLE OF CONTENTS

ABSTRACT i

ACKNOWLEDGEMENTS iv

TABLE OF CONTENTS vi

LIST OF ABBREVIATIONS xiii

Chapter 1 INTRODUCTION 1

1.1 Cancer 1

1.2 Tumour Hypoxia 3

1.2.1 Treating tumour hypoxia 6

1.3 Hypoxia-activated prodrugs (HAPs) 9

1.3.1 Selectivity of HAPs for hypoxic tissue 9

1.3.2 Classes of bioreductive HAPs 11

Quinones 12

N-Oxides 13

Nitroaromatics 15

1.3.3 Molecularly targeted HAPs 20

1.4 Improving the efficacy of HAPs in clinical trials 24

1.5 Imaging tumour hypoxia 26

1.5.1 Exogenous bioreductive molecules 26

1.5.2 *In situ* fluorescence imaging 28

1.6 Aims 36

Chapter 2 DESIGN, SYNTHESIS AND EVALUATION OF A NOVEL FLUOROGENIC BIOREDUCTIVE GROUP 39

2.1 Introduction 39

2.2 Design of the fluorogenic bioreductive group 41

2.3 Synthesis 44

2.3.1 Synthetic Route 1 44

2.3.2 Synthetic route 2 49

2.4 Selection of a biologically active cargo molecule 56

2.5 Evaluation of 2.49 as a fluorogenic HAP 60

2.5.1 A validation protocol 60

2.5.2 Zinc reduction assay and fragmentation analysis 61

2.5.3 Bioreduction using NADPH reductase 63

2.5.4 Cell treatment and cell lysis analysis 65

2.5.5 Activity of 2.49 against BRD4 68

2.6 Fluorescence Evaluation 69

2.7 Conclusion 74

Chapter 3 TOWARDS THE SYTNHESIS OF A NIR, FLUOROGENIC HYPOXIA-ACTIVATED DYE 76

3.1 Introduction 76

3.2 Synthesis of intermediates 3.9 and 3.10 79

3.3 Condensation reactions 81

3.4 Base-catalysed elimination reactions 85

3.5 Knoevenagel condensation of malononitrile 87

3.6 Pd-catalysed nitration 88

3.7 Diazotisation of 3.1 89

3.8 Synthesis of an NIR fluorogenic bioreductive group 94

3.9 Discussion of synthetic strategies 97

Chapter 4 BIOLOGICAL EVALUATION OF A FLUOROGENIC AZIDE-CONTAINING HYPOXIA-ACTIVATED DYE 99

4.1 Introduction 99

4.1.1 Azide-containing compounds as biological probes 99

4.1.2 Evidence for azides as bioreducible functionalities 101

4.2 Synthesis of an azide-containing fluorogenic NIR dye 104

4.3 Fluorometric analysis and zinc reduction assay 105

4.4 Mechanism of reduction 107

4.5 Enzymatic Analysis 110

4.5.1 Cytochrome P450 (CYP) NADPH reductase enzymes 110

4.5.2 Human Liver Microsomes 111

4.5.3 Cytochrome P450 (CYP) enzymes 113

4.6 Cell treatment and cell lysis analysis 119

4.7 Fluorescence Evaluation 121

4.7.1 Fluorescence cell sorting to evaluate *in vitro* reduction 121

4.7.2 Confocal Microscopy 124

4.7.3 Spheroids 125

4.8 The role of sulfur-containing species 129

4.9 Discussion 135

Chapter 5 EVALUATION AND SYNTHESIS OF A NOVEL NIR FLUOROGENIC HYPOXIA-ACTIVATED PRODRUG 136

5.1 Introduction 136

5.1.1 Selection of a NIR fluorophore 136

5.1.2 HAPs with dual delivery of cargo molecules 139

5.2 Selection of the biologically active cargo molecule 142

5.3 Synthesis 142

5.3.1 Synthesis of the nitrobenzyl bioreductive core 142

5.3.2 Synthesis of hypoxia-activated derivatives of NIR dye 5.1 150

5.4 Evaluation of bioreductive properties 151
5.4.1 Zinc reduction assay 151
5.4.2 Cytochrome P450 (CYP) NADPH reductase assay 153
5.4.3 *In vitro* analysis 160
5.5 Fluorescence Evaluation 162
5.5.1 Fluorimetry 162
5.5.2 Confocal microscopy 163
5.6 Conclusions 165
Chapter 6 GENERAL DISCUSSION AND FUTURE WORK 166
6.1 Conclusions 166
6.2 Improving properties of fluorogenic HAPs 167
6.2.1 Considering compound delivery and concentration 167
6.2.2 Considering preclinical and clinical applications 168
6.2.3 Considering delivery of the cargo molecule 168
6.2.4 Considering alternative imaging modalities 170
6.3 Concluding remarks 171
Chapter 7 EXPERIMENTAL METHODS 172
7.1 General Chemistry 172
7.1.1 NMR Spectroscopy 172
7.1.2 Mass Spectrometry 173
7.1.3 Melting points 174
7.1.4 Infrared spectra 174
7.1.5 Analytical thin layer chromatography 174
7.1.6 Silica gel flash column chromatography 174
7.1.7 Concentration *in vacuo* 175
7.1.8 Chemicals 175
7.1.9 Solvent purification 175
7.1.10 Compound purity 175
7.1.11 HPLC analysis of assay solutions 176

7.1.12 Fluorometric analysis 177
7.1.13 Zinc reduction assay 177
7.1.14 Steady state radiolysis 178
7.2 Synthetic Procedures 179
7.2.1 Chapter 2 compounds 179
2.1. 6-Nitroquinoline 179
2.16. 5-(Bromomethyl)-6-nitroquinoline 180
2.17. (6-Nitroquinolin-5-yl)methanol 181
2.18. (6-Chloroquinolin-5-yl)methanol 182
2.19. 6-Chloroquinoline-5-carbaldehyde 183
2.21. 5-Bromo-6-chloroquinoline 184
2.23. 5,8-Dibromo-6-chloroquinoline 185
2.25. 5-Bromo-6-chloro-2-isopropylquinoline 185
2.28. 6-Chloro-5-(((2-fluorobenzyl)oxy)methyl)quinoline 186
2.29. 6-Chloro-5-(((4-fluorobenzyl)oxy)methyl)quinoline 187
2.30. 5-((Benzyloxy)methyl)-6-chloroquinoline 188
2.31. (6-Chloroquinolin-5-yl)methyl acetate 189
2.32. 5-(((2-Fluorobenzyl)oxy)methyl)-6-nitroquinoline 190
2.33. 5-(((4-Fluorobenzyl)oxy)methyl)-6-nitroquinoline 192
2.36. 6-Nitroquinoline-5-carbaldehyde 193
2.37. 5-Bromo-6-nitroquinoline 194
2.40. 5-Amino-8-bromo-6-nitroquinoline 195
2.47. 6,6'-Dinitro-5,5'-biquinoline 196
2.49. (3-(3,5-Dimethylisoxazol-4-yl)-5-((6-nitroquinolin-5-yl)methoxy)phenyl)(phenyl)methanol 197
2.56. (6-Aminoquinolin-5-yl)methanol 198
7.2.2 Chapter 3 compounds 200
3.1. (*E*)-2-(2-(4-Aminostyryl)-4*H*-chromen-4-ylidene)malononitrile 200
3.2. (*E*)-2-(2-(4-Nitrostyryl)-4*H*-chromen-4-ylidene)malononitrile* 201
3.9. 2-Methyl-4*H*-chromen-4-one 202
3.10. 2-(2-Methyl-4*H*-chromen-4-ylidene)malononitrile 203
3.16. (*E/Z*)-2-(2-Methyl-4*H*-chromen-4-ylidene)-3-oxo-3-(piperidin-1-yl)propanenitrile 204

3.21. (*E*)-2-(2-(4-Hydroxystyryl)-4*H*-chromen-4-ylidene)malononitrile 205
3.24. (*E*)-2-(4-Nitrostyryl)-4*H*-chromen-4-one 206
3.25. 2-(1-(4-Nitrophenyl)-2-(4-oxo-4*H*-chromen-2-yl)ethyl)malononitrile 207
3.27. (*E*)-4-(2-(4-(Dicyanomethylene)-4*H*-chromen-2-yl)vinyl)phenyl trifluoromethanesulfonate 208
3.29. (*E*)-2-(2-(4-Azidostyryl)-4*H*-chromen-4-ylidene)malononitrile 209
3.34. Methyl 3-(bromomethyl)-4-nitrobenzoate 210
3.35. Methyl 3-(hydroxymethyl)-4-nitrobenzoate 211
3.37. Methyl 3-(((*tert*-butyldimethylsilyl)oxy)methyl)-4-nitrobenzoate 212
3.38. (3-(((*tert*-Butyldimethylsilyl)oxy)methyl)-4-nitrophenyl)methanol 213
3.39. 3-(((*tert*-Butyldimethylsilyl)oxy)methyl)-4-nitrobenzaldehyde 214

7.2.3 Chapter 5 compounds 216

5.1. (*E*)-1-Ethyl-2-(2-(6-hydroxy-2,3-dihydro-1*H*-xanthen-4-yl)vinyl)-3,3-dimethyl-3*H*-indol-1-ium iodide 216
5.8. (*E*)-2-(2-(6-((3-((3-(3,5-Dimethylisoxazol-4-yl)-5-((4-fluorophenyl)(hydroxy)methyl)phenoxy)methyl)-4-nitrobenzyl)oxy)-2,3-dihydro-1*H*-xanthen-4-yl)vinyl)-1-ethyl-3,3-dimethyl-3*H*-indol-1-ium iodide 217
5.15. (3-((5-(Bromomethyl)-2-nitrobenzyl)oxy)-5-(3,5-dimethylisoxazol-4-yl)phenyl)(4-fluorophenyl)methanol 219
5.16. 2,4-Bis(bromomethyl)-1-nitrobenzene 220
5.17. (4-Nitro-1,3-phenylene)dimethanol 221
5.18. (3-((3-(Bromomethyl)-4-nitrobenzyl)oxy)-5-(3,5-dimethylisoxazol-4-yl)phenyl)(4-fluorophenyl)methanol 222
5.20. 1-Ethyl-2,3,3-trimethyl-3*H*-indol-1-ium iodide 223
5.22. (*E*)-2-Chloro-3-(hydroxymethylene)cyclohex-1-ene-1-carbaldehyde 223
5.24. 2-((*E*)-2-((*E*)-2-Chloro-3-(2-((*E*)-1-ethyl-3,3-dimethylindolin-2-ylidene)ethylidene)cyclohex-1-en-1-yl)vinyl)-1-ethyl-3,3-dimethyl-3*H*-indol-1-ium iodide 224
5.26. 1-Ethyl-2-((*E*)-2-((*E*)-3-(2-((*E*)-1-ethyl-3,3-dimethylindolin-2-ylidene)ethylidene)-2-((4-nitrophenethyl)amino)cyclohex-1-en-1-yl)vinyl)-3,3-dimethyl-3*H*-indol-1-ium iodide 225
5.33. (*E*)-1-Ethyl-3,3-dimethyl-2-(2-(6-((4-nitrobenzyl)oxy)-2,3-dihydro-1*H*-xanthen-4-yl)vinyl)-3*H*-indol-1-ium iodide 226

7.3 Biological Methods 228

7.3.1 General biological laboratory and cell culture reagents 228
7.3.2 Hypoxia treatment 229
7.3.3 Enzyme treatments 229
7.3.4 Cell lines and culture 231
7.3.5 Cryropreservation of cell lines 233
7.3.6 Compound treatments of cells 233
7.3.7 Cell lysate HPLC analysis 234
7.3.8 Antibodies 235
7.3.9 Cell lysis and protein purification 236
7.3.10 Western blotting 236
7.3.11 RNA interference 237
7.3.12 Fluorescence microscopy 238
7.3.13 Spheroid growth and treatment 238
7.3.14 Spheroid immunofluorescence microscopy 239
7.3.15 Fluorescence automated cell sorting (FACS) 240
7.3.16 Clonogenic survival assay 240
7.3.17 Statistical analysis 241

REFERENCES 242

APPENDICES 268

A. List of publications and patents 268
B. Select ^{1}H, ^{13}C, and ^{19}F NMR Spectra 298
C. Single dose mean graph of Compound 2.48 384

LIST OF ABBREVIATIONS

ADP · adenosine diphosphate

AOAA · aminooxyacetic acid

aq. · aqueous

Ar · aromatic

ATR · ataxia telangiectasia and Rad3-related protein

a.u. · absorbance units

AZT · azidothymidine/Zidovudine

BET · bromodomain and extra-terminal domain family

BRD4 · bromodomain-containing protein 4

BSA · bovine serum albumin

Bu · butyl

^{t}Bu · *tert*-butyl

CBS · cystathionine beta synthase

Chk1 · checkpoint kinase 1

conc. · concentrated

COSY · homonuclear correlation spectroscopy

CSE · cystathionine gamma-lyase

CYP · cytochrome P450

DAPI · 4',6-Diamidino-2-phenylindole dihydrochloride

dba · dibenzylideneacetone

DCE · 1,2-dichloroethane

DDR · DNA damage response

DMF · dimethylformamide

DMSO · dimethyl sulfoxide

DNA · deoxyribonucleic Acid

DSB · double strand break

EGFR · epidermal growth factor receptor

EPR · enhanced permeability and retention

ESI · electrospray ionisation

eq. · equivalents

FACS · fluorescence automated cell sorting

FAD · flavin adenine dinucleotide

FBS · fetal bovine serum

FDA · food and drug administration (United States)

FI · field ionisation

FMN · flavin mononucleotide

× *g* · times gravity

g · grams

GSH · glutathione

h · hour(s)

HAP · hypoxia-activated prodrug

HBOT · hyperbaric oxygen therapy

HIF-1 · hypoxia-inducible factor 1

HMBC · heteronuclear multiple-bond correlation

HPLC · high-performance liquid chromatography

HSQC · heteronuclear single quantum coherence

Hz · hertz

IC_{50} · half inhibitory concentration

ICG · indocyanine green

^{i}Pr · *iso*-propyl

iNOS · nitric oxide synthase

J · coupling constant

LCMS · liquid chromatography-mass spectrometry

L-cys · L-cysteine

LDA · lithium diisopropylamide

Lit. · literature value

MHz · megahertz

min · minute(s)

MRI · magnetic resonance imaging

MS · mass spectrometry

mTOR · mechanistic target of rapamycin

m/z · mass divided by charge ratio

NADPH · nicotinamide adenine dinucleotide phosphate

NIR · near infrared

NMR · nuclear magnetic resonance

PAG · propargyl glycine

PBS · phosphate buffered saline

PDB ID · protein data bank identification

PE · petroleum ether

PET · positron emission tomography

Ph · phenyl

pO_2 · partial pressure of oxygen

ppm · parts per million

R_f · retention factor

RNA · ribonucleic acid

RT · room temperature

SAR · structure-activity relationship

sat. · saturated

SET · single electron transfer

siNT · short-noninterfering RNA

siRNA · short-interfering RNA

S_NAr · nucleophilic aromatic substitution

SPR · surface plasmon resonance

SSB · single strand break

TBS · tris-buffered saline

TBDMS · *tert*-Butyldimethylsilyl

TCA · trichloroacetic acid

TFA · trifluoroacetic acid

THF · tetrahydrofuran

TKI · tyrosine kinase inhibitor

TLC · thin layer chromatography

topo II · topoisomerase II

TPZ · tirapazamine

VEGF · vascular endothelial growth factor

WT · wild-type

Chapter 1

INTRODUCTION

1.1 Cancer

Cancer is a leading cause of death worldwide, accounting for 8.2 million deaths in 2012, and a further 14 million diagnoses.[1,2] Despite advances in the understanding of cancer biology, it is estimated that 1 in 2 people in the United Kingdom, born after 1960, will develop the disease.[3] Consequently, interrogation of the underpinning biology and tumourigenesis is the subject of intense global research,[4-6] and successfully treating cancer patients remains a significant challenge.[7,8]

Cancer is the term used to describe a broad range of diseases that can affect any area of the body. Normal, healthy cells become cancerous as a result of errors made during cell replication, introducing mutations to the genome.[9] Consequently, the precise characteristics of cancer are complex, and differ between affected tissues, and individual patients. In their seminal paper, Hanahan and Weinberg proposed key 'hallmarks' or traits common to all cancer types. Identification of these fundamental properties has aided clinicians and biologists to better understand tumour phenotypes, and discuss this complex disease.[10] These hallmarks include resistance to cell death, enhanced levels of cell replication, invasiveness towards healthy tissues, and

various other mechanisms to promote cancer cell survival.[10] A more detailed understanding of the operative machinery of tumour cells, has led to the more recent inclusion of further hallmarks; genomic instability, abnormal metabolic pathways, inflammation and evasion of the immune system (**Figure 1.1**).[6]

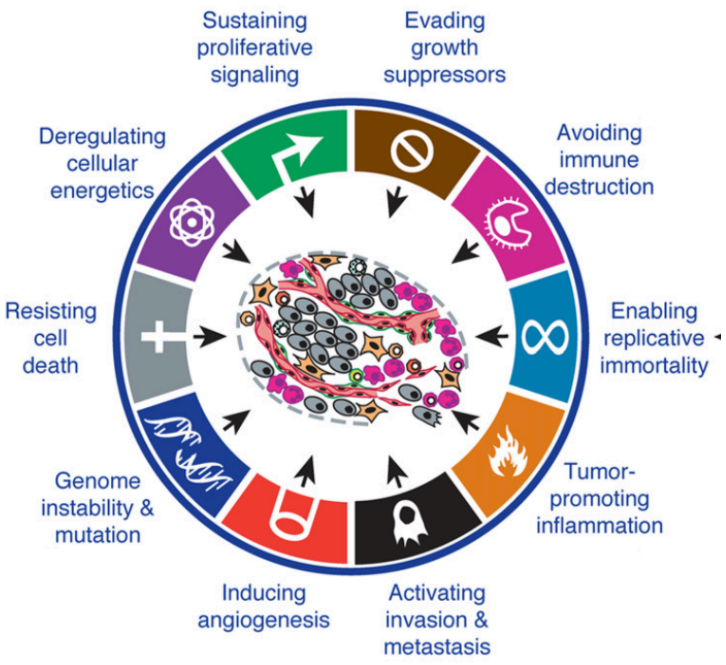

Figure 1.1. An illustration to show the variety and complexity of capabilities acquired by cancer cells to promote growth and survival. Adapted with permission: license number 3884141391482.[6]

Combinations of cancer hallmarks collectively influence the tumour phenotype. High metabolic demand of rapidly proliferating cancer cells, results in rapid consumption of oxygen within the tumour volume, causing the tumour to switch to abnormal metabolic pathways. The increased demand for oxygen ultimately leads to another hallmark of solid tumours: tumour hypoxia.

1.2 Tumour Hypoxia

Hypoxia (an inadequate supply of oxygen for normal cellular function) is a common feature of solid tumours, associated with poor patient prognosis, aggressive tumour phenotypes, and decreased genomic stability (**Figure 1.2**).[11,12] Increased resistance to both radiotherapy and chemotherapy, and a strong link with metastatic potential, makes treatment of hypoxic tumours a significant clinical challenge.[12]

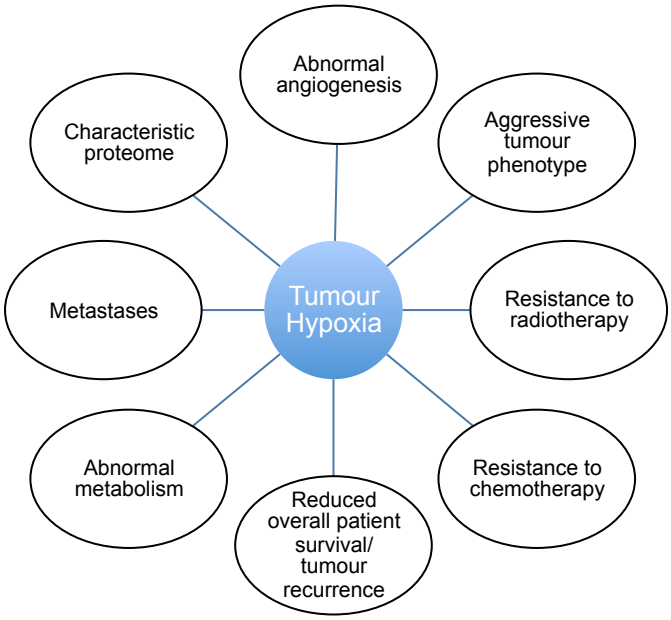

Figure 1.2. A relationship diagram to show the implications of tumour hypoxia on cell biology and treatment for patients.

Hypoxia arises due to an imbalance between oxygen availability and requirement. As tumour cells proliferate rapidly, their metabolic demand for oxygen exceeds supply, and the tumour induces the process of angiogenesis (new blood vessel formation) in an attempt to address the deficit.[13-15] However, the vasculature (blood vessel system) within a hypoxic tumour is highly abnormal, and although adequate to sustain the tumour, regions of low oxygen exist (**Figure 1.3**).[16,17] The condition of hypoxia can be dynamic within

the tumour, and areas can undergo reoxygenation as oxygen supply is restored.[18] Tumour hypoxia is found at distances typically >100 μm from the nearest blood vessel, and consequently, the oxygen deficiency moving away from a vessel is highly heterogeneous.[19-21]

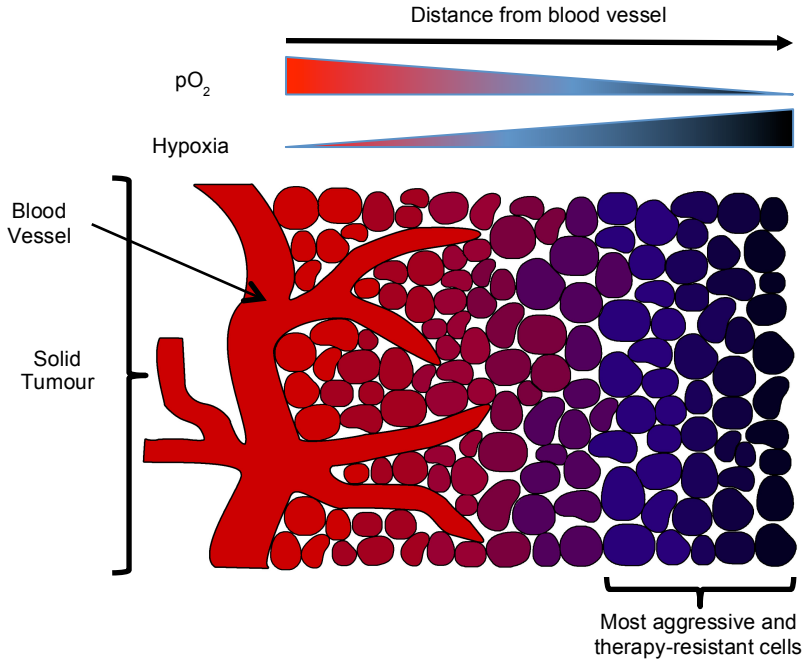

Figure 1.3. An illustration of the hypoxic tumour microenvironment. Tumour cells proximal to the blood vessel receive an adequate supply of O_2. However distal cells are increasingly starved of O_2. These hypoxic cells represent the most aggressive and therapy resistant cells. Image credit: Jonathan Ient, Hammond Laboratory.

Clinical trials have correlated tumour hypoxia with poor prognoses in patients with head and neck,[22] cervical[23] and prostate cancer.[24] The poor outcome for patients with hypoxic tumours, and the resistance of hypoxic tumours to conventional therapy, is starkly demonstrated by disease-free survival of patients with head and neck cancer, following radiation therapy (**Figure 1.4**).[25] Patient survival was determined to be 30% less where patients tested positive for tumour hypoxia, compared to those with normoxic tumours, over a period of 30 months.

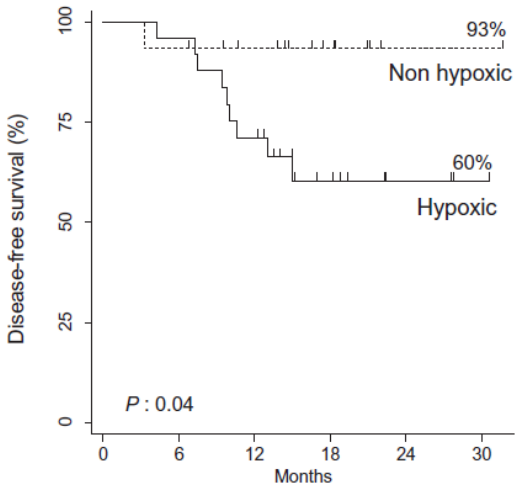

Figure 1.4. Disease free survival over a 30-month period of 40 patients with head and neck cancer following radiation therapy. Patients with hypoxic tumours suffered an approximate 30% increased mortality risk, compared to patients with normoxic tumours. Adapted with permission: license number 3903660025812.[25]

Representative partial pressures of oxygen (pO_2) in various types of solid tumour, and that of healthy tissue surrounding the tumour are shown in **Table 1.1**, as determined by the oxygen electrode.[16,26] A distinct difference between the pO_2 for healthy tissue, and the tumour is observed, indicating a poorly perfused vasculature and the presence of hypoxia. Tumour hypoxia is typically defined as a partial pressure of oxygen between 1 - 15 mmHg, or 0.1 – 2% atmospheric oxygen (pO_2 Air: 160 mmHg [21%]),[26] with severe hypoxia or anoxia defined as below 0.1% O_2.[27] However, the oxygen electrode is invasive, limited to surgically accessible tumours, and subjective with respect to the area of the tumour examined, and consequently is no longer commonly used.[26,28]

Table 1.1. Average partial pressures of oxygen (pO_2) in mmHg in various tumour cell types and the surrounding healthy tissue, as determined by an oxygen electrode. Red represents well oxygenated, and blue represents poorly oxygenated. Table adapted from data obtained from various patient cohorts. ND indicates data not available.[16,26]

Tumour type	Median tumour pO_2 (mmHg)	Median normal pO_2 (mmHg)
Glioblastoma	4.9	ND
Head and neck carcinoma	14.6	51.2
Lung	7.5	38.5
Breast	10.0	ND
Pancreatic	2.7	51.6
Cervical	3.0	51.0
Prostate	2.4	30.0
Soft-tissue sarcoma	6.2	ND

The data shown in **Table 1.1** highlights the variability of hypoxia between different tumour types, and gives some indication of the complexity of the condition, and why therefore it is difficult to treat effectively.

1.2.1 Treating tumour hypoxia

Patients with hypoxic tumours are significantly less likely to respond to all forms of therapy, including chemotherapy and radiotherapy.[22,29,30] Chemotherapy (the use of xenobiotics to treat tumours) relies on an efficient vasculature system for compound delivery to the tumour volume *via* the blood. However, the tortuous hypoxic vasculature hinders efficient compound delivery to the tumour volume.[31] Furthermore, radiotherapy (the use of radiation to kill cancer cells) relies on the presence of oxygen to be an effective method of treatment, through what is known as the oxygen enhancement effect.[22,32] Oxygen is required to permanently fix the damage caused to DNA during radiation therapy, through oxidative processes.[33] In the absence of oxygen, the required dose of radiation to achieve the same

biological response, can be up to three times greater than under conditions of adequate oxygen.[19,34] Furthermore, hypoxia promotes the metastatic potential of the tumour. Approximately 90% of deaths attributed to cancer do not arise from the primary tumour itself, but from invasion of other organs in the latter stages of the disease (metastases).[35] Patients with resectable hypoxic tumours often require follow up treatment, as secondary tumours are already developing.[36] However, removal of metastases is not always an option for patients. Consequently, hypoxia represents a major clinical challenge in the treatment of patients with solid tumours, and its negative implications has led to various strategies to improve outcome.

Hyperbaric oxygen therapy (HBOT) requires patients to inhale an oxygen enriched atmosphere, to increase delivery of oxygen to the tumour.[37] This technique improved the effectiveness of radiation (as determined by local tumour control) in a large multicentre clinical trial of patients with advanced uterine cervical cancer.[38] However, HBOT has not been implemented as a regular clinical procedure due to logistical difficulties of administering radiation in atmospheric chambers.[38]

An alternative strategy for radiosensitsation is administration of molecules capable of mimicking the role of oxygen in fixing radiation-induced DNA damage.[39] Nimorazole **1.2**, a nitroimidazole-based drug, was developed as a more potent radiosensitiser than the related, less efficient radiosensitiser, misonidazole **1.1** (**Figure 1.5**).[40] The electron-withdrawing nitroimidazole moiety can accept electrons produced during ionising radiation to form a radical **1.3**, like oxygen does to form superoxide. The nimorazole nitro radical **1.3** has similar reactivity to molecular superoxide towards DNA bases, making

damage to the DNA structure permanent.[41] Nimorazole improves disease-free survival and local tumour control in patients with head and neck cancer, who are receiving radiotherapy (**Figure 1.5**).[42] Nimorazole is now routinely used in Denmark as an accompaniment to radiation therapy, but additional clinical trials in other countries are on-going.[39]

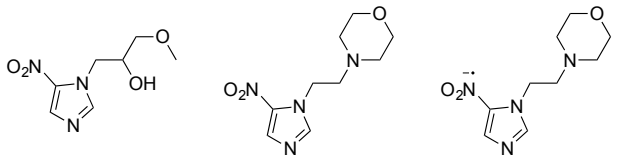

1.1 (Misonidazole) **1.2** (Nimorazole) **1.3**

Figure 1.5. The chemical structures of radiosensitising molecules; misonidazole **1.1**, nimorazole **1.2**, and the corresponding nitro radical of nimorazole, **1.3**.

The cellular response to low oxygen conditions results a unique proteome and hypoxic signature. The key transcriptional factor, hypoxia-inducible factor 1 (HIF-1), is stabilised under hypoxic conditions, resulting in up-regulation of HIF responsive genes to promote cell survival.[43] Conditions of low oxygen also result in the activation of pathways to repair DNA damage.[44] For example, inhibition of ataxia telangiectasia and Rad3-related protein (ATR), a key kinase involved in the hypoxic DNA damage response (DDR), results in increased sensitisation of hypoxic cells to radiation.[45] Hypoxic tumours can be sensitised to existing treatments, such as radiotherapy, by inhibiting proteins critical to hypoxic survival.[46] However, many of the pathways involved in the hypoxic response are also important for normal cell cycle progression.[47] Consequently, methods for targeting these molecules to hypoxia are desired. The characteristic low-oxygen environment, compared to normal tissues, presents a window of therapeutic opportunity to develop targeted therapies.[48] By exploiting the chemically reducing conditions

found in hypoxic regions, oxygen-sensitive molecules can be designed to selectively kill hypoxic cells. Therapies that belong to this class of treatment are described as hypoxia-activated prodrugs (HAPs).

1.3 Hypoxia-activated prodrugs (HAPs)

HAPs are biologically-inactive molecules that undergo enzyme-mediated reduction under conditions of reduced oxygen.[17] Bioreduction of HAPs causes a change in the chemical structure, transforming the prodrug into a biologically active form, to kill hypoxic cells. The use of prodrugs in cancer therapy is potentially a superior approach to conventional chemotherapy. Chemotherapeutics are extremely toxic, and cause adverse, and often intolerable side effects for patients.[49] By targeting drugs to hypoxia, these side effects could be reduced by enabling greater control over delivery.[50] HAPs are specifically designed to exploit the unique microenvironment found within hypoxic tumours for therapeutic advantage. Different classes of HAPs gain their requisite oxygen-sensitivity and hypoxic toxicity *via* different metabolic pathways, but all rely on enzyme-mediated reductive processes.

1.3.1 Selectivity of HAPs for hypoxic tissue

The majority of HAPs rely on the presence of one-electron reductase enzymes in tumour tissue, which are upregulated in hypoxic conditions.[51] Single electron transfer (SET) to the HAP is mediated by reductases, generating a radical species (**Scheme 1.1**).[52] Under normoxic (where an adequate oxygen supply is available) conditions, oxygen can scavenge the radical's electron, and oxidise the HAP back to its original state. This futile

redox process between enzyme, HAP, and oxygen, is critical in preventing unwanted activation of the prodrug in healthy, well-oxygenated tissues.[16] Under hypoxic conditions, however, further reduction by enzyme-mediated SETs can occur, resulting in biotransformation of the HAP to its active form. The oxygen sensitive chemical group is embedded in the HAP structure, and are henceforth referred to as bioreductive groups.

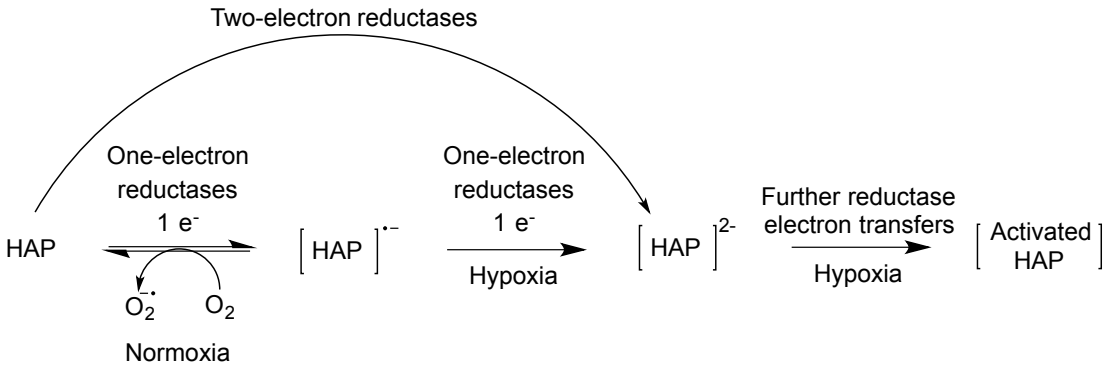

Scheme 1.1. The general mechanism of HAP activation by one-electron reductases. In the presence of oxygen the initial radical is quenched. Further reduction under hypoxic conditions results in activation of the HAP.

A number of one-electron reductases responsible for HAP activation have been identified, and their ability to do so relies on the class of bioreductive group employed.[53,54] Some HAPs can be reduced by two-electron reductases, consequently bypassing the mechanism of hypoxia-sensitivity by quenching of radicals by oxygen (**Scheme 1.1**).[17] Such prodrugs derive their oxygen sensitivity from competition with oxygen for electrons. Where oxygen levels are depleted, reduction of the HAP can occur.[55,56]

1.3.2 Classes of bioreductive HAPs

Early attempts to sensitise hypoxic tumours to radiation therapy, focused on molecules that mimic oxygen and its radiosensitising properties, such as nimorazole **1.2** (**Figure 1.5**).[40] It was noted that some of these molecules had enhanced toxicity against hypoxic cells in the absence of radiation, and therefore might be useful as targeted therapies.[57] Pioneering work by Wilson and co-workers demonstrated that the nitroaromatic, nitracrine **1.4**, showed 100,000-fold enhanced hypoxia-selective toxicity compared to the radiosensitiser misonidazole **1.1**, by intercalating DNA to induce damage (**Figure 1.6**).[58] Since these studies, a range of chemical functionalities have been identified as useful moieties to target hypoxia, including; quinones, *N*-oxides, and nitroaromatic compounds.[59]

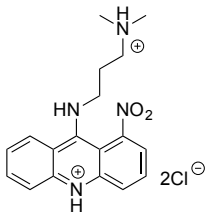

1.4 (Nitracrine)

Figure 1.6. Chemical structure of nitracrine **1.4**.

Quinone and *N*-Oxide based HAPs are typically activated at 'intermediate' levels of hypoxia (kO_2 [O_2 for 50% reduction inhibition] ~ 1 μM) owing to their reductive activation by two-electron reductases, and are described as Class I HAPs.[60] Nitroaromatic HAPs are reduced under conditions of 'acute' hypoxia (kO_2 ~ 0.1 μM), relying on single electron-reductase activity, and are referred to as Class II HAPs.[60] Different oxygen sensitivities of HAPs potentially enables tailoring of activation

according to the severity of hypoxia found in a tumour. It is, therefore, important to know the oxygen concentrations at which specific HAPs are activated, and to correlate this with a patient's tumour hypoxia when considering treatment.[17] However, accurately determining the severity of hypoxia, and therefore predicting the efficacy of any HAP, is a major clinical challenge, and evaluation of the degree of tumour hypoxia is not routine clinical practice.[28]

Quinones

The widely used quinone-based anticancer-drug, Mitomycin C **1.5**, targets cancer by cross-linking DNA, preventing cell replication (**Figure 1.7**).[61,62] During preclinical evaluation, **1.5** was noted to have enhanced toxicity against hypoxic cells compared to those in normoxia.[63] Subsequent development of derivatives of **1.5** led to molecules with improved hypoxia-specificity,[53] the most widely evaluated of which is the clinical candidate EO9 **1.6**, which demonstrates 30-fold enhanced cytotoxicity under hypoxic conditions following reduction to DNA damaging species **1.8** (**Figure 1.7**).[53,64] However, the poor pharmacokinetic profile of **1.6** has hindered evaluation in tumour types where local administration is not possible.[65] Paradoxically, the rapid urinary clearance of E09 **1.6** has led to its application as a treatment for metastatic bladder cancer, and has shown promising results for reducing disease recurrence in Phase II clinical trials.[66] A multicentre Phase III clinical trial, initiated in September 2015, is currently underway (NCT02563561).

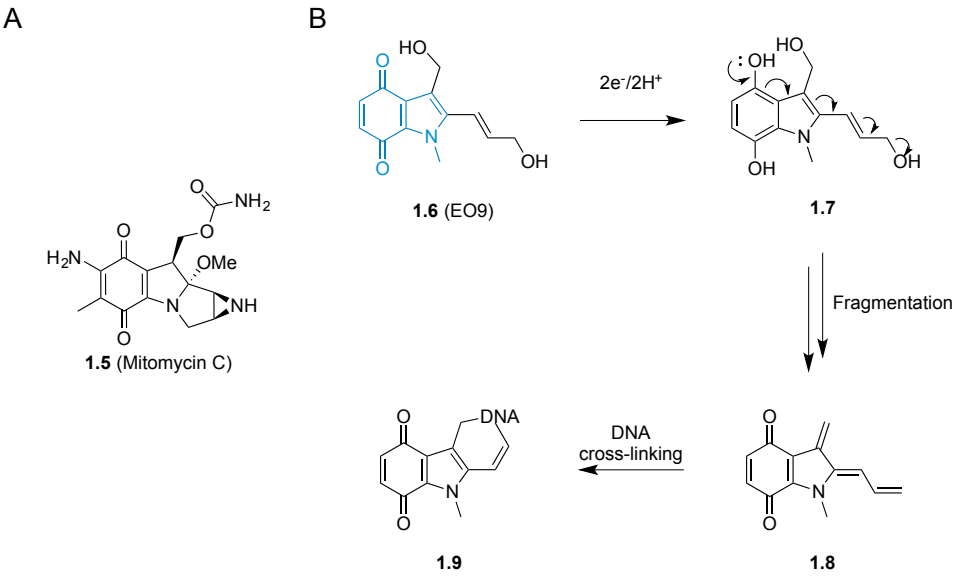

Figure 1.7. (A) The chemical structure of Mitomycin C **1.5**; (B) A scheme to show the mechanism of reduction of EO9 **1.6** under hypoxic conditions. The bioreductive quinone moiety is highlighted in blue. **1.6** can be reduced by one or two-electron reductases.[17]

N-Oxides

Both aliphatic and aromatic *N*-oxides have also undergone clinical and preclinical evaluation as HAPs.[17] Tirapazamine (TPZ) **1.10** is perhaps the most widely investigated HAP of this class, and induces DNA damage by formation of radicals **1.11** and **1.12** under hypoxic conditions (**Figure 1.8A**).[51] However, a Phase III clinical trial, in combination with chemotherapy, and radiation, determined that administration of TPZ **1.10** to patients with head and neck cancers led to no overall improvement in patient survival.[67] Criticisms of the head and neck cancer trial have, however, been made due to lack of stratification of patients with hypoxic tumours, and for the quality of radiation delivery.[67,68] Similar results were recorded in a more recent Phase III trial with patients suffering from cervical carcinomas, resulting in further speculation that successful clinical results may require the identification of patients with tumour hypoxia prior to initiation of the trial.[69] The lack of clinical

efficacy is also partially attributed to poor extravascular permeability of **1.10** in the tumour volume.[70] Consequently, analogues of **1.10** with improved pharmacokinetic profiles have been investigated, including SN30000 **1.13**, which is currently undergoing preclinical development (**Figure 1.8B**).[71,72]

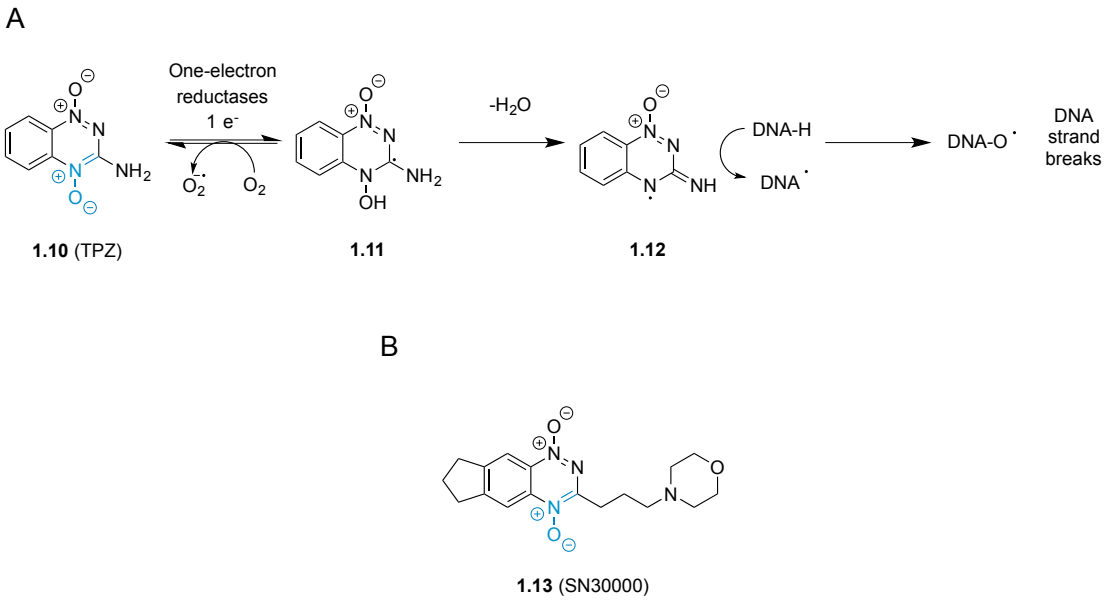

Figure 1.8. (A) A scheme to show the reduction mechanism of aromatic *N*-oxide TPZ **1.10**, mediated by one or two electron reductases. The bioreductive *N*-oxide moiety is highlighted in blue. Formation of radicals **1.11** and **1.12** causes radical damage to DNA, introducing irreversible DNA strand breaks; (B) Chemical structures of pharmacologically improved TPZ derivative, SN30000 **1.13**, activated by one-electron reductases.[73]

Another *N*-oxide based HAP, AQ4N **1.14**, inhibits topoisomerase II (topo II) and intercalates DNA, following reduction to the corresponding dimethyl amine **1.15**, under hypoxic conditions (**Scheme 1.2**). Topo II regulates the introduction, and repair of double strand breaks (DSBs) and single strand breaks (SSBs) in DNA in the event of DNA becoming tangled or broken during cell replication.[74] Inhibition of topo II results in apoptosis, and is the subject target of a recent Phase II clinical trial for patients with metastatic soft tissue sarcoma.[75] In addition to one-electron reductases, AQ4N **1.14** can be activated by two-electron reductases under hypoxic conditions.[76] Recent *in*

vitro studies demonstrated the effectiveness of combining AQ4N **1.14** with radiation, and highlights the importance of the 2-electron reductase haemoprotein, nitric oxide synthase (iNOS) for activation of the prodrug.[77,78] Furthermore, AQ4N **1.14** is reduced by the 2-electron reductases cytochrome P450s 2S1 and 2W1, which are highly upregulated in response to hypoxia.[56] Preclinical treatment of tumours with AQ4N **1.14** has been shown to improve sensitivity to radiotherapy.[76,79] Phase I clinical trials demonstrated that AQ4N **1.14** localised in hypoxia preferentially in a variety of tumour tissue types, and encouragingly was permeable across the blood-brain barrier, with no significant toxicity to patients.[80,81] AQ4N **1.14** is under evaluation in further Phase I/II clinical trials in patients with various solid tumour types, although progression has been hampered by lack of financial support.[82]

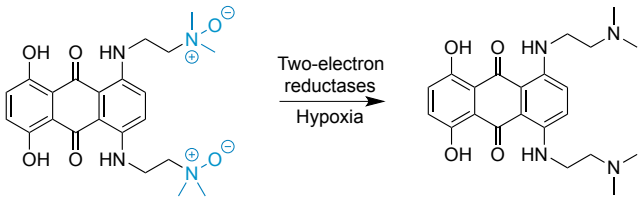

1.14 (AQ4N) **1.15** (AQ4)

Scheme 1.2. The mechanism of action of AQ4N **1.14**. Two-electron reductase activity results in reduction of the *N*-oxide functionality to afford AQ4 **1.15**, a topoisomerase II inhibitor.

Nitroaromatics

A variety of nitroaromatic-based bioreductive groups have been employed in the development of hypoxia-targeted compounds including; nitrofurans, nitrothiophenes, and perhaps more commonly, nitroimidazoles and nitrobenzyls.[47,83-87] Each of these bioreductive groups relies on reduction of the nitro functionality for their oxygen sensitivity, which occurs *via* a sequential one-electron reduction mechanism.[48] Transfer of a single electron

(SET) to a nitro group **1.16**, results in radical species **1.17**, which can be quenched by oxygen, back to **1.16**. This futile redox cycle ensures the bioreductive group is not activated in normal tissues. Under conditions of hypoxia, further SETs can occur, reducing the nitro functionality to the nitroso **1.18**, hydroxylamine **1.19** or amine **1.20** functionality (**Scheme 1.3**).[47]

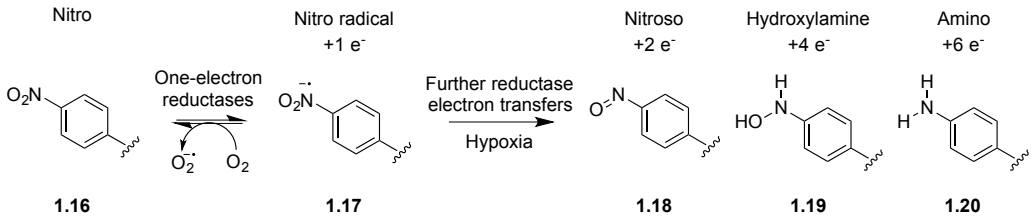

Scheme 1.3. Enzyme-mediated reduction of nitro groups occurs *via* sequential single electron transfers, to afford a variety of reduction intermediates. The nitro radical can be quenched by oxygen, affording oxygen sensitivity. The nitroaromatic class of bioreductive group is used as an example.

The sensitivity of nitro groups to SET reduction has been exploited in HAP development in two distinct ways: firstly, to furnish an amino group in a scaffold following nitro reduction; and secondly as a trigger group to induce prodrug fragmentation, and release a molecule of therapeutic interest.[17] An example of the former is the clinical candidate PR-104 **1.21**, which following phosphate hydrolysis to **1.21**, and reduction of the nitro group to the corresponding amine, furnishes activated nitrogen mustards **1.24** and **1.25**, capable of intercalating DNA in hypoxia, which causes cell-cycle arrest (**Scheme 1.4**).[88,89] Despite some underlying issues with dose related toxicity, **1.21** has undergone a variety of clinical trials.[84,90] A recent Phase I/II clinical trial demonstrated **1.21** to be particularly effective in combating tumours associated with acute myeloid leukaemia (NCT01037556), warranting further investigation of **1.21** in cancer therapy.[91]

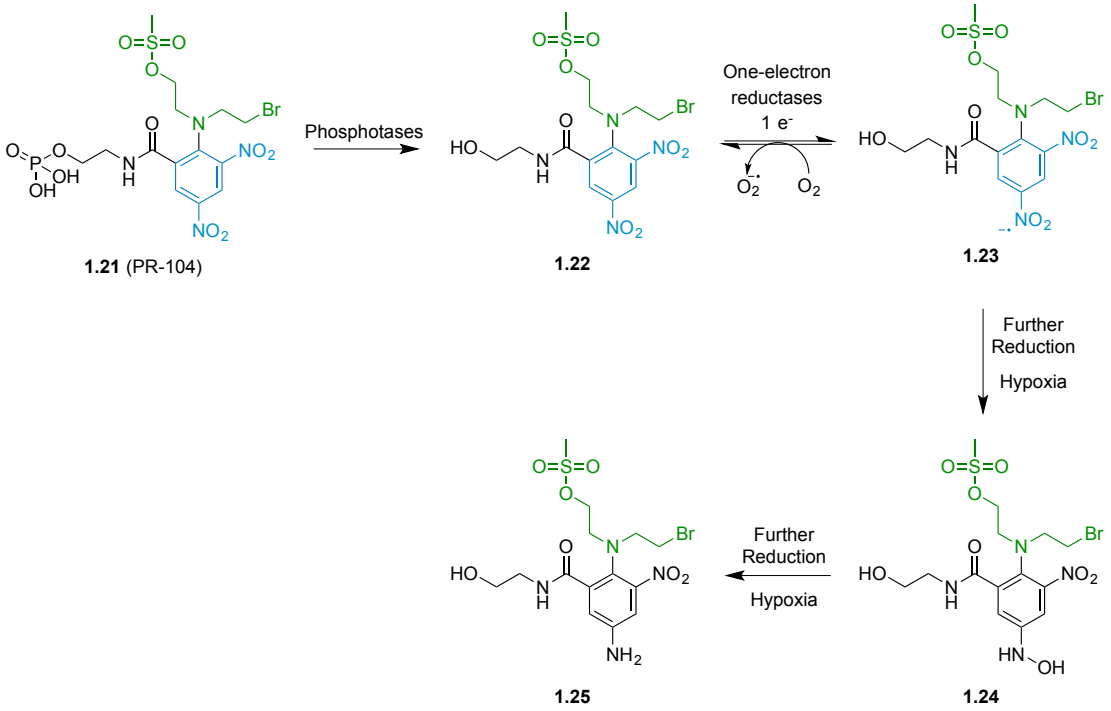

Scheme 1.4. The mechanism of reductive activation of PR-104 **1.21**, mediated by phosphatases and one or two electron reductases. The bioreductive moiety is highlighted in blue, and the DNA damaging nitrogen mustard in green. Reduction of the *para* nitro position affords hydroxylamine **1.24**, activating the nitrogen mustard component for DNA intercalation. Further reduction to the amine **1.25** also promotes the DNA damaging interaction.[89]

The second utility of nitroaromatic bioreductive groups – as trigger moieties to release a therapeutic molecule in hypoxia – will be the focus of the studies described in this dissertation. Enzymatic reduction of the electron-withdrawing nitro group to the corresponding electron donating amine results in a change in the electronic properties of the aromatic system. The increase in aromatic electron density following nitro group reduction has been exploited to promote prodrug fragmentation at the benzylic position (**Scheme 1.5**).[17,92] A cargo molecule of therapeutic interest is subsequently released. Before reduction occurs the prodrugs must be hydrolytically stable (with respect to hydrolysis at the benzylic position) and therefore, the cargo molecules are not released under normoxic conditions.

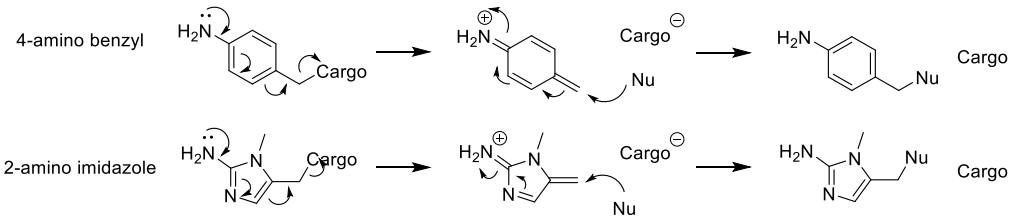

Scheme 1.5. Elimination causes fragmentation at the benzylic position of a hypoxia-activated prodrug to release the cargo molecule.[48]

The most clinically advanced HAP of this class is TH-302 **1.26**, a 2-nitroimidazole-based prodrug, which following activation in hypoxia, releases the nitrogen mustard **1.30**, a DNA alkylating agent (**Scheme 1.6**).[83] Only once fragmentation to release **1.30** is induced, can DNA alkylation occur **1.31**.[92] A recent *in vivo* study suggested that inhibition of vascular endothelial growth factor (VEGF; a driver of angiogenesis), and inhibition of HIF-1α (a driver of tumourigenesis), in combination with **1.26** could be an attractive therapeutic combination for treatment of sarcomas.[93] This work complemented the finding that TH-302 **1.26**, in combination with VEGF inhibitors, enhanced the efficacy of radiotherapy.[94] Further preclinical studies have shown the anti-tumour utility of TH-302 **1.26** is enhanced when combined with checkpoint-kinase 1 (Chk1) inhibitors, a key regulator of the cell cycle.[95] The enhancement of cytotoxicity was observed only in p53 (tumour suppressor gene)-deficient cells, compared to p53 proficient cells. Treatment of mice bearing renal cell carcinoma xenografts with TH-302 **1.26** in combination with inhibitors of the intracellular kinase mTOR (cell growth regulator), increased DNA damage, and decreased cell proliferation compared to individual treatments.[96]

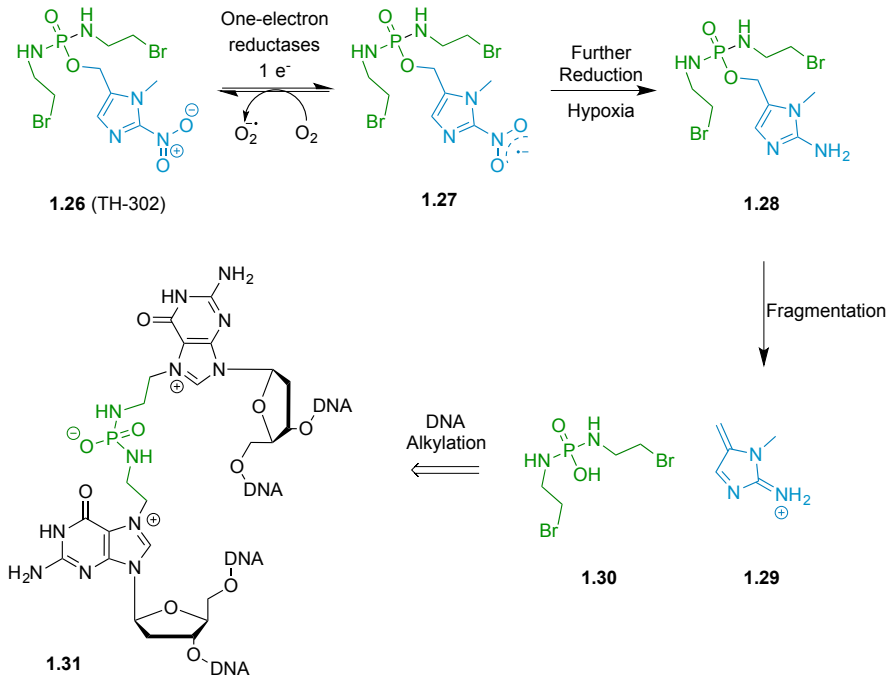

Scheme 1.6. The mechanism of reductive activation of TH-302 **1.26**, mediated by one-electron reductases. Under normoxic conditions, the HAP remains inactive. However, following reduction of the 2-nitroimidazole bioreductive group (blue) to the corresponding amine **1.28**, fragmentation occurs to release the nitrogen mustard **1.30** (green), which then alkylates basic residues in the DNA backbone causing irreversible DNA damage.[92]

Recent Phase III clinical trials (NCT01746979, NCT01440088) evaluated **1.26** as a combination therapy, with gemcitabine in patients with metastatic pancreatic cancer, and doxorubicin in patients with soft tissue sarcoma. However, these large trials, did not meet the primary end point of improving overall survival.[54] Similarly to TPZ **1.10** (**Figure 1.8**, Page 14) clinical trials, patients were not stratified for tumour hypoxia prior to initiation of the trial. Studies have shown that biomarkers for tumour hypoxia can be predict the sensitivity of non-small cell lung cancer and pancreatic adenocarcinoma xenografts to TH-302 **1.26** treatment.[97,98] The cytotoxic effects of TH-302 **1.26** are enhanced in combination with radiotherapy, offering another avenue of investigation for this HAP.[97]

The Phase III clinical trials of **1.26** has led investigators to reflect on the development of HAPs, and the rationale for targeting hypoxia in this way.[54] The release of, or formation of, DNA damaging agents from the HAP, results in the prodrug acting as a conventional, cell-damaging chemotherapy. Issues deriving from overlapping toxicity with standard chemotherapies during clinical trials has been cited as a limiting factor in the clinical progression of HAPs.[17,47] For example, a Phase Ib clinical trial determined that combination of standard chemotherapies, gemcitabine or docetaxel, with HAP PR-104 **1.21** (**Scheme 1.4**, Page 17) resulted in dose-limiting toxicity.[84] Consequently, a more refined, molecularly-based approach to treating tumour hypoxia with HAPs is being investigated.[90]

1.3.3 Molecularly targeted HAPs

The majority of HAPs developed to date have been molecules that become toxic in hypoxic tissue, resulting in DNA damage, and consequently stopping cell replication.[17] Delivering toxic agents, however, can cause damage to neighbouring healthy tissue, as these agents can diffuse out of the hypoxic areas.[53] Perhaps, a more elegant approach is the development of molecularly targeted HAPs, which deliver a ligand for protein inhibition to hypoxic regions.[48] By targeting proteins associated with tumourigenesis and survival, greater selectivity over healthy tissue can be achieved.

Early examples of targeting ligands with bioreductive groups include nitroaromatic prodrugs of a poly(ADP-ribose)polymerase (PARP, implicated in DNA damage repair) inhibitor, developed by Parveen and co-workers, and nitroaromatic derivatives of the anti-cancer drug paclitaxel developed by Damen and co-workers.[99,100] Subsequently, further work has demonstrated

the release of other biologically active molecules from bioreductive groups, including; steroids,[101] the anti-cancer drug doxorubicin,[102] and inhibitors of; lysyl oxidase,[103] DNA alkyltransferase ,[104] DNA-dependent protein kinase (DNA-PK, a protein implicated in repair of DNA double strand breaks),[105] topoisomerase I (implicated in DNA cleavage),[106] and VEGF receptor tyrosine kinase.[107]

A clinically advanced example of this approach is TH-4000 **1.32** (**Scheme 1.7**), which when activated in hypoxic tumours, releases an epidermal growth factor receptor (EGFR) tyrosine kinase inhibitor (TKI); a class of proteins heavily implicated in cancer growth.[108] **1.32** employs a 4-nitroimidazole bioreductive group, which under hypoxic conditions, fragments at the benzylic position to release inhibitor **1.34**. Preclinical data for **1.32** have only been disclosed in the form of abstracts.[109-111] Fragmentation of **1.32** is thought to occur *via* radical **1.33** in hypoxia, and does not require reduction to the corresponding amine or hydroxylamine. **1.32** is currently under evaluation in Phase II clinical trials for patients with advanced EGFR-mutant non-small cell lung cancer (NCT02454842), and for patients with metastatic neck, head, or skin squamous cell carcinoma (NCT02449681).

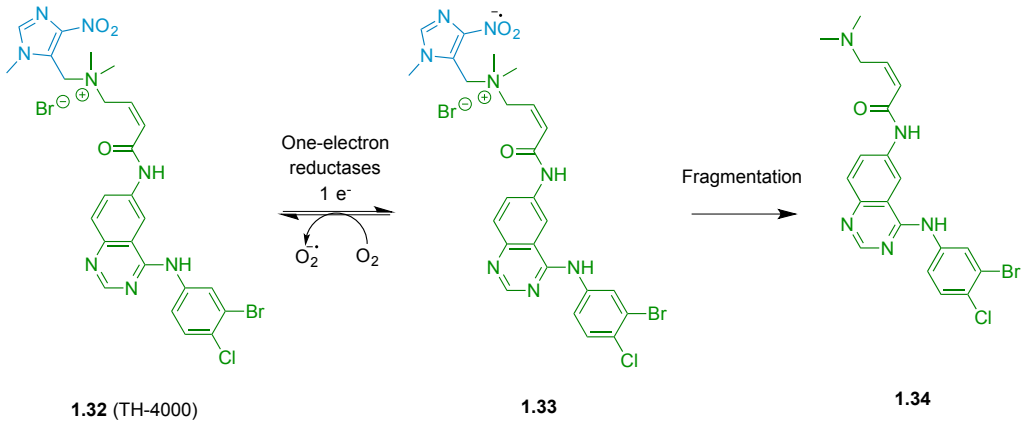

Scheme 1.7. The mechanism of action of TH-4000 **1.32**. Persistence of radical **1.33** under hypoxic conditions induces fragmentation to release the EGFR inhibitor **1.34**.[111]

Molecularly targeted HAPs can be designed to target a wide-variety of cellular pathways. Targeting Check-point kinase 1 (Chk1) is a long-standing attractive target in cancer therapy, as cancer cells which lose Chk1 function, cannot respond to replication stress, and consequently undergo apoptosis.[112] Chk1 is a key regulator of cell cycle progression, stalling mitosis until damaged DNA is repaired. The severe levels of hypoxia associated with radiation resistance induce a replication stress response, a key component of which is Chk1.[44] Inhibition of Chk1 blocks its function in the hypoxia-induced DNA damage response (DDR).[113] However, Chk1 activity is critical in all cells, and overlapping toxicity in combination with standard therapies, and cardiac problems, has hindered progression of Chk1 inhibitors in the clinic.[112] Delivering Chk1 inhibitors specifically in hypoxia could circumvent these issues, by targeting the most aggressive fraction of the tumour. Our laboratories developed CH-01 **1.35**, a hypoxia-activated Chk1 prodrug, which inhibits Chk1 only under hypoxic conditions following fragmentation to release the active drug **1.36** (**Figure 1.9**). Treatment of cancer cell lines with **1.35** caused loss of cell viability (**Figure 1.9B**) and elevated DNA damage in

human colorectal cancer (RKO) cells under hypoxic conditions, an observation consistent with inhibition of Chk1 (**Figure 1.9A**).[47]

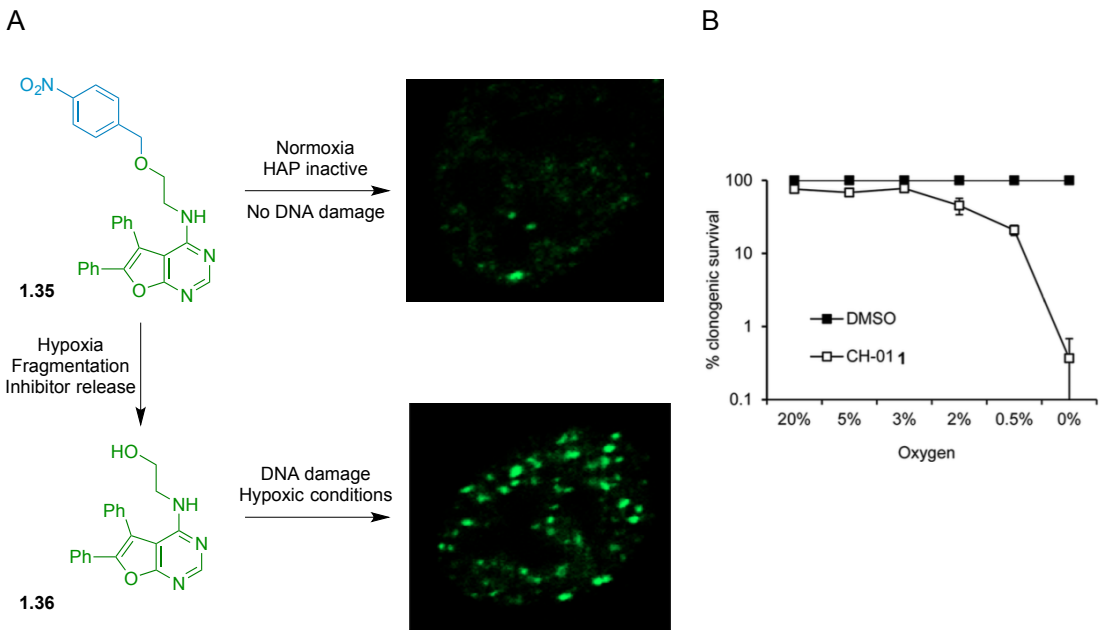

Figure 1.9. (A) Treatment of RKO cells under normoxic conditions with CH-01 **1.35** led to no induction of DNA damage. However, under hypoxic conditions, reduction and fragmentation occurs to release Chk1 inhibitor **1.36**, resulting in elevated levels of DNA damage. The bioreductive group is highlighted in blue, and the Chk1 inhibitor in green; (B) Colony survival curve showing survival of cells treated with CH-01 **1.35** under various oxygen conditions. Cell death is enhanced under hypoxic conditions. Adapted with permission *ACS Chem. Biol*. 2013; 8(7), 1451.[47]

The utility of molecularly targeted HAPs is only recently being explored, and is a promising therapeutic alternative to the delivery of indiscriminate cytotoxic agents to hypoxia, which can cause adverse side effects in healthy tissue.[90] A limitation of this approach, however, is that the inhibitor selected must be suitable for development into a HAP.[48] Alkylation of a key motif involved in the protein-ligand binding must sufficiently decrease ligand potency to avoid the inactive prodrug having effects in normoxia.[48] Consequently, the development of molecularly targeted HAPs requires careful consideration of ligand structure-activity relationships (SAR) and design of the

prodrug must aim to disrupt the ligand's activity. Such factors are considered in **Chapter 2.4** (Page 56), and also detailed further in **Appendix A.4**.

1.4 Improving the efficacy of HAPs in clinical trials

Despite some success in early-stage clinical trials and preclinical studies, the progression of HAPs to routine chemotherapeutics has been hampered by ineffectiveness in improving overall survival.[54,59] The predominant challenge in the clinic is routinely identifying, and evaluating the severity of tumour hypoxia between patients.[28] Development and refinement of hypoxic gene signatures across various cancer types could provide a powerful and effective prognostic method for evaluation of hypoxia. A meta-analysis of clinical studies revealed common genes associated with hypoxia in patients with in patients with head and neck, and breast cancers.[114] More recently, a hypoxic signature comprising of 15-genes was used to predict poorer clinical outcome of patients with hypoxic tumours, but also to predict their sensitivity to radiotherapy.[115]

Genetic profiling of tumours with high levels of HAP-activating reductase enzymes will ultimately enable improved selection of patients for HAP therapies. However, the enzymology involved in HAP activation is complex, and it is likely multiple enzymes will contribute to HAP activation in cells.[17,54] Overexpressing reductase enzymes enables comparison of the cellular activation of HAPs to that in wild type cells, and was used to implicate various one-electron reductase enzymes in the activation of SN30000 **1.13** (**Figure 1.8B**, Page 14).[71] However, artificial manipulation of the cellular proteome to study HAPs does not accurately represent endogenous cellular

conditions. Generation of gene knock-out cell lines offers promise for improving our understanding of HAP activation within a tumour.[54] Cytochrome p450 (CYP) reductase was recently shown to be the major determinant for successful hypoxic activation of the preclinical candidate SN30000 **1.13** and the clinical candidate TH-302 **1.26** (**Scheme 1.6**, Page 19), through generation of CYP reductase knock-out cell lines.[72] CYP reductase is a flavoprotein that has been heavily implicated as a one-electron reductase that has been shown to important for HAP activation in both preclinical and clinical studies.[17,116] In addition to TH-302 **1.26** and SN30000 **1.13**, CYP reductase is important in the activation of TPZ **1.10** (**Figure 1.8**, Page 14)[117] and also activates the molecularly targeted Chk1 HAP, CH-01 **1.35** (**Figure 1.9**, Page 23).[47] Screening tumour samples for essential reductase enzymes, and determining their expression under hypoxic conditions could enable improved identification of patients who will respond to HAP therapy.

A significant physiopathological issue for HAP therapy, is the delivery of any chemotherapeutic to a hypoxic tumour is limited by the poorly perfused vasculature.[73] Drug permeability through multiple cell layers, deep into the tumour tissue, is therefore a key consideration in HAP design. The HAP AQ4N **1.14** (**Scheme 1.2**, Page 15) was shown to permeate tumour tissue deeply in preclinical *in vivo* studies, an effect which was further enhanced in hypoxic conditions.[82] Careful refinement of pharmacokinetics could improve the efficacy of future bioreductive prodrugs. Predictive *in silico* models have previously been used to evaluate the pharmacokinetic profile of HAPs before selection as a candidate, as with SN30000 **1.13** (**Figure 1.8B**, Page 14).[70]

The ability to physically see hypoxia *in situ*, without removing the tumour, would be a powerful method for optimising both radiotherapy and treatment with HAPs.[118] Furthermore, visualisation of hypoxia would provide a real-time method for assessing tumour oxygenation throughout the course of treatment, and identifying the most therapy resistant and aggressive tumour cells. The following section considers the advances made in biomedical imaging of hypoxic tumours.

1.5 Imaging tumour hypoxia

1.5.1 Exogenous bioreductive molecules

Hypoxia-sensitive bioreductive molecules have been used clinically to visualise tumour hypoxia. Molecules comprising the 2-nitroimidazole bioreductive group have been employed as exogenous markers of hypoxia.[119] Nitroimidazole-containing hypoxic biomarkers, pimonidazole **1.37** and EF5 **1.39**, undergo bioreduction to the corresponding 2-aminoimidazole species selectively in hypoxic tissue (**Figure 1.10A**). Following immunostaining with selective antibodies, detailed studies of the severity and heterogeneity of the hypoxic microenvironment can be examined (**Figure 1.10B**).[120,121] However, these strategies require patient biopsies to be taken for immunostaining, and therefore is an invasive technique.[122]

A

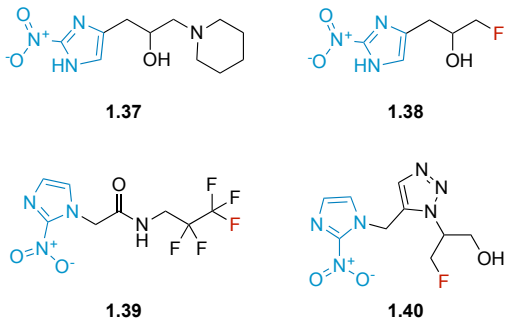

B

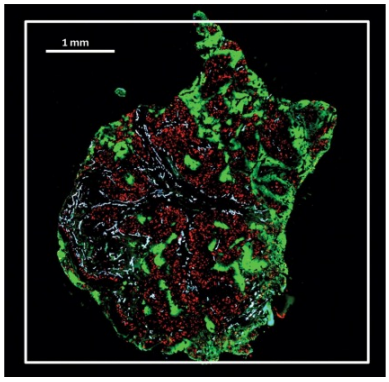

Figure 1.10. (A) Chemical structures of nitroimidazoles; pimonidazole **1.37**, ^{18}F-MISO **1.38**, ^{18}F-EF5 **1.39**, and ^{18}F-HX4 **1.40**. The bioreductive nitroimidazole groups are highlighted in blue, and radiolabelled fluorine in red. (B) Pimonidazole immunofluorescence staining (green) of a laryngeal carcinoma biopsy sample. Heterogeneity of hypoxia throughout the tumour sample can be seen and distinguished from proliferating cells (red). Adapted with permission: license number 3902451010116.[122]

Bioreductive hypoxia markers for use in non-invasive positron emission tomography (PET) imaging have also been developed (**Figure 1.10**A). These agents, which include **1.38**, **1.39**, and **1.40**, have been used for quantitative analysis of hypoxia within a tumour, and correlated hypoxia with poor prognosis in patients with glioblastomas.[123,124] ^{18}F-Misonidazole **1.38** (FMISO) is clinically the most studied PET biomarker for hypoxia, and has been used to evaluate oxygenation of a wide variety of cancers including head and neck, breast, renal and lung.[118] However, clinical acceptance of ^{18}F-FMISO **1.38** has been hampered by a poor pharmacokinetic profile, and high accumulation in normal tissues, resulting in a poor signal to noise ratio.[118] Other bioreductive PET imaging agents have subsequently been investigated. ^{18}F-EF5 **1.39** was shown to be a predictive biomarker for sensitivity to the HAP SN30000 **1.13** in a non-small cell lung cancer xenograft model, in combination with radiotherapy.[125] More recently, the PET tracer ^{18}F-HX4 **1.40** was used to monitor hypoxia in patients with head and neck cancer during radiotherapy, and was shown to be a positive marker for sensitivity of xenograft tumours to

TH-302 **1.26** in combination with radiotherapy.[97,126] Direct comparison of the hypoxia-targeted PET imaging agents available is difficult, owing to differential tumour permeability and variable hypoxia between patients.[28]

1.5.2 *In situ* fluorescence imaging

An alternative strategy undergoing preclinical development, is targeting fluorophores to hypoxia for use in optical imaging.[127] Optical imaging techniques utilise specialist cameras to visualise fluorophores that emit in the near-infrared (NIR) region of the electromagnetic spectrum (650-1000 nm).[128] These wavelengths are clinically favoured, as they avoid issues associated with tissue auto-fluorescence, and afford improved light penetrability through tissue.[129,130] Non-hypoxia targeted NIR cyanine dyes have been used in preclinical and clinical studies, to localise tumours, and to guide surgeons during resections.[131-136] The NIR cyanine dye, indocyanine green **1.41** (ICG) has been widely employed in clinical studies to evaluate tumours during surgery owing to fluorescence emission at approximately 800 nm (**Figure 1.11**).[136-139] ICG **1.41** is not targeted to tumours, but rather accumulates in them, due to the enhanced permeability and retention (EPR) effect, and is one of only two FDA approved NIR dyes for human studies.[31,140,141] Consequently, there is a need for development of novel NIR dyes, with improved pharmacokinetic and photophysical properties to better suit specific imaging requirements.[142]

A

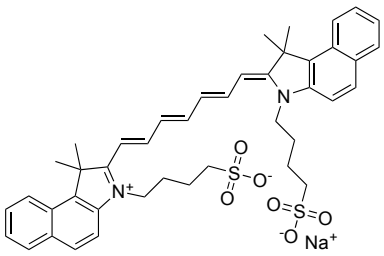

1.41

B

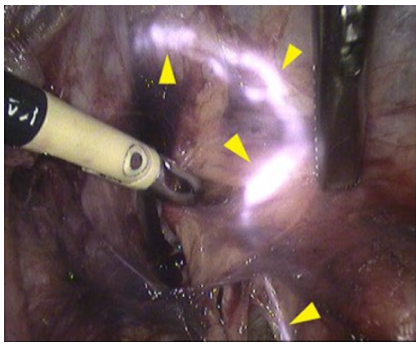

Figure 1.11. (A) The chemical structure of cyanine-based dye, indocyanine green **1.41** (ICG). (B) Intraoperative NIR fluorescence imaging in a female patient with gynaecological cancer. Fluorescence of ICG corresponds to lymphatic vessels and sentinel lymph node. Adapted with permission *BMC Res Notes*. 2015; 8: 608.[134]

Preclinical development of NIR fluorophores to target tumour hypoxia is on-going.[143-145] Nitroaromatic molecules have primarily been exploited in the design of these molecules, owing to their sensitivity to reductase enzymes under conditions of reduced oxygen. However, nitroaromatic bioreductive groups offer additional advantages with respect to fluorescence imaging. It is well-established that nitro groups are capable of quenching the fluorescence of a molecule (**Figure 1.12A**).[146,147] Upon absorption of a photon, electron transfer from the electronically excited state to the electron-deficient nitro group occurs. The energy absorbed by the nitro group is subsequently dissipated as vibrational energy. This process returns the molecule to the electronic ground state, and therefore quenches the fluorescence.[148] However, following nitro bioreduction to the corresponding amine, quenching of the excited state cannot occur, and fluorescence is restored (**Figure 1.12B**).[127] This photophysical property of nitro groups has been exploited to afford enhanced fluorescence signal in hypoxia following reduction, enabling improved imaging resolution and signal-background noise ratio compared to normoxic tissue. Molecules that become fluorescent in

response to certain stimuli can be defined as fluorogenic. Early pioneering work by Wardman and co-workers demonstrated this concept, employing acridine derivative **1.42** and napthalimide derivative **1.43**, both of which were shown to be activated in hypoxic cells, resulting in a 'switch-on' of fluorescence (**Figure 1.13**).[149-151]

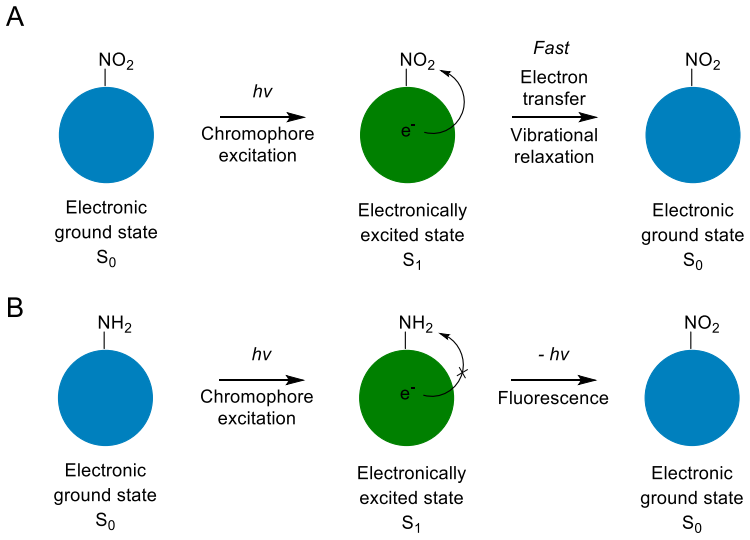

Figure 1.12. Absorption of a photon by a chromophore results in an electronically excited molecule. (A) Electron-deficient nitro groups accept the excited electron, and dissipate the energy as vibrational energy, preventing fluorescence. (B) Representative amino group cannot accept the excited electron. Fluorescence occurs by emission of this absorbed energy as a photon from S_1 to S_0.[148]

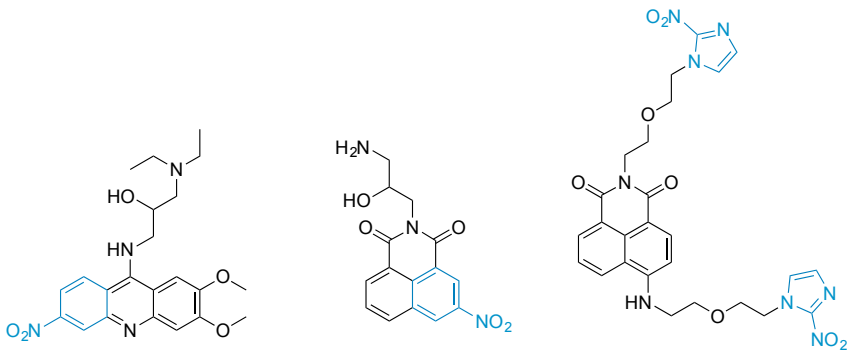

Figure 1.13. The chemical structures of fluorogenic hypoxia-activated markers **1.42**, **1.43** and **1.44**. The bioreductive moieties are highlighted in blue.[149,151,152]

The position of the nitro group is not limited to being embedded in the fluorophore structure as in **1.42** and **1.43**. Nitro-mediated quenching of fluorescence can also occur distally. Building upon the structure of **1.43**, nitroimidazole derivative **1.44** was shown to be approximately 20-fold more fluorescent under hypoxic conditions, corresponding to the reduced 2-aminoimidazole species, compared to normoxic conditions in a variety of human cancer cell lines (**Figure 1.13**).[152]

Owing to the clinical applications of ICG **1.41**, a number of hypoxia-targeted derivatives have been developed.[127,153] Recent work demonstrated cyanine derivative **1.45** as a useful NIR fluorogenic probe (λ_{ex}: 730 nm, $\lambda_{em:}$ 788 nm) for the visualisation of nitroreductase activity in hypoxic tumours *in vivo* and *in vitro* (**Figure 1.14**).[143] However, *in vivo* data was obtained by direct injection of **1.45** into the tumour volume, indicating the physiochemical properties of the probe may require further development to be suitable for intravenous administration.

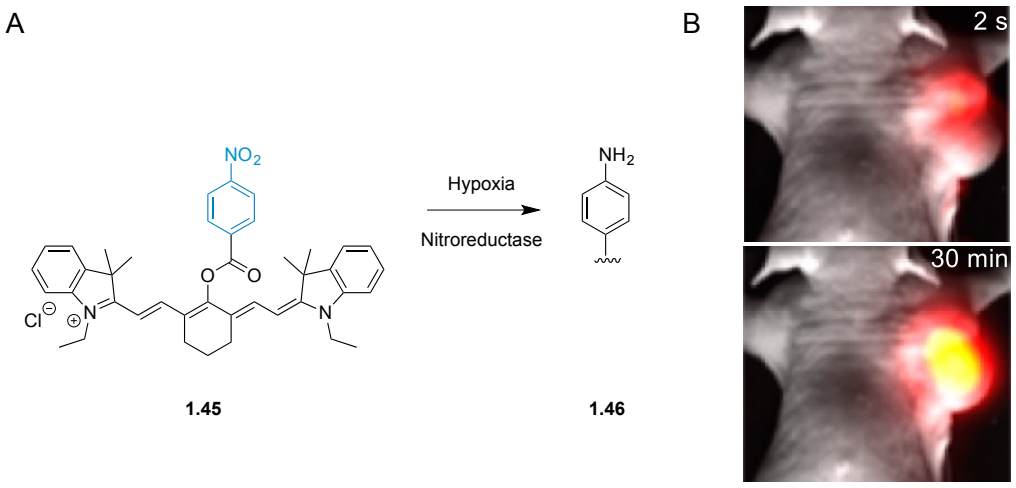

Figure 1.14. (A) Scheme to show reduction of **1.45** under hypoxic conditions results in fluorescent amino species **1.44**. The bioreductive group is highlighted in blue (B) Representative image of an A549 (lung cancer) tumour bearing mouse, treated with **1.45** Top: 2 seconds after injection, Bottom: after 30 minutes. Adapted with permission from *J. Am. Chem. Soc*., 2015, **137**, 6407-6416. © 2015 American Chemical Society.[143]

Other ICG **1.41** derivatives have incorporated 2-nitroimidazole linkers for hypoxia-sensitivity, including **1.47** and **1.48**.[154,155] Intravenous administration of **1.47** to tumour bearing mice resulted in enhanced fluorescence signal in the hypoxic areas of tumours after 3 hours, while retaining similar spectrophotometric properties to **1.41** (λ_{em}:780 nm) (**Figure 1.15**). Contraction of the central unsaturated carbon chain by 2 carbons, afforded derivative **1.48**. Despite blue-shifted fluorescence by approximately 100 nm, the quantum yield of **1.48** compared to **1.47** was improved 5-fold, and visualisation in tumour-bearing mice was enhanced.

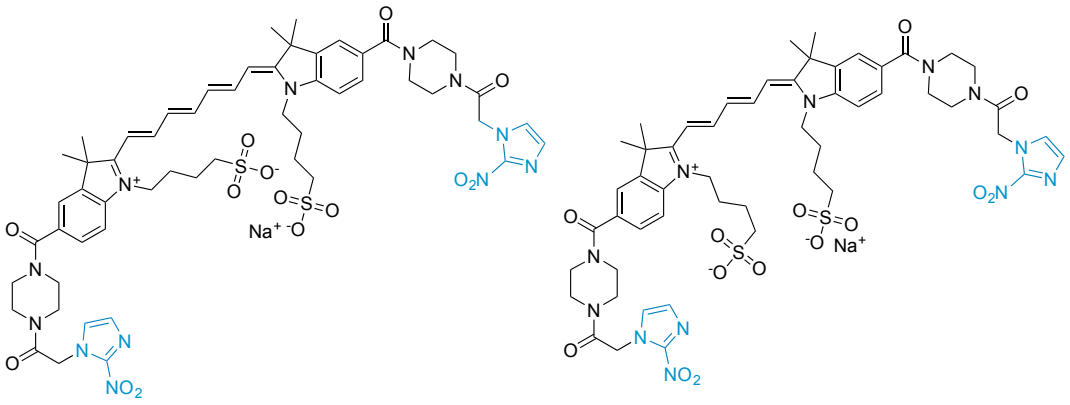

1.47 1.48

Figure 1.15. Chemical structure of hypoxia-targeted indocyanine green derivatives **1.47** and **1.48**. Fluorescence of **1.48** is blue shifted approximately 100 nm owing to the shorter central carbon chain compared to **1.47**, but offers 5-fold improvement in quantum yield, and improved *in vivo* imaging properties. The bioreductive groups are highlighted in blue.[154,155]

An alternative strategy for inducing a switch-on of fluorescence in hypoxia is adoption of the prodrug strategy, in which bioreduction induces a fragmentation step to release a cargo molecule. Alkylation of electron-rich moieties such as phenols or anilines is detrimental to the fluorescence of a molecule.[156] Where the cargo molecule selected is a fluorophore, fragmentation under hypoxic conditions can restore fluorescence. An example of this approach is compound **1.49**, which following reduction of the nitrobenzyl bioreductive group to the corresponding amine **1.50** under hypoxic conditions, fragmentation *via* a carbamate linker occurs to afford fluorescent dye **1.51** (**Scheme 1.8**).[157] The utility of this technology was demonstrated in A549 human lung carcinoma cells, resulting in fluorescence when cells were treated under hypoxic (1% O_2) conditions, but no fluorescence under normoxic conditions.

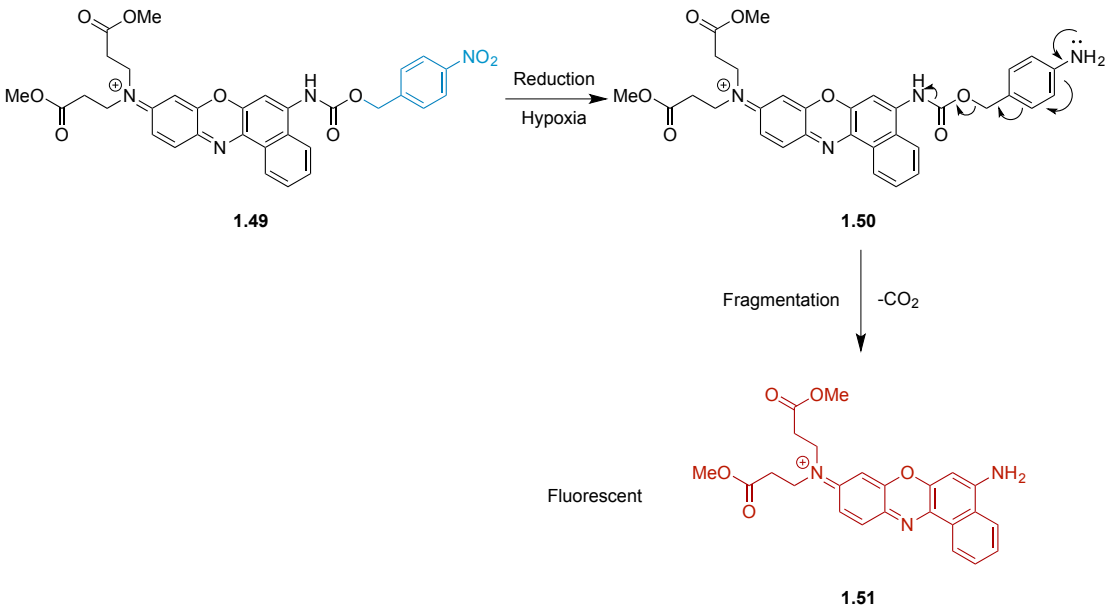

Scheme 1.8. Fluorogenic hypoxia-activated dye **1.49** undergoes enzymatic bioreduction under hypoxic conditions to the corresponding amine **1.50**. This induces a fragmentation process, in which carbon dioxide is eliminated to promote release of the amine functionality. The free amine then restores the fluorescence of dye **1.51**.[157]

Fluorescent compounds with emission towards, or within the NIR region of the electromagnetic spectrum rely on a push-pull mechanism of electron density throughout a conjugated structure. Disruption of the flow of electron density through the π-system disrupts the fluorescence of a molecule.[156,158] The indole-based fluorogenic compound **1.52** exploits this concept, to afford a hypoxia-sensitive dye.[159] The nitro group disrupts the push-pull electronic system, but following reduction to the corresponding amine **1.53** (λ_{em}: 560 nm) under hypoxic conditions, fluorescence is restored (**Scheme 1.9A**). Work by Moerner and co-workers exploited this concept further in the development of **1.54** (λ_{em}: 610 nm), which is reduced to fluorescent **1.55** by nitroreductase enzymes, for use in super-resolution microscopy to evaluate real time nitroreductase activity (**Scheme 1.9B**).[160]

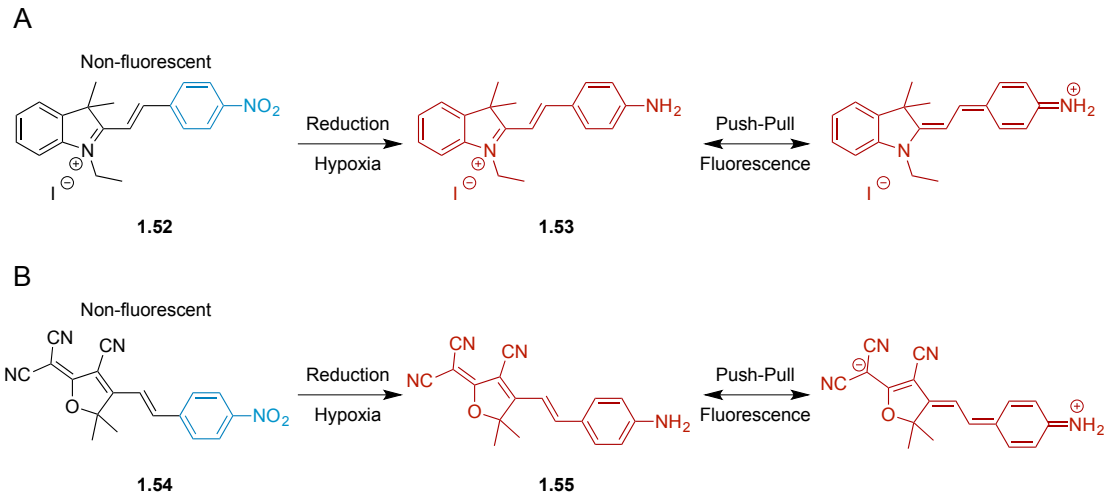

Scheme 1.9. Fluorogenic dyes **1.52** (A) and **1.54** (B) which rely on a push-pull mechanism of electron density through the conjugated system, following reduction to amines **1.53** and **1.55**, for efficient fluorescence emission. Where this fluorescence is disrupted, by introduction of a nitro group for example, fluorescence is quenched. The bioreductive group is highlighted in blue.[159,160]

Fluorescent reporters of biological environments, or processes, are clearly powerful tools in research.[161,162] Fluorogenic molecules such as those described above, afford a significant increase in fluorescence in response to the hypoxic microenvironment, reducing the signal-noise ratio when comparing hypoxia to normoxia. This is in contrast to PET imaging agents that rely on progressive accumulation in hypoxic tissue, and consequently results in high levels of background signal in surrounding tissue. The preclinical evaluation of hypoxia-targeted ICG derivatives described above indicates the potential utility of these molecules in identifying and targeting tumour hypoxia.

1.6 Aims

A number of preclinical and clinical studies have highlighted the importance of identifying tumour hypoxia before HAP administration to maximise efficacy of the therapy.[97,98] The success of HAPs in the clinic has been hampered by inadequate stratification of tumour hypoxia in patient samples.[54] The methods for identifying tumour hypoxia, and treating tumour hypoxia with HAPs are currently distinct. For example, use of the PET imaging agent ^{18}F-EF5 **1.39**, to identify tumour hypoxia prior to administration of HAPs such as TH-302 **1.26**, does not account for the differential pharmacokinetic profile of the two distinct molecules. The permeability of the two molecules is likely to differ significantly, as is their retention in the tumour volume and clearance. Consequently, the biodistribution of any HAP throughout a tumour volume is currently unclear.

We hypothesised that bioreductive imaging agents could be combined with prodrugs to both visualise and treat hypoxic tumours, simultaneously. Such a technology would afford a real-time readout of the delivery of a prodrug molecule to the tumour, while positively identifying the presence of tumour hypoxia. To address our hypothesis, fluorescence was selected as our imaging modality, owing to the broad variety of laboratory methods for fluorescence detection, and the vast library of fluorescent molecules that could be readily synthesised and chemically adapted.

Combination of the fluorescence quenching properties of nitro groups, their hypoxia sensitivity, and use as triggers for prodrug fragmentation presents an opportunity to develop novel, fluorogenic bioreductive groups.

Considering hypoxia-activated fluorogenic dyes, the bioreductive groups; 4-nitrobenzyl and 2-nitroimidazoles, have been employed to afford quenching of fluorescence, which then fragment following reduction in hypoxic conditions to release a fluorescent dye (**Figure 1.16A**).[127] Alternatively, the nitro functionality can be embedded in the fluorophore structure, causing the whole molecule to become fluorescent (**Figure 1.16B**).

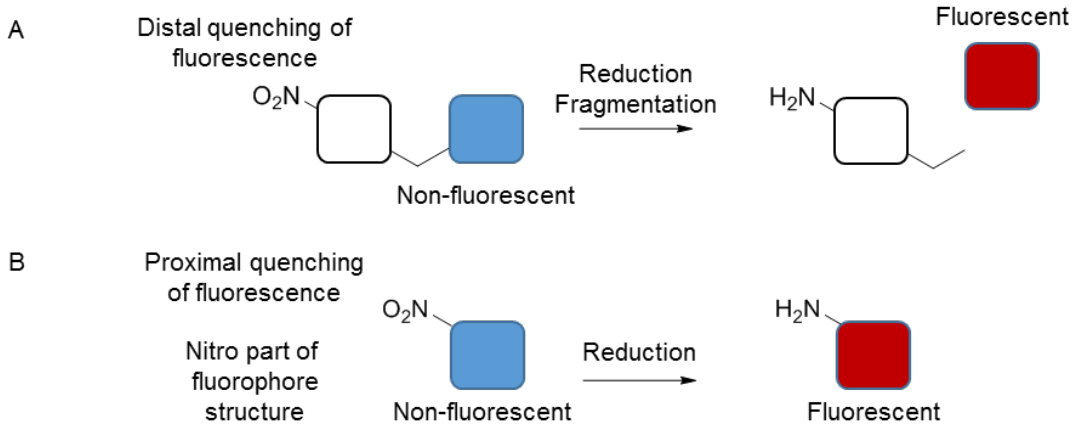

Figure 1.16. Nitro groups can quench the fluorescence by (A) distal quenching, and also by being (B) proximal to the fluorophore. When reduced to the amine species in hypoxia, fluorescence can be restored either by (A) a fragmentation step to release a fluorophore or (B) where the nitro group is embedded in the fluorophore structure, and no fragmentation step is required.

It was proposed that a hypoxia-activated fluorogenic dye, in which the nitro group was embedded in the structure, could be chemically manipulated to also act as a trigger of fragmentation following reduction (**Figure 1.17**). These fluorogenic bioreductive groups would become fluorescent upon activation in hypoxia, simultaneously delivering a biologically relevant cargo molecule through a fragmentation step.

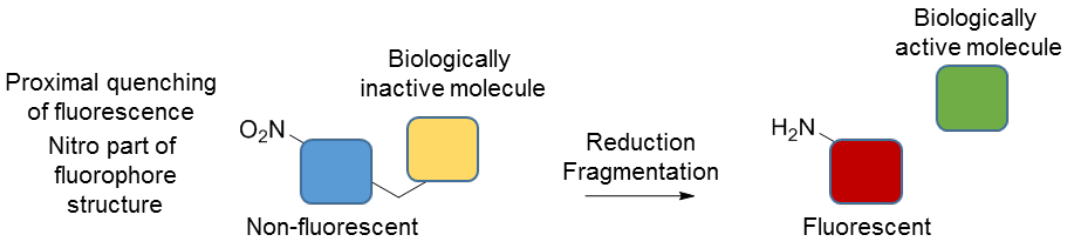

Figure 1.17. Schematic representation of a fluorogenic hypoxia-activated prodrug. Reduction of the nitro functionality to the amino species simultaneously induces fragmentation to release a biologically active molecule, and cause a switch-on of fluorescence.

With the aim of developing the first fluorogenic bioreductive group for delivery of a biologically active molecule to hypoxia, scaffolds suitable for chemical manipulation and for a 'switch-on' of fluorescence following reduction of a nitro group to the corresponding amine was considered.

Chapter 2

DESIGN, SYNTHESIS AND EVALUATION OF A NOVEL FLUOROGENIC BIOREDUCTIVE GROUP

2.1 Introduction

With the aim of developing a fluorogenic bioreductive group, fluorescent scaffolds suitable for synthetic introduction of a benzylic handle to attach a cargo molecule were considered (**Figure 1.17**, Page 38). Various nitro-functionalised heterocyclic compounds have been investigated as hypoxia-sensitive fluorescent markers.[127] Pioneering work by Olive and co-workers demonstrated the use of a fluorogenic nitroquinoline derivative to detect hypoxia *in vitro*, using fluorescence automated cell sorting (FACS).[163] Fluorogenic 6-nitroquinoline **2.1**, a structurally simple heterocyclic scaffold, undergoes NADPH reductase-mediated reduction to the fluorescent amine **2.2**, exclusively under hypoxic conditions (**Scheme 2.1**).[164,165]

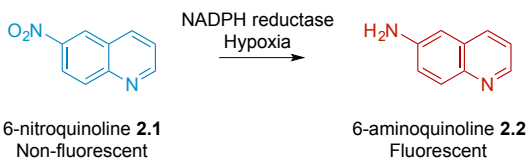

Scheme 2.1. 6-nitroquinoline **2.1** undergoes sequential single electron reductions under hypoxic conditions to afford the amino metabolite **2.2**. The nitro group quenches fluorescence of the quinoline, which is then restored upon reduction to **2.2**.

Fluorogenic *Oxo*-nitroquinoline **2.3**, a derivative of **2.1**, was reported to also be a substrate for NADPH reductase, affording fluorescent amine **2.4** under hypoxic conditions, but not normoxic conditions (**Scheme 2.2**).[166] Compound **2.3** was further evaluated in 22 different cancer cell lines to monitor one-electron reductase activity under hypoxic conditions, by fluorescence microscopy and FACS analysis. Enzymatic reduction of nitro **2.3** to amine **2.4** afforded a 'switch-on' of fluorescence, which was shown to correlate well with activation of HAP PR-104 **1.21** (**Scheme 1.4**, Page 17). The imaging properties of **2.4** indicated that introduction of an *N*-alkyl ester, and quinoline oxidation, was well tolerated with respect to fluorescence of the structurally simplified aminoquinoline **2.2** scaffold. Comparing the fluorescence of structurally diverse amines **2.4** and **2.2**, gave confidence to functionalisation of nitroquinolines to afford a fluorogenic bioreductive group.

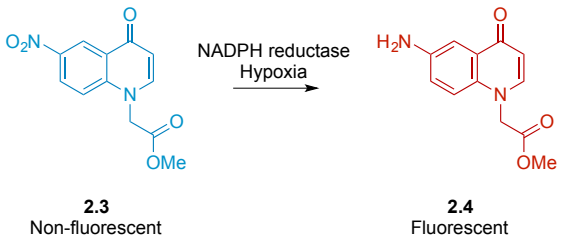

2.3
Non-fluorescent

2.4
Fluorescent

Scheme 2.2. Quinolone **2.3** is a fluorogenic marker of hypoxia. Reduction of the nitro group to the amino species **2.4** causes a switch on of fluorescence.[166]

Nitroquinolines have also been investigated by numerous academic research groups as molecules that become cytotoxic to cells in hypoxic conditions.[167-170] 3-nitroquinoline derivative **2.5** was reported to undergo enzymatic reduction to the corresponding amine **2.6** under hypoxic conditions (**Scheme 2.3**).[171] An intramolecular deprotonation from intermediate **2.7** causes an elimination to release **2.8**, a DNA alkylating agent. Compound **2.5**

was shown to cause enhanced cytotoxicity in hypoxic human colorectal adenocarcinoma (HT-29) cells, compared to those treated under normoxic conditions. This work represents an early example of drug delivery to hypoxia *via* an enzymatically promoted elimination.

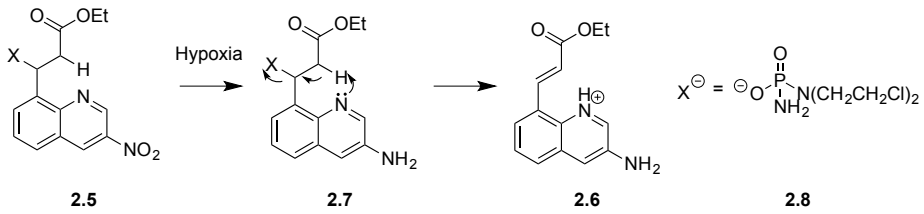

2.5 **2.7** **2.6** **2.8**

Scheme 2.3. Reduction of **2.5** under hypoxic conditions increases the basicity of the sp^2 hybridised nitrogen, promoting elimination to release phosphoramide mustard **2.8**, a DNA alkylating agent. The HAP **2.5** showed 11-fold enhanced cytotoxicity in HT-29 cells under hypoxic conditions, compared to normoxic conditions.[171]

Given the prevalence of nitroquinolines in the literature, particularly their application as HAPs and fluorogenic markers of hypoxia, nitroquinoline **2.1** was identified as an attractive start point for development of a fluorogenic bioreductive group. It was proposed that introduction of a benzylic handle for attachment of a biologically active cargo molecule, would transform **2.1** into a fluorogenic bioreductive group.

2.2 Design of the fluorogenic bioreductive group

A study into the fluorescence properties of aminoquinolines indicated that both 6- and 3-aminoquinoline are fluorescent, whereas 5- and 8-aminoquinoline are not.[172] These studies indicated that selection of suitable structural isomers of nitroquinoline **2.1** would be imperative for fluorescence following reduction of the nitro group. Owing to the reported sensitivity of **2.1** to the one-electron reductase; NADPH reductase, 6-nitroquinoline derivatives, rather than 3-nitro derivatives were investigated.[164]

The success of any HAP relies on efficient fragmentation to release the biologically active cargo molecule. Therefore, factors that promote the desired fragmentation step, following bioreduction, were considered. Under hypoxic conditions, nitro reduction of aromatic bioreductive groups causes an increase in electron density, which induces fragmentation at the benzylic position (**Scheme 1.5**, Page 18). It was hypothesised that positions on the quinoline ring, which have the greatest electron density, would facilitate this fragmentation. The *ortho* positions with respect to the nitro group were suitable for fragmentation to release a cargo molecule, as demonstrated by nitroquinolines **2.9** and **2.11**, and consequently were considered for modification with a methylene handle (**Scheme 2.4**).

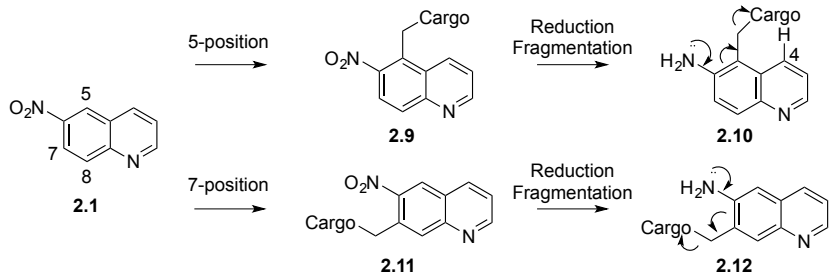

Scheme 2.4. The 5- **2.9** and 7-position **2.11** of nitroquinoline **2.1** are suitable for intramolecular elimination of a cargo molecule from the corresponding amino metabolites **2.10** and **2.12**, under hypoxic conditions.

Nitration of unsubstituted quinolines under acidic conditions, occurs preferentially at the 5- and 8-positions, due to greater effective electron density. It was hypothesised that modification at the 5-position would aid fragmentation of the HAP, relative to the less electron rich 7-position. There is also the possibility that hydrogen at the 4-position may clash sterically with the methylene group and cargo molecule of **2.10**, favouring elimination compared to **2.12** where this interaction would be absent (**Scheme 2.4**). Consequently

2.9 was selected as the synthetic target (**Scheme 2.5**). Upon bioreduction of **2.9** to amine **2.10** under hypoxic conditions, it was hypothesised that fluorescence of the quinoline would be restored, which would simultaneously induce fragmentation of a cargo compound (**Scheme 2.5**). It was suggested that following fragmentation, the electrophilic iminium ion **2.14**, would undergo rapid nucleophilic addition to re-aromatise, and afford the fluorescent amino derivative **2.15**. Possible nucleophilic species could be H_2O or high concentration intracellular thiols such as glutathione (GSH) or cysteine.[173]

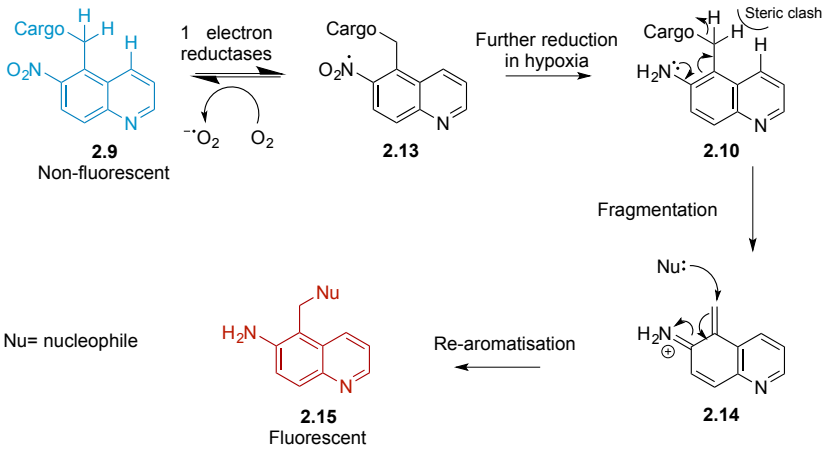

Scheme 2.5. A single electron transfer to the nitro group, affords radical **2.13**, which can be quenched by oxygen. Under hypoxic conditions, further reduction occurs to afford the fluorescent amino metabolite **2.10**. An intramolecular elimination releases the compounds cargo, to afford electrophile **2.14**, which undergoes nucleophilic rearomatisation to **2.15**.

In summary, following consideration of fluorescence and fragmentation properties, **2.9** was selected for evaluation as a fluorogenic bioreductive group, incorporating modification at the 5-position of 6-nitroquinoline **2.1**.

2.3 Synthesis

2.3.1 Synthetic Route 1

To install a biologically active cargo molecule onto **2.1**, a synthetic intermediate suitable for coupling was required. Bromide **2.16** would afford a chemical handle for introduction of a wide range of functional groups *via* S_N2-type chemistry. Therefore a retrosynthesis of **2.16** was devised (**Scheme 2.6**). Commercially available 6-Chloroquinoline **2.22** was hypothesised to undergo bromination preferentially at the 5-position due to the inductive effect of the chlorine (**Scheme 2.6**, Step v). Introduction of a carboxyl group *via* Grignard chemistry would rely on the comparatively weaker aryl C-Br ($E_{bond\ dissociation}$ = 346 kJ mol^{-1}) bond *vs* C-Cl ($E_{bond\ dissociation}$ = 407 kJ mol^{-1}) bond to afford the desired regiochemistry (**Scheme 2.6**, Step iv).[174] Subsequent reduction would afford alcohol **2.18** (**Scheme 2.6**, Step iii).

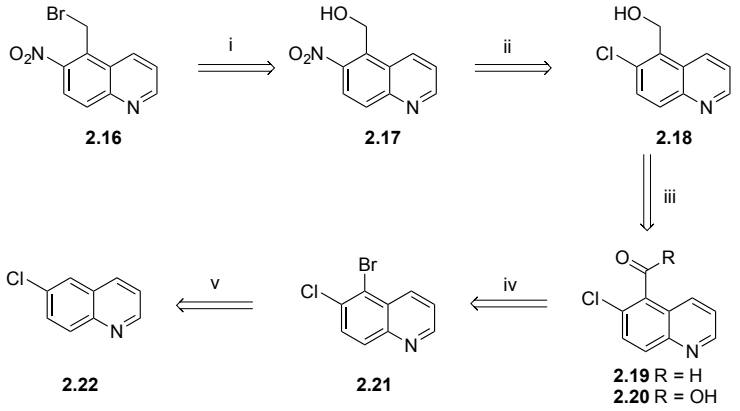

Scheme 2.6. Proposed retrosynthetic route to afford fluorogenic **2.16** for alkylation of a biologically active molecule: (i) Bromination; (ii) Palladium catalysed nitration of aryl chloride (iii) Reduction (iv) Grignard chemistry/acylation (v) Bromination.

Introduction of a nitro group, *via* palladium-catalysed nitration chemistry from chloride **2.18** (**Scheme 2.6**, Step ii),[175] was a potentially superior

approach to introduction of the nitro at an earlier stage, as a nitro group could reduce the propensity of **2.21** to undergo electrophilic aromatic substitution. Methylene alcohol **2.17** would offer scope for introduction of various functional handles if required, and could be converted to bromo derivative **2.16** by an Appel reaction or acid-catalysed S_N2 (**Scheme 2.6**, Step i).[176]

Bromination of **2.22** at the 5-position was achieved by addition of Br_2 in the presence of $AlCl_3$ to afford **2.21** (**Scheme 2.7**). After 24 hours, the reaction was judged to be complete by NMR analysis of the crude reaction mixture, and the product **2.21** isolated in 30% yield by silica gel column chromatography. Dibrominated side product **2.23** was also isolated in 12% yield. Increasing the reaction scale from 400 mg to 5 g, allowed more accurate, controlled addition of Br_2 to the reaction mixture, and consequently improved the yield of the desired product **2.21** to 69%.

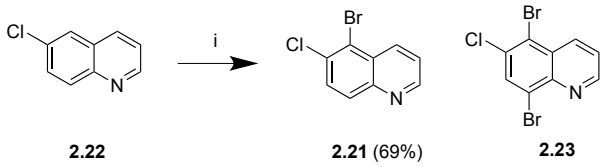

2.22 **2.21** (69%) **2.23**

Scheme 2.7. Bromination of **2.22**; *Reagents and conditions:* (i) $AlCl_3$ (3 eq.), Br_2 (1 eq.), 120 °C, 24 h, 69%.

With compound **2.21** in hand, introduction of a carbonyl-containing functionality, *via* formation of the corresponding Grignard reagent was investigated. Compound **2.21** was treated with 2 M ^{i}PrMgCl in THF to afford presumed intermediate **2.24** as the corresponding Grignard reagent (**Scheme 2.8**, Step i). Initial investigations focused on carboxylation of intermediate **2.24** by bubbling CO_2 through the reaction solution (**Scheme 2.8**, Step ii). TLC analysis ^{1}H NMR and mass spectrometry of the crude reaction

mixture suggested formation of the desired carboxyl product **2.20**. However, upon aqueous work-up the product could not be isolated, due to the propensity of **2.20** to reside in H_2O.

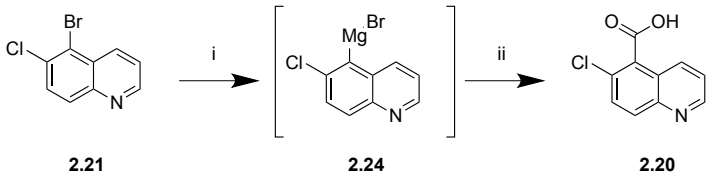

Scheme 2.8. Carboxylation/formylation of compound **2.21** *via* Grignard formation; *Reagents and conditions:* (i) 2 M ^{i}PrMgCl (1.0 eq.), THF, 0 °C, 2 h; (ii) CO_2 (g), 3.5 h.

Formation of the aldehyde **2.19** was subsequently investigated, by treatment of presumed intermediate **2.24** with DMF, furnishing the desired formylated product **2.19** in 23% yield (**Scheme 2.9**, Step ii). Side product **2.25**, resulting from insertion of ^{i}Pr at the 2-position, was also isolated. Simultaneous investigations into a single-pot reaction procedure found that reducing aldehyde **2.19** with $NaBH_4$ *in situ* led to a comparable yield of **2.18**, to first isolating **2.19**, then performing the reduction to **2.18** (**Scheme 2.9**).

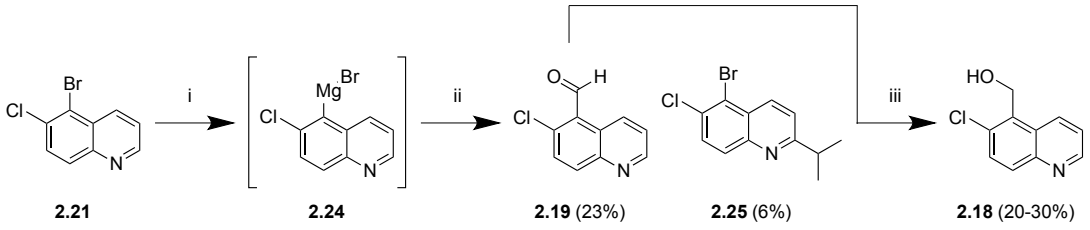

Scheme 2.9. Formylation of **2.21** *via* Grignard reagent formation; *Reagents and conditions:* (i) 2 M ^{i}PrMgCl (1.1 eq.), THF, 0 °C, 30 min; (ii) DMF (5 eq.), 0 °C, 4 h, 23%; (iii) $NaBH_4$ (2 eq.), THF, 0 °C, 4 h, 20-30%.

To improve the reaction yield, formation of the presumed intermediate **2.24** was investigated. Quinoline **2.21** was treated with 2 M ^{i}PrMgCl solution in THF, and the reaction was quenched with ice-cold H_2O at regular time intervals. Using ^{1}H NMR spectrometry to analyse the crude reaction mixture,

40 minutes was determined to be the optimal time for formation of presumed intermediate **2.24**. To further reduce unwanted side reactions, the addition of ^{i}PrMgCl was performed at −10 °C, instead of 0 °C. Following treatment of **2.24** with DMF, the presence of the desired aldehyde **2.19** was determined by TLC analysis. Subsequent reduction of **2.19** with $NaBH_4$ *in situ*, afforded **2.18** in an improved yield of 55%. Over three steps, these optimised conditions represent an effective yield of approximately 80% per step (**Scheme 2.10**).

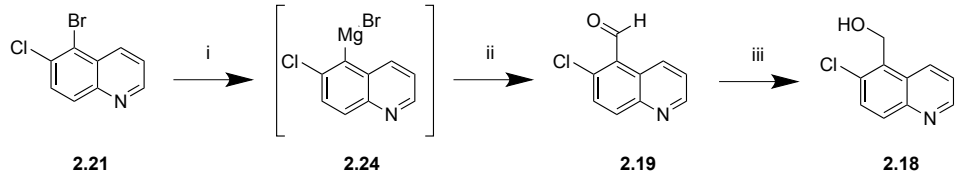

2.21 **2.24** **2.19** **2.18**

Scheme 2.10. Formylation of **2.21** *via* Grignard chemistry, followed by reduction of aldehyde **2.19**; *Reagents and conditions:* (i) 2 M ^{i}PrMgCl (1.2 eq.), THF, −10 °C, 1 h; (ii) DMF (5 eq.), −10 - 0 °C, 4 h; (iii) $NaBH_4$ (1 eq.), 0 °C, 1 h; 55% over 3 steps.

With methylene alcohol **2.18** in hand, introduction of a nitro group *via* palladium-catalysed nitration, to furnish **2.17** was investigated (**Scheme 2.11A**). To evaluate the nitration procedure, test substrate **2.22** was successfully investigated, affording **2.1** in 64% yield (**Scheme 2.11B**).[175]

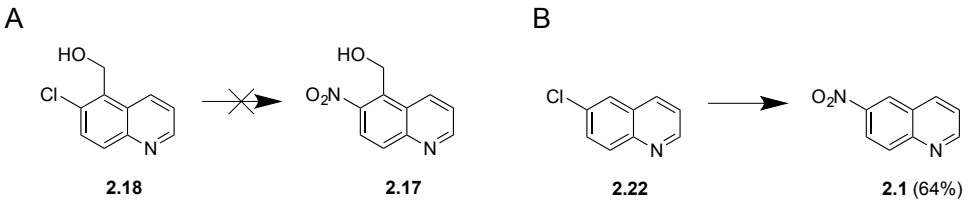

2.18 **2.17** **2.22** **2.1** (64%)

Scheme 2.11. (A) Attempted palladium-catalysed nitration of methylene alcohol **2.18**; (B) Nitration of 6-chloroquinoline **2.22**; *Reagents and conditions:* $NaNO_2$ (2 eq.), $Pd(dba)_3$ (0.5 mol%), ^{t}BuBrettPhos (1.2 mol%), ^{t}BuOH, 130 °C, 24 h, 64%.

Attempts to perform nitration on methylene alcohol **2.18** led to no formation of the product **2.17** as determined by TLC and mass spectrometry analysis. In two independent reactions, 75% and 80% of the starting material

2.18 was recovered by silica gel column chromatography, respectively. Increasing the catalyst loading (10 mol% $Pd_2(dba)_3$, 24 mol% ^{t}BuBrettPhos) also afforded no detectable conversion of **2.18**. These results suggested that either oxidative insertion, or reductive elimination with nitrite was not occurring. It was hypothesised that the primary alcohol moiety could be co-ordinating with the palladium centre after oxidative insertion, to form a 5-membered ring complex **2.27**. Such a structure could reduce the favourability of transmetallation, by increasing the overall stability of the palladium intermediate **2.26** (**Figure 2.1**). Consequently, nitrite co-ordination would be disfavoured, and reductive elimination to afford the desired product **2.17** prevented.

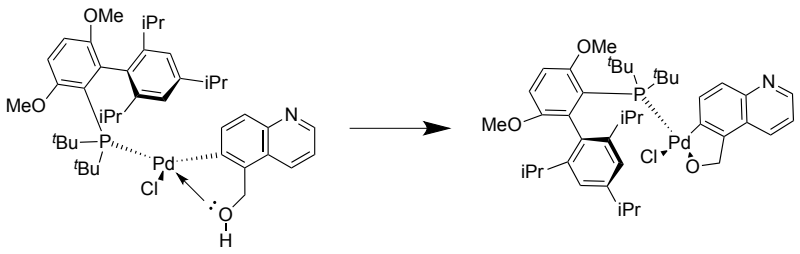

2.26 **2.27**

Figure 2.1. Hypothesised structure of the intermediate **2.26** following oxidative insertion. The lone pair of the primary alcohol may co-ordinate to the Pd centre forming a 5-membered ring **2.27**, thereby preventing approach of the nitrite anion, necessary for the desired reductive elimination.

To test this hypothesis, a number of ether derivatives of **2.18** were synthesised, and the nitration reaction attempted (**Scheme 2.12**). Successful conversion of the *ortho*-fluorobenzyl **2.28** and *para*-fluorobenzyl **2.29** derivatives to the corresponding nitro compound was achieved, with an increased catalyst loading compared to that used for 6-chloroquinoline **2.22**.

After purification, **2.32** and **2.33** were isolated in 68% and 38%, respectively (**Scheme 2.12**).

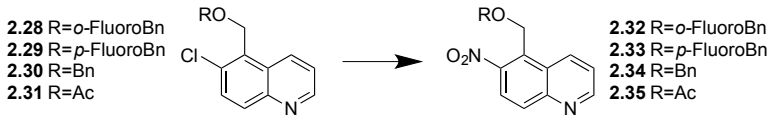

Scheme 2.12. Palladium-catalysed nitration of ether and acyl derivatives of methylene alcohol **2.18**; *Reagents and conditions:* (i) $NaNO_2$ (2 eq.), $Pd(dba)_3$ (2.5 mol%), ^{t}BuBrettPhos (6 mol%), ^{t}BuOH, 130 °C, 24 h.

Palladium-catalysed nitration of the benzyl **2.30** and acetylated **2.31** derivatives were also evaluated on a small scale (20 mg starting material). Benzyl derivative **2.30** was determined to undergo the desired nitration to compound **2.34** by mass spectrometry, ^{1}H NMR spectrometry, and TLC analysis of the crude reaction mixture. Evidence of the acetylated reaction product, **2.35**, was observed by mass spectrometry.

The palladium-catalysed nitration of ether derivatives **2.28-2.31** suggested that the presence of a primary alcohol in **2.18** prevented progression of the reaction (**Scheme 2.12**). By introducing alkyl/acyl groups at this position, co-ordination of the alcohol to the palladium centre was prevented, and the catalysis cycle progressed to afford the desired nitrated products. However, protection of **2.18** to achieve nitration, and subsequent deprotection, would incorporate two additional steps to the overall synthesis. Consequently, an alternative, more efficient synthetic strategy was investigated.

2.3.2 Synthetic route 2

As a result of the difficulties encountered with the nitration of **2.18**, an alternative, shorter synthesis was devised (**Scheme 2.13**). Employing

5-amino-6-nitroquinoline **2.38** as the commercially available starting material, provided functionalisation already installed at the desired positions. The amino group at the 5-position offered a chemical handle for the introduction of a halide *via* a Sandmeyer reaction to afford bromide **2.37** (**Scheme 2.13**, Step iv).[177] It was proposed that magnesium-halogen exchange with **2.37** would occur readily, due to the electron withdrawing effects of the *ortho* nitro group (**Scheme 2.13**, Step iii).[178] Subsequent formylation and reduction would afford the desired alcohol **2.17** (**Scheme 2.13**, Step ii), which could be converted to the desired bromide **2.16** (**Scheme 2.13**, Step i).

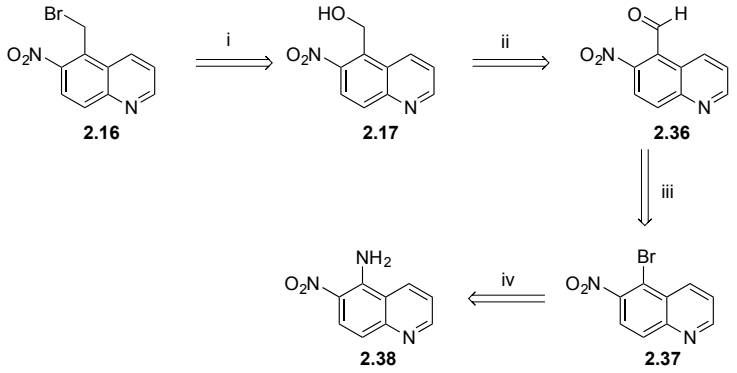

Scheme 2.13. Proposed retrosynthetic route to afford fluorogenic derivative **2.16** for alkylation of a biologically active cargo molecule: (i) Bromination; (ii) Reduction; (iii) Grignard chemistry/formylation; (iv) Sandmeyer bromination.

Initial attempts to brominate **2.38** employing a procedure with catalytic CuBr (1 mol%) led to a complex mixture of products as judged by TLC analysis.[179] However, evidence of the desired product **2.37** was observed by mass spectrometry. A copper-free procedure to generate bromodimethylsulfonium **2.39** *in situ* as the brominating reagent was also investigated (**Scheme 2.14**).[180] ^{1}H NMR analysis of the crude reaction mixture revealed a single reaction product, with the amino functionality still intact. Mass spectrometry and the emergence of a ^{1}H NMR singlet suggested

bromination at either the 7- or 8-position of the quinoline ring. This product was determined in subsequent investigations to be the 8-substituted isomer **2.40** (**Scheme 2.17**, Page 52).

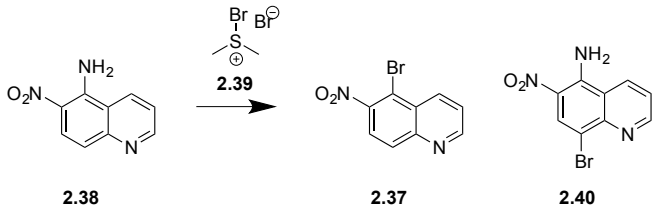

Scheme 2.14. Attempted copper free bromination of **2.38** by generating bromodimethylsulfonium **2.39** *in situ*. *Reagents and conditions:* $NaNO_2$ (4 eq.), aq. HBr (48% w/v) (4 eq.), DMSO, 35 °C. 2 h.

Following treatment of **2.38** with aq. HBr (48% *w/v*) and $NaNO_2$, analysis of the crude reaction mixture by ^{1}H NMR and mass spectroscopy indicated predominate conversion of the starting material to **2.40**. The formation of **2.40**, suggested an oxidative process was occurring to form Br_2 *in situ* from HBr and $NaNO_2$, enabling electrophilic aromatic substitution. It was hypothesised that using stoichiometric amounts of CuBr could promote the desired reaction, by forming a complex with bromide and nitrite anions in solution, thereby potentially reducing formation of Br_2. Furthermore, CuBr promotes reductive elimination of N_2 from a diazonium intermediate by single electron transfers, enabling reaction progression.[177]

Employing a procedure using excess CuBr (1.2 eq.) and $NaNO_2$ (1.2 eq.), the desired brominated product **2.37** was furnished in 18% yield (**Scheme 2.15**).[181] ^{1}H NMR and mass spectrometry analysis of the crude reaction mixture also suggested the presence of undesired side products **2.40**, and **2.41** (**Scheme 2.15**).

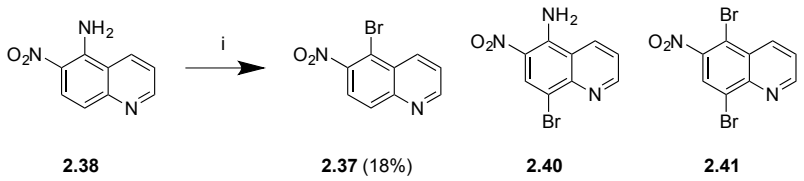

Scheme 2.15. Bromination of quinoline **2.38** using excess Cu(I)Br; *Reagents and conditions:* (i) Cu(I)Br (1.2 eq.), $NaNO_2$ (1.2 eq.), conc. HBr (aq.), 0 °C, 4 h,18%.

It was likely that delocalisation of the amino lone pair of **2.38** into the *ortho* nitro group would make nucleophilic addition with the nitrosonium electrophile (NO^+) less favourable, thereby preventing diazotisation to form intermediate **2.42** (**Scheme 2.16**).

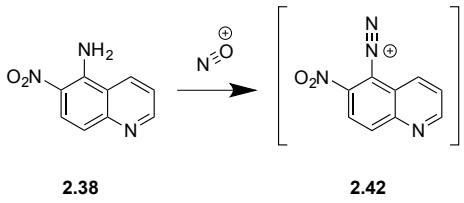

Scheme 2.16. The reactivity of the amine of compound **2.38,** to act as a nucleophile towards the nitrosonium electrophile is likely to be reduced due to deactivating inductive effects of the nitro group. The diazonium intermediate **2.42** is highly electron deficient with a nitro group adjacent.

To promote formation of presumed diazonium intermediate **2.42**, increasing the equivalents of $NaNO_2$ and therefore NO^+ *in situ*, was considered. Optimisation of the reaction conditions, employing 3 eq. $NaNO_2$, led to isolation product **2.37** in an improved yield of 51%, and a reduced yield of the undesired side product **2.40** (**Scheme 2.17**).

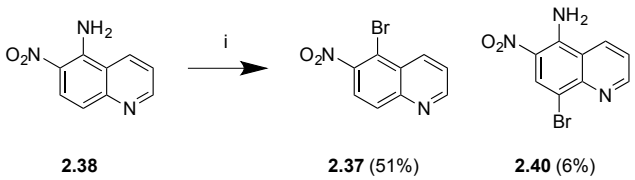

Scheme 2.17. Bromination of compound **2.38**; *Reagents and conditions:* (i) CuBr (1.2 eq.), $NaNO_2$ (3 eq.), aq. HBr, 0 °C, 3 h, 51%.

With the desired compound **2.37** in hand; introduction of the formyl functionality was investigated. The conditions previously used for formylation of the chloroquinoline **2.21** (**Scheme 2.9**, Page 46), afforded a complex mixture of products, as determined by TLC analysis (**Scheme 2.18**).

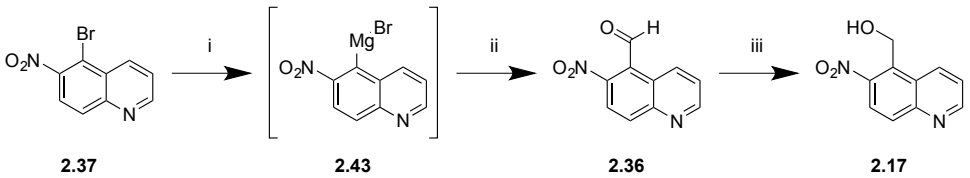

Scheme 2.18. Attempted formylation of **2.37**; *Reagents and conditions:* (i) 2 M ^{i}PrMgCl/THF (1.2 eq.), THF, −10 °C, 1 h; (ii) DMF (5 eq.), −10 - 0 °C, 4 h.

To determine whether the presumed Grignard intermediate **2.43** had formed, the reaction was investigated by quenching with H_2O at selected time intervals, and the crude reaction mixture was analysed by ^{1}H NMR spectrometry (**Scheme 2.19**, Step i). The expected product nitroquinoline **2.1** could not be detected when ^{i}PrMgCl was employed. However, use of a "turbo" Grignard (^{i}PrMgCl·LiCl) led to some formation of the desired product **2.1**, as determined by ^{1}H NMR analysis of the crude reaction mixture. Conversion of starting material using ^{i}PrMgCl·LiCl suggested that the presumed lithium intermediate **2.45**, with a small, hard counter cation, might be stabilised better than the analogous magnesium stabilised intermediate **2.44**.

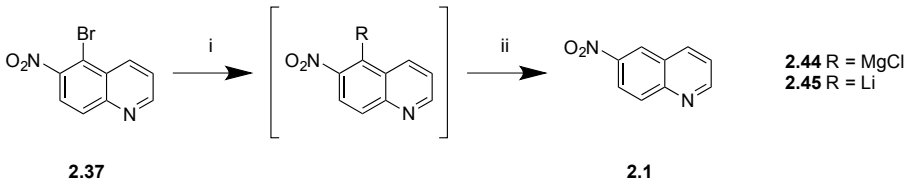

Scheme 2.19. Halogen lithium exchange may afford a more stable organoanion intermediate. **2.45**, compared to magnesium intermediate **2.44**; *Reagents and conditions*: **2.44** (i) 2 M ^{i}PrMgCl/THF (1.2 eq.), THF, −10 °C, 30 min; (ii) H_2O, 0 °C, 5 min; **2.45** (i) 1.3 M *n*-BuLi (1.2 eq.), THF, −10 °C, 30 min; (ii) H_2O, 0 °C, 5 min.

Treatment of **2.37** with *n*-BuLi for 30 min in THF at −70 °C, followed by quenching with H_2O, led to the formation of **2.1**, as determined by TLC analysis, ^{1}H NMR and mass spectrometry of the crude reaction mixture. Taking this reaction forward, formylation of the presumed organolithium intermediate **2.45** was investigated using distilled ethyl formate (EtOCHO) as the formylation reagent. It was hypothesised that the lower pKa of EtOH (pKa ~ 17) as the leaving group in EtOCHO, compared to Me_2NH (pKa ~ 37) for DMF, could accelerate formylation. Subsequent purification of the reaction mixture led to isolation of the desired aldehyde **2.36** in 10% yield (**Scheme 2.20**).

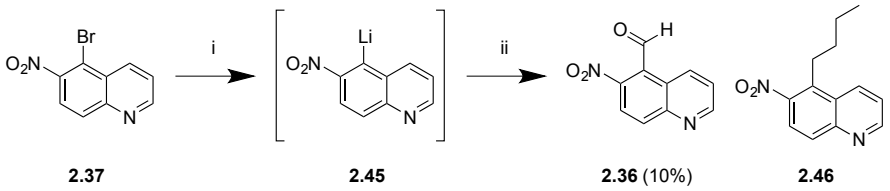

2.37 **2.45** **2.36** (10%) **2.46**

Scheme 2.20. Synthesis of aldehyde **2.36**; *Reagents and conditions:* (i) 2.3 M *n*-BuLi/hexanes (1 eq.), THF, −100 °C, EtOCHO (5 eq.), −100 °C → RT, 16 h, 10%.

^{1}H NMR and mass spectrometry analysis of the crude reaction mixture suggested that a number of side products had formed (**Scheme 2.20**). The dominant side product was likely to be **2.46**, arising from nucleophilic substitution of the intermediate **2.45** with butylbromide, as determined by ^{1}H NMR and mass spectrometry analysis of the crude reaction mixture. Alternatively, compound **2.46** could arise from an S_NAr reaction between *n*-BuLi and compound **2.37**. It was found that use of the milder organolithium reagent phenyl lithium (PhLi, pKa_H ~ 43), compared to *n*-BuLi (pKa_H ~ 50) afforded the desired aldehyde product **2.36** in an improved yield of 45% (**Scheme 2.21**).

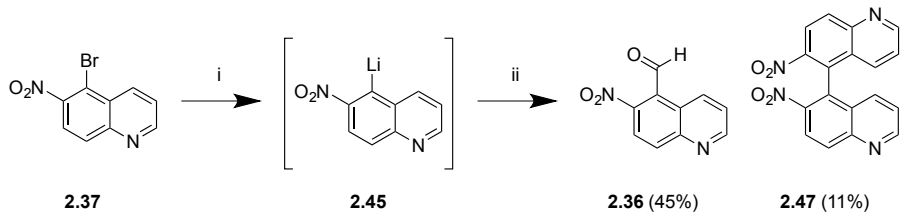

2.37 **2.45** **2.36** (45%) **2.47** (11%)

Scheme 2.21. Synthesis of aldehyde **2.36**; *Reagents and conditions:* (i) 1.75 M PhLi/THF (1 eq.), −78 °C, 45 min; (ii) EtOCHO (5 eq.), −78 °C → RT, 16 h, 45%.

On larger reaction scales (500 mg **2.37**), the reaction detailed in **Scheme 2.21** was found to be capricious, with yields ranging from 20-30%. Side products isolated from these reactions included the dimer **2.47** in 11% yield (**Scheme 2.21**). Slow addition of PhLi over 30 minutes, and EtOCHO as a solution (1 M, THF), to ensure effective heat dispersion throughout the reaction solution, led to no appreciable increase in yield of **2.36** (40-45%).

With aldehyde **2.36** in hand, reduction of the aldehyde moiety with $NaBH_4$ was attempted, furnishing methylene alcohol **2.17** in an excellent yield of 94% (**Scheme 2.22**). Treatment of methylene alcohol **2.17** with aq. HBr (48% *w/v*) afforded compound **2.16** in 84% yield (**Scheme 2.23**).

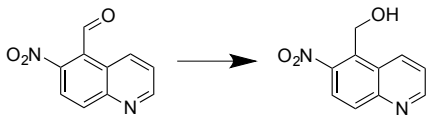

2.36 **2.17**

Scheme 2.22. Reduction of aldehyde **2.36**; *Reagents and conditions:* (i) $NaBH_4$ (1 eq.), 0 °C, 15 min, 94%.

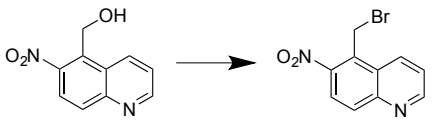

2.17 **2.16**

Scheme 2.23. Bromination of **2.17** by acid-catalysed nucleophilic substitution; *Reagents and conditions*: (i) HBr (48% aq.), 75 °C, 20 h, 84%.

In summary, starting from commercially available 5-amino-6-nitroquinoline **2.38**, a practical, four-step, synthetic route to furnish bromide **2.16**, suitable for use as an alkylating agent, was successfully devised. With **2.16** in hand, attention turned to introduction of a cargo molecule to evaluate **2.9** as a fluorogenic bioreductive group.

2.4 Selection of a biologically active cargo molecule

Epigenetic pathways have emerged as exciting targets in cancer therapy.[182,183] These pathways can control and manipulate the transcription of genes, by marking DNA with reversible chemical tags such as methylation, or by making reversible post-translational modifications to histone proteins.[184] The function of proteins that 'read' one such mark made to histones; acetylation of lysine, are called bromodomains and have been the subject of intense biological research.[185-187] A variety of chemical probes have been reported as tools to elucidate the role of bromodomains in living systems.[187,188] Using chemical tools to inhibit a bromodomain sub-family; called the bromodomain and extra-terminal domain (BET) family, is the subject of on-going investigations for the treatment of a number of cancer types.[189-191] A potential criticism of inhibiting epigenetic proteins is the essential role they play in managing the genome in non-diseased cells.[192] As such, the BET bromodomain inhibitors currently being evaluated in the clinic for cancer treatment show toxicity issues.[193-195] Consequently, there is a need to develop targeted epigenetic therapies, which avoid cytotoxicity in normal, healthy tissue. An attractive solution to this problem is developing BET bromodomain inhibitors as HAPs, which are selectively activated in hypoxic tumours.

Bromodomain-containing protein 4 (BRD4), a member of the BET family, has been impicated in *myc* driven tumours, and other aggressive forms of cancer.[196,197] Our laboratory has developed a series of compounds for the study of BRD4.[198,199] Compound **2.48** was identified as a BRD4 chemical probe with a reported IC_{50} value of 0.382 μM, as determined by an AlphaScreen® assay, and a K_D of 0.390 μM by surface plasmon resonance (SPR) (**Figure 2.2A**).[198] The anti-cancer activity of **2.48** was demonstrated against a variety of cancer cell lines (**Appendix C**). Furthermore, by means of clonogenic survival assays, **2.48** exhibited enhanced potency against oesophageal FLO-1 (**Figure 2.2B**) and OE21 (**Figure 2.2C**) cells under hypoxic conditions compared to normoxic conditions, suggesting **2.48** could be an effective molecule to target hypoxia.

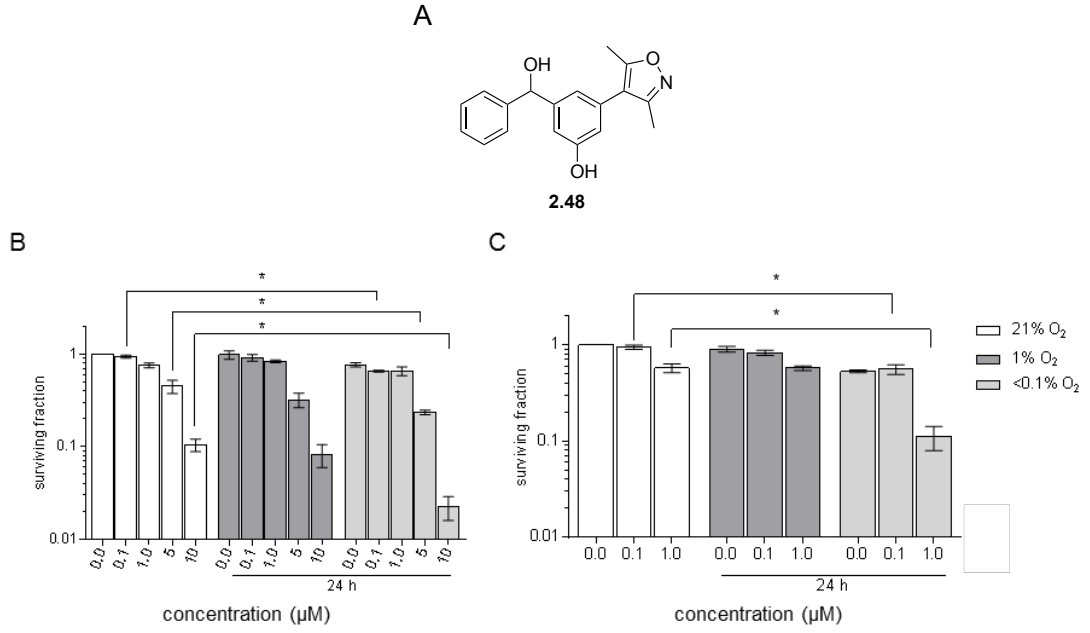

Figure 2.2. (A): Chemical structure of **2.48**; (B-C) Bar charts to show cell survival following treatment with **2.48** at the indicated concentrations for 24 h under normoxic (21% O_2), moderately hypoxic (1% O_2) and hypoxic (<0.1% O_2) conditions; (B) FLO-1 and (C) OE-21 oesophageal cancer cell lines. These data were provided by Dr Selvakumar Anbalagan (Hammond laboratory).

The X-ray crystal structure of **2.48** in complex with the first bromodomain of BRD4 displays an interaction of the phenol hydroxyl group with a conserved H_2O, which is located in the ZA channel (**Figure 2.3**).

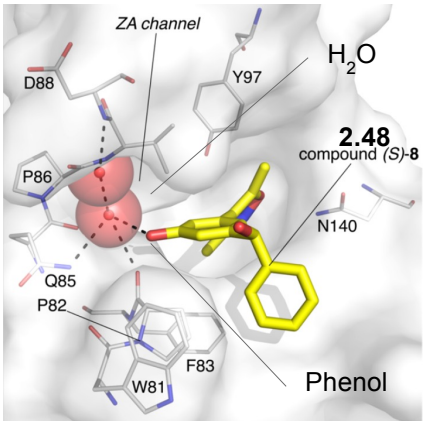

Figure 2.3. X-Ray crystal structure of **2.48** in complex with the first bromodomain of BRD4. The phenol functional group forms a hydrogen bond interaction with a conserved H_2O molecule. BRD4(1) PDB code: 3SVG. Adapted with permission.[198]

To be effective at targeting BRD4 in hypoxia, a HAP derivative of **2.48** must have poor potency against its target under normoxic conditions. This is critical so that normal, well-oxygenated tissues are not affected by phenotypic changes to BRD4 function. Only when the HAP is exposed to hypoxia would **2.48** be released, reinstating activity against BRD4. It was hypothesised that disrupting the phenol-H_2O binding interaction, by masking the phenol functionality with a bioreductive group, and thereby introducing a sterically demanding moiety, would significantly reduce the potency of **2.48** towards BRD4. To test our hypothesis, the fluorogenic bioreductive group, alkylating derivative, **2.16** was installed onto **2.48** at the phenol position. Alkylation was achieved by treatment of **2.48** under basic conditions with the bromo derivative **2.16** (**Scheme 2.24**) to afford **2.49** in 54% yield.

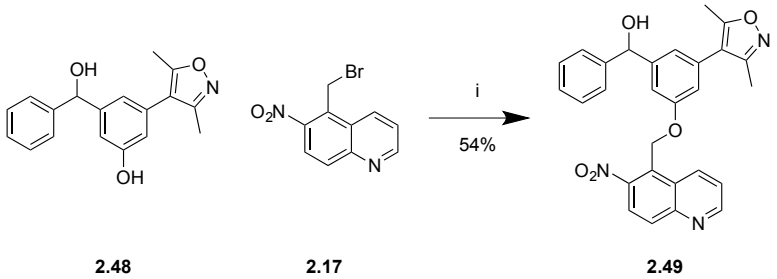

Scheme 2.24. Synthesis of fluorogenic hypoxia activated BRD4 inhibitor **2.49**; *Reagents and conditions:* (i) Cs_2CO_3, DMF, RT, 2 h, 54%. Compound **2.48** was provided as a gift from Dr David Hewings (Conway laboratory).

With compound **2.49** in hand, investigations into the utility of the molecule as a fluorogenic HAP were considered. Under hypoxic conditions, it was proposed that **2.49** would be a substrate for NADPH reductase, to afford fluorescent amine **2.51**, which undergoes subsequent fragmentation to release cargo **2.48** (**Scheme 2.25**).

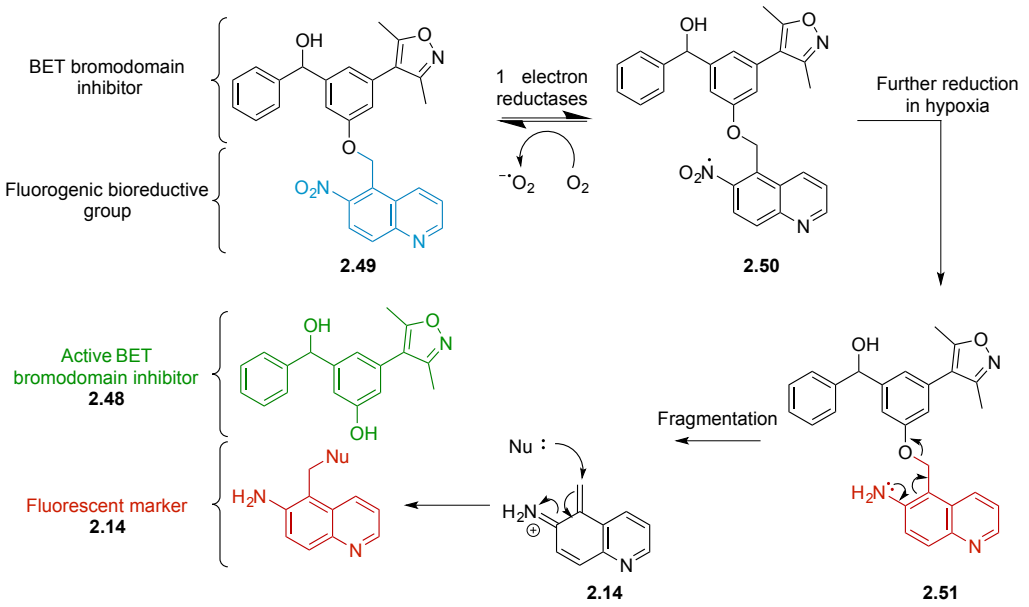

Scheme 2.25. A proposed mechanism of action for the fluorogenic HAP **2.49**. Single electron transfer (SET) to the nitro group forms a radical species **2.50**, which is quenched in the presence of oxygen back to **2.49**. Under hypoxic conditions, the radical persists, and further reduction occurs to afford amino species **2.51**. From amino species **2.51** an intramolecular elimination is enabled, causing fragmentation to release compound **2.48**, an active BET bromodomain inhibitor.

2.5 Evaluation of 2.49 as a fluorogenic HAP.

2.5.1 A validation protocol

Following synthesis, a series of experiments are required to biologically evaluate a novel HAP molecule, and determine its propensity to undergo reduction and fragmentation, prior to more complex biological interrogation. The studies detailed below were designed to be a simple and efficient method for performing preliminary HAP investigations (**Figure 2.4**).[48]

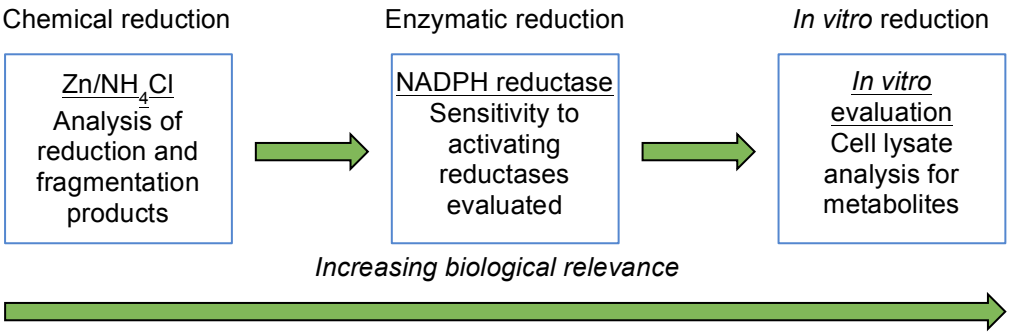

Figure 2.4. Evaluation protocol of hypoxia-activated prodrugs, increasing in biological relevance (**Appendix A.4**).

The initial validation step, employs zinc and ammonium chlordide as chemical reductants. This experiment has previously been used to afford insights into the mechanism of action, and fragmentation of HAPs.[47,200] The second step involves treatment of the candidate HAP with reductase enzymes, namely NADPH reductase which is heavily implicated in HAP activation, under hypoxic (<0.1% O_2) and normoxic (21% O_2) conditions.[72] Finally, cancer cell lines are treated with the candidate HAP under normoxic (21% O_2) and hypoxic (<0.1% O_2) conditions. The cell lysate is then analysed by HPLC/LCMS for hypoxia-specific reduction or fragmentation products of the HAP. Full details of this protocol may be found in **Appendix A.4**.

2.5.2 Zinc reduction assay and fragmentation analysis

Compound **2.49** was treated with zinc and ammonium chloride (1 % *w/v*) in DMF over 30 minutes. Aliquots of the reaction solution were taken at regular intervals, and analysed by HPLC for the presence of nitro reduction intermediates (**Figure 2.5**). The resulting data revealed induction of formation of nitroso **2.52** and amine **2.51**. No release of inhibitor **2.48** was detected over the time course of the assay, indicating that under the reaction conditions, the reduced amine intermediate **2.51** was stable.

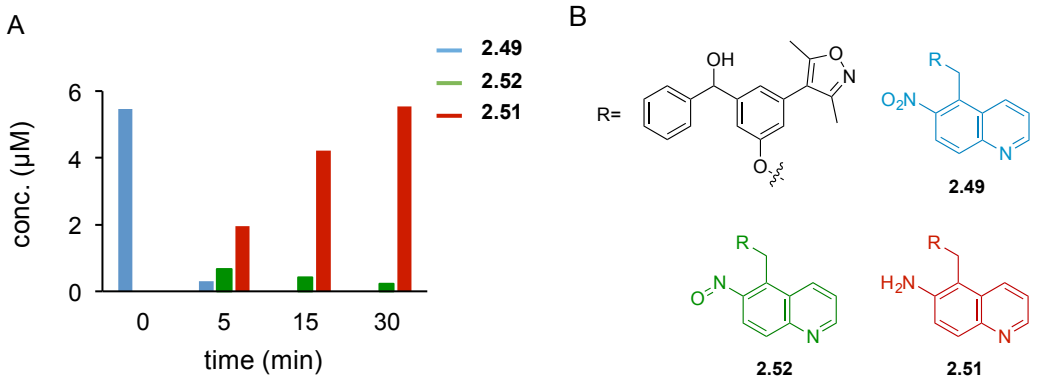

Figure 2.5. (A) Bar chart to show the concentrations of nitro **2.49**, nitroso **2.52** and amine **2.51** with time during zinc reduction of compound **2.49**. To determine concentrations, an assumption is made that the UV absorbance of the nitroso **2.52** and amine **2.51** derivatives is the same as that of the parent compound **2.49**. (B) Chemical structures of **2.49**, nitroso intermediate **2.52** and amine intermediate **2.51**. Colours correspond to the graph bars in A.

To evaluate whether the amine intermediate **2.52** was stable to more physiologically relevant aqueous conditions, an aliquot from Time=30 minutes was added to aqueous phosphate buffer, and the resulting solution was incubated at 37 °C for 24 hours. The 30-minute aliquot was selected due to almost complete conversion to the desired amine **2.51** (**Figure 2.5**). Subsequent HPLC analysis of the solution after this time revealed complete fragmentation of the amine intermediate **2.51** to afford inhibitor **2.48** (**Figure 2.6A**). Crucially, this fragmentation was not observed with the

corresponding parent nitro compound **2.49**, which was stable to hydrolysis (**Figure 2.6B**).

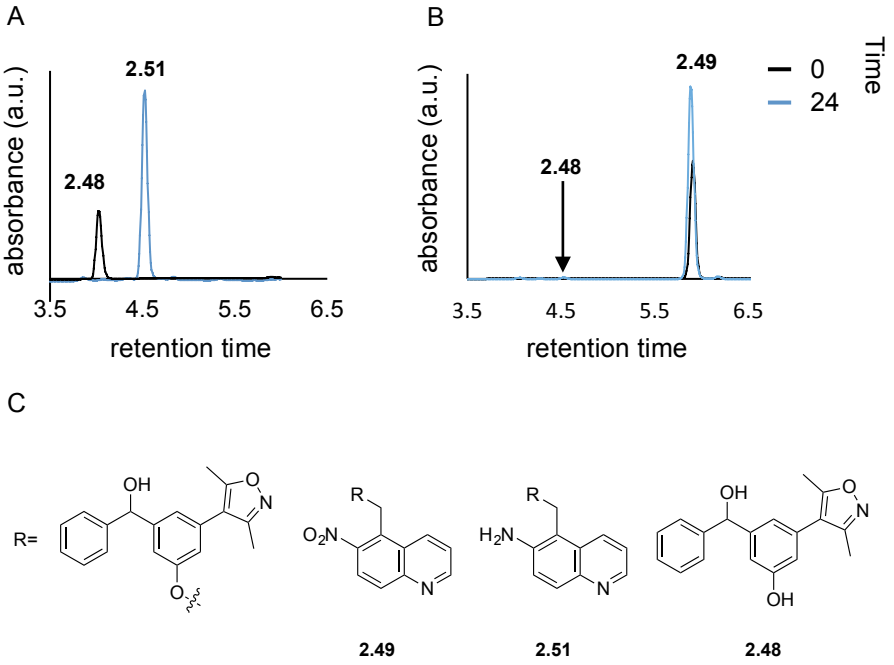

Figure 2.6. Absorbance (254 nm) charts to show the HPLC UV traces of (A) amine species **2.51** and (B) nitro **2.49** incubated with 0.1 M KH_2PO_4 buffer pH 7.4 at 37 °C for 24 h. The expected retention times of amine **2.51**, nitro **2.49** and inhibitor **2.48** are indicated by their respective compound numbers. Amine **2.51** was taken directly as an aliquot (5 µL) from the Zn reduction assay and injected into 95 µL of buffer; (C) Chemical structures of **2.49**, **2.51** and **2.48**.

The data shown suggest that reduction to the fluorescent amine **2.51** was required for fragmentation to occur under aqueous conditions, releasing **2.48** (**Figure 2.6A**). Contrastingly, nitro **2.49** did not undergo hydrolysis to release **2.48**, supporting our mechanism for elimination of a cargo molecule *via* the reduced amine **2.51** from the bioreductive group **2.9** (**Figure 2.6B**). These preliminary results showed promise for the utility of **2.9** as a bioreductive group. Consequently, fluorogenic HAP BET bromodomain inhibitor **2.49** was progressed to the next step of our validation protocol.

2.5.3 Bioreduction using NADPH reductase

NADPH reductase has been widely implicated in the bioreduction of nitroaromatic compounds under hypoxic conditions.[71] Compound **2.49** was treated with NADPH reductase under normoxic (21% O_2; **Figure 2.7A**) and hypoxic (<0.1% O_2; **Figure 2.7B**) conditions, and the concentrations of **2.49** and **2.48** determined by HPLC at times up to 24 hours.

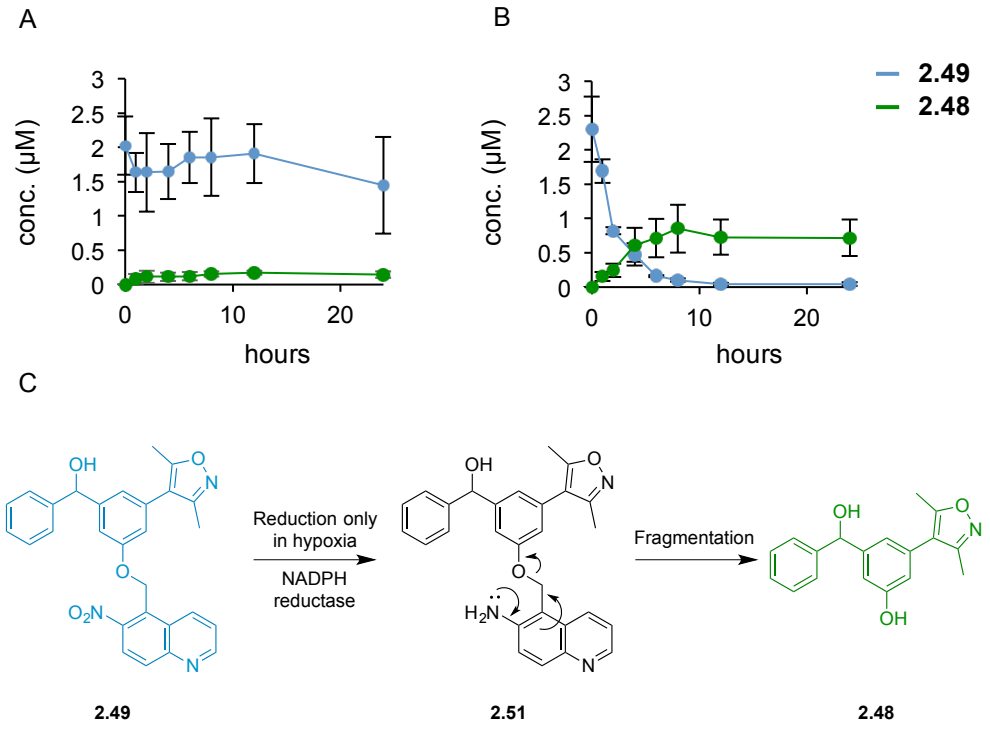

Figure 2.7. (A-B) Graphs to show the concentration of **2.49** and **2.48** with time during treatment of **2.49** (10 μM) with NADPH reductase enzymes over 24 h under (A) normoxic (21% O_2) and (B) hypoxic (<0.1% O_2) conditions. (C) Schematic showing the reduction and fragmentation of **2.49** under hypoxic conditions. Colours correspond to those in graphs A and B.

Under normoxic conditions, no increase in **2.48** concentration was observed, and the concentration of **2.49** remained largely consistent (**Figure 2.7A**). This result indicated that **2.49** was stable to NADPH reductase under normoxic conditions as predicted. In contrast, under hypoxic (<0.1% O_2) conditions, the concentration of **2.48** increased with time, concomitantly

with the decrease in **2.49** concentration (**Figure 2.7B**). Release of **2.48** from **2.49** under hypoxic conditions occurred progressively from 0-8 hours, further supporting our proposed mechanism, in which nitro reduction is a requirement for fragmentation to occur (**Figure 2.7C**).

Reduction products such as nitroso **2.52**, hydroxylamine **2.53** or amino **2.51** species were not detected by HPLC analysis under hypoxic conditions (**Figure 2.8A**). The absence of these intermediates may possibly reflect a rapid reduction of **2.49** and fragmentation of amine **2.51**. In contrast to **2.49**, reduction intermediates were detected for the HAP Chk1 inhibitor, CH-01 **1.35**, developed by our laboratory (**Figure 2.8B**; **Appendix A.1**).[47] It is possible that **2.49** undergoes more rapid bioreduction compared to the 4-nitrobenzyl group in CH-01 **1.35**, due to the extended aromacity of the quinoline ring, better stabilising radical nitro intermediate. Treatment of **1.35** with NADPH reductase under hypoxic conditions did not afford detectable amounts of Chk1 inhibitor **1.36** until 24-48 hours.[47] The difference in the fragmentation rates of **2.49** *vs* **1.35** is almost certainly a reflection of the better leaving group ability of a phenol **2.48** (pKa~10) compared to a primary alcohol **1.36** (pKa~16).

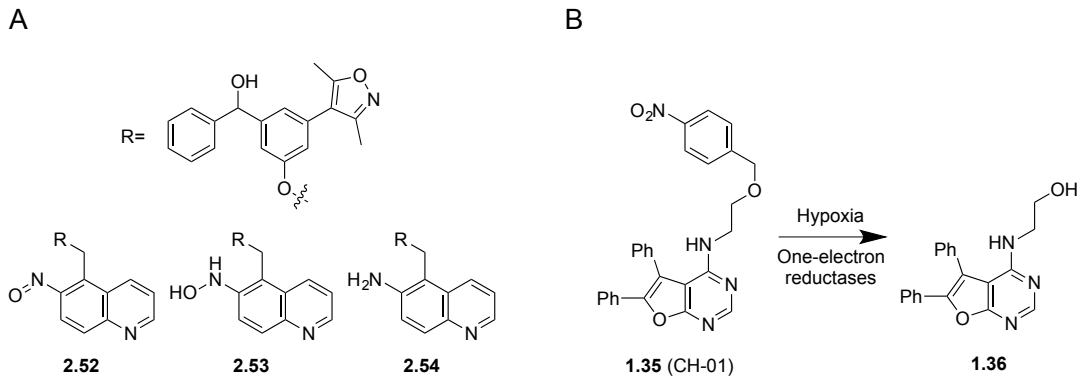

Figure 2.8. (A) Chemical structures of nitroso **2.52**, hydroxylamine **2.53**, and amino **2.51** reduction intermediates; (B) Schematic to show the transformation of CH-01 **1.35** under hypoxic conditions to a primary alcohol containing Chk1 inhibitor **1.36**.

Treatment of **2.49** with NADPH reductase provided validation for 5-methylene-6-nitroquinoline **2.9** as a novel bioreductive group. A clear oxygen dependency for activation was established. With these promising results in hand, the propensity of **2.49** to undergo oxygen sensitive bioreduction in cell-based assays was evaluated.

2.5.4 Cell treatment and cell lysis analysis

Our laboratory has previously used human colorectal carcinoma (RKO) cells in the evaluation of candidate hypoxia-activated prodrugs.[47] Consequently, RKO cells were employed for validation experiments, and were treated with **2.49** under hypoxic (<0.1% O_2) conditions for 2, 4, 8 or 24 hours. The cells were subsequently harvested, and the lysate was analysed by HPLC/LCMS for the presence of associated reduction and fragmentation products (**Figure 2.9**). Formation of the desired biologically-active cargo molecule **2.48** could not be detected. Furthermore, the concentration of **2.49** remained largely constant over the time course of the assay

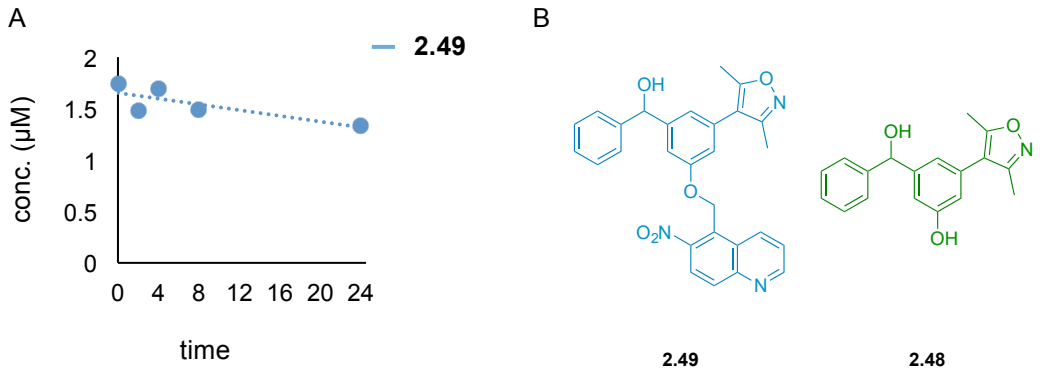

Figure 2.9. (A) Graph to show the concentration of **2.49** in RKO cell lysate (0.5×10^6 cells) after treatment with **2.49** (10 μM) for the indicated time under hypoxic (<0.1% O_2) conditions. Cells were lysed with 3% trichloroacetic acid (TCA). (B) Chemical structures of **2.49** and **2.48**.

Due to the lack of any observable reduction metabolites of **2.49**, extended treatment times were considered. RKO cells were treated with **2.49** for 24 hours under normoxic (21% O_2) and hypoxic (<0.1% O_2) conditions. The cells were lysed with MeCN and the lysate analysed by for the presence of **2.49** and associated reduction and fragmentation products. HPLC/LCMS analysis suggested the oxidised compound **2.54** was present (**Figure 2.10**).

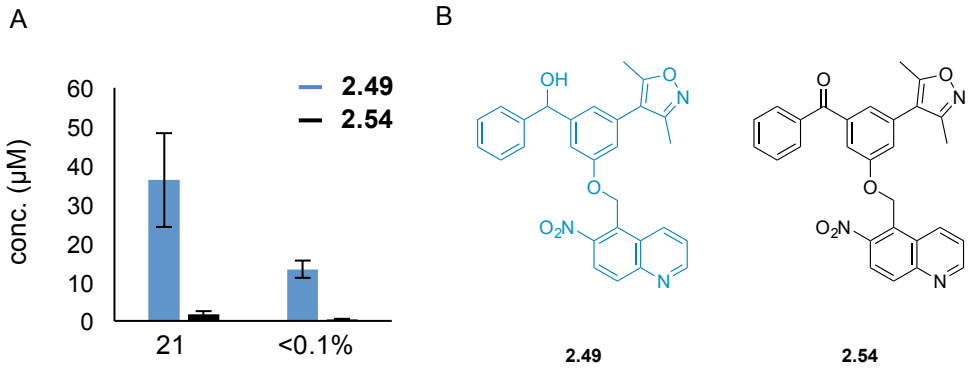

Figure 2.10. (A) Graph to show the concentrations of **2.49** and **2.54** in RKO cell lysate (0.5×10^6 cells) following treatment with **2.49** (10 μM) for 24 h under normoxic (21% O_2) and hypoxic (<0.1% O_2) conditions. Cells were lysed with MeCN; (B) Chemical structures of **2.49** and oxidised metabolite **2.54** at the secondary alcohol position. Colours correspond to the bars in graph A.

The presence of oxidised metabolite **2.54** suggested that **2.49** was cell permeable, and was undergoing an oxidative metabolic process. However,

reduction and fragmentation products could not be detected by HPLC/LCMS. The lower concentration of **2.49** detected in the cell lysate after treatment in hypoxia, compared to normoxia could be indicative of the reduced metabolic stability of **2.49** under hypoxic conditions. Alternatively, **2.49** could be undergoing reduction and fragmentation, but **2.48** was metabolised rapidly and consequently not detected by HPLC. Consequently, the metabolic stability of **2.49** was investigated.

Liver microsomes comprise a variety of enzymes involved in the metabolism of xenobiotics, and have been used as useful *in vitro* tools to predict stability of a drug *in vivo*.[201,202] Investigations using human microsome fractions revealed **2.49** $t_{1/2}$: 43.8 min under normoxic (21% O_2) conditions and $t_{1/2}$: 16.5 min under hypoxic (<0.1% O_2) conditions (**Figure 2.11**). Microsomal degradation of **2.49** was approximately 3-fold faster under hypoxic conditions, compared to normoxic.

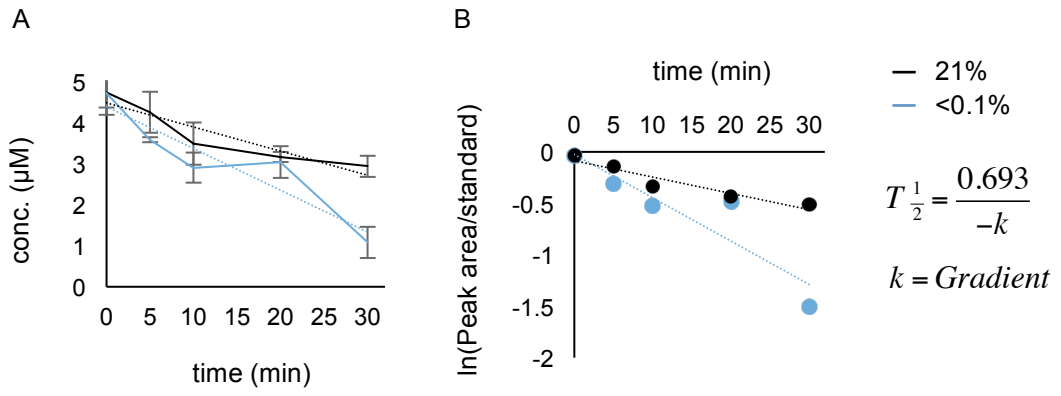

Figure 2.11. Compound **2.49** was treated with human liver microsomes under normoxic (21% O_2) and hypoxic (<0.1% O_2) conditions over 30 min. (A) Graph to show the concentration of **2.49** in the assay volume with time under normoxic (21% O_2) and hypoxic (<0.1% O_2) conditions (B) Graph to show the degradation of **2.49** compared to a 5 μM internal standard, with time, under normoxic and hypoxic conditions. The key shown relates to graphs A and B. The half-life of **2.49** was calculated from the gradient of the line of best fit (dashed) and calculated as indicated.[203]

Under hypoxic conditions, treatment of **2.49** with liver microsomes led to numerous metabolites, as determined by HPLC/LCMS, with indication to the presence of primary metabolites, including oxidation of the secondary alcohol **2.54**, and *para*-hydroxylation of the phenyl group **2.55** (**Figure 2.12**).

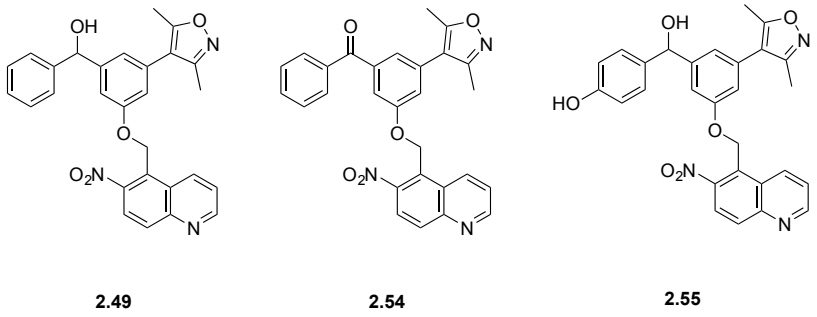

Figure 2.12. Chemical structures of compounds arising from primary metabolism of **2.49**.

These investigations suggest the presence of metabolic hotspots on **2.49**, which were located on the **2.48** fragment of the molecule. It was therefore likely that if **2.49** were undergoing reduction and fragmentation to release **2.48** under hypoxic conditions in cells, **2.48** was rapidly metabolised and consequently not detected *in vitro* by HPLC analysis. This hypothesis was supported by work conducted in our laboratory examining the metabolic stability of **2.48** and various analogues.[204]

2.5.5 Activity of 2.49 against BRD4

The IC_{50} of **2.48** against BRD4 (0.382 μM) was evaluated using an AlphaScreen® assay. Therefore, HAP analogue **2.49** was subject to identical analysis, allowing direct comparison of the inhibition activity.[205] Installation of the fluorogenic bioreductive group **2.9** onto the phenol position of **2.48** to yield **2.49** was not detrimental to potency against BRD4. Compound **2.49** was determined to have an IC_{50} of 0.749 μM representing a modest decrease in

potency compared to the parent compound, **2.48** (IC_{50} : 0.382 μM). As such, use of **2.49** as a prodrug to target BRD4 in hypoxia would result in a BRD4 dependent phenotype in both normoxic and hypoxic conditions. Therefore, **2.49** was unsuitable for evaluation as a HAP within the context of targeting BRD4 in hypoxic tumours. Despite this result, **2.49** was suitable for validation experiments of the novel fluorogenic hypoxia-activated bioreductive group **2.9** (**Scheme 2.5**, Page 43).

2.6 Fluorescence Evaluation

For 5-methylene-6-nitroquinoline **2.9** to be a useful fluorogenic bioreductive group, there must be an increase in fluorescence intensity upon reduction to the corresponding amine. To evaluate the fluorescence profile of **2.49** before, and after reduction of the nitro functionality to amine **2.51**, fluorometric analysis was performed (**Figure 2.13**).

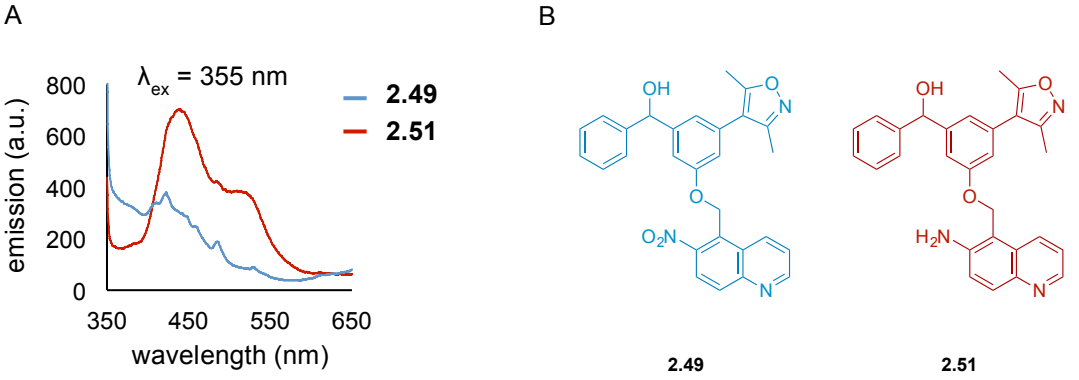

Figure 2.13. (A) Graph to show the fluorescence emission intensity (λ_{ex} 355 nm) of **2.49** (100 μM) and **2.51** (100 μM) in aq. NaH_2PO_4 buffer (15 mM, pH 7.4, 150 mM NaCl). A solution of **2.51** was prepared from the T=30 aliquot from the zinc reduction experiment (**Chapter 2.5.2**, Page 61). (B) Chemical structures of **2.49** and **2.51**. Colours correspond to the fluorescence emission spectra in A.

Amine **2.51** demonstrated enhanced fluorescence emission intensity of approximately 2.5-fold (λ_{em} = 450 nm) to 5-fold (λ_{em} = 510 nm) compared to

2.49, and therefore bioreductive group **2.9** can be termed as fluorogenic. Furthermore, the fluorescence spectrum of **2.51** is in good agreement with that reported for 6-aminoquinoline **2.2**, indicating that modifications to a 6-aminoquinoline **2.2** scaffold at the 5-position were well tolerated, with respect to the fluorescence profile.[165,172]

Having evaluated the fluorescence emission spectra for **2.49** and the reduction product, amine **2.51**, subsequent investigations focused on whether fluorescence would be observed after fragmentation. It was proposed that H_2O, an abundant cellular nucleophile, might react with the electrophilic iminium ion **2.14** *in vitro* (**Scheme 2.26**). Consequently, the fluorescence profiles of amine species **2.56** and nitro species **2.57** were evaluated (**Figure 2.14**).

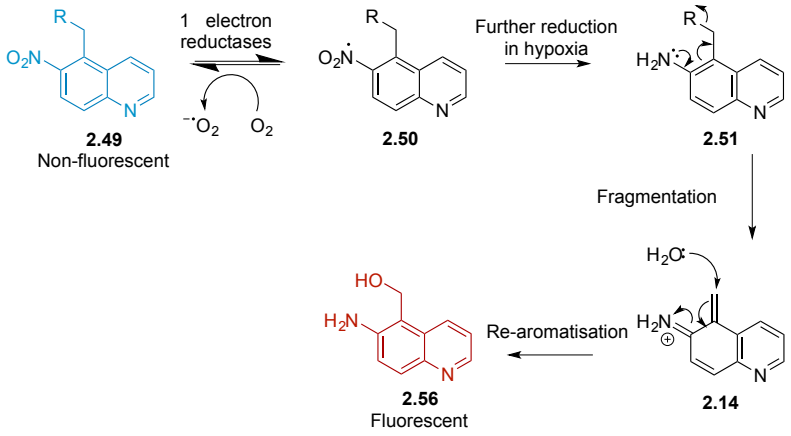

Scheme 2.26. Hypoxia-dependent reduction of **2.49** results in the amine metabolite **2.51**. After fragmentation an electrophile **2.14** is formed, which is quenched by intracellular nucleophiles, such as H_2O, which would afford amine **2.56**.

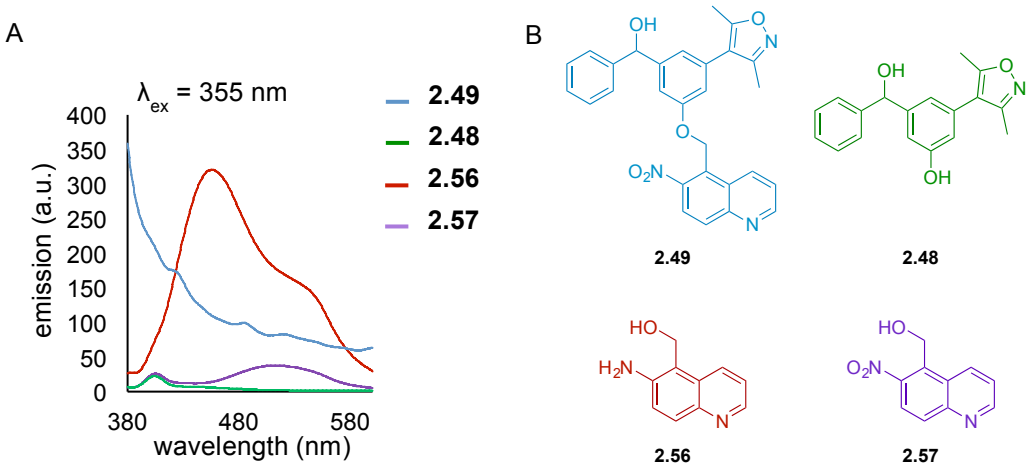

Figure 2.14. (A) Graph to show fluorescence emission spectra (λ_{ex} 355 nm) of 100 µM solutions of **2.49**, **2.48**, **2.56** and **2.57**. Fluorescence spectra were recorded in aqueous NaH_2PO_4 buffer (15 mM, pH 7.4, 150 mM NaCl). (B) Chemical structures of **2.49**, **2.48**, **2.56** and **2.57** colour coded to correspond to graph A.

Compound **2.56** exhibited approximately 300-fold greater fluorescence emission intensity (λ_{em} = 450 nm) than the analogous nitro compound **2.57**. However, when compared to parent fluorogenic HAP **2.49**, this fluorescence difference is reduced to approximately 3-fold (**Figure 2.14A**). This result suggests that **2.49** exhibits moderate inherent fluorescence in phosphate buffer. Interestingly, **2.48** and **2.57** as distinct compounds exhibited no appreciable fluorescence.

Studies introduced later in this study determined that fluorescence spectra of a fluorogenic compound obtained in ^{i}PrOH, were comparable to those obtained in cells by confocal microscopy (**Figure 4.19**, Page 128). Consequently spectra were also obtained in ^{i}PrOH. The fluorescence emission intensity of **2.56** at the previously employed concentration (100 µM) exceeded the detection limit of the spectrometer, and visual inspection of the solution in the spectrometer revealed strong fluorescence (**Figure 2.15A**). In contrast, no visual fluorescence was observed for nitro derivative **2.57** at the

same concentration. Dilution of each sample to 1 µM enabled evaluation by fluorometric analysis, and revealed approximately 450-fold greater fluorescence intensity of amine **2.56** compared to nitro analogues **2.57** and **2.49** (**Figure 2.15B**). Interestingly, the previously observed fluorescence of **2.49** in aqueous buffer was entirely abrogated in ^{i}PrOH.

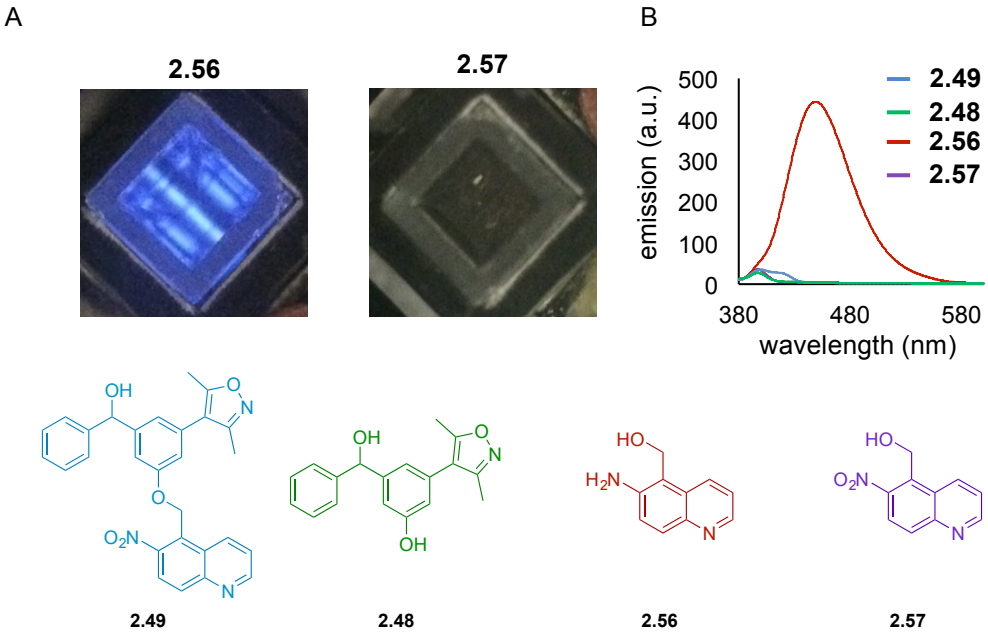

Figure 2.15. (A) Top views of the cuvette used in fluorescence spectroscopy. Visual fluorescence of 100 µM ^{i}PrOH solutions of amino **2.56** compared to nitro **2.57**; (B) Fluorescence emission spectra of 1 µM ^{i}PrOH solutions of **2.49**, **2.48**, **2.56**, and **2.57** (λ_{ex} 355 nm). (C) Chemical structures of **2.49**, **2.48**, **2.56**, and **2.57**. Colours correspond to graph B.

To ensure only fluorescent amino derivative **2.56** absorbed the fluorescence excitation light (λ_{ex} 355 nm), UV-Vis spectra were obtained (**Figure 2.16**). The fluorescent amine **2.56** showed absorption maximum ($\lambda_{max\ abs}$) at 360 nm. Critically, nitro-derivatives **2.49** and **2.57**, and cargo molecule **2.58** showed no absorption maximum at this wavelength.

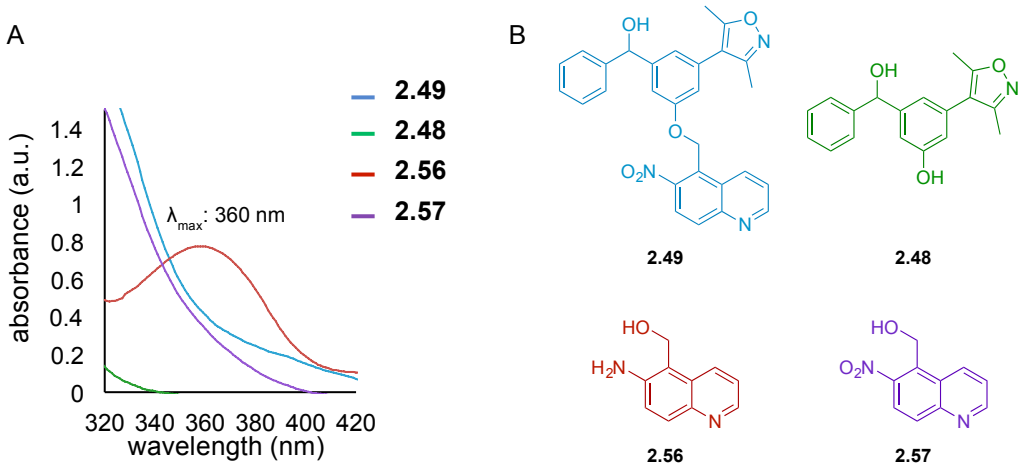

Figure 2.16. (A) Graph to show UV-Vis absorption spectra of aq. KH_2PO_4 solutions of **2.49**, **2.48**, **2.56** and **2.57** (500 μM, pH 7.4). (B) Chemical structures of **2.49**, **2.48**, **2.56**, and **2.57**. The colours correspond to graph A.

The suitability of amine **2.56** for fluorescence microscopy was evaluated by treating RKO cells with **2.56** (10 nm-500 μM) under normoxic (21% O_2) conditions, and following an incubation period of 2-8 hours, visualisation was performed. Unfortunately, fluorescence corresponding to **2.56** could not be detected *in vitro* under any of the treatment conditions investigated. The lack of fluorescence in cells treated with **2.56** suggested the molecule was either not suitable for fluorescence microscopy, or not cell membrane permeable. Considering a simplified structure, amine **2.2** (**Scheme 2.1**, Page 39) has proved useful in fluorescence studies to monitor enzyme activity, and to label molecules for HPLC analysis, but no use in fluorescence microscopy has been reported.[172,206]

2.7 Conclusion

In conclusion, 5-methylene-6-nitroquinoline **2.9** has been shown to be a novel, fluorogenic hypoxia-activated group. Conjugation of the group to a BET bromodomain inhibitor **2.48** afforded candidate fluorogenic HAP **2.49**. In the presence of oxygen **2.49** remains stable with respect to metabolism by NADPH reductase enzymes. However, in the absence of oxygen, nitro reduction occurred to afford to corresponding amine **2.51**, which fragments to release BET bromodomain inhibitor **2.48**. NADPH reductase has been identified as critical for the activation of HAPs in both pre-clinical and clinical studies, and so is encouraging for the use of fluorogenic bioreductive group **2.9** in future studies.[84,207] Using a zinc reduction assay, amine **2.51** was shown to trigger fragmentation to release cargo molecule **2.48**, whereas unreduced nitro analogue **2.49** was hydrolytically stable.

Evaluation of **2.49** in a human colorectal carcinoma (RKO) cells was inconclusive regarding hypoxia-dependent reduction and fragmentation to release **2.48**. Development of **2.48** analogues to improve metabolic stability, for incorporation into HAPs, would potentially aid *in vitro* HPLC analysis. Furthermore, introduction of structural diversity around the acetyl-lysine mimetic (the 3,5-dimethylisozaxole moiety) of **2.48** could provide alternative positions for the attachment of bioreductive group **2.9**. This could better reduce the potency of fluorogenic HAP **2.49**, compared to its biologically active cargo, **2.48**.

Reduction of **2.49** to the amine **2.51** resulted in an increase in fluorescence, indicating **2.49** could be a useful reporter of hypoxic conditions.

Furthermore, the rearomatised fluorogenic group **2.56**, a likely product of intracellular fragmentation, was shown to have ~450 fold greater fluorescence parent nitro **2.49** in ^{i}PrOH by fluorescence spectroscopy. Unfortunately, **2.56** could not be visualised in cells. It is possible that **2.56** was not cell permeable, and therefore could not be detected *in vitro* by microscopy. It is also possible that **2.56** is not bright enough, or the quantum yield too low, to be a useful compound for fluorescence microscopy. **2.56** therefore requires development into a brighter fluorophore.

This work represents the first ever demonstration of a bioreductive group that can deliver a cargo molecule of therapeutic interest, and simultaneously report on its bioreduction under hypoxic conditions. It is consequently the subject of a patent application.[208]

Chapter 3

TOWARDS THE SYTNHESIS OF A NIR, FLUOROGENIC HYPOXIA-ACTIVATED DYE

3.1 Introduction

Following development of 6-nitroquinoline **2.1** into a fluorogenic bioreductive group **2.9**, it was noted that improved spectrophotometric properties would be required for detailed fluorescence analysis of HAP activation in tumour models. The following design criteria were, therefore, considered for the next generation fluorogenic bioreductive group:

a) The emission maximum (λ_{max}) of the fluorophore
b) The synthetic scope for modification into a bioreductive group
c) The opportunity for installation of a nitro group, which upon reduction to the corresponding amine, would induce a 'switch-on' of fluorescence.

To be an effective *in vivo* fluorogenic bioreductive group, the fluorescent component must emit light within the near-infrared (λ_{max}: 650-1300 nm) region of the electromagnetic spectrum, where issues associated with tissue autofluorescence, and photon penetrability are reduced.[133] Biomedical NIR dyes have recently been employed *in vivo* to identify tumour margins during surgical resections,[209,210] and to identify

chemotherapy-therapy resistant metastases.[211] Therefore, only fluorophores that emit within this range were considered for development into a fluorogenic bioreductive group.

Aminostyryl chromenone derivative **3.1** was identified as a potentially suitable fluorophore for development into a fluorogenic bioreductive group. The electron-donating amine group, in conjugation with the electron-withdrawing cyano groups affords a push-pull system type fluorophore, with a reported λ_{max} within the NIR region (670 nm) (**Scheme 1.9**, Page 35).[212] Furthermore, **3.1** is reported to be suitable for two-photon microscopy; a useful technique for *in vivo* fluorescence imaging with improved tissue penetrability.[212,213]

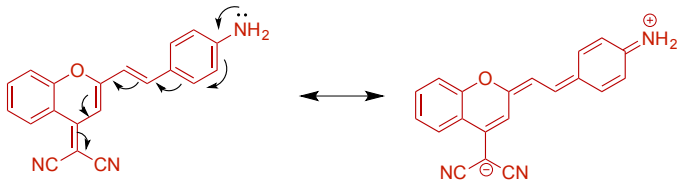

3.1

Scheme 3.1. Amine **3.1** is a two-photon NIR fluorophore with a λ_{max} ~ 670 nm. The push-pull system between the amine and cyano groups affords a favourable fluorescent profile.[212]

The amino functionality of **3.1** offered scope for installation of a nitro group, to afford a candidate fluorogenic hypoxia-activated dye **3.2** (**Scheme 3.2**). Nitro groups are established quenchers of molecular fluorescence,[148] and are sensitive to reduction by one-electron reductases under hypoxic conditions.[47] It was, therefore, hypothesised that following enzyme-mediated bioreduction to the corresponding amine, fluorescence of **3.1** would be restored to fluorescently mark hypoxic regions of a tumour model.

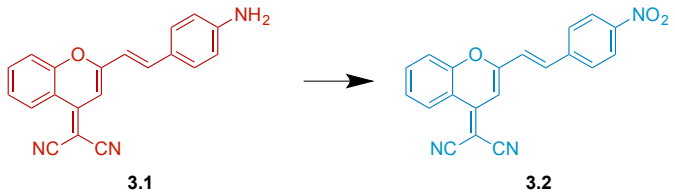

3.1 3.2

Scheme 3.2. Proposed transformation of fluorescent **3.1** into the fluorogenic, hypoxia-activated dye **3.2**. Bioreduction of the nitro functionality in hypoxia could restore fluorescence of the compound. Red indicates fluorescent and blue indicates non-fluorescent. *Proposed reagents: HCl aq., $NaNO_2$.*

Further scope for modifications to **3.2** was proposed to introduce a biologically relevant cargo molecule, therefore affording a novel fluorogenic bioreductive group **3.3** (**Scheme 3.3**). In contrast to generation one, the 6-nitroquinoline bioreductive group **2.9**, once **3.3** is enzymatically reduced by SET under hypoxic conditions, the release of the cargo molecule would be accompanied by fluorescence in the NIR region. The electrophile **3.6** produced in the fragmentation step was likely to undergo rearomatisation with intracellular nucleophiles, such as thiols or H_2O.[214]

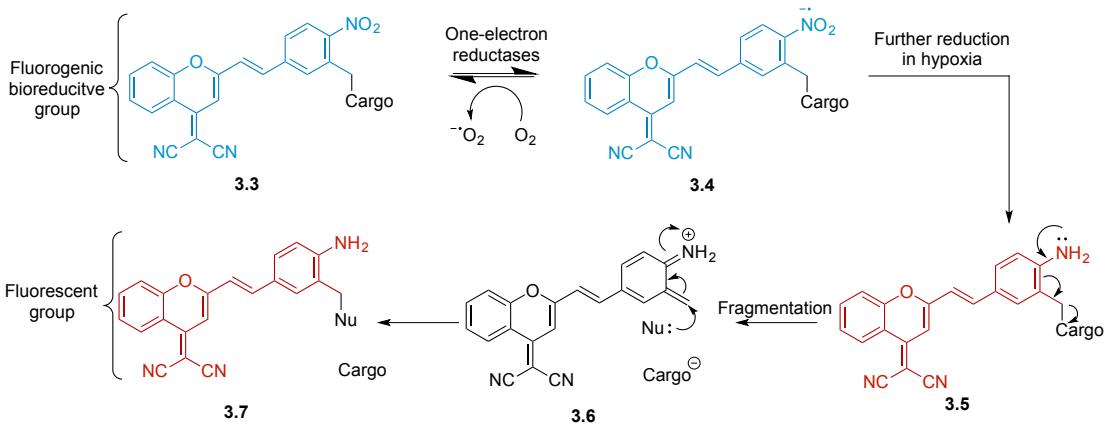

Scheme 3.3. Proposed introduction of a chemical handle *ortho* to the nitro group would allow introduction of a cargo molecule. Reduction by one-electron reductase enzymes under hypoxic conditions would yield the fluorescent group **3.5**, inducing fragmentation to release a cargo molecule. Rearomatisation by an intracellular nucleophile (Nu) would afford to fluorescent amine **3.7**. Blue structures indicate non-fluorescent, and red indicates fluorescent.

Validation of the nitro compound **3.2** as a NIR hypoxia-activated dye to afford amine **3.1** was considered vital before carrying out synthesis to make **3.3**. Consequently **3.2** was identified as the primary synthetic target for the purposes of validation of bioreductive and fluorescent properties. If these studies were successful, it was proposed to progress **3.2** for further development into the fluorogenic bioreductive group **3.3**.

3.2 Synthesis of intermediates 3.9 and 3.10

The amine **3.1** and nitro derivative **3.2** are structurally related by the styryl chromenone moiety (**Figure 3.1**). Consequently, the intermediates reported to obtain amine **3.1**, were also selected as the primary synthetic targets for use in synthesis of nitro **3.2**. Chromenone **3.9** and malononitrile derivative **3.10** were, therefore, synthesised with modifications to the reported procedure (**Scheme 3.4**).[212]

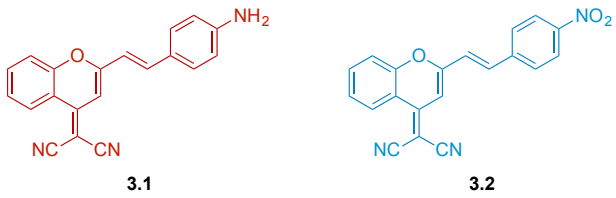

Figure 3.1. The chemical structures of amine **3.1** and the analogous nitro derivative **3.2**.

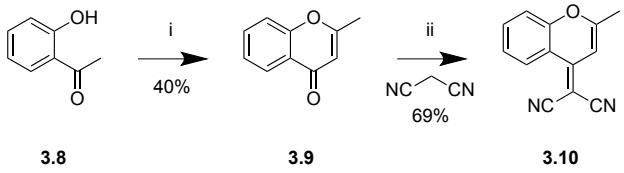

Scheme 3.4. Synthesis of intermediates **3.9** and **3.10**; *Reagents and conditions:* (i) Na (2.8 eq.), EtOAc, RT, 4 h; AcOH/H_2SO_4, 100 °C, 1 h, 40%; (ii) $CH_2(CN)_2$ (10 eq.), Ac_2O, 120 °C, 3 h, 69%.

Synthesis of chromenone **3.9** was achieved from commercially available 2-Hydroxyacetophenone **3.8** (40% yield) (**Scheme 3.4**, Step i). A Knoevenagel condensation of malononitrile with chromenone **3.9**, employing conditions previously described, was found to be capricious, affording **3.10** in variable yields (10%-25%).[212] Increasing the equivalents of malononitrile from 1.2 to 10 improved reaction progression, and following crystallisation, led to isolation of **3.10** in 69% yield (**Scheme 3.4**, Step ii).

An alternative strategy to furnish **3.10** was also investigated, based on the Vilsmeier-Haack formylation (**Scheme 3.5**).[215] Treatment of **3.9** with $POCl_3$ led to formation of a bright pink solution, suggesting formation of the chloro-oxonium cation **3.11**. Aqueous work-up of the reaction resulted in formation of the starting material **3.10**, indicating that chloro-oxonium species **3.11** was present. Subsequent addition of malononitrile to the reaction solution provided **3.10** in 61% yield.

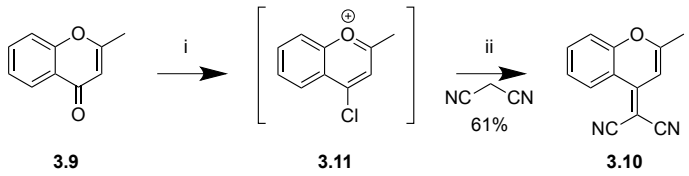

3.9 **3.11** **3.10**

Scheme 3.5. Synthesis of key intermediate **3.10** using $POCl_3$ to deoxygenate **3.9**; *Reagents and conditions:* (i) $POCl_3$ (1 eq.), RT, $CHCl_3$, 3 h ; (ii) $CH_2(CN)_2$ (1.1 eq.), Et_3N (3 eq.), RT, 72 h 61%.

Repetition of this reaction on larger scales (200 mg) was capricious affording **3.10** in variable yields (10-20%). It was hypothesised the variable yields were a result of localised heat spikes, arising from acid-base neutralisation upon addition of Et_3N (**Scheme 3.5**, Step ii). Consequently, the

previously employed condensation reaction with malononitrile (**Scheme 3.4**) was used for subsequent syntheses.

With key intermediates **3.9** and **3.10** in hand, a variety of synthetic strategies were investigated to afford the target nitro compound **3.2**.

3.3 Condensation reactions

Malononitrile-chromenone **3.10** has successfully been used in condensation reactions with aldehydes.[212,216] The reported synthesis of amine **3.1** employs a condensation reaction with 4-acetamidobenzaldehyde **3.12** to afford presumed intermediate **3.13** (**Scheme 3.6**). Subsequent deprotection of the acetyl group under acidic conditions was reported to yield amine **3.1**. The electron-withdrawing malononitrile group enhances the acidity of the methyl protons α to the aromatic chromenone ring, allowing **3.10** to act as a nucleophile upon deprotonation. To evaluate the condensation procedure, the reaction between **3.10** and **3.12** was carried out with modifications, leading to successful isolation of **3.1** (23% yield) (**Scheme 3.6**).

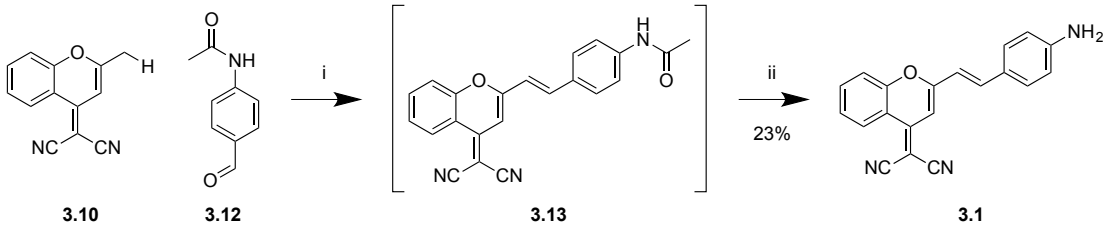

Scheme 3.6. Synthesis of amine **3.1**; *Reagents and conditions:* (i) **3.10** (1.1 eq.); toluene, AcOH (0.8 eq.), piperidine (0.5 eq.), 115 °C, 3 h; (ii) conc. aq. HCl/EtOH (2:3), 80 °C, 3 h, 23% over 2 steps.[212]

Based on these results, it was proposed that a condensation reaction between 4-nitrobenzaldehyde **3.14** and chromenone **3.10** would furnish the

desired nitro derivative **3.2**. Employing the conditions used for synthesis of **3.1**, the reaction was attempted (**Scheme 3.7**).

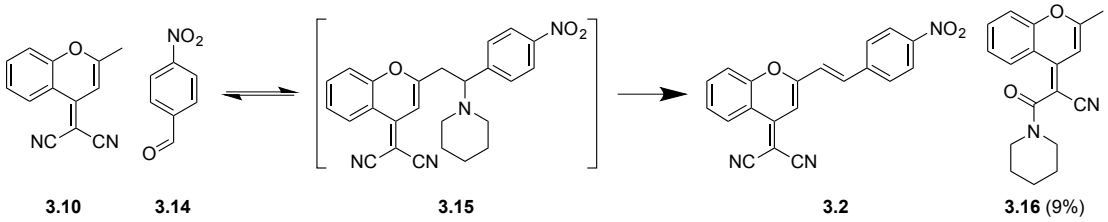

3.10 **3.14** **3.15** **3.2** **3.16** (9%)

Scheme 3.7. Attempted synthesis of **3.2** *via* a condensation reaction with **3.14** and **3.10**; *Reagents and conditions:* **3.14** (1.1 eq.), **3.10** (1 eq.) toluene, AcOH (6.6 eq.), piperidine (3.8 eq.), 110 °C, 3 h.

^{1}H NMR spectroscopy and TLC analysis of the crude reaction mixture revealed a mixture of products, of which starting materials **3.10** and **3.14**, were the predominant components. Following purification by silica gel column chromatography, a mixture of products was obtained, including compound **3.16** arising from nitrile hydrolysis (9% yield). The presence of **3.16** indicated that the equivalents of piperidine used in the condensation reaction protocol were too high. Consequently, the equivalents of AcOH and piperidine were reduced from that reported (8.7 eq. and 5 eq. respectively),[212] approximately 5-fold to 1.8 eq. and 1.1 eq. respectively. Under these conditions, the reaction solution was clear yellow, indicating red-coloured starting material **3.10** was being consumed, and was in contrast to previous reaction attempts where the reaction solution was dark brown. After 30 minutes a golden yellow precipitate formed, which was filtered and dried *in vacuo*. Analysis of the precipitate by accurate mass spectrometry (FI^{+}) revealed the desired mass of the product **3.2** (**Figure 3.2**).

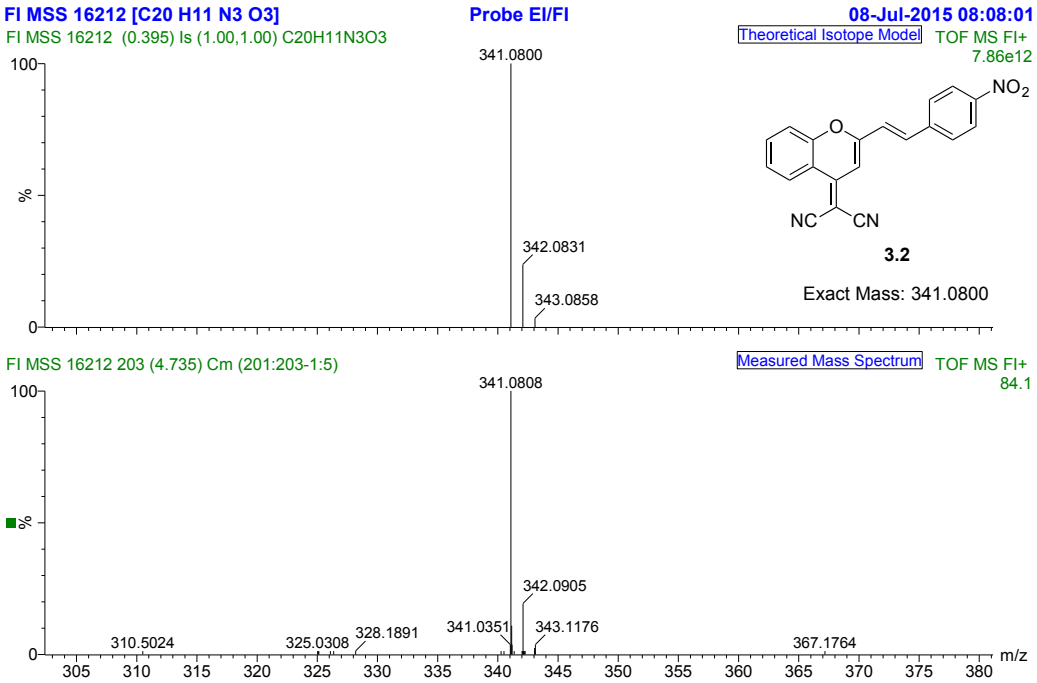

Figure 3.2. Accurate mass spectrometric analysis of the reaction precipitate, showing good agreement between theoretical and measured masses of compound **3.2** to 4 decimal places. The structure of **3.2** is inset. Error between calculated and measured masses: 2.34 ppm.

The solubility of the precipitate was extremely poor in common NMR solvents (DMSO-d_6, toluene-d_8, acetone-d_6). Pyridine-d_6 was found to be more suitable, and ^{1}H NMR analysis revealed a mixture of products. Unfortunately, further purification by silica gel column chromatography led to no isolation of the desired product **3.2** due to the insolubility of the precipitate in organic solvents.

Further analysis of the reaction mixture by low-resolution mass spectrometry suggested the presence of the proposed condensation intermediate **3.15** (**Scheme 3.7**). This indicated that elimination of piperidine to afford **3.2** was not readily occurring. This was likely due to the electron-withdrawing effect of the *para*-nitro group, making developing positive charge at the benzylic position in the elimination transition state **3.17**, thermodynamically unfavourable (**Figure 3.3**). To investigate this hypothesis,

a variety of *para*-substituted benzaldehydes were selected. The condensation reaction between **3.10** and benzaldehydes; 4-nitro **3.14** (*para*-Hammet constant [σ_p]: 0.78), 4-chloro **3.18** (σ_p: 0.23), 4-acetamido **3.12** (σ_p: 0.00), and 4-hydroxy **3.19** (σ_p: −0.37) were investigated (**Scheme 3.8**).[217] The Hammet constants provided give an indication of the substituents ability to withdraw electron density from the aromatic ring. Where the value is higher, the electron-deficiency is greater.

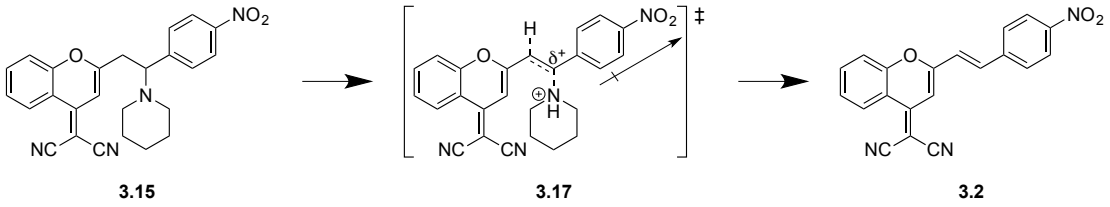

Figure 3.3. Proposed transition state of elimination **3.17** to afford product **3.2**. Developing positive charge at the benzylic position is likely to be thermodynamically unfavourable, due to the electron-drawing nitro group.

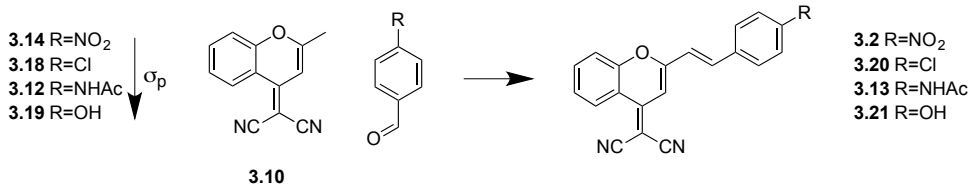

Scheme 3.8. Synthesis of **3.1** analogues using aldehydes of varying electronic properties; *Reagents and conditions:* Aldehyde (1.2 eq.), AcOH (6.6 eq.), piperidine (3.8 eq.), toluene, 95 °C, 24 h. **3.21**: 56%; **3.13**: 45%.

It was found that 4-Hydroxybenxaldehyde **3.19** readily underwent condensation to afford **3.21** in 56% yield. Reaction with the less electron rich acetamido aldehyde **3.12** furnished the precipitate of **3.13** in 45% yield (which was used without further purification and deacetylated to afford **3.1** in 23% yield). The chloro aldehyde **3.18** and nitro aldehyde **3.14** afforded no desired products, as determined by TLC analysis and ^{1}H NMR spectroscopy. These data revealed a correlation between the electron donating properties of the

aldehyde's *para* substituent, and the propensity for elimination to occur under the reaction conditions (**Scheme 3.8**). Consequently, kinetically driven reactions were investigated.

3.4 Base-catalysed elimination reactions

Previous condensation reactions investigated (**Chapter 3.3**, Page 81) suggested an electron-donating group was critical for the elimination step to occur under thermodynamic conditions. It was suggested that elimination could be favoured under kinetically controlled conditions, by promoting double bond formation at the electron-deficient benzylic position (**Scheme 3.9**). Consequently, a variety of bases were investigated to examine if elimination could be kinetically driven (**Table 3.1**).

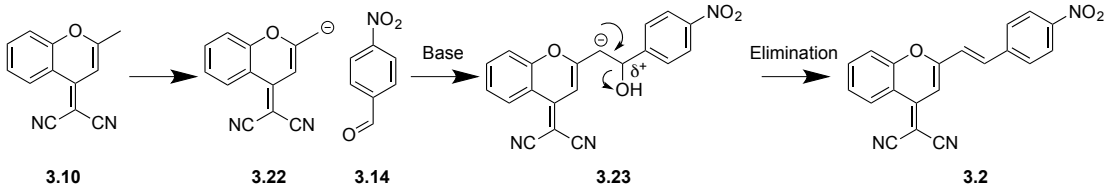

Scheme 3.9. Attempted synthesis of **3.2** under basic conditions.

Table 3.1. Attempted conditions for the base-promoted condensation of **3.10** with **3.14**.

Base	Equivalents	Temperature (°C)	Solvent	Time (h)
Cs_2CO_3	5	65	DMF	3
Cs_2CO_3/piperidine	1.2	RT	DMF	24
Cs_2CO_3/piperidine	1.2	RT	THF	24
Na/MeOH	5	75	MeOH	3
Pyridine	5	65	THF	3
2 M LDA/THF	3	RT	THF	24

Under basic conditions, chromenone **3.10** formed a deep blue solution from red, suggesting deprotonation of the methyl position to afford anion **3.22**. However, upon addition of 4-Nitrobenzaldehyde **3.14**, no product was formed under any of the reaction conditions investigated, as determined by ^{1}H NMR spectroscopy and TLC analysis of the crude reaction mixture. It was proposed that the basic conditions used could be promoting nitrile hydrolysis, leading to a variety of undesired products and unreacted starting material. To investigate this hypothesis, a condensation reaction with 4-Nitrobenzaldehyde **3.14** and chromenone **3.9** was investigated, employing NaOMe as the base (**Scheme 3.10**). During the reaction, a pale yellow precipitate formed, which after filtration and washing with MeOH, was determined to be the desired nitrostyryl chromenone **3.24** (61% yield).

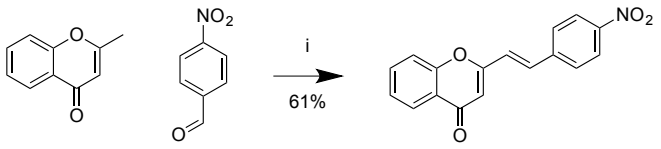

Scheme 3.10. Synthesis of **3.24**; *Reagents and conditions:* (i) Na (5 eq.), MeOH, 4-nitrobenzaldehyde **3.14** (1.2 eq.), 75 °C, 2 h, 61%.

Isolation of **3.24** indicated that presence of the malononitrile in compound **3.10** made it an unsuitable material for use with strong bases. The temperature of the condensation between malononitrile chromenone **3.10** and 4-Nitrobenzaldehyde **3.14** (**Scheme 3.8**, Page 84) was reduced to ambient temperature, and after 2 h a dark green precipitate formed. However, the precipitate was extremely insoluble in organic solvents, and ^{1}H NMR analysis of the precipitate was inconclusive.

3.5 Knoevenagel condensation of malononitrile

Synthesis of nitrostyryl chromenone **3.24** (**Scheme 3.10**) presented an opportunity to furnish **3.2** *via* an alternative synthetic strategy. It was envisioned that the ketone functionality of **3.24** could undergo a condensation reaction with malononitrile (**Scheme 3.11**). ^{1}H NMR spectroscopy and TLC analysis of the crude reaction mixture revealed a mixture of products, which could not be separated by column chromatography. It was proposed that using a Lewis acid could promote addition of malononitrile into the carbonyl group. Subsequently, **3.24** was treated with $BF_3{\cdot}Et_2O$ and a basic solution of malononitrile, followed by heat under reflux of the reaction solution (**Scheme 3.12**).

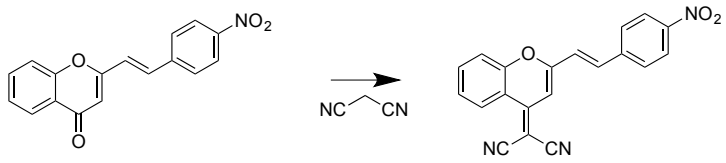

3.24 **3.2**

Scheme 3.11. Attempted synthesis of **3.2** by condensation with malononitrile; *Reagents and conditions:* $CH_2(CN)_2$ (10 eq.), Ac_2O, 110 °C, 3 h.

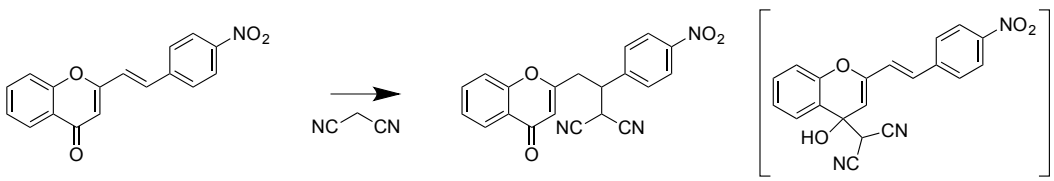

3.24 **3.25** (16%) **3.26**

Scheme 3.12. Attempted condensation of malononitrile with **3.24**; *Reagents and conditions:* BF_3:Et_2O (1.2 eq.), malononitrile (1.2 eq.), NaH (2 eq.), THF, RT, 1 h.

TLC analysis of the reaction mixture indicated multiple products in the reaction solution, of which one spot was dominant (**Scheme 3.12**). Mass spectrometry analysis suggested the presence of the proposed 1,2-addition

intermediate **3.26**. However, following purification and isolation, the structural isomer **3.25** was determined to be the dominant product, in 16% yield. Use of the stronger Lewis acid $AlCl_3$ yielded similar results by TLC analysis. These results were perhaps unsurprising considering hard-soft arguments. Malononitrile (pKa ~ 11) is a soft nucleophile or Michael donor, and would favour 1,4- or 1,6- conjugate addition into **3.24** over 1,2- addition. Consequently, alternative strategies were investigated.

3.6 Pd-catalysed nitration

Chemistry employing Pd catalysis for the introduction of a nitro functionality was previously used to install a nitro group from an aryl halide (**Chapter 2.3.1**, Page 44). This chemistry was reported to be more thermodynamically favourable employing aryl triflates rather than aryl chlorides.[218] Consequently, previously synthesised hydroxyl derivative **3.21** (**Scheme 3.8**, Page 84) was converted to the corresponding triflate **3.27** in 35% yield, and the nitration attempted (**Scheme 3.13**).

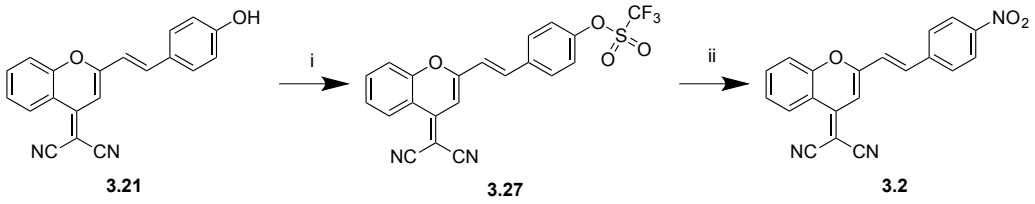

Scheme 3.13. Attempted Pd catalysed nitration to afford **3.2** *via* synthesis of the corresponding triflate **3.27**; *Reagents and conditions:* (i) Triflic anhydride (1.5 eq.), pyridine, 0 °C → RT, 20 min, 35%; (ii) $Pd_2(dba)_3$ (2.5 mol%), ^{t}BuBrettPhos (1.2 mol%), $NaNO_2$ (2 eq.), ^{t}BuOH, 80 °C, 24 h.

Under the reaction conditions, compound **3.2** was not detected by TLC analysis or ^{1}H NMR spectroscopy of the crude reaction mixture. Increasing the reaction temperature to 95 °C led to UV visualisation of a new spot by

TLC analysis. Subsequent low-resolution mass spectrometry of the reaction mixture suggested product **3.2** formation *m/z* 342.1 ($[M+H]^+$). Purification by silica gel chromatography led to isolation of an unknown reaction product. Subsequent high-resolution mass spectrometry revealed the desired mass 341.0806 (**3.2** requires 341.0800). However, ^{1}H NMR analysis of the isolated spot revealed multiple products were present. Further purification led to decomposition of the product, indicating instability of the reaction mixture to silica gel column chromatography.

It is unclear whether the desired product **3.2** was a major or minor component of the reaction mixture due to unsuccessful purification. Despite some success in synthesising **3.2** as determined by mass spectrometry, the product could not be isolated, and consequently an alternative strategy was investigated.

3.7 Diazotisation of 3.1

The literature reported that fluorescent amino compound **3.1** undergoes diazotisation to form presumed salt **3.28**, which following treatment with NaN_3 furnishes azide **3.29** (**Scheme 3.14**).[212] Amino compound **3.1** was previously furnished by condensation of **3.29** with 4-Acetamidobenzaldehyde **3.12**, followed by deacetylation in 23% yield (**Scheme 3.6**). To evaluate the propensity of **3.1** to undergo diazotisation, a model reaction was performed empoying NaN_3, to successfully furnish **3.29** (56% yield) (**Scheme 3.14**). It was subsequently proposed that, treatment of **3.1** with $NaNO_2$, instead of NaN_3, would afford the desired nitro derivative **3.2** (**Scheme 3.15**).

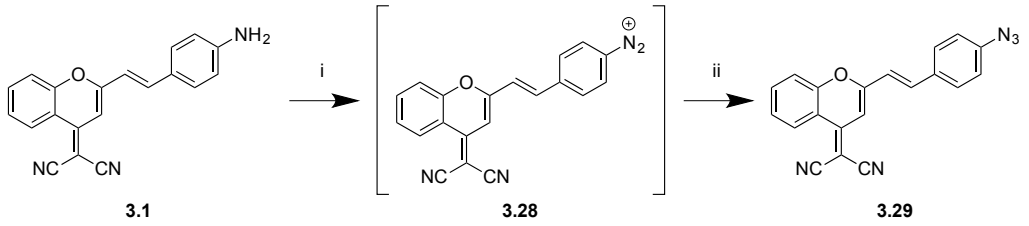

Scheme 3.14. Diazotisation of **3.1** to yield the presumed diazonium intermediate **3.28**, which can be transformed into the azide compound **3.29** on treatment with NaN_3. *Reagents and conditions*: (i) aq. $NaNO_2$ (5.3 eq.), aq. 5 M HCl; (ii) NaN_3 (21 eq.), 0 °C, 1 h, 56%.

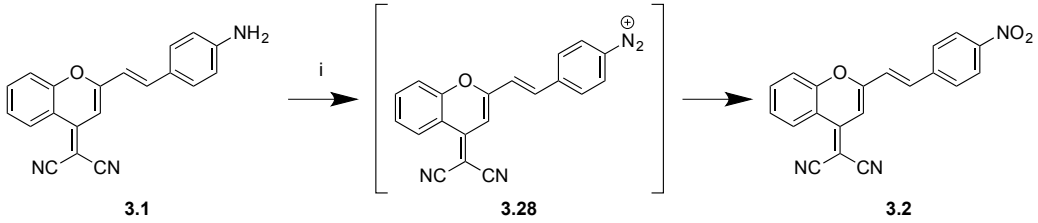

Scheme 3.15. Synthesis of **3.2** *via* formation of the diazonium salt **3.28** of **3.1**; *Reagents and conditions:* (i) aq. $NaNO_2$ (10 eq.), AcOH, RT, 15 h, 63%.

TLC analysis of the crude nitration reaction mixture indicated the formation of a new product (**Scheme 3.15**). Subsequent purification by column chromatography led to the formation of new products, suggesting the compound formed was unstable on silica. The reaction was repeated under reduced time of 2 hours, and aqueous work-up carried out before purification. Upon work-up, an orange precipitate formed, which was filtered and dried under reduced pressure. ^{1}H NMR spectroscopy of the precipitate revealed a single product, with the correct number of protons predicted for the desired nitro product **3.2**. Consequently, the ^{1}H NMR spectra of the precipitate and starting material **3.1** were compared (**Figure 3.4**). These ^{1}H NMR data were consistent with expected resonance peaks for the desired product **3.2**, as the electron withdrawing nitro group would cause the observed downfield chemical shift in the proton resonances, compared to **3.1**. In addition, proton

resonances corresponding to the amino functionality could not be detected in the ^{1}H NMR spectrum.

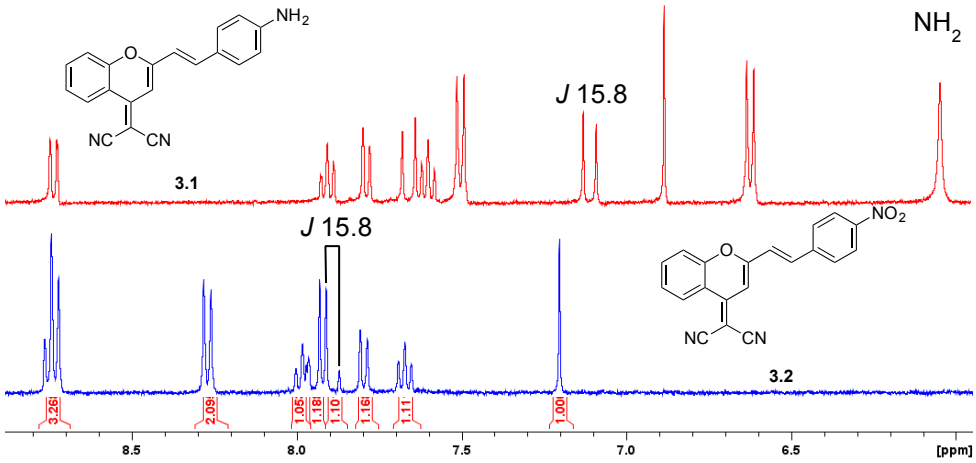

Figure 3.4. Comparison of proton NMR spectra (DMSO-d_6) of **3.1** (red) and the isolated precipitate [**3.2**] (blue). Analysis reveals loss of the amine (NH_2) peak, and maintenance of the *trans* double bond coupling. Integral values add up to the required 11 protons for **3.2**.

Examination of the ^{13}C NMR spectrum revealed the appearance of a resonance signal consistent with that expected for a nitro-substituted aromatic carbon (δ 146.6 ppm), which was absent in the starting material **3.1**. Analysis by HBMC and HSQC revealed the resonance was actually the carbon *para* to the nitro position, and that the nitro-substituted carbon signal was at lower chemical shift (δ 114.5 ppm) (**Figure 3.5**). This carbon resonance indicates a more shielded carbon-nitrogen bond, compared to that typically expected for aryl-nitro compounds. The shielding effect of nitro groups on carbon in electron deficient systems has been reported, and is demonstrated by comparing ^{13}C resonance signals of nitrobenzene (δ 148.1 ppm) with *p*-fluoronitrobenzene (δ 144.3 ppm).[219,220]

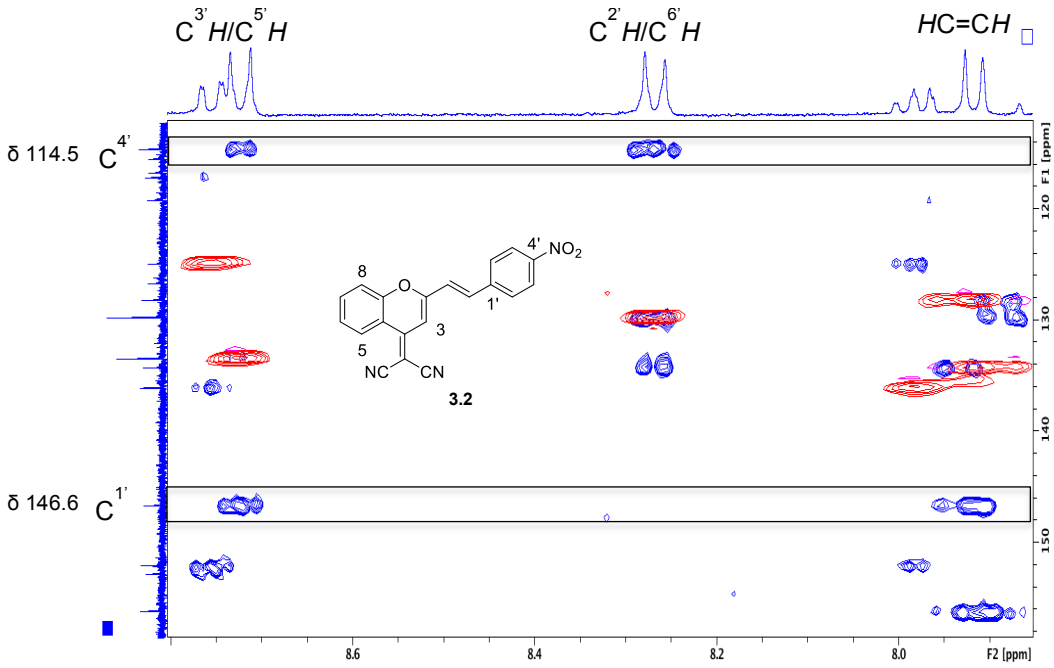

Figure 3.5. Spectra to show the HMBC (blue) and HSQC (red) 2D spectra of precipitate **3.2**. HMBC resonance signals indicate the ^{13}C resonance for the carbon *ipso* to the nitro group ($C^{4'}$) is at 114.4 ppm, as shown by coupling to the aromatic ring. The carbon *para* to the nitro group ($C^{1'}$) is at 146.6 ppm, as shown by coupling to the double bond, and the protons *ortho* to the nitro group.

Infrared spectroscopy of the solid indicated the presence of strong absorption bands consistent with those expected for nitro group stretches (1504, 1334). Comparison to the starting material **3.1** revealed the absence of these peaks, but corresponded well with other absorption frequencies, including the presence of nitrile stretches at approximately 2210 cm^{-1} (**Figure 3.6**). Comparison with chromenone-nitro analogue **3.24** revealed a similar fingerprint region, and stretches consistent with those of a nitro group. Comparison with **3.21**, which would be expected to have similar electronic properties to **3.1** due to the electron-donating hydroxyl substituent, revealed similarly weak IR absorption bands, giving strength to the proposed push-pull resonance structure previously discussed (**Scheme 3.1**, Page 77).

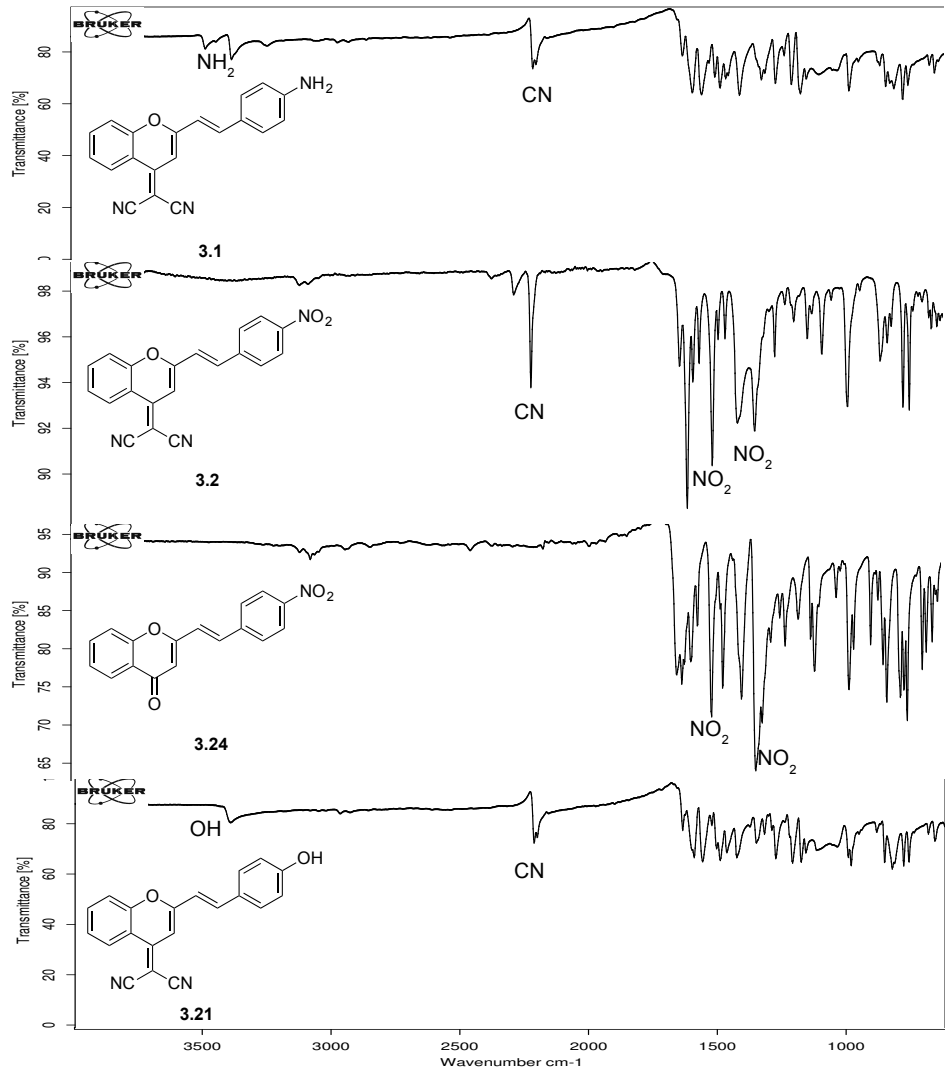

Figure 3.6. Infrared absorption spectra for amine **3.1**, nitro **3.2**, chromenone-nitro analogue **3.24** and hydroxyl analogue **3.21**.

High-resolution mass spectrometry (FI^+) indicated the molecular weight of the solid was 357.0710, which differed from 341.0800 required for compound **3.2**. However, it is possible that **3.2** did not ionise under the mass spectrometry conditions: a hypothesis supported by the weak intensity of the mass spectrum obtained. Interestingly, the recorded mass (357.0710) correlated with a nitro-peroxide structure **3.30** (**Figure 3.7**). However, it is not clear whether such structures are likely to form in field ionisation techniques.

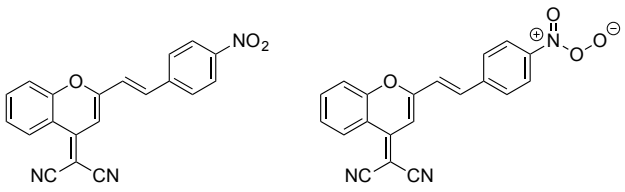

3.2 Exact Mass: 341.0800 **3.30** Exact Mass: 357.0750

Figure 3.7. Structures of **3.2** and the peroxide derivative **3.30** labelled with their corresponding masses (1 mole) in grams to 4 d.p. Error: 14 ppm for peroxide structure.

Full experimental data for this precipitate can be found in **Chapter 7.2** (Page 201) and spectra in **Appendix B**. The spectroscopic data presented are consistent with the proposed structure, **3.2**. However, without conclusive characterisation by mass spectrometry, and issues surrounding compound solubility, it was deemed inappropriate to progress the compound for biological evaluation.

3.8 Synthesis of an NIR fluorogenic bioreductive group

Attempted syntheses of **3.2** suggested that poor solubility in organic solvents was hindering isolation of the desired product. The fraction of sp^3-hybridised carbons to the total number of carbons in a molecule (Fsp^3) has been correlated with successful translation of molecules from the laboratory to preclinical and clinical testing.[221] The Fsp^3 of **3.2** is 0, offering some indication as to the reasons for its poor solubility. It was hypothesised that disruption of planar interactions between molecules of **3.2** could improve solubility and purification.[222] Subsequently, a retrosynthesis of a fluorogenic bioreductive group derivative **3.31** (Fsp^3 0.05), suitable as an alkylating agent, was proposed, by incorporating an sp^3 hybridised bromo-methylene group (**Scheme 3.16**).

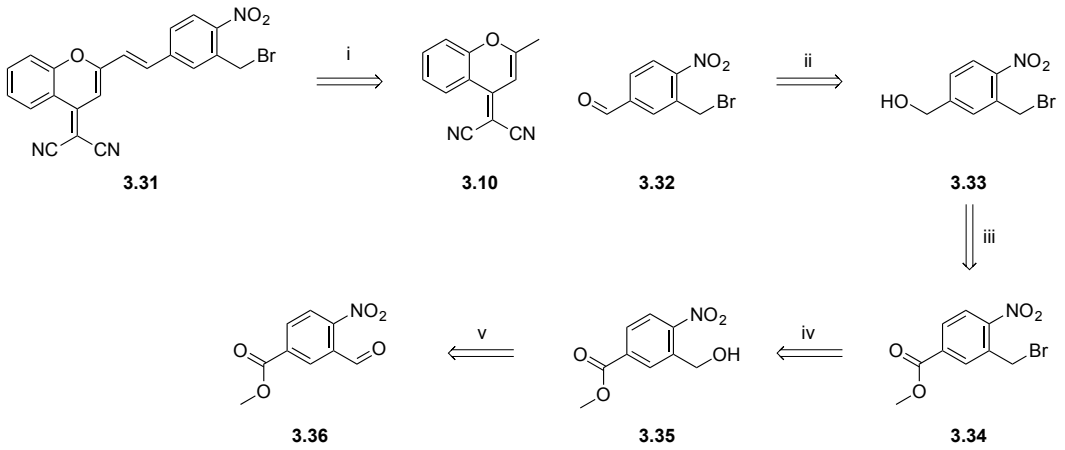

3.31 3.10 3.32 3.33 3.34 3.35 3.36

Scheme 3.16. Proposed retrosynthesis of methylene functionalised compound **3.31** for use as a alkylating bioreductive group; (i) Condensation, (ii) Oxidation, (iii) Reduction, (iv) Appel reaction, (v) Reduction.

Commercially available **3.36** was hypothesised to undergo aldehyde reduction to alcohol **3.35** (**Scheme 3.16**, Step v), which could be converted to the corresponding bromide **3.34** (**Scheme 3.16**, Step iv). Reduction of the ester of **3.34** would afford alcohol **3.33** (**Scheme 3.16**, Step iii), which could be readily oxidised to the desired aldehyde **3.32** (**Scheme 3.16**, Step ii). Condensation reactions between **3.10** and **3.14** had previously afforded the desired nitro product **3.2**, as determined by mass spectrometry, but purification was unsuccessful (**Figure 3.2**, Page 83). It was proposed that a condensation reaction between **3.10** and **3.32** would possibly enable purification of product **3.31** by introduction of an sp^3-hybridised methylene bromide (**Scheme 3.16**, Step i).

Compound **3.36** was treated with $NaBH_4$ to yield methylene alcohol **3.35** in 69% yield (**Scheme 3.17**, Step i). A subsequent Appel reaction afforded the bromo intermediate **3.34** in excellent 81% yield (**Scheme 3.17**, Step ii). Reduction of the methyl ester **3.34** with $NaBH_4$ proved to be

unsuccessful, with loss of bromine observed by ^{1}H NMR and mass spectrometry analysis of the crude reaction mixture.

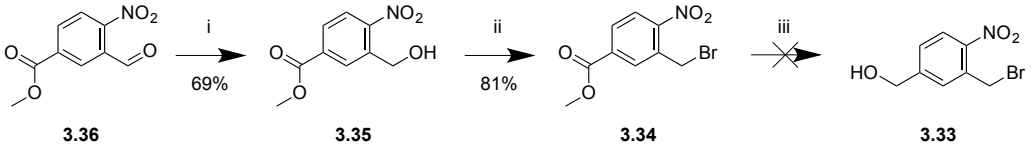

Scheme 3.17. Towards the synthesis of **3.33**; *Reagents and conditions:* (i) $NaBH_4$ (0.25 eq.), MeOH/THF, RT, 15 h, 69%; (ii) PPh_3 (1.1 eq.), CBr_4 (1.1 eq.), RT, 5 h, 81%; (iii) $NaBH_4$ (4 eq.), MeOH/THF, RT, 4 h.

An alternative functional group to bromine was proposed to circumvent the problems encountered with $NaBH_4$ reduction, and subsequently, protection of methylene alcohol **3.35** as a silyl ether was investigated (**Scheme 3.18**). The *tert*-Butyldimethylsilyl (TBDMS) protecting group was selected due to its steric bulk, which was hypothesised to further reduce the planarity of the desired product. Protection of **3.35** with a TBDMS group afforded **3.37** in 81% yield, which following reduction to **3.38** (60% yield), and then oxidation, furnished the desired *para* substituted aldehyde **3.39** (67% yield).

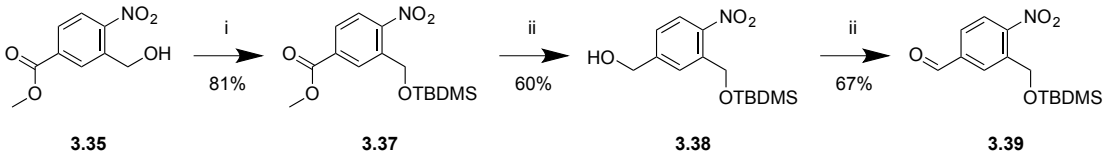

Scheme 3.18. Synthesis of aldehyde **3.39**; *Reagents and conditions:* (i) TBDMSCl (2 eq.), imidazole (2 eq.) DMF, RT, 1 h, 81%; (ii) $NaBH_4$ (2 eq.), MeOH/THF, RT, 15 h, 60% over 2 steps (i-ii); MnO_2 (10 eq.), CH_2Cl_2, acetone, RT, 3 d, 67%.

With protected aldehyde **3.39** successfully isolated, a condensation reaction to afford **3.40** was investigated (**Scheme 3.19**). Analysis of the crude reaction mixture by ^{1}H NMR spectroscopy and TLC revealed the presence of aldehyde **3.39** and the absence of the desired reaction product **3.40**. It is

plausible that progression of the condensation reaction relies on the product being insoluble in the reaction mixture, therefore driving the equilibrium by removing it from the reaction.

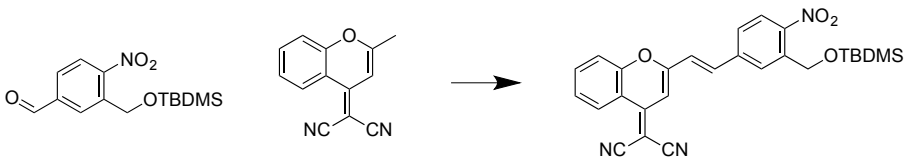

3.39 **3.10** **3.40**

Scheme 3.19. Attempted synthesis of TBDMS protected product **3.40**; *Reagents and conditions:* Piperidine (0.5 eq.), AcOH (0.8 eq.), Toluene, 110 °C, 3 h.

3.9 Discussion of synthetic strategies

In an attempt to synthesise **3.2** a number of synthetic strategies were employed. Despite careful consideration and rigorous analysis, isolation of **3.2** in sufficient quantities for biological evaluation and complete characterisation, remained elusive. The following issues were identified as being associated with these uncertainties:

a) Precipitates isolated potentially containing **3.2** were highly insoluble in organic solvents, making NMR analysis and further purification difficult.
b) **3.2** appeared to not ionise well in either electrospray ionisation or field ionisation techniques. This characteristic made absolute confirmation of the compound's structural formula difficult.

The product isolated through diazonium chemistry (**Chapter 3.7**, Page 89), was identified as having spectroscopic properties in good agreement with those anticipated for **3.2**. However, mass spectrometry analysis did not confirm the desired product mass. It was significant that this precipitate was isolated by filtration of an aqueous work-up, indicating that in

reactions, which may have contained the product, **3.2** may have been lost following aqueous work-up. Alternative synthetic strategies did afford detection of the product by mass spectrometry, but subsequent purification by silica gel chromatography was unsuccessful. These experiments suggest the product was unstable to purification by conventional methods.

Chapter 4

BIOLOGICAL EVALUATION OF A FLUOROGENIC AZIDE-CONTAINING HYPOXIA-ACTIVATED DYE

4.1 Introduction

4.1.1 Azide-containing compounds as biological probes

Azides, an energy rich functional group, have long enjoyed exploration within the context of organic chemistry; as intermediates in the synthesis of pharmaceutical heterocycles, as promoters of rearrangements, and in CH activation.[223] Organic azides transcend the interface between chemistry and biology, and have been employed as useful molecules in light-activated probes, and in labelling proteins *in vitro*.[161,223,224] A particularly attractive feature of organic azides is their high kinetic stability within the cellular environment, and resistance to aerobic oxidation.[225] Furthermore, azides are known to be inert to reaction with biologically abundant nucleophiles, in particular water and amines, and demonstrate limited reactivity with intracellular thiols.[225-228] The biological stability of azides has resulted in them being extensively used in the visualisation of biological processes and cell infrastructure. Exploitation of Huisgen [3+2] cycloadditions between azides and alkynes, an example of click chemistry, is perhaps the most widely utilised azide reaction in chemical biology (**Scheme 4.1**).[229] Copper-free or

strain-promoted click chemistry has enabled selective labelling of intracellular proteins without the cytotoxicity issues associated with copper *in vitro*.[230,231] Furthermore, such chemical tools have been developed to be fluorogenic, enhancing intracellular fluorescence resolution following triazole formation, both *in vitro* and *in vivo*.[231]

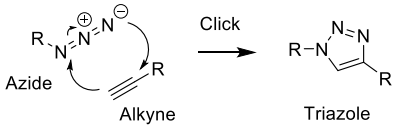

Scheme 4.1. An example of click chemistry involving a 1,3-dipolar cycloaddition between an alkyne and azide, to afford the corresponding triazole.

Click chemistry has also been exploited to develop DNA sequences linked by triazole moieties, which demonstrate enhanced kinetic stability compared to phosphate linkers, and undergo transcription with endogenous DNA polymerase enzymes.[232,233] Such work represents steps towards the total synthesis and assembly of genomes. Further applications of click-chemistry include *in vivo* targeting of therapeutic nanoparticles to tumours by forming liposomes.[234]

The recent explosion of azide-containing compounds as sensors of hydrogen sulfide, an emerging important signalling molecule in biological systems, demonstrates the scope for development of fluorogenic molecules based on reduction of azides to the corresponding amine.[235,236] Following the initial report of these fluorogenic azide compounds by Lippert, Chang and co-workers, focus has remained on their utility as sensors of hydrogen sulfide.[235,237] Consequently, the utility of fluorogenic azides within the context of alternative cellular reduction mechanisms has received little attention.

4.1.2 Evidence for azides as bioreducible functionalities

Despite extensive investigation within the context of click-chemistry, the behaviour of azides under variable physiological conditions, and particularly their metabolism, is relatively poorly understood. The limited reports that do exist suggest that electron-deficient aryl azides **4.1** and **4.2**, undergo reduction to afford the corresponding amines **4.3** and **4.4**, when incubated with mouse liver microsomes in the absence of air (**Scheme 4.2A**).[238] Further evidence for oxygen-dependent metabolism of azides includes studies into the pharmacokinetics of the anti-viral drug, AZT **4.5**, which undergoes anaerobic metabolism to a toxic side product AMT **4.6** in the presence of human liver microsomes (**Scheme 4.2B**).[239] Microsomes are frequently employed in laboratory-based metabolism studies of xenobiotics.[240,241] This fraction of liver homogenate contains water-soluble enzymes, isolated by centrifugation, and is particularly high in levels of cytochrome P450 (CYP) enzymes, which are broadly responsible for clearance of drugs in the human body.[242-244] Pan-Zhou and co-workers linked the importance of CYP activity to the *in vivo* metabolism of **4.5** to **4.6**.[239]

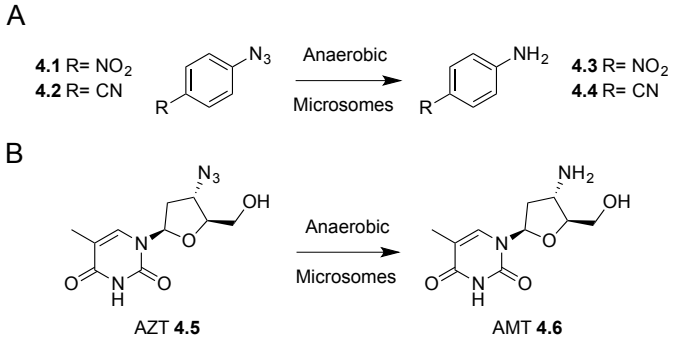

Scheme 4.2. Examples of oxygen-dependent reduction of azide-containing compounds. (A) Electron deficient aromatic azides **4.1** and **4.2** undergo reduction to the corresponding amines **4.3** and **4.4** in the presence of mouse microsomes under anerobic conditions.[238] (B) The anti-viral drug AZT **4.5** undergoes metabolism to the amine AMT **4.6** in the presence of human liver microsomes under anaerobic conditions.[239]

Reports of azide reduction under anaerobic conditions suggests that azide groups could be exploited in the development of HAPs.[238,245] Few examples exist of using this functional group to target hypoxia, or indeed in drug development, which given their widely accepted bio-stability could be considered surprising. Damen and co-workers synthesised derivatives of the commonly used anti-cancer drug paclitaxel for targeting hypoxia, and employed a 4-azidobenzyl bioreductive group, amongst others.[100] However, evaluation of their compounds included preliminary data in which only toxicity against cancer cell lines was examined, and treatments under hypoxic conditions were not investigated. Kotra and co-workers developed an azide-nucleoside prodrug for anti-viral therapy, which was shown to undergo bioreduction *in vivo* to the corresponding amine.[246] However, similarly, no application to hypoxia or cancer therapy was made.

With the above studies in mind, exploitation of azide-containing compounds as sensors of low oxygen conditions, and to target tumour hypoxia was investigated. Given the favourable NIR fluorescent properties of amine **3.1** (λ_{max}: 670 nm) (**Chapter 3.1**, Page 76), the utility of azide **3.29** (**Chapter 3.7**, Page 89) as a fluorogenic probe for detection of hypoxia was considered (**Scheme 4.3**). The push-pull electronic donation from the amine, through the conjugated system to the nitrile groups, affords **3.1** favourable fluorescence properties (**Scheme 1.9**, Page 35). In contrast, the azide **3.29** reduces donation of electronic density into the aromatic system, and is consequently non-fluorescent.[212]

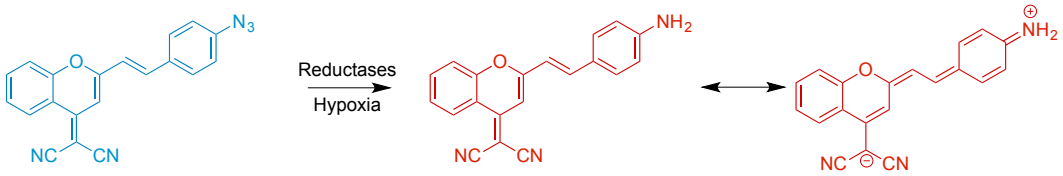

3.29 3.1

Scheme 4.3. It was hypothesised that **3.29** could be a substrate for enzymatic reduction under hypoxic conditions, affording the fluorescent compound **3.1** (resonance structure to show push-pull electronic system, right) and therefore acting as a marker of hypoxia.

Hypoxia-dependent, enzyme-mediated reduction of **3.29** could be a useful model for investigating azide groups as bioreductive moieties. Reduction of **3.29** *in vitro* and *in vivo* was likely to result in fluorescent amine **3.1**, the presence of which could be evaluated by fluorescence microscopy, HPLC analysis, cell-sorting techniques and various other laboratory based assays. Consequently, **3.29** was synthesised, with the aim of demonstrating the suitability in a variety of 2D and 3D tumour models to report on variable oxygen tensions, and also to elucidate the mechanism of oxygen-dependent reduction of azides.

4.2 Synthesis of an azide-containing fluorogenic NIR dye

Employing the synthetic route previously described (**Chapter 3.3**, Page 81) **3.29** was synthesised with modifications to the reported procedure (**Scheme 4.4**).[212]

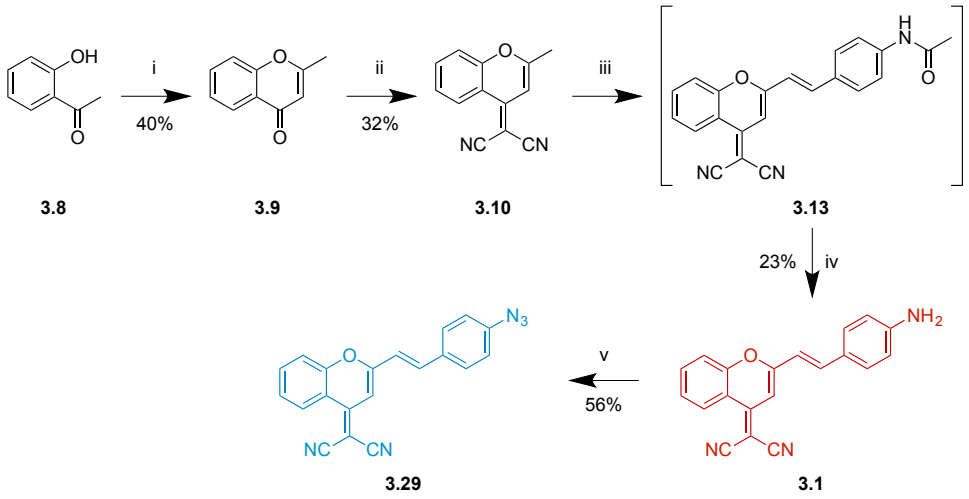

Scheme 4.4. Synthesis of **3.29**; *Reagents and conditions:* (i) Na (2.8 eq.), EtOAc, RT, 4 h; $AcOH/H_2SO_4$, 100 °C, 1 h, 40%; (ii) $CH_2(CN)_2$ (10 eq.), Ac_2O, 120 °C, 3 h, 69%; (iii) 4-Acetamidobenzaldehyde **3.12** (1.1 eq.), toluene, AcOH/piperidine, 110 °C, 3 h; (iv) HCl/EtOH aq., 100 °C, 3 h, 23% over 2 steps; (v) $NaNO_2$, aq. HCl, NaN_3, 0 °C-5 °C, 1 h, 56%. Red indicates fluorescent and blue non-fluorescent.

Treatment of commercially available 2-Hydroxyacetophenone **3.8** with sodium metal in ethyl acetate, followed by heating under reflux under acidic conditions afforded chromenone **3.9** in moderate yield (40%). Chromenone **3.9**, heated under reflux with malononitrile, furnished the chromenone derivative **3.10** *via* a Knoevenagel condensation.[247] A condensation reaction with 4-Acetamidobenzaldehyde **3.12**, afforded intermediate **3.13**, which was taken forward without further purification. Treatment of **3.13** under reflux in acidic conditions resulted in hydrolysis of the acetylamino group, to afford the desired fluorescent amine **3.1** (23% yield). The fluorogenic azide compound **3.29** was then synthesised *via* formation of the diazonium salt of **3.1**, and

subsequent treatment with sodium azide (56% yield). Further synthetic details can be found in **Chapter 3.2** (Page 79).

With the target compounds in hand, the biological utility of azide **3.29** as a fluorogenic marker of hypoxia was investigated. The protocol developed by our laboratory for the evaluation of hypoxia-activated probes was followed, employing assays of progressively increasing biological relevance (**Chapter 2.5**, Page 60).[48]

4.3 Fluorometric analysis and zinc reduction assay

The utility of any fluorogenic probe relies on a distinct difference between the baseline fluorescence of the probe, and its 'active' fluorescent form.[162] For **3.29** to be a useful marker of hypoxia, **3.29** must show little fluorescence compared to its metabolite **3.1**. Therefore, the fluorescence spectra of azide **3.29** and amine **3.1** were first compared as solutions in ^{i}PrOH (**Figure 4.1**).

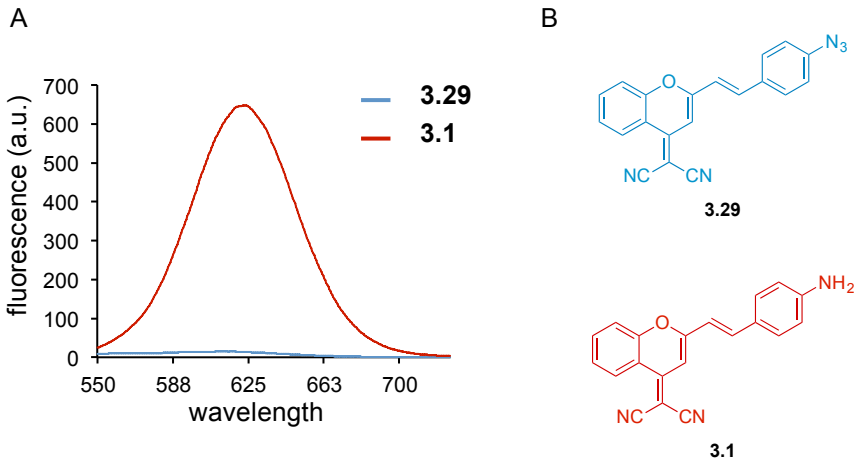

Figure 4.1. (A) The fluorescence emission spectra of **3.29** and **3.1** in ^{i}PrOH (50 µM, λ_{ex} 515 nm). (B) Chemical structures of **3.29** and **3.1**. The colours indicated correspond to those used in graph A.

Amine **3.1** was approximately 650-fold more fluorescent (λ_{max} 620 nm) than the corresponding azide **3.29**, indicating that azide **3.29** was fluorogenic with respect to reduced amine **3.1** (**Figure 4.1A**). Furthermore, the spectra obtained for **3.29** and **3.1** were in good agreement with the previously reported spectroscopic data.[212] It was subsequently decided to investigate whether fluorescence could be correlated with the degree of reduction of azide **3.29** to the corresponding amine **3.1**. An ^{i}PrOH solution of azide **3.29** was treated with zinc and ammonium chloride, and the fluorescence of the reaction solution recorded at selected intervals (**Figure 4.2A**).

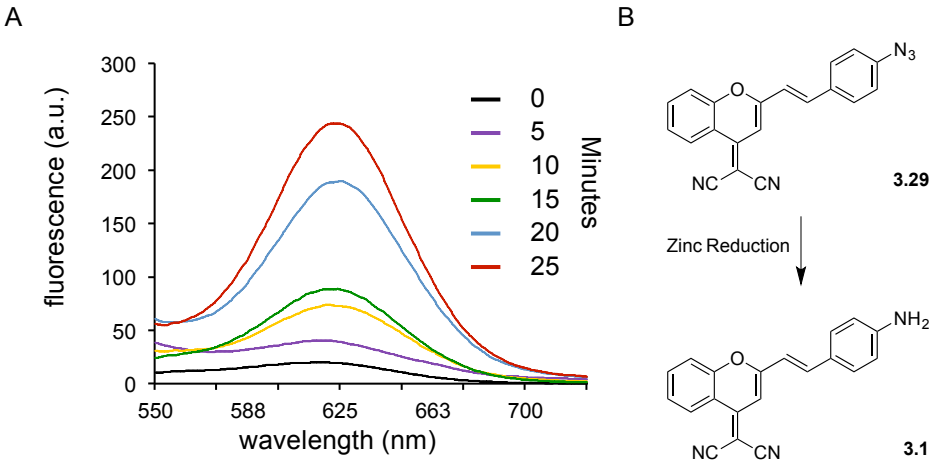

Figure 4.2. (A) Graph to show the fluorescence emission spectra (λ_{ex}: 515 nm) of **3.29** undergoing zinc reduction with time. A solution of **3.29** (50 µM) in ^{i}PrOH (900 µL) was treated with aq. NH_4Cl (100 µL, 10% *w/v*) and zinc dust (1 mg). The fluorescence spectrum was recorded at regular intervals. (B) Schematic to show the zinc mediated reduction of **3.29** to **3.1**.

Employing the same excitation wavelength (λ_{ex} 515 nm) a time-dependent increase in fluorescence was observed, the fluorescence spectra of which was directly comparable with that of purified amine **3.1** (λ_{max}: 620 nm) (**Figure 4.1A**). The similarity of the fluorescence profiles indicated that **3.1** was the reduction product, which was subsequently confirmed by HPLC analysis at the end of the time course.

In conclusion, amine **3.1** was found to be over 600-fold more fluorescent than the corresponding azide **3.29**, and therefore, **3.29** was confirmed to be fluorogenic. Despite the recorded λ_{max} (620 nm) of **3.1** being just outside of the NIR region (λ_{em}: 650-1300 nm), it was decided that the spectrophotometric profile was sufficient for further fluorescence analysis.[133] Consequently, the mechanism of azide reduction, and its sensitivity to the presence of oxygen was investigated.

4.4 Mechanism of reduction

Radiolysis has been widely used to evaluate the reduction mechanism of bioreductive prodrugs,[41] and affords information about sensitivity of HAPs one-electron reductases by mimicking single-electron transfers.[92,248] Radiolysis has previously been shown to reduce sulfonyl azides to the corresponding sulfonamides.[249] Tanabe and co-workers also demonstrated the reduction of an azide-uridine derivative following irradiation under hypoxic conditions.[250] However, to the best of our knowledge, this technique has not yet been used to evaluate the reduction mechanism of azide compounds, and more importantly, within the context of bioreductives. To determine whether azide **3.29** was reduced by sequential, single electron transfers, an ^{i}PrOH solution of **3.29** was irradiated with γ-rays under anaerobic conditions, and aliquots of the assay solution analysed by HPLC at selected time points (**Figure 4.3**).

Irradiation of the reaction solution causes formation of ^{i}PrO radicals *in situ*. These radicals can then act as electron carriers for reduction of the azide moiety of **3.29**. Under anaerobic conditions, the concentration of **3.29**

decreased in a linear fashion with time, corresponding to a linear increase in the concentration of **3.1** (**Figure 4.3B**). The inverse concentration relationship between **3.29** and **3.1** indicates that azide **3.29** is directly reduced to amine **3.1**, and that no stable intermediates are formed. Furthermore, the formation of **3.1** under anaerobic conditions indicates that reduction of the azide of **3.29** occurs *via* a mechanism of sequential single electron transfers.

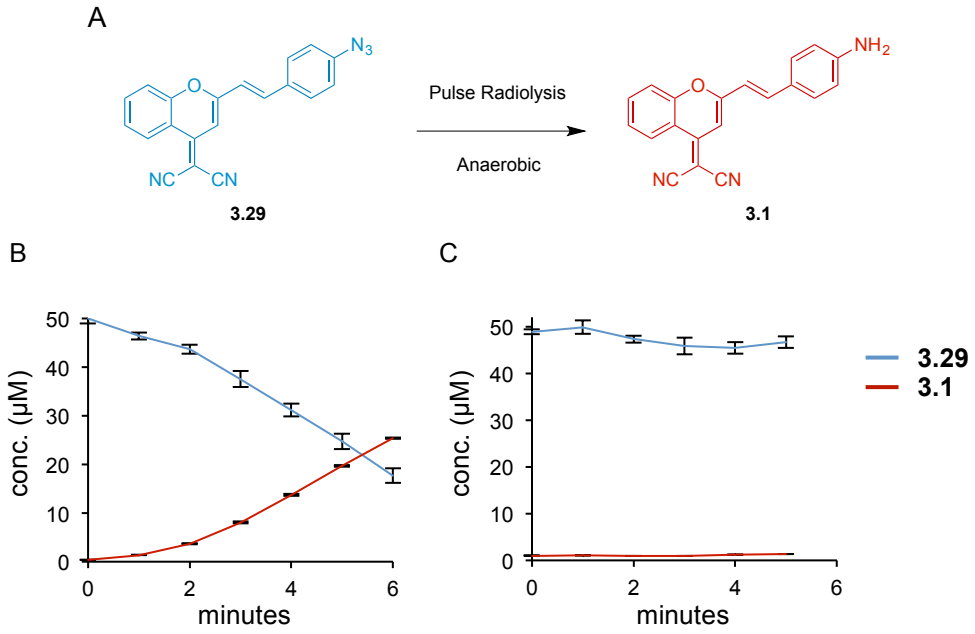

Figure 4.3. (A) Schematic to represent the reduction of **3.29** to **3.1** under steady state radiolysis. Colours correspond to those in graphs B and C. (B-C) Graphs to show the concentrations of **3.29** and **3.1** with time following irradiation (14 Gy/min) of 50 μM solutions in aq. KH_2PO_4 buffered ^{i}PrOH (pH 7.4) under an N_2O atmosphere with (B) no oxygen (C) 2% O_2. Aliquots from the assay volume were taken at regular intervals and analysed by HPLC. The key shown corresponds to graphs B and C.

It has been reported that sodium azide is capable of quenching singlet oxygen, and *vice versa*.[251] Such a relationship indicates that oxygen would be able to quench the azide radical **4.7**, corresponding to a single electron transfer (**Scheme 4.5**). To determine whether the reduction occurred *via* **4.7**, radiolysis was repeated in the presence of 2% oxygen (**Figure 4.3C**). Under these conditions, the formation of **3.1** was entirely abrogated and the

concentration of **3.29** remained constant, indicating oxygen was able to quench the initial azide radical species **4.7**, and therefore, no further reduction to **3.1** could occur. A mechanism for the oxygen-sensitive reduction of **3.29** to **3.1** is proposed below, and is hypothesised to progress *via* elimination of nitrogen gas (**Scheme 4.5**).[252]

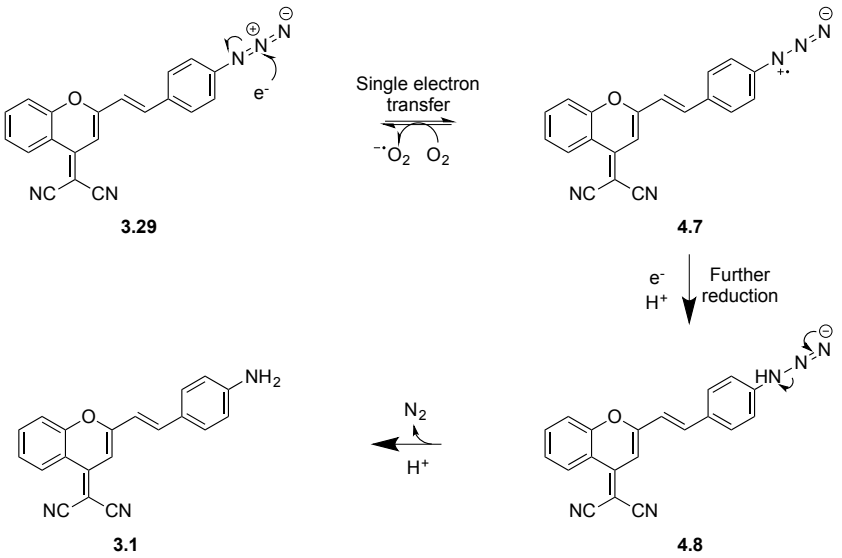

Scheme 4.5. Proposed reduction mechanism of the azide functionality of **3.29** involving sequential single electron transfers to yield fluorescent **3.1**, *via* elimination of nitrogen gas. The stoichiometry of the reduction is suggested to require 2 electrons per molecule of **3.29**.

In conclusion, the azide group of **3.29** was shown to undergo reduction by a mechanism of single electron transfers, which was inhibited in the presence of oxygen. The steady state radiolysis experiments chemically demonstrate the proposed reduction mechanism shown in **Scheme 4.5**. However, this result does not preclude two-electron reductase activity *in vivo*. Consequently, **3.29** was evaluated in enzyme-based reduction assays.

4.5 Enzymatic Analysis

Following the validation protocol for hypoxia-activated prodrugs, **3.29** was progressed to *in vitro* validation with a variety of human enzymes under both normoxic and hypoxic conditions.

4.5.1 Cytochrome P450 (CYP) NADPH reductase enzymes

Radiolysis experiments suggested that azide **3.29** might be a substrate for reduction by one-electron reductases. Despite the azide functionality being structurally distinct to a nitro group, the propensity of NADPH reductase enzymes to reduce **3.29** was investigated (**Figure 4.4**).

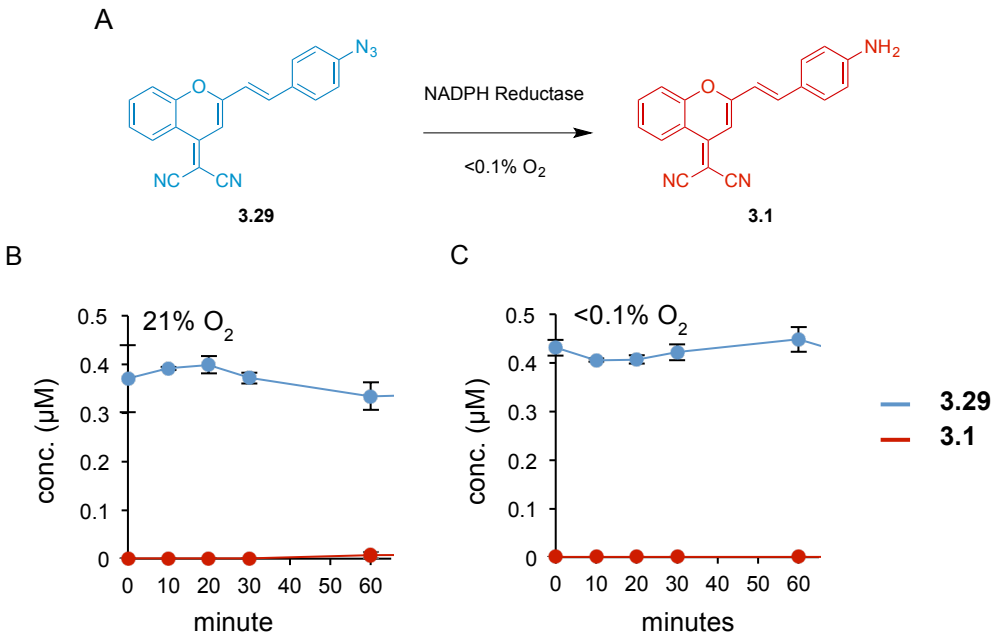

Figure 4.4. (A) Scheme to show the investigated reduction of **3.29** to its amino metabolite **3.1** following treatment with NADPH reductase enzymes under hypoxic conditions. (B-C) Graphs to show the concentration of **3.29** and **3.1** during treatment with NADPH reductase enzymes under (B) normoxic (21% O_2) and (C) hypoxic (<0.1% O_2) conditions. Aliquots from the assay volume were taken at regular intervals and analysed by HPLC.

Under both normoxic and hypoxic conditions, no reduction of azide **3.29** to amine **3.1** was observed. Throughout the time course of the assay, the concentration of azide **3.29** remained constant, indicating no other metabolic

processes were occurring. The lack of NADPH reductase activity suggests enzymatic reduction of the azide group could proceed *via* a distinct mechanism, compared to that proposed for nitro groups. Consequently, alternative human enzymes were considered.

4.5.2 Human Liver Microsomes

Previous studies suggested that mouse liver microsomes could promote the reduction of the electron-deficient azide **4.1** to the corresponding amine **4.3** under conditions of depleted oxygen (**Scheme 4.6A**).[238] However, where more electron rich substrates were investigated, such as methoxy **4.9** reduction was not observed (**Scheme 4.6B**).

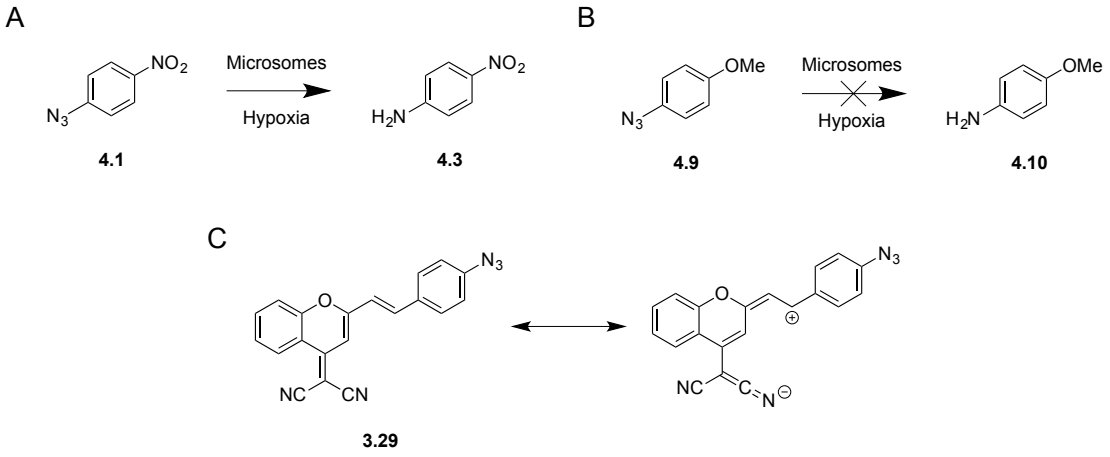

Scheme 4.6. (A) Treatment of electron-deficient aryl azide compound **4.1** with mouse liver microsomes under conditions of depleted oxygen afforded the amine **4.3**. (B) As in A, where more electron rich substrates, such as **4.9**, were used no reduction occurred. (C) Resonance structure of **3.29** showing the chromenone moiety can act as an electron withdrawing substituent *para* to the azide group.

Similarly to **4.1**, azide **3.29** comprises an electron-withdrawing substituent *para* to the azide functionality (**Scheme 4.6C**). Therefore, it was hypothesised that azide **3.29** may also be a suitable substrate for microsome-mediated reduction (**Figure 4.5**). Under normoxic conditions, no detectable formation of **3.1** with time was observed (**Figure 4.5A**). In contrast,

under hypoxic conditions, the concentration of **3.1** increased in a linear fashion with time (**Figure 4.5B**). The absence of oxygen was therefore determined to be imperative for the microsomal reduction of azide **3.29** to the corresponding amine **3.1**.

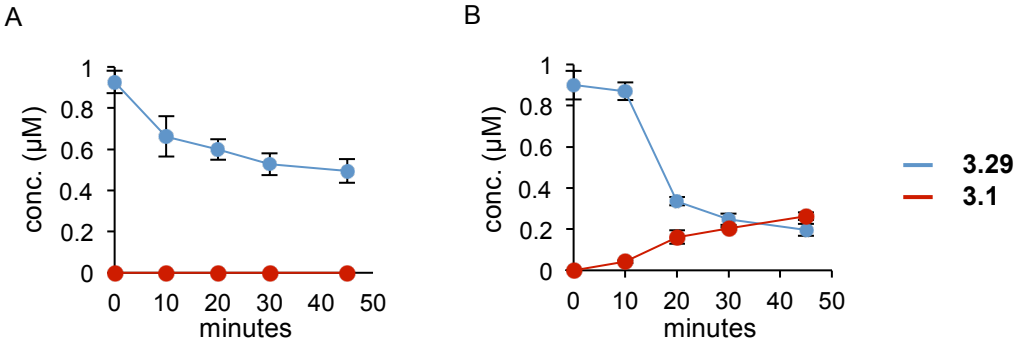

Figure 4.5. Graphs to show the concentrations of **3.29** and **3.1** with time following treatment with human liver microsomes. The assay volume was treated under (A) normoxic (21% O_2) and (B) hypoxic (<0.1% O_2) conditions. Aliquots were taken at regular intervals and the concentrations of **3.29** and **3.1** determined by HPLC analysis.

Both mouse and human liver microsomes have been widely used as prognostic for the stability of drug candidates *in vivo*.[253,254] The time dependent decrease in **3.29** concentration under normoxic conditions, and greater concentration decrease in **3.29** than formation of **3.1** under hypoxic conditions, suggested other metabolic processes could be occurring (**Figure 4.5**). Subsequently, it was determined that **3.29** had approximately 3-fold greater stability under normoxic conditions ($T_{1/2}$: 53 minutes) than hypoxic conditions ($T_{1/2}$: 18 minutes) (**Figure 4.6**). The reduced rate of degradation of **3.29** under normoxic conditions was encouraging for the stability of **3.29** *in vivo*.[255] Liver microsome-mediated reduction of **3.29** revealed a strong oxygen dependency, and good stability under normoxic conditions, warranting further investigation of the enzymes potentially responsible.

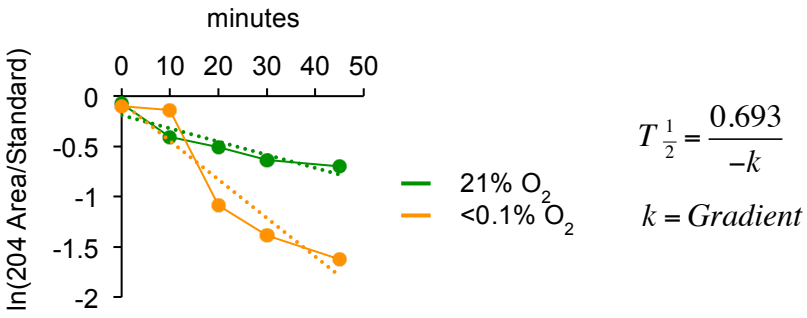

Figure 4.6. A graph to show microsomal degredation of **3.29** under normoxic (21% O_2), and hypoxic (<0.1% O_2) conditions over 45 min. The half-life of **3.29** was calculated from the gradient of the line of best fit (dashed line) and calculated as indicated.[203]

4.5.3 Cytochrome P450 (CYP) enzymes

Human liver microsomes comprise a large number of enzymes, and consequently, it was not clear which enzymes, or combination of enzymes, were responsible bioreduction of azide **3.29** to amine **3.1**. The liver microsomes used were reported to contain a variety CYP enzymes, uridine glucuronide transferases, and flavin monooxygenases.[242] Given reported the reported activity of CYP enzymes reducing the anti-viral drug AZT, it was hypothesised that the CYP component of the microsomal fraction could be responsible for the reduction of azide **3.29**, under anaerobic conditions.[239] Five purified CYP enzymes, commonly used in metabolism studies, were subsequently employed,[256,257] and **3.29** was treated with each enzyme individually under variable oxygen conditions, and the assay solution analysed for the concentration of amine **3.1** (**Figure 4.7**).

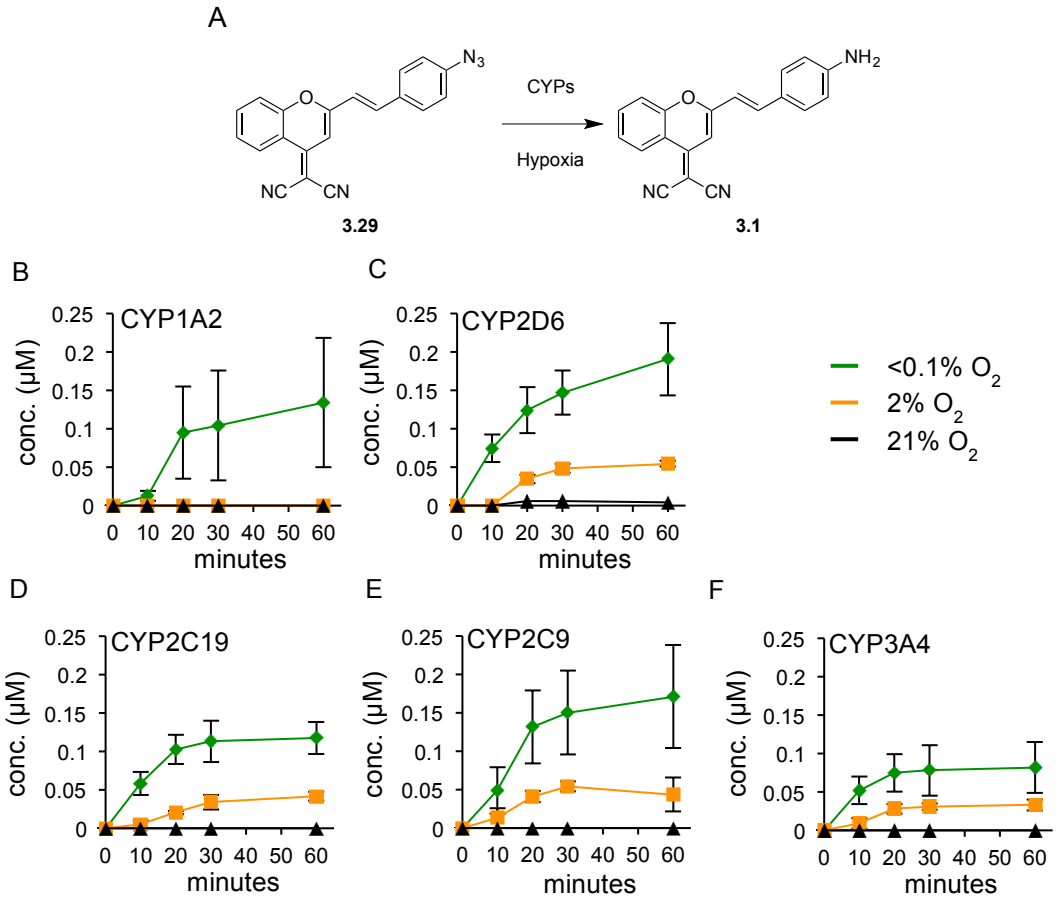

Figure 4.7. (A) Schematic to show evaluation of the CYP mediated reduction of **3.29** to **3.1** under variable oxygen conditions. (B-F) Graphs to show the concentration of **3.1** with time during treatment with the indicated CYP enzyme. The activity of each enzyme was evaluated under hypoxic (<0.1% O_2), moderately hypoxic (2% O_2), and normoxic (21% O_2) conditions. Aliquots from the assay volume were taken at regular intervals and analysed by HPLC.

Under hypoxic conditions, **3.29** underwent efficient reduction to fluorescent amino species **3.1**, with each of the individual enzymes investigated (**Figure 4.7**, **B-F**). The efficiency of this enzyme-mediated reduction decreased under moderately hypoxic (2% O_2) conditions, and was entirely abrogated under normoxic conditions. Evaluation of the reduction of **3.29** with CYP1A2 revealed strong oxygen sensitivity, with the formation of **3.1** being completely inhibited in the presence of 2% oxygen (**Figure 4.7B**). Under hypoxic conditions, enzymes CYP2D6 and 2C9 demonstrated the greatest propensity for the reduction of **3.29** (**Figure 4.7**, **C**, **E**, respectively)

yielding the greatest concentrations of amine **3.1**. CYP2D6 has been reported as being responsible for the hepatic metabolism of approximately 25% of all xenobiotics.[258] Comparison of the concentrations of **3.29** and **3.1** with time under hypoxic conditions revealed an inverse relationship, indicating **3.29** was not undergoing any other prominent metabolic processes (**Figure 4.8**).

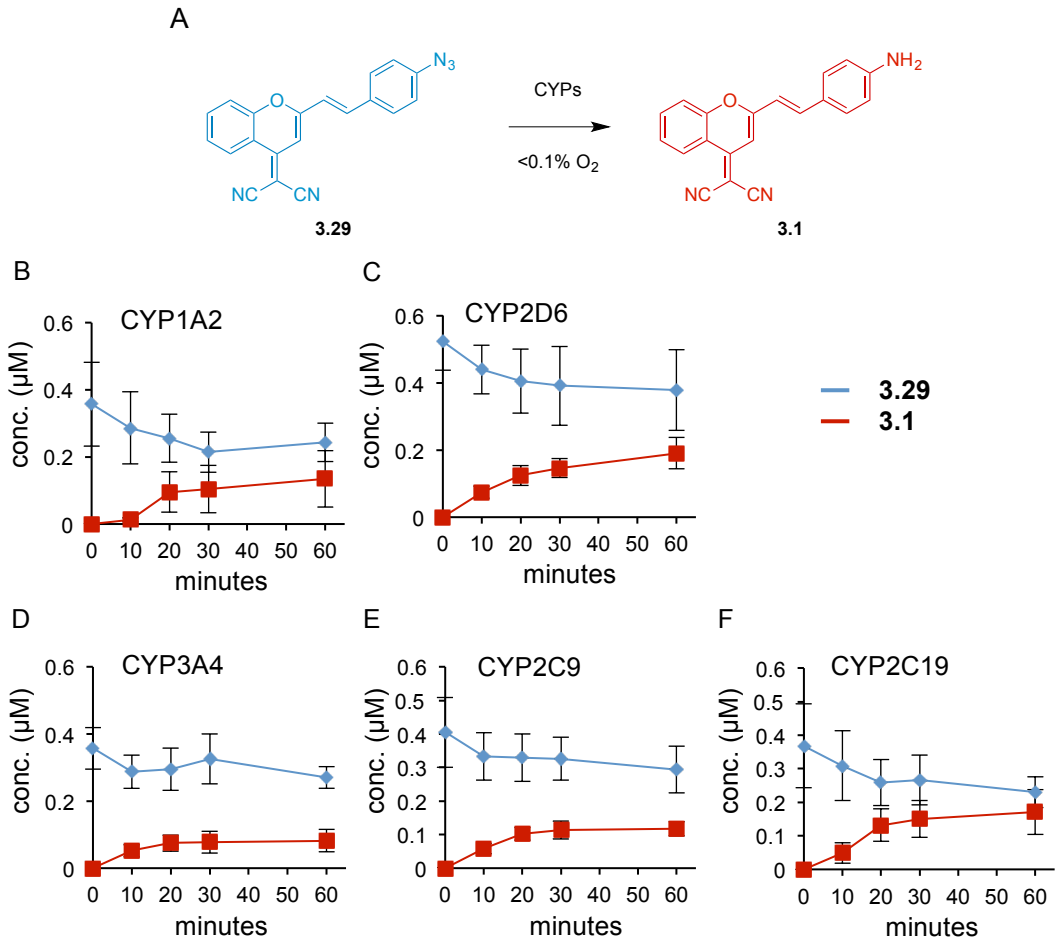

Figure 4.8. (A) Schematic to show the CYP-mediated reduction of **3.29** to **3.1** under hypoxic (<0.1% O_2) conditions. Colours correspond to graphs B-F. (B-F) Graphs to show the concentrations of **3.29** and **3.1** during treatment with the indicated enzymes under hypoxic (<0.1% O_2) conditions. Aliquots from the assay volume were taken at regular intervals and analysed by HPLC. The key shown corresponds to graphs B-F.

The activity of all 5 enzymes towards reduction of **3.29** under conditions of reduced oxygen indicated that the CYP enzyme family was broadly capable of azide reduction, regardless of isoform. To evaluate

whether this activity was specific to the structure of **3.29**, an alternative, commercially available and structurally distinct azide substrate, 7-azido-4-methylcoumarin **4.11**, was selected for investigation.[259] **4.11** was treated with the CYP enzymes that demonstrated the greatest propensity for reduction of **3.29** (**Figure 4.7**): CYPs 2D6 and 2C9 under normoxic (**Figure 4.9**, B, D) and hypoxic conditions (**Figure 4.9**, C, E).

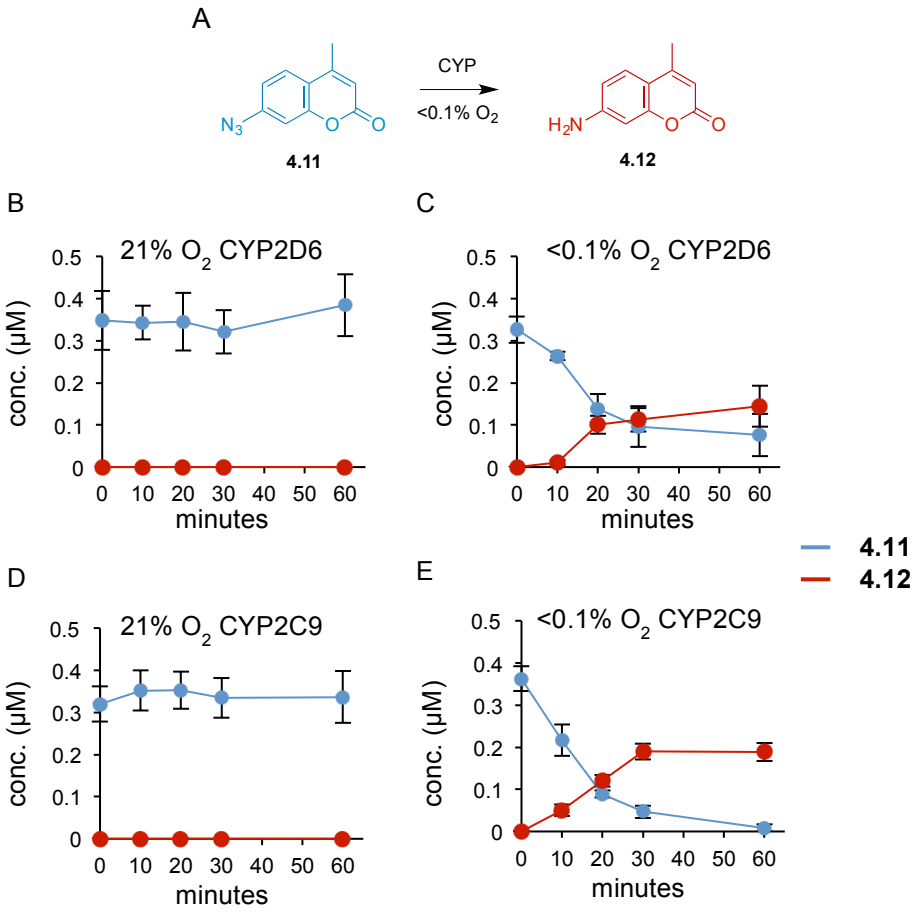

Figure 4.9. (A) Scheme to show the reduction of **4.11** to its amino metabolite **4.12** following treatment with CYPs under hypoxic conditions. Colours correspond to graphs B-E. (B-E) Graphs to show the concentrations of **4.11** and **4.12** during treatment with the indicated enzyme under normoxic (21% O_2) and hypoxic (<0.1% O_2) conditions. Aliquots from the assay volume were taken at regular intervals and analysed by HPLC. The key shown corresponds to graphs B-E.

Compound **4.11** was determined to undergo CYP-mediated reduction to the amino metabolite **4.12**, only under hypoxic conditions. The depreciation

in concentration of **4.11** had an inverse relationship with an increase in **4.12**, indicating that no other prominent metabolic processes were occurring (**Figure 4.9**, C, E). The oxygen sensitive CYP-mediated reduction of **4.11**, suggests that azide reduction under hypoxic conditions by CYPs could be widely applicable.

For CYP-mediated azide reduction to occur, co-ordination of nitrogen to the haem centre of the enzyme is required to facilitate electron transfers.[260,261] Evidence for this mechanism is demonstrated by the abrogation of microsomal azide reduction in the presence of oxygen, and furthermore, abrogation in the presence of carbon monoxide - even where oxygen is absent.[239,262] Carbon monoxide binds strongly to the iron centre of haemoproteins through a sigma bonding interaction, and π-backbonding from the metal centre, thereby blocking access of the azide.[263] Oxygen binds to haem in a similar way, and blocks binding interactions with the azide substrate (**Scheme 4.7**).

Under conditions of reduced oxygen, the CYP450-mediated bioreduction of azides is thought to proceed *via* a nitrene intermediate (**Scheme 4.7B**).[261] The mechanism of oxidation of a substrate RH, to the corresponding alcohol ROH by molecular oxygen is also shown for comparison, in which an Fe(III) intermediate precedes Fe(IV) in the catalytic cycle (**Scheme 4.7C**). In contrast, azide reduction is proposed to occur *via* a two-electron reduction *via* Fe(II) to Fe(IV) to eliminate N_2, and form the corresponding nitrene. Using engineered CYP450 enzymes, Arnold and co-workers elegantly exploited this mechanism to perform a variety of

chemical transformations on sulfonyl azides including; CH aminations,[264,265] aziridations,[266] and allylic amine synthesis.[267]

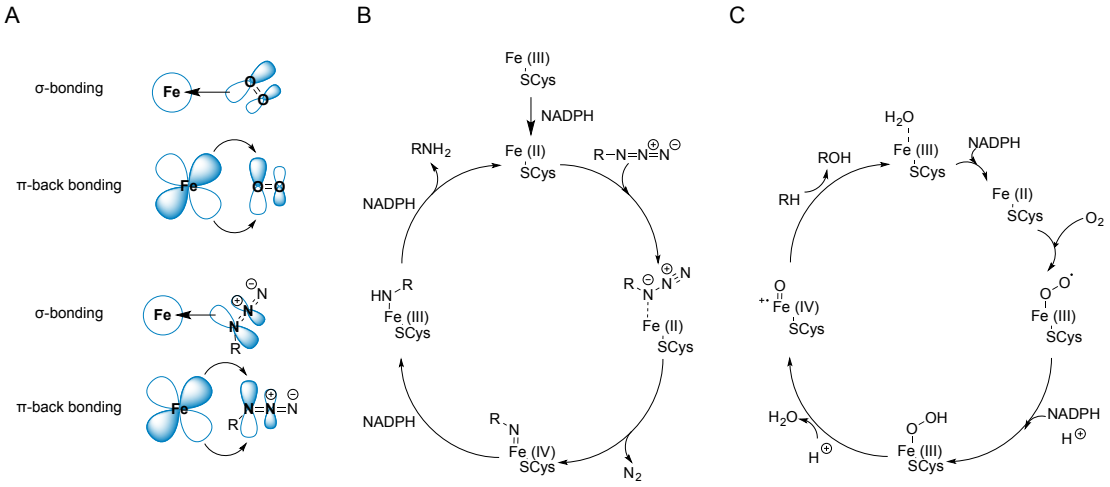

Scheme 4.7. (A) Orbital diagrams to show the bonding interactions between an iron centre, and ligands: oxygen (top) and azide (bottom). Oxygen and azides donate electron density to iron *via* σ-bonds, and this interaction is strengthened iron donating electron density to the ligands by π-backbonding. (B) Where oxygen is absent, the azide co-ordinates and the catalytic cycle progresses to eliminate nitrogen gas, *via* a presumed nitrene intermediate. Adapted with permission.[268] (C) Mechanism of oxidation of a substrate RH by molecular oxygen for comparison. Adapted with permission.[269] Copyright © 2004 American Chemical Society.

In summary, azide **3.29** was shown to be a substrate for a wide variety of common CYP enzymes in an oxygen dependent manner. Furthermore, no other metabolic processes could be detected by HPLC analysis. Under hypoxic conditions, the efficiency of reduction of **3.29** was enhanced, which was hypothesised to be a consequence of competitive binding between oxygen and azide **3.29**, and a mechanism is proposed. Reduction of azides *via* co-ordination to the haem centre of CYPs has common ground with the two-electron reduction of the clinical candidate HAP, AQ4N **1.14**, which is also sensitive to CYP reduction under hypoxic conditions (**Scheme 1.2**, Page 15).[17]

4.6 Cell treatment and cell lysis analysis

Following enzymatic analysis of **3.29**, the compound was progressed for evaluation in human cancer cell lines under variable oxygen conditions.[48] These experiments would allow determination of whether the oxygen-dependent enzymatic reduction of **3.29** was translatable to the complex cellular environment. CYP enzymes were identified as efficient mediators of reduction of **3.29** (**Chapter 4.5.3**, Page 113), and consequently the hepatic human cancer cell line HepG2 was selected for validation, owing to their elevated expression levels of CYP enzymes compared to other tissue types.[270] HepG2 cells were treated with **3.29** under normoxic or hypoxic conditions for defined periods of time. The cells were then harvested, lysed, and the lysate analysed by HPLC (**Figure 4.10A**).

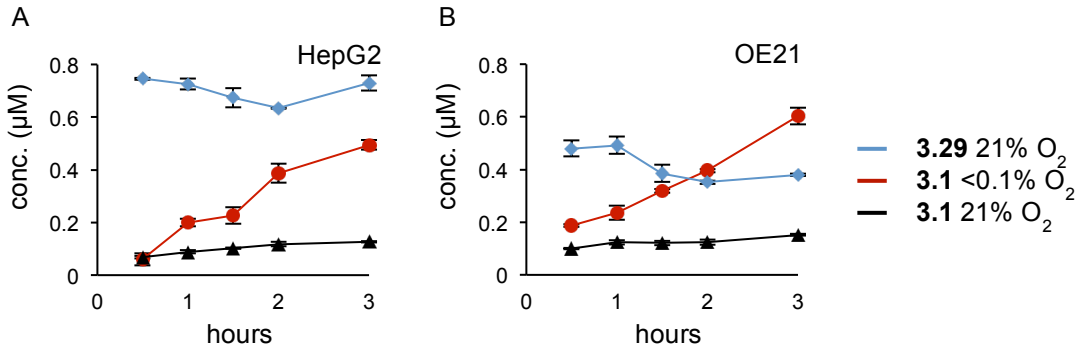

Figure 4.10. Graphs to show the cellular concentrations (0.25 million^{-1}) of **3.29** and **3.1** under normoxic (21% O_2) and hypoxic (<0.1% O_2) conditions following treatment with **3.29** (1 μM) for the indicated time. Cells were harvested, lysed and the lysate analysed by HPLC to determine the concentrations. (A) HepG2 cells (B) OE21 cells.

Determination of the concentrations of **3.29** and **3.1** revealed a strong linear induction in concentration of amine **3.1** with time, under hypoxic conditions. In contrast, under normoxic conditions, the formation of **3.1** was abrogated, and the concentration of **3.29** remained largely constant. The

stability of **3.29** in HepG2 cells under normoxic conditions indicated no other metabolic processes were occurring. The oesophageal cancer cell line OE21, was also investigated to determine whether the observed activity of **3.29** was specific to HepG2 cells (**Figure 4.10B**). Similarly to HepG2 cells, OE21 cells efficiently reduced **3.29** to **3.1** under hypoxic conditions. The activity of OE21 cells with respect to reduction of **3.29** was abrogated under normoxic conditions.

To determine whether treatment of cells with **3.29** resulted in cytotoxicity, a colony survival assay was performed in OE21 cells. Colonies were left to grow for 10 days, following treatment with **3.29** from 0-24 hours, under normoxic and hypoxic conditions, (**Figure 4.11**). No significant associated toxicity to cells, relative to the DMSO control, was observed and therefore **3.29** was suitable for progression in other cell-based assays.

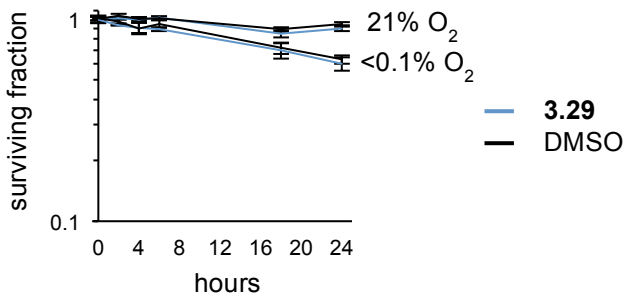

Figure 4.11. Graph to show the surviving fraction of cells in a colony survival assay, following treatment with **3.29** (1 μM) for the indicated period of time. Colonies were left to grow for 10 days, stained and then counted.

4.7 Fluorescence Evaluation

4.7.1 Fluorescence cell sorting to evaluate *in vitro* reduction

Fluorescence automated cell sorting (FACS) is a useful technique for quantifying fluorescence from individual cells within a population, and can therefore be used to count cells.[18] In line with previous investigations, the same cells lines; HepG2 and OE21 cells, were treated with **3.29** under normoxic and hypoxic conditions. The fluorescence of the cells was subsequently analysed using FACS (**Figure 4.12**).

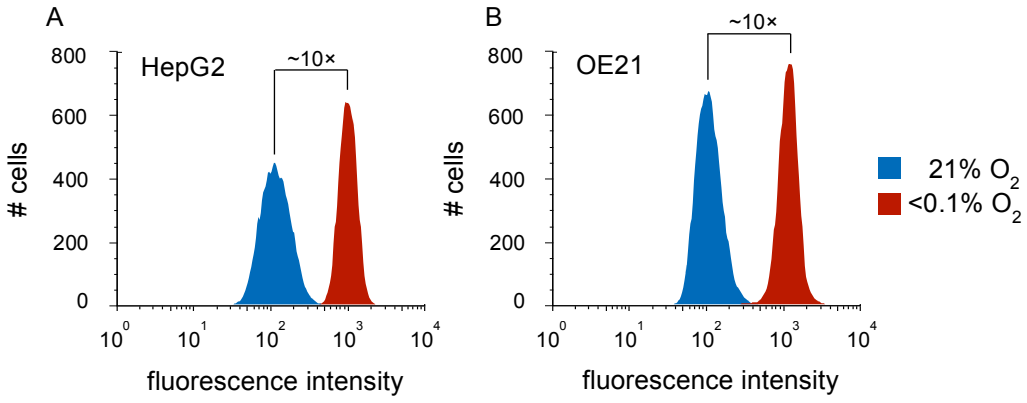

Figure 4.12. FACS histograms showing the fluorescence of cells (logarithmic) versus the number of cells, following treatment with **3.29** (1 μM) under normoxic (21% O_2) and hypoxic (<0.1% O_2) conditions for 4 h. Fluorescence was detected in the red region of the electromagnetic spectrum (A) HepG2. (B) OE21.

By considering the apex of each histogram plot, the fluorescence of HepG2 cells treated with **3.29** under hypoxic conditions can be calculated as ~10-fold greater, compared to cells treated with **3.29** under normoxic conditions (**Figure 4.12**A). Similar increases in OE21 cell fluorescence under hypoxic conditions; compared to normoxic conditions were observed (**Figure 4.12B**).

The studies presented thus far consider the reduction of **3.29** under severely hypoxic (<0.1% O_2) and normoxic (21% O_2) conditions. However, the degree of hypoxia within solid tumours fluctuates dramatically, and is heterogeneous throughout.[271] Consequently, the reduction sensitivity of **3.29** to variable oxygen concentrations is critical for specifically targeting hypoxic conditions. Subsequently, azide **3.29** reduction under a range of hypoxic conditions was evaluated, and the fluorescence of the cells following treatment analysed by FACS (**Figure 4.13**).

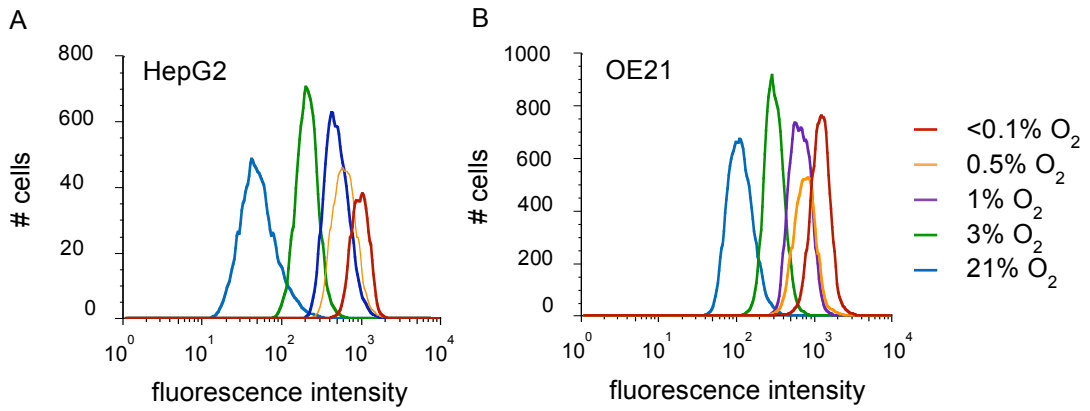

Figure 4.13. FACS histogram plots showing the fluorescence intensity of cells (logarithmic) versus the number of cells, following treatment with **3.29** (1 μM) under the indicated oxygen conditions for 4 h. (A) HepG2. (B) OE21.

The fluorescence intensity of cells correlated with the oxygen concentration in an inverse relationship (**Figure 4.13A**). An increase in fluorescence intensity was observed with the severity of hypoxia. Furthermore, the oxygen dependence of **3.29** reduction could be visually observed by examination of the cell pellets prior to FACS analysis (**Figure 4.14**). As reported in **Chapter 7.2.2** (Page 200), purified amine **3.1** is red in colour. A strong induction of a red colour was observed with decreasing oxygen concentration, indicating the formation of **3.1**.

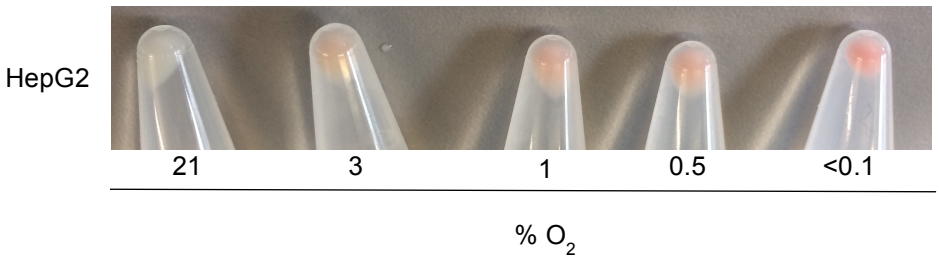

Figure 4.14. A photograph to show the cell pellets of HepG2 cells treated with **3.29** (1 μM) for 4 h under conditions of the indicated oxygen concentration. The red colour indicates increasing amounts of reduction product, amine **3.1**.

The lifetime of fluorescent amine **3.1** is important in the identification of tumour regions that have been hypoxic, and subsequently undergone reoxygenation. To evaluate the stability of amine **3.1** once formed, HepG2 cells treated with **3.29** under hypoxic conditions were transferred to normoxic conditions, and the fluorescence of cells evaluated by FACS analysis at selected times (**Figure 4.15A**).

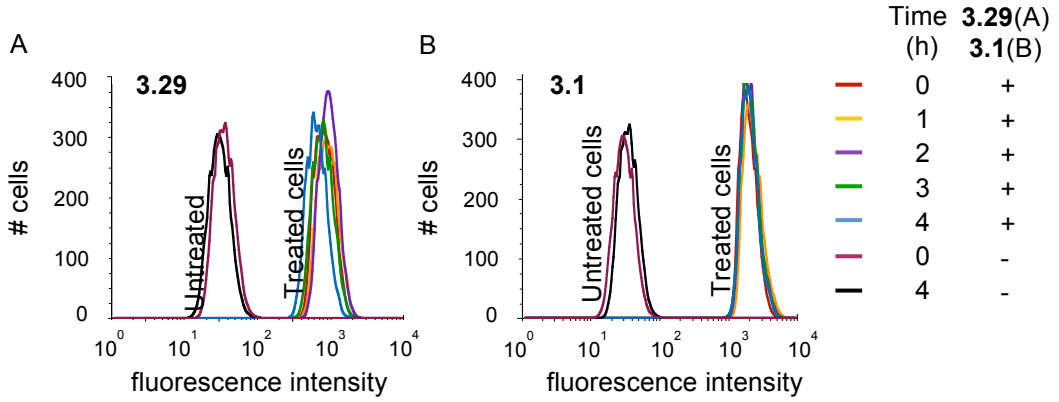

Figure 4.15. FACS histograms showing the fluorescence of cells (logarithmic) versus the number of cells. (A) HepG2 cells following treatment with **3.29** (1 μM) under hypoxic (<0.1% O_2) conditions for 4 h were transferred to normoxic (21% O_2) conditions for the indicated time and then cell fluorescence analysed by FACS. (B) As in A, but treated with fluorescent amine **3.1** (1 μM).

The fluorescence intensity of HepG2 cells pre-treated with **3.29** under hypoxic conditions for 4 hours, remained stable following transfer to normoxic conditions over 4 hours. No decrease in fluorescence indicated amine **3.1** was

stable with respect to reoxygenation over the experiment time course, and was not being degraded in a metabolically active hepatic cell line (**Figure 4.15A**). To confirm this result, cells were directly treated with amine **3.1** under the same experimental conditions, and no decrease in fluorescence intensity was observed (**Figure 4.15B**).

4.7.2 Confocal Microscopy

Confocal microscopy is used for high-resolution fluorescence imaging of cells, and can monitor intracellular proteins and processes in real time.[272,273] Following evaluation of oxygen-dependent fluorogenic properties by FACS analysis, **3.29** was progressed for evaluation by confocal microscopy. In a continuation of previous experiments, HepG2 and OE21 cells were treated with **3.29** under normoxic and hypoxic conditions, and following nuclear staining with DAPI, were imaged (**Figure 4.16**).

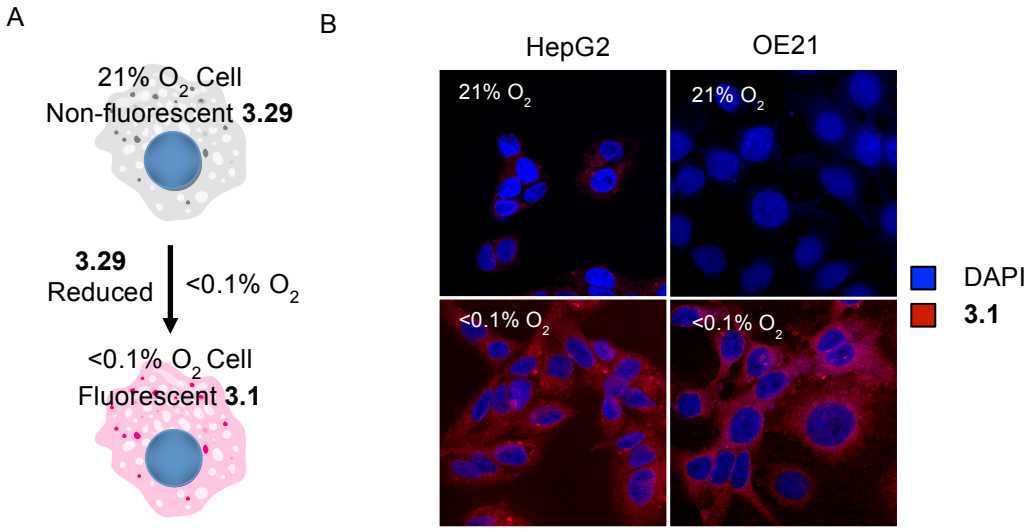

Figure 4.16. (A) Schematic to show cells treated with **3.29** become fluorescent under hypoxic conditions, corresponding to reduction to fluorescent amine **3.1**. Under normoxic conditions no reduction occurs, and therefore no fluorescence is observed. (B) Images taken by confocal microscopy showing the cellular fluorescence associated with **3.1** (red) under normoxic (21% O_2) and hypoxic (<0.1% O_2) conditions. Blue fluorescence is DAPI, which was used as a nuclear stain. HepG2 and OE21 cells were evaluated.

A strong induction of fluorescence associated with **3.1** was observed where cells were exposed to hypoxia, in both HepG2 and OE21 cells. The cellular localisation of fluorescence associated with **3.1** appeared to be exclusively in the cytoplasm, indicating that activation of **3.29** was in this area of the cell. Negligible fluorescence associated with **3.1** was observed where cells were treated under normoxic conditions. The confocal microscopy images taken support the fluorescence intensities observed by FACS analysis, and further validate the hypoxia-dependent reduction of azide **3.29** to amine **3.1** *in vitro*.

4.7.3 Spheroids

Spheroids are proliferating tumour cells, growing in a 3D framework, and typically represent a sphere. As spheroids grow, the environment of the comprising cells more accurately represents that of a tumour, compared to experiments with cell monolayers. Spheroids are useful models for examining the complex oxygen conditions found within a tumour.[274] As the radius of a spheroid increases, the concentration of oxygen decreases towards the centre: a consequence of the diffusion limit of oxygen (100-200 μm), and also increased oxygen consumption of cells.[35] As a result, the centres of spheroids are hypoxic.

FACS analysis of cells treated with **3.29** under variable hypoxia revealed a well-defined fluorescence oxygen dependency (**Figure 4.13**, Page 122). Therefore, it was hypothesised that **3.29** might be suitable for evaluation of the complex oxygen gradients found in spheroids. Furthermore, treatment of spheroids with **3.29** would afford information regarding the ability of **3.29** to permeate through multiple cell layers, and indicate whether **3.29**

might be suitable for progression to *in vivo* analysis. Consequently, human colorectal (HCT116) spheroids were grown to diameters where hypoxia would be present (500-600 μm), such that the spheroid radius was greater than the diffusion limit of oxygen through cell layers.[274] Spheroids were initially treated with **3.1**, and the distribution of fluorescence assessed by confocal microscopy following cryogenic sectioning (**Figure 4.17**). DAPI was used as a nuclear stain. Fluorescence associated with **3.1** was observed throughout the spheroid section in a uniform fashion, indicating that **3.1** was cell permeable across multiple cell layers. Having validated that fluorescent **3.1** could be visualised in spheroid sections, the distribution and activation of fluorogenic **3.29** was investigated.

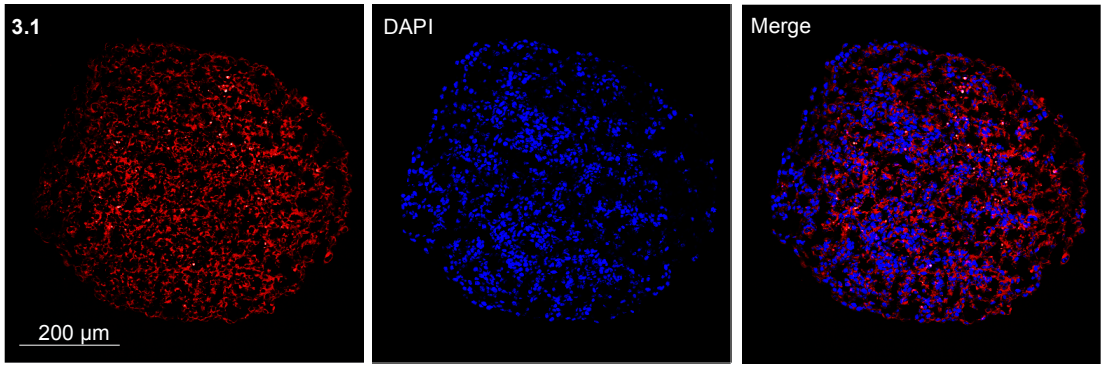

Figure 4.17. Confocal microscopy images of HCT116 spheroid sections treated with **3.1** (20 μM) for 6 h. DAPI (blue) was used as a nuclear stain and **3.1** (red) distribution throughout the spheroid was analysed.

To ensure that **3.29** was only undergoing activation in hypoxic regions, spheroids were also treated with pimonidazole **1.37** as a positive control for hypoxia. Following treatment with **3.29** and pimonidazole **1.37**, the spheroids were sectioned, stained, and imaged by confocal microscopy (**Figure 4.18**). DAPI was used as a nuclear stain.

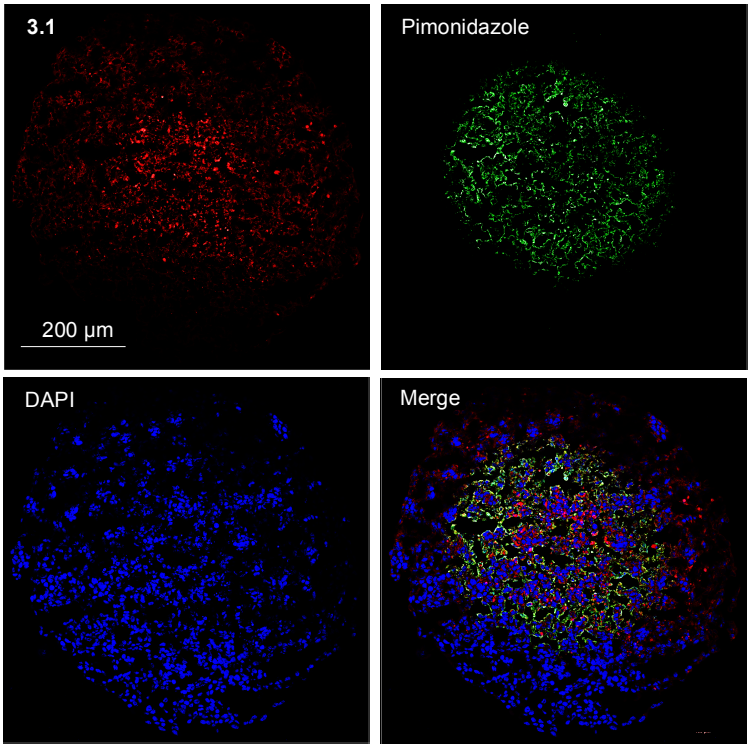

Figure 4.18. Confocal microscopy images of HCT116 spheroid sections treated with **3.29** (20 µM) and pimonidazole **1.37** (40 µM) for 6 h. DAPI (blue) was used as a nuclear stain, pimonidazole (green) was used to positively identify hypoxic regions, and **3.1** (red) distribution throughout the spheroid was analysed.

Elevated fluorescence intensity associated with **3.1** was observed in the central regions of the spheroid, which closely correlated with hypoxic regions of the spheroid as determined by pimonidazole immunofluorescence staining. The identification of enhanced **3.1** fluorescence in the core of the spheroid indicated that **3.29** was permeable across multiple cell layers, and was undergoing activation primarily when exposed to hypoxia. In order to confirm the fluorescence observed was that of **3.1**, a confocal fluorescence spectrum was obtained, and compared directly to that of purified **3.1** (**Figure 4.19A**).

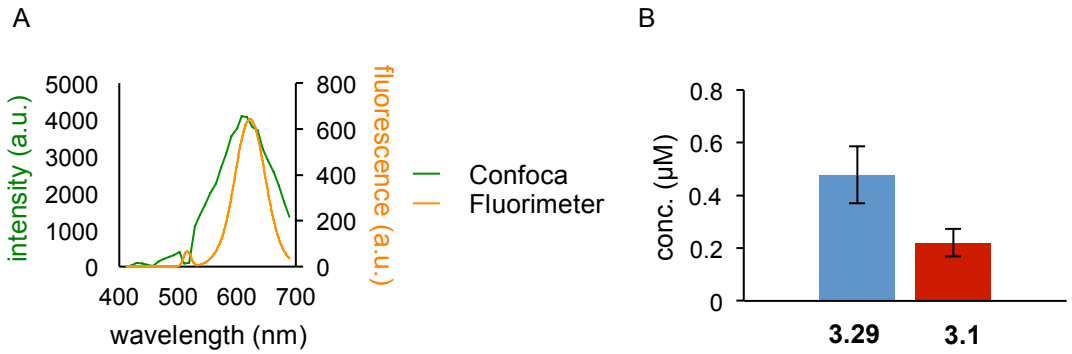

Figure 4.19. (A) Fluorescence spectra obtained by confocal lambda scan analysis (λ_{ex}: 514 nm) of the light associated with **3.1** in **Figure 4.18**, compared to a fluorescence spectrum (λ_{ex}: 515 nm) of purified **3.1** (50 μM) in ^{i}PrOH from **Figure 4.1**. (B) A graph to show the concentration of **3.29** and **3.1** per 9 spheroids. Spheroids were collected, lysed in MeCN and the supernatant analysed by HPLC.

The spectrum obtained by confocal microscopy agreed well with that of **3.1** obtained by fluorimetry, with similar emission maxima at 620 nm. Furthermore, the similarity of the spectra obtained suggested ^{i}PrOH might be a useful solvent for mimicking the fluorescence of a fluorophore in a cellular environment. To further confirm that **3.1** was present in spheroids treated with **3.29**, spheroids were disaggregated, lysed and the cell lysate analysed by HPLC for the presence of **3.29** and **3.1** (**Figure 4.19B**). Amine **3.1** was detected in the lysed spheroids, indicating that reduction of **3.29** was occurring efficiently in hypoxic regions.

For all of the spheroid experiments conducted, HCT116 cells were used owing to their propensity for successful spheroid formation and growth.[18] Attempts to grow spheroids using the cell lines throughout this study, OE21 and HepG2, proved unsuccessful. It is unclear why OE21 and HepG2 cell lines did not form spheroids, although it is known that some cell types are not suitable for such 3D studies.[274] The fluorescence located in the hypoxic regions of the HCT116 spheroid, following treatment with **3.29**, is indicative of

another cell line in which oxygen-dependent reduction of **3.29** occurs (**Figure 4.18**).

4.8 The role of sulfur-containing species

Azide containing compounds have been reported to be susceptible to thiol-mediated reduction to the corresponding amine species.[227] The stability of **3.29** with respect to common intracellular thiols, glutathione (GSH) and L-cysteine (L-cys), was subsequently examined. **3.29** was treated with either GSH or L-cys under normoxic and hypoxic (to ensure no oxidation of the thiol moiety was occurring in air) conditions, and the presence of **3.1** determined by HPLC analysis (**Figure 4.20**). Reduced product, amine **3.1** could not be detected by HPLC analysis after 16 hours treatment with GSH or L-cys, indicating **3.29** was stable with respect to reduction by the thiols evaluated.

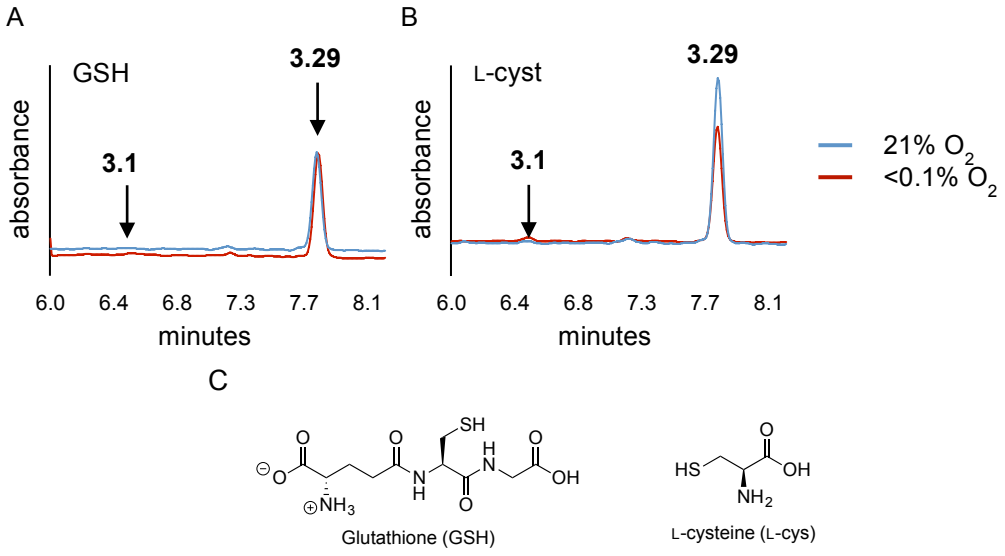

Figure 4.20. Graphs to show the UV absorbance spectra (420 nm visualisation) of aq. **3.29** (1 μM) treated with (A) GSH (1 mM) or (B) L-cyst under normoxic (21% O_2) and hypoxic (<0.1% O_2) conditions for 16 h. The expected retention times of **3.29** and **3.1** are indicated. (C) Chemical structures of GSH and L-cysteine.

Azide **3.29** was reported to be sensitive to reduction through exogenous administration of NaHS, a source of the primary thiol, hydrogen sulfide.[212] However, reduction of **3.29** by endogenous H_2S was not examined, and exogenous administration of H_2S sources is thought to have detrimental effects on cell biology.[275] Consequently, the role of H_2S in the intracellular reduction of azide **3.29** to amine **3.1** was investigated.

Recent reports have suggested an important role for H_2S in cancer biology, and that elevated cellular levels of H_2S may be indicative of oxidative stress, and its concentration is elevated under hypoxic conditions.[276] H_2S has been shown to drive tumour growth and angiogenesis in colon cancer,[277] and in renal cell carcinoma,[278] indicating this small molecule is involved in a variety of tumourigenesis pathways and could possibly be a novel cancer therapy target.[279] H_2S has also been linked to increased tumour radioresistance.[280] Quantification of endogenous H_2S has been an on-going scientific challenge, however, recently developed fluorescent chemical probes have been detected intracellular H_2S, including levels found in mitochondria.[236,281]

Cellular production of hydrogen sulfide is primarily regulated by the enzymes cystathionine-β-synthase (CBS) and cystathionine-γ-lyase (CSE).[276] Furthermore, it has been suggested that CBS is primarily responsible for H_2S production in tumours,[277,282] and has been identified as a HIF-1 target, resulting in up-regulation in hypoxia.[283]

Despite poor potency and selectivity, aminooxyacetic acid (AOAA) **4.13**, and propargyl glycine (PAG) **4.14** are routinely used inhibitors of CBS

and CSE respectively, in a wide range of research areas *in vitro* and *in vivo*, ranging from cancer therapy, to embryonic development, to obesity.[259,284-287] Inhibition of CBS with AOAA **4.13** was shown to reduce the growth of colorectal (HCT116) xenografts in mice, whereas CSE inhibition with PAG **4.14** had no effect, both of which results were consistent with enzyme knock-down studies.[277] Both AOAA **4.13** and PAG **4.14** are effective only when used in mM concentrations.[284] Consequently, employing reported inhibitor concentrations, HepG2 cells were treated with PAG **4.14** (5 mM),[278,288,289] AOAA **4.13** (1 mM),[277,287,290] or a combination under hypoxic conditions to reduce H_2S production, and assess their effect on the reduction of **3.29** to amine **3.1**, the concentrations of which in the cell lysate were determined by HPLC analysis (**Figure 4.21**).

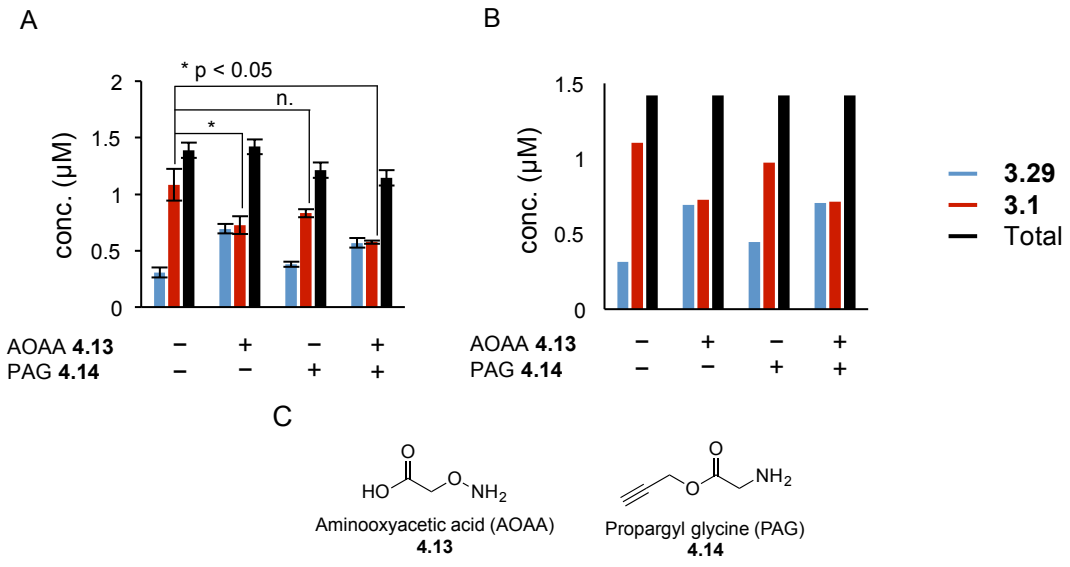

Figure 4.21. (A) Bar chart to show the concentrations of **3.29** (blue), **3.1** (red) and the total concentration (black) of both **3.29** and **3.1** per 0.25 million cells treated with the indicated inhibitor. Cells were pre-treated for 3 h with inhibitors (PAG **4.14** 50 μM, AOAA **4.13** 10 μM) followed by treatment with **3.29** (1 μM) and the inhibitors (PAG **4.14** 5 mM, AOAA **4.13** 1 mM) for 4 h. Cells were harvested, lysed and the lysate analysed by HPLC to determine the concentrations of **3.29** and **3.1**. (B) Bar chart to show the data in A with normalised total concentration of **3.29** and **3.1**. (C) Chemical structures of PAG and AOAA.

Inclusion of the total concentration of **3.29** and **3.1** (black bars) (**Figure 4.21A**) provides a good indication as to whether the same number of cells were harvested and lysed for analysis. Where cells were treated with inhibitors, a depleted concentration of **3.1** was revealed, relative to an untreated control. Treatment with AOAA **4.13** significantly ($p<0.05$) reduced the concentration of **3.1** (red bars). However, treatment with PAG **4.14** was determined to be not significant (n.s) (**Figure 4.21A**). Normalisation of the total concentration of **3.29** and **3.1** (black bars) enabled greater appreciation of the data set out in **Figure 4.21A** with respect to depletion of amine **3.1** concentration (**Figure 4.21B**).

The significant reduction in amine **3.1** formation where cells were treated with AOAA **4.13** suggests that inhibition of CBS, and therefore H_2S production, may affect the reduction of **3.29** *in vitro* under hypoxic conditions. However, formation of **3.1** was not entirely abrogated, suggesting that reduction by H_2S was not the only mechanistic pathway for azide **3.29** reduction under hypoxic conditions. It should be noted that no positive control for action of the inhibitors was used, and consequently the resulting inhibition data is only indicative of the role of CBS and CSE.

Despite being widely used as an inhibitors of CBS and CSE, the broader selectivity profile of AOAA **4.13** and PAG **4.14** against other cellular targets are unclear.[284,291] Both PAG **4.14** and AOAA **4.13** are known to target other PLP(pyridoxal-5′-phosphate)-dependent enzymes to which CBS and CSE belong.[292] In addition, treatment of cells with AOAA **4.13**, which is an acid, led to a visually appreciable change in the colour of cell growth medium, at the treatment doses employed. Such a colour change is indicative of

significant changes in pH of the medium. Therefore the effect of AOAA **4.13** treatment on reduction of **3.1** may be due to compromised cellular function under experimental conditions. To evaluate whether AOAA **4.13** impacted the production of **3.1** from **3.29** *via* inhibition of CBS and therefore reduced H_2S levels, or through off-target cell effects, short-interfering RNA (siRNA) was used. The expression of CBS in OE21 cells was knocked-down, using siRNA. The depleted protein levels confirmed by western blot analysis (**Figure 4.22A**).

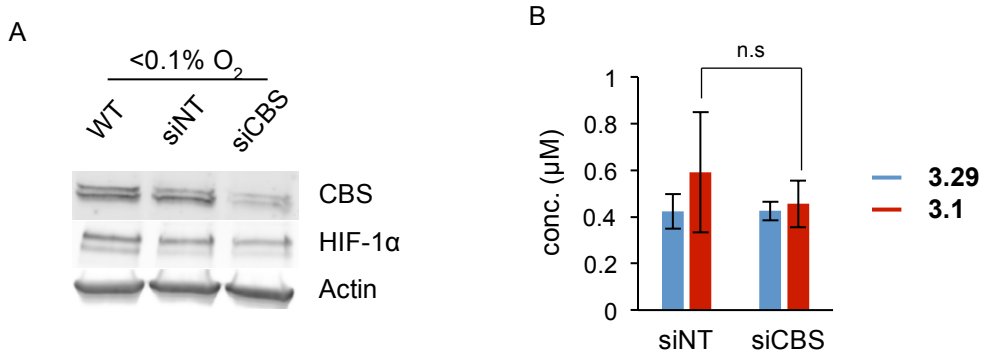

Figure 4.22. (A) Western blot to show depleted levels of CBS in OE21 cells when treated with the corresponding siRNA; siCBS. The presence of HIF-1α was used as a control for hypoxia, and actin as a loading control. Depletion represents approximately 30% of normal CBS levels, as determined by LiCor analysis. (B) A graph to show the concentrations of **3.29** and **3.1** per 0.5 million cells with normal CBS function (siNT) and reduced CBS levels (siCBS), following treatment with **3.29** (1 μM) for 4 h under hypoxic conditions. Cells were harvested, lysed, and the lysate analysed by HPLC analysis.

OE21 cells with depleted (~70% depletion) CBS levels were treated with **3.29** under hypoxic conditions, and the cell lysate analysed by HPLC. Examination of the resulting HPLC data revealed no significant difference in the concentration of amine **3.1** in cells depleted of CBS, compared to a control with normal CBS levels (**Figure 4.22B**). The comparable concentrations of **3.1** suggested that CBS expression was not a major determinant in the reduction of **3.29** under the experimental conditions employed.

In contrast to inhibition of CBS with AOAA **4.14** (**Figure 4.21A**), knockdown of the protein did not result in a statistically significant decrease in formation of amine **3.1**. It is possible that AOAA **4.14** treatment compromised normal cellular function through off-target effects, and therefore affected reduction of **3.29** under hypoxic conditions. However, decreasing cellular CBS by siRNA, to approximately 30% compared to control cells, would be predicted to have a significant effect on H_2S production.[282] Endogenous H_2S in cells could contribute to the reduction of **3.29** to **3.1**. However, following inhibition and knock-down studies, the role of H_2S was likely to not be the predominant mechanism of activation in cells.

4.9 Discussion

The fluorogenic, azide containing compound **3.29** was shown to be sensitive to hypoxia-dependent reduction, to yield fluorescent amine **3.1**. A variety of 2D and 3D cellular assays were employed, and **3.29** was demonstrated to be a useful fluorogenic marker of hypoxic in confocal microscopy and spheroid sections. In contrast to nitro-based bioreductives, azide **3.29** was not reduced by NADPH reductase under hypoxic conditions. However, a number of individual CYP enzymes were identified as being capable of this reductive transformation. Despite reports of H_2S activity towards the reduction of azides, the data presented suggests the role of hydrogen sulfide in reduction of **3.29** was limited under cellular conditions. These studies provided interesting insights into the utility of azide compounds in the development of bioreductive dyes, and particularly their biostability under conditions of reduced oxygen. To the best of our knowledge, this work represents the first demonstration of azide compounds to target hypoxia, and offers promise for further study of this energy rich functional group as a hypoxia-sensitive moiety.

Chapter 5

EVALUATION AND SYNTHESIS OF A NOVEL NIR FLUOROGENIC HYPOXIA-ACTIVATED PRODRUG

5.1 Introduction

5.1.1 Selection of a NIR fluorophore

The established biomedical use of cyanine-based fluorophores, such as ICG **1.41**, makes them attractive for incorporation into a fluorogenic bioreductive prodrug (**Chapter 1.5.2**, Page 28).[127,293] The NIR dye **5.1** was identified as a cyanine-fluorescein-derived dye with a similar Stokes-shift to **1.41**, and a λ_{max} of approximately 716 nm (**Figure 5.1**).[156] Furthermore, **5.1** has been employed in a variety of *in vitro* and *in vivo* studies, including imaging of tumour models in mice.[156,294,295]

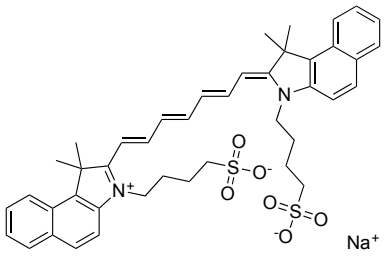

1.41 (ICG)

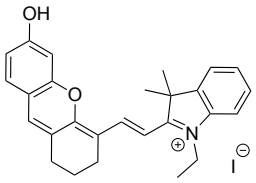

5.1

Figure 5.1. Chemical structures of ICG **1.41** (λ_{ex}: 780 nm, λ_{em}: ~800 nm) and **5.1** (λ_{ex}: ~690 nm, λ_{em}: ~716 nm).

Alkylation of the phenol group of **5.1** is known to quench fluorescence of the molecule.[156] Alkylation alters the donation of electron density from the phenolate group into the conjugated push-pull type system, thereby modulating fluorescence. The importance of the free phenol group for fluorescence was exploited in the development of the bioreductive fluorogenic dye **5.2** (**Scheme 5.1**).[296] In response to nitroreductase enzymes in a zebrafish model, fluorogenic **5.2** undergoes hypoxia-dependent reduction to the corresponding amine **5.3**, inducing fragmentation to release NIR dye **5.1** and restore fluorescence (**Scheme 5.1**).

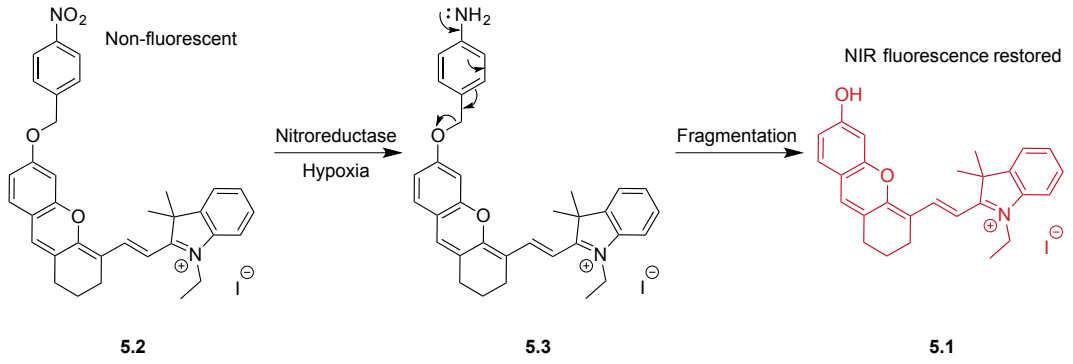

Scheme 5.1. Fluorogenic hypoxia-activated dye **5.2** is sensitive to nitroreductase-mediated reduction of the 4-nitrobenzyl bioreductive group, under hypoxic conditions. Reduction to amine **5.3** induces fragmentation to release **5.1** and restore fluorescence.[296]

It was hypothesised that similar fluorogenic properties could be introduced by replacing the hydroxyl group with other electron donating substituents, such as an amino group. The amine derivative **5.4** has recently been shown to be a useful fluorescent marker in tumour bearing mice, with a similar fluorescent profile to hydroxyl analogue **5.1**.[297,298] Transformation of the amino functionality into a nitro group could quench the fluorescence of **5.4** (**Figure 1.12**, Page 30), affording an alternative fluorogenic hypoxia-activated dye **5.5** (**Scheme 5.2**).

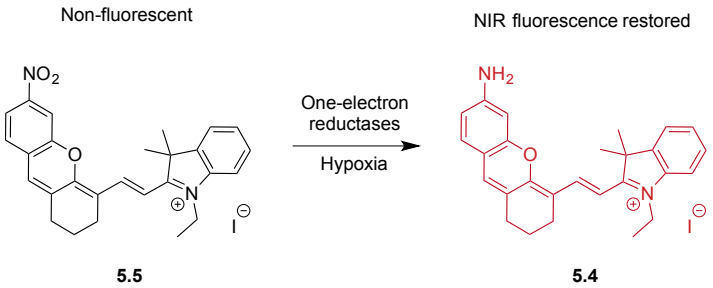

Scheme 5.2. Installation of an electron-withdrawing nitro group instead of an electron-donating phenol group is hypothesised to quench fluorescence. Under hypoxic conditions, the nitro group undergoes reduction to the electron donating amino group, therefore likely restoring fluorescence of the molecule.

The development of nitro derivative **5.5** into a fluorogenic bioreductive group **5.6** was also considered, which would fragment *via* the reduced amine species **5.7** to release a cargo molecule. Fragmentation of a nitroaromatic bioreductive compound relies on increased electron density in the aromatic ring following reduction to the amine (**Scheme 5.2A**).

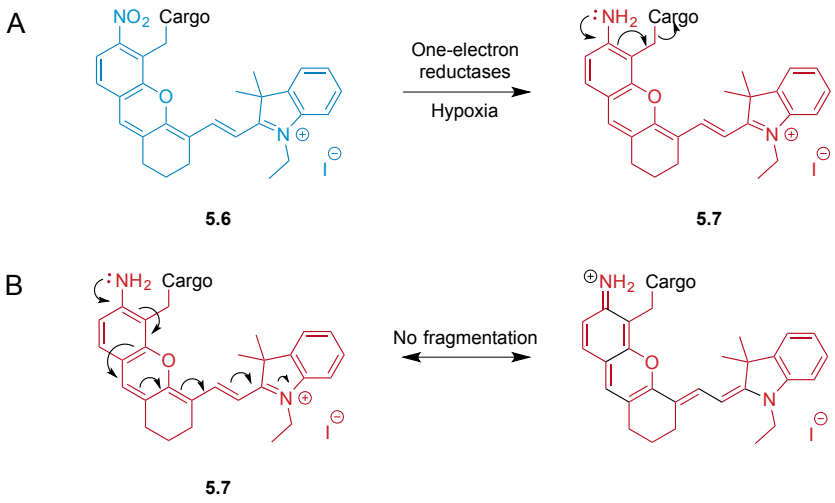

Figure 5.2. (A) Synthesis of **5.6** would afford a fluorogenic bioreductive group, which following reduction to amine **5.7** in hypoxia would become fluorescent, and fragment to release a cargo molecule. (B) Resonance structure of amine **5.7** showing the extended conjugated system might prevent fragmentation to release the cargo molecule.

Common bioreductive groups for induction of fragmentation, such as imidazoles or benzyl groups, comprise single aromatic rings (**Scheme 1.5**, Page 18). However, in the proposed NIR bioreductive group **5.6**, the aromatic

system, into which the amino group of **5.7** donates electron density, is extended with a conjugated, electron-withdrawing indole present (**Scheme 5.2B**). Therefore, following reduction, the effective increase in electron density within the aromatic structure is less in **5.7**, compared to benzyl or imidazole groups. Consequently the fragmentation to release the cargo molecule might be inefficient.

5.1.2 HAPs with dual delivery of cargo molecules

The studies detailed in this dissertation have focused on integrating the hypoxia-sensitive nitro group into the fluorogenic scaffold, such as 5-methylene-6-nitroquinoline **2.9** (Page 43) and the NIR fluorogenic nitro-styrylchromenone **3.3** (Page 78). However, development of highly conjugated NIR dyes could possibly be compromised by poor fragmentation (**Scheme 5.2**). To maintain efficient fragmentation, a bioreductive group was considered which would deliver both NIR fluorophore **5.1** and a cargo molecule, under hypoxic conditions. To the best of our knowledge there are no examples of HAPs, which fragment to release two cargo molecules. A nitro benzyl bioreductive group was considered for introduction of dual delivery capabilities. Functionalisation with an additional methylene group would afford two positions (*ortho* and *para*) for installation of a cargo molecule, as in molecule **5.8** (**Scheme 5.3**). Consequently, the bioreductive candidate **5.8** was identified as the primary synthetic target.

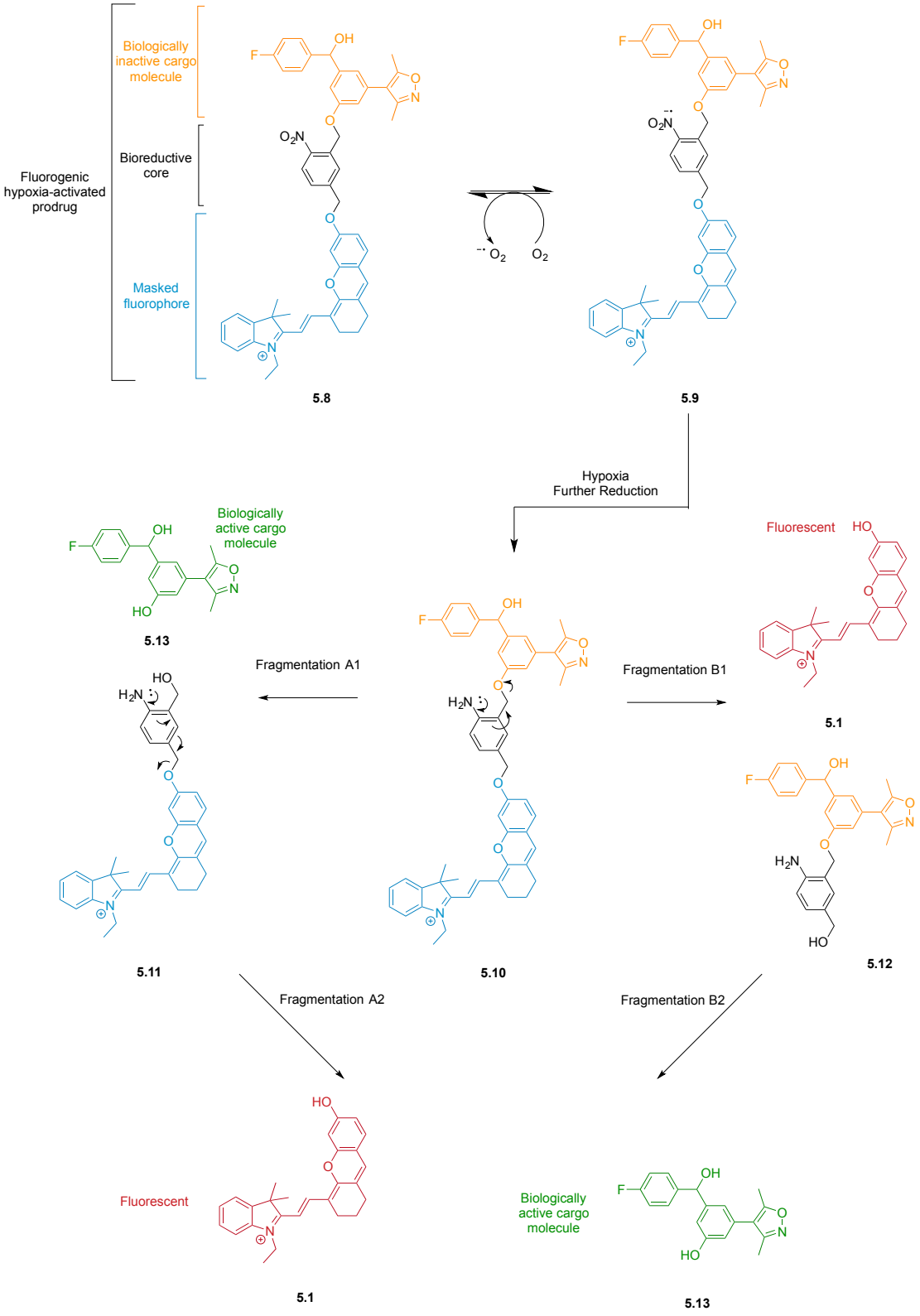

Scheme 5.3. Proposed mechanism of hypoxia-dependent reduction and fragmentation of **5.8**. The bioreductive nitrobenzyl core is oxygen sensitive, and when reduced to the corresponding amine **5.10**, can fragment to release a NIR fluorophore **5.1** and the biologically active cargo molecule **5.13**.

It is likely that the lower phenol group pKa of dye **5.1** (pKa ~ 5.6 [calculated]) compared to cargo molecule **5.13** (pKa ~ 11) will kinetically favour fragmentation pathway B over fragmentation pathway A (**Scheme 5.3**).[48,156] Consequently, methods of maximising fragmentation to release **5.13** were considered. It was proposed that installation of a cargo molecule **5.13** at the 2-benzyl position of the bioreductive group would accelerate fragmentation through an intramolecular hydrogen bond between the reduced amino group and phenoxide as in compound **5.10** (**Figure 5.3**). Furthermore, it might be that the steric clash between cargo molecule **5.13** and the amino group at the 2-position could further accelerate fragmentation. Both hydrogen bonding, and steric clash would be absent if the cargo molecule were installed at the 4-position as in compound **5.14** (**Figure 5.3**).

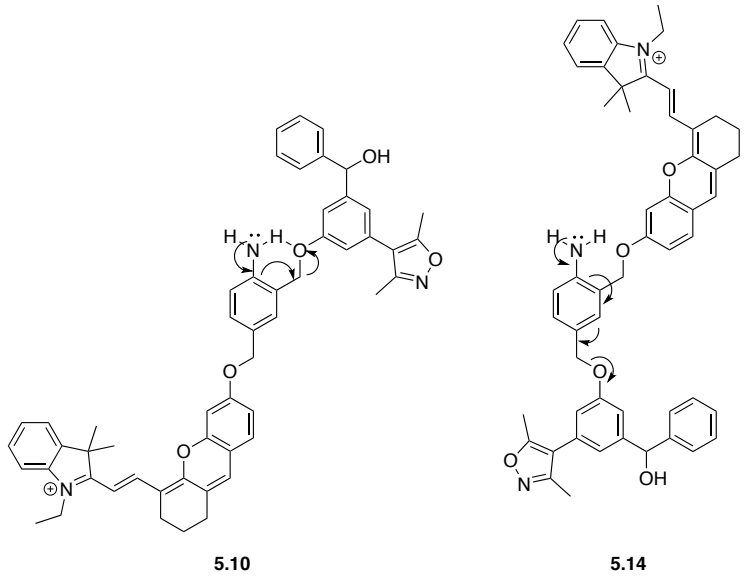

Figure 5.3. Representative structures to show possible hydrogen bonding interaction in amine **5.10** to accelerate fragmentation of cargo compound **5.13**, which is absent in the 4-substituted analogue **5.14**.

Compound **5.8** in which the cargo molecule **5.13** is at the 2-position, and NIR dye **5.1** at the 4-position was consequently selected for synthesis,

with the intention of determining whether a central bioreductive core could be used to deliver two cargo molecules under hypoxic conditions.

5.2 Selection of the biologically active cargo molecule

The BET bromodomain inhibitor **2.48** has previously been employed as a cargo molecule for a candidate fluorogenic bioreductive prodrug (**Chapter 2.4**, Page 56). During the course of the studies detailed in this dissertation, the metabolic profile of **2.48** was examined and analogues made to improve its stability *in vivo*.[204] The fluoro analogue **5.13** was hypothesised to have improved resistance to oxidation of the phenyl ring in liver microsomes compared to **2.48**. Phenyl ring oxidation had previously been observed in metabolism studies of **2.49** (**Figure 2.12**, Page 68) and it was hypothesised that introduction of a fluoro group might block this metabolism site. Consequently, compound **5.13** was selected as the cargo molecule.[299]

5.3 Synthesis

5.3.1 Synthesis of the nitrobenzyl bioreductive core

A retrosynthesis was proposed, in which the central nitrobenzyl bioreductive core **5.16** was used as an alkylating agent to sequentially install **5.13** (**Scheme 5.4**, Step ii) and NIR dye **5.1** (**Scheme 5.4**, Step i).

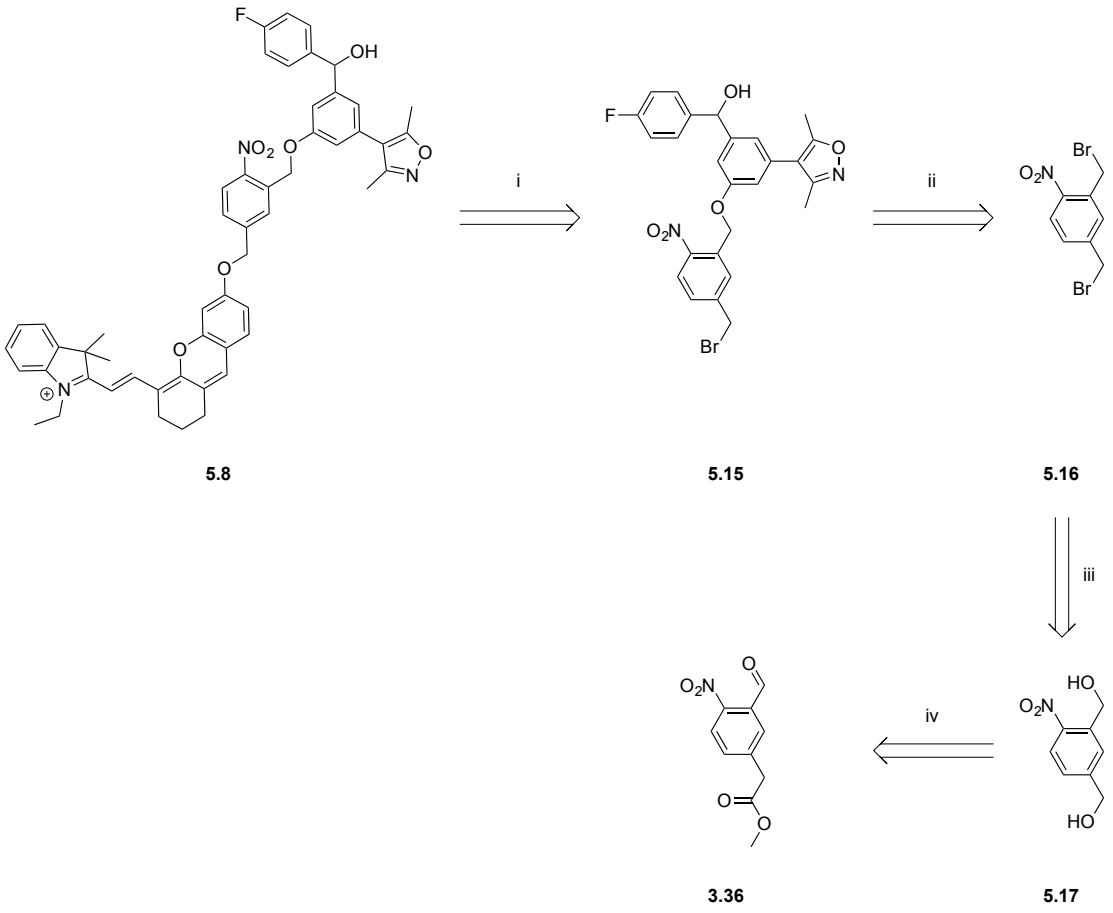

Scheme 5.4. Proposed retrosynthesis of **5.8** in which **5.16** is used as an alkylating agent to introduce **5.13** and dye **5.1** sequentially; (i) Base (ii) Base (iii) conc. HBr (iv) $NaBH_4$.

Reduction of commercially available **3.36** would afford the dimethylene alcohol **5.17** (**Scheme 5.4**, Step iv). Conversion of **5.17** to the dibromide **5.16** could be achieved by nucleophilic substitution in HBr (**Scheme 5.4**, Step iii). The regiochemistry of alkylating **5.13** using bromobenzyl derivative **5.16** was unclear (**Scheme 5.4**, Step ii). Alkylation at the 2-position as in structure **5.15** was likely to be sterically less favourable. However, due to the inductive effect of the *ortho* nitro group, alkylation at the 2-position could be kinetically favourable compared to the 4-position. Separation of any regioisomers would afford methylene bromide **5.15** to allow installation of NIR dye **5.1** and afford desired compound **5.8** (**Scheme 5.4**, Step i).

Compound **3.36** was treated with $NaBH_4$ to furnish dimethylene alcohol **5.17** in 39% yield (**Scheme 5.5**, Step i). Bromination of **5.17** was achieved by acid-catalysed nucleophilic substitution in concentrated aqueous HBr to furnish **5.16** in 50% yield (**Scheme 5.5**, Step ii).

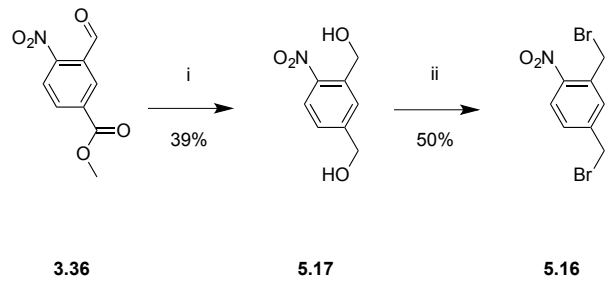

3.36 **5.17** **5.16**

Scheme 5.5. Borohydride reduction of **3.36** to afford dimethylene alcohol **5.17** and subsequent bromination to afford **5.16**; *Reagents and conditions*: (i) $NaBH_4$ (3 eq.), MeOH, THF, 0 °C → RT, 15 h, 39%; (ii) conc. aq. HBr. 65 °C, 24 h, 50%.

Having synthesised the central nitrobenzyl core **5.16** for use as an alkylating agent, installation of **5.13** at the benzylic positions was investigated (**Scheme 5.6**). As expected, a mixture of regioisomers was isolated, arising from alkylation at the benzylic 2-position **5.15** and the 4-position **5.18**. The similar isolated yields for each regioisomer suggested the reaction was not regioselective. However, it was possible to separate **5.15** and **5.18** using silica gel column chromatography.

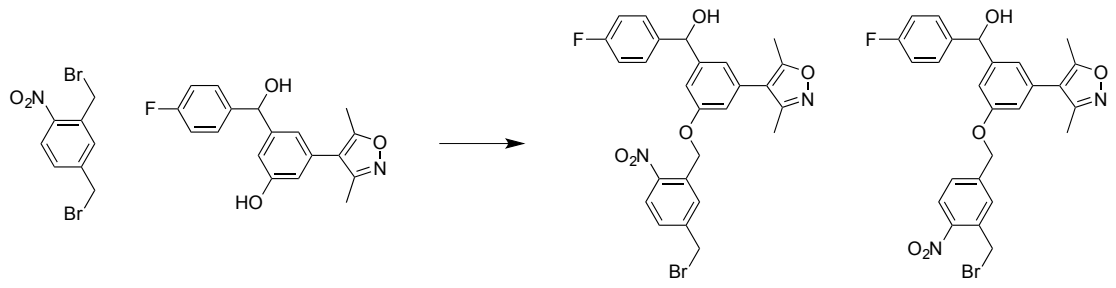

5.16 **5.13** **5.15** (20%) **5.18** (17%)

Scheme 5.6. Alkylation of **5.13** using **5.16** leads to a mixture of regioisomers **5.15** and **5.18** in an isolated 1.2:1 ratio; *Reagents and conditions*: Cs_2CO_3 (1 eq.), DMF, 0 °C → 35 °C, 3 h. Compound **5.13** was provided as a gift from Ray Berkeley (Conway laboratory).

Therefore, **5.15** was furnished in three steps with the desired cargo compound **5.13** at the 2-position of the bioreductive nitrobenzyl group. With key intermediate **5.15** in hand; synthesis and installation of NIR dye **5.1**, to furnish the desired fluorogenic HAP **5.8**, was investigated. The synthesis of NIR dye **5.1** had been previously reported by Yuan, Zhu and co-workers, and the synthesis of key intermediates was investigated.[156] Using commercially available **5.19**, which was alkylated using ethyl iodide under reflux to afford **5.20** in excellent yield (91%) (**Scheme 5.7**).[300]

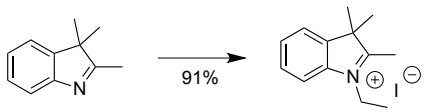

5.19 **5.20**

Scheme 5.7. Alkylation of **5.19** to afford the iodo salt **5.20**; *Reagents and conditions*: EtI (1.5 eq.), 70 °C 24 h, 91%.

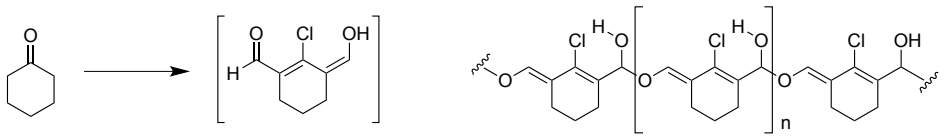

5.21 **5.22** **5.23**

Scheme 5.8. Attempted synthesis of intermediate **5.22** and plausible polymeric structure of isolated product **5.23**; *Reagents and conditions*: $POCl_3$ (4.0 eq.), DMF/CH_2Cl_2 (1:1 *v/v*), 0 °C → 70 °C, 3 h.

Attempts to synthesise intermediate **5.22** focused on reports by Samanta, Chang and co-workers, which suggested **5.22** could be isolated as yellow crystals, following quenching of the reaction solution on ice (**Scheme 5.8**).[301] However, the reported procedure led to the formation of a black precipitate. Attempted purification of the precipitate using silica gel column chromatography proved unsuccessful. ^{1}H NMR spectroscopy of the black precipitate revealed **5.22** was not the dominant product, as determined by the

absence of an aldehyde resonance peak. However, ^{1}H NMR spectroscopy did indicate successful substitution at the 2- and 6-positions of cyclohexanone **5.21**, and furthermore, the desired mass was present in low-resolution mass spectrometry analysis. It was suggested that the black precipitate isolated was a mixture of polymers **5.23**, and consequently ^{1}H NMR analysis was inconclusive.

Despite incomplete characterisation of the black precipitate, the solid was taken forward synthetically to examine whether **5.22** was present. A condensation reaction between iodo-indole salt **5.20** and the black precipitate was consequently investigated (**Scheme 5.9**).[302] Chloro cyanine **5.24** was isolated as a green solid contaminated with starting material indole **5.20**, as determined by ^{1}H and ^{13}C NMR spectroscopy. The synthesis of the desired product **5.24** indicated the black precipitate did indeed contain compound **5.22**, and was likely to be a polymer **5.23**, as hypothesised.

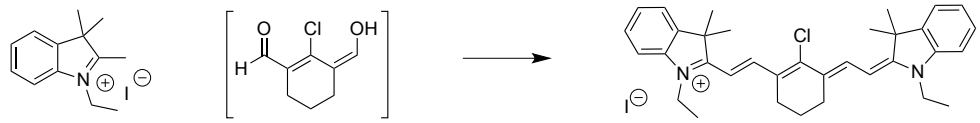

5.20 **5.22** **5.24**

Scheme 5.9. Synthesis of the chloro derivative **5.24** by condensation reaction between **5.20** and **5.22**; *Reagents and conditions*: NaOAc (1.1 eq.) **5.20** (2.0 eq.), RT, 2 h.

To evaluate the suitability of chloro intermediate **5.24** for nucleophilic substitution reaction, the compound was treated with amine **5.25** to afford **5.26** in 22% yield (**Scheme 5.10**). A nitroimidazole derivative of compound **5.26** has previously been reported as suitable for the detection of hypoxia, suggesting **5.26** could also be used as a fluorescent marker of reduced oxygen in cells.[302]

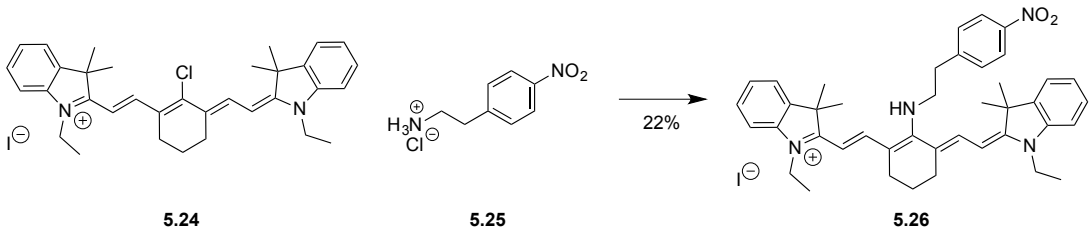

5.24 5.25 5.26

Scheme 5.10. Synthesis of aminoethylbenzyl derivative **5.26** indicating **5.24** was suitable for S_NAr substitution reactions; *Reagents and conditions*: **5.25** (1.3 eq.), Et_3N (2.0 eq.), DMF, 55 °C, 3 h, 22%.

Treatment of compound **5.24** with resorcinol **5.27** under basic conditions was reported to afford NIR dye **5.1** *via* a retro-Knoevenagel condensation (**Scheme 5.11**).[296] Attempts to synthesise **5.1** employing the reported procedures, led to the successful detection of **5.1** by TLC analysis, and mass spectrometry.[156,296] Attempts to purify the product by silica gel, and aluminium (neutral and basic) column chromatography, however, afforded impure samples of the product in less than 3% yield. TLC analysis suggested multiple products were present in the reaction mixture. Consequently, a proposed reaction mechanism was examined (**Scheme 5.12**).[156] An S_NAr reaction by resorcinol **5.27** affords intermediate **5.28** (**Scheme 5.12**). The electron-donating ability of the second phenol group is likely to be critical for ring closing formation to form intermediate **5.29**. The final stage of the reaction requires elimination of the indole moiety **5.31**, which is reported to be favoured by the presence of trace amounts of water in the reaction.[297] Consequently, the first two stages of the reaction are favoured by basic conditions, and the final stage requires neutral conditions.

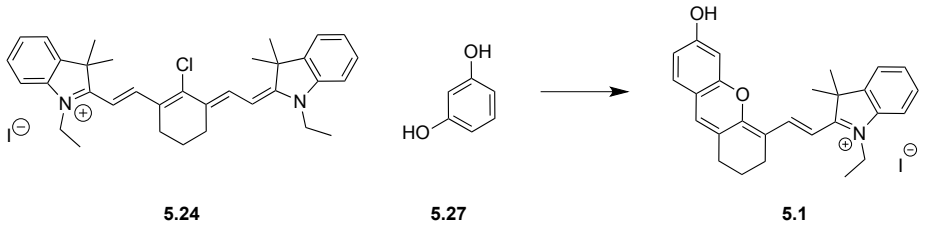

5.24 **5.27** **5.1**

Scheme 5.11. Attempted synthesis of **5.1**; *Reagents and conditions*: (A) K_2CO_3 (1.2 eq.), **5.27** (1.2 eq.), MeCN, 50 °C, 4 h;[296] (B): NaH (2.1 eq.), **5.27** (2.1 eq.), DMF, 50 °C, 4 h.[156]

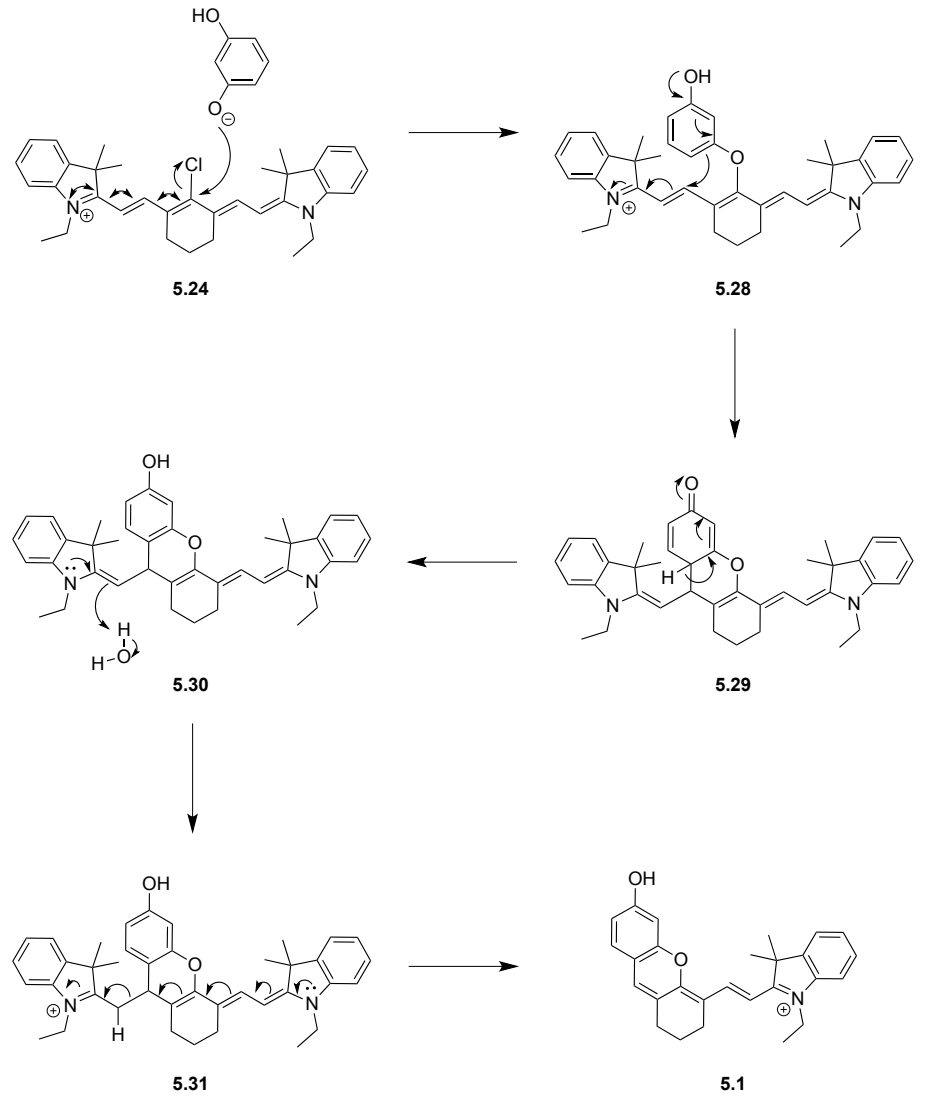

5.24 **5.28** **5.29** **5.30** **5.31** **5.1**

Scheme 5.12. A proposed mechanism of formation of **5.1** *via* a retro-Knoevenagel condensation of **5.24** with resorcinol **5.27**. The electron-donating ability of the phenol group in intermediate **5.28** is critical for cyclisation to occur, affording intermediate **5.30**. Elimination of the indole moiety can then afford **5.1**.

It was noted that K_2CO_3 was only sparingly soluble in MeCN (**Scheme 5.11**, Conditions A), which was likely to affect the efficiency of the conjugate addition of **5.27** and cyclisation to afford intermediate **5.30** (**Scheme 5.12**). Use of Cs_2CO_3 to improve base solubility in the reaction mixture led to no appreciable increase in conversion to the product, as determined by TLC analysis. Consequently, Et_3N was used as a soluble organic base for subsequent reactions. It was hypothesised that less polar solvents than MeCN or DMF could reduce solvation of the reaction intermediates, possibly promoting progression of the reaction. Starting materials **5.24** and **5.27** were found to be soluble in 1,2-dichloroethane (DCE), and the reaction was subsequently attempted under reflux (**Scheme 5.13**).

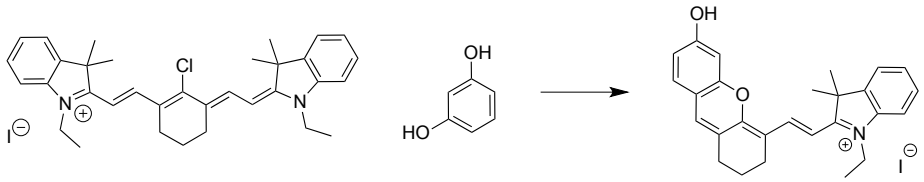

5.24 **5.27** **5.1**

Scheme 5.13. Synthesis of NIR dye **5.1**; *Reagents and conditions*: Resorcinol **5.27** (1.5 eq.), Et_3N (4 eq.), DCE, 90 °C, 4 h.

Analysis of the reaction mixture by TLC revealed a mixture of products. However, TLC analysis suggested an improved conversion to the desired product **5.1** compared to previous attempts. Purification of the reaction mixture using silica gel column chromatography led to isolation of impure product **5.1** (445 mg, 1.00 g reaction scale) that was inseparable from impurities, even following further chromatography. A sample of this product (90 mg) was purified using semi-preparative HPLC, to afford the desired product **5.1** (45 mg).

5.3.2 Synthesis of hypoxia-activated derivatives of NIR dye 5.1

With NIR dye **5.1** in hand alkylation to introduce a bioreductive core, conjugated to the BET bromodomain inhibitor **5.13**, was investigated. Alkylation of **5.1** with nitrobenzyl has been shown to afford **5.33**; a useful reporter of nitroreductase activity in zebrafish.[296] Consequently, **5.33** was synthesised in 18% yield as a control compound, which lacks a biologically-relevant cargo molecule at the *ortho* position as in target compound **5.8** (**Scheme 5.14**).

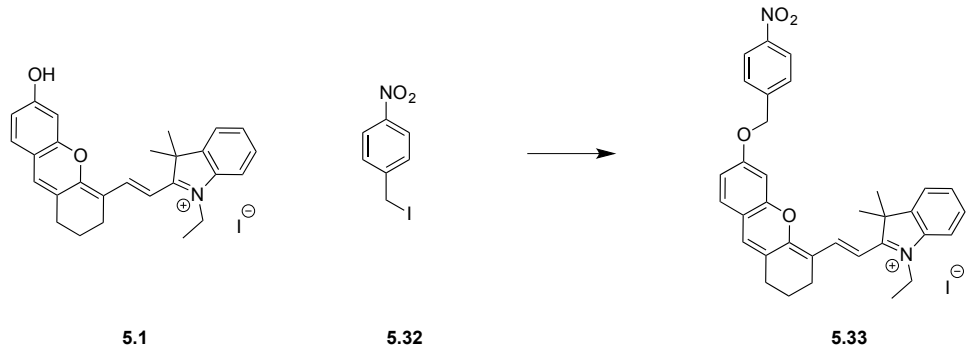

5.1 **5.32** **5.33**

Scheme 5.14. Synthesis of hypoxia-activated dye **5.33**, a reporter of nitroreductase activity; *Reagents and conditions*: 4-Nitrobenzyl iodide **5.32** (1.1 eq.), Et_3N (1 eq.), $CHCl_3$, 55 °C, 16 h, 18%.

Employing the previously synthesised bromobenzyl **5.15** with compound **5.13** preinstalled (**Scheme 5.6**, Page 144), alkylation of **5.1** was attempted (**Scheme 5.15**). With the desired fluorogenic HAP candidate **5.8** synthesised in 23% yield, it was next determined whether the central nitrobenzyl bioreductive core could undergo hypoxia-dependent activation to deliver the NIR fluorophore **5.1**, and the cargo BET bromodomain inhibitor **5.13** (**Scheme 5.3**, Page 140).

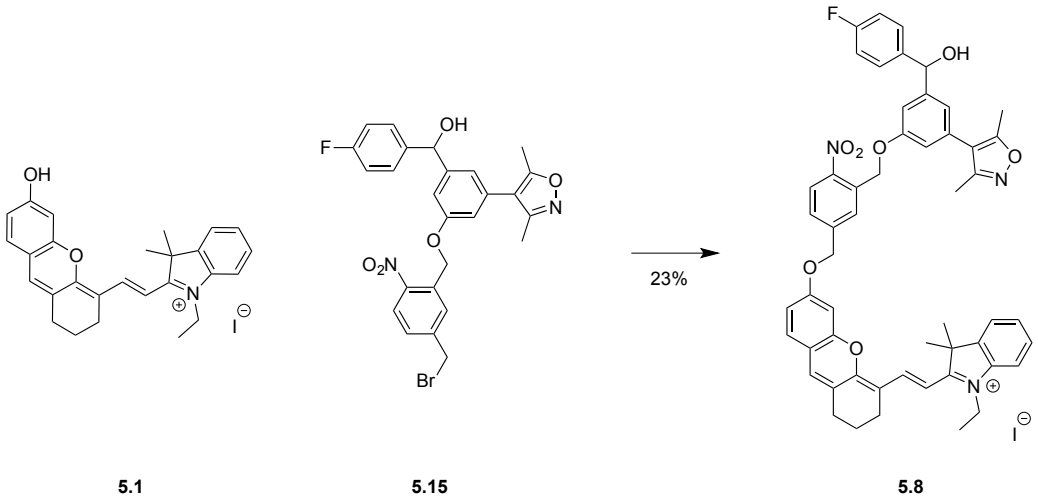

5.1 **5.15** **5.8**

Scheme 5.15. Synthesis of fluorogenic hypoxia-activated compound **5.8**; *Reagents and conditions*: **5.1** (1 eq.), Et_3N (2 eq.), $CHCl_3$, 55 °C, 16 h, 23%.

5.4 Evaluation of bioreductive properties

With **5.8**, and control compounds **5.1** and **5.33** in hand, validation experiments for bioreductive molecules, reported by our laboratories, were conducted.[48]

5.4.1 Zinc reduction assay

Compounds **5.8** and **5.33** were treated separately with zinc and ammonium chloride, and the assay solution analysed by HPLC for reduction products at selected time points (**Figure 5.4**). Treatment of **5.8** revealed reduction to the hydroxylamine **5.34**, and an increase in the concentration of fragmentation product, NIR dye **5.1** with time. However, neither the BET bromodomain inhibitor **5.13**, nor amine **5.10** (Page 140) could be identified by HPLC analysis (**Scheme 5.3**, Page 140). Furthermore, the introduction of zinc to the reaction mixture led to a sharp decrease in the concentration of **5.8**, relative to the starting time point. These data suggested that **5.8** was unstable with respect to zinc reduction.

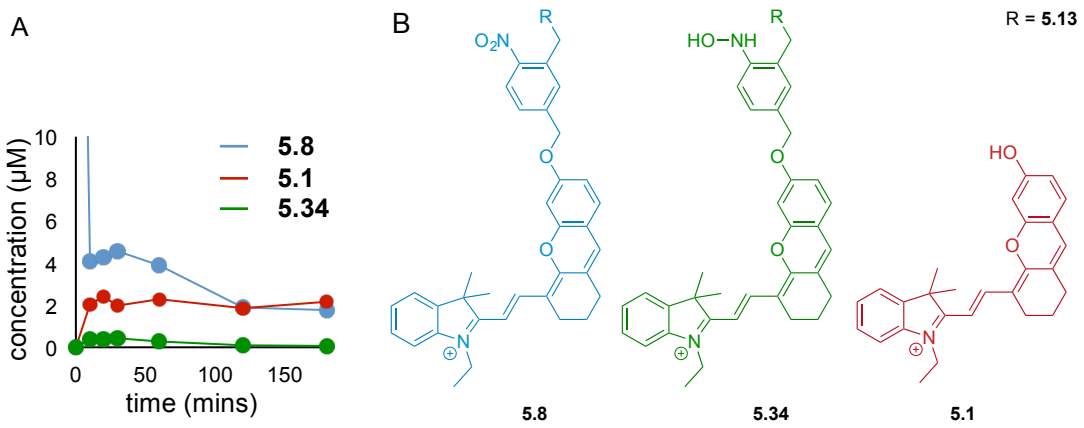

Figure 5.4. (A) Graph to show concentrations of the shown compounds with time following zinc reduction of **5.8** (100 μM) in DMF with NH_4Cl. Concentrations in the assay volume were determined by HPLC analysis. (B) Structures of the detected reduction intermediates. The colours shown correspond to those in the graph.

Similar results were obtained with the structurally simplified nitrobenzyl control compound **5.33** under the same assay conditions (**Figure 5.5**). The concentrations of reduction intermediates; hydroxylamine **5.35** and nitroso **5.36**, peaked at 10 minutes, before decreasing with time. This decrease corresponded to an increase in the concentration of NIR dye **5.1**, indicating fragmentation from the reduction products.

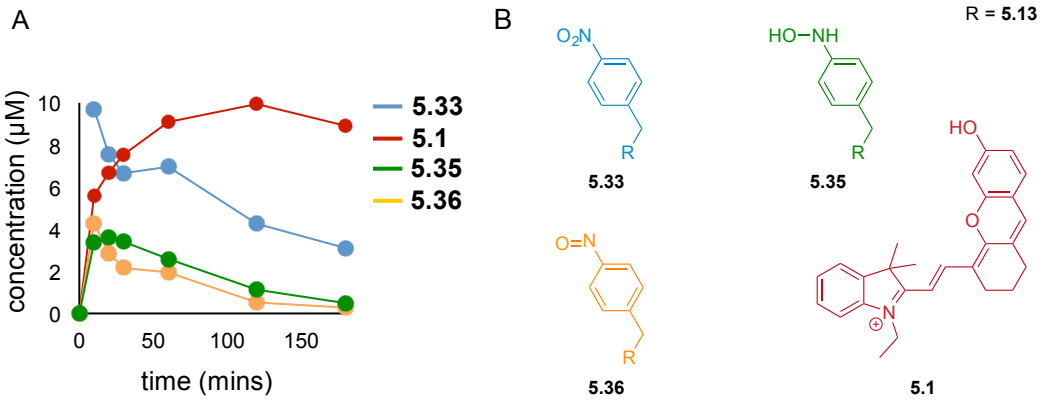

Figure 5.5. (A) Graph to show concentrations of the shown compounds with time following zinc reduction of **5.33** (100 μM) in DMF with NH_4Cl. Concentrations in the assay volume were determined by HPLC analysis. (B) Structures of the detected reduction intermediates. The colours shown correspond to those in the graph.

It was noted that zinc reduction of **5.8** and **5.33** did not result in concentrations of NIR dye **5.1** comparable to the starting concentration of the assay solution (100 μM). Consequently, the stability of NIR dye **5.1** to zinc reduction was investigated (**Figure 5.6**). Upon addition of zinc, a rapid decrease in the concentration of **5.1** was observed within 10 minutes, and continued to depreciate over the time course of the experiment. The depletion of **5.1** concentration suggested instability with respect to zinc reduction.

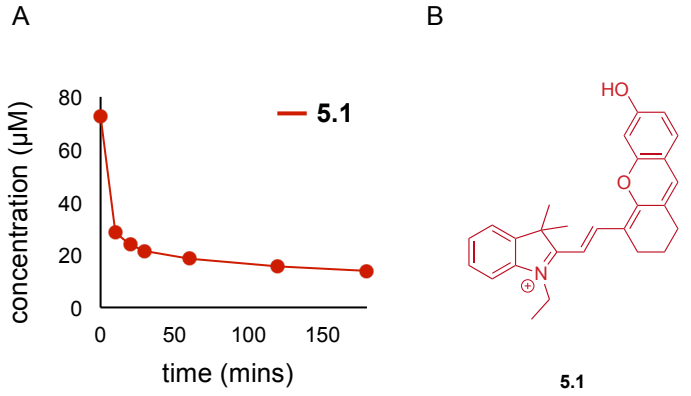

Figure 5.6. (A) Graph to show concentrations of NIR dye **5.1** with time following zinc reduction of **5.1** (100 μM) in DMF with NH_4Cl. (B) Structure of NIR dye **5.1**. The colour shown corresponds to that in the graph.

These data collectively suggest treatment of molecules containing **5.1** with zinc, results in compound decomposition, and therefore the assay was unsuitable for determining reduction and fragmentation. Consequently, fluorogenic HAP candidate **5.8** and fluorogenic dye **5.33** were progressed to enzyme-based reduction assays, the next stage of our validation protocol.

5.4.2 Cytochrome P450 (CYP) NADPH reductase assay

Compounds **5.8** and **5.33** were subject to treatment with NADPH reductase enzymes under normoxic and hypoxic conditions (**Figure 5.7**). The concentrations of **5.8** and **5.33** decreased over time, indicating the

compounds were precipitating out of solution. Furthermore, no other metabolites could be detected by HPLC analysis.

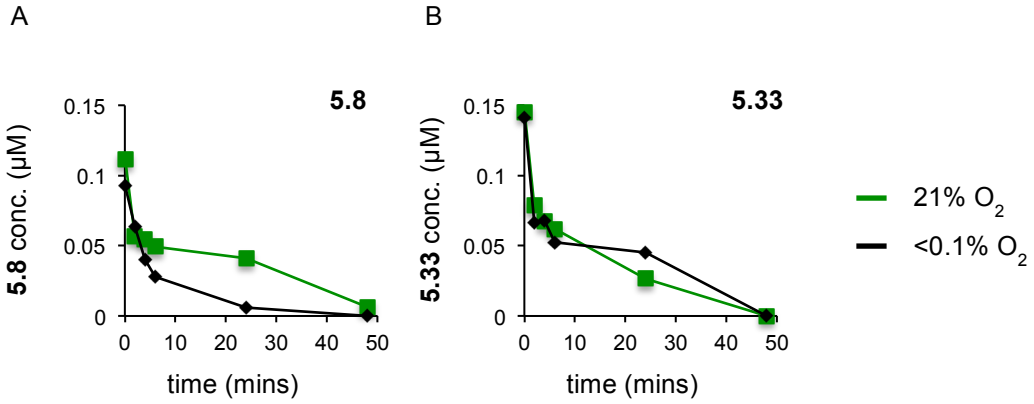

Figure 5.7. Graphs to show the concentrations of (A) **5.8** and (B) **5.33** following treatment with NADPH reductase enzymes under normoxic (21% O_2) and hypoxic (<0.1% O_2) conditions. Concentrations were determined by HPLC analysis from the assay volume.

It was hypothesised that the compounds were aggregating to the protein in solution. Cyclodextrins are commonly used to enhance the solubility of compounds in biochemical assays and prevent such interactions.[95] Consequently, **5.8** and **5.33** were treated with NADPH reductase enzymes in the presence of 100 μM α-cyclodextrin (**Figure 5.8**). Analysis of compound concentration by HPLC revealed an improvement in the solubility over the assay time course. However, reduction metabolites could not be detected by HPLC analysis even at extended time points of 24 and 48 hours (later time points not shown).

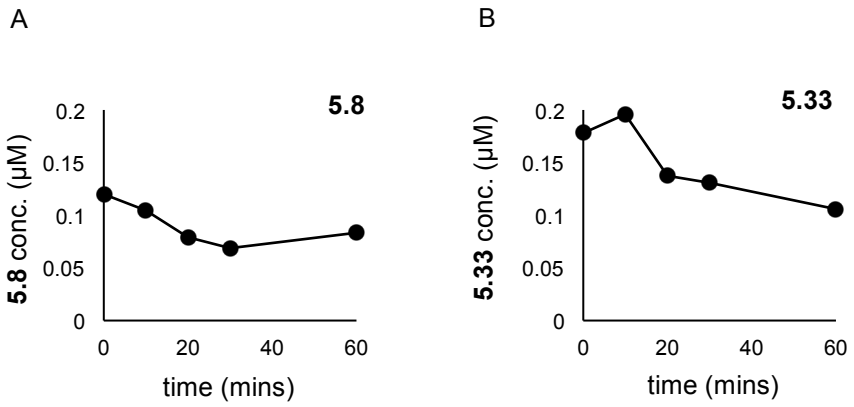

Figure 5.8. Graphs to show the concentration of (A) **5.8** and (B) **5.33** following treatment with NADPH reductase enzymes and α-cyclodextrin (100 μM) under hypoxic (<0.1% O_2) conditions.

The absence of reduction metabolites suggested that both compounds **5.8** and **5.33** were not substrates for NADPH reductase enzymes, or that they aggregated in solution preferentially, or crashed out when not associated with cyclodextrin. Consequently, the crystal structure of human NADPH reductase (PDB ID: 3QE2) was considered (**Figure 5.9**).[303] The enzyme is a homodimer, in which each protein units binding site contains three co-factors: NADPH, FAD, and FMN (**Figure 5.9A**). The nicotinamide moiety of NADPH is disordered, and consequently, only the adenosine diphosphate (ADP) moiety is observed in the crystal structure (**Figure 5.9B**). The crystal structure suggests the binding pocket of subunit B is more solvent exposed, and consequently, this pocket was selected for consideration in docking studies (**Figure 5.9**).

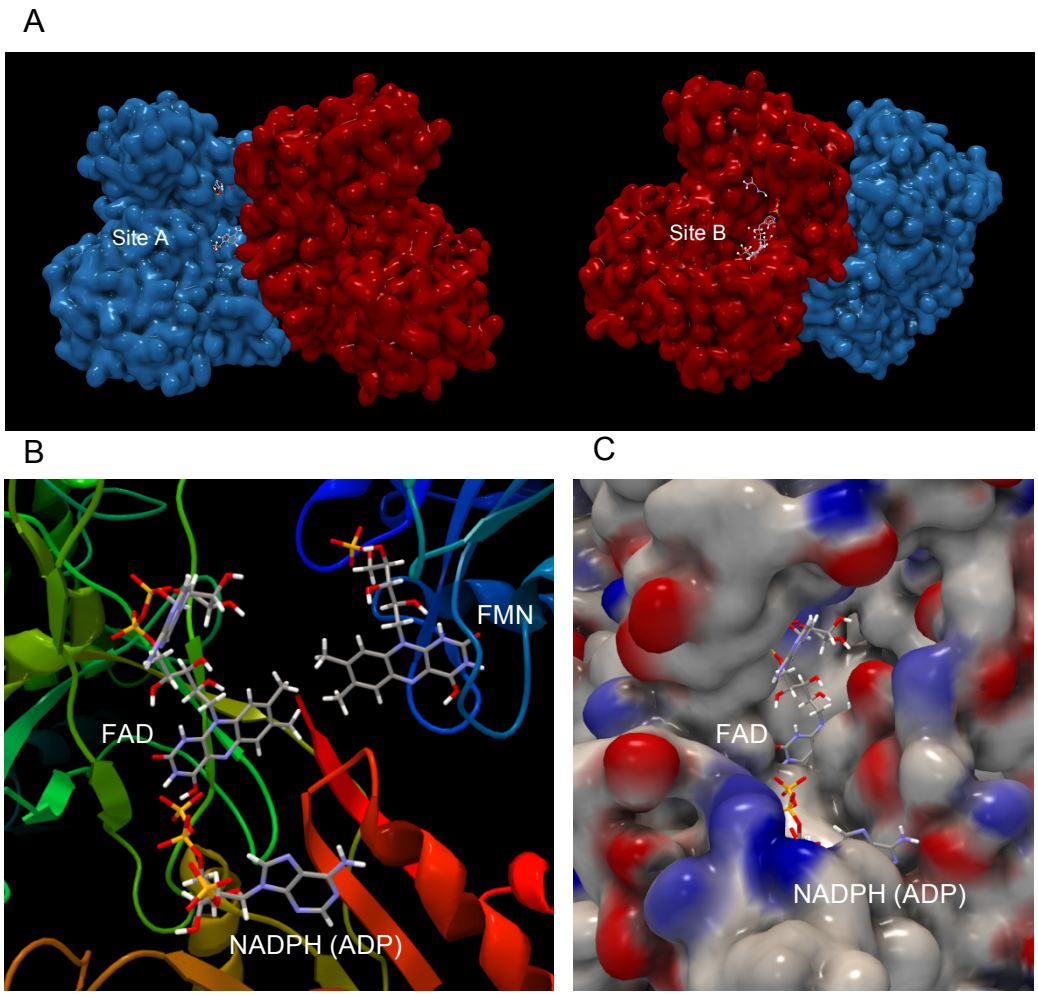

Figure 5.9. (A) Crystal structure of homodimeric NADPH reductase, and the binding sites of each constituent protein subunit. Protein represented by space filling; (B) Binding domain of subunit B. Co-factors are NADPH, FAD, and FMN. PDB ID: 3QE2.[303] NADPH is disordered in the crystal structure, and hence ADP is shown; (C) Charge surface representation of binding domain B; red positive, blue negative, white hydrophobic region. NADPH and FAD are more solvent exposed in the binding site than FMN.

The precise mechanism of NADPH reductase-mediated electron transfer to nitro groups is unclear.[17] However, the broader activity of NADPH reductase is reported to proceed *via* reduction of FAD by NADPH.[17] The resulting $FADH_2$ species is then capable of acting as a one, or two electron donor.[54,304] The cofactor FMN binds more deeply in the protein structure, and therefore is likely to be less accessible (**Figure 5.9C**). Therefore, it was hypothesised that reduction of bioreductive nitroaryl groups occurs *via* reduced FAD (**Scheme 5.16**). Assuming the mechanism proposed is

plausible, the proximity of the nitro group to FAD would be important for efficient electron transfer. The nitrogen at the 4-position, which was considered in subsequent docking studies, is highlighted in red.

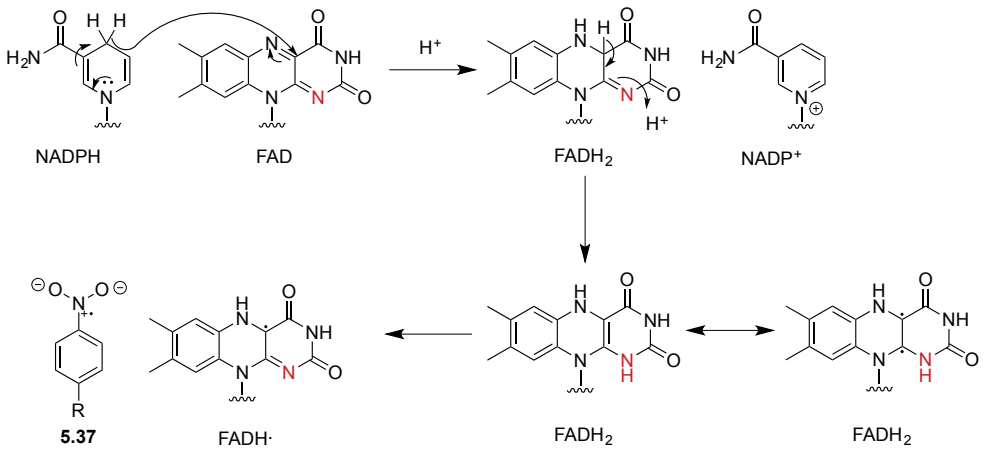

Scheme 5.16. Possible mechanism of reduction of a nitroaromatic group in the binding domain of NADPH reductase. Reduction of FAD by NADPH affords intermediate $FADH_2$, which can act as a one or two electron reductant.[54] Nitroaromatic bioreductive groups are possibly reduced by $FADH_2$ to give radical species **5.37**. The nitrogen at the four position, considered in subsequent docking studies, is highlighted in red.

Docking is a computational method for evaluating the interactions between two molecules, including ligands and proteins, and has widely been used in preliminary ligand screening studies.[305] Consequently, docking of compounds **5.8** and **5.33** into the binding site of NADPH reductase was evaluated, and results in which the bioreductive nitroaromatic group was in the proximity of FAD were considered (**Figure 5.10**). CLC Drug Discovery Workbench version 3.0 was the docking software used, and the docking site radius was 13 Å.

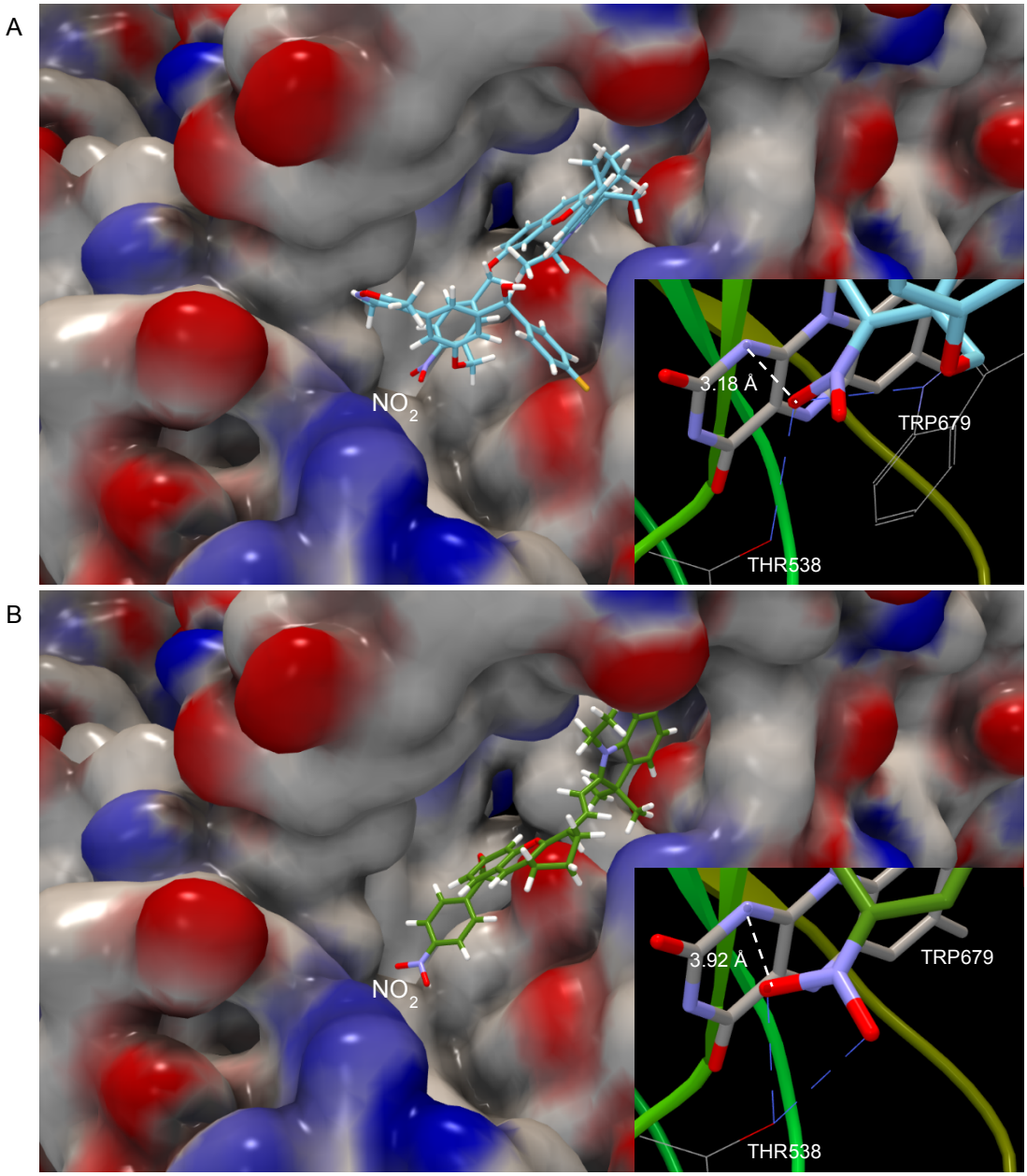

Figure 5.10. Docking results of (A) **5.8** and (B) **5.33** in the binding domain of NADPH reductase where the nitroaromatic bioreductive group is orientated towards the cofactor FAD. Insets show hydrogen bonding interactions of the nitro groups (blue dashed lines), and their respective distances to nitrogen at the four position of FAD, a likely site of electron transfer.[54] Calculations were made omitting the presence of NADPH.

The distance between the nitro group and the indicated nitrogen of FAD were calculated to be 3.91 Å and 3.18 Å for **5.8** and **5.33**, respectively, both of which are within ranges of electron transfer.[304] The docking calculations suggest both compounds **5.8** and **5.33** are plausible substrates for NADPH reductase, but offer no comparison to the likelihood of this binding

interaction. Consequently, identical calculations were performed on known substrates; CH-01 **1.35** and TH-302 **1.26**, and the binding affinities of similar nitro group conformations compared to **5.8** and **5.33** (**Table 5.1**).[47,72]

Table 5.1. Scores from docking results of the indicated compounds in binding conformations where the nitroaryl group is proximal to the cofactor FAD.

Compound	Flexible Bonds	H bond score	Steric interaction score	Ligand conformation penalty	Distance $N\text{-}NO_2$ (Å)	Overall
5.8	12	−7.14	−43.41	9.82	3.179	-40.72
5.33	7	−3.67	−42.21	5.06	3.915	-46.82
TH-302 **1.26**	10	−8.19	−34.56	6.42	2.871	−36.33
CH-01 **1.35**	9	−6.0	−37.26	6.10	4.634	−37.16

The more negative the overall score, the more favourable binding is predicted to be. Interestingly, compounds **5.8** and **5.33** were predicted to be stronger binders in this conformation than **1.26** and **1.35**. However, it should be noted that these calculations are a model, and it is likely binding parameters are inaccurate and do not take into account desolvation energies. In spite of this, the docking results indicate that both **5.8** and **5.33** are predicted to be substrates of NADPH reductase, and their access the binding pocket is not sterically prohibited. Therefore, given these results, **5.8** and **5.33** are plausible substrates of NADPH reductase, it is likely the compounds aggregated in solution, and consequently underwent no enzyme-mediated bioreduction.

5.4.3 *In vitro* analysis

Despite the unsuitability of **5.8** and **5.33** for use in the NADPH reductase assay, the compounds were progressed to *in vitro* cellular reduction assays. Human colorectal RKO cells have been shown to be a suitable cell line for evaluation of bioreductive compounds in hypoxia.[47] Consequently, RKO cells were treated with compounds **5.8** and **5.33** for 24 hours, and the cell lysate analysed by HPLC for metabolites (**Figure 5.11**). No metabolites corresponding to reduction of the nitro group of **5.33** were detected in cells under normoxic or hypoxic conditions. However, cells treated with **5.8** under hypoxic conditions revealed the presence of the reduced amino compound **5.10**, fragmentation intermediate **5.11**, and NIR dye **5.1** (**Figure 5.11A**). These products were absent when cells were treated with **5.8** under normoxic conditions (**Figure 5.11A**).

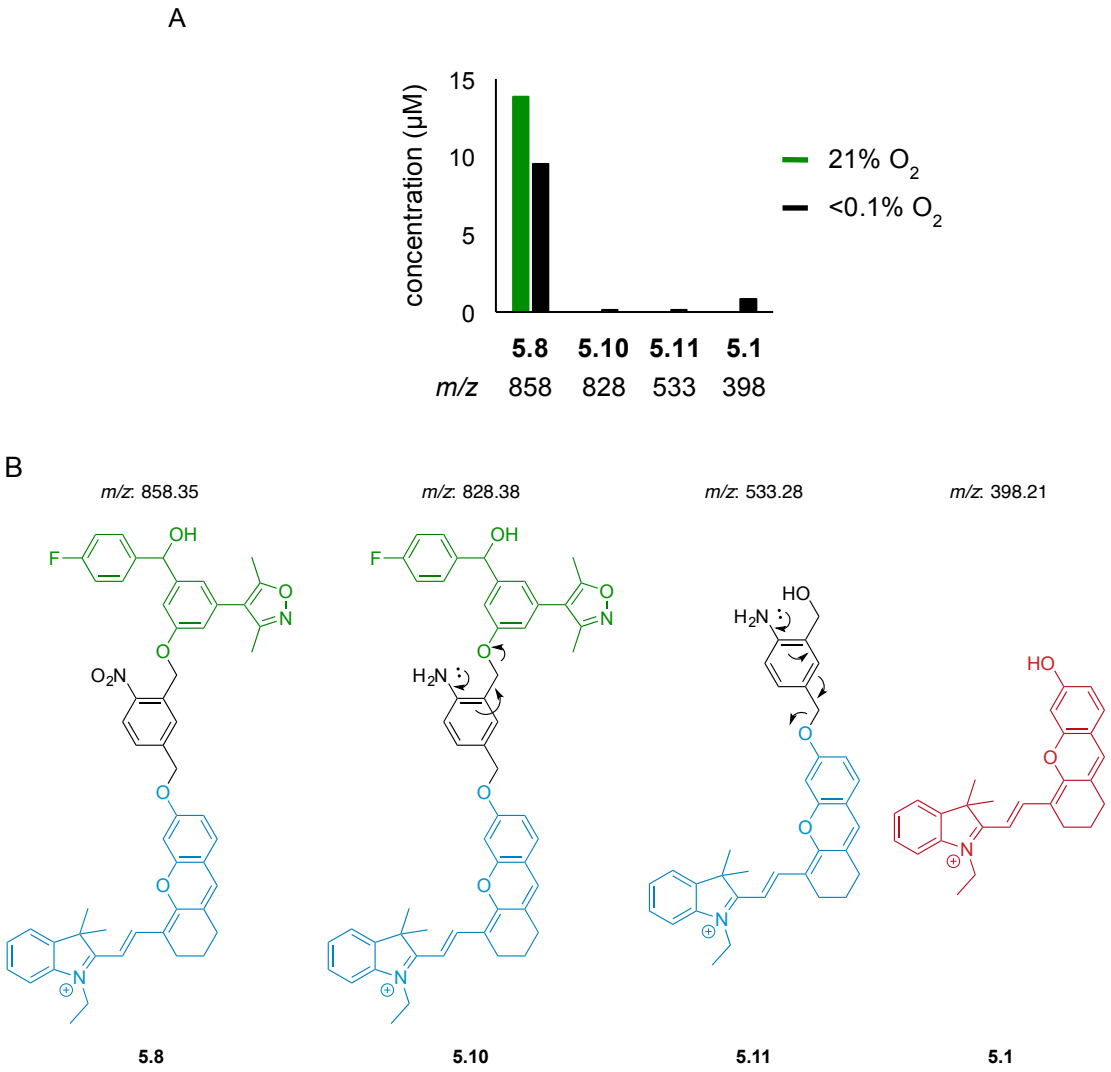

Figure 5.11. (A) Bar chart to show cell lysate concentrations of the indicated compounds following treatment with **5.8** for 24 h. The LCMS mass to charge ratios (*m/z*) of the peaks used to positively identify metabolites are also shown. The UV absorption (610 nm) of metabolites **5.10** and **5.11** is assumed to be the same as **5.8** (B) Chemical structures of compounds observed by LCMS.

These data indicate **5.8** was cell permeable, and undergoing the proposed oxygen-sensitive bioreductive pathway to the amine **5.10**, inducing fragmentation to release BET bromodomain inhibitor **5.13** and NIR dye **5.1** (**Scheme 5.3**, Page 140). Despite the BET bromodomain inhibitor **5.13** not being detected by LCMS analysis, the presence of fragmentation intermediate **5.11** is indicative that **5.13** is released as proposed. BET bromodomain inhibitor **5.13** is a poor chromophore compared to NIR dye **5.1**, making its

visualisation by HPLC at comparable concentrations difficult. To the best of our knowledge, this is the first demonstration of a nitrobenzyl bioreductive group fragmenting at two, distinct positions to deliver two, different cargo molecules. However, the concentration of **5.8** remained dominant in the cell lysate, indicating the reduction and fragmentation process was inefficient.

5.5 Fluorescence Evaluation

5.5.1 Fluorimetry

The NIR dye **5.1** is reported to have a maximum λ_{abs} at 690 nm, corresponding to a fluorescence maximum at λ_{em} 716 m (pH 7.4 PBS/MeOH 1:1).[156] The fluorescence spectra of NIR dye **5.1**, **5.8** and **5.33** were subsequently recorded and compared (**Figure 5.12A**). In our hands, the fluorescence emission intensity was greatest at λ_{ex} 670 nm in MeOH/PBS, rather than 690 nm as reported.[156] As previously discussed (**Chapter 4.7.2**, Page 124), fluorescence spectra in ^{i}PrOH may be a good indication of fluorescence observed by confocal microscopy. Evaluation of fluorescence in ^{i}PrOH revealed maximum fluorescence emission intensity of NIR dye **5.1** when excited at 690 nm (**Figure 5.12B**). Critically, in both solvents, **5.8** and **5.33** exhibited negligible fluorescence emission compared to **5.1**, indicating their suitability for use as fluorogenic molecules. Where the phenol position is alkylated as in **5.8** and **5.33**, fluorescence is quenched, and is only restored when fragmentation occurs to release free phenol **5.1**.

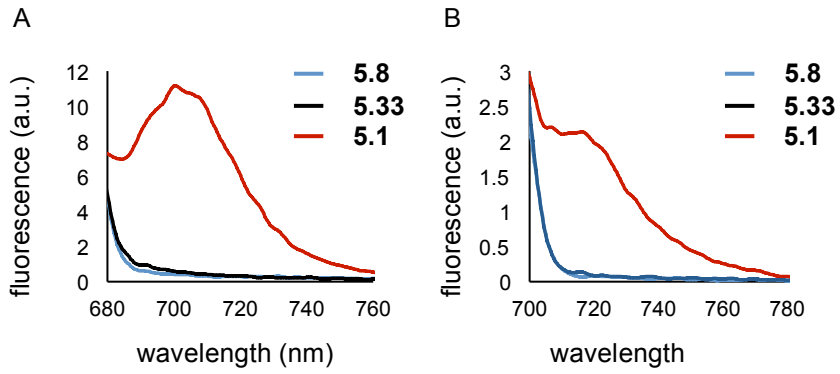

Figure 5.12. Fluorescence emission spectra of compounds **5.8**, **5.33**, and **5.1**. (A) λ_{ex}: 670 nm, pH 7.4, 1:1 PBS/MeOH; (B) λ_{ex}: 690 nm, ^{i}PrOH.

5.5.2 Confocal microscopy

It was unclear whether compound **5.1** would be suitable for use in confocal microscopy as the excitation wavelength required (670-690 nm) exceeded the longest wavelength laser (633 nm) available to us at the time of writing. Confocal fluorescence microscopy with compounds **5.8**, **5.33**, and **5.1** could reveal useful information about their membrane permeability. It was hypothesised that the inefficiency of reduction and fragmentation observed *in vitro* (**Chapter 5.4.3**, Page 160) was a consequence of the compounds being stuck in the cell membrane. Fluorometric analysis suggested that employing a λ_{ex} of 633 nm (the longest wavelength confocal laser available) the fluorescence emission intensity of **5.1** would still be greater than **5.8** or **5.33** (**Figure 5.13A**). However, treatment of RKO cells with each compound independently did not afford the expected enhanced fluorescence for NIR dye **5.1** (**Figure 5.13**, **B-D**).

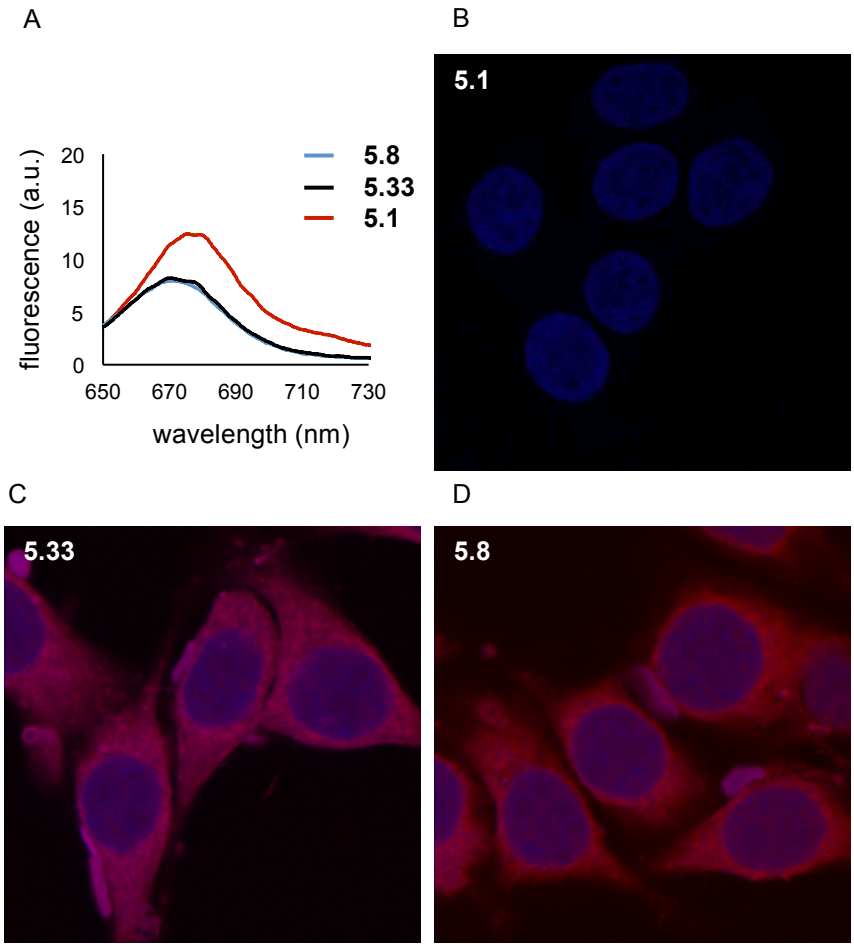

Figure 5.13. (A) Fluorescence emission spectra of compounds **5.8**, **5.33**, and **5.1** in ^{i}PrOH, λ_{ex}: 633 nm. (B-D) Fluorescence confocal microscopy images of RKO cells treated with 1 μM (B) **5.1**, (C) **5.33**, and (D) **5.8** for 3 h under normoxic conditions. λ_{ex}: 633 nm. Nuclei were stained with DAPI (blue).

The images obtained suggested that NIR dye **5.1** had reduced cell permeability compared to compounds **5.33** and **5.8**, and therefore fluorescence was not detected (**Figure 5.13B**). If **5.1** is not cell membrane permeable, this may be advantageous when released from **5.8** under hypoxic conditions, as the NIR dye **5.1** would remain trapped inside cells. Fluorescence distribution throughout the cell cytoplasm indicated both **5.33** and **5.8** were membrane permeable, and also possibly nuclear membrane permeable (**Figure 5.13**, **C-D**). Given **5.8** fragments to release a BET

bromodomain inhibitor upon reduction, localisation in the nucleus is a favourable area for delivery of its therapeutic cargo.

5.6 Conclusions

Prior to this study, it was unclear whether nitrobenzyl bioreductive groups could be modified to fragment to deliver two distinct cargo molecules from a single bioreductive core, following reduction under hypoxic conditions. Compound **5.8** was synthesised for biological evaluation as a fluorogenic bioreductive molecule, which fragmented to release a BET bromodomain inhibitor **5.13**, and a near infrared fluorophore **5.1**. Treatment of RKO cells with **5.8** revealed reduction of the nitrobenzyl group exclusively under hypoxic conditions. Furthermore, the amino species fragmented to release both the BET bromodomain inhibitor, and the NIR dye. However, the concentration of the reduction products of **5.8** detected in RKO cells was a small fraction (approximately 5%) of the overall dose. Consequently, methods for improving the reduction and fragmentation of **5.8** need to be considered. Possible methods for achieving this are discussed in **Chapter 6.2** (Page 167).

Chapter 6

GENERAL DISCUSSION AND FUTURE WORK

6.1 Conclusions

The aim of this study was to develop a fluorogenic, bioreductive group, suitable for selective delivery of a cargo molecule of therapeutic interest, under hypoxic conditions. The first example of fluorogenic bioreductive group to target hypoxia **2.9**, based on 6-Nitroquinoline, was designed and synthesised. A novel fluorogenic HAP **2.49** was synthesised, and shown to release a BET bromodomain inhibitor **2.48**, following enzymatic reduction under hypoxic conditions (**Figure 2.7**, Page 63). Under normoxic conditions, the fluorogenic bioreductive group remained stable with respect to hydrolysis. Reduction of **2.49** to the amino derivative **2.51** led to an increase in fluorescence intensity, demonstrating **2.49** is fluorogenic (**Figure 2.13**, Page 69). This work subsequently led to the submission of a patent application (**Appendix A.2**).

Consideration of a fluorogenic bioreductive group, with improved spectrophotometric properties for biomedical imaging, led to the evaluation of NIR dye **3.1** (**Scheme 3.2**, Page 78). Synthesis of the nitro derivative **3.2** was synthetically challenging, but despite this, spectroscopic data indicated the desired molecule was made. The poor solubility of **3.2** and lack of absolute

characterisation resulted in the compound not being progressed for further evaluation. However, synthesis of the azide derivative **3.29** provided an opportunity to investigate the utility of azides in hypoxia-targeted molecules (**Scheme 4.3**, Page 103). The oxygen dependent reduction of azide **3.29** occurred with a variety of human cytochrome P450 enzymes (**Figure 4.7**, Page 114). Furthermore, similar oxygen-dependent reduction was observed in human cancer cell lines in a variety of 2D and 3D tumour models. These results have implications for the use of azides in other cell-based assays, and to our knowledge are the first demonstrations of exploiting oxygen-dependent reduction of azides to target hypoxia in cancer.

Further work to improve the imaging properties of a fluorogenic HAP led to the synthesis and biological evaluation of cyanine derivatives (**Scheme 5.3**, Page 140). Treatment of human cancer cells under hypoxic conditions with a novel fluorogenic HAP **5.8**, revealed selective delivery of NIR dye **5.1** and BET bromodomain inhibitor **5.13** (**Figure 5.11**, Page 161). This work demonstrated the first indication that a nitrobenzyl bioreductive core could be modified to fragment twice, delivering two different cargo molecules. However, the efficiency of the reduction and fragmentation was shown to be capricious, and therefore requires optimisation.

6.2 Improving properties of fluorogenic HAPs

6.2.1 Considering compound delivery and concentration

One challenge facing development of fluorogenic HAPs is reconciling the concentration of cargo molecule required to cause a phenotypic effect (inhibition of a protein target, toxicity or otherwise), with the sensitivity of the

fluorescent group for imaging. To have maximal effect, cargo molecules with high potency against their targets, in combination with excellent quantum yield, far-NIR emitting, fluorescent dyes is desirable. Designing fluorogenic HAPs with these considerations in mind, will potentially minimise the dose required in preclinical studies.

6.2.2 Considering preclinical and clinical applications

ICG **1.41** is currently one of only two clinically approved NIR dyes for use in biomedical imaging (**Figure 5.1**, Page 136).[137] However, ICG **1.41** has its limitations, including poor pharmacokinetic profile, and poor quantum yield.[142] Consequently, new dyes are urgently required for improved optical imaging in the clinic. Many new NIR dyes have undergone preclinical evaluation, but progression to the clinic has thus far not been investigated.[306]

Considering preclinical applications, fluorogenic HAPs could ultimately be useful tools for detailed examination of *in vivo* xenograft sections, enabling study of the biodistribution of HAPs throughout a hypoxic tumour. Interrogation of HAP cellular permeability and localisation could positively inform the design of future HAPs.

6.2.3 Considering delivery of the cargo molecule

Dyes which fluoresce towards, or within, the NIR are highly conjugated, and often electron deficient aromatic systems. As the aromatic system increases in size, the efficiency of fragmentation to release a cargo molecule is compromised (**Figure 5.2**, Page 138). Alternative fragmentation modalities may need to be considered to improve fragmentation kinetics. Delivery of cargo molecules may be improved by introducing ring closing mechanisms

(**Scheme 6.1**), or improving thermodynamic favourability for fragmentation by introduction of carboxy linkers (**Scheme 6.2**).[206]

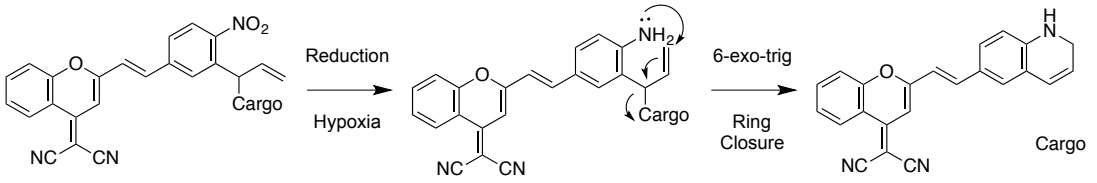

6.1 **6.2** **6.3**

Scheme 6.1. Reduction of nitro **6.1** to the corresponding amine **6.2**, could enable a 6-exo-trig ring closure, favoured by Baldwin's rules, to eliminate the cargo molecule and form hydro-quinoline derivative **6.3**.[307]

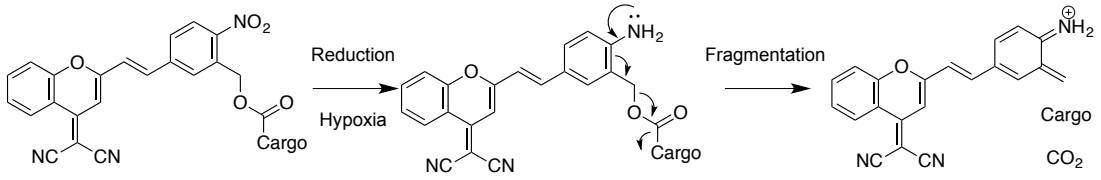

6.4 **6.5** **6.6**

Scheme 6.2. Reduction of nitro **6.4** to the corresponding amine **6.5** results in fragmentation to release the cargo molecule, and is entropically favoured by concomitant elimination of carbon dioxide.

It is generally accepted that fragmentation of HAPs to release a cargo molecule, is favoured by decreasing the pKa of the leaving group.[48] However, to date, there has been no detailed analysis comparing the pKa of a leaving group with the rate of fragmentation. Furthermore, the variation in fragmentation rates to release a cargo molecule, with different bioreductive groups has not been investigated. Such information would be extremely useful in selecting suitable molecules for development into molecularly targeted HAPs.

The studies detailed in this dissertation focus on the utility of bioreductive groups which following bioreduction in hypoxia, become fluorescent and fragments to release a biologically active cargo molecule.

Detecting activation of such fluorogenic HAPS by fluorescence does not preclude that the molecule has not yet fragmented, and consequently the cargo molecule remains biologically inactive. Development of fluorogenic HAPs that become fluorescent following fragmentation, rather than following bioreduction, would improve our understanding of delivery of the cargo molecules in hypoxic tumours.

6.2.4 Considering alternative imaging modalities

Fluorescence imaging is a powerful modality for interrogating biological systems. Recently, with the advent of novel microscopes, fluorescence has found clinical applications in guiding surgeons during procedures, and in *in vivo* imaging.[129] Fluorescent dyes offer a relatively low cost method for visualising tissues, but their application is limited by the relatively poor tissue penetrability (mm-cm), meaning only superficial tissues can be visualised.

Future development of HAPs may benefit from incorporation of alternative imaging modalities, such as PET or MRI. Many bioreductive PET agents have already undergone clinical evaluation, indicating their combination with drug delivery may be a favourable avenue for investigation (**Figure 6.1**).[126] For example, the clinical candidate TH-302 **1.26** could be modified to incorporate the structure of clinical PET tracer FMISO **1.38** to afford **6.6**. More recently, the demonstration of oxygen-enhanced MRI opens a window of opportunity for utilising another powerful and widely used biomedical imaging method for the development of imagable HAPs to target hypoxia.[308]

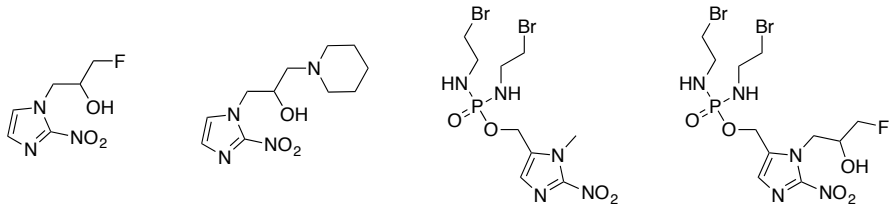

1.38 **1.37** **1.26** **6.6**

Figure 6.1. Chemical structures of clincal hypoxia-activated PET tracer FMISO **1.38**, hypoxia-marker pimonidazole **1.37**, clinical candidate TH-302 **1.26**, and proposed modified TH-302 **6.6** to make the 2-nitroimidazole bioreductive group a potentially useful PET tracer.

6.3 Concluding remarks

Fluorogenic hypoxia-activated prodrugs have the potential to be powerful informative tools to evaluate tumour hypoxia, but also to simultaneously treat tumours. The success of these therapies in the clinic hinges on successfully identifying patients will be sensitive to treatment by better understanding their biodistribution in a tumour, and the oxygenation of the tumour regions they occupy. Fluorogenic, or more generally, HAPs that can be imaged, provide an avenue for doing this. Current methods employed in small-scale studies, involve separate administration of a hypoxia-tracer, followed by the HAP, ignoring the distinct pharmacokinetic profiles of the individual molecules.[125] Combining imaging and therapy, will be an important step forward in improving delivery and treatment of hypoxic tumours.

Chapter 7

EXPERIMENTAL METHODS

7.1 General Chemistry

7.1.1 NMR Spectroscopy

^{1}H NMR spectra were recorded on Bruker DPX400 (400 MHz), Bruker DQX400 (400 MHz), Bruker AVC500 (500 MHz), Brucker AV700 (700 MHz) or Bruker AVG400 (400 MHz) spectrometers using deuterochloroform (unless indicated otherwise) as a reference for the internal deuterium lock. The chemical shift data for each signal are given as δ_H in units of parts per million (ppm) relative to non-deuterated trace solvent.[309] The multiplicity of each signal is indicated by s (singlet); d (doublet); dd (doublet of doublets), ddd (doublet of doublet of doublets), t (triplet), tt (triplet of triplets), q (quartet), qn (quintet), sp (septet), or m (multiplet). The number of protons (n) for a given resonance signal is indicated by nH. Coupling constants *J* are quoted in Hz and are recorded to the nearest 0.1 Hz. Identical proton coupling constants *J* are averaged in each spectrum and reported to the nearest 0.1 Hz. The coupling constants are determined by analysis using Bruker TopSpin software. Spectra were assigned using COSY, HSQC and HMBC experiments, as necessary.

^{13}C NMR spectra were recorded on a Bruker AVC500 (126 MHz) spectrometer in the stated solvents, with broadband proton decoupling and an internal deuterium lock. The chemical shift data for each signal are given as δ_C in units of parts per million (ppm) relative to trace non-deuterated solvent.[309] The shift values of resonances are quoted to 1 decimal place, and were determined using Bruker TopSpin software. Where appropriate, coupling constants *J* are quoted in Hz and are recorded to the nearest 0.1 Hz. ^{13}C spectra were assigned using 2D NMR experiments including COSY, HMBC and HSQC.

^{19}F NMR spectra were recorded on a Bruker AVB500 (470 MHz), Bruker AVF400 (376 Hz), AVH400 (376 Hz) or Bruker AVN400 (376 MHz) spectrometer using a broadband proton decoupling pulse sequence and deuterium internal lock. The chemical shift for each signal are given as δ_F in units of parts per million (ppm) relative to trifluoromethane where δ_F = 0.00 ppm.

7.1.2 Mass Spectrometry

Spectra were acquired on a Micromass LCT Premier Spectrometer, VG platform spectrometer, or Agilent 6120 spectrometer (low resolution). Electrospray ionisation spectra were obtained on Micromass LCT Premier and Bruker MicroTOF spectrometers, operating in positive or negative mode as indicated, from solutions of MeOH or MeCN. *m/z* values are reported in Daltons and followed by their percentage abundance in parentheses. Electron ionisation/field ionisation (EI/FI) was carried out on a Waters GCT with a temperature programmed solids probe inlet. Samples were introduced in glass tips directly into the source where they were vaporised and analysed. In

EI the ionisation is by electron impact, electrons being provided by a filament. In FI the ionisation is in an intense electric field that causes quantum electron tunnelling of a valence electron.

7.1.3 Melting points

Melting points were determined using a Leica Galen III hot stage microscope and are uncorrected. The solvents of crystallisation are shown in parentheses.

7.1.4 Infrared spectra

Infrared (IR) spectra were obtained from neat samples, either as solids or liquids using a diamond ATR module. The spectra were recorded on a Bruker Tensor 27 spectrometer. Absorption maxima are recorded in wavenumbers (cm^{-1}), and reported as s (strong), m (medium), w (weak) or br (broad).

7.1.5 Analytical thin layer chromatography

Thin layer chromatography (TLC) was carried out on normal phase Merck silica gel 60 F_{254} aluminium-supported chromatography sheets. Visualisation was by absorption of UV light (λ_{max} 254 and 365 nm), or thermal development after dipping in one of: (a) ethanolic phosphomolybdic acid (PMA) or ninhydrin; (b) aqueous potassium permanganate, potassium carbonate and sodium hydroxide.[310]

7.1.6 Silica gel flash column chromatography

Silica gel flash column chromatography was performed manually using VWR Prolabo silica gel 60 (240-400 mesh) under a positive pressure of nitrogen.

7.1.7 Concentration *in vacuo*

In vacuo refers to the removal of solvent under reduced pressure using a Büchi™ rotary evaporator.

7.1.8 Chemicals

Chemicals were purchased from Sigma Aldrich UK, Fisher Scientific and Alfa Aesar UK, and were used as supplied unless otherwise stated. PE refers to the fraction of light petroleum ether boiling within the range of 40-60 °C. Brine refers to a saturated aqueous solution of sodium chloride.

7.1.9 Solvent purification

Anhydrous solvents were obtained under the following conditions: Diethyl ether, toluene, dichloromethane and tetrahydrofuran were dried by passing through a column of activated basic alumina according to the Grubbs' procedure.[311] Anhydrous *N,N*-Dimethylformamide and methanol were purchased from Sigma Aldrich UK in SureSeal™ bottles and used without further purification. All other solvents were used as supplied (analytical or HPLC grade) without purification. Anhydrous tetrahydrofuran (THF) was distilled from sodium metal, using benzophenone as an indicator.[312] Degassed *tert*-butanol was obtained using a freeze-thaw procedure under vacuum.

7.1.10 Compound purity

Compound purity was determined by HPLC, and was carried out on a Waters system (2695 pump/autosampler 2996 diode array detector and ZQ2000 mass spectrometer). The column was a Hichrom RPB, 5 μm, 100 × 3.2 mm at 35 °C. The purity of compound **5.26** was determined on a Waters

XSelect CSH C18 XP, 2.5µm, 100 x 2.1 mm, at 35 °C. Unless otherwise stated, the elutants were 10 mM formic acid in Millipore H_2O (A), and acetonitrile (B), and the flow rate was 0.5 mL/min. Compound purities were determined at a UV absorbance of 254 nm, unless indicated otherwise.

Microanalyses were obtained from the Elemental Analysis Service, London Metropolitan University, London. The experimental elemental percentages were required to be within ±0.3 of the predicted elemental percentages.

7.1.11 HPLC analysis of assay solutions

Aliquots taken from chemical and biological assays were evaluated on the same system as that described in **Chapter 7.1.10**. For each sample, UV spectra were collected between 260-800 nm, and mass spectra collected for *m/z* ratios from 260-900. These ranges were reduced where appropriate. The injection volume for each sample was 25 µL.

Concentrations of compounds in assay aliquots were determined by means of calibration curves. Calibration curves were obtained from solutions of each compound in DMSO (1-2 mM) and were diluted in MeCN. The final concentrations were 5 µM, 2.5 µM, 1.25 µM, 0.625 µM, 0.3125 µM, and 0.15625 µM. The peak area for each concentration was plotted against concentration, and a line of best fit introduced, such that the intercept was 0.

Table 7.1 describes the methods of HPLC elution for each compound. The peak area for each compound was evaluated at the indicated wavelength (λ_{vis}). Unless otherwise indicated, elutant A refers to 10 mM formic acid in Millipore H_2O, and elutant D refers to acetonitrile. Together, A and D make

100% of the elutant. In all cases, after the 6 min gradient had finished, %D final was held for 2 min, followed by an immediate return to %D Start for 2 min. The overall run time per sample was, therefore, 10 min. The flow rate was 0.5 mL/min.

Table 7.1. Tables of conditions used for HPLC analysis

Compound	Gradient (%D Start→%D Final)	λ_{vis} (nm)
2.48	30→95	254
2.49	30→95	254
3.1	30→95	420
3.29	30→95	420
5.1	50→95	610
5.8	50→95	610
5.13	30→95	254
5.33	50→95	610

7.1.12 Fluorometric analysis

Fluorescence spectra were obtained using a Perkin Elmer LS 50 B luminescence spectrometer. Samples were evaluated in a 1 mL quartz cuvette, and excited at the indicated wavelength.

7.1.13 Zinc reduction assay

Zinc reduction was performed using zinc dust (Sigma-Aldrich), ammonium chloride (Fisher Scientific), DMF (Sigma-Aldrich), DMSO (Sigma-Aldrich), and 2-Propanol (^{i}PrOH, Sigma-Aldrich). T=0 refers to the aliquot/fluorescence spectrum taken before the addition of zinc dust. Two methods were used:

(a) HPLC analysis method: To a solution of **2.49** (1 mg, 0.002 mmol, 1 eq.) in DMF (2 mL), was added aq. NH_4Cl (20 µL, 10% w/v) and zinc dust (4 mg, 0.061 mmol, 30 eq.). The reaction mixture was stirred at ambient temperature for 16 h. Aliquots (200 µL) were taken at the indicated time intervals, the solution centrifuged at 17000 × *g* to remove any sediment, and the supernatant analysed by HPLC. The same procedure was used for compounds **3.1**, **3.8** and **3.33**.

(b) Fluorometric analysis method: To a 1 mL quartz-cuvette containing ^{i}PrOH (850 µL) was added a DMSO solution of compound **3.29** (50 µL, 1 mM stock), and aq. NH_4Cl (100 µL, 1% *w/v*). Zinc dust (approximately 1 mg) was added to the solution, and fluorescence spectra were recorded at the indicated time intervals. The cuvette was physically shaken between time intervals. An excitation wavelength of 515 nm was used. The same procedure was used for compounds **3.1**, **3.8** and **3.33**.

7.1.14 Steady state radiolysis

A 1 mL solution of **3.29** (50 µM) in 1:1 *v/v* ^{i}PrOH and 4 mM $KHPO_4$ buffer (pH 7.4) was made. The solution was transferred to a glass HPLC vial (2.5 mL), sealed, and degassed for 15 min with N_2O gas. A T=0 aliquot (50 µL) was taken. The vial was irradiated for 6 min at 14 Gy/min, in a Caesium-137 GSR D1 irradiator (Gamma-service Medical GmbH, Leipzig, Germany) and aliquots (50 µL) taken at minute intervals. The aliquots were analysed by HPLC as described in **Chapter 7.1.11** (Page 176).

7.2 Synthetic Procedures

7.2.1 Chapter 2 compounds

2.1. 6-Nitroquinoline

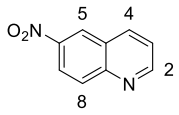

To a flame dried microwave vial under an argon atmosphere, 6-Chloroquinoline **2.22** (164 mg, 1.0 mmol, 1.0 eq.), $Pd_2(dba)_3$ (4.5 mg, 5.0 µmol, 0.5 mol%), ^{t}BuBrettPhos[175,313] (6 mg, 12.4 µmol, 1.2 mol%), and $NaNO_2$ (138 mg, 2.0 mmol, 2.0 eq.) were added. The vial was evacuated and backfilled with argon 3 times. Degassed ^{t}BuOH (2 mL), and TDA (*tris*(3,6-dioxaheptyl)amine) (16 µL, 16.2 mg, 50.0 µmol, 5 mol%) were syringed in. The reaction mixture was heated under reflux at 130 °C for 24 h, cooled to ambient temperature, and H_2O (10 mL) added. The organic components were extracted with EtOAc (3 × 10 mL), the organic phases combined, washed with H_2O (3 × 10 mL), dried over $MgSO_4$, filtered and concentrated *in vacuo*. The residue was adsorbed onto Celite® and the product purified by silica gel column chromatography, eluting with PE and EtOAc (20% EtOAc), to yield **2.1** (111 mg, 64%) as a colourless solid: R_f: 0.37 (EtOAc - PE 1:1); mp: 148-150 °C (EtOAc) [Lit. 149-151 °C][175]; ^{1}H (200 MHz, $CDCl_3$): 9.09 (1H, d, *J* 4.0, C_2H), 8.80 (1H, d, *J* 2.5, C_5H), 8.48 (1H, dd, J_1 9.2, J_2 2.5, C_7H), 8.37 (1H, d, *J* 8.3, C_4H), 8.26 (1H, d, *J* 9.2, C_8H), 7.58 (1H, dd, J_1 8.3, J_2 4.0, C_3H); LRMS: *m/z* (ES^+) 175.1 ($[M+H]^+$, 100%); This data is in good agreement with literature values.[175]

2.16. 5-(Bromomethyl)-6-nitroquinoline

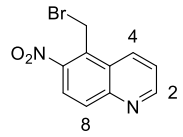

A solution of alcohol **2.17** (20 mg, 0.10 mmol, 1.0 eq.) in conc. aq. HBr (48% *w/v*, 0.2 mL) was stirred at 75 °C for 20 h. The reaction solution was cooled to ambient temperature, H_2O (10 mL) added, and adjusted to pH 7 with solid K_2CO_3. The organic components were extracted with EtOAc (3 × 3 mL), the organic phases combined, dried over $MgSO_4$, filtered and concentrated *in vacuo* to yield **2.16** (22 mg, 84%) as an orange crystalline solid: R_f: 0.33 (EtOAc - PE 1:1); mp: 112-114 °C (EtOAc); $\bar{\nu}_{max}$ (solid) cm^{-1}: 3089 (w, Ar CH), 1518 (s, NO_2 asym), 1343 (s, NO_2 sym); ^1H NMR (500 MHz, $CDCl_3$): 9.11 (1H, dd, J_1 4.2, J_2 1.6, C^2H), 8.67 (1H, d, J 8.7, C^4H), 8.24 (1H, s, J 9.2, C^8H), 8.14 (1H, d, J 9.2, C^7H), 7.70 (1H, dd, J_1 8.7, J_2 4.2, C^3H), 5.11 (2H, s, CH_2Br); ^{13}C NMR (126 MHz, $CDCl_3$): 153.3 (C^2), 149.5 (C^{8a}), 146.6 (C^6), 133.9 (C^4), 132.6 (C^8), 129.3 (C^5), 126.6 (C^{4a}), 124.4 (C^7), 123.1 (C^3), 22.6 (CH_2Br); HRMS: *m/z* (EI^+) [Found $(M[^{79}Br])^+$ 265.9686, $(M[^{81}Br])^+$ 267.9675. $C_{10}H_7BrN_2O_2$ requires $(M[^{79}Br])^+$ 265.9691, $(M[^{81}Br])^+$ 267.9670; LRMS: *m/z* (EI^+) 289.2 ($[M+Na]^+$, 100%); Anal. calculated for: C, 45.0; H, 2.6; N, 10.5; Found: C, 45.1; H, 2.8; N, 10.5.

2.17. (6-Nitroquinolin-5-yl)methanol

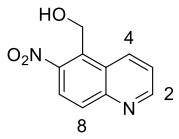

To a solution of aldehyde **2.36** (100 mg, 0.50 mmol, 1.0 eq.) in distilled THF (4 mL), $NaBH_4$ (9 mg, 0.50 mmol, 1.0 eq.) was added portion-wise at 0 °C and the reaction solution stirred for 15 min. MeOH (2 mL) and aq. HCl (1 mL, 1 M) were added and the reaction mixture concentrated *in vacuo*. The resulting residue was dissolved in EtOAc (15 mL), washed with H_2O (3 × 15 mL), sat. aq. $NaHCO_3$ (2 × 10 mL), dried over $MgSO_4$, filtered and concentrated *in vacuo*. The resulting residue was adsorbed onto Celite®, and the product purified by silica gel column chromatography, eluting with PE and EtOAc (40% EtOAc), to yield **2.17** (95 mg, 94%) as a pale yellow solid: R_f: 0.30 (EtOAc); mp: 139-141 °C (EtOAc); $\bar{\nu}_{max}$ (solid) cm^{-1}: 3102 (br, OH), 1601 (w, C=N), 1532 (s, NO_2 asym), 1324 (s, NO_2 sym); ^1H NMR (500 MHz, $CDCl_3$): 9.09 (1H, dd, J_1 4.2, J_2 1.6, C^2H), 8.79 (1H, d, J 8.7, C^4H), 8.23 (1H, d, J 9.2, C^8H), 8.11 (1H, d, J 9.2, C^7H), 7.65 (1H, dd, J_1 8.7, J_2 4.2, C^3H), 5.14 (2H, s, CH_2OH); ^{13}C NMR (126 MHz, $CDCl_3$): 153.2 (C^2), 149.6 (C^{8a}), 147.8 (C^6), 134.6 (C^4), 132.5 (C^5), 131.9 (C^8), 127.5 (C^{4a}), 123.7 (C^7), 123.2 (C^3), 55.7 ($C^{5'}$); HRMS: *m/z* (FI^+) [Found $(M)^+$ 204.0541, $(M[^{13}C])^+$ 205.0533. $C_{10}H_8N_2O_3$ requires $(M)^+$ 204.0535, $(M[^{13}C])^+$ 205.0565]; LRMS: *m/z* (ES^+) 205.1 ($[M+H]^+$, 100%); Anal. calculated for: C, 58.8; H, 4.0; N, 13.7. Found: C, 58.8; H, 3.8; 13.7.

2.18. (6-Chloroquinolin-5-yl)methanol

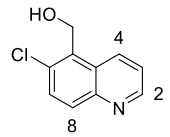

To a solution of **2.19** (1 g, 4.1 mmol, 1.0 eq.) in THF (10 mL), ^{i}PrMgCl (2 M soln. in THF, 2.47 mL, 4.9 mmol, 1.2 eq.) was added drop-wise at −10 °C. The solution was stirred for at −10 °C for 1 h, and DMF (1.6 mL, 20.5 mmol, 5.0 eq.) was added drop-wise. The reaction solution was stirred at 0 °C for 4 h, and then quenched by addition of EtOH (2 mL). $NaBH_4$ (160 mg, 4.1 mmol, 1.0 eq.) was added portion-wise at 0 °C, and stirred for 1 h at 0 °C. The reaction solution was quenched by addition of H_2O (6 mL) drop-wise over 5 min, and the reaction solution was concentrated *in vacuo*. The resulting slurry was extracted with EtOAc (3 × 30 mL), washed with sat. aq. $NaHCO_3$ solution (3 × 15 mL), brine (3 × 15 mL), dried over Na_2SO_4, filtered and concentrated *in vacuo*. The residue was adsorbed onto Celite®, and the product purified by silica gel column chromatography, eluting with PE, EtOAc and Et_3N (49% EtOAc, 1% Et_3N), and crystallised from $CHCl_3$ to yield **2.18** (403 mg, 55%) as colourless crystals: R_f: 0.50 (EtOAc); mp: 182-184 °C ($CHCl_3$); $\bar{\nu}_{max}$ (solid) cm^{-1}: 3142 (br, OH), 1486 (m, C=C); ^{1}H NMR (500 MHz, $CDCl_3$): 8.92 (1H, d, *J* 4.2, C^2*H*), 8.60 (1H, d, *J* 8.5, C^4*H*), 8.02 (1H, d, *J* 9.0, C^7*H*), 7.68 (1H, d, *J* 9.0, C^7*H*), 7.51 (1H, dd, J_1 8.5, J_2 4.2, C^3*H*), 5.28 (2H, s, C$^{1'}$*H*$_2$), 2.15 (1H, s, C$^{1'}$H$_2$O*H*); ^{13}C NMR (126 MHz, $CDCl_3$): 150.5 (C^2), 147.4 (C^{8a}), 133.3 (C^5), 133.1 (C^4), 132.7 (C^6), 131.5 (C^8), 130.9 (C^7), 128.4 (C^{4a}), 122.3 (C^3), 58.9 (C$^{1'}$); HRMS: *m/z* (ESI$^+$) [Found (M+H)$^+$ 194.0361. $C_{10}H_8ClNO$ requires (M+H)$^+$ 194.0367]; LRMS: *m/z* (ESI$^+$) 194.1 ([M+H]$^+$,

100%), 196.1 ([M+H]$^+$ 32%); Anal. calculated for $C_{10}H_8ClNO$: C, 62.0; H, 4.2; N, 7.2. Found: C, 62.1; H, 4.2; N, 7.2.

2.19. 6-Chloroquinoline-5-carbaldehyde

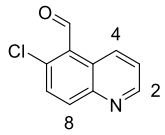

To a solution of **2.21** (500 mg, 2.1 mmol, 1.0 eq.) in anhydrous THF (5 mL), was added ^{i}PrMgCl (2 M in THF, 1.03 mL, 2.1 mmol, 1.0 eq.) drop-wise at 0 °C. The solution was stirred at 0 °C for 1 h, and DMF (0.8 mL, 10.3 mmol, 5.0 eq.) was added drop-wise. The reaction solution was gradually warmed to ambient temperature over 18 h, and then quenched by addition of H_2O (10 mL). The organic components were extracted with EtOAc (2 × 50 mL), the organic phases combined, washed with brine (2 × 50 mL), dried over Na_2SO_4, filtered, and concentrated *in vacuo*. The residue was adsorbed onto Celite®, and the product purified by silica gel column chromatography, eluting with PE and EtOAc (gradient, 0-100% EtOAc). The product was crystallised from Et_2O to yield **2.19** (91 mg, 23%) as yellow crystals: R_f: 0.78 (EtOAc - PE 1:1); mp: 124-126 °C (Et_2O); $\bar{\nu}_{max}$ (solid) cm^{-1}: 1683 (s, C=O), 1490 (m, C=C); ^{1}H (500 MHz, $CDCl_3$): 10.86 (1H, s, C^{5}C*H*O), 9.45 (1H, dd, J_1 8.8, J_2 1.5, C^2*H*), 8.96 (1H, dd, J_1 4.2, J_2 1.5, C^4*H*), 8.26 (1H, d, J 8.9, C^8*H*), 7.74 (1H, d, J 8.9, C^7*H*), 7.58 (1H, dd, J_1 8.8, J_2 4.2, C^3*H*); ^{13}C NMR (126 MHz, $CDCl_3$): 192.2 (*C*HO), 151.5 (C^4), 147.1 (C^{8a}), 141.3 (C^6), 137.3 (C^8), 133.5 (C^2), 131.4 (C^7), 127.3 (C^{4a}), 127.0 (C^5), 124.3 (C^3); HRMS: *m/z* (ESI$^+$) [Found (M+H)$^+$ 192.023. $C_{10}H_6ClNO$ requires (M+H)$^+$ 192.0211];

LRMS: *m/z* (ESI$^+$) 192.1 ([M+H]$^+$, 100%); Anal. calculated for $C_{10}H_6ClNO$: C, 62.7; H, 3.2; N, 7.3. Found C, 62.8; H, 3.1; N, 7.4.

2.21. 5-Bromo-6-chloroquinoline

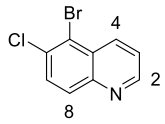

To a mixture of 6-Chloroquinoline **2.22** (5.0 g, 31.0 mmol, 1.0 eq.) and aluminium chloride (12.2 g, 93.0 mmol, 3.0 eq.), was added bromine (1.6 mL, 5.0 g, 31.0 mmol, 1.0 eq.) drop-wise over 0.5 h at 120 °C. The reaction mixture was stirred at 120 °C for 24 h, cooled to ambient temperature, MeOH/H_2O (1:1 *v/v*, 10 mL) added drop-wise, and concentrated *in vacuo*. The residue was dissolved in CH_2Cl_2 (25 mL), washed with sat. aq. $NaHCO_3$ (3 × 10 mL), dried over Na_2SO_4, filtered, and concentrated *in vacuo*. The residue was adsorbed onto Celite® and the product purified by silica gel column chromatography, eluting with PE and CH_2Cl_2 (gradient, 60-100% CH_2Cl_2), and crystallised from Et_2O, to yield **2.21** (5.1 g, 69%) as a colourless crystalline solid: R_f: 0.32 (CH_2Cl_2); mp: 63-65 °C (Et_2O) [Lit. 62-63 °C][314]; $\bar{\nu}_{max}$ (solid) cm^{-1}: 3034 (w, Ar C-H), 1579 (m, Ar C=C); ^{1}H NMR (500 MHz, $CDCl_3$): 8.92 (1H, d, *J* 4.2, C^2*H*), 8.59 (1H, d, *J* 8.5, C^4*H*), 8.04 (1H, d, *J* 9.0, C^8*H*), 7.76 (1H, d, *J* 9.0, C^7*H*), 7.54 (1H, dd, J_1 8.5, J_2 4.2, C^3*H*); ^{13}C NMR (126 MHz, $CDCl_3$): 150.9 (C^2), 147.3 (C^{8a}), 136.0 (C^4), 133.8 (C^6), 130.9 (C^7), 130.1 (C^8), 128.9 (C^{4a}), 122.9 (C^3), 121.6 (C^5); HRMS: *m/z* (FI$^+$) [Found (M[^{35}Cl^{79}Br])$^+$ 241.9368. C_9H_5ClNBr requires (M[^{35}Cl^{79}Br])$^+$ 241.9346; LRMS: *m/z* (ESI$^+$) 243.9 ([M+H]$^+$, 100%), 241.9 ([M+H]$^+$, 90%), 245.93 ([M+H]$^+$, 80%). These data are in good agreement with literature values.[314]

2.23. 5,8-Dibromo-6-chloroquinoline

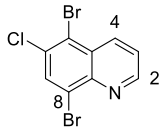

Further elution in the purification of compound **2.21** gave compound **2.23**. Crystallisation from Et_2O afforded **2.23** (96 mg, 12%) as a colourless crystalline solid: R_f: 0.51 (CH_2Cl_2); mp: 153-155 °C (Et_2O); $\bar{\nu}_{max}$ (solid) cm^{-1}: 3078 (w, Ar C-H), 1568 (m, Ar C=C); ^1H NMR (500 MHz, $CDCl_3$): 9.04 (1H, dd, J_1 4.2, J_2 1.4, C^2H), 8.62 (1H, dd, J_1 8.6, J_2 1.4, C^4H), 8.15 (1H, s, C^7H), 7.60 (1H, dd, J_1 8.6, J_2 4.2, C^3H); ^{13}C NMR (126 MHz, $CDCl_3$): 151.7 (C^2), 144.4 (C^{8a}), 136.8 (C^4), 133.9 (C^7), 133.8 (C^6), 129.7 (C^{4a}), 125.3 (C^8), 123.7 (C^3), 121.4 (C^5); HRMS: *m/z* (FI^+) [Found $(M[^{35}Cl^{79}Br^{81}Br])^+$ 320.8350. $C_9H_4ClNBr_2$ requires $(M[^{35}Cl^{79}Br^{81}Br])^+$ 320.8374; LRMS: *m/z* (ESI^+) 321.9 $([M+H]^+$, 100%); Anal. calculated for $C_9H_4Br_2ClN$: C, 33.6; H, 1.3; N, 4.4. Found: C, 33.8; H, 1.2; N, 4.5.

2.25. 5-Bromo-6-chloro-2-isopropylquinoline

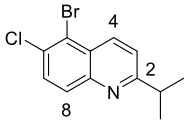

Further elution from purification of compound **2.19** yielded **2.25** (30 mg, 6%) as a yellow oil: R_f: 0.55 (EtOAc - PE 1:9); $\bar{\nu}_{max}$ (neat) cm^{-1}: 2963 (s, CH_3), 1605 (s, C=N), 1340 (m, $CH(CH_3)_2$) 1280 (m, $CH(CH_3)_2$); ^1H (500 MHz, $CDCl_3$): 8.45 (1H, d, *J* 8.8, C^4H), 7.94 (1H, d, *J* 9.0, C^8H), 7.69 (1H, d, *J* 9.0, C^7H), 7.43 (1H, d, *J* 8.8, C^3H), 3.26 (1H, sp, *J* 7.0, $CHCH_3$), 1.39 (6H, d, *J* 7.0, $CHCH_3$); ^{13}C NMR (126 MHz, $CDCl_3$): 168.5 (C^2), 146.8 (C^{8a}), 136.3 (C^4), 132.5 (C^6), 130.5 (C^8), 129.9 (C^7), 127.7 (C^5), 121.4 (C^3), 121.3 (C^{4a}), 37.0

(C^2CH), 22.5 ($CH(CH_3)$); HRMS: *m/z* (ESI^+) [Found $(M[^{35}Cl^{79}Br]+H)^+$ 283.9834. $C_{12}H_{11}BrClN$ requires $(M[^{35}Cl^{79}Br]+H)^+$ 283.9836]; LRMS: *m/z* (ESI^+) 286.0 ($[M(^{35}Cl^{81}Br)+H]^+$, 100%), 284.0 ($[M(^{35}Cl^{79}Br)+H]^+$, 80%); Anal. calculated for $C_{12}H_{11}BrClN$: C, 50.7; H, 3.9; N, 4.9. Found C, 50.7; H, 4.1; N, 5.0.

2.28. 6-Chloro-5-(((2-fluorobenzyl)oxy)methyl)quinoline

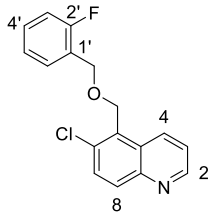

To a solution of **2.18** (60 mg, 0.31 mmol, 1.0 eq.) in DMF (1.0 mL), was added 2-Fluorobenzyl bromide (42 µL, 68 mg, 0.40 mmol, 1.1 eq.) and NaH (60% dispersion in mineral oil, 62 mg, 1.55 mmol, 5.0 eq.). The reaction mixture was stirred at ambient temperature for 0.5 h and then quenched by addition of MeOH (5 mL) drop-wise. The organic components were extracted with EtOAc (3 × 10 mL), the organic phases were combined, washed with H_2O (3 × 10 mL), dried over Na_2SO_4, filtered and concentrated *in vacuo*. The residue was adsorbed onto Celite® and the product purified by silica gel column chromatography, eluting with PE and EtOAc (20% EtOAc) to yield **2.28** (70 mg, 74%) as a colourless solid: R_f: 0.40 (EtOAc – PE 1:1); mp: 49-51 °C (EtOAc); $\bar{\nu}_{max}$ (solid) cm^{-1}: 1489 (m, C=C), 1082 (s, C-F); ^1H NMR (500 MHz, $CDCl_3$): 8.90 (1H, d, *J* 4.2, C^2H), 8.50 (1H, d, *J* 8.5, C^4H), 8.01 (1H, d, *J* 9.0, C^8H), 7.67 (1H, d, *J* 9.0, C^7H), 7.45 (1H, dd, J_1 8.5, J_2 4.2, C^3H), 7.38 (1H, dd, J_1 7.5, J_2 7.5, $C^{6'}H$), 7.29-7.26 (1H, m, $C^{4'}H$), 7.11 (1H, dd, J_1 7.5, J_2 7.5, $C^{5'}H$), 7.04 (1H, dd, J_1 9.5, J_2 9.5, $C^{3'}H$), 5.17 (2H, s, C^5CH_2O), 4.69

(2H, s, C$^{1'}$CH_2O); ^{13}C NMR (126 MHz, $CDCl_3$): 162.4 (d, $J_{C\text{-}F}$ 247.2, C$^{2'}$), 150.5 (C^{2}), 147.4 (C^{8a}), 133.4 (C^{6}), 133.2 (C^{4}), 131.7 (C^{7}), 130.8 (C^{8}), 130.6 (C^{5}), 130.4 (d, $J_{C\text{-}F}$ 3.8, C$^{6'}$), 129.8 (d, $J_{C\text{-}F}$ 7.6, C$^{4'}$), 128.8 (C^{4a}), 125.0 (d, $J_{C\text{-}F}$ 14.2, C$^{1'}$), 124.2 (d, $J_{C\text{-}F}$ 3.8, C$^{5'}$), 122.1 (C^{3}), 115.4 (d, $J_{C\text{-}F}$ 21.4, C$^{3'}$), 66.2 (d, $J_{C\text{-}F}$ 3.8, C$^{1'}$CH_2O), 66.0 (C$^{5'}$CH_2O); ^{19}F NMR (470 MHz, $CDCl_3$): −118.6; HRMS: *m/z* (ESI$^+$) [Found (M+H)$^+$ 302.0747. $C_{17}H_{13}ClFNO$ requires (M+H)$^+$ 302.0742]; LRMS: *m/z* (ESI$^+$) 302.1 ([M+H]$^+$, 100%) 304.1 ([M+H]$^+$, 32%); Anal. calculated for $C_{17}H_{13}ClFNO$: C, 67.7; H, 4.3; N, 4.6. Found: C, 67.6; H, 4.5; N, 4.6.

2.29. 6-Chloro-5-(((4-fluorobenzyl)oxy)methyl)quinoline

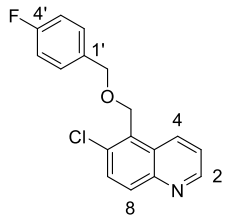

To a solution of **2.18** (70 mg, 0.36 mmol, 1.0 eq.) in DMF (1.3 mL), was added 4-Fluorobenzyl bromide (45 µL, 68 mg, 0.40 mmol, 1.1 eq.) and NaH (60% dispersion in mineral oil, 72 mg, 1.81 mmol, 5.0 eq.). The reaction mixture was stirred at ambient temperature for 0.5 h and quenched by addition of MeOH (5 mL) drop-wise. The organic components were extracted with EtOAc (3 × 10 mL), the organic phases combined, washed with H_2O (3 × 10 mL), dried over Na_2SO_4, filtered, and concentrated *in vacuo*. The residue was adsorbed onto Celite® and the product purified by silica gel column chromatography, eluting with PE and EtOAc (20% EtOAc) to yield **2.29** (82 mg, 75%) as a colourless solid: R_f: 0.55 (EtOAc - Pet 1:1); mp: 63-65 °C (EtOAc); $\bar{\nu}_{max}$ (solid) cm^{-1}: 1461 (s, C=C), 1219 (s, C-F) 1025 (s,

C-Cl); ^{1}H NMR (500 MHz, $CDCl_3$): 8.92 (1H, d, *J* 4.2, $C^{2}H$), 8.50 (1H, d, *J* 8.6, $C^{4}H$), 8.04 (1H, d, *J* 9.0, $C^{8}H$), 7.69 (1H, d, *J* 9.0, $C^{7}H$), 7.47 (1H, dd, J_1 8.6, J_2 4.2, $C^{3}H$), 7.33-7.28 (2H, m, $C^{2'}H$, $C^{6'}H$), 7.01-6.99 (2H, m, $C^{5'}H$, $C^{3'}H$), 5.14 (2H, s, $C^{5}CH_2O$), 4.56 (2H, s, $C^{1'}CH_2O$); ^{13}C NMR (126 MHz, $CDCl_3$): 162.4 (d, $J_{C\text{-}F}$ 246.2, $C^{4'}$), 150.1 (C^{2}), 147.0 (C^{8a}), 133.6 (d, $J_{C\text{-}F}$ 2.9, $C^{1'}$), 133.4 (C^{6}), 133.2 (C^{4}), 131.4 (C^{8}), 130.8 (C^{7}), 130.6 (C^{5}), 129.6 (d, $J_{C\text{-}F}$ 8.0, $C^{2'}/C^{6'}$), 128.6 (C^{4a}), 122.0 (C^{3}), 115.2 (d, $J_{C\text{-}F}$ 20.8, $C^{5'}/C^{3'}$), 71.7 ($C^{1'}CH_2O$), 65.5 ($C^{5}CH_2O$); ^{19}F NMR (470 MHz, $CDCl_3$): −114.4; HRMS: *m/z* (ESI^+) [Found $(M+Na)^+$ 324.0563. $C_{17}H_{13}ClFNO$ requires $(M+Na)^+$ 324.0562]; LRMS: *m/z* (ESI^+) 302.1 ($[M+H]^+$, 100%) 304.1 ($[M+H]^+$, 32%); Analytical HPLC (RPB C18 column [100 mm × 3.2 mm, 35 °C]; 90:10 H_2O 10 mM FA/H_2O:MeCN → 95:5 MeCN:10 mM FA/H_2O; 6 min, 3 min hold) Ret. Time = 7.30 min, Purity: >99%.

2.30. 5-((Benzyloxy)methyl)-6-chloroquinoline

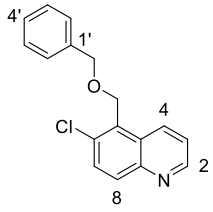

To a solution of **2.18** (40 mg, 0.21 mmol, 1.0 eq.) in DMF (1 mL), was added NaH (60% dispersion in mineral oil, 41 mg, 1.05 mmol, 5.0 eq.) portion-wise at ambient temperature. The reaction mixture was stirred for 5 min, Benzyl bromide (30 µL, 43 mg, 0.24 mmol, 1.2 eq.) was added drop-wise, stirred for 15 min, and then MeOH (10 mL) added. The organic components were extracted with EtOAc (3 × 10 mL), the organic layers combined, washed with brine (3 × 10 mL), dried over $MgSO_4$, filtered, and concentrated *in vacuo*. The residue was adsorbed onto Celite® and the

product purified by silica gel column chromatography, eluting with PE and EtOAc (50% EtOAc), to yield **2.30** (45 mg, 77%) as a colourless solid: R_f: 0.63 (EtOAc); mp: 46-48 °C (EtOAc); $\bar{\nu}_{max}$ (solid) cm^{-1}: 1592 (m, C=N), 1497 (m, C=C); ^1H NMR (500 MHz, $CDCl_3$): 8.91 (1H, s, C^2H), 8.50 (1H, d, *J* 8.6, C^4H), 8.02 (1H, d, *J* 9.1, C^8H), 7.68 (1H, d, *J* 9.1, C^7H), 7.45 (1H, dd, J_1 8.6, J_2 = 4.2, C^3H), 7.35 (2H, s, $C^{2'/6'}H$), 7.34 (2H, s, $C^{3'/5'}H$), 7.28-7.32 (1H, m, $C^{4'}H$), 5.15 (2H, s, C^5CH_2O), 4.62 (2H, s, $C^{1'}CH_2O$); ^{13}C NMR (126 MHz, $CDCl_3$): 150.5 (C^2), 147.5 (C^{8a}), 138.0 ($C^{1'}$), 133.5 (C^5), 133.3 (C^4), 131.7 (C^8), 130.9 (C^{4a}), 130.8 (C^7), 128.8 (C^6), 128.6 ($C^{2'/6'}$), 128.1 ($C^{3'/5'}$), 128.0 ($C^{4'}$), 122.0 (C^3), 72.8 ($C^{1'}CH_2O$), 65.7 (C^5CH_2O); HRMS: *m/z* (ESI^+) [Found $(M+Na)^+$ 306.0648. $C_{17}H_{14}ClNO$ requires $(M+Na)^+$ 306.0656]; LRMS: *m/z* (ESI^+) 284.1 ($[M(^{35}Cl)+H]^+$, 100%), 286.1 ($[M(^{37}Cl)+H]^+$, 30%); Analytical HPLC (RPB C18 column [100 mm × 3.2 mm, 35 °C]; 90:10 H_2O 10 mM FA/H_2O:MeCN → 95:5 MeCN:10 mM FA/H_2O; 6 min, 3 min hold) Ret. Time = 7.42 min, Purity: >99%.

2.31. (6-Chloroquinolin-5-yl)methyl acetate

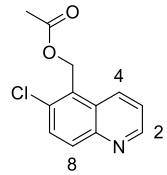

To a solution of **2.18** (50 mg, 0.26 mmol, 1.0 eq.) in pyridine (104 µL, 102 mg, 1.30 mmol, 5.0 eq.), was added Ac_2O (27 µL, 0.29 mmol, 1.1 eq.) drop-wise at 0 °C. The reaction mixture was heated to 30 °C for 1 h, cooled to ambient temperature and 1 M aq. $CuSO_4$ (20 mL) was added. The organic components were extracted with EtOAc (2 × 15 mL), the organic phases combined, washed with 1 M aq. $CuSO_4$ (2 × 20 mL), brine (2 × 20 mL), dried over $MgSO_4$, filtered, and concentrated *in vacuo*. The residue was adsorbed

onto Celite® and the product purified by silica gel column chromatography, eluting with PE and EtOAc (40% EtOAc), to yield **2.31** (36 mg, 60%) as a colourless solid: R_f: 0.62 (EtOAc); mp: 64-67 °C (EtOAc); $\bar{\nu}_{max}$ (solid) cm^{-1}: 3043 (w, Ar C-H), 1727 (s, C=O), 1242 (s, C-O); ^{1}H NMR (500 MHz, $CDCl_3$): 8.93 (1H, d, *J* 4.1, C^2H), 8.39 (1H, d, *J* 8.6, C^4H), 8.06 (1H, d, *J* 9.0, C^7H), 7.71 (1H, d, *J* 9.0, C^8H), 7.49 (1H, dd, J_1 8.6, J_2 4.1, C^3H), 5.70 (2H, s, C^5CH_2O), 2.08 (3H, s, CO_2CH_3); ^{13}C NMR (126 MHz, $CDCl_3$): 170.9 (CO_2CH_3), 150.6 (C^2), 147.2 (C^{8a}), 134.6 (C^{4a}), 132.33 (C^4), 132.29 (C^7), 131.0 (C^8), 128.7 (C^5), 128.4 (C^6), 122.4 (C^3), 59.7 (C^5CH_2O), 20.9 (CO_2CH_3); HRMS: *m/z* (ESI^+) [Found $(M+H)^+$ 236.0467. $C_{12}H_{10}ClNO_2$ requires $(M+H)^+$236.0473]; LRMS: *m/z* (ESI^+) 236.1 ($[M+H]^+$, 100%) 238.1 ($[M+H]^+$, 32%); Analytical HPLC (RPB C18 column [100 mm × 3.2 mm, 35 °C]; 90:10 H_2O 10 mM FA/H_2O:MeCN → 95:5 MeCN:10 mM FA/H_2O; 6 min, 3 min hold) Ret. Time = 5.92 min, Purity: >99%.

2.32. 5-(((2-Fluorobenzyl)oxy)methyl)-6-nitroquinoline

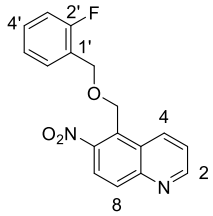

To a flame dried microwave vial under an argon atmosphere, **2.28** (50 mg, 0.17 mmol, 1.0 eq.), $Pd_2(dba)_3$ (3.8 mg, 4.20 µmol, 2.5 mol%), ^{t}BuBrettPhos[175,313] (4.8 mg, 9.90 µmol, 6 mol%), and $NaNO_2$ (23 mg, 0.34 mmol, 2.0 eq.) were added. The vial was evacuated and backfilled with argon 3 times, and degassed ^{t}BuOH (0.5 mL), and TDA (*tris*(3,6-dioxaheptyl)amine) (3 µL, 3 mg, 9.38 µmol, 5 mol%) were syringed in. The

reaction mixture was heated under reflux at 130 °C for 24 h, cooled to ambient temperature, EtOAc (10 mL) added, filtered through Celite®, and concentrated *in vacuo*. The resulting residue was adsorbed onto Celite®, and the product purified by silica gel column chromatography, eluting with PE and EtOAc (20% EtOAc), to yield **2.32** (34 mg, 68%) as a pale yellow solid: R_f: 0.31 (EtOAc - PE 1:1); mp: 87-89 °C (EtOAc); $\bar{\nu}_{max}$ (solid) cm^{-1}: 1532 (s, NO_2 asym), 1365 (s, NO_2 sym), 1075 (s, CH_2OCH_2); ^1H (500 MHz, $CDCl_3$): 9.04 (1H, dd, J_1 4.2, J_2 1.6, C^2H), 8.68 (1H, d, J 8.8, C^4H), 8.16 (1H, d, J 9.2, C^7H), 8.00 (1H, d, J 9.2, C^8H), 7.57 (1H, dd, J_1 8.7, J_2 4.2, C^3H), 7.35 (1H, td, J_1 7.5, J_2 1.6, $C^{6'}H$), 7.28 (1H, m, $C^{4'}H$), 7.11 (1H, td, J_1 7.5, J_2 0.9, $C^{5'}H$), 7.04 (1H, t, J 9.2, $C^{3'}H$), 5.16 (2H, s, C^5CH_2O), 4.70 (2H, s, $C^{1'}CH_2O$); ^{13}C NMR (126 MHz, $CDCl_3$): 160.9 (d, $J_{C\text{-}F}$ 247.3, $C^{2'}$), 152.7 (C^2), 148.9 (C^{8a}), 148.2 (C^{4a}), 134.9 (C^4), 131.9 (C^7), 130.5 (d, $J_{C\text{-}F}$ 4.0, $C^{6'}$), 130.0 (d, $J_{C\text{-}F}$ 8.3, $C^{4'}$), 128.8 (C^6), 127.5 (C^5), 124.3 ($C^{1'}$), 124.20 ($C^{5'}$), 124.17 ($C^{3'}$), 123.4 (C^8), 122.7 (C^3), 115.5 (d, $J_{C\text{-}F}$ 21.4, $C^{3'}$), 66.8 (d, $J_{C\text{-}F}$ 3.7, $C^{1'}CH_2O$), 63.9 (C^5CH_2O); ^{19}F NMR (376 MHz, $CDCl_3$): −118.5; HRMS: *m/z* (ESI^+) [Found $(M+Na)^+$ 335.0811. $C_{17}H_{13}FN_2O_3$ requires $(M+Na)^+$ 335.0802]; LRMS: *m/z* (ESI^+) 313.1 ($[M+H]^+$, 100%), 314.1 ($[M+H]^+$, 18%). Analytical HPLC (RPB C18 column [100 mm × 3.2 mm, 35 °C]; 90:10 H_2O 10 mM FA/H_2O:MeCN → 95:5 MeCN:10 mM FA/H_2O; 6 min, 3 min hold) Ret. Time = 6.81 min, Purity: >99%.

2.33. 5-(((4-Fluorobenzyl)oxy)methyl)-6-nitroquinoline

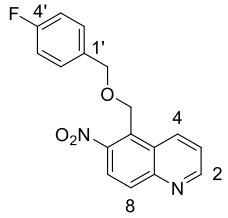

To a flame dried microwave vial under an argon atmosphere, **2.29** (50 mg, 0.17 mmol, 1.0 eq.), $Pd_2(dba)_3$ (3.8 mg, 4.20 µmol, 2.5 mol%), ^{t}BuBrettPhos[175,313] (4.8 mg, 9.90 µmol, 6 mol%), and $NaNO_2$ (23 mg, 0.34 mmol, 2.0 eq.) were added. The vial was evacuated and backfilled with argon 3 times, and degassed ^{t}BuOH (0.5 mL), and TDA (*tris*(3,6-dioxaheptyl)amine) (3 µL, 3 mg, 9.38 µmol, 5 mol%) were syringed in. The reaction mixture was heated under reflux at 130 °C for 24 h., cooled to ambient temperature, EtOAc (10 mL) added, filtered through a pad of Celite®, and concentrated *in vacuo*. The resulting residue was adsorbed onto Celite®, and the product purified by silica gel column chromatography, eluting with PE and EtOAc (20% EtOAc), to yield **2.33** (20 mg, 38%) as a pale yellow solid: R_f: 0.42 (EtOAc – PE 1:1); mp: 69-71 °C (EtOAc); $\bar{\nu}_{max}$ (solid) cm^{-1}: 3053 (w, Ar C-H), 1525 (s, NO_2 asym), 1345 (s, NO_2 sym), 1087 (s, CH_2OCH_2); ^{1}H NMR (500 MHz, $CDCl_3$): 9.06 (1H, dd, J_1 4.2, J_2 1.4, C_2H), 8.66 (1H, d, J 8.7, C^4H), 8.20 (1H, d, J 9.2, C^8H), 8.00 (1H, d, J 9.2, C^7H), 7.58 (1H, dd, J_1 8.7, J_2 4.2, C^3H), 7.32-7.27 (2H, m, $C^{2'}H/C^{6'}H$), 7.05-7.00 (2H, m, $C^{3'}H/C^{5'}H$), 5.12 (2H, s, C^5CH_2O), 4.59 (2H, s, $C^{1'}CH_2O$); ^{13}C NMR (126 MHz, $CDCl_3$): 162.7 (d, $J_{C\text{-}F}$ 246.0, $C^{4'}$), 152.9 (C^2), 149.1 (C^{8a}), 148.4 (C^6), 134.9 (C^4), 133.16 (d, $J_{C\text{-}F}$ 2.9, $C^{1'}$), 132.0 (C^8), 129.95 (d, $J_{C\text{-}F}$ 8.7, $C^{2'}/C^{6'}$), 129.0 (C^5), 127.6 (C^{4a}), 123.6 (C^7), 122.9 (C^3), 115.6 (d, $J_{C\text{-}F}$ 22.0, $C^{3'}/C^{5'}$), 72.7

($C^{1'}CH_2O$), 63.7 (C^5CH_2O); ^{19}F NMR (376 MHz, $CDCl_3$): −114.0; HRMS: *m/z* (ESI$^+$) [Found $(M+Na)^+$ 335.0795. $C_{17}H_{13}FN_2O_3$ requires $(M+Na)^+$ 335.0802]; LRMS: *m/z* (ES^+) 313.1 ($[M+H]^+$, 100%); Analytical HPLC (RPB C18 column [100 mm × 3.2 mm, 35 °C]; 90:10 H_2O 10 mM FA/H_2O:MeCN → 95:5 MeCN:10 mM FA/H_2O; 6 min, 3 min hold) Ret. Time = 6.84 min, Purity: 97.3%.

2.36. 6-Nitroquinoline-5-carbaldehyde

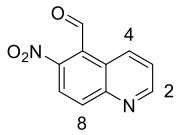

To a solution of **2.37** (50 mg, 0.20 mmol, 1.0 eq.) in distilled THF (2 mL), was added Phenyl lithium (1.75 M in THF, 113 µL, 0.20 mmol, 1.0 eq.) drop-wise at −78 °C. The reaction solution was stirred for 0.5 h, then distilled EtOCHO (160 µL, 1.0 mmol, 5.0 eq.) was added drop-wise at −78 °C. The reaction solution was gradually warmed to ambient temperature over 18 h, and concentrated *in vacuo*. The resulting residue was adsorbed onto Celite® and the product purified by silica gel column chromatography, eluting with PE and EtOAc (40% EtOAc), followed by crystallisation from MeCN, to yield **2.36** (18 mg, 45%) as pale orange needles: R_f: 0.19 (EtOAc - PE 1:1); mp: 165-167 °C (MeCN); $\bar{\nu}_{max}$ (solid) cm^{-1}: 3078 (w, Ar C-H), 1688 (s, C=O), 1598 (m, C=N), 1519 (s, NO_2 asym), 1492 (m, C=C), 1378 (s, NO_2 sym); ^1H NMR (500 MHz, $CDCl_3$): 10.58 (1H, s, $C^{5'}HO$), 9.13 (1H, dd, J_1 4.2, J_2 1.5, C^2H), 8.74 (1H, dd, J_1 8.7, J_2 1.5, C^4H), 8.40 (2H, s, C^7H/C^8H), 7.64 (1H, dd, J_1 8.7, J_2 4.2, C^3H); ^{13}C NMR (126 MHz, $CDCl_3$): 189.2 ($C^{5'}HO$), 154.1 (C^2), 149.9 (C^{8a}), 146.8 (C^6), 135.2 (C^4), 134.8 (C^8/C^7), 131.9 (C^5), 124.8 (C^{4a}), 124.0

(C^3), 123.0 (C^7/C^8); HRMS: *m/z* (FI^+) [Found $(M)^+$ 202.0378, $(M[^{13}C])^+$ 203.0397. $C_{10}H_6N_2O_3$ requires $(M)^+$ 202.0378, $(M[^{13}C])^+$ 203.0408; LRMS: *m/z* (ESI^+) 203.1 ($[M+H]^+$, 100%); Anal. calculated for: C, 59.4; H, 3.0; N, 13.9. Found: C, 59.5; H, 2.9; N, 13.7.

2.37. 5-Bromo-6-nitroquinoline

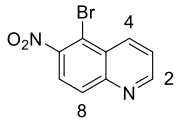

To a solution of 5-Amino-6-nitroquinoline **2.38** (5.0 g, 25.5 mmol, 1.0 eq.) and CuBr (4.6 g, 31.8 mmol, 1.2 eq.) in aq. HBr (15% *w/v*, 375 mL), aq. $NaNO_2$ (7.9 M, 79 mmol, 3.1 eq.) was added drop-wise, and stirred at ambient temperature for 3 h. The reaction solution was adjusted to pH 7 by addition of sat. aq. $NaHCO_3$, followed by addition of sat. aq. EDTA (15 mL), and the reaction mixture stirred at ambient temperature for 0.5 h. The organic components were extracted with EtOAc (5 × 50 mL), the organic phases combined, washed with sat. aq. EDTA (3 × 30 mL), sat aq. $Na_2S_2O_3$ (3 × 30 mL), brine (3 × 30 mL), dried over $MgSO_4$, filtered, and concentrated *in vacuo*. The residue was adsorbed onto Celite® and the product purified by silica gel column chromatography, eluting with PE and EtOAc (33% EtOAc), to yield **2.37** (3.4 g, 13.5 mmol, 51%) as a colourless solid: R_f: 0.41 (PE -EtOAc 3:2); mp: 138-140 °C (EtOAc); $\bar{\nu}_{max}$ (solid) cm^{-1}: 1590 (w, C=N), 1519 (s, NO_2 asym), 1485 (m, C=C), 1352 (s, NO_2 sym); ^1H NMR (500 MHz, $CDCl_3$): 9.07 (1H, dd, J_1 4.2, J_2 1.5, C^2H), 8.76 (1H, d, J 8.6, C^4H), 8.20 (1H, d, J 9.0, C^8H), 7.99 (1H, d, J 9.0, C^7H), 7.66 (1H, dd, J_1 8.6, J_2 4.2, C^3H); ^{13}C NMR (126 MHz, $CDCl_3$): 153.4 (C^2), 149.0 (C^{8a}), 148.6 (C^6), 137.4 (C^4),

131.0 (C^7), 128.1 (C^{4a}), 124.3 (C^8), 124.0 (C^3), 115.3 (C^6); HRMS: *m/z* (FI^+) [Found $(M[^{79}Br])^+$ 251.9539, $(M[^{81}Br])^+$ 253.9523. $C_9H_5BrN_2O_2$ requires $(M[^{79}Br])^+$ 251.9534, $(M[^{81}Br])^+$ 253.9515; LRMS: *m/z* (ES^+) 130.2 (100%), 253.0 ($[M+H]^+$, 33%), 255.0, ($[M+H]^+$, 33%)); Anal. calculated for: C, 42.7; H, 2.0; N, 11.1. Found: C, 42.6; H, 1.9; N, 11.2.

2.40. 5-Amino-8-bromo-6-nitroquinoline

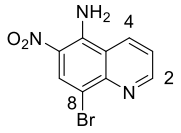

To a solution of 5-Amino-6-nitroquinoline **2.38** (1.0 g, 5.3 mmol, 1.0 eq.) and CuBr (0.9 g, 6.4 mmol, 1.2 eq.) in aq. HBr (15% *w/v*, 30 mL), aq. $NaNO_2$ (7.9 M, 1.09 g, 15 mmol, 2.8 eq.) was added drop-wise, and stirred vigorously at ambient temperature for 2 h. The reaction solution was adjusted to pH 7 by addition of sat. aq. $NaHCO_3$, followed by addition of sat. aq. EDTA (15 mL), and the reaction mixture was stirred at ambient temperature for 0.5 h. The organic components were extracted with EtOAc (5 × 50 mL), the organic phases combined, washed with sat. aq. EDTA (3 × 30 mL), sat aq. $Na_2S_2O_3$ (3 × 30 mL), brine (3 × 30 mL), dried over $MgSO_4$, filtered, and concentrated *in vacuo*. The residue was adsorbed onto Celite® and the product purified by silica gel column chromatography, eluting with PE and EtOAc (gradient, 30-100% EtOAc), followed by crystallisation from EtOAc, to yield **2.40** (87 mg, 6%) as a yellow solid: R_f: 0.71 (EtOAc); mp: > 300 °C (EtOAc); $\bar{\nu}_{max}$ (solid) cm^{-1}: 3395 (m, NH_2), 1629 (m, C-NH_2), 1616 (s, NO_2 asym), 1370 (s, NO_2 sym); ^1H (500 MHz, DMSO-d_6): 9.10-9.06 (2H, m, C^2H, C^3H), 8.87 (2H, bs, C^5NH_2), 8.51 (s, 1H, C^7H), 7.72 (1H, dd, J_1 8.4, J_2 4.4,

C^{3}*H*); ^{13}C NMR (126 MHz, DMSO- d_6): 154.0 (C^{2}), 147.3 (C$^{8a/5}$), 145.8 (C$^{5/8a}$), 133.9 (C^{4}), 127.9 (C^{7}), 124.9 (C^{6}), 121.9 (C^{3}), 120.6 (C^{4a}), 109.0 (C^{8}); HRMS *m/z* (FI^{+}) [Found (M[^{79}Br])$^{+}$ 266.9649, (M[^{81}Br])$^{+}$ 268.9646; $C_9H_6BrN_3O_2$ requires (M[^{79}Br])$^{+}$ 266.9643, (M[^{81}Br])$^{+}$ 268.9624; LRMS: *m/z* (ESI^{+}) 157.1 (100%), 268.0 ([M+H]$^{+}$, 25%), 270.0 ([M+H]$^{+}$, 25%); Anal. calculated for: C, 40.3; H, 2.3; N, 15.7. Found: C, 40.4, H; 2.15; N, 15.6.

2.47. 6,6'-Dinitro-5,5'-biquinoline

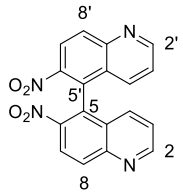

To a solution of **2.37** (500 mg, 1.98 mmol, 1.0 eq.) in distilled THF (20 mL), Phenyl lithium (1.75 M in THF, 1.1 mL, 1.98 mmol, 1.0 eq.) was drop-wise at −78 °C and the reaction solution stirred for 45 min. Distilled EtOCHO (1 M in THF) (9.9 mL, 9.92 mmol, 5.0 eq.) was added drop-wise at − 78 °C. The reaction solution was allowed to gradually warm to ambient temperature whilst stirring over 18 h, and concentrated *in vacuo*. The resulting residue was adsorbed onto Celite®, and the product purified by silica gel column chromatography, eluting with EtOAc, to yield **2.47** (76 mg, 11%) as a black solid: R_f: 0.17 (EtOAc); mp: > 300 °C (EtOAc); $\bar{\nu}_{max}$ (solid) cm^{-1}: 3057 (w, Ar C-H), 1519 (s, NO_2 asym), 1334 (s, NO_2 sym); ^{1}H NMR (500 MHz, $CDCl_3$): 9.07 (2H, dd, J_1 4.2, J_2 1.8, C$^{2/2'}$*H*), 8.57 (2H, d, *J* 9.2, C$^{7/7'}$*H*), 8.45 (2H, d, *J* 9.2, C$^{8/8'}$*H*), 7.40-7.31 (4H, m, C$^{4/4'}$*H*); ^{13}C NMR (126 MHz, $CDCl_3$): 153.8 (C$^{2/2'}$), 149.5 (C$^{8a/8a'}$), 145.6 (C$^{6/6'}$), 135.0 (C$^{4/4'}$), 132.5 (C$^{8/8'}$), 129.7 (C$^{5/5'}$), 127.4 (C$^{4a/4a'}$), 124.4 (C$^{7/7'}$), 123.6 (C$^{3/3'}$); HRMS: *m/z* (ESI^{+}) [Found (M+Na)$^{+}$

369.0600. $C_{18}H_{10}N_4O_4$ requires $(M+Na)^+$ 369.0594]; LRMS: *m/z* (ESI^+) 347.0 ($[M+H]^+$, 100%); Anal. calculated for: C, 62.4; H, 2.9; N, 16.2. Found: C, 62.3; H, 2.8; N, 16.1.

2.49. (3-(3,5-Dimethylisoxazol-4-yl)-5-((6-nitroquinolin-5-yl)methoxy)phenyl)(phenyl)methanol

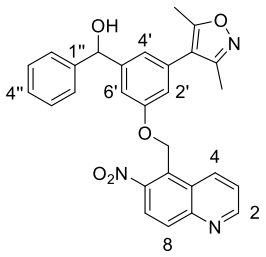

To a solution of **2.48** (70 mg, 0.24 mmol, 1.0 eq.) in DMF (1.2 mL), solid Cs_2CO_3 (77 mg, 0.24 mmol, 1.0 eq.) was added, and stirred at ambient temperature for 20 min. A solution of **2.16** (63 mg, 0.24 mmol, 1.0 eq.) in DMF (1.2 mL) was added drop-wise to the reaction mixture and stirred at ambient temperature for 2 h. H_2O (5 mL) was added, and the organic components extracted with EtOAc (2 × 10 mL). The aq. layer was adjusted to pH 7 with 1 M aq. HCl, and the organic components extracted with EtOAc (2 × 10 mL). The organic phases were combined, washed with H_2O (3 × 5 mL), brine (3 × 5 mL), dried over Na_2SO_4, filtered, and concentrated *in vacuo*. The resulting residue was adsorbed onto Celite®, and the product purified using silica gel column chromatography, eluting with PE and EtOAc (50% EtOAc), to yield **2.49** (62 mg, 54%) as a colourless solid: R_f: 0.18 (EtOAc - PE 1:1); mp: 75-77 °C (Et_2O); $\bar{\nu}_{max}$ (solid) cm^{-1}: 3324 (br, OH), 1531 (s, NO_2 asym), 1322 (s, NO_2 sym), 1023 (s, CH_2OCH_2); ^1H NMR (500 MHz, $CDCl_3$): 9.08 (1H, dd, J_1 4.2, J_2 1.6, C^2H), 8.63 (1H, d, J 8.4, C^4H), 8.27 (2H, d, J 9.2, C^8H), 8.08 (2H, d, J 9.2, C^7H), 7.60 (1H, dd, J_1 8.4, J_2 4.2, C^3H), 7.42-7.34 (4H, m, $C^{2''}H$,

$C^{3''}H$, $C^{5''}H$, $C^{6''}H$), 7.33-7.28 (1H, m, $C^{4''}H$), 7.09 (1H, s, $C^{6'}H$), 6.89 (1H, s, $C^{4'}H$), 6.74 (1H, s, $C^{2'}H$), 5.86 (1H, s, C*H*OH), 5.66 (2H, s, CH_2O), 2.35 (3H, s, CH_3CN/CH_3CO), 2.20 (3H, s, CH_3CN/CH_3CO); ^{13}C NMR (126 MHz, $CDCl_3$): 165.6 (CH_3CO/CH_3CN), 158.6 ($C^{1''}$), 158.6 (CH_3CO/CH_3CN), 153.1 (C^{2}), 149.2 (C^{8a}), 148.4 (C^{6}), 146.5 ($C^{1'}$), 143.5 ($C^{5'}$), 134.7 (C^{4}), 132.7 (C^{8}), 132.4 ($C^{3'}$), 128.9 ($C^{3''}/C^{5''}$), 128.2 ($C^{4''}$), 127.6 (C^{4a}/C^{5}), 126.7 ($C^{2''}/C^{6''}$), 123.8 (C^{7}), 123.2 (C^{3}), 121.1 ($C^{4'}$), 116.3 ($CC(CH_3)$), 115.2 ($C^{2'}$), 112.0 ($C^{6'}$), 76.3 (*C*HOH), 62.3 (CH_2O), 11.8 (CH_3CO/CH_3CN), 11.0 (CH_3CN/CH_3CO); HRMS: *m/z* (ESI^+) [Found $(M+Na)^+$ 504.1531. $C_{28}H_{23}N_3O_5$ requires $(M+Na)^+$ 504.1530]; LRMS: *m/z* (ESI^+) 482.1 ($[M+H]^+$, 100%); Analytical HPLC (RPB C18 column [100 mm × 3.2 mm, 35 °C]; 70:30:0.1 H_2O:MeCN:TFA → 95:5:0.1 MeCN:H_2O:TFA; 6 min, 3 min hold) Ret. Time = 5.89 min, Purity: 96.9%.

2.56. (6-Aminoquinolin-5-yl)methanol

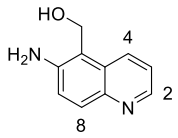

To a solution of **2.17** (53 mg, 0.26 mmol, 1 eq.) in DMF (1.0 mL), was added aq. NH_4Cl (10% *w/v*, 0.25 mL) and Zn dust (506 mg, 7.70 mmol, 30.0 eq.) was added, and stirred at ambient temperature for 2 h. H_2O (10 mL) was added, the organic components extracted with EtOAc (3 × 10 mL), the organic phases combined, washed with H_2O (3 × 10 mL), brine (2 × 10 mL), dried over $MgSO_4$, filtered and concentrated *in vacuo*. The resulting residue was adsorbed onto Celite® and the product purified by silica gel column chromatography, eluting with EtOAc, to yield **2.56** (39 mg, 85%) as a

hygroscopic yellow solid: R_f: 0.31 (EtOAc); $\bar{\nu}_{max}$ (solid) cm^{-1}: 3360 (br, OH), 1520 (m, C=N), 1342 (m, C-NH_2); ^1H NMR (500 MHz, $CDCl_3$): 8.52 (1H, d, *J* 4.0, C^2H), 8.46 (1H, d, *J* 8.6, C^4H), 7.79 (1H, d, *J* 8.8, C^8H), 7.43 (1H, dd, J_1 8.6, J_2 4.0, C^3H), 7.32 (1H, d, *J* 8.8, C^7H), 4.99 (2H, s, CH_2OH); ^{13}C NMR (126 MHz, $CDCl_3$): 147.0 (C^{8a}), 146.1 (C^2), 143.6 (C^6), 132.7 (C^4), 130.3 (C^{4a}), 129.9 (C^8), 124.2 (C^7), 122.5 (C^3), 115.0 (C^5), 56.3 (CH$_2$OH); HRMS: *m/z* (ESI^+) [Found $(M+H)^+$ 175.0862. $C_{10}H_{11}N_2O$ requires $(M)^+$ 175.0866]; LRMS: *m/z* (ESI^+) 175.1 ($[M+H]^+$, 100%); Analytical HPLC (RPB C18 column [100 mm × 3.2 mm, 35 °C]; 95:5:0.1 H_2O:MeCN:TFA → 70:30:0.1 MeCN:H_2O:TFA; 6 min, 3 min hold) Ret. Time = 2.07 min, Purity: 96.7%.

7.2.2 Chapter 3 compounds

3.1. (*E*)-2-(2-(4-Aminostyryl)-4*H*-chromen-4-ylidene)malononitrile

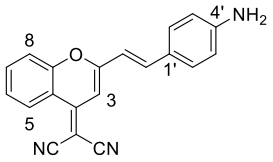

To a solution of **3.10** (130 mg, 0.63 mmol, 1.0 eq.) and 4-Acetamidobenzaldehyde **3.12** (110 mg, 0.67 mmol, 1.1 eq.) in toluene (2 mL), AcOH (30 µL, 32 mg, 0.52 mmol, 0.8 eq.) and piperidine (30 µL, 26 mg, 0.30 mmol, 0.5 eq.) was added drop-wise. The reaction mixture was heated under reflux at 115 °C for 3 h, cooled to ambient temperature, and the precipitate filtered and dried under reduced pressure. The precipitate was suspended in a mixture of conc. aq. HCl and EtOH (2:3, 50 mL), and heated under reflux at 80 °C for 3 h. The reaction mixture was cooled to ambient temperature, the pH adjusted to 7 using solid K_2CO_3, and H_2O (50 mL) added. The organic components were extracted with EtOAc (1 × 50 mL), dried over $MgSO_4$, filtered and concentrated *in vacuo*. The resulting residue was adsorbed onto Celite®, and the product purified by silica gel column chromatography, eluting with PE and acetone (gradient, 20-40% acetone), followed by crystallisation from toluene, to yield **3.1** (30 mg, 23%) as dark crimson crystals: R_f: 0.19 (acetone - PE 3:7); mp: 262-265 °C (toluene) [Lit. 243-245 °C][212]; $\bar{\nu}_{max}$ (solid) cm^{-1}: 3372 (br, N-H), 2202 (w, C≡N), 1621 (w, C=C(CN)$_2$); ^{1}H NMR (500 MHz, DMSO-d_6): 8.73 (1H, dd, J_1 8.5, J_2 1.3, C^5*H*), 7.92-7.87 (1H, m, C^7*H*), 7.78 (1H, dd, J_1 8.5, J_2 1.1, C^8*H*), 7.65 (1H, d, *J* 15.8, C*H*C$^{1'}$), 7.61-7.57 (1H, m, C^6*H*), 7.50 (1H, d, *J* 8.6, C$^{2'}$*H*/C$^{6'}$*H*), 7.10 (1H, d, *J* 15.8, C^{2}C*H*), 6.89 (1H, s, C^3*H*), 6.62 (2H, d, *J* 8.6, C$^{3'}$*H*/C$^{5'}$*H*), 6.03 (2H, s,

C$^{4'}$NH_2); ^{13}C NMR (126 MHz, DMSO-d_6): 159.8 (C^{2}), 152.6 (C^{4}), 152.14 (C^{8a}), 152.09 (C$^{4'}$), 140.7 (*C*HC$^{1'}$), 135.1 (C^{7}), 130.7 (C$^{2'}$/C$^{6'}$), 126.0 (C^{6}), 124.6 (C^{8}), 122.3 (C$^{1'}$), 119.0 (C^{5}), 117.9 (*C*N), 117.3 (C^{4a}), 116.5 (*C*N), 113.8 (C$^{3'}$/C$^{5'}$), 112.4 (C^{2}*C*H), 104.9 (C^{3}), 57.6 (*C*(CN)$_2$); HRMS: *m/z* (ESI$^+$) [Found (M+H)$^+$ 312.11309. $C_{20}H_{13}N_3O$ requires (M+H)$^+$ 312.11314]; LRMS: *m/z* (ESI$^+$) 312.1 ([M+H]$^+$, 100%); Analytical HPLC (RPB C18 column [100 mm × 3.2 mm, 35 °C]; 70:30:0.1 H_2O:MeCN:TFA → 95: 5:0.1 MeCN:H_2O:TFA; 6 min, 3 min hold) Ret. Time = 6.34 min, Purity: 97.1%.; These data are in good agreement with literature values.[173,212]

3.2. (*E*)-2-(2-(4-Nitrostyryl)-4*H*-chromen-4-ylidene)malononitrile*

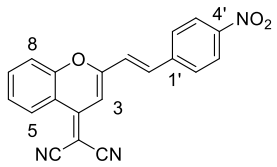

To a solution of **3.1** (16 mg, 0.05 mmol, 1.0 eq.) in AcOH (0.8 mL), aq. $NaNO_2$ (0.2 mL, 47 mg, 0.68 mmol, 13.0 eq.) was added drop-wise and stirred at ambient temperature for 15 h. The precipitate was filtered, washed with H_2O (3 × 5 mL), EtOAc (3 × 5 mL) and dried *in vacuo* to yield **3.2** (11 mg, 63%) as a brown solid: $\bar{\nu}_{max}$ (solid) cm^{-1}: 2210 (m, C≡N), 1632 (m, C=C(CN)$_2$), 1504 (NO_2), 1334 (NO_2); ^{1}H NMR (500 MHz, acetone-d_6): 8.75 (1H, d, *J* 8.0, C^{5}*H*), 8.74 (1H, d, *J* 8.8, C$^{3'}$*H*/C$^{5'}$*H*), 8.27 (1H, d, *J* 8.8, C$^{2'}$*H*/C$^{6'}$*H*), 7.98 (1H, dd, J_1 8.0, J_2 8.0, C^{7}*H*), 7.95 (1H, d, *J* 15.8, C^{2}C*H*), 7.89 (1H, d, *J* 15.8, C$^{1'}$C*H*), 7.79 (1H, d, *J* 8.0, C^{8}*H*), 7.67 (1H, dd, J_1 8.0, J_2 8.0, C^{6}*H*), 7.20 (1H, s, C^{3}*H*); ^{13}C NMR (126 MHz, acetone-d_6): 156.1 (C^{2}), 152.8 (C^{4}), 152.0 (C^{8a}), 146.6 (C$^{1'}$), 136.1 (C^{7}), 134.2 (C$^{1'}$*C*H), 133.4 (C$^{3'}$/C$^{5'}$), 129.7 (C$^{2'}$/C$^{6'}$), 128.2

(C^2CH), 126.6 (C^6), 124.9 (C^5), 119.2 (C^8), 117.1 (C^{4a}), 116.7 ($C(CN)_2$), 115.5 ($C(CN)_2$), 114.5 ($C^{4'}$), 110.3 (C^3), 62.9 ($C(CN)_2$);

*Characterisation of this compound is incomplete, as mass spectrometry data could not be obtained.

3.9. 2-Methyl-4*H*-chromen-4-one

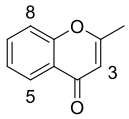

To a solution of 2-Hydroxyacetophenone **3.8** (17.0 mL, 0.13 mol, 1.0 eq.) in EtOAc (450 mL) under an argon atmosphere, Na (8.0 g, 0.35 mol, 2.8 eq.) was added portion-wise. The reaction mixture was stirred at ambient temperature for 4 h, and the precipitate filtered and dried under reduced pressure. The precipitate was dissolved in H_2O (100 mL), then AcOH (40 mL) was added, followed by drop-wise addition of conc. H_2SO_4 (10 mL). The reaction mixture was heated under reflux for 1 h, cooled to ambient temperature, ice-cold water (100 mL) added portion-wise, and the pH adjusted to 7 with solid $NaHCO_3$. The organic components were extracted with toluene (4 × 50 mL), the organic phases combined, washed with brine (1 × 100 mL), dried over Na_2SO_4, filtered and concentrated *in vacuo*. The resulting residue was adsorbed onto Celite®, and the product purified by silica gel column chromatography, eluting with PE and Et_2O (gradient, 50-100% Et_2O) to afford **3.9** (5.4 g, 40%) as a colourless solid: R_f: 0.40 (EtOAc - PE 1:4); mp: 58-60 °C (EtOAc) [Lit. 55-56 °C][315]; $\bar{\nu}_{max}$ (solid) cm^{-1}: 1688 (s, C=O); ^1H NMR (400 MHz, $CDCl_3$): 8.14 (1H, dd, C^5H, J_1 7.9, J_2 1.5), 7.60-7.50 (1H, m, C^7H), 7.40-7.30 (2H, m, C^6H/C^8H), 6.14 (1H, s, C^3H), 2.34 (3H, s, C^2CH_3);

^{13}C NMR (126 MHz, $CDCl_3$): 177.9, 166.1, 156.2, 133.2, 125.2, 124.7, 123.2, 117.7, 110.3, 20.6; LRMS: *m/z* (ESI^+) 161.1 ($[M+H]^+$, 100%); Analytical HPLC (RPB C18 column [100 mm × 3.2 mm, 35 °C]; 90:10 10 mM FA/H_2O:MeCN → 95: 5:0.1 MeCN: 10 mM/H_2O; 6 min, 3 min hold) Ret. Time = 5.94 min, Purity: 98.3%. These data are in good agreement with the literature values. [315,316]

3.10. 2-(2-Methyl-4*H*-chromen-4-ylidene)malononitrile

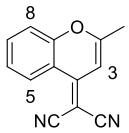

To a solution of **3.9** (1.6 g, 1.0 mmol, 1.0 eq.) in Ac_2O (10 mL), was added malononitrile (6.6 g, 10.0 mmol, 10.0 eq.). The reaction mixture was heated at 100 °C for 3 h, and cooled to ambient temperature. MeOH (20 mL) was added, the reaction mixture stirred at 50 °C for 20 min, and concentrated *in vacuo*. The product was crystallised from the resulting residue with Et_2O (1.42 g), and recrystallised from MeOH, to yield **3.10** (0.66 g, 69%) as pale red crystals: R_f: 0.35 (acetone - PE 1:4); mp: 184-186 °C (MeOH); $\bar{\nu}_{max}$ (solid) cm^{-1}: 2202 (s, C≡N), 1635 (s, C=C(CN)$_2$); ^{1}H NMR (500 MHz, $CDCl_3$): 8.94-8.90 (1H, m, C^5*H*), 7.74-7.69 (1H, m, C^7*H*), 7.48-7.43 (2H, m, C^6*H*/C^8*H*), 6.72 (1H, s, C^3*H*), 2.44 (3H, s, C^{2}C*H*$_3$); ^{13}C NMR (126 MHz, $CDCl_3$): 161.9 (C^2), 153.3 (C^{8a}), 153.0 (C^4), 134.8 (C^7), 126.4 (C^5), 125.9 (C^8), 119.0 (C^6), 117.7 (C^{4a}), 116.8 (CN), 115.8 (CN), 105.8 (C^3), 62.4 (*C*(CN)$_2$), 20.8 (*C*H$_3$); HRMS: *m/z* (ESI^+) [Found $(M+Na)^+$ 231.0533. $C_{13}H_8N_2O$ requires $(M+Na)^+$ 231.0529]; LRMS: *m/z* (ESI^+) 231.0 ($[M+Na]^+$, 100%); Analytical HPLC (RPB C18 column [100 mm × 3.2 mm, 35 °C]; 90:10 10 mM FA/H_2O:MeCN → 95:

5:0.1 MeCN: 10 mM/H_2O; 6 min, 3 min hold) Ret. Time = 6.64 min, Purity: >99%. These data are in good agreement with literature values.[212]

3.16. (*E/Z*)-2-(2-Methyl-4*H*-chromen-4-ylidene)-3-oxo-3-(piperidin-1-yl)propanenitrile

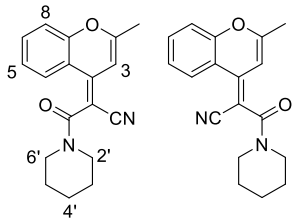

To a solution of **3.10** (25 mg, 0.12 mmol, 1.0 eq.) in toluene (4 mL), was added 4-Nitrobenzadehyde **3.14** (22 mg, 0.15 mmol, 1.2 eq.), AcOH (45 µL, 47 mg, 0.79 mmol, 6.6 eq.) and piperidine (45 µL, 39 mg, 0.45 mmol, 3.8 eq.) at ambient temperature. The reaction mixture was heated under reflux for 18 h, cooled to ambient temperature and concentrated *in vacuo*. The resulting residue was adsorbed onto Celite®, and the product purified by silica gel column chromatography, eluting with PE and acetone (10% acetone) to yield **3.16** (3 mg, 9%) as a red solid (isomer configuration not determined): R_f: 0.55 (acetone – PE 1:4); mp: 137-140 °C (acetone); $\bar{\nu}_{max}$ (solid) cm^{-1}: 1728 (s, C=O); ^1H NMR (500 MHz, acetone-d_6): 8.16 (1H, dd, J_1 8.0, J_2 1.5, C^5H), 7.61-7.57 (1H, m, C^7H), 7.35 (1H, s, C^3H), 7.37-7.33 (1H, m, C^6H), 7.28 (1H, dd, J_1 8.2, J_2 0.9, C^8H), 3.55-3.50 (4H, m, $C^{2'}H_2$/ $C^{6'}H_2$), 2.49 (3H, s, C^2CH_3), 1.73-1.66 (6H, m, $C^{3'}H_2$/ $C^{4'}H_2$/ $C^{5'}H_2$); ^{13}C NMR (126 MHz, acetone-d_6): 162.6 (C^4C), 162.0 (*C*O), 158.2 (*C*N), 153.6 (C^{8a}), 146.5 (C^4), 132.6 (C^7), 125.2 (C^5), 124.9 (C^6), 118.1 (C^{4a}), 117.6 (C^8), 106.2 (C^3), 99.1 (C^2), 51.3 ($C^{2'}$/$C^{6'}$), 26.8 ($C^{3'}$/$C^{5'}$), 25.3 (C^2CH_3), 25.1 ($C^{4'}$); HRMS: *m/z* (ESI^+) [Found $(M+Na)^+$ 317.1269. $C_{18}H_{18}N_2O_2$ requires $(M+Na)^+$ 317.1260]; LRMS: *m/z* (ESI^+) 295.0

([M+H]$^+$, 100%); Analytical HPLC (RPB C18 column [100 mm × 3.2 mm, 35 °C]; 90:10 H_2O 10 mM FA/H_2O:MeCN → 95:5 MeCN:10 mM FA/H_2O; 6 min, hold 3 min) Ret. Time = 7.94 min, Purity: >99%.

3.21. (*E*)-2-(2-(4-Hydroxystyryl)-4*H*-chromen-4-ylidene)malononitrile

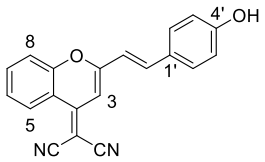

To a solution of **3.10** (25 mg, 0.12 mmol, 1.0 eq.) in toluene (3 mL), was added 4-Hydroxybenzaldehyde **3.19** (18 mg, 0.15 mmol, 1.2 eq.) followed by drop-wise addition of a mixture of AcOH and piperidine (1:1 *v/v*, 90 µL). The reaction mixture was heated under reflux for 18 h, cooled to ambient temperature and concentrated *in vacuo*. The resulting residue was adsorbed onto Celite®, and the product purified by silica gel column chromatography, eluting with PE and acetone (10% acetone) to yield **3.21** (12 mg, 58%) as a red solid: R_f: 0.12 (acetone - PE 1:4); mp: 260-262 °C (acetone); $\bar{\nu}_{max}$ (solid) cm^{-1}: 3389 (br, OH), 2204 (w, C≡N), 1624 (w, C=C(CN)$_2$); ^{1}H NMR (700 MHz, acetone-d_6): 8.90-8.86 (1H, m, C^5*H*), 7.89-7.92 (1H, m, C^7*H*), 7.78 (1H, d, *J* 16.0, C*H*C$^{1'}$), 7.78-7.74 (1H, m, C^8*H*), 7.67 (2H, d, *J* 8.6, C$^{2'}$*H*/ C$^{6'}$*H*), 7.62-7.57 (1H, m, C^6*H*), 7.21 (1H, d, *J* 16.0, C^{2}C*H*), 6.94 (2H, d, *J* 8.6, C$^{3'}$*H*/ C$^{5'}$*H*), 6.91 (1H, s, C^3*H*); ^{13}C NMR (176 MHz, acetone-d_6): 161.0 (C$^{4'}$), 159.9 (C^2), 154.0 (C^{8a}), 153.6 (C^4), 140.2 (C*H*C$^{1'}$), 136.1 (C^7), 131.2 (C$^{2'}$/C$^{6'}$), 128.1 (C$^{1'}$), 126.9 (C^6), 126.2 (C^5), 119.9 (C^8), 118.7 (C^{4a}), 118.0 (*C*N), 117.1 (C$^{3'}$/C$^{5'}$), 117.0 (C^2*C*H), 116.6 (C(*C*N)$_2$), 106.8 (C^3), 61.8 (*C*(CN)$_2$); HRMS: *m/z* (ESI$^-$) [Found (M-H)$^-$ 311.0813. $C_{20}H_{12}N_2O_2$ requires (M-H)$^-$ 311.0826]; LRMS: *m/z* (ESI$^+$) 311.0 ([M+H]$^+$, 100%); Analytical

HPLC (RPB C18 column [100 mm × 3.2 mm, 35 °C]; 90:10 10 mM FA/H_2O:MeCN → 95: 5:0.1 MeCN: 10 mM/H_2O; 6 min) Ret. Time = 6.65 min, Purity: >99%. These data are in good agreement with literature values.[216]

3.24. (*E*)-2-(4-Nitrostyryl)-4*H*-chromen-4-one

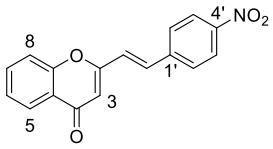

To MeOH (2.5 mL), Na metal (20 mg, 0.83 mmol, 5 eq.) was added portion-wise, and the reaction mixture stirred at ambient temperature for 10 min, or until the Na metal was consumed. To the NaOMe solution, compound **3.9** (22 mg, 0.14 mmol, 1.0 eq.) was added, and the reaction mixture stirred at ambient temperature for 5 min. 4-Nitrobenzaldehyde **3.14** (25 mg, 0.17 mmol, 1.2 eq.) was added, and the reaction mixture heated under reflux for 2 h. The precipitate was filtered, dried under reduced pressure, and washed with MeOH (10 mL) to yield **3.24** (25 mg, 61%) as a yellow solid: R_f: 0.40 (acetone - 3:7); mp: 283-285 °C (MeOH) [282-283 °C][317]; $\bar{\nu}_{max}$ (solid) cm^{-1}: 1623 (s, C=O), 1508 (s, NO_2 asym), 1337 (s, NO_2 sym); ^{1}H NMR (500 MHz, DMSO-d_6): 8.31 (2H, d, *J* 8.8, $C^{3'}H/C^{5'}H$), 8.04 (1H, dd, J_1 8.0, J_2 1.7, C^5H), 8.00 (2H, d, *J* 8.8, $C^{2'}H/C^{6'}H$), 7.85 (1H, dd, J_1 7.6, J_2 1.4, C^7H), 7.84 (1H, d, *J* 16.2, C^2CH), 7.73 (1H, d, *J* 8.2, C^8H), 7.50 (1H, dd, J_1 7.5, J_2 1.0, C^6H), 7.48 (1H, d, *J* 16.2, $CHC^{1'}$), 6.57 (1H, s, C^3H); ^{13}C NMR (126 MHz, DMSO-d_6): 177.2 (C^4), 160.9 (C^2), 155.6 (C^{8a}), 147.6 ($C^{4'}$), 141.6 ($C^{1'}$), 134.6 (C^7), 134.0 (C^2CH), 128.8 ($C^{2'}/C^{6'}$), 125.5 ($CHC^{1'}$), 125.1 (C^6), 124.9 (C^5), 124.2 ($C^{5'}/C^{3'}$), 123.6 (C^{4a}), 118.3 (C^8), 111.5 (C^3); HRMS: *m/z* (ESI^+) [Found $(M+Na)^+$ 316.0582. $C_{17}H_{11}NO_4$ requires $(M+Na)^+$ 316.0580];

LRMS: *m/z* (ESI$^+$) 294.1 ([M+H]$^+$, 100%); Analytical HPLC (RPB C18 column [100 mm × 3.2 mm, 35 °C]; 70:30:0.1 H_2O:MeCN:TFA → 95: 5:0.1 MeCN:H_2O:TFA; 6 min, 3 min hold) Ret. Time = 5.96 min, Purity: 96.6%. These data are in good agreement with literature values.[317]

3.25. 2-(1-(4-Nitrophenyl)-2-(4-oxo-4*H*-chromen-2-yl)ethyl)malononitrile

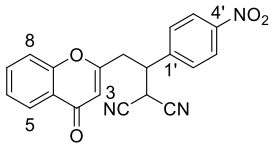

To a solution of **3.24** (30 mg, 0.10 mmol, 1.0 eq.) in THF (3 mL), was added BF_3:Et_2O (15 µL, 0.12 mmol, 1.2 eq.) and the solution was stirred at ambient temperature for 0.5 h. A solution of malononitrile (8 mg, 0.12 mmol, 1.2 eq.) and NaH (60% dispersion mineral oil, 5 mg, 0.20 mmol, 2.0 eq.) in THF (2 mL) was added drop-wise at ambient temperature and stirred for 1 h. Further NaH (60% dispersion mineral oil, 5 mg, 0.2 mmol, 2.0 eq.) was added, the reaction mixture heated under reflux for 18 h, cooled to ambient temperature, and concentrated *in vacuo*. The resulting residue was adsorbed onto Celite®, and the product purified by silica gel column chromatography, eluting with PE and acetone (20% acetone) to yield **3.25** (5.8 mg, 16%) as a yellow solid: R_f: 0.24 (acetone - PE 3:7); mp: 198-201 °C (acetone); $\bar{\nu}_{max}$ (solid) cm^{-1}: 2360 (m, C≡N), 1738 (s, C=O), 1653 (m, C=C(CN)$_2$), 1512 (s, NO_2 asym), 1346 (s, NO_2 sym); ^{1}H NMR (500 MHz, DMSO-d_6): 8.26 (2H, d, *J* 8.5, C$^{3'}$*H*/C$^{5'}$*H*), 7.92 (1H, dd, *J* 7.9, *J* 1.6, C^5*H*), 7.80 (2H, d, *J* 8.5, C$^{2'}$*H*/C$^{6'}$*H*), 7.79-7.74 (1H, m, C^7*H*), 7.53 (1H, d, *J* 8.4, C^8*H*), 7.43 (1H, dd, J_1 7.5, J_2 1.0, C^6*H*), 6.29 (1H, s, C^3*H*), 5.52 (1H, d, *J* 6.3, C*H*(CN)$_2$), 4.39 (1H, m, C*H*C$^{1'}$), 3.40 (2H, d, *J* 7.2, C^{2}CH_2); ^{13}C NMR (126 MHz, DMSO-d_6):

176.8 (C^4), 164.8 (C^2), 156.0 (C^{8a}), 147.7 ($C^{4'}$), 144.0 ($C^{1'}$), 134.4 (C^7), 130.0 ($C^{2'}/C^{6'}$), 125.6 (C^6), 124.9 (C^5), 123.9 ($C^{3'}/C^{5'}$), 123.0 (C^{4a}), 118.2 (C^8), 112.9 (*C*N), 112.7 (*C*N), 111.7 (C^3), 41.7 (*C*H$C^{1'}$), 35.7 (C^2*CH*), 28.6 ($C^{3'}$); HRMS: *m/z* (ESI^+) [Found $(M+H)^+$ 360.0980. $C_{20}H_{13}N_3O_4$ requires $(M+H)^+$ 360.0979]; LRMS: *m/z* (ESI^+) 360.2 ($[M+H]^+$, 100%).

3.27. (*E*)-4-(2-(4-(Dicyanomethylene)-4*H*-chromen-2-yl)vinyl)phenyl trifluoromethanesulfonate

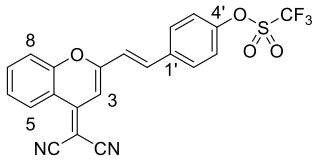

To a solution of **3.21** (840 mg, 2.69 mmol, 1.0 eq.) in pyridine (20 mL), was added triflic anhydride (678 µL, 1.14 g, 4.04 mmol, 1.5 eq.) drop-wise at 0 °C and the solution was stirred for 10 min, followed by stirring at ambient temperature for a further 10 min, and then quenched by addition of 1 M aq. HCl (10 mL). The organic components were extracted with EtOAc (3 × 30 mL), the organic phases combined, washed with aq. $CuSO_4$ (0.2 M, 2 × 20 mL), sat. aq. EDTA (2 × 20 mL), brine (2 × 20 mL), dried over $MgSO_4$, filtered and concentrated *in vacuo*. The resulting residue was adsorbed onto Celite®, and the product purified by silica gel column chromatography, eluting with PE and acetone (10% acetone) to yield **3.27** (420 mg, 35%) as a yellow solid: R_f: 0.33 (acetone - PE 1:4); mp: 179-182 °C (acetone); $\bar{\nu}_{max}$ (solid) cm^{-1}: 2212 (s, C≡N), 1638 (m, C=C$(CN)_2$), 1419 (s, S=O), 1134 (s, S=O); ^{1}H NMR (500 MHz, acetone-d_6): 8.89 (1H, dd, J_1 8.4, J_2 1.2, C^5*H*), 8.04-8.00 (2H, m, $C^{2'}$*H*/$C^{6'}$*H*), 7.99-7.94 (1H, m, C^7*H*), 7.91 (1H, d, *J* 16.0, C^2C*H*), 7.82-7.78 (1H, dd, J_1 8.4, J_2 1.0, C^8*H*), 7.68-7.62 (1H, m, C^6*H*), 7.62-7.58 (2H, m, $C^{3'}$*H*/$C^{5'}$*H*),

7.55 (1H, d, *J* 16.0, C*H*C$^{1'}$), 7.05 (1H, s, C^{3}*H*); ^{13}C NMR (126 MHz, acetone-d_6): 158.3 (C^{2}), 153.7 (C^{4}), 153.3 (C^{8a}), 151.2 (C$^{4'}$), 137.1 (C^{2}C*H*), 136.9 (C$^{1'}$), 136.2 (C^{7}), 131.0 (C$^{2'}$/C$^{6'}$), 127.0 (C^{6}), 126.1 (C^{5}), 123.1 (C$^{3'}$/C$^{5'}$), 122.5 (C*H*C$^{1'}$), 120.6 (*C*F$_3$), 119.9 (C^{8}), 118.4 (C^{4a}), 117.5 (C(*C*N)$_2$), 116.1 (C(*C*N)$_2$), 108.4 (C^{3}), 63.6 (*C*(CN)$_2$); ^{19}F NMR (376 MHz, acetone-d_6): −74.1; HRMS: *m/z* (FI$^+$) [Found (M)$^+$ 444.0391. $C_{21}H_{11}N_2O_4F_3S$ requires (M)$^+$ 444.0392]; Analytical HPLC (RPB C18 column [100 mm × 3.2 mm, 35 °C]; 90:10 H_2O 10 mM FA/H_2O:MeCN → 95:5 MeCN:10 mM FA/H_2O; 6 min, 3 min hold) Ret. Time = 8.14 min, Purity: 98.6%.

3.29. (*E*)-2-(2-(4-Azidostyryl)-4*H*-chromen-4-ylidene)malononitrile

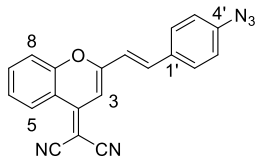

To a solution of **3.1** (26 mg, 0.08 mmol, 1.0 eq.) in aq. HCl (5 M, 5 mL), was added aq. $NaNO_2$ (29 mg, 0.42 mmol, 5.3 eq., 0.3 mL) drop-wise at 0 °C and the reaction mixture was stirred for 10 min. To the reaction mixture, aq. NaN_3 (109 mg, 1.68 mmol, 21 eq., 0.9 mL) was added drop-wise, and stirred at 0 °C – 5 °C for 1 h. H_2O (20 mL) was then added, the organic components were extracted with EtOAc (2 × 50 mL), the organic phases were combined, dried over $MgSO_4$, filtered and concentrated *in vacuo*. The resulting residue was adsorbed onto Celite®, and the product purified using silica gel column chromatography, eluting with PE and acetone (40% acetone), to yield **3.29** (15 mg, 56%) as a yellow/orange solid: R_f: 0.65 (acetone - PE 4:6); mp: 188-191 °C (acetone); $\bar{\nu}_{max}$ (solid) cm^{-1}: 2208 (m, C≡N), 2119 (m, N≡N), 1631 (m, C=C(CN)$_2$); ^{1}H NMR (500 MHz, acetone-d_6): 8.89 (1H, dd, J_1 8.4,

J_2 1.2, C^8*H*), 7.98-7.92 (1H, m, C^7*H*), 7.90-7.84 (3H, m, C$^{3'}$*H*/C$^{5'}$*H*/C^{2}C*H*), 7.80 (1H, dd, J_1 8.5, J_2 1.0, C^5*H*), 7.67-7.62 (1H, m, C^6*H*), 7.41 (1H, d, *J* 16.1, C*H*C$^{1'}$), 7.20 (2H, d, *J* 8.5, C$^{2'}$*H*/C$^{6'}$*H*), 6.99 (C^3*H*); ^{13}C NMR (126 MHz, acetone-d_6): 159.2 (C^2), 153.9 (C^4), 153.5 (C^{8a}), 143.0 (C$^{4'}$), 138.7 (*C*HC$^{1'}$), 136.2 (C^6), 133.3 (C$^{1'}$), 130.9 (C$^{2'}$/C$^{6'}$), 127.0 (C^7), 126.2 (C^5), 120.8 (C$^{3'}$/C$^{5'}$), 120.1 (C^2*C*H), 120.0 (C^8), 118.6 (C^{4a}), 117.8 (C(*C*N)$_2$), 116.4 (C(*C*N)$_2$), 107.8 (C^3), 62.9 (*C*(CN)$_2$); HRMS: *m/z* (FI$^+$) [Found (M)$^+$ 337.0985. $C_{20}H_{11}N_5O$ requires (M)$^+$ 337.0964]; Analytical HPLC (RPB C18 column [100 mm × 3.2 mm, 35 °C]; 70:30:0.1 H_2O:MeCN:TFA → 95: 5:0.1 MeCN:H_2O:TFA; 6 min; 3 min hold) Ret. Time = 7.64 min, Purity: >99%. These data are in good agreement with the literature values.[212]

3.34. Methyl 3-(bromomethyl)-4-nitrobenzoate

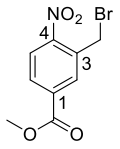

To a solution of **3.35** (100 mg, 0.47 mmol, 1.0 eq.) in CH_2Cl_2 (2.4 mL) under an argon atmosphere, was added triphenylphosphine (136 mg, 0.52 mmol, 1.1 eq.) and tetrabromomethane (173 mg, 0.52 mmol, 1.1 eq.). The reaction mixture was stirred vigorously at ambient temperature for 5 h, and concentrated *in vacuo*. The resulting residue was adsorbed onto Celite® and the product purified using silica gel column chromatography, eluting with PE and Et_2O (20% Et_2O) to yield **3.34** (104 mg, 0.38 mmol, 81%) as a colourless solid: R_f: 0.66 (Et_2O – PE, 1:1); mp: 114-116 °C; $\bar{\nu}_{max}$ (solid) cm^{-1}: 1717 (s, C=O), 1525 (s, NO_2 asym), 1434 (s, C-O), 1353 (m, NO_2 sym); ^{1}H NMR (500 MHz, $CDCl_3$): 8.23 (1H, d, *J* 1.8, C^2*H*), 8.12 (1H, dd, *J* 8.5,

J 1.8, C^5*H*), 8.05 (1H, d, *J* 8.5, C^6*H*), 4.83 (2H, s, C*H*$_2$Br), 3.99 (3H, s, OC*H*$_3$); ^{13}C NMR (126 MHz, $CDCl_3$): 164.8 (C=O), 150.6 (C^4), 134.7, 133.9 (C^1/C^3), 133.2 (C^3/C^1), 130.7 (C^6), 125.7 (C^5), 53.2 (O*C*H$_3$), 28.3 (*C*H$_2$Br); HRMS: *m/z* (FI$^+$) [Found (M)$^+$ 272.9635. $C_9H_8BrNO_4$ requires (M)$^+$ 272.9637]; Analytical HPLC (RPB C18 column [100 mm × 3.2 mm, 35 °C]; 90:10:0.1 H_2O:MeCN:TFA → 95:5:0.1 MeCN:H_2O:TFA; 6 min, 3 min hold) Ret. Time = 6.66 min, Purity: 97.2%.

3.35. Methyl 3-(hydroxymethyl)-4-nitrobenzoate

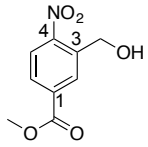

To a solution of Methyl-3-formyl-4-nitrobenzoate **3.36** (1.0 g, 4.8 mmol, 1.0 eq.) in MeOH/THF (1:4 *v/v*, 20 mL), was added $NaBH_4$ (91 mg, 2.4 mmol, 0.25 eq.) portion-wise at ambient temperature and stirred for 15 h. The reaction mixture was concentrated *in* vacuo, H_2O (15 mL) added, and the organic components extracted with $CHCl_3$ (3 × 15 mL). The organic phases were combined, washed with brine (1 × 30 mL), dried over $MgSO_4$, filtered, and concentrated and dried *in vacuo* to yield **3.35** (696 mg, 69%) as an orange solid: R_f: 0.44 (Et_2O – PE, 1:1); mp: 51-54 °C; $\bar{\nu}_{max}$ (solid) cm^{-1}: 3263 (br, OH), 1721 (s, C=O), 1520 (s, NO_2 asym), 1339 (m, NO_2 sym); ^{1}H NMR (500 MHz, $CDCl_3$): 8.44-8.41 (1H, m, C$_2$*H*), 8.14-8.06 (2H, m, C^5*H*, C^6*H*), 5.02 (2H, s, C*H*$_2$OH), 3.97 (3H, s, C*H*$_3$); ^{13}C NMR (126 MHz, $CDCl_3$): 165.4 (*C*OOMe), 150.0 (C^4), 137.3 (C^3), 134.9 (C^1), 131.0 (C^2), 129.6 (C^6), 125.1 (C^5), 62.4 (CH_2), 53.2 (O*C*H$_3$); HRMS: *m/z* (ESI$^+$) [Found (M+Na)$^+$ 234.03740, $C_9H_9NO_5$ requires (M+Na)$^+$ 234.03729]; LRMS: *m/z* (ESI$^+$) 234.1 ([M+Na]$^+$,

100%); Analytical HPLC (RPB C18 column [100 mm × 3.2 mm, 35 °C]; 90:10 10 mM FA/H_2O:MeCN → 95:5 MeCN:10 mM FA/H_2O; 6 min) Ret. Time = 5.39 min, Purity: 94.8%.

3.37. Methyl 3-(((*tert*-butyldimethylsilyl)oxy)methyl)-4-nitrobenzoate

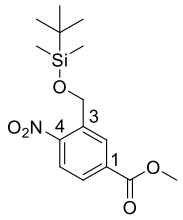

To a solution of **3.35** (265 mg, 1.26 mmol, 1.0 eq.) in DMF (4.5 mL), imidazole (170 mg, 2.51 mmol, 2 eq.) was added. TBDMSCl (378 mg, 2.51 mmol, 2 eq.) was then added portion-wise, and the reaction solution stirred at ambient temperature for 1 h. H_2O (20 mL) was added and the organic components were extracted with Et_2O (20 mL). The organic layer was washed with H_2O (3 × 20 mL), dried over $MgSO_4$, filtered, and concentrated *in vacuo*. The resulting residue was adsorbed onto Celite®, and the product purified by silica gel column chromatography, eluting with PE and Et_2O (5% Et_2O) to yield **3.37** (332 mg, 1.02 mmol, 81%) as a colourless solid: R_f: 0.65 (Et_2O – PE, 1:9); mp: 42-44 °C; $\bar{\nu}_{max}$ (solid) cm^{-1}: 1723 (s, C=O), 1525 (s, NO_2 asym), 1301 (s, NO_2 sym); ^1H NMR (500 MHz, $CDCl_3$): 8.56 (1H, s, C^2H), 8.19-8.00 (2H, m, C^5H, C^6H), 5.09 (2H, s, CH_2OSi), 3.96 (3H, s, OCH_3), 0.99 (9H, s, $C(CH_3)_3$), 0.16 (6H, s, $Si(CH_3)_2$); ^{13}C NMR (126 MHz, $CDCl_3$): 165.3 (*C*OOMe), 148.8 (C^4), 138.4 (C^3), 134.4 (C^1), 129.7 (C^2), 128.6 (C^5), 124.5 (C^6), 61.8 (C^3CH_2), 52.8 ($COOCH_3$), 25.7 ($C(CH_3)_3$), 18.7 ($C(CH_3)_3$), −5.6 ($Si(CH_3)_2$); HRMS: *m/z* (ESI^+) [Found $(M+Na)^+$ 348.1247, $C_{15}H_{23}NO_5Si$ requires $(M+Na)^+$ 348.1243]; Analytical HPLC (RPB C18 column [100 mm ×

3.2 mm, 35 °C]; 90:10 10 mM FA/H_2O:MeCN → 95:5 MeCN:10 mM FA/H_2O; 6 min) Ret. Time = 8.56 min, Purity: >99%.

3.38. (3-(((*tert*-Butyldimethylsilyl)oxy)methyl)-4-nitrophenyl)methanol

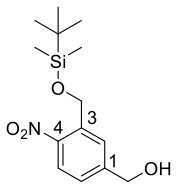

To a solution of **3.37** (828 mg, 3.92 mmol, 1.0 eq.) in DMF (8 mL), was added imidazole (533 mg, 7.84 mmol, 2 eq.). TBDMSCl (1.30 g, 8.63 mmol, 2.2 eq.) was then added portion-wise, and the reaction solution stirred at ambient temperature for 1 h. H_2O (30 mL) was added, and the organic components were extracted with Et_2O (30 mL). The organic layer was washed with H_2O (3 × 20 mL), dried over $MgSO_4$, filtered and concentrated *in vacuo*. The resulting residue was dissolved in MeOH (10 mL) and THF (20 mL). To the reaction solution, $NaBH_4$ (446 mg, 11.8 mmol, 3.0 eq.) was added portion-wise, and stirred at ambient temperature for 15 h. The reaction solution was concentrated *in vacuo*, and the resulting residue dissolved in Et_2O (30 mL). The organic components were washed with H_2O (30 mL), dried over $MgSO_4$, filtered and concentrated *in vacuo*. The resulting residue was adsorbed onto Celite®, and the product purified by silica gel column chromatography, eluting with PE and Et_2O (30% Et_2O) to yield **3.38** (682 mg, 2.30 mmol, 60%) as a colourless solid: R_f: 0.45 (Et_2O – PE, 3:7); mp: 56-58 °C; $\bar{\nu}_{max}$ (solid) cm^{-1}: 3220 (br, OH), 1516 (s, NO_2 asym), 1335 (s, NO_2 sym); ^{1}H NMR (500 MHz, $CDCl_3$): 8.10 (1H, d, *J* 8.7,C^5*H*), 7.88 (1H, s, C^2*H*), 7.42 (1H, d, *J* 8.7, C^6*H*), 5.10 (2H, s, CH_2OSi), 4.82 (2H, s, CH_2OH), 0.97 (9H, s, C(CH_3)$_3$), 0.16 (6H, s, Si(CH_3)$_2$); ^{13}C NMR (126 MHz, $CDCl_3$):

147.5 (C^4), 145.6 (C^1), 138.9 (C^3), 125.8 (C^2), 125.23 (C^6), 125.18 (C^5), 64.5 (CH_2OH), 62.4 (C^3CH_2), 26.1 ($C(CH_3)_3$), 18.5 ($C(CH_3)_3$), −5.2 ($Si(CH_3)_2$); HRMS: *m/z* (ESI^+) [Found $(M+Na)^+$ 320.1299, $C_{15}H_{23}NO_5Si$ requires $(M+Na)^+$ 320.1289]; Analytical HPLC (RPB C18 column [100 mm × 3.2 mm, 35 °C]; 90:10 10 mM FA/H_2O:MeCN → 95:5 MeCN:10 mM FA/H_2O; 6 min, 3 min hold) Ret. Time = 7.64 min, Purity: 96.5%.

3.39. 3-(((*tert*-Butyldimethylsilyl)oxy)methyl)-4-nitrobenzaldehyde

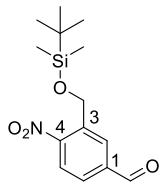

To a solution of **3.38** (70 mg, 0.24 mmol, 1.0 eq.) in CH_2Cl_2 (3 mL) and acetone (0.3 mL), MnO_2 (205 mg, 2.40 mmol, 10 eq.) was added and the reaction mixture stirred at ambient temperature for 3 days. The reaction was filtered through Celite®, and the Celite® washed with CH_2Cl_2 (30 mL). The filtrate was concentrated *in vacuo*. The resulting residue was adsorbed onto Celite®, and the product purified by silica gel column chromatography, eluting with PE and Et_2O (20% Et_2O) to yield **3.39** (47 mg, 0.16 mmol, 67%) as a colourless solid: R_f: 0.80 (Et_2O – PE, 4:6); mp: 24-25 °C; $\bar{\nu}_{max}$ (solid) cm^{-1}: 1702 (s, C=O), 1525 (s, NO_2 asym), 1309 (m, NO_2 sym); ^1H NMR (500 MHz, $CDCl_3$): 8.42-8.39 (1H, m, C^2H), 8.19 (1H, d, *J* 8.2, C^5H), 7.95-7.92 (1H, m, C^6H), 5.13 (2H, s, C^3CH_2), 0.99 (9H, s, $C(CH_3)_3$), 0.18 (6H, s, $Si(CH_3)_2$); ^{13}C NMR (126 MHz, $CDCl_3$): 190.9 (C=O), 149.7 (C^4), 139.5 (C^3), 139.4 (C^1), 130.5 (C^2), 127.9 (C^6), 125.5 (C^5), 61.9 (C^3CH_2), 26.1 ($C(CH_3)_3$), 18.5 ($C(CH_3)_3$), −5.2 ($Si(CH_3)_2$); HRMS: *m/z* (ESI^+) [Found $(M+MeOH+Na)^+$ 350.1393, $C_{14}H_{21}NO_4Si$ requires $(M+MeOH+Na)^+$ 350.1394]; Analytical HPLC

(RPB C18 column [100 mm × 3.2 mm, 35 °C]; 90:10 10 mM FA/H_2O:MeCN → 95:5 MeCN:10 mM FA/H_2O; 6 min, 3 min hold) Ret. Time = 8.15 min, Purity: >99%.

7.2.3 Chapter 5 compounds

5.1. (*E*)-1-Ethyl-2-(2-(6-hydroxy-2,3-dihydro-1*H*-xanthen-4-yl)vinyl)-3,3-dimethyl-3*H*-indol-1-ium iodide

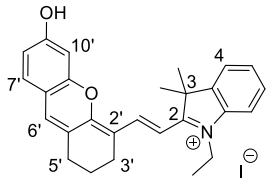

To a solution of **5.24** (1.00 g, 1.57 mmol, 1.0 eq.) in 1,2-Dichloroethane (40 mL), was added Resorcinol **5.27** (260 mg, 2.36 mmol, 1.5 eq.) and Et_3N (0.41 mL, 0.30 g, 6.28 mmol, 4.0 eq.). The reaction mixture was heated under reflux at 90 °C for 4 h, then cooled to ambient temperature, and concentrated *in vacuo*. The resulting residue was adsorbed onto Celite®, and the product purified using silica gel column chromatography, eluting with CH_2Cl_2 and MeOH (gradient, 2→3% MeOH) to yield **5.1** (445 mg) as an impure green/blue metallic solid. 90 mg of **5.1** was further purified by semi-preparative HPLC (Phenomenex Luna C18(2) 10 µm column [250 × 10 mm], 55:45:0.1 MeCN:H_2O:TFA → 90:10:0.1 MeCN:H_2O:TFA; 5 min, 5 mL/min, Ret Time = 3.80) to yield **5.1** (45 mg) as a green/blue solid: R_f: 0.07 (MeOH – CH_2Cl_2, 6:94); mp: 256-258 °C; $\bar{\nu}_{max}$ (solid) cm^{-1}: 1673 (m, C=O), 1530 (s, C=N), 1457 (s, C=C), 1166 (s, C-O), 1110 (s, C-O); ^{1}H NMR (500 MHz, MeOD-d_4): 8.77 (d, 1H, *J* 15.1, $C^{2'}CH$), 7.65 (d, 1H, *J* 7.4, C^7H), 7.55-7.49 (m, 2H, C^6H, C^4H), 7.46-7.39 (m, 3H, $C^{6'}H$, $C^{7'}H$, C^5H), 6.88-6.84 (m, 2H, $C^{8'}H$, $C^{10'}H$), 6.47 (d, 1H, *J* 15.1, C^2CH), 4.37 (q, 2H, *J* 7.3, NCH_2CH_3), 2.79 (t, 2H, *J* 6.0, $C^{5'}H_2$), 2.73 (t, 2H, *J* 6.1, $C^{3'}H_2$), 1.99-1.90 (m, 2H, $C^{4'}H_2$), 1.82 (s, 6H, $C(CH_3)_2$), 1.47 (t, 3H, *J* 7.3, NCH_2CH_3); ^{13}C NMR (126 MHz, MeOD-d_4): 176.7 (C^2), 162.7 ($C^{9'}$), 162.6 ($C^{1'a}$), 155.2 ($C^{10'a}$), 145.8

($C^{2'}CH$), 142.3 (C^{3a}), 141.5 (C^{7a}), 135.2 ($C^{6'}$), 129.4 ($C^{7'}$), 129.1 (C^{6}), 127.0 (C^{5}), 126.4 ($C^{5'a}$), 122.7 (C^{4}), 115.3 ($C^{6'a}$), 114.7 ($C^{8'}/C^{10'}$), 114.4 ($C^{2'}$), 112.3 (C^{7}), 102.5 ($C^{2}CH$), 101.9 ($C^{8'}/C^{10'}$), 50.6 (C^{3}), 40.2 (CH_2CH_3), 28.9 ($C^{5'}$), 27.2 ($C(CH_3)_2$), 24.0 ($C^{3'}$), 20.7 ($C^{4'}$), 11.6 (CH_2CH_3); ^{19}F NMR (376 MHz, MeOD-d_4): −76.9, <0.0001% *w/w* TFA; HRMS: *m/z* (ESI^+) [Found $(M-I)^+$ 398.21149, $C_{29}H_{28}NO_4F_3$ requires $(M-I)^+$ 398.21146]; Analytical HPLC (RPB C18 column [100 mm × 3.2 mm, 35 °C]; 50:50:0.1 H_2O:MeCN:TFA → 95:5:0.1 MeCN:H_2O:TFA, 6 min) Ret. Time = 4.05 min, Purity: >99%.

5.8. (*E*)-2-(2-(6-((3-((3-(3,5-Dimethylisoxazol-4-yl)-5-((4-fluorophenyl)(hydroxy)methyl)phenoxy)methyl)-4-nitrobenzyl)oxy)-2,3-dihydro-1*H*-xanthen-4-yl)vinyl)-1-ethyl-3,3-dimethyl-3*H*-indol-1-ium iodide

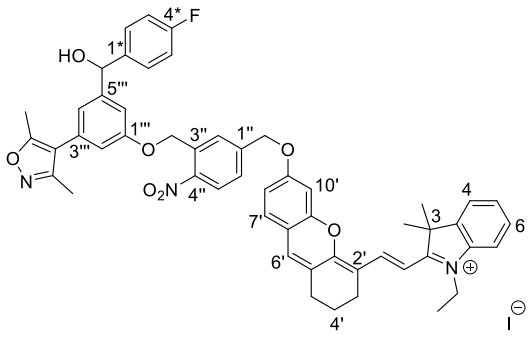

To a solution of **5.15** (10 mg, 0.02 mmol, 1.0 eq.) and **5.1** (10.8 mg, 0.02 mmol, 1 eq.) in $CHCl_3$ (0.25 mL), was added Et_3N (5.6 µL, 4.1 mg, 0.04 mmol, 2.0 eq.). The reaction solution was heated to 55 °C for 16 h, cooled to ambient temperature, and concentrated *in vacuo*. From the resulting residue, the product was purified, by semi-preparative HPLC (Phenomenex Luna C18(2) 10 µm column [250 × 10 mm]; 65:35:0.1 MeOH:H_2O:TFA → 90:10:0.1 MeOH:H_2O:TFA; 7 min, 5 mL/min) to yield **5.8** (4.5 mg, 23%) as a

blue solid: R_f: 0.19 (Acetone – PE, 4:6); mp: 115-118 °C; $\bar{\nu}_{max}$ (solid) cm^{-1}: 1571 (s, C=N), 1525 (m, NO_2 asym), 1439 (s, C=C), 1341 (m, NO_2 sym), 1188 (s, C-O), 1115 (m, C-F); ^{1}H NMR (500 MHz, MeOD-d_4): 8.75 (1H, d, J 14.9 $C^{2'}CH$), 8.23 (1H, d, J 8.4, $C^{5''}H$), 7.95 (1H, s, $C^{2''}H$), 7.74-7.69 (1H, m, $C^{6''}H$), 7.60-7.52 (3H, m, $C^{7}H$, $C^{10'}H$, $C^{8'}H$), 7.46-7.37 ($4H_2$), 2.74 (2H, t, J 6.3, $C^{3'}CH_2$), 2.30 (3H, s, CH_3CN/CH_3CO), 2.13 (3H, s, CH_3CN/CH_3CO), 1.96 (2H, tt, J_1 6.3, J 6.3, $C^{4'}H_2$), 1.79 (6H, s, $C^3(CH_3)_2$), 1.50 (3H, t, J 7.3, NCH_2CH_3); ^{13}C NMR (126 MHz, MeOD-d_4): 179.1 (C^2), 167.0 (CH_3CO/ CH_3CN), 163.6 (J_{C-F} 241.5, C^{4*}), 164.5 ($C^{9'a}$), 162.9 ($C^{10'a}$), 162.8 ($C^{1'a}$), 159.9 (CH_3CO/CH_3CN), 159.8 ($C^{1'''}$), 155.7 ($C^{7'a}$), 148.8 ($C^{3'''}$), 148.5 ($C^{4''}$), 147.4 ($C^{2'}CH$), 144.7 ($C^{3''}$), 143.7 (C^{3a}), 142.6 (C^{7a}), 142.0 (J_{C-F} 2.3, C^{1*}), 135.2 ($C^{1''}$), 134.7 ($C^{6'}$), 132.9 ($C^{5'''}$), 130.4 ($C^{10'}$/$C^{8'}$), 130.3 ($C^{7'}$), 129.6 (J_{C-F} 8.0, C^{2*}/C^{6*}), 129.0 ($C^{5'a}$), 128.7 (C^5), 128.5 ($C^{2''}$), 128.4 ($C^{6''}$), 126.7 ($C^{5''}$), 123.9 ($C^{10'}$/$C^{8'}$), 121.5 ($C^{2'''}$), 117.6 ($C^{3'''}C$), 116.1 (J_{C-F} 22.0, C^{3*}/C^{5*}), 115.8 ($C^{2'}$), 115.3 ($C^{2'''}H$), 115.2 ($C^{6'''}H$), 113.9 (C^7), 113.7 ($C^{4'''}$), 104.9 (C^2CH), 102.9 ($C^{2''}H$), 75.9 (, 70.5 ($C^{1''}CH_2O$), 68.3 ($C^{3''}CH_2O$), 52.1 (C^3), 41.6 (NCH_2CH_3), 30.2 ($C^{3'}H_2$), 28.3 $C^3(CH_3)_2$, 25.2 ($C^{5'}H_2$), 21.8 ($C^{4'}H_2$), 13.0 (NCH_2CH_3), 11.9 (CH_3CN/CH_3CO), 11.0 (CH_3CN/CH_3CO); ^{19}F NMR (376 MHz, MeOD-d_4): −117.4 ($C^{4*}F$), −77.0 <0.0001% *w/w* TFA; HRMS: *m/z* (ESI^+) [Found $(M-I)^+$ 858.3542, $C_{55}H_{49}N_3O_9F_4$ requires $(M-I)^+$ 858.3549]; Analytical HPLC (RPB C18 column [100 mm × 3.2 mm, 35 °C]; 40:60:0.1 H_2O:MeCN:TFA → 100:0:0.1 MeCN:H_2O:TFA, 6 min) Ret. Time = 5.36 min, Purity: >99%.

5.15. (3-((5-(Bromomethyl)-2-nitrobenzyl)oxy)-5-(3,5-dimethylisoxazol-4-yl)phenyl)(4-fluorophenyl)methanol

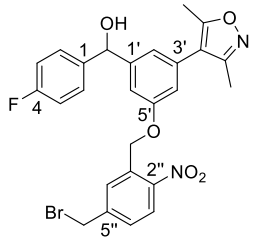

To a solution of **5.13** (82.5 mg, 0.278 mmol, 1.0 eq.) in DMF (2.5 mL), was added Cs_2CO_3 (90 mg, 0.278 mmol, 1 eq.) under an argon atmosphere. The reaction mixture was stirred at ambient temperature for 10 min, then added drop-wise to a solution of **5.16** (172 mg, 0.556 mmol, 2 eq.) in DMF (2.5 mL) at 0 °C, under an argon atmosphere. The reaction mixture was stirred at 0 °C for 1 h, Cs_2CO_3 (45 mg, 0.5 eq.) was added and stirred for a further 1 h at ambient temperature. The reaction mixture was then heated to 35 °C for 15 min, cooled to ambient temperature, and concentrated *in vacuo*. To the resulting residue, EtOAc (25 mL), and 1 M aq. HCl (20 mL) were added. The organic components were extracted into the EtOAc, the organic layer washed with H_2O (3 × 20 mL), dried over $MgSO_4$, filtered and concentrated *in vacuo*. The resulting residue was adsorbed onto Celite®, and the product purified using silica gel column chromatography, eluting with PE and acetone (gradient, 10→20% acetone) to yield **5.15** (29 mg, 20%) as a colourless solid: R_f: 0.61 (Acetone – PE, 4:6); mp: 132-134 °C; $\bar{\nu}_{max}$ (solid) cm^{-1}: 3339 (br, OH), 1589 (s, C=N), 1521 (s, NO_2 sym), 1339 (s, NO_2 asym); ^1H NMR (500 MHz, $CDCl_3$): 8.15 (1H, d, *J* 8.5, $C^{3''}H$), 7.88 (1H, d, *J* 1.8, $C^{6''}H$), 7.52 (1H, dd, J_1 8.5, J_2 1.8, $C^{4''}H$), 7.32-7.39 (2H, m, C^2H, C^6H), 7.00-7.07 (3H, m, C^3H, C^5H, $C^{2'}H$), 6.86-6.88 (1H, m, $C^{4'}H$), 6.76-6.79 (1H, m,

C$^{6'}$*H*), 5.85 (1H, s, C*H*OH), 5.47 (2H, s, CH_2O), 4.51 (2H, s, CH_2Br), 2.46 (1H, d, *J* 3.0, O*H*), 2.36 (3H, s, CH_3CN/CH_3CO), 2.21 (3H, s, CH_3CN/CH_3CO); ^{13}C NMR (126 MHz, $CDCl_3$): 165.6 (CH_3*C*ON), 162.5 (d, $J_{C\text{-}F}$ 242.0, C^4), 158.60 (C$^{5'}$), 158.58 (CH_3*C*NO), 146.5 (C$^{3'}$), 146.3 (C$^{2''}$), 144.4 (C$^{5''}$), 139.3 (d, $J_{C\text{-}F}$ 2.9, C^1), 134.3 (C$^{1''}$), 132.4 (C$^{1'}$), 129.2 (C$^{6''}$), 129.1 (C$^{4''}$), 128.4 (d, $J_{C\text{-}F}$ 8.0, C^2/C^6), 125.9 (C$^{3''}$), 120.7 (C$^{4'}$), 116.4 (C$^{3'}$*C*CON), 115.7 (d, $J_{C\text{-}F}$ 21.0, C^3/C^5), 115.0 (C$^{6'}$), 112.4 (C$^{2'}$*H*), 75.7 (C*H*OH), 67.1 (*C*H_2O), 31.1 (*C*H_2Br), 11.8 (*C*H_3CN/*C*H_3CO), 11.0 (*C*H_3CN/*C*H_3CO); HRMS: *m/z* (ESI$^+$) [Found (M+FA+H)$^+$ 585.06881, $C_{26}H_{22}N_2O_5FBr$ requires (M+FA+H)$^+$ 585.06782]; Analytical HPLC (RPB C18 column [100 mm × 3.2 mm, 35 °C]; 90:10:0.1 H_2O:MeCN:TFA → 95:5:0.1 MeCN:H_2O:TFA, 6 min) Ret. Time = 7.30 min, Purity: >99%.

5.16. 2,4-Bis(bromomethyl)-1-nitrobenzene

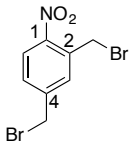

To a solution of **5.17** (66 mg, 0.36 mmol, 1 eq.), aq. HBr (48% *w/v*, 1 mL) was added, stirred at 65 °C for 24 h, and cooled to ambient temperature. H_2O (5 mL) was added, the pH adjusted to 7 using solid K_2CO_3, and the organic components extracted using $CHCl_3$ (2 × 5 mL). The organic phases were combined, dried over $MgSO_4$, filtered, concentrated and dried *in vacuo* to yield **5.16** (55 mg, 50%) as an orange/yellow oil: R_f: 0.64 (Et_2O - PE 2:8); $\bar{\nu}_{max}$ (neat) cm^{-1}: 1520 (s, NO_2 asym), 1340 (s, NO_2 sym); ^{1}H NMR (500 MHz, $CDCl_3$): 8.03 (1H, d, *J* 8.4, C^6*H*), 7.59 (1H, d, *J* 2.0, C^3*H*), 7.50 (1H, dd, J_1 8.4, J_2 2.0, C^5*H*), 4.82 (2H, s, C^{2}CH_2), 4.48 (2H, s, C^{4}CH_2); ^{13}C NMR

(126 MHz, $CDCl_3$): 147.5 (C^1), 144.0 (C^4), 133.7 (C^2), 133.2 (C^3), 130.2 (C^5), 126.3 (C^6), 30.7 (C^4CH_2), 28.9 (C^2CH_2); HRMS: *m/z* (FI^+) [Found $(M)^+$ 308.8843 ($^{79}Br^{81}Br$), $C_8H_7Br_2NO_2$ requires $(M)^+$ ($^{79}Br^{81}Br$) 308.8823]; Analytical HPLC (RPB C18 column [100 mm × 3.2 mm, 35 °C]; 90:10 10 mM FA/H_2O:MeCN → 95:5 MeCN:10 mM FA/H_2O; 6 min, 3 min hold) Ret. Time = 6.92 min, Purity: >99%.

5.17. (4-Nitro-1,3-phenylene)dimethanol

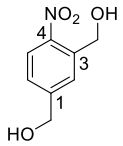

To a solution of Methyl-3-formyl-4-nitrobenzoate **3.36** (500 mg, 2.4 mmol, 1.0 eq.) in a mixture of MeOH and THF (1:4, *v/v*, 10 mL) under an argon atmosphere, was added $NaBH_4$ (273 mg, 7.2 mmol, 3.0 eq.) portion-wise at 0 °C. The reaction solution was gradually warmed to ambient temperature over 15 h, quenched by addition of 1 M aq. HCl (1 mL) and concentrated *in vacuo*. The resulting residue was dissolved in $CHCl_3$ (5 mL), and washed with H_2O (10 mL). The aqueous phase was saturated with solid NaCl, the organic components extracted with $CHCl_3$ (2 × 10 mL), the organic phases combined, dried over $MgSO_4$, filtered and concentrated *in vacuo*. From the resulting residue, the product was crystallised from $CHCl_3$ to yield **5.17** (170 mg, 1.0 mmol, 39%) as a white crystalline solid: R_f: 0.37 (Et_2O – PE 4:6); mp: 82-85 °C [Lit. 92-94 °C][318]; $\bar{\nu}_{max}$ (solid) cm^{-1}: 3242 (br, OH), 1512 (s, NO_2 asym), 1330 (s, NO_2 sym); ^1H NMR (500 MHz, CDCl3): 8.12 (1H, d, *J* 8.3, C^5H) 7.74 (1H, s, C^2H), 7.47 (1H, d, *J* 8.3, C^6H), 4.99 (2H, d, *J* 4.35, C^3CH_2), 4.84 (2H, d, *J* 4.35, C^1CH_2), 2.53 (1H, s, OH), 1.92 (1H, s, OH);

^{13}C NMR (126 MHz, $CDCl_3$): 147.8 (C^1), 146.8 (C^4), 137.3 (C^3), 127.8 (C^2), 126.3 (C^6), 125.7 (C^5), 62.8 (C^3CH_2), 64.2 (C_1CH_2); HRMS: *m/z* (ESI^+) [Found $(M+Na)^+$ 206.04249, $C_8H_9NO_4$ requires $(M+Na)^+$ 206.04238]; LRMS: *m/z* (ESI^+) 206.1 ($[M+Na]^+$, 100%); Analytical HPLC (RPB C18 column [100 mm × 3.2 mm, 35 °C]; 90:10:0.1 H_2O:MeCN:TFA → 95: 5:0.1 MeCN:H_2O:TFA; 6 min) Ret. Time = 4.20 min, Purity: 93.8%. These data are in good agreement with literature values.[318]

5.18. (3-((3-(Bromomethyl)-4-nitrobenzyl)oxy)-5-(3,5-dimethylisoxazol-4-yl)phenyl)(4-fluorophenyl)methanol

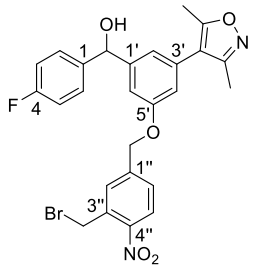

Procedure as described for compound **5.15** to yield **5.18** (25 mg, 17%) as a yellow oil: R_f: 0.58 (Acetone – PE, 4:6); $\bar{\nu}_{max}$ (neat) cm^{-1}: 3351 (br, OH), 1589 (s, C=N), 1524 (s, NO_2 asym), 1341 (NO_2 sym), 1218 (C-O); ^{1}H NMR (500 MHz, $CDCl_3$): 8.07 (1H, d, *J* 8.4,$C^{5''}H$), 7.62 (1H, d, *J* 1.8, $C^{2''}H$), 7.53 (1H, dd, J_1 8.4, J_2 1.8, $C^{6''}H$), 7.38-7.31 (2H, m, C^3H, C^5H), 7.07-7.01 (2H, m, C^2H, C^6H), 7.01-6.98 (1H, m, $C^{2'}H$) 6.88-6.85 (1H, m, $C^{4'}H$), 6.76-6.72 (1H, m, $C^{6'}H$), 5.84 (1H, d, *J* 2.5, C*H*OH), 5.14 (2H, s, CH_2O), 4.84 (2H, s, CH_2Br), 2.37 (1H, d, *J* 2.5, CHO*H*), 2.35 (3H, s, CH_3CN/CH_3CO), 2.21 (3H, s, CH_3CN/CH_3CO); ^{13}C NMR (126 MHz, $CDCl_3$): 165.7 (CH_3CO), 162.5 ($J_{C\text{-}F}$ 246.6, C^4), 158.59 ($C^{5'}$/CH_3CN), 158.56 ($C^{5'}$/CH_3CN), 147.4 ($C^{4''}$), 146.2 ($C^{3'}$), 143.4 ($C^{1''}$), 139.3 ($J_{C\text{-}F}$ 2.9, C^1), 133.5 ($C^{3''}$), 132.4 ($C^{1'}$), 130.9 ($C^{2''}$), 128.4

($J_{C\text{-}F}$ 8.0, C^2/C^6), 127.9 ($C^{6''}$), 126.1 ($C^{5''}$), 120.6 ($C^{4'}$), 116.3 ($C^{3'}$*C*CON), 115.7 ($J_{C\text{-}F}$ 21.6, C^3/C^5), 115.0 ($C^{6'}$), 111.7 ($C^{2'}$), 75.4 (*C*HOH), 68.6 (*C*H_2O), 28.9 (*C*H_2Br), 11.8 (*C*H_3CN/*C*H_3CO), 11.0 (*C*H_3CN/*C*H_3CO); HRMS: *m/z* (ESI^+) [Found $(M+FA+H)^+$ 585.06812, $C_{26}H_{22}N_2O_5FBr$ requires $(M+FA+H)^+$ 585.06782]; Analytical HPLC (RPB C18 column [100 mm × 3.2 mm, 35 °C]; 90:10:0.1 H_2O:MeCN:TFA → 95:5:0.1 MeCN:H_2O:TFA, 6 min) Ret. Time = 7.30 min, Purity: >99%.

5.20. 1-Ethyl-2,3,3-trimethyl-3*H*-indol-1-ium iodide

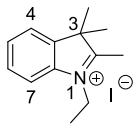

A mixture of 2,3,3-Trimethylindolenine **5.19** (4.4 mL, 4.36 g, 27.5 mmol, 1.0 eq.) and iodoethane (3 mL, 6.84 g, 41.2 mmol, 1.5 eq.) was heated under reflux at 70 °C for 24 h. The reaction mixture was cooled to ambient temperature, the precipitate filtered, washed with EtOAc (4 × 15 mL) and dried *in vacuo* to yield **5.20** (7.9 g, 91%) as a purple crystalline solid: mp: 210-214 °C (EtOAc) [Lit. 165-166 °C][319]; $\bar{\nu}_{max}$ (solid) cm^{-1}: 3027 (w, Ar C-H), 1460 (m, C=C); ^{1}H NMR (400 MHz, DMSO-d_6): 8.01-7.93 (1H, m, C^4*H*), 7.87-7.81 (1H, m, C^6*H*), 7.66-7.58 (2H, m, C^5*H*, C^7*H*), 4.49 (2H, q, *J* 7.3, C$H_2$$CH_3$), 2.83 (3H, s, C^2CH_3), 1.53 (6H, s, C^3(CH_3)$_2$), 1.44 (3H, t, *J* 7.3, CH_2CH_3); LRMS: *m/z* (ESI^+) 188.2 ([M-I]$^+$, 100%). These data are in good agreement with literature values.[319]

5.22. (*E*)-2-Chloro-3-(hydroxymethylene)cyclohex-1-ene-1-carbaldehyde

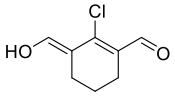

To a solution of Cyclohexanone **5.21** (5.0 mL, 4.7 g, 48.3 mmol, 1.0 eq.) in DMF/CH_2Cl_2 (1:1 *v/v*, 40 mL), $POCl_3$ (18.0 mL, 29.6 g, 193.0 mmol, 4.0 eq.) was added drop-wise at 0 °C, and the reaction mixture heated under reflux for 3 h. The reaction mixture was cooled to ambient temperature, poured onto ice (~ 100 g) and warmed to ambient temperature over 18 h. The precipitate was filtered, dried *in vacuo* and used without further purification. ^{1}H NMR (500 MHz, acetone-d_6): 2.46 (4H, t, *J* 6.2), 1.67 (2H, qn, *J* 6.2); LRMS: *m/z* (ESI$^+$) 173.1 ([M+H]$^+$, 100%).[301]

5.24. 2-((*E*)-2-((*E*)-2-Chloro-3-(2-((*E*)-1-ethyl-3,3-dimethylindolin-2-ylidene)ethylidene)cyclohex-1-en-1-yl)vinyl)-1-ethyl-3,3-dimethyl-3*H*-indol-1-ium iodide

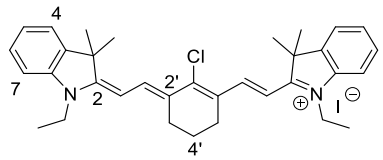

To solution of **5.20** (0.17 g, 1.28 mmol, 2.3 eq.) in Ac_2O (5 mL), NaOAc (0.08 g, 0.98 mmol, 0.75 eq.) and [precipitate] **5.22** (0.8 g, 3.0 mmol, 1.0 eq.) was added, stirred at ambient temperature for 2 h, and concentrated *in vacuo*. The resulting residue washed with Et_2O (3 × 10 mL), boiling EtOAc (4 × 15 mL), and dried *in vacuo*, to yield **5.24** (0.3 g) as an impure green solid, and used without further purification. ^{1}H NMR (400 MHz, $CDCl_3$): 8.31 (2H, d, *J* 14.0, $C^{2'}CH$), 7.44-7.20 (6H, m, C^4H, C^5H, C^6H), 7.16 (2H, d, *J* 7.7, C^7H), 6.24 (2H, d, *J* 14.0, C^2CH), 4.26 (4H, q, *J* 7.3, CH_2CH_3), 2.79 (4H, t, *J* 5.9, $C^{3'}H_2/C^{5'}H_2$), 2.03-1.93 (2H, m, $C^{4'}H_2$), 1.71 (12H, s, C^3CH_3), 1.45 (6H, t, CH_2CH_3); LRMS: *m/z* (ESI$^+$) 511.3 ([M-I]$^+$, 100%). These data are in good agreement with literature values.[300,301]

5.26. 1-Ethyl-2-((*E*)-2-((*E*)-3-(2-((*E*)-1-ethyl-3,3-dimethylindolin-2-ylidene)ethylidene)-2-((4-nitrophenethyl)amino)cyclohex-1-en-1-yl)vinyl)-3,3-dimethyl-3*H*-indol-1-ium iodide

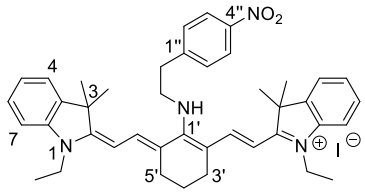

To a solution of **5.24** (1.28 g, 2.0 mmol, 1.0 eq.) in DMF (20 mL), was 2-(4-Nitrobenzyl)ethylamine hydrochloride **5.25** (0.54 g, 2.7 mmol, 1.3 eq.) and Et_3N (0.74 mL, 0.53 g, 4.0 mmol, 2.0 eq.). The reaction solution was stirred at 55 °C for 3 h, cooled to ambient temperature and concentrated *in vacuo*. The resulting residue was dissolved in EtOAc (30 mL), washed with H_2O (2 × 20 mL), brine (2 × 20 mL), dried over $MgSO_4$, filtered and concentrated *in vacuo*. The resulting residue was adsorbed onto Celite®, and the product purified by silica gel column chromatography, eluting with EtOAc and MeOH (20% MeOH) to yield **5.26** (0.26 g, 22%) as a deep blue solid: R_f: 0.4 (EtOAc - MeOH 8:2); mp: 149-152 °C (MeOH); $\bar{\nu}_{max}$ (solid) cm^{-1}: 2926 (w, CH_2CH_3), 1515 (m, NO_2 asym), 1273 (m, NO_2 sym), 1106 (m, C-N), 769 (m, Ar CH); ^1H NMR (500 MHz, $CDCl_3$): 10.55 (1H, s, N*H*), 8.09 (2H, d, *J* 8.6, $C^{3''}H/C^{5''}H$), 7.72 (2H, d, *J* 12.2, $C^{2'}CH$), 7.46 (2H, d, *J* 8.6, $C^{2''}H/C^{6''}H$), 7.28-7.23 (4H, m, C^6H/C^4H), 7.04 (2H, dd, J_1 7.4, J_2 7.4, C^5H), 6.81 (2H, d, *J* 7.4, C^7H), 5.49 (2H, d, *J* 12.2, C^2CH), 4.23 (2H, s, $NHCH_2$), 3.80 (4H, d, *J* 6.6 CH_2CH_3), 3.56 (2H, t, *J* 6.5, $C^{1''}CH_2$), 2.32 (4H, t, *J* 6.2, $C^{3'}H_2/C^{5'}H_2$), 1.70 (12H, s, C^3CH_3), 1.54-1.44 (2H, m, $C^{4'}H_2$), 1.32 (6H, t, *J* 6.6, CH_2CH_3); ^{13}C NMR (126 MHz, $CDCl_3$): 171.1 ($C^{1'}$), 166.5 (C^2), 147.5 ($C^{1''}$), 146.7 ($C^{4''}$), 142.8 (C^{7a}), 140.7 (C^{3a}), 137.4 ($C^{2'}CH$), 130.3 ($C^{2''}/C^{6''}$), 128.1 (C^4/C^6), 123.6

($C^{3''}/C^{5''}$), 122.5 (C^5H), 122.3 (C^4/C^6), 119.9 ($C^{2'}$), 107.8 (C^7), 93.2 (C^2CH), 50.4 ($NHCH_2$), 47.8 (C^3), 37.8 (CH_2CH_3), 36.8 $C^{1''}CH_2$), 28.9 (C^3CH_3), 25.6 ($C^{3''}/C^{5''}$), 21.5 ($C^{4''}$), 11.5 (CH_2CH_3); HRMS: *m/z* (ESI^+) [Found $(M\text{-}I)^+$ 641.3844. $C_{42}H_{49}N_4O_2I$ requires $(M\text{-}I)^+$ 641.3850]; LRMS: *m/z* (ESI^+) 641.4 ($[M\text{-}I]^+$, 100%); Analytical HPLC (Waters XSelect CSH C18 XP, 100 x 2.1 mm, 2.5µm, 35 °C]; 70:30 10 mM FA/H_2O:MeCN → 95:5 MeCN:10 mM FA/H_2O; 10 min) Ret. Time = 10.50 min, Purity: >99%.

5.33. (*E*)-1-Ethyl-3,3-dimethyl-2-(2-(6-((4-nitrobenzyl)oxy)-2,3-dihydro-1*H*-xanthen-4-yl)vinyl)-3*H*-indol-1-ium iodide

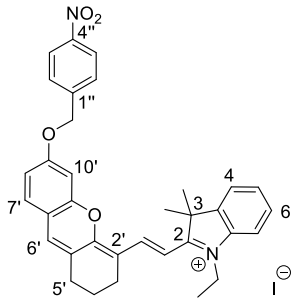

To a solution of **5.1** (50 mg, 0.10 mmol, 1.0 eq.) in $CHCl_3$ (0.5 mL), was added Et_3N (13.5 µL, 9.8 mg, 0.095 mmol, 1 eq.) and 4-Nitrobenzyl iodide **5.32** (27.5 mg, 0.105 mmol, 1.1 eq.). The reaction solution was heated to 55 °C for 16 h, cooled to ambient temperature, and concentrated *in vacuo*. From the resulting residue, the product was purified, by semi-preparative HPLC (Phenomenex Luna C18(2) 10 µm column [250 × 10 mm]; 65:35:0.1 MeOH:H_2O:TFA → 83:17:0.1 MeOH:H_2O:TFA; 10 min, 5 mL/min) to yield **5.33** (11 mg, 18%) as a blue solid: R_f: 0.23 (MeOH – CH_2Cl_2, 4:96); mp: 128-130 °C; $\bar{\nu}_{max}$ (solid) cm^{-1}: 1529 (s, NO_2 asym), 1425 (s, C=C), 1372 (m, NO_2 sym), 1113 (s, C-O); ^1H NMR (500 MHz, MeOD-d_4): 8.77 (1H, d, *J* 15.0, $C^{2'}CH$), 8.34-8.29 (2H, m, $C^{3''}H$, $C^{5''}H$), 7.76 (2H, d, *J* 8.6, $C^{2''}H$, $C^{6''}H$),

7.67 (1H, d, *J* 7.3, $C^{7}H$), 7.59-7.45 (4H, m, $C^{7'}H$, $C^{6}H$, $C^{5}H$, $C^{4}H$), 7.39 (1H, s, $C^{6'}H$), 7.13 (1H, d, *J* 2.4, $C^{10'}H$), 7.08 (1H, dd, J_1 8.7, J_2 2.3, $C^{8'}H$), 6.53 (1H, d, *J* 15.0, $C^{2}CH$), 5.43 (2H, s, $C^{1''}CH_2$), 4.41 (2H, q, *J* 7.3, CH_2CH_3), 2.79 (2H, t, *J* 5.8, $C^{5'}H$), 2.73 (2H, t, *J* 5.8, $C^{3'}H$), 1.94 (tt, 2H, J_1 5.8, J_2 5.8, $C^{4'}H$), 1.82 (6H, s, $C(CH_3)_2$), 1.49 (3H, t, *J* 7.3, CH_2CH_3); ^{13}C NMR (126 MHz, MeOD-d_4): 178.9 (C^{2}), 163.1 ($C^{9'}$), 162.9 ($C^{1'a}$), 155.8 ($C^{10'a}$), 149.2 ($C^{4''}$), 147.2 ($C^{2'}CH$), 145.5 ($C^{1''}$), 143.7 (C^{3a}), 142.5 (C^{7a}), 134.7 ($C^{6'}$), 130.3 ($C^{7'}$), 130.2 (C^{6}), 129.2 ($C^{2''}$, $C^{6''}$), 129.0 ($C^{5'a}$), 128.6 (C^{5}), 124.8 ($C^{3''}$, $C^{5''}$), 123.8 (C^{7}), 117.7 ($C^{6'a}$), 115.7 ($C^{2'}$), 114.9 ($C^{8'}$), 113.8 (C^{4}), 104.7 ($C^{2}CH$), 102.9 ($C^{10'}$), 70.6 ($C^{1''}CH_2$), 52.3 (C^{3}), 41.5 (CH_2CH_3), 30.2 ($C^{5'}$), 28.2 ($C(CH_3)_2$), 25.2 ($C^{3'}$), 21.8 ($C^{4'}$), 13.0 (CH_2CH_3); ^{19}F NMR (376 MHz, MeOD-d_4): −77.2, <0.0001% *w/w* TFA; HRMS: *m/z* (ESI^+) [Found $(M\text{-}I)^+$ 533.2431, $C_{36}H_{33}N_2O_6F_3$ requires $(M\text{-}I)^+$ 533.2435]; Analytical HPLC (RPB C18 column [100 mm × 3.2 mm, 35 °C]; 50:50:0.1 H_2O:MeCN:TFA →95:5:0.1 MeCN:H_2O:TFA, 6 min) Ret. Time = 6.16 min, Purity: >99%. These data are in good agreement with the reported values.[296]

7.3 Biological Methods

7.3.1 General biological laboratory and cell culture reagents

Laboratory plastic ware was supplied by CoStar® and Corning®. **Table 7.2** describes the general biological laboratory reagents used. All glassware used was autoclaved prior to use.

Table 7.2. General biological laboratory reagents

Name	Supplier
Acetonitrile	Sigma-Aldrich UK
Agarose	Sigma-Aldrich UK
β-mercaptoethanol	Fischer Scientific
Blocking buffer LiCor	LiCor
BSA (bovine serum albumin)	Fisher Scientific
Bromophenol blue	Fisher Scientific
DMEM (Dublecco's modified Eagle's medium)	Sigma-Aldrich UK
DharmaFECT 1	Fisher Scientific
DMSO (dimethylsulfoxide)	Fisher Scientific
Ethanol	Fisher Scientific
FBS (foetal bovine serum)	Autogen Bioscience
NEM (*N*-ethylmaleimide)	Sigma-Aldrich UK
Paraformaldehyde	Fisher Scientific
PBS (phosphate-buffered saline)	Fisher Scientific
ProLong® Gold	Invitrogen/Life technologies
RPMI medium	Sigma-Aldrich UK
Trypsin 0.05% EDTA	Sigma-Aldrich UK
Triton-X-100	Fisher Scientific
Tween 20	Fisher Scientific
Urea	Fisher Scientific

7.3.2 Hypoxia treatment

Hypoxia treatments were carried out using a Bactron II anaerobic chamber (Shel Lab®), or a Bactron EZ anaerobic chamber (Shel Lab®). Chambers were under a positive pressure of an anaerobic nitrogen gas mixture. No oxygen was supplied; however, it is not possible to guarantee 0% oxygen due to potential leaks. It is estimated that the oxygen concentration at a given time is no higher than 0.1%. Therefore, the oxygen tension for experiments carried out in these chambers are referred to as <0.1% O_2 throughout this dissertation. For experiments performed in the anaerobic chamber, glass dishes for plating cells, and glass vials for enzymatic assays were used, with the exception of clonogenic survival assays. This is because plastic is thought to be able to retain oxygen. An *in vivo* 400 (Ruskinn) hypoxic chamber or Whitley H35 hypoxystation (Don Whitley Scientific®) was used for oxygen concentrations of 3%-0.2%. The oxygen tensions of the chambers were routinely tested using an OxyLite probe (Oxford Optronix). A Forma Series II (TheroScientific®) incubator was used for an oxygen concentration of 5%.

7.3.3 Enzyme treatments

All of the purified enzymes used were purchased from Cypex Limited. (Dundee, UK) and were used as supplied. Purified cytochrome P450 reductase (cat.no CYP004) was purchased individually. Purified cytochrome P450s 1A2, 2D6, 2C9, C219 and 3A4 (cat. no. CYP051) were purchased as a high reductase bactosome kit.

An NADPH regenerating system was used in each assay. Solution A (20×, Corning®, 451220) and Solution B (200×, Corning®, 451200) were used as supplied. Solution A and Solution B comprise the following:

(a) Solution A: 26 mM $NADP^+$, 66 mM $MgCl_2$, 66 mM glucose-6-phosphate in H_2O

(b) Solution B: 40 units/mL glucose-6-phosphate dehydrogenase in 5 mM sodium citrate

In all cases, Millipore™ water and 0.5 M K_2HPO4 buffer (BD Gentest™) were used. The composition of 1 mL of assay solution for a typical assay with cytochrome p450 reductase is detailed in **Table 7.3**.

Table 7.3. NADPH reductase assay - the requisite components of an NADPH reductase assay, and the volumes of each required per 1 mL assay volume.

Name	Volume in 1 mL assay	Final Concentration
0.5 M K_2HPO_4	200 µL	100 mM
Solution A (20×)	50 µL	1×
Solution B (200×)	10 µL	1×
H_2O	730 µL	
P450 Reductase	9 µL	92 pmol/mL
Substrate (1 mM DMSO)	1 µL	1 µM

Substrates were introduced to the assay volume last, and T=0 aliquots taken at this time. Aliquots (50 µL) were taken at the desired time points, and the reaction quenched by addition into MeCN (50 µL). Samples were then centrifuged at 17000 × *g* for 10 minutes, and the supernatant analysed by

HPLC. All substrates were used at 1 μM final concentration in the assay volume, with the exception of compound **2.49** (10 μM final, 10 mM DMSO).

For alternative cytochrome P450 enzymes, the volume of enzyme added was adjusted to maintain a final enzyme concentration of 92 pmol/mL. Any volume alterations were compensated for by adjustment of the volume of H_2O, as described in **Table 7.4**.

Table 7.4. Cytochrome P450 reduction assays – volume of enzymes required and the corresponding amount of H_2O per 1 mL assay volume.

CYP Enzyme (Supplier conc. nmol/mL)	Volume in 1 mL assay	Volume H_2O
1A2R (5.4)	17 μL	723 μL
2C19 (4.2)	22 μL	718 μL
2C9HR (2.8)	33 μL	707 μL
2D6 (3.3)	29 μL	711 μL
3A4R (6.1)	15 μL	725 μL

Human liver microsomes, pooled from 50 individual donors (ThermoFisher Scientific, HMMCPL) were used as supplied. Per assay volume, the reaction was set up as described in **Table 7.3**, except 725 μL of H_2O was added, and 15 μL of microsomes as supplied.

7.3.4 Cell lines and culture

RKO colorectal cells, HepG2 hepatic cells, OE21 oesophageal cells and HCT116 colorectal cells were used in this study. Cells came from Public Health England. RKO cells, HepG2 cells and H1299 cells were cultured in DMEM supplemented with 10% FBS, in a standard humidified incubator at

37 °C and 5% CO_2. OE21 cells were cultured under the same conditions with RPMI instead of DMEM. All experiments were performed at a cell confluency of 65-75%.

Cells were cultured with 100 U/mL penicillin and 0.1 mg/mL streptomycin. Penicillin-Streptomycin solution (Sigma-Aldrich, 100×, cat. no. P4333) was aliquoted (5 mL), and stored at −20 °C. When required, the aliquot was thawed at ambient temperature, added to media (500 mL) directly.

Cells were passaged 3-4 times per week. A cell suspension was prepared by removal of the medium, washing with PBS, followed by addition of Trypsin-EDTA solution for 1-5 minutes to trypsinise the cells. The Trypsin-EDTA solution was inactivated by the addition of fresh media. The cell density was determined by the addition of cell suspension (10 µL) to a Neuenbauer haemocytometer chamber. Cells were counted in the standard manner. The desired number of cells for each experiment was then seeded in fresh media.

Cells were routinely tested for the presence of mycoplasma using the PlasmoTest™ kit (InvivoGen). Cells were grown in antibiotic-free media for 24 hours, then harvested when 90-100% confluent. Cells were then heated for 15 minutes at 100°C. The resulting suspension (50 µL) was added to HEK-Blue cells (200 µL, 1-3.5×10^5 cells/mL) in HEK-Blue™ detection medium (InvivoGen). Cells were plated, in duplicate in a 96-well plate, together with positive and negative controls provided by the manufacturer. The plates were then incubated under normal tissue culture conditions for 24 hours. After this time, the wells were examined for the appearance of a blue colour, which

indicated the presence of lipoprotein expressed by bacteria and mycoplasma. A pink colour indicated a negative result, suggesting absence of mycoplasma.

7.3.5 Cryopreservation of cell lines

Cells were grown to 70% confluence, trypsinised with Trypsin-EDTA solution, and resuspended in 5 mL of fresh media. The cells were pelleted by centrifugation at 4500 × *g* for 5 minutes at ambient temperature. The media supernatant was removed, and the cell pellet re-suspended in 1 mL of freezing media (10% FBS, 80% media, 10% DMSO) and stored in a 1.5 mL cryovial (ThermoScientific Nunc™, cat. no. 5001-1020) for freezing. The vial was insulated by wrapping with tissue, before transferal to liquid nitrogen for long-term storage.

When required, cells were removed from liquid nitrogen, rapidly thawed in a water bath at 37 °C, and transferred to 5 mL of pre-warmed media. Cells were pelleted by centrifuged at 4500 × *g* for 5 minutes at ambient temperature. The supernatant was removed and the pelleted cells were re-suspended in fresh media. The cell suspension was then transferred to a 75 cm^3 flask and incubated under normal conditions.

7.3.6 Compound treatments of cells

Cells were treated with the indicated compounds, at the indicated concentrations, as a solution made in fresh media. Drug stocks in DMSO (1000 ×) were diluted in media 1:1000 to the desired concentration (1 ×), such that the overall DMSO concentration was ≤0.5% in the media.

For inhibition of cystathionine-β-synthase, cells were pre-treated with 10 μM of aminooxyacetic acid (AOAA **4.13**, Sigma-Aldrich, C13408)

for 3 hours, followed by treatment with 1 mM AOAA **4.13** and 1 μM **3.29** for 4 hours. For inhibition of cystathionine γ-lyase, cells were treated with 50 μM of DL-propargylglycine (PAG **4.14**, Sigma-Aldrich, P7888) for 3 hours followed by treatment with 5 mM PAG **4.14** and 1 μM **3.29** for 4 hours.

7.3.7 Cell lysate HPLC analysis

Cells were seeded at a density of 0.5×10^5 - 1×10^6 cells per 6 cm dish and incubated for 15 hours. Cells were treated then as detailed in **Chapter 7.3.6**, and treated under conditions of the indicated oxygen pressure, for the indicated period of time. Cells were then harvested, pelleted by centrifugation at 4500 × *g*, and lysed with 50 μL of MeCN. The solution was centrifuged at 17000 × *g* to remove cell debris, and the supernatant analysed by HPLC.

7.3.8 Antibodies

Primary antibodies

Table 7.5. Primary antibodies used for western blotting and IF

Name	Species	Dilution	Clone ID	Supplier/cat. no.
β-Actin	Mouse	1:10000	AC-15	Santa Cruz Biotechnology/sc-69878
CBS	Rabbit	1:500		Sigma-Aldrich/ HPA001223
CYP1A2	Mouse	1:1000	3B8C1	Abcam®/3B8C1
CYP2C19	Rabbit	1:1000		Abcam®/ab83233
CYP2C9	Rabbit	1:1000		Abcam®/ab4236
CYP2D6	Rabbit	1:500		Abcam®/ab62204
CYP3A4	Rabbit	1:250		Abcam®/ab135813
HIF-1α	Mouse	1:500	54/HIF-1α	Becton Dickinson Biosciences/610959
Pimonidazole	Mouse	1:100	4.3.11.3	Hypoxyprobe/ HP1-100

Secondary antibodies

Table 7.6. Secondary antibodies used for western blotting

Name	Dilution	Application	Supplier/cat. no.
Alexa-Fluor 680 goat anti-mouse IgG (H+L)	1:10000	WB	Invitrogen/A21057
Alexa-Fluor 680 goat anti-rabbit IgG (H+L)	1:10000	WB	Invitrogen/A21076
IRDye 800CW donkey anti-mouse IgG	1:10000	WB	LiCor/926-32212
Alexa-Fluor 488 goat anti-mouse	1: 500	IF	Invitrogen/A11017

7.3.9 Cell lysis and protein purification

Media was removed from the cells, followed by washing with PBS. The cells were scraped into 1 mL of PBS, and then pelleted by centrifugation at 4500 × *g*. The supernatant was removed, and the cell pellet lysed in 40-100 µL of UTB (9 M urea, 75 mM Tris HCl, pH 7.5, 0.1 M ß-mercaptoethanol). The resulting UTB solutions were then sonicated for 20 seconds, followed by centrifugation for 15 minutes at 17000 × *g* at 4 °C to remove cell debris. The supernatant was transferred to a clean Eppendorf. A Nanodrop meter was used for protein quantification, using 2 µL of supernatant per measurement. Absorbance was detected at 280 nm, using UTB as a blank. Three measurements were made per supernatant, and the average taken as the final protein concentration. The appropriate volume of sample (typically corresponding to 20-50 µg of protein) was added to 5 µL of sample buffer (3.3% SDS, 6 M urea, 17 mM Tris-HCl (pH 7.5), 0.07 M β-mercaptoethanol, 0.01% bromophenol blue). Each sample was heated at 100 °C for 10 minutes. The gels used were 10% pre-cast polyacrylamide Mini-PROTEAN TGX™ gels (Bio-Rad, cat. no. 4561033) and were electrophoresed for 60-70 minutes at 120-150 V. 5 µL of a protein ladder (Bio-Rad, Precision) was loaded to enable analysis of the molecular weight of bands.

7.3.10 Western blotting

Proteins in the electrophoresed gels were transferred onto PVDF membranes (Trans-Blot® Turbo™ Transfer Pack, BioRad) by a Trans-Blot® Turbo™ transfer system. Transfers were run for 7 minutes at 25 V. The membrane was then blocked for 1 hour using a 1:1 mixture of LiCor buffer and tris-buffered saline solution (TBS, 50 mM Tris-HCl, pH 7.6, 150 mM

NaCl). Primary antibodies were diluted in a 1:1 mixture of LiCor buffer and TBS-Tween (0.1% Tween). The membranes were treated with primary antibodies for 16 hours at 4 °C, whilst shaking. The dilutions used for each primary antibody used are given in **Table 7.5**. After this time, the membrane was washed with TBS-Tween for 10 minutes, followed by washing a further two times. The membrane was then treated with the appropriate secondary antibody, diluted in a 1:1 mixture of LiCor buffer:TBS-Tween, for 2 hours at ambient temperature, whilst shaking. The dilutions used for each secondary antibody used are given in **Table 7.6**. The membrane was then washed in TBS-Tween for 10 minutes, twice, followed by a 10 minute wash in TBS. Membranes were then developed using an Odyssey infrared imaging system.

7.3.11 RNA interference

ON-Target*plus* SMARTpool human cystathionine-β-synthase siRNA (Dharmacon®, cat. no. L-008617-00) and ON-Target*plus* control non-targeting siRNA (Dharmacon®, D-001810-10) were transfected into cells using DharmaFECT 1 at a final concentration of 50 nm. Cells were seeded at a density of 2.5×10^5 cells per 3.5 mm well/plate, in antibiotic free media. The following day, cells were transfected. The H_2O used was DEPC treated. The following solutions were made:

Tube A: 5μL 20 μM aq. siRNA, 20 μL H_2O, 25 μL media (−FBS, −P/S)

Tube B: 5 μL DharmaFECT, 345 μL media (−FBS, −P/S)

Each tube was incubated at ambient temperature for 5 minutes, followed by drop-wise addition of Tube A to Tube B with frequent shaking. The resulting solution: A+B was then left to incubate for 20 minutes. The

media from the cells to be transfected was removed, 1.6 mL of fresh media added, followed by drop-wise addition of 400 µL of A+B. Cells were then incubated for 24 hours at 37 °C before replacing the media with fresh media. Cells were then incubated for a further 24 hours at 37 °C before treatment and harvesting.

7.3.12 Fluorescence microscopy

0.5-1×10^6 cells were seeded in 6 cm dishes containing cover slips, and left to adhere for 16 hours. The media was removed, and replaced with fresh media containing the desired compound (1 µM), and the cells treated under 21% or <0.1% O_2 for 4 hours. After this time, the media was removed, and the cells washed in PBS for 5 minutes, twice. The cells were fixed with 4% paraformaldehyde solution (4% *w/v* paraformaldehyde, 2% *w/v* sucrose, PBS) for 10 minutes at ambient temperature, and washed twice with PBS for 5 minutes. The cells were then treated with DAPI solution (0.1 µg/mL, PBS) for 10 minutes at ambient temperature, followed by washing with PBS for 5 minutes, twice. The cover slips were then carefully removed, and mounted onto slides with ProLong® Gold mounting medium (Invitrogen/Life technologies). The slides were left to dry for 24 hours before analysis using a LSM780 (Carl Zeiss Microscopy Ltd) confocal microscope.

7.3.13 Spheroid growth and treatment

Spheroids were grown with HCT116 colorectal cells using the liquid overlay method. [274,320] A solution of 1% agarose/PBS was prepared and heated in a microwave to ensure a homogeneous solution. 100 µL of the solution was added to wells in a 96-well plate, and allowed to cool, and set at ambient temperature for 15 minutes. The base of each well was examined for

bubbles in the agarose. If bubbles were present, the wells were marked, and discarded. 100 µL of media (DMEM, 10% FBS, P/S) was added to each well, and the plate incubated at 37 °C for 1 hour. HCT116 cells (500/well) were seeded in 100 µL of media, and the plates incubated for 3 days at 37 °C to allow initiation of spheroid growth. Every two subsequent days, 100 µL of media was removed from each well, and replaced with 100 µL fresh media. Spheroids were grown to 500-650 µm in diameter (requiring 10-12 days of growth) before treatment.

7.3.14 Spheroid immunofluorescence microscopy

Spheroids were treated with compound **3.1** (20 µM), or **3.29** (20 µM) and pimonidazole (40 µM), for the indicated time. Spheroids were harvested from their wells, the media removed, and fixed in 4% paraformaldehyde at 4 °C for 16 hours. The 4% paraformaldehyde was removed, and the spheroids treated with 30% sucrose (*w/v*, PBS) for 3 hours before mounting in OCT embedding medium (ThermoScientific). Spheroids were sectioned as 5 µM thick slices using a cryostat, mounted onto slides, and stored at −80 °C. Sections were then rehydrated in 0.1% PBS-Tween (*v/v*, PBS) and blocked with 1% bovine serum albumin (BSA) (*w/v*, PBS-Tween) for 2 hours at ambient temperature. The sections were washed with 0.1% PBS-Tween for 10 minutes, twice, before treatment with pimonidazole primary antibody (Hypoxyprobe) for 2 hours at a dilution of 1:100 (*v/v*, 1% BSA). After this time, sections were washed with 0.1% PBS-Tween for 10 minutes, and treated with AlexaFluor 488 green secondary antibody at a dilution of 1:500 (*v/v*, 1% BSA). Sections were then washed with PBS-Tween, stained with DAPI solution (0.1 µg/mL, PBS), and the slides mounted using ProLong® Gold mounting

medium (Invitrogen/Life technologies). Slides were left to dry for 24 hours before analysis. Slides were analysed using a LSM780 (Carl Zeiss Microscopy Ltd) confocal microscope, and measured using Zeiss ZEN 2012 software.

7.3.15 Fluorescence automated cell sorting (FACS)

0.5-1×10^6 cells were seeded in 6 cm dished and left to adhere for 16 hours. After this time, the media was removed, and replaced with fresh media containing either compound **3.1** (1 μM) or compound **3.29** (1 μM) for 4 hours under the indicated oxygen concentration. Following treatment, the media was removed, the cells washed in PBS, and pelleted through centrifugation at 4500 × *g* for 5 minutes, and the PBS removed. The cell pellet was then re-suspended in 1 mL Trypsin-EDTA solution and incubated at 37 °C for 5 minutes. The trypsin was removed by centrifugation at 4500 × *g* for 5 minutes, the cell pellet re-suspended in 1 mL 4% paraformaldehyde solution, and shaken at ambient temperature for 10 minutes. The cells were pelleted through centrifugation at 4500 × *g* for 5 minutes, the 4% paraformaldehyde solution removed, and the cell pellet re-suspended in PBS. Cells were also used without fixing with 4% paraformaldehyde, where samples were analysed immediately after the termination of the experiment. Analysis was carried out for a cell count of 10000 using a Becton-Dickinson FACScan. Samples were analysed using FlowJo software (Treestar, Ashland OR 97520) and CellQuest Pro software.

7.3.16 Clonogenic survival assay

Cells (300) were seeded in 3.5 cm wells (6-well plates) and left to adhere for 5 hours. The media was removed, replaced with fresh media

containing **3.29** (1 μM), or DMSO as a control. The cells were treated under 21% and <0.1% O_2 for 2, 4, 6, 18 or 24 hours. After each time, the media was removed, and replaced with fresh media, before transferal to an incubator at 37 °C. Colonies (>50 cells) were left to develop for 10 days and visualised with methylene blue stain (50% MeOH, 20% EtOH in PBS, 1% methylene blue (Fisher BioReagents).

7.3.17 Statistical analysis

Statistical analyses were carried out using Microsoft Excel software. The standard error (S.E) was calculated using the following formula:

$$S.E = \frac{S.D}{\sqrt{n}}$$

Wherein S.D is the standard deviation, and n is the number of samples. Statistical significance was determined using Student's T test.

REFERENCES

(1) International Agency for Research on Cancer. Globocan 2012: Estimated Cancer Incidence, Mortality and Prevalence Worldwide in 2012. *World Health Organisation* **2013**.

(2) Cancer Research UK: World Cancer Factsheet. *Cancer Research UK* **2014**.

(3) Cancer Research UK: Cancer Risk Statistics for the UK. *Cancer Research UK* **2016**.

(4) Torjesen, I. Cancer Research UK Will Increase Its Research Spending by 50% Over the Next Five to 10 Years. *BMJ (Clinical research edition)* **2014**, *348*, g3012.

(5) Worldwide Cancer Research: Annual Review 2014/15. *Worldwide Cancer Research (formerly American Institute of Cancer Research)* **2015**.

(6) Hanahan, D.; Weinberg, R. A. Hallmarks of Cancer: the Next Generation. *Cell* **2011**, *144* (5), 646–674.

(7) Sharma, R. A.; Plummer, R.; Stock, J. K.; Greenhalgh, T. A.; Ataman, O.; Kelly, S.; Clay, R.; Adams, R. A.; Baird, R. D.; Billingham, L.; Brown, S. R.; Buckland, S.; Bulbeck, H.; Chalmers, A. J.; Clack, G.; Cranston, A. N.; Damstrup, L.; Ferraldeschi, R.; Forster, M. D.; Golec, J.; Hagan, R. M.; Hall, E.; Hanauske, A.-R.; Harrington, K. J.; Haswell, T.; Hawkins, M. A.; Illidge, T.; Jones, H.; Kennedy, A. S.; McDonald, F.; Melcher, T.; O'Connor, J. P. B.; Pollard, J. R.; Saunders, M. P.; Sebag-Montefiore, D.; Smitt, M.; Staffurth, J.; Stratford, I. J.; Wedge, S. R.; NCRI CTRad Academia-Pharma Joint Working Group. Clinical Development of New Drug-Radiotherapy Combinations. *Nat. Rev. Clin. Oncol.* **2016**, *10.1038/nrclinonc.2016.79* (Ahead of Print).

(8) Burki, T. K. Lack of Access to Targeted Cancer Therapy. *Lancet Oncol.* **2015**, *16* (13), e482.

(9) Alexandrov, L. B.; Nik-Zainal, S.; Wedge, D. C.; Aparicio, S. A. J. R.; Behjati, S.; Biankin, A. V.; Bignell, G. R.; Bolli, N.; Borg, A.; Børresen-Dale, A.-L.; Boyault, S.; Burkhardt, B.; Butler, A. P.; Caldas, C.; Davies, H. R.; Desmedt, C.; Eils, R.; Eyfjörd, J. E.; Foekens, J. A.; Greaves, M.; Hosoda, F.; Hutter, B.; Ilicic, T.; Imbeaud, S.; Imielinsk, M.; Jäger, N.; Jones, D. T. W.; Jones, D.; Knappskog, S.; Kool, M.; Lakhani, S. R.; López-Otín, C.; Martin, S.; Munshi, N. C.; Nakamura, H.; Northcott, P. A.; Pajic, M.; Papaemmanuil, E.; Paradiso, A.; Pearson, J. V.; Puente, X. S.; Raine, K.; Ramakrishna, M.; Richardson, A. L.; Richter, J.; Rosenstiel, P.; Schlesner, M.; Schumacher, T. N.; Span, P. N.; Teague, J. W.; Totoki, Y.; Tutt, A. N. J.; Valdés-Mas, R.; van Buuren, M. M.; van t Veer, L.; Vincent-

Salomon, A.; Waddell, N.; Yates, L. R.; Zucman-Rossi, J.; Andrew Futreal, P.; McDermott, U.; Lichter, P.; Meyerson, M.; Grimmond, S. M.; Siebert, R.; Campo, E.; Shibata, T.; Pfister, S. M.; Campbell, P. J.; Stratton, M. R. Signatures of Mutational Processes in Human Cancer. *Nature* **2013**, *500* (7463), 415–421.

(10) Hanahan, D.; Weinberg, R. A. The Hallmarks of Cancer. *Cell* **2000**.

(11) Bristow, R. G.; Hill, R. P. Hypoxia and Metabolism. Hypoxia, DNA Repair and Genetic Instability. *Nat. Rev. Cancer.* **2008**, *8* (3), 180–192.

(12) Vaupel, P. Hypoxia and Aggressive Tumor Phenotype: Implications for Therapy and Prognosis. *The Oncologist* **2008**, *13*, 21–26.

(13) Pugh, C. W.; Ratcliffe, P. J. Regulation of Angiogenesis by Hypoxia: Role of the HIF System. *Nat. Med.* **2003**, *9* (6), 677–684.

(14) Lee, S. L. C.; Rouhi, P.; Dahl Jensen, L.; Zhang, D.; Ji, H.; Hauptmann, G.; Ingham, P.; Cao, Y. Hypoxia-Induced Pathological Angiogenesis Mediates Tumor Cell Dissemination, Invasion, and Metastasis in a Zebrafish Tumor Model. *PNAS USA* **2009**, *106* (46), 19485–19490.

(15) Facciabene, A.; Peng, X.; Hagemann, I. S.; Balint, K.; Barchetti, A.; Wang, L.-P.; Gimotty, P. A.; Gilks, C. B.; Lal, P.; Zhang, L.; Coukos, G. Tumour Hypoxia Promotes Tolerance and Angiogenesis via CCL28 and Treg Cells. *Nature* **2011**, *475* (7355), 226–230.

(16) Brown, J. M.; Wilson, W. R. Exploiting Tumour Hypoxia in Cancer Treatment. *Nat. Rev. Cancer.* **2004**, *4* (6), 437–447.

(17) Wilson, W. R.; Hay, M. P. Targeting Hypoxia in Cancer Therapy. *Nat. Rev. Cancer.* **2011**, *11*, 1–18.

(18) Pires, I. M.; Bencokova, Z.; Milani, M.; Folkes, L. K.; Li, J.-L.; Stratford, M. R.; Harris, A. L.; Hammond, E. M. Effects of Acute Versus Chronic Hypoxia on DNA Damage Responses and Genomic Instability. *Cancer Res.* **2010**, *70* (3), 925–935.

(19) Thomlinson, R. H.; Gray, L. H. The Histological Structure of Some Human Lung Cancers and the Possible Implications for Radiotherapy. *Br. J. Cancer* **1955**, *9* (4), 539–549.

(20) Grimes, D. R.; Kannan, P.; Warren, D. R.; Markelc, B.; Bates, R.; Muschel, R.; Partridge, M. Estimating Oxygen Distribution From Vasculature in Three-Dimensional Tumour Tissue. *J. R. Soc. Interface* **2016**, *13* (116), 1–12.

(21) Olive, P. L.; Vikse, C.; Trotter, M. J. Measurement of Oxygen Diffusion Distance in Tumor Cubes Using a Fluorescent Hypoxia Probe. *Int. J. Radiat. Oncol. Biol. Phys.* **1992**, *22* (3), 397–402.

(22) Nordsmark, M.; Bentzen, S. M.; Rudat, V.; Brizel, D.; Lartigau, E.; Stadler, P.; Becker, A.; Adam, M.; Molls, M.; Dunst, J.; Terris, D. J.; Overgaard, J. Prognostic Value of Tumor Oxygenation in 397 Head and Neck Tumors After Primary Radiation Therapy. an International Multi-Center Study. *Radiother. Oncol.* **2005**, *77* (1), 18–24.

(23) Nordsmark, M.; Loncaster, J.; Aquino-Parsons, C.; Chou, S.-C.; Ladekarl, M.; Havsteen, H.; Lindegaard, J. C.; Davidson, S. E.; Varia, M.; West, C.; Hunter, R.; Overgaard, J.; Raleigh, J. A. Measurements of Hypoxia Using Pimonidazole and Polarographic Oxygen-Sensitive Electrodes in Human Cervix Carcinomas.

Radiother. Oncol. **2003**, *67* (1), 35–44.
(24) Chopra, S.; Foltz, W. D.; Milosevic, M. F.; Toi, A.; Bristow, R. G.; Ménard, C.; Haider, M. A. Comparing Oxygen-Sensitive MRI (BOLD R2*) with Oxygen Electrode Measurements: a Pilot Study in Men with Prostate Cancer. *Int. J. Radiat. Biol.* **2009**, *85* (9), 805–813.
(25) Mortensen, L. S.; Johansen, J.; Kallehauge, J.; Primdahl, H.; Busk, M.; Lassen, P.; Alsner, J.; Sørensen, B. S.; Toustrup, K.; Jakobsen, S.; Petersen, J.; Petersen, H.; Theil, J.; Nordsmark, M.; Overgaard, J. FAZA PET/CT Hypoxia Imaging in Patients with Squamous Cell Carcinoma of the Head and Neck Treated with Radiotherapy: Results From the DAHANCA 24 Trial. *Radiother. Oncol.* **2012**, *105* (1), 14–20.
(26) Carreau, A.; Hafny-Rahbi, B. E.; Matejuk, A.; Grillon, C.; Kieda, C. Why Is the Partial Oxygen Pressure of Human Tissues a Crucial Parameter? Small Molecules and Hypoxia. *J. Cell. Mol. Med.* **2011**, *15* (6), 1239–1253.
(27) Bertout, J. A.; Patel, S. A.; Simon, M. C. The Impact of O2 Availability on Human Cancer. *Nat. Rev. Cancer* **2008**, *8* (12), 967–975.
(28) Hammond, E. M.; Asselin, M.-C.; Forster, D.; O'Connor, J. P. B.; Senra, J. M.; Williams, K. J. The Meaning, Measurement and Modification of Hypoxia in the Laboratory and the Clinic. *Clin. Oncol. (R. Coll. Radiol.)* **2014**, *26* (5), 277–288.
(29) Höckel, M.; Schlenger, K.; Aral, B.; Mitze, M.; Schaffer, U.; Vaupel, P. Association Between Tumor Hypoxia and Malignant Progression in Advanced Cancer of the Uterine Cervix. *Cancer Res.* **1996**, *56* (19), 4509–4515.
(30) Saggar, J. K.; Tannock, I. F. Chemotherapy Rescues Hypoxic Tumor Cells and Induces Their Reoxygenation and Repopulation--an Effect That Is Inhibited by the Hypoxia-Activated Prodrug TH-302. *Clin. Cancer Res.* **2015**, *21* (9), 2107–2114.
(31) Minchinton, A. I.; Tannock, I. F. Drug Penetration in Solid Tumours. *Nat. Rev. Cancer* **2006**, *6* (8), 583–592.
(32) Hall, E. J.; Giaccia, A. J. *Radiobiology for the Radiologist,* 6th ed.; Lippincott Williams & Wilkins, **2006**.
(33) Grimes, D. R.; Partridge, M. A Mechanistic Investigation of the Oxygen Fixation Hypothesis and Oxygen Enhancement Ratio. *Biomed. Phys. Eng. Express* **2015**, *1* (4), 045209.
(34) Höckel, M.; Vaupel, P. Tumor Hypoxia: Definitions and Current Clinical, Biologic, and Molecular Aspects. *J. Natl. Cancer Inst.* **2001**, *93* (4), 266–276.
(35) Gilkes, D. M.; Semenza, G. L.; Wirtz, D. Hypoxia and the Extracellular Matrix: Drivers of Tumour Metastasis. *Nat. Rev. Cancer* **2014**, *14* (6), 430–439.
(36) Nardo, B.; Serafini, S.; Ruggiero, M.; Grande, R.; Fugetto, F.; Zullo, A.; Novello, M.; Rizzuto, A.; Bonaiuto, E.; Vaccarisi, S.; Cavallari, G.; Serra, R.; Cannistrà, M.; Sacco, R. Liver Resection for Metastases From Colorectal Cancer in Very Elderly Patients: New Surgical Horizons. *Int. J. Surg.* **2016**, *10.1016/j.ijsu.2016.06.014* (Ahead of Print).

(37) Overgaard, J. Hypoxic Radiosensitization: Adored and Ignored. *J. of Clin. Oncol.* **2007**, *25* (26), 4066–4074.
(38) Saunders, M.; Dische, S. Clinical Results of Hypoxic Cell Radiosensitisation From Hyperbaric Oxygen to Accelerated Radiotherapy, Carbogen and Nicotinamide. *Br. J. Cancer Suppl.* **1996**, *27*, S271–S278.
(39) Horsman, M. R.; Overgaard, J. The Impact of Hypoxia and Its Modification of the Outcome of Radiotherapy. *J. Rad. Res.* **2016**, *10.1093/jrr/rrw007* (Ahead of Print).
(40) Wardman, P. Chemical Radiosensitizers for Use in Radiotherapy. *Clin. Oncol. (R. Coll. Radiol.)* **2007**, *19* (6), 397–417.
(41) O'Neill, P.; Wardman, P. Radiation Chemistry Comes Before Radiation Biology. *Int. J. Radiat. Biol.* **2009**, *85* (1), 9–25.
(42) Overgaard, J.; Hansen, H. S.; Overgaard, M.; Bastholt, L.; Berthelsen, A.; Specht, L.; Lindeløv, B.; Jørgensen, K. A Randomized Double-Blind Phase III Study of Nimorazole as a Hypoxic Radiosensitizer of Primary Radiotherapy in Supraglottic Larynx and Pharynx Carcinoma. Results of the Danish Head and Neck Cancer Study (DAHANCA) Protocol 5-85. *Radiother. Oncol.* **1998**, *46* (2), 135–146.
(43) Semenza, G. L. Targeting HIF-1 for Cancer Therapy. *Nat. Rev. Cancer* **2003**, *3* (10), 721–732.
(44) Hammond, E. M.; Dorie, M. J.; Giaccia, A. J. Inhibition of ATR Leads to Increased Sensitivity to Hypoxia/Reoxygenation. *Cancer Res.* **2004**, *64* (18), 6556–6562.
(45) Pires, I. M.; Olcina, M. M.; Anbalagan, S.; Pollard, J. R.; Reaper, P. M.; Charlton, P. A.; McKenna, W. G.; Hammond, E. M. Targeting Radiation-Resistant Hypoxic Tumour Cells Through ATR Inhibition. *Br. J. Cancer* **2012**, *107* (2), 291–299.
(46) Olcina, M.; Lecane, P. S.; Hammond, E. M. Targeting Hypoxic Cells Through the DNA Damage Response. *Clin. Cancer Res.* **2010**, *16* (23), 5624–5629.
(47) Cazares-Körner, C.; Pires, I. M.; Swallow, I. D.; Grayer, S. C.; O'Connor, L. J.; Olcina, M. M.; Christlieb, M.; Conway, S. J.; Hammond, E. M. CH-01 Is a Hypoxia-Activated Prodrug That Sensitizes Cells to Hypoxia/Reoxygenation Through Inhibition of Chk1 and Aurora a. *ACS Chem. Biol.* **2013**, *8* (7), 1451–1459.
(48) O'Connor, L. J.; Cazares-Körner, C.; Saha, J.; Evans, C. N. G.; Stratford, M. R. L.; Hammond, E. M.; Conway, S. J. Design, Synthesis and Evaluation of Molecularly Targeted Hypoxia-Activated Prodrugs. *Nat. Protoc.* **2016**, *11* (4), 781–794.
(49) Sunakawa, Y.; Bekaii-Saab, T.; Stintzing, S. Reconsidering the Benefit of Intermittent Versus Continuous Treatment in the Maintenance Treatment Setting of Metastatic Colorectal Cancer. *Cancer Treat. Rev.* **2016**, *45*, 97–104.
(50) Liapis, V.; Labrinidis, A.; Zinonos, I.; Hay, S.; Ponomarev, V.; Panagopoulos, V.; DeNichilo, M.; Ingman, W.; Atkins, G. J.; Findlay, D. M.; Zannettino, A. C. W.; Evdokiou, A. Hypoxia-activated pro-drug TH-302 exhibits potent tumor suppressive activity and cooperates with chemotherapy against osteosarcoma. *Cancer Lett.* **2015**, *357*

(1), 160–169.
(51) Guise, C. P.; Mowday, A. M.; Ashoorzadeh, A.; Yuan, R.; Lin, W.-H.; Wu, D.-H.; Smaill, J. B.; Patterson, A. V.; Ding, K. Bioreductive Prodrugs as Cancer Therapeutics: Targeting Tumor Hypoxia. *Chin. J. Cancer* **2014**, *33* (2), 80–86.
(52) Wardman, P.; Dennis, M. F.; Everett, S. A.; Patel, K. B.; Stratford, M. R. L.; Tracy, M. Radicals From One-Electron Reduction of Nitro Compounds, Aromatic N-Oxides and Quinones: the Kinetic Basis for Hypoxia-Selective, Bioreductive Drugs. *Biochem. Soc. Symp.* **1995**, *61*, 171–194.
(53) McKeown, S. R.; Cowen, R. L.; Williams, K. J. Bioreductive Drugs: From Concept to Clinic. *Clinical Oncology* **2007**, *19* (6), 427–442.
(54) Hunter, F. W.; Wouters, B. G.; Wilson, W. R. Hypoxia-Activated Prodrugs: Paths Forward in the Era of Personalised Medicine. *Br. J. Cancer* **2016**, *114* (10), 1071–1077.
(55) Raleigh, S. M.; Wanogho, E.; Burke, M. D.; McKeown, S. R.; Patterson, L. H. Involvement of Human Cytochromes P450 (CYP) in the Reductive Metabolism of AQ4N, a Hypoxia Activated Anthraquinone Di-N-Oxide Prodrug. *Int. J. Radiat. Oncol. Biol. Phys.* **1998**, *42* (4), 763–767.
(56) Nishida, C. R.; Lee, M.; de Montellano, P. R. O. Efficient Hypoxic Activation of the Anticancer Agent AQ4N by CYP2S1 and CYP2W1. *Mol. Pharmacol.* **2010**, *78* (3), 497–502.
(57) Fielden, E. M.; Adams, G. E.; Cole, S.; Naylor, M. A.; O'Neill, P.; Stephens, M. A.; Stratford, I. J. Assessment of a Range of Novel Nitro-Aromatic Radiosensitizers and Bioreductive Drugs. *Int. J. Radiat. Oncol. Biol. Phys.* **1992**, *22* (4), 707–711.
(58) Wilson, W. R.; Denny, W. A.; Twigden, S. J.; Baguley, B. C.; Probert, J. C. Selective Toxicity of Nitracrine to Hypoxic Mammalian Cells. *Br. J. Cancer* **1984**, *49* (2), 215–223.
(59) Hay, M. P.; Hicks, K. O.; Wang, J. Hypoxia-Directed Drug Strategies to Target the Tumor Microenvironment. *Adv. Exp. Med. Biol.* **2014**, *772*, 111–145.
(60) Foehrenbacher, A.; Secomb, T. W.; Wilson, W. R.; Hicks, K. O. Design of Optimized Hypoxia-Activated Prodrugs Using Pharmacokinetic/Pharmacodynamic Modeling. *Front. Oncol.* **2013**, *3*, 314.
(61) Petrelli, F.; Ghidini, A.; Inno, A.; Barni, S. Mitomycin-C+Fluoropyrimidines in Heavily Pretreated Metastatic Colorectal Cancer: a Systematic Review and Evidence Synthesis. *Anticancer Drugs* **2016**, *27* (6), 488–495.
(62) Zargar, H.; Aning, J.; Ischia, J.; So, A.; Black, P. Optimizing Intravesical Mitomycin C Therapy in Non-Muscle-Invasive Bladder Cancer. *Nat. Rev. Urol.* **2014**, *11* (4), 220–230.
(63) Stratford, I. J.; Stephens, M. A. The Differential Hypoxic Cytotoxicity of Bioreductive Agents Determined in Vitro by the MTT Assay. *Int. J. Radiat. Oncol. Biol. Phys.* **1989**, *16* (4), 973–976.
(64) Hendriks, H. R.; Pizao, P. E.; Berger, D. P.; Kooistra, K. L.; Bibby, M. C.; Boven, E.; Dreef-van der Meulen, H. C.; Henrar, R. E. C.; Fiebig, H. H.; Double, J. A.; Hornstra, H. W.; Pinedo, H. M.; Workman, P.;

Schwartsmann, G. EO9: a Novel Bioreductive Alkylating Indoloquinone with Preferential Solid Tumour Activity and Lack of Bone Marrow Toxicity in Preclinical Models. *Eur. J. Cancer* **1993**, *29* (6), 897–906.

(65) Phillips, R. M.; Hendriks, H. R.; Peters, G. J.; EORTC-Pharmacology and Molecular Mechanism Group. EO9 (Apaziquone): From the Clinic to the Laboratory and Back Again. *Br. J. Pharmacol.* **2013**, *168* (1), 11–18.

(66) Hendricksen, K.; Cornel, E. B.; de Reijke, T. M.; Arentsen, H. C.; Chawla, S.; Witjes, J. A. Phase 2 Study of Adjuvant Intravesical Instillations of Apaziquone for High Risk Nonmuscle Invasive Bladder Cancer. *J. Urol.* **2012**, *187* (4), 1195–1199.

(67) Rischin, D.; Peters, L. J.; O'Sullivan, B.; Giralt, J.; Fisher, R.; Yuen, K.; Trotti, A.; Bernier, J.; Bourhis, J.; Ringash, J.; Henke, M.; Kenny, L. Tirapazamine, Cisplatin, and Radiation Versus Cisplatin and Radiation for Advanced Squamous Cell Carcinoma of the Head and Neck (TROG 02.02, HeadSTART): a Phase III Trial of the Trans-Tasman Radiation Oncology Group. *J. Clin. Oncol.* **2010**, *28* (18), 2989–2995.

(68) Peters, L. J.; O'Sullivan, B.; Giralt, J.; Fitzgerald, T. J.; Trotti, A.; Bernier, J.; Bourhis, J.; Yuen, K.; Fisher, R.; Rischin, D. Critical Impact of Radiotherapy Protocol Compliance and Quality in the Treatment of Advanced Head and Neck Cancer: Results From TROG 02.02. *J. Clin. Oncol.* **2010**, *28* (18), 2996–3001.

(69) DiSilvestro, P. A.; Ali, S.; Craighead, P. S.; Lucci, J. A.; Lee, Y.-C.; Cohn, D. E.; Spirtos, N. M.; Tewari, K. S.; Muller, C.; Gajewski, W. H.; Steinhoff, M. M.; Monk, B. J. Phase III Randomized Trial of Weekly Cisplatin and Irradiation Versus Cisplatin and Tirapazamine and Irradiation in Stages IB2, IIA, IIB, IIIB, and IVA Cervical Carcinoma Limited to the Pelvis: a Gynecologic Oncology Group Study. *J. Clin. Oncol.* **2014**, *32* (5), 458–464.

(70) Hicks, K. O.; Siim, B. G.; Jaiswal, J. K.; Pruijn, F. B.; Fraser, A. M.; Patel, R.; Hogg, A.; Liyanage, H. D. S.; Dorie, M. J.; Brown, J. M.; Denny, W. A.; Hay, M. P.; Wilson, W. R. Pharmacokinetic/Pharmacodynamic Modeling Identifies SN30000 and SN29751 as Tirapazamine Analogues with Improved Tissue Penetration and Hypoxic Cell Killing in Tumors. *Clin. Cancer Res.* **2010**, *16* (20), 4946–4957.

(71) Wang, J.; Guise, C. P.; Dachs, G. U.; Phung, Y.; Hsu, A. H.-L.; Lambie, N. K.; Patterson, A. V.; Wilson, W. R. Biochemical Pharmacology. Identification of one-electron reductases that activate both the hypoxia prodrug SN30000 and diagnostic probe EF5. *Biochemical Pharmacol.* **2014**, *91* (4), 436–446.

(72) Hunter, F. W.; Young, R. J.; Shalev, Z.; Vellanki, R. N.; Wang, J.; Gu, Y.; Joshi, N.; Sreebhavan, S.; Weinreb, I.; Goldstein, D. P.; Moffat, J.; Ketela, T.; Brown, K. R.; Koritzinsky, M.; Solomon, B.; Rischin, D.; Wilson, W. R.; Wouters, B. G. Identification of P450 Oxidoreductase as a Major Determinant of Sensitivity to Hypoxia-Activated Prodrugs. *Cancer Res.* **2015**, *75* (19), 4211–4223.

(73) Hicks, K. O.; Pruijn, F. B.; Sturman, J. R.; Denny, W. A.; Wilson, W.

R. Multicellular Resistance to Tirapazamine Is Due to Restricted Extravascular Transport. *Cancer Res.* **2003**, *63* (18), 5970–5977.

(74) Peters, K. B.; Brown, J. M. Tirapazamine. *Cancer Res.* **2002**, *62* (18), 5248–5253.

(75) Gupta, S.; Gouw, L.; Wright, J.; Chawla, S.; Pitt, D.; Wade, M.; Boucher, K.; Sharma, S. Phase II Study of Amrubicin (SM-5887), a Synthetic 9-Aminoanthracycline, as First Line Treatment in Patients with Metastatic or Unresectable Soft Tissue Sarcoma: Durable Response in Myxoid Liposarcoma with TLS-CHOP Translocation. *Invest. New Drugs* **2016**, *34* (2), 243–252.

(76) Williams, K. J.; Albertella, M. R.; Fitzpatrick, B.; Loadman, P. M.; Shnyder, S. D.; Chinje, E. C.; Telfer, B. A.; Dunk, C. R.; Harris, P. A.; Stratford, I. J. In Vivo Activation of the Hypoxia-Targeted Cytotoxin AQ4N in Human Tumor Xenografts. *Mol. Cancer Ther.* **2009**, *8* (12), 3266–3275.

(77) Mehibel, M.; Singh, S.; Cowen, R. L.; Williams, K. J.; Stratford, I. J. Radiation Enhances the Therapeutic Effect of Banoxantrone in Hypoxic Tumour Cells with Elevated Levels of Nitric Oxide Synthase. *Oncol. Rep.* **2016**, *35* (4), 1925–1932.

(78) Nishida, C. R.; Ortiz de Montellano, P. R. Reductive Heme-Dependent Activation of the N-Oxide Prodrug AQ4N by Nitric Oxide Synthase. *J. Med. Chem.* **2008**, *51* (16), 5118–5120.

(79) McKeown, S. R.; Friery, O. P.; McIntyre, I. A.; Hejmadi, M. V.; Patterson, L. H.; Hirst, D. G. Evidence for a Therapeutic Gain When AQ4N or Tirapazamine Is Combined with Radiation. *Br. J. Cancer Suppl.* **1996**, *27*, S39–S42.

(80) Albertella, M. R.; Loadman, P. M.; Jones, P. H.; Phillips, R. M.; Rampling, R.; Burnet, N.; Alcock, C.; Anthoney, A.; Vjaters, E.; Dunk, C. R.; Harris, P. A.; Wong, A.; Lalani, A. S.; Twelves, C. J. Hypoxia-Selective Targeting by the Bioreductive Prodrug AQ4N in Patients with Solid Tumors: Results of a Phase I Study. *Clin. Cancer Res.* **2008**, *14* (4), 1096–1104.

(81) Papadopoulos, K. P.; Goel, S.; Beeram, M.; Wong, A.; Desai, K.; Haigentz, M.; Milián, M. L.; Mani, S.; Tolcher, A.; Lalani, A. S.; Sarantopoulos, J. A Phase 1 Open-Label, Accelerated Dose-Escalation Study of the Hypoxia-Activated Prodrug AQ4N in Patients with Advanced Malignancies. *Clin. Cancer Res.* **2008**, *14* (21), 7110–7115.

(82) Trédan, O.; Garbens, A. B.; Lalani, A. S.; Tannock, I. F. The Hypoxia-Activated ProDrug AQ4N Penetrates Deeply in Tumor Tissues and Complements the Limited Distribution of Mitoxantrone. *Cancer Res.* **2009**, *69* (3), 940–947.

(83) Duan, J.-X.; Jiao, H.; Kaizerman, J.; Stanton, T.; Evans, J. W.; Lan, L.; Lorente, G.; Banica, M.; Jung, D.; Wang, J.; Ma, H.; Li, X.; Yang, Z.; Hoffman, R. M.; Ammons, W. S.; Hart, C. P.; Matteucci, M. Potent and Highly Selective Hypoxia-Activated Achiral Phosphoramidate Mustards as Anticancer Drugs. *J. Med. Chem.* **2008**, *51* (8), 2412–2420.

(84) McKeage, M. J.; Jameson, M. B.; Ramanathan, R. K.; Rajendran, J.; Gu, Y.; Wilson, W. R.; Melink, T. J.; Tchekmedyian, N. S. PR-104 a

Bioreductive Pre-Prodrug Combined with Gemcitabine or Docetaxel in a Phase Ib Study of Patients with Advanced Solid Tumours. *BMC Cancer* **2012**, *12*, 496.

(85) Thomson, P.; Naylor, M. A.; Everett, S. A.; Stratford, M. R. L.; Lewis, G.; Hill, S.; Patel, K. B.; Wardman, P.; Davis, P. D. Synthesis and Biological Properties of Bioreductively Targeted Nitrothienyl Prodrugs of Combretastatin a-4. *Mol. Cancer Ther.* **2006**, *5* (11), 2886–2894.

(86) Everett, S. A.; Naylor, M. A.; Patel, K. B.; Stratford, M. R.; Wardman, P. Bioreductively-Activated Prodrugs for Targeting Hypoxic Tissues: Elimination of Aspirin From 2-Nitroimidazole Derivatives. *Bioorg. Med. Chem. Lett.* **2003**, *9* (9), 1267–1272.

(87) Li, Z.; Li, X.; Gao, X.; Zhang, Y.; Shi, W.; Ma, H. Nitroreductase Detection and Hypoxic Tumor Cell Imaging by a Designed Sensitive and Selective Fluorescent Probe, 7-[(5-Nitrofuran-2-Yl)Methoxy]-3 H-Phenoxazin-3-One. *Anal. Chem.* **2013**, *85* (8), 3926–3932.

(88) Guise, C. P.; Abbattista, M. R.; Tipparaju, S. R.; Lambie, N. K.; Su, J.; Li, D.; Wilson, W. R.; Dachs, G. U.; Patterson, A. V. Diflavin Oxidoreductases Activate the Bioreductive Prodrug PR-104A Under Hypoxia. *Mol. Pharmacol.* **2011**, *81* (1), 31–40.

(89) Patterson, A. V.; Ferry, D. M.; Edmunds, S. J.; Gu, Y. Mechanism of Action and Preclinical Antitumor Activity of the Novel Hypoxia-Activated DNA Cross-Linking Agent PR-104. *Clin. Cancer Res.* **2007**, *13* (13), 3922–3932.

(90) Phillips, R. M. Targeting the Hypoxic Fraction of Tumours Using Hypoxia-Activated Prodrugs. *Cancer Chemother. Pharmacol.* **2016**, *77* (3), 441–457.

(91) Konopleva, M.; Thall, P. F.; Yi, C. A.; Borthakur, G.; Coveler, A.; Bueso-Ramos, C.; Benito, J.; Konoplev, S.; Gu, Y.; Ravandi, F.; Jabbour, E.; Faderl, S.; Thomas, D.; Cortes, J.; Kadia, T.; Kornblau, S.; Daver, N.; Pemmaraju, N.; Nguyen, H. Q.; Feliu, J.; Lu, H.; Wei, C.; Wilson, W. R.; Melink, T. J.; Gutheil, J. C.; Andreeff, M.; Estey, E. H.; Kantarjian, H. Phase I/II Study of the Hypoxia-Activated Prodrug PR104 in Refractory/Relapsed Acute Myeloid Leukemia and Acute Lymphoblastic Leukemia. *Haematologica* **2015**, *100* (7), 927–934.

(92) Meng, F.; Evans, J. W.; Bhupathi, D.; Banica, M.; Lan, L.; Lorente, G.; Duan, J. X.; Cai, X.; Mowday, A. M.; Guise, C. P.; Maroz, A.; Anderson, R. F.; Patterson, A. V.; Stachelek, G. C.; Glazer, P. M.; Matteucci, M. D.; Hart, C. P. Molecular and Cellular Pharmacology of the Hypoxia-Activated Prodrug TH-302. *Mol. Cancer Ther.* **2012**, *11* (3), 740–751.

(93) Yoon, C.; Chang, K. K.; Lee, J. H.; Tap, W. D.; Hart, C. P.; Simon, M. C.; Yoon, S. S. Multimodal Targeting of Tumor Vasculature and Cancer Stem-Like Cells in Sarcomas with VEGF-a Inhibition, HIF-1α Inhibition, and Hypoxia-Activated Chemotherapy. *Oncotarget* **2016**, *7* (28), 42844–42858.

(94) Yoon, C.; Lee, H.-J.; Park, D. J.; Lee, Y.-J.; Tap, W. D.; Eisinger-Mathason, T. S. K.; Hart, C. P.; Choy, E.; Simon, M. C.; Yoon, S. S. Hypoxia-Activated Chemotherapeutic TH-302enhances the Effects of VEGF-a Inhibitionand Radiation on Sarcomas. *Br. J. Cancer* **2015**,

113 (1), 46–56.
(95) Meng, F.; Bhupathi, D.; Sun, J. D.; Liu, Q.; Ahluwalia, D.; Wang, Y.; Matteucci, M. D.; Hart, C. P. Enhancement of Hypoxia-Activated Prodrug TH-302 Anti-Tumor Activity by Chk1 Inhibition. *BMC Cancer* **2015**, *15* (422), 1–17.
(96) Sun, J. D.; Ahluwalia, D.; Liu, Q.; Li, W.; Wang, Y.; Meng, F.; Bhupathi, D.; Matteucci, M. D.; Hart, C. P. Combination Treatment with Hypoxia-Activated Prodrug Evofosfamide (TH-302) and mTOR Inhibitors Results in Enhanced Antitumor Efficacy in Preclinical Renal Cell Carcinoma Models. *Am. J. Cancer Res.* **2015**, *5* (7), 2139–2155.
(97) Peeters, S. G. J. A.; Zegers, C. M. L.; Biemans, R.; Lieuwes, N. G.; van Stiphout, R. G. P. M.; Yaromina, A.; Sun, J. D.; Hart, C. P.; Windhorst, A. D.; van Elmpt, W.; Dubois, L. J.; Lambin, P. TH-302 in Combination with Radiotherapy Enhances the Therapeutic Outcome and Is Associated with Pretreatment [18F]HX4 Hypoxia PET Imaging. *Clin. Cancer Res.* **2015**, *21* (13), 2984–2992.
(98) Zhang, X.; Wojtkowiak, J. W.; Martinez, G. V.; Cornnell, H. H.; Hart, C. P.; Baker, A. F.; Gillies, R. MR Imaging Biomarkers to Monitor Early Response to Hypoxia-Activated Prodrug TH-302 in Pancreatic Cancer Xenografts. *PLoS ONE* **2016**, *11* (5), e0155289.
(99) Parveen, I.; Naughton, D. P.; Whish, W. J.; Threadgill, M. D. 2-Nitroimidazol-5-Ylmethyl as a Potential Bioreductively Activated Prodrug System: Reductively Triggered Release of the PARP Inhibitor 5-Bromoisoquinolinone. *Bioorg. Med. Chem. Lett.* **1999**, *9* (14), 2031–2036.
(100) Damen, E. W. P.; Nevalainen, T. J.; van den Bergh, T. J. M.; de Groot, F. M. H.; Scheeren, H. W. Synthesis of Novel Paclitaxel Prodrugs Designed for Bioreductive Activation in Hypoxic Tumour Tissue. *Bioorg. Med. Chem.* **2002**, *10* (1), 71–77.
(101) Ferrer, S.; Naughton, D. P.; Threadgill, M. D. 1H NMR Studies on the Reductively Triggered Release of Heterocyclic and Steroid Drugs From 4,7-Dioxoindole-3-Methyl Prodrugs. *Tetrahedron* **2003**.
(102) Hay, M. P.; Wilson, W. R.; Denny, W. A. Nitroarylmethylcarbamate Prodrugs of Doxorubicin for Use with Nitroreductase Gene-Directed Enzyme Prodrug Therapy. *Bioorg. Med. Chem.* **2005**, *13* (12), 4043–4055.
(103) Granchi, C.; Funaioli, T.; Erler, J. T.; Giaccia, A. J.; Macchia, M.; Minutolo, F. Bioreductively Activated Lysyl Oxidase Inhibitors Against Hypoxic Tumours. *Chem. Med. Chem.* **2009**, *4* (10), 1590–1594.
(104) Zhu, R.; Liu, M.-C.; Luo, M.-Z.; Penketh, P. G.; Baumann, R. P.; Shyam, K.; Sartorelli, A. C. 4-Nitrobenzyloxycarbonyl Derivatives of O(6)-Benzylguanine as Hypoxia-Activated Prodrug Inhibitors of O(6)-Alkylguanine-DNA Alkyltransferase (AGT), Which Produces Resistance to Agents Targeting the O-6 Position of DNA Guanine. *J. Med. Chem.* **2011**, *54* (21), 7720–7728.
(105) Lindquist, K. E.; Cran, J. D.; Kordic, K.; Chua, P. C.; Winters, G. C.; Tan, J. S.; Lozada, J.; Kyle, A. H.; Evans, J. W.; Minchinton, A. I. Selective Radiosensitization of Hypoxic Cells Using BCCA621C: a Novel Hypoxia Activated Prodrug Targeting DNA-Dependent Protein

Kinase. *Tumor Microenvironment and Therapy* **2013**, *1*.
(106) Zhang, Z.; Tanabe, K.; Hatta, H.; Nishimoto, S.-I. Bioreduction Activated Prodrugs of Camptothecin: Molecular Design, Synthesis, Activation Mechanism and Hypoxia Selective Cytotoxicity. *Org. Biomol. Chem.* **2005**, *3* (10), 1905–1910.
(107) Blanche, E. A.; Maskell, L.; Colucci, M. A.; Whatmore, J. L. Synthesis of Potential Prodrug Systems for Reductive Activation. Prodrugs for Anti-Angiogenic Isoflavones and VEGF Receptor Tyrosine Kinase Inhibitory Oxindoles. *Tetrahedron* **2009**.
(108) Karnthaler-Benbakka, C.; Groza, D.; Kryeziu, K.; Pichler, V.; Roller, A.; Berger, W.; Heffeter, P.; Kowol, C. R. Tumor-Targeting of EGFR Inhibitors by Hypoxia-Mediated Activation. *Angew. Chem. Int. Ed.* **2014**, *53* (47), 12930–12935.
(109) Patterson, A.; Silva, S.; Jackson, V. The Hypoxia-Activated EGFR-TKI TH-4000: Preclinical Profile and Ongoing Clinical Studies in NSCLC, SCCHN, and SCCS. *14th International Tumor Microenvironment Workshop: Hypoxia, Angiogensis and Vasculature*. 14th International Tumor Microenvironment Workshop: Hypoxia, Angiogenesis and Vasculature: Vancouver 2015.
(110) Patterson, A. V.; Silva, S.; Guise, C.; Bull, M.; Abbattista, M.; Hsu, A.; Sun, J. D.; Hart, C. P.; Pearce, T. E.; Smaill, J. B. TH-4000, a Hypoxia-Activated EGFR/Her2 Inhibitor to Treat EGFR-TKI Resistant T790M-Negative NSCLC. *ASCO Meeting Abstracts* **2015**, *33* (15_suppl), e13548.
(111) Patterson, A. V.; Silva, S.; Guise, C.; Abbattista, M.; Bull, M.; Hsu, H.-L.; Hart, C.; Sun, J.; Grey, A.; Ashoorzadeh, A.; Anderson, R.; Smaill, J. B. Abstract 5358: the Hypoxia-Activated EGFR-TKI TH-4000 Overcomes Erlotinib-Resistance in Preclinical NSCLC Models at Plasma Levels Achieved in a Phase 1 Clinical Trial. *Cancer Res.* **2015**, *75* (15 Supplement), 5358–5358.
(112) Sakurikar, N.; Eastman, A. Will Targeting Chk1 Have a Role in the Future of Cancer Therapy? *J. Clin. Oncol.* **2015**, *33* (9), 1075–1077.
(113) Dillon, M. T.; Good, J. S.; Harrington, K. J. Clinical Oncology. *Clin. Oncol.* **2014**, *26* (5), 257–265.
(114) Buffa, F. M.; Harris, A. L.; West, C. M.; Miller, C. J. Large Meta-Analysis of Multiple Cancers Reveals a Common, Compact and Highly Prognostic Hypoxia Metagene. *Br. J. Cancer* **2010**, *102*, 428–435.
(115) Toustrup, K.; Sørensen, B. S.; Nordsmark, M.; Busk, M.; Wiuf, C.; Alsner, J.; Overgaard, J. Development of a Hypoxia Gene Expression Classifier with Predictive Impact for Hypoxic Modification of Radiotherapy in Head and Neck Cancer. *Cancer Res.* **2011**, *71* (17), 5923–5931.
(116) Ross, D.; Beall, H. D.; Siegel, D.; Traver, R. D. Enzymology of Bioreductive Drug Activation. *Br. J. Cancer* **1996**, *74* ((Suppl. XXVII)), S1–S8.
(117) Patterson, A. V.; Barham, H. M.; Chinje, E. C. Importance of P450 Reductase Activity in Determining Sensitivity of Breast Tumour Cells to the Bioreductive Drug, Tirapazamine (SR 4233). *Br. J. Cancer* **1995**, *72*, 1144–1150.

(118) Fleming, I. N.; Manavaki, R.; Blower, P. J.; West, C.; Williams, K. J.; Harris, A. L.; Domarkas, J.; Lord, S.; Baldry, C.; Gilbert, F. J. Imaging Tumour Hypoxia with Positron Emission Tomography. *Br. J. Cancer* **2015**, *112* (2), 238–250.
(119) Sun, X.; Niu, G.; Chan, N.; Shen, B.; Chen, X. Tumor Hypoxia Imaging. *Mol. Imaging Biol.* **2011**, *13* (3), 399–410.
(120) Nordsmark, M.; Loncaster, J.; Aquino-Parsons, C.; Chou, S.-C.; Gebski, V.; West, C.; Lindegaard, J. C.; Havsteen, H.; Davidson, S. E.; Hunter, R.; Raleigh, J. A.; Overgaard, J. The Prognostic Value of Pimonidazole and Tumour pO2 in Human Cervix Carcinomas After Radiation Therapy: a Prospective International Multi-Center Study. *Radiother. Oncol.* **2006**, *80* (2), 123–131.
(121) Wang, J.; Foehrenbacher, A.; Su, J.; Patel, R.; Hay, M. P.; Hicks, K. O.; Wilson, W. R. The 2-Nitroimidazole EF5 Is a Biomarker for Oxidoreductases That Activate the Bioreductive Prodrug CEN-209 Under Hypoxia. *Clin. Cancer Res.* **2012**, *18* (6), 1684–1695.
(122) Bussink, J.; van Herpen, C. M. L.; Kaanders, J. H. A. M.; Oyen, W. J. G. PET-CT for Response Assessment and Treatment Adaptation in Head and Neck Cancer. *Lancet Oncol.* **2010**, *11* (7), 661–669.
(123) Spence, A. M.; Muzi, M.; Swanson, K. R.; O'Sullivan, F.; Rockhill, J. K.; Rajendran, J. G.; Adamsen, T. C. H.; Link, J. M.; Swanson, P. E.; Yagle, K. J.; Rostomily, R. C.; Silbergeld, D. L.; Krohn, K. A. Regional Hypoxia in Glioblastoma Multiforme Quantified with [18F]Fluoromisonidazole Positron Emission Tomography Before Radiotherapy: Correlation with Time to Progression and Survival. *Clin. Cancer Res.* **2008**, *14* (9), 2623–2630.
(124) Swanson, K. R.; Chakraborty, G.; Wang, C. H.; Rockne, R.; Harpold, H. L. P.; Muzi, M.; Adamsen, T. C. H.; Krohn, K. A.; Spence, A. M. Complementary but Distinct Roles for MRI and 18F-Fluoromisonidazole PET in the Assessment of Human Glioblastomas. *J. Nucl. Med.* **2009**, *50* (1), 36–44.
(125) Chitneni, S. K.; Bida, G. T.; Yuan, H.; Palmer, G. M.; Hay, M. P.; Melcher, T.; Wilson, W. R.; Zalutsky, M. R.; Dewhirst, M. W. 18F-EF5 PET Imaging as an Early Response Biomarker for the Hypoxia-Activated Prodrug SN30000 Combined with Radiation Treatment in a Non-Small Cell Lung Cancer Xenograft Model. *J. Nucl. Med.* **2013**, *54* (8), 1339–1346.
(126) Zegers, C. M. L.; Hoebers, F. J. P.; van Elmpt, W.; Bons, J. A.; Öllers, M. C.; Troost, E. G. C.; Eekers, D.; Balmaekers, L.; Arts-Pechtold, M.; Mottaghy, F. M.; Lambin, P. Evaluation of Tumour Hypoxia During Radiotherapy Using [(18)F]HX4 PET Imaging and Blood Biomarkers in Patients with Head and Neck Cancer. *Eur. J. Nucl. Med. Mol. Imaging* **2016**, *10.1007/s00259-016-3429-y* (Ahead of Print).
(127) Elmes, R. B. P. Bioreductive Fluorescent Imaging Agents: Applications to Tumour Hypoxia. *Chem. Commun. (Camb.)* **2016**, *52* (58), 8935–8956.
(128) Ntziachristos, V. Going Deeper Than Microscopy: the Optical Imaging Frontier in Biology. *Nat. Methods* **2010**, *7* (8), 603–614.
(129) Vahrmeijer, A. L.; Hutteman, M.; van der Vorst, J. R.; van de Velde,

C. J. H.; Frangioni, J. V. Image-Guided Cancer Surgery Using Near-Infrared Fluorescence. *Nat. Rev. Clin. Oncol.* **2013**, *10* (9), 507–518.
(130) Iqbal, H.; Pan, Q. Image Guided Surgery in the Management of Head and Neck Cancer. *Oral Oncol.* **2016**, *57*, 32–39.
(131) Liu, S.; Zheng, Y.; Volpi, D.; El-Kasti, M.; Klotz, D.; Tullis, I.; Henricks, A.; Campo, L.; Myers, K.; Laios, A.; Thomas, P.; Ng, T.; Dhar, S.; Becker, C.; Vojnovic, B.; Ahmed, A. A. Toward Operative in Vivo Fluorescence Imaging of the C-Met Proto-Oncogene for Personalization of Therapy in Ovarian Cancer. *Cancer* **2014**, *121* (2), 202–213.
(132) van der Vorst, J. R.; Hutteman, M.; Mieog, J. S. D.; de Rooij, K. E.; Kaijzel, E. L.; Löwik, C. W. G. M.; Putter, H.; Kuppen, P. J. K.; Frangioni, J. V.; van de Velde, C. J. H.; Vahrmeijer, A. L. Near-Infrared Fluorescence Imaging of Liver Metastases in Rats Using Indocyanine Green. *J. Surg. Res.* **2012**, *174* (2), 266–271.
(133) Frangioni, J. V. In Vivo Near-Infrared Fluorescence Imaging. *Curr. Opin. Chem. Biol.* **2003**, *7* (5), 626–634.
(134) Laios, A.; Volpi, D.; Tullis, I. D. C.; Woodward, M.; Kennedy, S.; Pathiraja, P. N. J.; Haldar, K.; Vojnovic, B.; Ahmed, A. A. A Prospective Pilot Study of Detection of Sentinel Lymph Nodes in Gynaecological Cancers Using a Novel Near Infrared Fluorescence Imaging System. *BMC Research Notes* **2015**, *8* (608), 1–9.
(135) Judy, R. P.; Keating, J. J.; DeJesus, E. M.; Jiang, J. X.; Okusanya, O. T.; Nie, S.; Holt, D. E.; Arlauckas, S. P.; Low, P. S.; Delikatny, E. J.; Singhal, S. Quantification of Tumorfluorescence During Intraoperativeoptical Cancer Imaging. *Sci. Rep.* **2015**, *5:16208*, 1–11.
(136) Digonnet, A.; van Kerckhove, S.; Moreau, M.; Willemse, E.; Quiriny, M.; Ahmed, B.; de Saint Aubain, N.; Andry, G.; Bourgeois, P. Near Infrared Fluorescent Imaging After Intravenous Injection of Indocyanine Green During Neck Dissection in Patients with Head and Neck Cancer: a Feasibility Study. *Head Neck* **2016**, *38 Suppl 1*, E1833–E1837.
(137) Porcu, E. P.; Salis, A.; Gavini, E.; Rassu, G.; Maestri, M.; Giunchedi, P. Indocyanine Green Delivery Systems for Tumour Detection and Treatments. *Biotechnol. Adv.* **2016**, *34* (5), 768–789.
(138) Kaibori, M.; Matsui, K.; Ishizaki, M.; Iida, H.; Okumura, T.; Sakaguchi, T.; Inoue, K.; Ikeura, T.; Asano, H.; Kon, M. Intraoperative Detection of Superficial Liver Tumors by Fluorescence Imaging Using Indocyanine Green and 5-Aminolevulinic Acid. *Anticancer Res.* **2016**, *36* (4), 1841–1849.
(139) Keating, J.; Tchou, J.; Okusanya, O.; Fisher, C.; Batiste, R.; Jiang, J.; Kennedy, G.; Nie, S.; Singhal, S. Identification of Breast Cancer Margins Using Intraoperative Near-Infrared Imaging. *J. Surg. Oncol.* **2016**, *113* (5), 508–514.
(140) Ishizawa, T.; Masuda, K.; Urano, Y.; Kawaguchi, Y.; Satou, S.; Kaneko, J.; Hasegawa, K.; Shibahara, J.; Fukayama, M.; Tsuji, S.; Midorikawa, Y.; Aburatani, H.; Kokudo, N. Mechanistic Background and Clinical Applications of Indocyanine Green Fluorescence Imaging of Hepatocellular Carcinoma. *Ann. Surg. Oncol.* **2014**, *21* (2), 440–448.

(141) Gibbs, S. L. Near Infrared Fluorescence for Image-Guided Surgery. *Quant. Imaging Med. Surg.* **2012**, *2* (3), 177–187.
(142) Alander, J. T.; Kaartinen, I.; Laakso, A.; Pätilä, T.; Spillmann, T.; Tuchin, V. V.; Venermo, M.; Välisuo, P. A Review of Indocyanine Green Fluorescent Imaging in Surgery. *Int. J. Biomed. Imaging* **2012**, *2012*, 940585.
(143) Li, Y.; Sun, Y.; Li, J.; Su, Q.; Yuan, W.; Dai, Y.; Han, C.; Wang, Q.; Feng, W.; Li, F. Ultrasensitive Near-Infrared Fluorescence-Enhanced Probe for in VivoNitroreductase Imaging. *J. Am. Chem. Soc.* **2015**, *137* (19), 6407–6416.
(144) Okuda, K.; Okabe, Y.; Kadonosono, T.; Ueno, T.; Youssif, B. G. M.; Kizaka-Kondoh, S.; Nagasawa, H. 2-Nitroimidazole-Tricarbocyanine Conjugate as a Near-Infrared Fluorescent Probe for in VivoImaging of Tumor Hypoxia. *Bioconjugate Chem.* **2012**, *23* (3), 324–329.
(145) McCormack, E.; Silden, E.; West, R. M.; Pavlin, T.; Micklem, D. R.; Lorens, J. B.; Haug, B. E.; Cooper, M. E.; Gjertsen, B. T. Nitroreductase, a Near-Infrared Reporter Platform for in Vivo Time-Domain Optical Imaging of Metastatic Cancer. *Cancer Res.* **2013**, *73* (4), 1276–1286.
(146) Munkholm, C.; Parkinson, D. R.; Walt, D. R. Intramolecular Fluorescence Self-Quenching of Fluoresceinamine. *J. Am. Chem. Soc.* **1990**, *112* (7), 2608–2612.
(147) Rtishchev, N. I.; Samoilov, D. V.; Martynova, V. P.; El'tsov, A. V. Luminescence Properties of Nitro Derivatives of Fluorescein. *Russ. J. Gen. Chem.* **2001**, *71* (9), 1467–1478.
(148) Ueno, T.; Urano, Y.; Kojima, H.; Nagano, T. Mechanism-Based Molecular Design of Highly Selective Fluorescence Probes for Nitrative Stress. *J. Am. Chem. Soc.* **2006**, *128* (33), 10640–10641.
(149) Begg, A. C.; Engelhardt, E. L.; Hodgkiss, R. J.; McNally, N. J.; Terry, N. H.; Wardman, P. Nitroakridin 3582: a Fluorescent Nitroacridine Stain for Identifying Hypoxic Cells. *Br. J. Radiol.* **1983**, *56* (672), 970–973.
(150) Wardman, P.; Clarke, E. D.; Hodgkiss, R. J.; Middleton, R. W.; Parrick, J.; Stratford, M. R. Nitroaryl Compounds as Potential Fluorescent Probes for Hypoxia. I. Chemical Criteria and Constraints. *Int. J. Radiat. Oncol. Biol. Phys.* **1984**, *10* (8), 1347–1351.
(151) Stratford, M. R.; Clarke, E. D.; Hodgkiss, R. J.; Middleton, R. W.; Wardman, P. Nitroaryl Compounds as Potential Fluorescent Probes for Hypoxia. II. Identification and Properties of Reductive Metabolites. *Int. J. Radiat. Oncol. Biol. Phys.* **1984**, *10* (8), 1353–1356.
(152) Liu, Y.; Xu, Y.; Qian, X.; Liu, J.; Shen, L.; Li, J. Novel Fluorescent Markers for Hypoxic Cells of Naphthalimides with Two Heterocyclic Side Chains for Bioreductive Binding. *Bioorg. Med. Chem.* **2006**, *14*, 2935–2941.
(153) Luo, S.; Zhang, E.; Su, Y.; Cheng, T.; Shi, C. A Review of NIR Dyes in Cancer Targeting and Imaging. *Biomaterials* **2011**, *32* (29), 7127–7138.
(154) Xu, Y.; Zanganeh, S.; Mohammad, I.; Aguirre, A.; Wang, T.; Yang, Y.; Kuhn, L.; Smith, M. B.; Zhu, Q. Targeting Tumor Hypoxia with 2-Nitroimidazole-Indocyanine Green Dye Conjugates. *J. Biomed. Opt.*

2013, *18* (6), 0660091–11.
(155) Zhou, F.; Zanganeh, S.; Mohammad, I.; Dietz, C.; Abuteen, A.; Smith, M. B.; Zhu, Q. Targeting Tumor Hypoxia: a Third Generation 2-Nitroimidazole-Indocyanine Dye-Conjugate with Improved Fluorescent Yield. *Org. Biomol. Chem.* **2015**, *13* (46), 11220–11227.
(156) Yuan, L.; Lin, W.; Zhao, S.; Gao, W.; Chen, B.; He, L.; Zhu, S. A Unique Approach to Development of Near-Infrared Fluorescent Sensors for in Vivo Imaging. *J. Am. Chem. Soc.* **2012**, *134* (32), 13510–13523.
(157) Guo, T.; Cui, L.; Shen, J.; Zhu, W.; Xu, Y.; Qian, X. A Highly Sensitive Long-Wavelength Fluorescence Probe for Nitroreductase and Hypoxia: Selective Detection and Quantification. *Chem. Commun.* **2013**, *49* (92), 10820–10822.
(158) Lord, S. J.; Conley, N. R.; Lee, H.-L. D.; Samuel, R.; Liu, N.; Twieg, R. J.; Moerner, W. E. A Photoactivatable Push−Pull Fluorophore for Single-Molecule Imaging in Live Cells. *J. Am. Chem. Soc.* **2008**, *130* (29), 9204–9205.
(159) Yuan, J.; Xu, Y.-Q.; Zhou, N.-N.; Wang, R.; Qian, X.-H.; Xu, Y.-F. A Highly Selective Turn-on Fluorescent Probe Based on Semi-Cyanine for the Detection of Nitroreductase and Hypoxic Tumor Cell Imaging. *RSC Adv.* **2014**, *4* (99), 56207–56210.
(160) Lee, M. K.; Williams, J.; Twieg, R. J.; Rao, J.; Moerner, W. E. Enzymatic Activation of Nitro-Aryl Fluorogens in Live Bacterial Cells for Enzymatic Turnover-Activated Localization Microscopy. *Chem. Sci.* **2013**, *4* (1), 220–225.
(161) Grammel, M.; Hang, H. C. Chemical Reporters for Biological Discovery. *Nat. Chem. Biol.* **2013**, *9* (8), 475–484.
(162) Chan, J.; Dodani, S. C.; Chang, C. J. Reaction-Based Small-Molecule Fluorescent Probes for Chemoselective Bioimaging. *Nat. Chem.* **2012**, *4* (12), 973–984.
(163) Olive, P. L. Cellular Metabolism of Fluorescent Nitroheterocycles. *Int. J. Radiat. Oncol. Biol. Phys.* **1984**, *10* (8), 1357–1360.
(164) Rajapakse, A.; Gates, K. S. Hypoxia-Selective, Enzymatic Conversion of 6-Nitroquinoline Into a Fluorescent Helicene: Pyrido[3,2- F]Quinolino[6,5- C]Cinnoline 3-Oxide. *J. Org. Chem.* **2012**, *77* (7), 3531–3537.
(165) Rajapakse, A.; Linder, C.; Morrison, R. D.; Sarkar, U.; Leigh, N. D.; Barnes, C. L.; Daniels, J. S.; Gates, K. S. Enzymatic Conversion of 6-Nitroquinoline to the Fluorophore 6-Aminoquinoline Selectively Under Hypoxic Conditions. *Chem. Res. Toxicol.* **2013**, *26* (4), 555–563.
(166) Su, J.; Guise, C. P.; Wilson, W. R. FSL-61 Is a 6-Nitroquinolone Fluorogenic Probe for One-Electron Reductases in Hypoxic Cells. *Biochem. J.* **2013**, *452* (1), 79–86.
(167) Siim, B. G.; Atwell, G. J.; Anderson, R. F.; Wardman, P.; Pullen, S. M.; Wilson, W. R.; Denny, W. A. Hypoxia-Selective Antitumor Agents. 15. Modification of Rate of Nitroreduction and Extent of Lysosomal Uptake by Polysubstitution of 4-(Alkylamino)-5-Nitroquinoline Bioreductive Drugs. *J. Med. Chem.* **1997**, *40* (9), 1381–1390.
(168) Denny, W. A.; Atwell, G. J.; Roberts, P. B.; Anderson, R. F.; Boyd,

M.; Lock, C. J. L.; Wilson, W. R. Hypoxia-Selective Antitumor Agents. 6. 4-(Alkylamino)Nitroquinolines: a New Class of Hypoxia-Selective Cytotoxins. *J. Med. Chem.* **1992**, *35* (26), 4832–4841.

(169) Wilson, W. R.; Siim, B. G.; Denny, W. A.; van Zijl, P. L.; Taylor, M. L.; Chambers, D. M.; Roberts, P. B. 5-Nitro-4-(N,N-Dimethylaminopropylamino)Quinoline (5-Nitraquine), a New DNA-Affinic Hypoxic Cell Radiosensitizer and Bioreductive Agent: Comparison with Nitracrine. *Rad. Res.* **1992**, *131* (3), 257–256.

(170) Couch, G. D.; Burke, P. J.; Knox, R. J.; Moody, C. J. Synthesis of 2-Aryl-6-Methyl-5-Nitroquinoline Derivatives as Potential Prodrug Systems for Reductive Activation. *Tetrahedron* **2008**, *64* (12), 2816–2823.

(171) Firestone, A.; Mulcahy, R. T.; Borch, R. F. Nitroheterocycle Reduction as a Paradigm for Intramolecular Catalysis of Drug Delivery to Hypoxic Cells. *J. Med. Chem.* **1991**, *34* (9), 2933–2935.

(172) Struwe, W. B.; Rudd, P. M. Aminoquinolines as Fluorescent Labels for Hydrophilic Interaction Liquid Chromatography of Oligosaccharides. *Biol. Chem.* **2012**, *393* (8), 757–765.

(173) Wu, X.; Sun, X.; Guo, Z.; Tang, J.; Shen, Y.; James, T. D.; Tian, H.; Zhu, W. In Vivo and in Situ Tracking Cancer Chemotherapy by Highly Photostable NIR Fluorescent Theranostic Prodrug. *J. Am. Chem. Soc.* **2014**, *136* (9), 3579–3588.

(174) Sheppard, T. D. Metal-Catalysed Halogen Exchange Reactions of Aryl Halides. *Org. Biomol. Chem.* **2009**, *7* (6), 1043–1052.

(175) Fors, B. P.; Buchwald, S. L. Pd-Catalyzed Conversion of Aryl Chlorides, Triflates, and Nonaflates to Nitroaromatics. *J. Am. Chem. Soc.* **2009**, *131* (36), 12898–12899.

(176) O'Connor, L. J.; Cazares-Körner, C.; Saha, J.; Evans, C. N. G.; Stratford, M. R. L.; Hammond, E. M.; Conway, S. J. Efficient Synthesis of 2-Nitroimidazole Derivatives and the Bioreductive Clinical Candidate Evofosfamide (TH-302). *Org. Chem. Front.* **2015**, *2* (9), 1026–1029.

(177) Hodgson, H. H. *The Sandmeyer Reaction.*; American Chemical Society, 1947.

(178) Sapountzis, I.; Knochel, P. General Preparation of Functionalized O-Nitroarylmagnesium Halides Through an Iodine–Magnesium Exchange. *Angew. Chem. Int. Ed.* **2002**, *41* (9), 1610–1611.

(179) Lee, Y. M.; Moon, M. E.; Vajpayee, V.; Filimonov, V. D.; Chi, K.-W. Efficient and Economic Halogenation of Aryl Amines via Arenediazonium Tosylate Salts. *Tetrahedron* **2010**, *66* (37), 7418–7422.

(180) Baik, W.; Luan, W.; Lee, H. J.; Yoon, C. H.; Koo, S.; Kim, B. H. Efficient One-Pot Transformation of Aminoarenes to Haloarenes Using Halodimethylisulfonium Halides Generated in Situ. *Can. J. Chem.* **2005**, *83* (3), 213–219.

(181) Gracia Ferrer, J.; Pages Santacana, L. M. 3-(5-Amino-6-Oxo-1,6-Dihydropyridazin-3-Yl)-Biphenyl Derivatives as PDE4 Inhibitors. European Patent Office December 14, 2011.

(182) Rodríguez-Paredes, M.; Esteller, M. Cancer Epigenetics Reaches Mainstream Oncology. *Nat. Med.* **2011**, *17* (3), 330–339.

(183) Ahuja, N.; Sharma, A. R.; Baylin, S. B. Epigenetic Therapeutics: a New Weapon in the War Against Cancer. *Annu. Rev. Med.* **2016**, *67*, 73–89.
(184) Conway, S. J.; Woster, P. M.; Shen, J.-K.; Georg, G.; Wang, S. Epigenetics: Novel Therapeutics Targeting Epigenetics. *J. Med. Chem.* **2015**, *58* (2), 523–524.
(185) Filippakopoulos, P.; Knapp, S. Targeting Bromodomains: Epigenetic Readers of Lysine Acetylation. *Nat. Rev. Drug Disc.* **2014**, *13* (5), 337–356.
(186) Smith, S. G.; Zhou, M.-M. The Bromodomain: a New Target in Emerging Epigenetic Medicine. *ACS Chem. Biol.* **2016**, *11* (3), 598–608.
(187) Brand, M.; Measures, A. M.; Wilson, B. G.; Cortopassi, W. A.; Alexander, R.; Höss, M.; Hewings, D. S.; Rooney, T. P. C.; Paton, R. S.; Conway, S. J. Small Molecule Inhibitors of Bromodomain-Acetyl-Lysine Interactions. *ACS Chem. Biol.* **2015**, *10* (1), 22–39.
(188) Theodoulou, N. H.; Tomkinson, N. C. O.; Prinjha, R. K.; Humphreys, P. G. Progress in the Development of Non-BET Bromodomain Chemical Probes. *Chem. Med. Chem.* **2016**, *11* (5), 477–487.
(189) Garcia, P. L.; Miller, A. L.; Kreitzburg, K. M.; Council, L. N.; Gamblin, T. L.; Christein, J. D.; Heslin, M. J.; Arnoletti, J. P.; Richardson, J. H.; Chen, D.; Hanna, C. A.; Cramer, S. L.; Yang, E. S.; Qi, J.; Bradner, J. E.; Yoon, K. J. The BET Bromodomain Inhibitor JQ1 Suppresses Growth of Pancreatic Ductal Adenocarcinoma in Patient-Derived Xenograft Models. *Oncogene* **2016**, *35* (7), 833–845.
(190) Roe, J.-S.; Mercan, F.; Rivera, K.; Pappin, D. J.; Vakoc, C. R. BET Bromodomain Inhibition Suppresses the Function of Hematopoietic Transcription Factors in Acute Myeloid Leukemia. *Mol. Cell* **2015**, *58* (6), 1028–1039.
(191) Shu, S.; Lin, C. Y.; He, H. H.; Witwicki, R. M.; Tabassum, D. P.; Roberts, J. M.; Janiszewska, M.; Huh, S. J.; Liang, Y.; Ryan, J.; Doherty, E.; Mohammed, H.; Guo, H.; Stover, D. G.; Ekram, M. B.; Peluffo, G.; Brown, J.; D'Santos, C.; Krop, I. E.; Dillon, D.; McKeown, M.; Ott, C.; Qi, J.; Ni, M.; Rao, P. K.; Duarte, M.; Wu, S.-Y.; Chiang, C.-M.; Anders, L.; Young, R. A.; Winer, E. P.; Letai, A.; Barry, W. T.; Carroll, J. S.; Long, H. W.; Brown, M.; Liu, X. S.; Meyer, C. A.; Bradner, J. E.; Polyak, K. Response and Resistance to BET Bromodomain Inhibitors in Triple-Negative Breast Cancer. *Nature* **2016**, *529* (7586), 413–417.
(192) Azad, N.; Zahnow, C. A.; Rudin, C. M.; Baylin, S. B. The Future of Epigenetic Therapy in Solid Tumours--Lessons From the Past. *Nat. Rev. Clin. Oncol.* **2013**, *10* (5), 256–266.
(193) Stathis, A.; Zucca, E.; Bekradda, M.; Gomez-Roca, C.; Delord, J.-P.; La Motte Rouge, de, T.; Uro-Coste, E.; de Braud, F.; Pelosi, G.; French, C. A. Clinical Response of Carcinomas Harboring the BRD4-NUT Oncoprotein to the Targeted Bromodomain Inhibitor OTX015/MK-8628. *Cancer Discovery* **2016**, *6* (5), 492–500.
(194) Treppendahl, M. B.; Kristensen, L. S.; Grønbæk, K. Predicting Response to Epigenetic Therapy. *J. Clin. Invest.* **2014**, *124* (1), 47–55.

(195) Theodoulou, N. H.; Tomkinson, N. C.; Prinjha, R. K.; Humphreys, P. G. Clinical Progress and Pharmacology of Small Molecule Bromodomain Inhibitors. *Curr. Opin. Chem. Biol.* **2016**, *33*, 58–66.
(196) Henssen, A.; Althoff, K.; Odersky, A.; Beckers, A.; Koche, R.; Speleman, F.; Schäfers, S.; Bell, E.; Nortmeyer, M.; Westermann, F.; Preter, K. D.; Florin, A.; Heukamp, L.; Spruessel, A.; Astrahanseff, K.; Lindner, S.; Sadowski, N.; Schramm, A.; Astorgues-Xerri, L.; Riveiro, M. E.; Eggert, A.; Cvitkovic, E.; Schulte, J. H. Targeting MYCN-Driven Transcription by BET-Bromodomain Inhibition. *Clin. Cancer Res.* **2015**, *22* (10), 2470–2481.
(197) Lovén, J.; Hoke, H. A.; Lin, C. Y.; Lau, A.; Orlando, D. A.; Vakoc, C. R.; Bradner, J. E.; Lee, T. I.; Young, R. A. Selective Inhibition ofTumor Oncogenes by Disruption of Super-Enhancers. *Cell* **2013**, *153* (2), 320–334.
(198) Hewings, D. S.; Fedorov, O.; Filippakopoulos, P.; Martin, S.; Picaud, S.; Tumber, A.; Wells, C.; Olcina, M. M.; Freeman, K.; Gill, A.; Ritchie, A. J.; Sheppard, D. W.; Russell, A. J.; Hammond, E. M.; Knapp, S.; Brennan, P. E.; Conway, S. J. Optimization of 3,5-Dimethylisoxazole Derivatives as Potent Bromodomain Ligands. *J. Med. Chem.* **2013**, *56* (8), 3217–3227.
(199) Hewings, D. S.; Wang, M.; Philpott, M.; Fedorov, O.; Uttarkar, S.; Filippakopoulos, P.; Picaud, S.; Vuppusetty, C.; Marsden, B.; Knapp, S.; Conway, S. J.; Heightman, T. D. 3,5-Dimethylisoxazoles Act as Acetyl-Lysine-Mimetic Bromodomain Ligands. *J. Med.Chem.* **2011**, *54* (19), 6761–6770.
(200) Shigenaga, A.; Ogura, K.; Hirakawa, H.; Yamamoto, J.; Ebisuno, K.; Miyamoto, L.; Ishizawa, K.; Tsuchiya, K.; Otaka, A. Development of a Reduction-Responsive Amino Acid That Induces Peptide Bond Cleavage in Hypoxic Cells. *Chem. Bio. Chem.* **2012**, *13* (7), 968–971.
(201) Riley, R. J.; McGinnity, D. F.; Austin, R. P. A Unified Model for Predicting Human Hepatic, Metabolic Clearance From in Vitro Intrinsic Clearance Data in Hepatocytes and Microsomes. *Drug Metab. Dispos.* **2005**, *33* (9), 1304–1311.
(202) McGinnity, D. F.; Soars, M. G.; Urbanowicz, R. A.; Riley, R. J. Evaluation of Fresh and Cryopreserved Hepatocytes as in Vitro Drug Metabolism Tools for the Prediction of Metabolic Clearance. *Drug Metab. Dispos.* **2004**, *32* (11), 1247–1253.
(203) Obach, R. S. Prediction of Human Clearance of Twenty-Nine Drugs From Hepatic Microsomal Intrinsic Clearance Data: an Examination of in Vitro Half-Life Approach and Nonspecific Binding to Microsomes. *Drug Metab. Dispos.* **1999**, *27* (11), 1350–1359.
(204) Jennings, L. E. Development of Ligands to Target Bromodomain-Histone Interactions, University of Oxford, 2015, pp 1–397.
(205) Federov, O. *With Thanks to Dr Oleg Federov for Performing the AlphaScreen Assay.*; Structural Genomics Consortium, Oxford.
(206) Huang, W.; Hicks, S. N.; Sondek, J.; Zhang, Q. A Fluorogenic, Small Molecule Reporter for Mammalian Phospholipase C Isozymes. *ACS Chem. Biol.* **2011**, *6* (3), 223–228.
(207) Su, J.; Gu, Y.; Pruijn, F. B.; Smaill, J. B.; Patterson, A. V.; Guise, C. P.; Wilson, W. R. Zinc Finger Nuclease Knock-Out of

NADPH:Cytochrome P450 Oxidoreductase (POR) in Human Tumor Cell Lines Demonstrates That Hypoxia-Activated Prodrugs Differ in POR Dependence. *J. Biol. Chem.* **2013**, *288* (52), 37138–37153.

(208) O'Connor, L. J.; Conway, S. J.; Hammond, E. M. Fluorogenic Protecting Group. US Patent Office May 21, 2015.

(209) Boonstra, M. C.; Tolner, B.; Schaafsma, B. E.; Boogerd, L. S. F.; Prevoo, H. A. J. M.; Bhavsar, G.; Kuppen, P. J. K.; Sier, C. F. M.; Bonsing, B. A.; Frangioni, J. V.; van de Velde, C. J. H.; Chester, K. A.; Vahrmeijer, A. L. Preclinical Evaluation of a Novel CEA-Targeting Near-Infrared Fluorescent Tracer Delineating Colorectal and Pancreatic Tumors. *Int. J. Cancer* **2015**, *137* (8), 1910–1920.

(210) DeLong, J. C.; Chakedis, J. M.; Hosseini, A.; Kelly, K. J.; Horgan, S.; Bouvet, M. Indocyanine Green (ICG) Fluorescence-Guided Laparoscopic Adrenalectomy. *J. Surg. Oncol.* **2015**, *112* (6), 650–653.

(211) Cocco, E.; Shapiro, E. M.; Gasparrini, S.; Lopez, S.; Schwab, C. L.; Bellone, S.; Bortolomai, I.; Sumi, N. J.; Bonazzoli, E.; Nicoletti, R.; Deng, Y.; Saltzman, W. M.; Zeiss, C. J.; Centritto, F.; Black, J. D.; Silasi, D.-A.; Ratner, E.; Azodi, M.; Rutherford, T. J.; Schwartz, P. E.; Pecorelli, S.; Santin, A. D. Clostridium Perfringens Enterotoxin C-Terminal Domain Labeled to Fluorescent Dyes for in Vivo Visualization of Micrometastatic Chemotherapy-Resistant Ovarian Cancer. *Int. J. Cancer* **2015**, *137* (11), 2618–2629.

(212) Sun, W.; Fan, J.; Hu, C.; Cao, J.; Zhang, H.; Xiong, X.; Wang, J.; Cui, S.; Sun, S.; Peng, X. A Two-Photon Fluorescent Probe with Near-Infrared Emission for Hydrogen Sulfide Imaging in Biosystems. *Chem. Commun.* **2013**, *49* (37), 3890.

(213) Katona, G.; Szalay, G.; Maák, P.; Kaszás, A.; Veress, M.; Hillier, D.; Chiovini, B.; Vizi, E. S.; Roska, B.; Rózsa, B. Fast Two-Photon in Vivo Imaging with Three-Dimensional Random-Access Scanning in Large Tissue Volumes. *Nat. Methods* **2012**, *9* (2), 201–208.

(214) Colucci, M. A.; Moody, C. J.; Couch, G. D. Natural and Synthetic Quinones and Their Reduction by the Quinone Reductase Enzyme NQO1: From Synthetic Organic Chemistry to Compounds with Anticancer Potential. *Org. Biomol. Chem.* **2008**, *6* (4), 637–656.

(215) Blaser, D.; Calmes, M.; Daunis, J.; Natt, F. Improvement of the Vilsmeier-Haack Reaction. *Org. Prep. Proc. Int.* **1993**, *25* (3), 338–341.

(216) Li, M.; Wu, X.; Wang, Y.; Li, Y.; Zhu, W.; James, T. D. A Near-Infrared Colorimetric Fluorescent Chemodosimeter for the Detection of Glutathione in Living Cells. *Chem. Commun.* **2014**, *50* (14), 1751–1753.

(217) Hansch, C.; Leo, A.; Taft, R. W. A Survey of Hammett Substituent Constants and Resonance and Field Parameters. *Chem. Rev.* **1991**, *91*, 165–195.

(218) Fors, B. P.; Dooleweerdt, K.; Zeng, Q.; Buchwald, S. L. An Efficient System for the Pd-Catalyzed Cross-Coupling of Amides and Aryl Chlorides. *Tetrahedron* **2009**, *65* (33), 6576–6583.

(219) Olah, G. A.; Fung, A. P.; Rawdah, T. N. Preparation and Carbon-13 Nuclear Magnetic Resonance Structural Study of Protonated,

Methylated, and SbF5- or BF3-Complexed Nitroalkanes and Nitroarenes. *J. Org. Chem.* **1980**, *45*, 4149–4153.
(220) Cecchi, L.; Melani, F.; De Sio, F. Carbon-13 NMR Study of 1-Methyl-3-Phenyl-4-Diazo-5-Benzoylamidopyrazole and Other Model Pyrazole Compounds. *J. Het. Chem.* **1985**, *22* (4), 951–952.
(221) Lovering, F.; Bikker, J.; Humblet, C. Escape From Flatland: Increasing Saturation as an Approach to Improving Clinical Success. *J. Med. Chem.* **2009**, *52* (21), 6752–6756.
(222) Ishikawa, M.; Hashimoto, Y. Improvement in Aqueous Solubility in Small Molecule Drug Discovery Programs by Disruption of Molecular Planarity and Symmetry. *J. Med. Chem.* **2011**, *54* (6), 1539–1554.
(223) Bräse, S.; Gil, C.; Knepper, K.; Zimmermann, V. Organic Azides: an Exploding Diversity of a Unique Class of Compounds. *Angew. Chem. Int. Ed.* **2005**, *44* (33), 5188–5240.
(224) Poloukhtine, A. A.; Mbua, N. E.; Wolfert, M. A.; Boons, G.-J.; Popik, V. V. Selective Labeling of Living Cells by a Photo-Triggered Click Reaction. *J. Am. Chem. Soc.* **2009**, *131* (43), 15769–15776.
(225) Prescher, J. A.; Bertozzi, C. R. Chemistry in Living Systems. *Nat. Chem. Biol.* **2005**, *1* (1), 13–21.
(226) Cretton, E. M.; Xie, M. Y.; Goudgaon, N. M.; Schinazi, R. F.; Chu, C. K.; Sommadossi, J. P. Catabolic Disposition of 3'-Azido-2',3'-Dideoxyuridine in Hepatocytes with Evidence of Azido Reduction Being a General Catabolic Pathway of 3'-Azido-2“,3-”Dideoxynucleosides. *Biochem. Pharmacol.* **1992**, *44* (5), 973–980.
(227) Staros, J. V.; Bayley, H.; Standring, D. N.; Knowles, J. R. Reduction of Aryl Azides by Thiols: Implications for the Use of Photoaffinity Reagents. *Biochem. Biophys. Res. Comm.* **1978**, *80* (3), 568–572.
(228) Griffin, R. J. The Medicinal Chemistry of the Azido Group. *Prog. Med. Chem.* **1994**, *31*, 121–232.
(229) Jewett, J. C.; Bertozzi, C. R. Cu-Free Click Cycloaddition Reactions in Chemical Biology. *Chem. Soc. Rev.* **2010**, *39* (4), 1272–1279.
(230) Nikić, I.; Kang, J. H.; Girona, G. E.; Aramburu, I. V.; Lemke, E. A. Labeling Proteins on Live Mammalian Cells Using Click Chemistry. *Nat. Protoc.* **2015**, *10* (5), 780–791.
(231) Shieh, P.; Dien, V. T.; Beahm, B. J.; Castellano, J. M.; Wyss-Coray, T.; Bertozzi, C. R. CalFluors: a Universal Motif for Fluorogenic Azide Probes Across the Visible Spectrum. *J. Am. Chem. Soc.* **2015**, *137* (22), 7145–7151.
(232) El-Sagheer, A. H.; Sanzone, A. P.; Gao, R.; Tavassoli, A.; Brown, T. Biocompatible Artificial DNA Linker That Is Read Through by DNA Polymerases and Is Functional in Escherichia Coli. *PNAS USA* **2011**, *108* (28), 11338–11343.
(233) Birts, C. N.; Sanzone, A. P.; El-Sagheer, A. H.; Blaydes, J. P.; Brown, T.; Tavassoli, A. Transcription of Click-Linked DNA in Human Cells. *Angew. Chem. Int. Ed.* **2014**, *53* (9), 2362–2365.
(234) Koo, H.; Lee, S.; Na, J. H.; Kim, S. H.; Hahn, S. K.; Choi, K.; Kwon, I. C.; Jeong, S. Y.; Kim, K. Bioorthogonal Copper-Free Click Chemistry in Vivo for Tumor-Targeted Delivery of Nanoparticles. *Angew. Chem. Int. Ed.* **2012**, *51* (47), 11836–11840.

(235) Henthorn, H. A.; Pluth, M. D. Mechanistic Insights Into the H 2S-Mediated Reduction of Aryl Azides Commonly Used in H 2S Detection. *J. Am. Chem. Soc.* **2015**, *137* (48), 15330–15336.
(236) Lin, V. S.; Chen, W.; Xian, M.; Chang, C. J. Chem Soc Rev. *Chem. Soc. Rev.* **2015**, *44*, 4596–4618.
(237) Lippert, A. R.; New, E. J.; Chang, C. J. Reaction-Based Fluorescent Probes for Selective Imaging of Hydrogen Sulfide in Living Cells. *J. Am. Chem. Soc.* **2011**, *133* (26), 10078–10080.
(238) Nicholls, D.; Gescher, A.; Griffin, R. J. Medicinal Azides. Part 8. the in Vitro Metabolism of P-Substituted Phenyl Azides. *Xenobiotica* **1991**, *21* (7), 935–943.
(239) Pan-Zhou, X. R.; Cretton-Scott, E.; Zhou, X. J.; Yang, M. X.; Lasker, J. M.; Sommadossi, J. P. Role of Human Liver P450s and Cytochrome B5 in the Reductive Metabolism of 3'-Azido-3'-Deoxythymidine (AZT) to 3“-Amino-3-”Deoxythymidine. *Biochem. Pharmacol.* **1998**, *55* (6), 757–766.
(240) Shaik, A. N.; Bohnert, T.; Williams, D. A.; Gan, L. L.; LeDuc, B. W. Mechanism of Drug-Drug Interactions Between Warfarin and Statins. *J. Pharm. Sci.* **2016**, *105* (6), 1976–1986.
(241) Mao, J.; Tay, S.; Khojasteh, C. S.; Chen, Y.; Hop, C. E. C. A.; Kenny, J. R. Evaluation of Time Dependent Inhibition Assays for Marketed Oncology Drugs: Comparison of Human Hepatocytes and Liver Microsomes in the Presence and Absence of Human Plasma. *Pharm. Res.* **2016**, *33* (5), 1204–1219.
(242) Beaufay, H. Analytical Study of Microsomes and Subcellular Membranes From Rat Liver: III. *J. Cell Biol.* **1974**, *61* (1), 213–231.
(243) Ogu, C. C.; Maxa, J. L. Drug Interactions Due to Cytochrome P450. *Proc. (Bayl Univ Med Cent)* **2000**, *13* (4), 421–423.
(244) Liu, X.; Hu, L.; Ge, G.; Yang, B.; Ning, J.; Sun, S.; Yang, L. Quantitative Analysis of Cytochrome P450 Isoforms in Human Liver Microsomes by the Combination of Proteomics and Chemical Probe-Based Assay. *Proteomics* **2014**, *14*, 1943–1951.
(245) Kamali, F.; Gescher, A.; Slack, J. A. Medicinal Azides. Part 3. the Metabolism of the Investigational Antitumour Agent Meta-Azidopyrimethamine in Mouse Tissue in Vitro. *Xenobiotica* **1988**, *18* (10), 1157–1164.
(246) Kotra, L. P.; Manouilov, K. K.; Cretton-Scott, E.; Sommadossi, J. P.; Boudinot, F. D.; Schinazi, R. F.; Chu, C. K. Synthesis, Biotransformation, and Pharmacokinetic Studies of 9-(Beta-D-Arabinofuranosyl)-6-Azidopurine: a Prodrug for Ara-a Designed to Utilize the Azide Reduction Pathway. *J. Med. Chem.* **1996**, *39* (26), 5202–5207.
(247) Mowry, D. T. The Knoevenagel Condensation of Aryl Alkyl Ketones with Malononitrile. *J. Am. Chem. Soc.* **1945**, *67* (7), 1050–1051.
(248) Wardman, P.; Priyadarsini, K. I.; Dennis, M. F.; Everett, S. A.; Naylor, M. A.; Patel, K. B.; Stratford, I. J.; Stratford, M. R.; Tracy, M. Chemical Properties Which Control Selectivity and Efficacy of Aromatic N-Oxide Bioreductive Drugs. *Br. J. Cancer Suppl.* **1996**, *27*, S70–S74.
(249) Reagan, M. T.; Nickon, A. The Photolysis of Sulfonyl Azides in

Isopropyl Alcohol. *J. Am. Chem. Soc.* **1968**, *90* (15), 4096–4105.
(250) Tanabe, K.; Ishizaki, J.; Ando, Y.; Ito, T.; Nishimoto, S.-I. Bioorganic & Medicinal Chemistry Letters. *Bioorg. Med. Chem. Lett.* **2012**, *22* (4), 1682–1685.
(251) Bancirova, M. Sodium Azide as a Specific Quencher of Singlet Oxygen During Chemiluminescent Detection by Luminol and Cypridina Luciferin Analogues. *Luminescence* **2011**, *26* (6), 685–688.
(252) Benati, L.; Bencivenni, G.; Leardini, R.; Minozzi, M.; Nanni, D.; Scialpi, R.; Spagnolo, P.; Zanardi, G. Radical Reduction of Aromatic Azides to Amines with Triethylsilane. *J. Org. Chem.* **2006**, *71* (15), 5822–5825.
(253) Grime, K. H.; Barton, P.; McGinnity, D. F. Application of in Silico, in Vitro and Preclinical Pharmacokinetic Data for the Effective and Efficient Prediction of Human Pharmacokinetics. *Mol. Pharm.* **2013**, *10* (4), 1191–1206.
(254) Chan, T. S.; Yu, H.; Moore, A.; Khetani, S. R.; Kehtani, S. R.; Tweedie, D. Meeting the Challenge of Predicting Hepatic Clearance of Compounds Slowly Metabolized by Cytochrome P450 Using a Novel Hepatocyte Model, HepatoPac. *Drug Metab. Dispos.* **2013**, *41* (12), 2024–2032.
(255) Tucker, G. T.; Houston, J. B.; Huang, S. M. Optimizing Drug Development: Strategies to Assess Drug Metabolism/Transporter Interaction Potential-Toward a Consensus. *Br. J. Clin. Pharmacol.* **2001**; *52* (1), pp 107–117.
(256) Cenacchi, V.; Battaglia, R.; Cinato, F.; Riccardi, B.; Spinabelli, D.; Brogin, G.; Puccini, P.; Pezzetta, D. In Vitroand in Vivometabolism of CHF 6001, a Selective Phosphodiesterase (PDE4) Inhibitor. *Xenobiotica* **2015**, *45* (8), 693–710.
(257) Renwick, A. B.; Surry, D.; Price, R. J.; Lake, B. G.; Evans, D. C. Metabolism of 7-Benzyloxy-4-Trifluoromethylcoumarin by Human Hepatic Cytochrome P450 Isoforms. *Xenobiotica* **2008**, *30* (10), 955–969.
(258) Wang, B.; Yang, L.-P.; Zhang, X.-Z.; Huang, S.-Q.; Bartlam, M.; Zhou, S.-F. New Insights Into the Structural Characteristics and Functional Relevance of the Human Cytochrome P450 2D6 Enzyme. *Drug Metab. Rev.* **2009**, *41* (4), 573–643.
(259) Thorson, M. K.; Majtan, T.; Kraus, J. P.; Barrios, A. M. Identification of Cystathionine B-Synthase Inhibitors Using a Hydrogen Sulfide Selective Probe. *Angew. Chem. Int. Ed.* **2013**, *52* (17), 4641–4644.
(260) Singh, R.; Kolev, J. N.; Sutera, P. A.; Fasan, R. Enzymatic C(Sp 3)-H Amination: P450-Catalyzed Conversion of Carbonazidates Into Oxazolidinones. *ACS Catal.* **2015**, *5* (3), 1685–1691.
(261) Giovani, S.; Singh, R.; Fasan, R. Chemical Science. *Chem. Sci.* **2015**, *7*, 234–239.
(262) Eagling, V. A.; Howe, J. L.; Barry, M. J.; Back, D. J. The Metabolism of Zidovudine by Human Liver Microsomes in Vitro: Formation of 3“-Amino-3-”Deoxythymidine. *Biochemical Pharmacology* **1994**, *48* (2), 267–276.
(263) Caughey, W. S. Carbon Monoxide Bonding in Hemeproteins; *Annals. New York Acad. Sci.* **1970**; 148–153.

(264) McIntosh, J. A.; Coelho, P. S.; Farwell, C. C.; Wang, Z. J.; Lewis, J. C.; Brown, T. R.; Arnold, F. H. Enantioselective Intramolecular C-H Amination Catalyzed by Engineered Cytochrome P450 Enzymes in Vitro and in Vivo. *Angew. Chem. Int. Ed.* **2013**, *52* (35), 9309–9312.
(265) Hyster, T. K.; Farwell, C. C.; Buller, A. R.; McIntosh, J. A.; Arnold, F. H. Enzyme-Controlled Nitrogen-Atom Transfer Enables Regiodivergent C–H Amination. *J. Am. Chem. Soc.* **2014**, *136*, 15505–15508.
(266) Farwell, C. C.; Zhang, R. K.; McIntosh, J. A.; Hyster, T. K.; Arnold, F. H. Enantioselective Enzyme-Catalyzed Aziridination Enabled by Active-Site Evolution of a Cytochrome P450. *ACS Cent. Sci.* **2015**, *1* (2), 89–93.
(267) Prier, C. K.; Hyster, T. K.; Farwell, C. C.; Huang, A.; Arnold, F. H. Asymmetric Enzymatic Synthesis of Allylic Amines: a Sigmatropic Rearrangement Strategy. *Angew. Chem. Int. Ed.* **2016**, *128* (15), 4789–4793.
(268) Singh, R.; Bordeaux, M.; Fasan, R. P450-Catalyzed Intramolecular Sp 3C–H Amination with Arylsulfonyl Azide Substrates. *ACS Catal.* **2014**, *4* (2), 546–552.
(269) Meunier, B.; De Visser, S. P.; Shaik, S. Mechanism of Oxidation Reactions Catalyzed by Cytochrome P450 Enzymes. *Chem. Rev.* **2004**, *104*, 3947–3980.
(270) Westerink, W. M. A.; Schoonen, W. G. E. J. Cytochrome P450 Enzyme Levels in HepG2 Cells and Cryopreserved Primary Human Hepatocytes and Their Induction in HepG2 Cells. *Toxicol. In Vitro* **2007**, *21* (8), 1581–1591.
(271) Yasui, H.; Matsumoto, S.; Devasahayam, N.; Munasinghe, J. P.; Choudhuri, R.; Saito, K.; Subramanian, S.; Mitchell, J. B.; Krishna, M. C. Low-Field Magnetic Resonance Imaging to Visualize Chronic and Cycling Hypoxia in Tumor-Bearing Mice. *Cancer Res.* **2010**, *70* (16), 6427–6436.
(272) Leung, B. O.; Chou, K. C. Review of Super-Resolution Fluorescence Microscopy for Biology. *Appl. Spect.* **2011**, *65* (9), 967–980.
(273) Fernández-Suárez, M.; Ting, A. Y. Fluorescent Probes for Super-Resolution Imaging in Living Cells. *Nat. Rev. Mol. Cell Biol.* **2008**, *9* (12), 929–943.
(274) Friedrich, J.; Seidel, C.; Ebner, R.; Kunz-Schughart, L. A. Spheroid-Based Drug Screen: Considerations and Practical Approach. *Nat. Protoc.* **2009**, *4* (3), 309–324.
(275) Olson, K. R. A Theoretical Examination of Hydrogen Sulfide Metabolism and Its Potential in Autocrine/Paracrine Oxygen Sensing. *Resp. Phys. Neurobiol.* **2013**, *186* (2), 173–179.
(276) Olson, K. R. Hydrogen Sulfide as an Oxygen Sensor. *Antiox. Redox Signaling* **2015**, *22* (5), 377–397.
(277) Szabo, C.; Coletta, C.; Chao, C.; Módis, K.; Szczesny, B.; Papapetropoulos, A.; Hellmich, M. R. Tumor-Derived Hydrogen Sulfide, Produced by Cystathionine-B-Synthase, Stimulates Bioenergetics, Cell Proliferation, and Angiogenesis in Colon Cancer. *PNAS USA* **2013**, *110* (30), 12474–12479.
(278) Sonke, E.; Verrydt, M.; Postenka, C. O.; Pardhan, S.; Willie, C. J.;

Mazzola, C. R.; Hammers, M. D.; Pluth, M. D.; Lobb, I.; Power, N. E.; Chambers, A. F.; Leong, H. S.; Sener, A. Nitric Oxide. *Nitric Oxide* **2015**, *49* (C), 26–39.

(279) Hellmich, M. R.; Coletta, C.; Chao, C.; Szabo, C. The Therapeutic Potential of Cystathionine B-Synthetase/Hydrogen Sulfide Inhibition in Cancer. *Antiox. Redox Signaling* **2015**, *22* (5), 424–448.

(280) ZHANG, J.; XIE, Y.; XU, Y.; PAN, Y.; SHAO, C. Hydrogen Sulfide Contributes to Hypoxia-Induced Radioresistance on Hepatoma Cells. *J. Rad. Res.* **2011**, *52* (5), 622–628.

(281) Bae, S. K.; Heo, C. H.; Choi, D. J.; Sen, D.; Joe, E.-H.; Cho, B. R.; Kim, H. M. A Ratiometric Two-Photon Fluorescent Probe Reveals Reduction in Mitochondrial H 2S Production in Parkinson's Disease Gene Knockout Astrocytes. *J. Am. Chem. Soc.* **2013**, *135* (26), 9915–9923.

(282) Bhattacharyya, S.; Saha, S.; Giri, K.; Lanza, I. R.; Nair, K. S.; Jennings, N. B.; Rodriguez-Aguayo, C.; Lopez-Berestein, G.; Basal, E.; Weaver, A. L.; Visscher, D. W.; Cliby, W.; Sood, A. K.; Bhattacharya, R.; Mukherjee, P. Cystathionine Beta-Synthase (CBS) Contributes to Advanced Ovarian Cancer Progression and Drug Resistance. *PLoS ONE* **2013**, *8* (11), e79167.

(283) Takano, N.; Peng, Y.-J.; Kumar, G. K.; Luo, W.; Hu, H.; Shimoda, L. A.; Suematsu, M.; Prabhakar, N. R.; Semenza, G. L. Hypoxia-Inducible Factors Regulate Human and Rat Cystathionine B-Synthase Gene Expression. *Biochem. J.* **2014**, *458* (2), 203–211.

(284) Asimakopoulou, A.; Panopoulos, P.; Chasapis, C. T.; Coletta, C.; Zhou, Z.; Cirino, G.; Giannis, A.; Szabo, C.; Spyroulias, G. A.; Papapetropoulos, A. Selectivity of Commonly Used Pharmacological Inhibitors for Cystathionine B Synthase (CBS) and Cystathionine Γ Lyase (CSE). *Br. J. Pharmacol.* **2013**, *169* (4), 922–932.

(285) Ning, N.; Zhu, J.; Du, Y.; Gao, X.; Liu, C.; Li, J. Dysregulation of Hydrogen Sulphide Metabolism Impairs Oviductal Transport of Embryos. *Nat. Commun.* **2014**, *5*, 4107.

(286) Tsai, C.-Y.; Peh, M. T.; Feng, W.; Dymock, B. W.; Moore, P. K. Hydrogen Sulfide Promotes Adipogenesis in 3T3L1 Cells. *PLoS ONE* **2015**, *10* (3), e0119511.

(287) Korangath, P.; Teo, W. W.; Sadik, H.; Han, L.; Mori, N.; Huijts, C. M.; Wildes, F.; Bharti, S.; Zhang, Z.; Santa-Maria, C. A.; Tsai, H.; Dang, C. V.; Stearns, V.; Bhujwalla, Z. M.; Sukumar, S. Targeting Glutamine Metabolism in Breast Cancer with Aminooxyacetate. *Clin. Cancer Res.* **2015**, *21* (14), 3263–3273.

(288) Pupo, E.; Pla, A. F.; Avanzato, D.; Moccia, F.; Cruz, J.-E. A.; Tanzi, F.; Merlino, A.; Mancardi, D.; Munaron, L. Hydrogen Sulfide Promotes Calcium Signals and Migration in Tumor-Derived Endothelial Cells. *Free Radic. Biol. Med.* **2011**, *51* (9), 1765–1773.

(289) PAN, Y.; Zhou, C.; Yuan, D.; ZHANG, J.; SHAO, C. Radiation Exposure Promotes Hepatocarcinoma Cell Invasion Through Epithelial Mesenchymal Transition Mediated by H 2S/CSE Pathway. *Rad. Res.* **2016**, *185* (1), 96–105.

(290) Chao, C.; Zatarain, J. R.; Ding, Y.; Coletta, C.; Mrazek, A. A.; Druzhyna, N.; Johnson, P.; Chen, H.; Hellmich, J. L.; Asimakopoulou,

A.; Yanagi, K.; Olah, G.; Szoleczky, P.; Törö, G.; Bohanon, F. J.; Cheema, M.; Lewis, R.; Eckelbarger, D.; Ahmad, A.; Módis, K.; Untereiner, A.; Szczesny, B.; Papapetropoulos, A.; Zhou, J.; Hellmich, M. R.; Szabo, C. Cystathionine-Beta-Synthase Inhibition for Colon Cancer: Enhancement of the Efficacy of Aminooxyacetic Acid via the Prodrug Approach. *Mol. Med.* **2016**, *22* (10.2119/molmed.2016.00102).

(291) Wallach, D. P. Studies on the GABA Pathway. I. the Inhibition of Gamma-Aminobutyric Acid-Alpha-Ketoglutaric Acid Transaminase in Vitro and in Vivo by U-7524 (Amino-Oxyacetic Acid). *Biochem. Pharmacol.* **1961**, *5*, 323–331.

(292) Whiteman, M.; Le Trionnaire, S.; Chopra, M.; Fox, B.; Whatmore, J. Emerging Role of Hydrogen Sulfide in Health and Disease: Critical Appraisal of Biomarkers and Pharmacological Tools. *Clin. Sci.* **2011**, *121* (11), 459–488.

(293) Solomon, M.; Liu, Y.; Berezin, M. Y.; Achilefu, S. Optical Imaging in Cancer Research: Basic Principles, Tumor Detection, and Therapeutic Monitoring. *Med. Princ. Pract.* **2011**, *20* (5), 397–415.

(294) Chen, H.; Lin, W.; Yuan, L. Construction of a Near-Infrared Fluorescence Turn-on and Ratiometric Probe for Imaging Palladium in Living Cells. *Org. Biomol. Chem.* **2013**, *11* (12), 1938–1941.

(295) Zhang, L.; Zheng, X. E.; Zou, F.; Shang, Y.; Meng, W.; Lai, E.; Xu, Z.; Liu, Y.; Zhao, J. A Highly Selective and Sensitive Near-Infrared Fluorescent Probe for Imaging of Hydrogen Sulphide in Living Cells and Mice. *Sci. Rep.* **2016**, *6* (18868), 1–10.

(296) Li, Z.; He, X.; Wang, Z.; Yang, R.; Shi, W.; Ma, H. *In Vivo* Imaging and Detection of Nitroreductase in Zebrafish by a New Near-Infrared Fluorescence on-Off Probe. *Biosens. Bioelectron.* **2015**, *63* (C), 112–116.

(297) Chen, H.; Dong, B.; Tang, Y.; Lin, W. Construction of a Near-Infrared Fluorescent Turn-on Probe for Selenol and Its Bioimaging Application in Living Animals. *Chemistry* **2015**, *21* (33), 11696–11700.

(298) Kong, F.; Liang, Z.; Luan, D.; Liu, X.; Xu, K.; Tang, B. A Glutathione (GSH)-Responsive Near-Infrared (NIR) Theranostic Prodrug for Cancer Therapy and Imaging. *Anal. Chem.* **2016**, *88* (12), 6450–6456.

(299) Smith, D. A. *Metabolism, Pharmacokinetics, and Toxicity of Functional Groups*; Royal Society of Chemistry, 2010.

(300) Xu, K.; Qiang, M.; Gao, W.; Su, R.; Li, N.; Gao, Y.; Xie, Y.; Kong, F.; Tang, B. A Near-Infrared Reversible Fluorescent Probe for Real-Time Imaging of Redox Status Changes in Vivo. *Chem. Sci.* **2013**, *4* (3), 1079–1086.

(301) Samanta, A.; Vendrell, M.; Das, R.; Chang, Y.-T. Development of Photostable Near-Infrared Cyanine Dyes. *Chem. Commun.* **2010**, *46* (39), 7406–7408.

(302) Xu, K.; Wang, F.; Pan, X.; Liu, R.; Ma, J.; Kong, F.; Tang, B. High Selectivity Imaging of Nitroreductase Using a Near-Infrared Fluorescence Probe in Hypoxic Tumor. *Chem. Commun.* **2013**, *49* (25), 2554.

(303) Xia, C.; Panda, S. P.; Marohnic, C. C.; Martásek, P.; Masters, B. S.; Kim, J.-J. P. Structural Basis for Human NADPH-Cytochrome P450 Oxidoreductase Deficiency. *PNAS USA* **2011**, *108* (33), 13486–13491.
(304) Murataliev, M. B.; Feyereisen, R.; Walker, F. A. Electron Transfer by Diflavin Reductases. *Biochim. Biophys. Acta* **2004**, *1698* (1), 1–26.
(305) Hewings, D. S.; Rooney, T. P. C.; Jennings, L. E.; Hay, D. A.; Schofield, C. J.; Brennan, P. E.; Knapp, S.; Conway, S. J. Progress in the Development and Application of Small Molecule Inhibitors of Bromodomain–Acetyl-Lysine Interactions. *J. Med. Chem.* **2012**, *55* (22), 9393–9413.
(306) Escobedo, J. O.; Rusin, O.; Lim, S.; Strongin, R. M. NIR Dyes for Bioimaging Applications. *Curr. Opin. Chem. Biol.* **2010**, *14*, 64–70.
(307) Alabugin, I. V.; Gilmore, K. Finding the Right Path: Baldwin "Rules for Ring Closure" and Stereoelectronic Control of Cyclizations. *Chem. Commun. (Camb.)* **2013**, *49* (96), 11246–11250.
(308) O'Connor, J. P. B.; Boult, J. K. R.; Jamin, Y.; Babur, M.; Finegan, K. G.; Williams, K. J.; Little, R. A.; Jackson, A.; Parker, G. J. M.; Reynolds, A. R.; Waterton, J. C.; Robinson, S. P. Oxygen-Enhanced MRI Accurately Identifies, Quantifies, and Maps Tumor Hypoxia in Preclinical Cancer Models. *Cancer Res.* **2016**, *76* (4), 787–795.
(309) Fulmer, G. R.; Miller, A. J. M.; Sherden, N. H.; Gottlieb, H. E.; Nudelman, A.; Stoltz, B. M.; Bercaw, J. E.; Goldberg, K. I. NMR Chemical Shifts of Trace Impurities: Common Laboratory Solvents, Organics, and Gases in Deuterated Solvents Relevant to the Organometallic Chemist. *Organometallics* **2010**, *29* (9), 2176–2179.
(310) Pirrung, M. C. *The Synthetic Organic Chemist's Companion; Appendix 3: Recipes for TLC Stains*; John Wiley & Sons, Inc., **2007**; pp 171–172.
(311) Pangborn, A. B.; Giardello, M. A.; Grubbs, R. H. Safe and Convenient Procedure for Solvent Purification. *Organometallics* **1996**, *15*, 1518–1520.
(312) Armarego, W.; Chai, C. *Purification of Laboratory Chemicals*, 7 ed.; Butterworth-Heinemann, 2012.
(313) Maimone, T. J.; Milner, P. J.; Kinzel, T.; Zhang, Y.; Takase, M. K.; Buchwald, S. L. Evidence for in Situ Catalyst Modification During the Pd-Catalyzed Conversion of Aryl Triflates to Aryl Fluorides. *J. Am. Chem. Soc.* **2011**, *133* (45), 18106–18109.
(314) Gordon, M.; Hamilton, H. J.; Adkins, C.; Hay, J.; Pearson, D. E. Synthesis of Some Halogenated Quinolines. *J. Het. Chem.* **1967**, *4* (3), 410–412.
(315) Shaw, A. Y.; Chang, C.-Y.; Liau, H.-H.; Lu, P.-J.; Chen, H.-L.; Yang, C.-N.; Li, H.-Y. European Journal of Medicinal Chemistry. *Eur. J. Med. Chem.* **2009**, *44* (6), 2552–2562.
(316) Zhao, J.; Zhao, Y.; Fu, H. Transition-Metal-Free Intramolecular Ullmann-Type O-Arylation: Synthesis of Chromone Derivatives. *Angew. Chem. Int. Ed.* **2011**, *50* (16), 3769–3773.
(317) Barros, A. I. R. N. A.; Silva, A. M. S. Synthesis and Structure Elucidation of Three Series of Nitro-2-Styrylchromones Using 1D and 2D NMR Spectroscopy. *Magn. Reson. Chem.* **2009**, *47* (10), 885–

896.
(318) Polaske, N. W.; Szalai, M. L.; Shanahan, C. S.; McGrath, D. V. Convergent Synthesis of Geometrically Disassembling Dendrimers Using Cu(I)-Catalyzed C−O Bond Formation. *Org. Lett.* **2010**, *12* (21), 4944–4947.
(319) Yuan, L.; Lin, W.; Song, J. Ratiometric Fluorescent Detection of Intracellular Hydroxyl Radicals Based on a Hybrid Coumarin-Cyanine Platform. *Chem. Commun.* **2010**, *46* (42), 7930–7932.
(320) Carlsson, J.; Yuhas, J. M. Liquid-Overlay Culture of Cellular Spheroids. In *Spheroids in Cancer research*; Recent Results in Cancer Research; Springer Berlin Heidelberg: Berlin, Heidelberg, 1984; Vol. 95, pp 1–23.

APPENDICES

A. List of publications and patents

1. CH-01 is a hypoxia-activated prodrug that sensitises cells to hypoxia through inhibition of Chk1 and Aurora A. C. Cazares-Körner, L J O'Connor *et al. ACS Chem. Biol.* **8(7)**, 1451–1459 (2013)…….**269**

2. Fluorogenic Protecting Group. L J O'Connor, S. J. Conway, E. M. Hammond. 2015, WO/2015/071665 A1 20150521……...**278**

3. Efficient synthesis of 2-nitroimidazole derivatives and the bioreductive clinical candidate Evofosfamide (TH 302); L. J O'Connor *et al. Org. Chem. Front.* **2**, 1026-1029 (2015)……...**280**

4. Design, Synthesis & Evaluation of molecularly targeted hypoxia-activated prodrugs; L J O'Connor *et al. Nature Protocols* **11**, 781–794 (2016)…….**284**

5. CYP450 Enzymes Effect Oxygen-dependent Reduction of an Azide-based Fluorogenic Dye. L J. O'Connor *et al.* (2016). (Manuscript in preparation)

B. Select ^{1}H, ^{13}C, and ^{19}F NMR Spectra

Selected ^{1}H and ^{13}C spectra are included for novel compounds of interest, and compounds tested in biological assays..…….....**298**

C. Single dose mean graph of Compound 2.48

Data showing mean growth development of various cancer cell lines treated with **2.48**……..……....**384**

ACS chemical biology

ACS AuthorChoice

Articles

pubs.acs.org/acschemicalbiology

Terms of Use

CH-01 is a Hypoxia-Activated Prodrug That Sensitizes Cells to Hypoxia/Reoxygenation Through Inhibition of Chk1 and Aurora A

Cindy Cazares-Körner,[†,‡,§] Isabel M. Pires,[†,§,⊥] I. Diane Swallow,[‡,§] Samuel C. Grayer,[‡] Liam J. O'Connor,[†,‡] Monica M. Olcina,[†] Martin Christlieb,[†] Stuart J. Conway,*[,‡] and Ester M. Hammond*[,†]

[†]Cancer Research U.K./MRC Gray Institute for Radiation Oncology and Biology, Department of Oncology, University of Oxford, Old Road Campus Research Building, Oxford OX3 7DQ, U.K.

[‡]Department of Chemistry, Chemistry Research Laboratory, University of Oxford, Mansfield Road, Oxford OX1 3TA, U.K.

Supporting Information

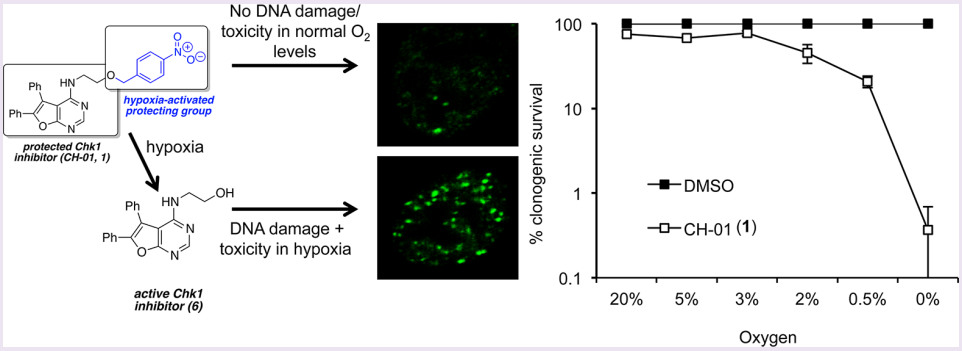

ABSTRACT: The increased resistance of hypoxic cells to all forms of cancer therapy presents a major barrier to the successful treatment of most solid tumors. Inhibition of the essential kinase Checkpoint kinase 1 (Chk1) has been described as a promising cancer therapy for tumors with high levels of hypoxia-induced replication stress. However, as inhibition of Chk1 affects normal replication and induces DNA damage, these agents also have the potential to induce genomic instability and contribute to tumorigenesis. To overcome this problem, we have developed a bioreductive prodrug, which functions as a Chk1/Aurora A inhibitor specifically in hypoxic conditions. To achieve this activity, a key functionality on the Chk1 inhibitor (CH-01) is masked by a bioreductive group, rendering the compound inactive as a Chk1/Aurora A inhibitor. Reduction of the bioreductive group nitro moiety, under hypoxic conditions, reveals an electron-donating substituent that leads to fragmentation of the molecule, affording the active inhibitor. Most importantly, we show a significant loss of viability in cancer cell lines exposed to hypoxia in the presence of CH-01. This novel approach targets the most aggressive and therapy-resistant tumor fraction while protecting normal tissue from therapy-induced genomic instability.

It is clear that the identification and exploitation of the differences between cancer and normal cells is essential for the design of effective therapeutics. The replicative stress response (RSR), which is characterized by Ataxia telangiectasia mutated rad3 related kinase-Checkpoint kinase 1 (ATR-Chk1) signaling, is elevated in numerous cancer cell types.[1] Targeting ATR/Chk1 has been proposed to sensitize cancer cells to DNA damage and to be particularly effective in those that have lost p53-mediated control of the G_1 checkpoint.[2] Recently, targeting the RSR through inhibition of the ATR-Chk1 pathway was proposed as an effective means of treating tumors with high levels of oncogene-mediated replication stress.[3,4] For example, tumors with elevated MYC levels have been shown to be sensitive to ATR/Chk1 inhibition.[3,5−8] Both ATR and Chk1 inhibitors have been developed, although ATR inhibition has yet to be evaluated in the clinic.[9−14] Clinical studies using Chk1 inhibitors in combination with standard DNA damaging chemotherapeutics have shown some success in combination with, for example, gemcitabine, irinotecan, and paclitaxel.[15,16] Recently, studies demonstrating that cancer cells with high levels of oncogene-mediated replication stress or inherent DNA damage show increased sensitivity to Chk1 inhibition have raised the possibility of using Chk1 inhibitors as single agents.[7] The enthusiasm for inhibiting kinases with roles in the cell cycle is somewhat tempered due to their roles in normal, unperturbed, replication.[17] It cannot be forgotten, for example, that Chk1 is an essential gene, the loss of which leads to embryonic lethality and which perhaps more significantly has been found to be altered in human cancers.[18] Indeed, a recent study demonstrated that while significant suppression of ATR

Received: September 3, 2012
Accepted: April 18, 2013
Published: April 18, 2013

ACS Publications © 2013 American Chemical Society

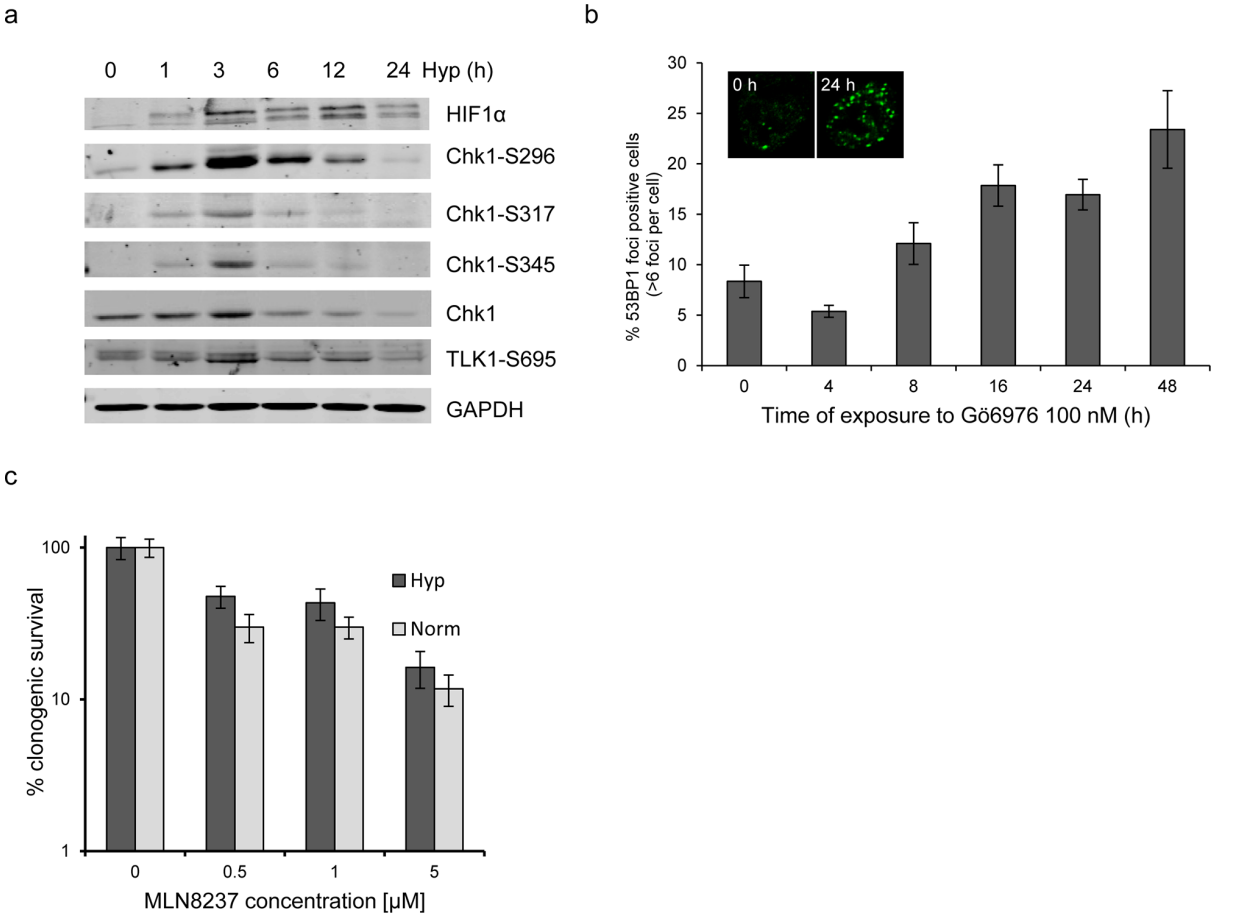

Figure 1. Targeting Chk1/Aurora A inhibition to hypoxic cells. (a) Chk1 is phosphorylated and active in hypoxic conditions. RKO cells were exposed to hypoxia (≤0.02% O_2) for the times indicated, and Western blotting was carried out. (b) Increasing exposure time to Gö6976 (100 nM) led to an accumulation of cells with >6 nuclear 53BP1 foci in WI38 cells. The inset shows an example of the 53BP1 foci observed. (c) RKO cells were treated with the Aurora A kinase inhibitor MLN8237 at the concentrations indicated in either normoxic or hypoxic (≤0.02% O_2) conditions for 16 h. A colony survival assay is shown.

activity led to loss of cell viability, ATR-haploinsufficiency promoted tumorigenesis.[4]

In addition to tolerating high levels of oncogene-mediated replication stress, tumors exist and thrive in conditions of low oxygen concentration (hypoxia). The degree of tumor hypoxia correlates well with resistance to therapy including radio/chemotherapy and surgery as well as an increased likelihood of metastasis.[19,20] In conditions of severe hypoxia (<0.1% O_2) a unique DNA damage response (DDR) occurs, which is characterized by both ATR and Ataxia telangiectasia mutated kinase (ATM) activity in the absence of detectable DNA damage.[21,22] In response to these conditions the levels of nucleotides rapidly fall, and this correlates with a complete replication arrest. The RSR initiated in severe hypoxia includes Chk1, and loss/inhibition of Chk1 has been demonstrated to sensitize cells to hypoxia/reoxygenation.[23]

An elegant approach to exploiting the low levels of oxygenation in tumors is through the use of agents that are activated by these conditions, commonly known as bioreductive prodrugs or hypoxic cytotoxins (recently reviewed in ref 24). These compounds contain functional groups that are susceptible to *in vivo* reduction under conditions of low oxygen concentration. Although there are five chemical moieties that have been demonstrated to undergo metabolism in hypoxia, the most common approach employs nitroaromatic derivatives, such as the 4-nitrobenzyl, 4-nitrofuryl, and 2-nitroimidazole groups.[24] The nitro group undergoes nitroreductase-mediated one electron reduction to a radical anion *in vivo*, which is rapidly oxidized by molecular oxygen under normoxic conditions, forming superoxide and rendering this pathway unproductive. Under hypoxic conditions, the radical anion is not reoxidized but undergoes further reduction to form a nitroso group, hydroxylamine, or an amine. While the nitro group has no available lone pair and is mesomerically and inductively electron-withdrawing, the nitroso group, the hydroxylamine, and the amine groups have an available lone pair and hence are mesomerically electron-donating. This reversal in reactivity has been harnessed to activate compounds selectively under hypoxic conditions. The majority of these compounds are based on increasing the electrophilicity of alkylating agents that then confer general toxicity in the hypoxic region. A number of these agents have been described, including tirapazamine (TPZ), AQ4N, PR-104A, CEN-209, RH-1, and TH-302.[25−28] TPZ has been tested in a number of clinical trials including a recent large randomized multicenter phase III trial combined with radiotherapy for head and neck cancers. This trial reported no benefit, although there were major deficiencies in the treatment of a subset of patients that

dx.doi.org/10.1021/cb4001537 | *ACS Chem. Biol.* 2013, 8, 1451−1459

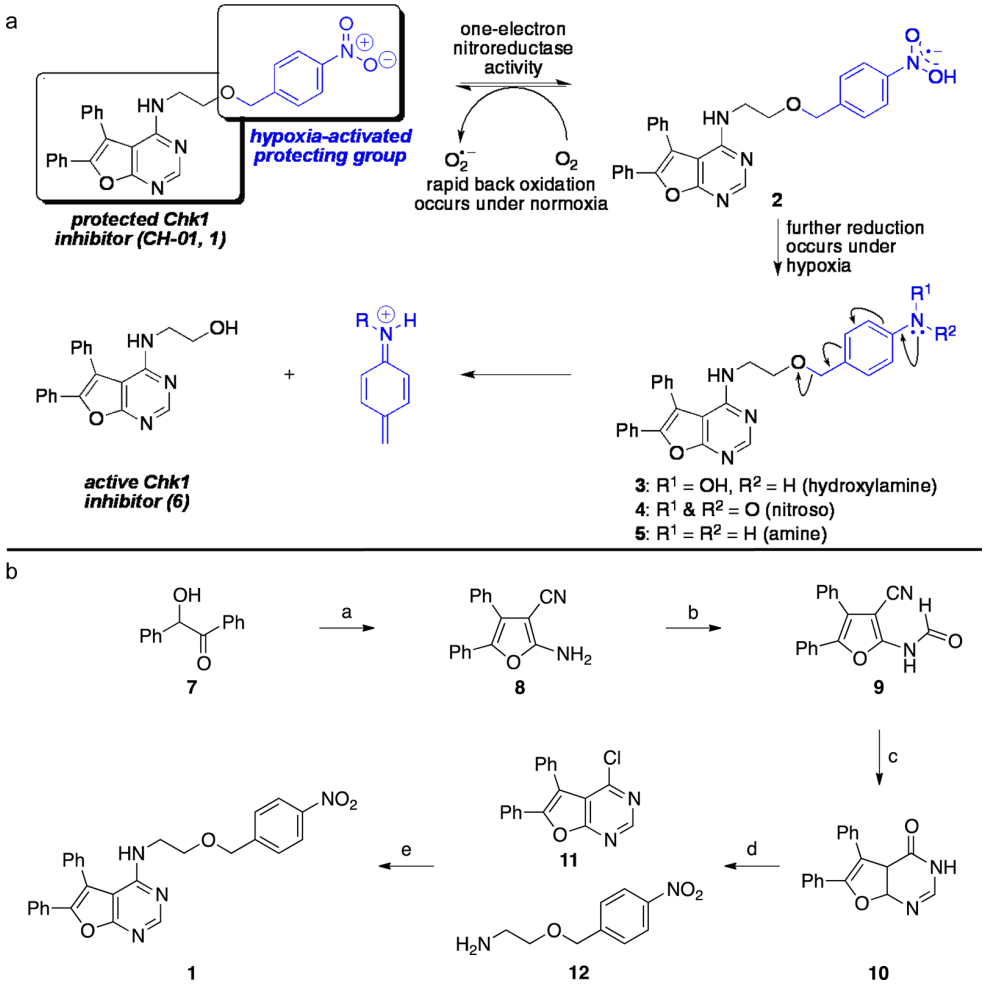

Figure 2. The concept of the hypoxia-activated Chk1 inhibitor CH-01 and its synthesis. (a) Attachment of the 4-nitrobenzyl group to the terminal hydroxyl group renders the Chk1 inhibitor **6** inactive. Under hypoxic conditions, the nitro group is reduced forming an electron-donating substituent, which ejects the active Chk1 inhibitor **6**. (b) Reagents and conditions: (a) malononitrile, Et_2NH, dioxane, reflux, 16 h, 75%; (b) acetic formic anhydride, 85 °C, 6 h; (c) neat, 220 °C, 30 min, 51% over two steps; (d) $POCl_3$, 55 °C, 2 h, 81%; (e) Et_3N, DMF, 80 °C, 6 h, 93%.

could be responsible for this.[29,30] Subsequently, analogues of TPZ have been described, one of which, CEN-209, is likely to be tested clinically in the near future.[31] More recently, TH-302 has undergone extensive preclinical testing and has been tested in a phase II trial for advanced pancreatic cancer and a phase III soft-tissue sarcoma trial.[32] Several factors are critical to the future success of bioreductive prodrugs, including the challenges of delivering such agents to hypoxic tumor cells and the need to identify biomarkers, which predict those tumors most likely to respond.

The majority of the bioreductive prodrugs described to date are designed to release a DNA damaging cytotoxin and therefore, once activated, act similarly to conventional chemotherapeutic agents. This approach raises the possibility of overlapping toxicities when these agents are combined with standard therapies. An alternative application of a hypoxia-activated group is to mask a drug, which acts as a protein ligand, to prevent binding to its target. This would render the compound inactive until the bioreductive group is removed under hypoxic conditions. Given that this strategy potentially allows targeting of promising cancer therapies to hypoxic tumors, it is surprising that it has not been more widely employed, although there are a few reports in the literature. Zhang et al. applied this strategy to the synthesis of three hypoxia-activated derivatives of 20(*S*)-camptothecin.[33] They demonstrated that a 4-nitrobenzyl derivative conferred some selectivity for hypoxic cells over normal cells. Granchi et al. described nitrobenzyl and nitrofuryl bioreductive prodrugs that release an inhibitor of the lysyl oxidase (LOX) protein in hypoxia.[34] In this instance the approach was beneficial as the released compound, BAPN, is a relatively nonselective LOX inhibitor with multiple biological interactions. Zhu et al. synthesized 4-nitrobenzyl derivatives of O^6-benzylguanine, which is an inhibitor of the resistance protein O^6-alkylguanine alkyltransferase (AGT).[35] It was demonstrated that the *gem*-dimethyl-4-nitrobenzyl analogue was effective in sensitizing laromustine-resistant DU145 human prostate carcinoma cells to laromustine under hypoxic conditions. Here, we describe CH-01, which is a proof-of-concept compound that we propose is activated as a Chk1 and Aurora kinase A inhibitor after the hypoxia-promoted loss of the 4-nitrobenzyl group. Clonogenic survival assays demonstrate that CH-01 (**1**) had little or no effect on cells in normal oxygen conditions; conversely, hypoxic cells were extremely sensitive to CH-01. Of the tumor cell lines

dx.doi.org/10.1021/cb4001537 | *ACS Chem. Biol.* 2013, 8, 1451−1459

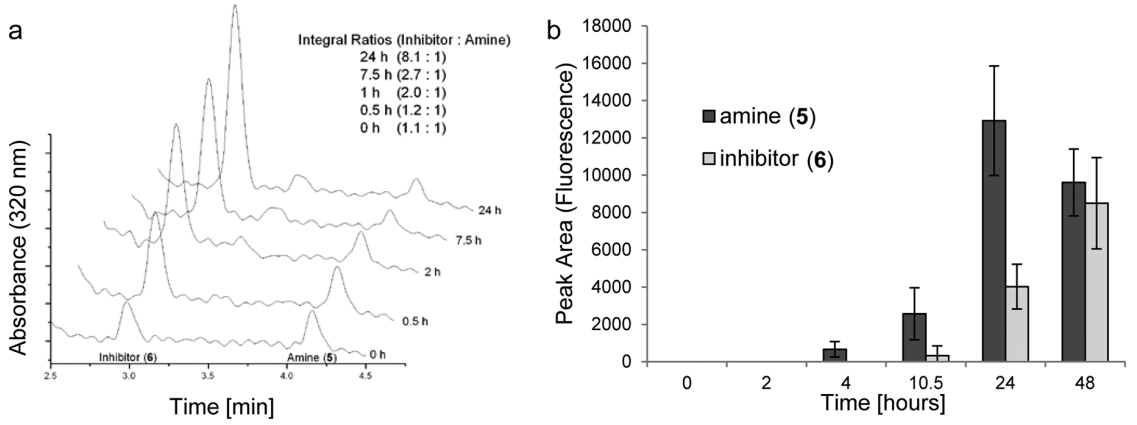

Figure 3. CH-01 is reduced and fragments in hypoxic conditions. CH-01 was subjected to different reduction conditions, and the resulting metabolites were analyzed by HPLC. A combination of photodiode array spectrophotometer, mass spectrometer, and fluorescence spectrophotometer (λ_{ex} 320 nm, λ_{em} 380 nm) was used to detect and characterize the metabolites. (a) CH-01 was subjected to zinc reduction for 1 h, and this solution was injected into potassium phosphate buffer pH 7.4. Incubation at 37 °C and analysis of the supernatant reveal loss of the amine **5** and formation of the active inhibitor **6**. (b) Bactosomal human NADPH-CYP reductase reduces CH-01 (**1**) to the amine **5** under hypoxic conditions (≤0.02% O_2). Over 24 h amine **5** accumulates and fragments to release the active inhibitor **6**.

tested, the sensitivity to CH-01 correlated with the baseline levels of DNA damage/replication stress. Therefore this strategy allows us to concentrate Chk1/Aurora kinase A inhibition in hypoxic cells, targeting the most aggressive tumor fraction, while protecting normal tissue.

RESULTS AND DISCUSSION

We have shown that depletion or inhibition of Chk1 sensitizes cells to hypoxia/reoxygenation.[22,36] The biological reasons behind this observation include our finding that Chk1 has a role to play in reoxygenation-induced replication restart, as well as normal replication.[23] In order to further validate Chk1 as a molecular target in hypoxic conditions, we have considered its autophosphorylation site serine 296 and the ATR-mediated phosphorylations on serine residues 317 and 345 as well as the total levels of Chk1. Chk1 was rapidly phosphorylated at all tested residues (Figure 1a). To verify that the hypoxia-mediated phosphorylation of Chk1 correlated with Chk1 activity, the levels of the Chk1 target Tousled-like kinase 1 (TLK1) are also shown.[37] As described previously, the total levels of Chk1 decrease during increasing exposure to hypoxia.[23] It is clear caution is warranted when considering the inhibition of essential genes such as Chk1. To demonstrate this point we exposed nontransformed human fetal lung fibroblasts (WI38) to a well-characterized Chk1 inhibitor, Gö6976, in the absence of additional stress. Increasing exposure to Gö6976 led to a significant accumulation of cells with more than six 53 binding protein 1 (53BP1) foci indicating that prolonged exposure to a Chk1 inhibitor leads to accumulation of DNA damage, which could in turn affect genome stability (Figure 1b). In order to target Chk1 kinase inhibition to the hypoxic regions of tumors, we synthesized a bioreductive Chk1 inhibitor, CH-01 (**1**). CH-01 is based on the Chk1 inhibitor **6** (Figure 2a) reported by Foloppe et al.[38] During the course of this work, compound **6** was also shown to inhibit Aurora kinase A.[39] Inhibitors of Aurora kinases have been tested clinically and show some promise; however, these agents have not been tested specifically in hypoxic conditions.[40] In order to investigate the potential benefit of Aurora A inhibition in hypoxic cells, we incubated RKO cells with the known selective Aurora A inhibitor MLN8237 in both normoxic and hypoxic conditions. The colony survival assay shown demonstrates that cells in both normoxia and hypoxia are sensitive to inhibition of Aurora A (Figure 1c).

Synthesis of a Bioreductive Chk1/Aurora A Inhibitor. Compound **6** was selected for its chemical simplicity and the well-defined Chk1 structure–activity relationships (SAR) reported around this scaffold. Compound **6** inhibits Chk1 kinase in an ATP competitive manner with a reported IC_{50} value of 20.9 μM, and the SAR showed that addition of a large substituent in place of the hydroxyl group resulted in a significant reduction in Chk1 affinity. Examination of an X-ray crystal structure of **6** bound to the ATP binding site of Chk1 reveals that the hydroxyl group binds oriented into a pocket, which is too small to accommodate a substituent such as the 4-nitrobenzyl group. This observation was corroborated by docking studies (see Supplementary Figure S1). Consequently we designed compound **1**, which we predicted to be inactive as a Chk1 inhibitor until the 4-nitrobenzyl group is removed in hypoxia (Figure 2a). Structure–activity studies have shown that compound **6** inhibits Aurora kinase A with an IC_{50} value of 309 nM.[39] In addition, these studies showed that larger groups, including 4-aminophenyl derivatives, were tolerated in place of the hydroxyl group. To predict whether addition of a 4-nitrobenzyl group would reduce the compound's affinity for Aurora kinase A, we undertook docking studies. These studies suggested that although both compound **1** and compound **5** would bind to Aurora kinase A with a reduced affinity compared to that of compound **6**, they could potentially still be accommodated in the ATP-binding site (see Supplementary Figure S2A and B). Compound **1** was synthesized using conditions similar to those reported by Foloppe (Figure 2b). Benzoin (**7**) was condensed with malononitrile to give 2-aminofuran **8**. Reaction with acetic formic anhydride afforded the formamide **9**, which cyclized to give **10** upon heating. Treatment of **10** with phosphorus oxychloride furnished the chloride **11**, which underwent facile reaction with *O*-(4-nitrobenyl)ethanolamine (**12**) to give the final product (**1**). Analysis of compound **1** in a radioactive (^{33}P-ATP) filter-binding assay revealed no activity against either Chk1 or Aurora kinase A at concentrations up to 100 μM (Supplementary

dx.doi.org/10.1021/cb4001537 | ACS Chem. Biol. 2013, 8, 1451–1459

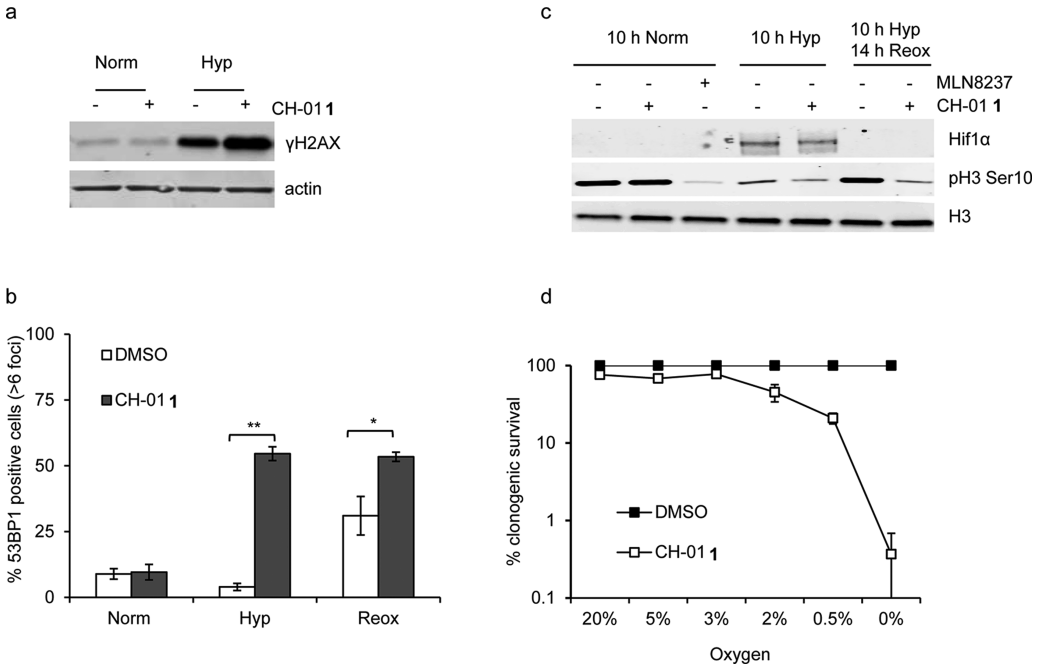

Figure 4. CH-01 induces DNA damage and is toxic in hypoxic conditions. (a) RKO cells were exposed to normoxia or hypoxia (≤0.02% O_2) for 6 h in the presence or absence of 25 μM CH-01 (**1**). Western blots for γH2AX and actin are shown. (b) RKO cells were exposed to normoxia or hypoxia (≤0.02% O_2) for 6 h and hypoxia followed by 18 h of reoxygenation ± **1** (25 μM). The graph shows the percentage of cells with >6 nuclear 53BP1 foci. Significance values: * $p < 0.05$; ** $p < 0.0001$. (c) RKO cells were exposed to hypoxia for the time periods indicated with either **1** (25 μM), MLN8237 (500 nM) or, as a control, DMSO. The levels of phosphorylated histone 3 (pH3 Ser10) were determined by Western blotting. Histone 3 (H3) is shown as loading control. (d) Clonogenic assays were carried out on RKO cells exposed to the oxygen tensions indicated for 24 h in the presence of 25 μM **1** or DMSO.

Figure S3). Conversely, compound **6** showed IC_{50} values of 1.75 and 0.81 μM against Chk1 and Aurora kinase A, respectively.

Mechanism of CH-01 Action. To determine whether **1** fragmented under reducing conditions as predicted, we carried out two reductions in progressively more biologically relevant conditions. Shigenaga et al. have previously employed zinc in aqueous ammonium chloride to reduce a 4-nitrobenzyl group to a 4-aminobenzyl group and hence demonstrate hypoxic activation of a peptide.[41] Using similar conditions of zinc and ammonium chloride in *N*,*N*-dimethylformamide (DMF), we demonstrated that **1** was reduced to give the nitroso compound **4** (confirmed by mass spectrometry) and the amine **5** after a period of 60 min (Supplementary Figure S4a). Upon exposure to aqueous conditions (potassium phosphate buffer, pH 7.4), HPLC analysis indicated that compounds **4** and **5** fragmented to give the active kinase inhibitor **6** (Figure 3a and Supplementary Figure S4b). Encouraged that we had proved reduction of **1** could induce fragmentation in buffer, we treated **1** with bactosomal human NADPH-CYP reductase in potassium phosphate buffer with the exclusion of oxygen. Under these conditions reduction of the 4-nitrobenzyl group of **1** to the 4-aminobenzyl derivative **5** was observed and fragmentation to the active inhibitor **6** occurred. When this experiment was repeated in the presence of oxygen, no reduction or production of compound **6** was observed (Figure 3b and data not shown). These results indicate that the nitrobenzyl group is reduced under purely chemical conditions and by reductase enzymes in hypoxic conditions. The reduced products fragment to give the active kinase inhibitor **6** in a manner consistent with the proposed *in vitro* mode of activation for compound **1**.

In Hypoxic Conditions CH-01 Leads to Loss of Cell Viability. Loss or inhibition of Chk1 has been shown to induce DNA damage due to impaired replisome stability and DNA repair.[42] Therefore, we investigated whether CH-01 (**1**) induced DNA damage in normoxia, hypoxia, and after reoxygenation. Initially, we carried out Western blotting for γH2AX and determined that the presence of **1** in hypoxic conditions led to an increase in the hypoxia-induced γH2AX signal (Figure 4a). As the robust induction of γH2AX by hypoxia alone makes this signal difficult to quantify we used the formation of 53BP1 foci as an alternative measure of DNA damage. As shown previously, hypoxia alone did not induce an accumulation of 53BP1 foci, although subsequent reoxygenation did cause DNA damage.[21] In contrast, exposure to **1** in hypoxia alone led to the accumulation of 53BP1 foci in over 50% of the cells (Figure 4b). These data indicate that CH-01 leads to the accumulation of DNA damage only in hypoxic conditions.

To confirm that **6** inhibits Aurora A/B, we treated RKO cells with CH-01 (**1**) in hypoxic conditions and then carried out Western blotting for histone-3 phosphorylated at serine 10, which is a characterized target of Aurora A/B.[43] Treatment of RKO cells in normoxia with MLN8237 demonstrated that phosphorylation of pH3 at ser10 can be inhibited through Aurora A inhibition. In contrast, **1** has no effect on this signal in normoxic conditions, indicating that this compound does not inhibit Aurora A/B. In response to hypoxia the pH3 ser10 signal decreased, and this decrease was exacerbated in the presence of **1**. After subsequent reoxygenation a clear and

dx.doi.org/10.1021/cb4001537 | *ACS Chem. Biol.* 2013, 8, 1451–1459

significant reduction of pH3 Ser10 was observed when RKO cells were incubated with **1** during hypoxia prior to reoxygenation (Figure 4c). These data suggest that **1** is reduced and fragmented to give **6**, which inhibits both Chk1 and Aurora A/B. This dual inhibition is beneficial as both Chk1 and Aurora A are involved in cell cycle progression and are therapeutic targets. Next, we exposed RKO cells to **1** and incubated the cells in oxygen concentrations ranging from 20% to ≤0.02% O_2 (Figure 4d). A colony survival assay was carried out at each of the oxygen tensions indicated and demonstrates a significant oxygen-dependent loss of viability. Most importantly, at oxygen levels associated with normal tissues (3% O_2 and above) there was little or no effect on cell viability.

It was important to determine that the biological effects observed were due to the release of **6** and not the bioreductive cage. Cells were exposed to the nonbioreductive inhibitor **6**, compound **13**, which releases EtOH under hypoxic conditions, and CH-01 (**1**, Figure 5a,b). As expected, RKO cells were

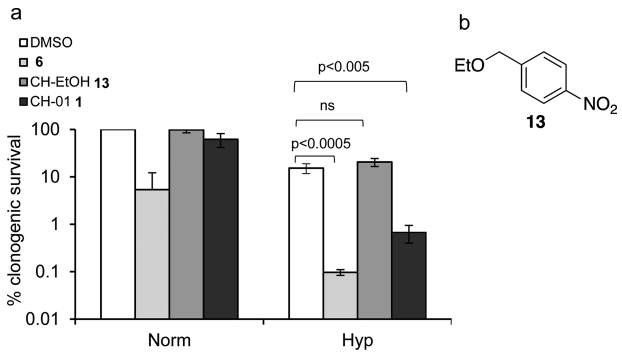

Figure 5. The biological activity of CH-01 is not associated with the bioreductive group. (a) Clonogenic assays were carried out using RKO cells exposed to DMSO, 25 μM inhibitor **6**, 25 μM CH-EtOH **13** or 25 μM CH-01 **1** for 24 h in either normoxia or hypoxia (≤0.02% O_2). (b) The structure of compound **13**, which ejects EtOH under hypoxic conditions.

sensitive to Chk1 inhibitor **6** ,and this sensitivity was increased in hypoxic conditions as previously reported. In contrast, **1** had no significant effect on the normoxic cells but significantly increased the sensitivity to hypoxia/reoxygenation. Importantly, compound **13** did not decrease cell viability, suggesting that the release of the reduced nitrobenzyl group side product alone is not cytotoxic.

Up to this point our studies had been restricted to the RKO cell line. However, we proposed that different cells lines would show varying degrees of sensitivity to **1**. To investigate this hypothesis further we used three lung cancer cell lines (A549, H1299, and H1975) to determine the effect of **1** in normoxia and hypoxia. Recent, reports suggest that the baseline levels of DNA damage and/or replication stress contribute to the relative sensitivity to Chk1 inhibitors. We proposed that this might also be the case for inhibitors of alternative kinases involved in the cell cycle and so might predict sensitivity to inhibition of Chk1 and Aurora A by **1**. Therefore, before testing the effect of **1** on cell viability in hypoxic conditions, we measured the basal levels of DNA damage and replication stress in these 3 cell lines. This measurement was achieved by staining for both 53BP1 and γH2AX, which are markers of DNA damage and/or replication stress (Figure 6a,b). In each cell line a significant proportion of the cells were found to be positive for these markers, although both the H1299 and H1975 cell line had higher levels of 53BP1/γH2AX positive cells than the A549s. Interestingly, large nuclear bodies were seen in the H1299 cell line, which were reminiscent of the recently described Oct-1, PTF, transcription (OPT) domains.[44] These data suggest that the A549 cell line should show the least sensitivity to **1** in hypoxic conditions. To test this hypothesis, the cell lines were exposed to **1** for 24 h in either normoxia or hypoxia (≤0.02% O_2). As predicted all three-cell lines were sensitive to **1** in hypoxic conditions, and of the three the A549 cells were the least sensitive. However, despite the relatively similar levels of DNA damage seen in the H1299 and H1975 cell lines, the latter were significantly more sensitive to **1**. Our data demonstrate that all four of the cell lines tested show increased sensitivity to **1** in hypoxia and that the degree of sensitivity can, in part, be determined by the basal levels of DNA damage/replication stress. In order to use an agent such as **1** most effectively, the degree of tumor hypoxia would have to be determined prior to treatment.[45−47] It is clear that nonhypoxic tumors would not respond and the more hypoxic the greater the predicted response (Figure 4d). However, the sensitivity to **1** is also determined by additional factors including the levels of DNA damage/replication arrest. We propose that **1** and derivatives would be effective against tumors with high levels of hypoxia or oncogene-mediated replication stress. In mildly hypoxic tumors, which are less susceptible to Chk1 inhibition due to low levels of replication stress for example, we predict that combining **1** with standard therapies would be effective.

Conclusions. We confirm earlier findings that inhibition of Chk1 is a valid approach to target hypoxic cancer cells. In addition, we have demonstrated that hypoxic cells show similar levels of sensitivity to inhibition of the Aurora A kinase as cells in normoxia. Here, we describe a bioreductive Chk1/Aurora A inhibitor, CH-01 (**1**), which selectively inhibits Chk1/Aurora A in hypoxic conditions and leads to significant loss of viability in the cancer cell lines tested. Although a proof-of-concept compound, the selective activity demonstrated by **1** suggests the potential for the bioreductive release of targeted therapies and demonstrates this approach as a promising strategy for the targeted application of cancer chemotherapeutics.

METHODS

Cell Lines. RKO (colorectal), A549, H1299, and H1975 (lung) cancer cell lines were cultured in DMEM medium containing 10% FBS, penicillin (100 U/mL) and streptomycin (100 μg/mL). WI38 nontransformed human fetal lung fibroblasts were grown in DMEM medium with 15% FBS. All cell lines were originally obtained from the ATCC and routinely mycoplasma tested and found to be negative. With the exception of colony survival experiments all others were carried out with cells at 75% confluence.

Chemical Synthesis. Details of the chemical synthesis and analytical data for the compounds described are available in the Supporting Information. Gö6976 was obtained from Sigma-Aldrich and MLN8237 from Selleckchem.

Hypoxia Treatment. Hypoxia treatments were carried out in a Bactron II (Shell laboratories), In vivo 400 (Ruskinn), or Heracell mixed gas incubator (Fisher Scientific) depending on the level of hypoxia required.

Clonogenic Assay. Colonies (>50 cells) were left to form for 10 days and visualized with methylene blue stain (70% methanol in PBS, 1% methylene blue (Fisher BioReagents)).

Western Blotting. Cells were lysed in UTB (9 M urea, 75 mM Tris-HCl pH 7.5 and 0.15 M β-mercaptoethanol) and sonicated briefly. Antibodies used were Chk1-S296, Chk1-S317, Chk1-S345,

dx.doi.org/10.1021/cb4001537 | ACS Chem. Biol. 2013, 8, 1451−1459

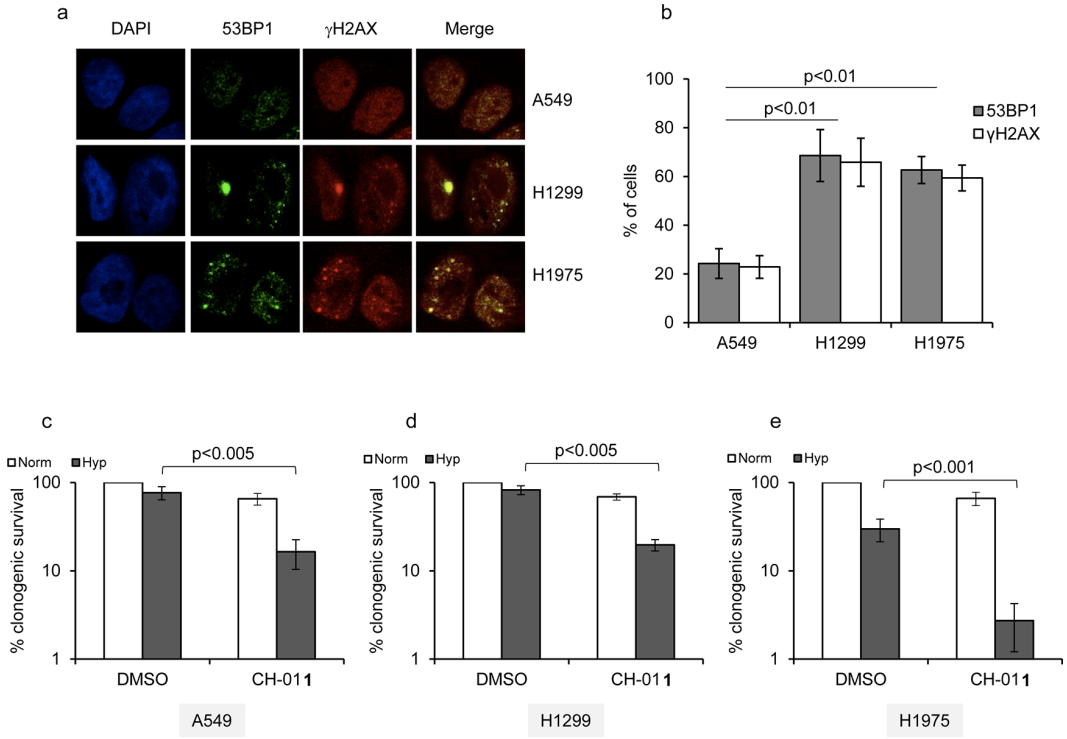

Figure 6. The sensitivity of cell lines to CH-01 correlates with levels of DNA damage and replication stress. (a) Endogenous DNA damage for each cell line was determined in the absence of additional stress by staining for the presence of 53BP1 (green) and γH2AX (red). (b) Graph represents the quantification of the percentage of cells with more than 6 53BP1 foci (black) or the presence of γH2AX foci positive staining (white) for the three cell lines. The three lung cancer cell lines A549 (c), H1299 (d), and H1975 (e) were exposed to DMSO or 25 μM CH-01 for 24 h in normoxia or hypoxia (≤0.02% O_2), and colony survival assays were carried out.

HIF1α (BD Biosciences), Chk1, γH2AX (Upstate-Millipore), H3-S10, TLK-S695 (Cell Signaling), and GAPDH (Fitzgerald Industries). The Odyssey infrared system was used for imaging (LI-COR Biosciences).

Zinc Reduction of 1. To a solution of **1** (1 mg, 0.0021 mmol) in DMF (2 mL) were added aqueous ammonium chloride (20 μL, 10% w/v) and zinc powder (5 mg, 0.0765 mmol, 36 equiv). The resulting mixture was stirred at ambient temperature for 16 h. Aliquots (200 μL) were taken at designated times (where $T = 0$ refers to before the addition of zinc powder), and the mixture was analyzed by HPLC.

Buffer Treatment of 5. For every time point of interest, 5 μL of the $T = 1$ h aliquot from the zinc reduction was injected into 95 μL of potassium phosphate buffer solution (pH 7.4), and the resulting suspensions were incubated at 37 °C. At designated times the suspensions were centrifuged. The supernatant was collected, and the precipitates were dissolved in acetonitrile. Both fractions were analyzed by HPLC.

Reductase Assay. Bactosomal human NADPH-CYP reductase (Cypex, 12.7 mg/mL, 13900 nmol/min/mL) was used in combination with an NADPH-regenerating system (BD Biosciences), and the assay was carried out according to the manufacturer's protocol (BD Biosciences application note 467) at a CH-01 concentration of 250 nM. Vials were deoxygenated by bubbling nitrogen prior to P540 addition and then transferred into a Bactron II (Shell laboratories). Samples were taken at different time points and analyzed by HPLC.

Immunofluorescence. Staining for 53BP1 (Novus Biologicals) and γH2AX foci was carried out as previously described.[21] Due to the presence of 1−2 53BP1 foci in the nuclei of unstressed cells, induction of DNA damage was quantified by counting cells with more than 6 foci. Cells were visualized using a Nikon 90i microscope.

HPLC Analysis. HPLC (Waters 2695 system) comprised an RPB column (100 mm × 3.2 mm, 35 °C). Separation was achieved at a flow rate of 0.5 mL/min with a gradient of 60−95% acetonitrile in 10 mM formic acid over 6 min. Detection used a photodiode array spectrophotometer (Waters 2996), a mass spectrometer (Waters Micromass ZQ mass spectrometer), and a fluorescence spectrophotometer (Waters 474) with λ_{ex} 320 nm, λ_{em} 380 nm. Injections of 10 μL were made.

Statistical Analysis. Statistical significance of differences between means of at least $n = 3$ experiments was determined using Student's t test (P-values indicated accordingly in figure legend or main text). Error bars represent ± SEM.

■ ASSOCIATED CONTENT

Ⓢ Supporting Information

Supplementary figures, general experimental, experimental procedures, and ^1H and ^{13}C NMR spectra. This material is available free of charge via the Internet at http://pubs.acs.org.

■ AUTHOR INFORMATION

Corresponding Author

*E-mail: ester.hammond@oncology.ox.ac.uk; stuart.conway@chem.ox.ac.uk.

Present Address

⊥University of Hull, Department of Biological Sciences, Hull HU6 7RX, U.K.

Author Contributions

§These authors contributed equally to this work.

Notes

The authors declare no competing financial interest.

■ ACKNOWLEDGMENTS

The authors thank M. Stratford, L. Folkes, P. Wardman, and P. O'Neill for useful discussions. E.M.H., I.M.P., and C.C.-K. are

funded by Cancer Research UK (C6515/A9321 awarded to E.M.H.). Additional funding was provided by the Oxford Cancer Research Centre development fund (awarded to E.M.H.). S.J.C. thanks the Department of Chemistry, University of Oxford, for research support.

REFERENCES

(1) Halazonetis, T. D., Gorgoulis, V. G., and Bartek, J. (2008) An oncogene-induced DNA damage model for cancer development. *Science 319*, 1352−1355.

(2) Chen, T., Stephens, P. A., Middleton, F. K., and Curtin, N. J. (2012) Targeting the S and G2 checkpoint to treat cancer. *Drug Discovery Today 17*, 194−202.

(3) Murga, M., Campaner, S., Lopez-Contreras, A. J., Toledo, L. I., Soria, R., Montana, M. F., D'Artista, L., Schleker, T., Guerra, C., Garcia, E., Barbacid, M., Hidalgo, M., Amati, B., and Fernandez-Capetillo, O. (2011) Exploiting oncogene-induced replicative stress for the selective killing of Myc-driven tumors. *Nat. Struct. Mol. Biol. 18*, 1331−1335.

(4) Gilad, O., Nabet, B. Y., Ragland, R. L., Schoppy, D. W., Smith, K. D., Durham, A. C., and Brown, E. J. (2010) Combining ATR suppression with oncogenic Ras synergistically increases genomic instability, causing synthetic lethality or tumorigenesis in a dosage-dependent manner. *Cancer Res. 70*, 9693−9702.

(5) Cole, K. A., Huggins, J., Laquaglia, M., Hulderman, C. E., Russell, M. R., Bosse, K., Diskin, S. J., Attiyeh, E. F., Sennett, R., Norris, G., Laudenslager, M., Wood, A. C., Mayes, P. A., Jagannathan, J., Winter, C., Mosse, Y. P., and Maris, J. M. (2011) RNAi screen of the protein kinome identifies checkpoint kinase 1 (CHK1) as a therapeutic target in neuroblastoma. *Proc. Natl. Acad. Sci. U.S.A. 108*, 3336−3341.

(6) Hoglund, A., Nilsson, L. M., Muralidharan, S. V., Hasvold, L. A., Merta, P., Rudelius, M., Nikolova, V., Keller, U., and Nilsson, J. A. (2011) Therapeutic implications for the induced levels of Chk1 in Myc-expressing cancer cells. *Clin. Cancer Res. 17*, 7067−7079.

(7) Ferrao, P. T., Bukczynska, E. P., Johnstone, R. W., and McArthur, G. A. (2011) Efficacy of CHK inhibitors as single agents in MYC-driven lymphoma cells. *Oncogene 31*, 1661−1672.

(8) Cavelier, C., Didier, C., Prade, N., Mansat-De Mas, V., Manenti, S., Recher, C., Demur, C., and Ducommun, B. (2009) Constitutive activation of the DNA damage signaling pathway in acute myeloid leukemia with complex karyotype: potential importance for checkpoint targeting therapy. *Cancer Res. 69*, 8652−8661.

(9) Pires, I. M., Olcina, M. M., Anbalagan, S., Pollard, J. R., Reaper, P. M., Charlton, P. A., McKenna, W. G., and Hammond, E. M. (2012) Targeting radiation-resistant hypoxic tumour cells through ATR inhibition. *Br. J. Cancer 107*, 291−299.

(10) Peasland, A., Wang, L. Z., Rowling, E., Kyle, S., Chen, T., Hopkins, A., Cliby, W. A., Sarkaria, J., Beale, G., Edmondson, R. J., and Curtin, N. J. (2011) Identification and evaluation of a potent novel ATR inhibitor, NU6027, in breast and ovarian cancer cell lines. *Br. J. Cancer 105*, 372−381.

(11) Toledo, L. I., Murga, M., Zur, R., Soria, R., Rodriguez, A., Martinez, S., Oyarzabal, J., Pastor, J., Bischoff, J. R., and Fernandez-Capetillo, O. (2011) A cell-based screen identifies ATR inhibitors with synthetic lethal properties for cancer-associated mutations. *Nat. Struct. Mol. Biol. 18*, 721−727.

(12) Ma, C. X., Janetka, J. W., and Piwnica-Worms, H. (2011) Death by releasing the breaks: CHK1 inhibitors as cancer therapeutics. *Trends Mol. Med. 17*, 88−96.

(13) Reaper, P. M., Griffiths, M. R., Long, J. M., Charrier, J. D., Maccormick, S., Charlton, P. A., Golec, J. M., and Pollard, J. R. (2011) Selective killing of ATM- or p53-deficient cancer cells through inhibition of ATR. *Nat. Chem. Biol. 7*, 428−430.

(14) Prevo, R., Fokas, E., Reaper, P. M., Charlton, P. A., Pollard, J. R., McKenna, W. G., Muschel, R. J., and Brunner, T. B. (2012) The novel ATR inhibitor VE-821 increases sensitivity of pancreatic cancer cells to radiation and chemotherapy. *Cancer Biol. Ther. 13*, 1072−1081.

(15) Blasina, A., Hallin, J., Chen, E., Arango, M. E., Kraynov, E., Register, J., Grant, S., Ninkovic, S., Chen, P., Nichols, T., O'Connor, P., and Anderes, K. (2008) Breaching the DNA damage checkpoint via PF-00477736, a novel small-molecule inhibitor of checkpoint kinase 1. *Mol. Cancer Ther. 7*, 2394−2404.

(16) Janetka, J. W., Ashwell, S., Zabludoff, S., and Lyne, P. (2007) Inhibitors of checkpoint kinases: from discovery to the clinic. *Curr. Opin. Drug Discovery Devel 10*, 473−486.

(17) Syljuasen, R. G., Sorensen, C. S., Hansen, L. T., Fugger, K., Lundin, C., Johansson, F., Helleday, T., Sehested, M., Lukas, J., and Bartek, J. (2005) Inhibition of human Chk1 causes increased initiation of DNA replication, phosphorylation of ATR targets, and DNA breakage. *Mol. Cell. Biol. 25*, 3553−3562.

(18) Carrassa, L., and Damia, G. (2011) Unleashing Chk1 in cancer therapy. *Cell Cycle 10*, 2121−2128.

(19) Vaupel, P., and Hockel, M. (2003) Tumor oxygenation and its relevance to tumor physiology and treatment. *Adv. Exp. Med. Biol. 510*, 45−49.

(20) Brown, J. M., and Giaccia, A. J. (1998) The unique physiology of solid tumors: opportunities (and problems) for cancer therapy. *Cancer Res. 58*, 1408−1416.

(21) Bencokova, Z., Kaufmann, M. R., Pires, I. M., Lecane, P. S., Giaccia, A. J., and Hammond, E. M. (2009) ATM activation and signaling under hypoxic conditions. *Mol. Cell. Biol. 29*, 526−537.

(22) Olcina, M., Lecane, P. S., and Hammond, E. M. (2010) Targeting hypoxic cells through the DNA damage response. *Clin. Cancer Res. 16*, 5624−5629.

(23) Pires, I. M., Bencokova, Z., Milani, M., Folkes, L. K., Li, J. L., Stratford, M. R., Harris, A. L., and Hammond, E. M. (2010) Effects of acute versus chronic hypoxia on DNA damage responses and genomic instability. *Cancer Res. 70*, 925−935.

(24) Wilson, W. R., and Hay, M. P. (2011) Targeting hypoxia in cancer therapy. *Nat. Rev. Cancer 11*, 393−410.

(25) Evans, J. W., Chernikova, S. B., Kachnic, L. A., Banath, J. P., Sordet, O., Delahoussaye, Y. M., Treszezamsky, A., Chon, B. H., Feng, Z., Gu, Y., Wilson, W. R., Pommier, Y., Olive, P. L., Powell, S. N., and Brown, J. M. (2008) Homologous recombination is the principal pathway for the repair of DNA damage induced by tirapazamine in mammalian cells. *Cancer Res. 68*, 257−265.

(26) Albertella, M. R., Loadman, P. M., Jones, P. H., Phillips, R. M., Rampling, R., Burnet, N., Alcock, C., Anthoney, A., Vjaters, E., Dunk, C. R., Harris, P. A., Wong, A., Lalani, A. S., and Twelves, C. J. (2008) Hypoxia-selective targeting by the bioreductive prodrug AQ4N in patients with solid tumors: results of a phase I study. *Clin. Cancer Res. 14*, 1096−1104.

(27) Jameson, M. B., Rischin, D., Pegram, M., Gutheil, J., Patterson, A. V., Denny, W. A., and Wilson, W. R. (2010) A phase I trial of PR-104, a nitrogen mustard prodrug activated by both hypoxia and aldo-keto reductase 1C3, in patients with solid tumors. *Cancer Chemother. Pharmacol. 65*, 791−801.

(28) Wang, J., Foehrenbacher, A., Su, J., Patel, R., Hay, M. P., Hicks, K. O., and Wilson, W. R. (2012) The 2-nitroimidazole EF5 is a biomarker for oxidoreductases that activate the bioreductive prodrug CEN-209 under hypoxia. *Clin. Cancer Res. 18*, 1684−1695.

(29) Rischin, D., Peters, L. J., O'Sullivan, B., Giralt, J., Fisher, R., Yuen, K., Trotti, A., Bernier, J., Bourhis, J., Ringash, J., Henke, M., and Kenny, L. (2010) Tirapazamine, cisplatin, and radiation versus cisplatin and radiation for advanced squamous cell carcinoma of the head and neck (TROG 02.02, HeadSTART): a phase III trial of the Trans-Tasman Radiation Oncology Group. *J. Clin. Oncol. 28*, 2989−2995.

(30) Peters, L. J., O'Sullivan, B., Giralt, J., Fitzgerald, T. J., Trotti, A., Bernier, J., Bourhis, J., Yuen, K., Fisher, R., and Rischin, D. (2010) Critical impact of radiotherapy protocol compliance and quality in the treatment of advanced head and neck cancer: results from TROG 02.02. *J. Clin. Oncol. 28*, 2996−3001.

(31) Hunter, F. W., Wang, J., Patel, R., Hsu, H. L., Hickey, A. J., Hay, M. P., and Wilson, W. R. (2012) Homologous recombination repair-dependent cytotoxicity of the benzotriazine di-N-oxide CEN-209:

comparison with other hypoxia-activated prodrugs. *Biochem. Pharmacol. 83*, 574−585.
(32) Sun, J. D., Liu, Q., Wang, J., Ahluwalia, D., Ferraro, D., Wang, Y., Duan, J. X., Ammons, W. S., Curd, J. G., Matteucci, M. D., and Hart, C. P. (2012) Selective tumor hypoxia targeting by hypoxia-activated prodrug TH-302 inhibits tumor growth in preclinical models of cancer. *Clin. Cancer Res. 18*, 758−770.
(33) Zhang, Z., Tanabe, K., Hatta, H., and Nishimoto, S. (2005) Bioreduction activated prodrugs of camptothecin: molecular design, synthesis, activation mechanism and hypoxia selective cytotoxicity. *Org. Biomol. Chem. 3*, 1905−1910.
(34) Granchi, C., Funaioli, T., Erler, J. T., Giaccia, A. J., Macchia, M., and Minutolo, F. (2009) Bioreductively activated lysyl oxidase inhibitors against hypoxic tumours. *ChemMedChem 4*, 1590−1594.
(35) Zhu, R., Liu, M. C., Luo, M. Z., Penketh, P. G., Baumann, R. P., Shyam, K., and Sartorelli, A. C. (2011) 4-nitrobenzyloxycarbonyl derivatives of O(6)-benzylguanine as hypoxia-activated prodrug inhibitors of O(6)-alkylguanine-DNA alkyltransferase (AGT), which produces resistance to agents targeting the O-6 position of DNA guanine. *J. Med. Chem. 54*, 7720−7728.
(36) Hammond, E. M., Dorie, M. J., and Giaccia, A. J. (2004) Inhibition of ATR leads to increased sensitivity to hypoxia/reoxygenation. *Cancer Res. 64*, 6556−6562.
(37) Pires, I. M., Bencokova, Z., McGurk, C., and Hammond, E. M. (2010) Exposure to acute hypoxia induces a transient DNA damage response which includes Chk1 and TLK1. *Cell Cycle 9*, 2502−2507.
(38) Foloppe, N., Fisher, L. M., Howes, R., Kierstan, P., Potter, A., Robertson, A. G., and Surgenor, A. E. (2005) Structure-based design of novel Chk1 inhibitors: insights into hydrogen bonding and protein-ligand affinity. *J. Med. Chem. 48*, 4332−4345.
(39) Coumar, M. S., Chu, C. Y., Lin, C. W., Shiao, H. Y., Ho, Y. L., Reddy, R., Lin, W. H., Chen, C. H., Peng, Y. H., Leou, J. S., Lien, T. W., Huang, C. T., Fang, M. Y., Wu, S. H., Wu, J. S., Chittimalla, S. K., Song, J. S., Hsu, J. T., Wu, S. Y., Liao, C. C., Chao, Y. S., and Hsieh, H. P. (2010) Fast-forwarding hit to lead: aurora and epidermal growth factor receptor kinase inhibitor lead identification. *J. Med. Chem. 53*, 4980−4988.
(40) Manchado, E., Guillamot, M., and Malumbres, M. (2012) Killing cells by targeting mitosis. *Cell Death Differ. 19*, 369−377.
(41) Shigenaga, A., Ogura, K., Hirakawa, H., Yamamoto, J., Ebisuno, K., Miyamoto, L., Ishizawa, K., Tsuchiya, K., and Otaka, A. (2012) Development of a reduction-responsive amino acid that induces peptide bond cleavage in hypoxic cells. *ChemBioChem 13*, 968−971.
(42) Sorensen, C. S., and Syljuasen, R. G. (2011) Safeguarding genome integrity: the checkpoint kinases ATR, CHK1 and WEE1 restrain CDK activity during normal DNA replication. *Nucleic Acids Res.*, DOI: 10.1093/nar/gkr697 .
(43) Crosio, C., Fimia, G. M., Loury, R., Kimura, M., Okano, Y., Zhou, H., Sen, S., Allis, C. D., and Sassone-Corsi, P. (2002) Mitotic phosphorylation of histone H3: spatio-temporal regulation by mammalian Aurora kinases. *Mol. Cell. Biol. 22*, 874−885.
(44) Harrigan, J. A., Belotserkovskaya, R., Coates, J., Dimitrova, D. S., Polo, S. E., Bradshaw, C. R., Fraser, P., and Jackson, S. P. (2011) Replication stress induces 53BP1-containing OPT domains in G1 cells. *J. Cell Biol. 193*, 97−108.
(45) Buffa, F. M., Harris, A. L., West, C. M., and Miller, C. J. (2010) Large meta-analysis of multiple cancers reveals a common, compact and highly prognostic hypoxia metagene. *Br. J. Cancer 102*, 428−435.
(46) Moon, E. J., Brizel, D. M., Chi, J. T., and Dewhirst, M. W. (2007) The potential role of intrinsic hypoxia markers as prognostic variables in cancer. *Antioxid. Redox Signaling 9*, 1237−1294.
(47) Ebbesen, P., Pettersen, E. O., Gorr, T. A., Jobst, G., Williams, K., Kieninger, J., Wenger, R. H., Pastorekova, S., Dubois, L., Lambin, P., Wouters, B. G., Van Den Beucken, T., Supuran, C. T., Poellinger, L., Ratcliffe, P., Kanopka, A., Gorlach, A., Gasmann, M., Harris, A. L., Maxwell, P., and Scozzafava, A. (2009) Taking advantage of tumor cell adaptations to hypoxia for developing new tumor markers and treatment strategies. *J. Enzyme Inhib. Med. Chem. 24* (Suppl 1), 1−39.

(12) International Application Status Report

Received at International Bureau: 19 November 2014 (19.11.2014)
Information valid as of: 28 April 2015 (28.04.2015)
Report generated on: 06 April 2016 (06.04.2016)

(10) Publication number:
WO2015/071665

(43) Publication date:
21 May 2015 (21.05.2015)

(26) Publication language:
English (EN)

(21) Application Number:
PCT/GB2014/053363

(22) Filing Date:
13 November 2014 (13.11.2014)

(25) Filing language:
English (EN)

(31) Priority number(s):
1320211.4 (GB)

(31) Priority date(s):
15 November 2013 (15.11.2013)

(31) Priority status:
Priority document received (in compliance with PCT Rule 17.1)

(51) International Patent Classification:
C07D 215/18 (2006.01); ***C07D 311/58*** (2006.01); **A61P 35/00** (2006.01); **A61K 31/47** (2006.01)

(71) Applicant(s):
ISIS INNOVATION LIMITED [GB/GB]; Ewert House Ewert Place Summertown Oxford Oxfordshire OX2 7SG (GB) *(for all designated states)*

(72) Inventor(s):
CONWAY, Stuart; University of Oxford Chemistry Research Laboratory 12 Mansfield Road Oxford Oxfordshire OX1 3TA (GB)
O'CONNOR, Liam; CRUK/MRC Oxford Institute for Radiation Oncology Old Road Campus Research Building Roosevelt Drive Oxford Oxfordshire OX3 7DQ (GB)
HAMMOND, Ester; Gray Institute for Radiation Oncology & Biology Old Road Campus Research Building Roosevelt Drive Oxford Oxfordshire OX3 7DQ (GB)

(74) Agent(s):
SIMONS, Amanda Louise; 14 South Square Gray's Inn London Greater London WC1R 5JJ (GB)

(54) Title (EN): FLUOROGENIC PROTECTING GROUP

(54) Title (FR): GROUPE DE PROTECTION FLUOROGÈNE

(57) Abstract:
(EN): A fluorogenic compound comprising a biologically active component and a hypoxia- activated protecting group which is fluorogenic. The biologically active component is bound to the fluorogenic component at an active binding position such that activity of the biologically active compound is suppressed until the protecting group is released. The protecting group is cleaved under hypoxic conditions, releasing the active compound and a fluorescent compound. The compounds can therefore be used in the treatment of hypoxia- related disease and disorder, such as tumour, and enable imaging of the release of the biologically active compound.

(FR): Cette invention concerne un composé fluorogène comprenant un composant biologiquement actif et un groupe de protection activé par l'hypoxie qui est fluorogène. Le composant biologiquement actif est lié au composant fluorogène à une position de liaison active telle que l'activité du composé biologiquement actif est supprimée tant que le groupe de protection n'est pas libéré. Le groupe de protection est clivé dans des conditions hypoxiques, libérant le composé actif et un composé fluorescent. Les composés peuvent par conséquent être utilisés dans le traitement d'une maladie ou d'un trouble lié à l'hypoxie, tel qu'une tumeur, et permettent l'imagerie de la libération du composé biologiquement actif.

International search report:
Received at International Bureau: 22 December 2014 (22.12.2014) [EP]

International Report on Patentability (IPRP) Chapter II of the PCT:
Not available

(81) Designated States:

AE, AG, AL, AM, AO, AT, AU, AZ, BA, BB, BG, BH, BN, BR, BW, BY, BZ, CA, CH, CL, CN, CO, CR, CU, CZ, DE, DK, DM, DO, DZ, EC, EE, EG, ES, FI, GB, GD, GE, GH, GM, GT, HN, HR, HU, ID, IL, IN, IR, IS, JP, KE, KG, KN, KP, KR, KZ, LA, LC, LK, LR, LS, LU, LY, MA, MD, ME, MG, MK, MN, MW, MX, MY, MZ, NA, NG, NI, NO, NZ, OM, PA, PE, PG, PH, PL, PT, QA, RO, RS, RU, RW, SA, SC, SD, SE, SG, SK, SL, SM, ST, SV, SY, TH, TJ, TM, TN, TR, TT, TZ, UA, UG, US, UZ, VC, VN, ZA, ZM, ZW

European Patent Office (EPO) : AL, AT, BE, BG, CH, CY, CZ, DE, DK, EE, ES, FI, FR, GB, GR, HR, HU, IE, IS, IT, LT, LU, LV, MC, MK, MT, NL, NO, PL, PT, RO, RS, SE, SI, SK, SM, TR

African Intellectual Property Organization (OAPI) : BF, BJ, CF, CG, CI, CM, GA, GN, GQ, GW, KM, ML, MR, NE, SN, TD, TG

African Regional Intellectual Property Organization (ARIPO) : BW, GH, GM, KE, LR, LS, MW, MZ, NA, RW, SD, SL, ST, SZ, TZ, UG, ZM, ZW

Eurasian Patent Organization (EAPO) : AM, AZ, BY, KG, KZ, RU, TJ, TM

ORGANIC CHEMISTRY
FRONTIERS

RESEARCH ARTICLE

View Article Online
View Journal | View Issue

CrossMark click for updates

Cite this: *Org. Chem. Front.*, 2015, **2**, 1026

Efficient synthesis of 2-nitroimidazole derivatives and the bioreductive clinical candidate Evofosfamide (TH-302)†

Liam J. O'Connor,[a,b] Cindy Cazares-Körner,[a,b] Jaideep Saha,[a] Charles N. G. Evans,[a,b] Michael R. L. Stratford,[b] Ester M. Hammond*[b] and Stuart J. Conway*[a]

Received 2nd July 2015,
Accepted 7th July 2015

DOI: 10.1039/c5qo00211g

rsc.li/frontiers-organic

Hypoxia, regions of low oxygen, occurs in a range of biological environments, and is involved in human diseases, most notably solid tumours. Exploiting the physiological differences arising from low oxygen conditions provides an opportunity for development of targeted therapies, through the use of bioreductive prodrugs, which are selectively activated in hypoxia. Herein, we describe an improved method for synthesising the most widely used bioreductive group, 2-nitroimidazole. The improved method is applied to an efficient synthesis of the anti-cancer drug Evofosfamide (TH-302), which is currently in Phase III clinical trials for treatment of a range of cancers.

Published on 10 July 2015. Downloaded on 06/04/2016 16:58:48.

Hypoxia, an inadequate supply of oxygen, is found in many biological contexts, including bacterial biofilms,[1] plant root nodules,[2,3] and human disease – most notably solid malignant tumours.[4,5] Tumour hypoxia arises from the high metabolic demands of the solid tumour, which results in a disorganised vasculature, and poor oxygen supply to regions of the tumour. The presence of hypoxia in solid tumours correlates with an increased likelihood of tumour metastasis, resistance to all modalities of treatment, and consequently a poor patient prognosis.[6] Hypoxic cells are resistant to radiotherapy because radiation-induced DNA damage relies on the generation of reactive oxygen species, and thus occurs in an oxygen-dependent manner. The disruption in tumour vasculature also results in poor delivery of chemotherapeutic agents, reducing the effectiveness of such drugs. Consequently, the hypoxic tumour volume comprises the most aggressive tumour fraction, which is also therapy resistant.[6] Therefore, overcoming the challenge of effectively targeting these cells is critical to the successful treatment of solid tumours, and improvement in patient prognosis.

Despite these complications, the reduced oxygen levels present an opportunity to exploit the chemical difference in physiological conditions within regions of hypoxia. Bioreductive prodrugs can be used to target therapeutic compounds to regions of hypoxia, affording enhanced precision in therapeutic compound delivery.[7] A number of chemical functionalities, which are selectively reduced under hypoxic conditions *via* enzymatic metabolism, have been employed in these prodrugs. The moieties used in such prodrugs include nitroaryl groups, quinones and *N*-oxides.[7–12]

The nitroimidazole group has been widely used in the development of bioreductive prodrugs and imaging agents. It has found application in anaerobic antibacterial treatments including metronidazole,[13,14] in anti-parasitic drug candidates,[15] and also in anti-cancer agents. A notable anti-cancer therapeutic that utilises this bioreductive principle is Evofosfamide (TH-302, Fig. 1).[16] Under conditions of normal oxygen

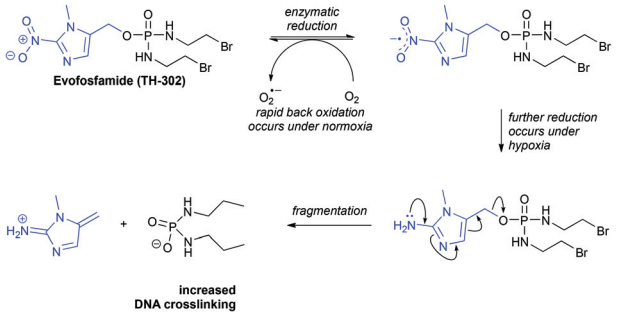

Fig. 1 The 2-nitroimidazole-containing bioreductive prodrug Evofosfamide (TH-302) is activated under hypoxic conditions. Under conditions of normal oxygen concentration (normoxia) the nitro group undergoes a process of futile cycling. Under hypoxia, the nitro group is reduced resulting in fragmentation to release the active drug, which crosslinks DNA.

[a]*Department of Chemistry, Chemistry Research Laboratory, University of Oxford, Mansfield Road, Oxford, OX1 3TA, UK. E-mail: stuart.conway@chem.ox.ac.uk*
[b]*Cancer Research UK/MRC Oxford Institute for Radiation Oncology, Department of Oncology, University of Oxford, Old Road Campus Research Building, Oxford, OX3 7DQ, UK*

†Electronic supplementary information (ESI) available: Full experimental details, ^{1}H, ^{13}C and ^{31}P NMR spectra, HPLC purity details for TH-302. See DOI: 10.1039/c5qo00211g

This journal is © the Partner Organisations 2015

Published on 10 July 2015. Downloaded on 06/04/2016 16:58:48.

concentration (normoxia) the nitro group undergoes a process of futile cycling. In hypoxic conditions the nitro group is reduced, resulting in fragmentation to release the active drug. Consequently, increased DNA crosslinking occurs selectively in hypoxia. TH-302 is in advanced Phase II clinical trials for a variety of cancers (ClinicalTrials.gov Identifiers: NCT02093962; NCT01403610; NCT02402062; NCT00742963). It has also recently entered Phase III trials, in combination with other therapeutics, for treatment of metastatic pancreatic cancer and metastatic soft tissue sarcoma (ClinicalTrials.gov Identifiers: NCT01746979; NCT01440088).

Despite the frequent use of 2-nitroimidazole derivatives as bioreductive prodrugs, existing literature procedures[17] for the synthesis of this group are capricious, time intensive, and afford low yields in our hands. There is, consequently, a need for a reliable, time efficient and higher-yielding synthesis of the key synthetic intermediates that can be used for the synthesis of bioreductive prodrugs. Here, we report a time efficient and repeatable synthesis of the aminoimidazole-based ester **4** in yields of 48–54% over three steps. This compound can readily be converted to the nitroimidazole **7**. Methods to transform the ester (**7**) into a range of useful synthetic handles are described. Finally, the alcohol **8** is employed to complete an efficient synthesis of the bioreductive prodrug TH-302.

To synthesise the key 2-aminoimidazole intermediate **4**, we initially investigated the procedure of Cavalleri *et al.*,[18] but we were not successful in synthesising the *N*-methyl-β,β-diethoxyalanine ethyl ester required for this route. We therefore investigated a one-pot procedure developed by Matteucci *et al.*, which was disclosed in the patent literature (Scheme 1A).[17] Formylation of sarcosine methyl ester (**1**), at both the α-carbon and the secondary amine, was achieved by treatment with sodium hydride and ethyl formate to afford **2**. The unwanted formyl group on the secondary amine was removed by heating under reflux in acidic EtOH to give the presumed intermediate **3**. Subsequent treatment with cyanamide under reflux in aqueous acetate-buffered conditions furnished the desired 2-aminoimidazole (**4**) in yields that typically ranged from 10–25%, over five repeats of the reaction (n = 5). It should be noted that this procedure was reported on an 82 g scale, and is perhaps less suitable for the scale of 2–3 g, which we employed. Our investigations into an alternative reported synthesis[19] were equally variable in the yield of the key intermediate (**4**).

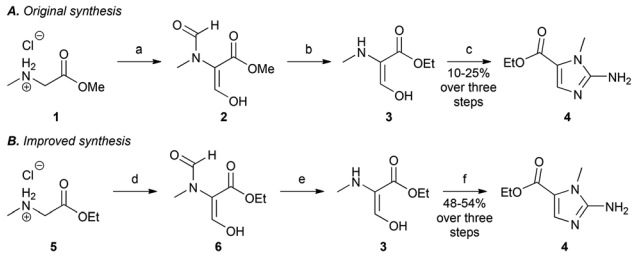

Scheme 1 The original and optimised synthetic routes for the 2-aminoimidazole ester **4**. A. Reagents and conditions: a. EtOCHO, NaH, 16 h; b. EtOH, conc. HCl, 90 °C, 2 h; c. AcOH (aq.), NaOAc, NH_2CN, 100 °C, 1.5 h; 10–25% over three steps (n = 5). B. Reagents and conditions: d. EtOCHO, THF, NaH, 3 h; e. EtOH, conc. HCl, 90 °C, 2 h; f. EtOH, H_2O, NH_2CN, pH 3, 100 °C, 1.5 h; 48–54% over three steps (n = 5).

When seeking to develop a more robust synthesis we identified the first step, in which the diformylated product (**2**) is furnished, as being especially capricious. In particular, the solubility of sarcosine methyl ester hydrochloride (**1**) in ethyl formate is moderate, and this step often failed to proceed, even when the starting material (**1**) was ground to a powder in an attempt to improve its solubility. We, therefore, hypothesised that the low yield of this reaction was linked to the poor solubility of **1** under the reaction conditions. To address this issue, THF was employed as co-solvent along with ethyl formate (1 : 1) to improve the solubility of the reactants. These modified conditions led to an improvement in the overall yield of the 2-aminoimidazole (**4**), ranging from 30–35%, over three steps (n = 3). In addition, THF as a co-solvent provided greater temperature control of the highly exothermic reaction, presumably resulting from improved heat transfer, and dilution of the reactants. A further improvement in yield was achieve by employing sarcosine ethyl ester hydrochloride (**5**) as the starting material (Scheme 1B), as this compound has improved solubility under the reaction conditions, compared to **1**. We also noted that the initial formylation step was time intensive, requiring at least 16 h for completion. As the sarcosine ethyl ester (**5**) is more soluble than the methyl ester (**1**), we hypothesised that this would increase the reaction rate. This proved to be the case, and after a substantially shorter time period, of 3 h (on a 2 g scale), a milky yellow suspension formed suggesting the presence of the desired *N*-formylated enolate (**6**). Given the advantages of using the sarcosine ethyl ester hydrochloride (**5**), we proceeded with the synthesis using this starting material.

To further improve the synthesis, we speculated that the conditions previously employed to form 2-aminoimidazole **4**, which involved heating under reflux in aqueous acetate-buffered conditions, would likely result in ethyl ester hydrolysis, depreciating the overall reaction yield. In addition, we speculated that a large excess of cyanamide would force the equilibrium towards the desired product. Therefore, the conditions for formation of the 2-aminoimidazole (**4**) were modified, such that intermediate (**3**) was treated with excess cyanamide under reflux in 70% aqueous EtOH (v/v). To minimise ester hydrolysis, the reaction solution was adjusted to pH 3–4 using 2 M aqueous NaOH. The product (**4**) was isolated by concentration *in vacuo* followed by adjustment of the pH to 8–9 with solid K_2CO_3, and filtration of the precipitate (Scheme 1B). This method resulted in reproducible yields of 48–54% (n = 5) for compound **4**, representing a yield of approximately 80% per step, and an improvement on the previously employed methods, which gave yields of 10–25%.

With the key 2-aminoimidazole intermediate (**4**) in hand, we sought to introduce the nitro functionality *via* diazotisation

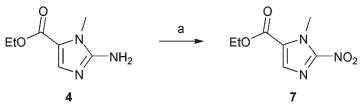

Scheme 2 Diazotisation and nitration of **4**. Reagents and conditions: AcOH, $NaNO_2$ (aq), rt, 4 h, 72%.

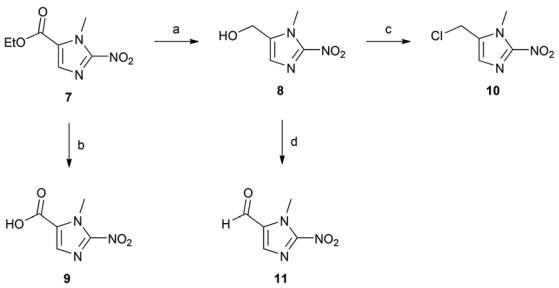

Scheme 3 The introduction of versatile synthetic handles on to the 2-nitroimidazole ring. Reagents and conditions: a. $NaBH_4$, THF, MeOH, 0 °C → rt, 2 h, 66%; b. NaOH (aq.), rt, 2 h, 95%; c. $SOCl_2$, pyridine, CH_2Cl_2, 0 °C → rt, 2 h, 66%; d. MnO_2, acetone, CH_2Cl_2, 3 d, 52%.

of the amino group (Scheme 2). Using the procedure reported by Matteucci *et al.*,[17] which employed a 4.8 M aqueous solution of $NaNO_2$, we found yields of the 2-nitroimidazole product (**7**) were typically 10–20% lower than the reported value of 62%. This procedure was reported on a 37 g scale, and the conditions used seem to be less suitable for more moderate scales of 2–5 g. To minimise the volume of water in the reaction, we used a saturated aqueous solution of $NaNO_2$, and increased the volume of AcOH in the reaction mixture from 50% to 66% (v/v). These modified conditions reliably afforded compound **7** in a yield of 72% (n = 3), and seem optimal for the introduction of the nitro group on a moderate scale.

The 2-nitroimidazole ester **7** represents a versatile synthetic intermediate, which can be transformed into a number of useful compounds that possess suitable chemical handles for attachment to a range of complementary functionalities. Here we include procedures for synthesis of the alcohol (**8**), carboxyl (**9**), chloride (**10**), and carbaldehyde (**11**) derivatives (Scheme 3).[18,20] Each of these intermediates is a useful synthetic substrate for the development of bioreductive prodrugs or dyes.

To demonstrate the utility of our improved synthetic route, we applied it to the synthesis of the Phase III clinical candidate, and bioreductive prodrug, Evofosfamide (TH-302, Scheme 4).

The bromoisophosphoramide mustard intermediate (Br-IPM, **13**), was synthesised from the corresponding 2-bromoethylamine hydrobromide salt (**12**), employing the method reported by Duan *et al.*[16] Subsequent treatment of (**13**) with the 2-nitroimidazole alcohol (**8**) under Mitsunobu conditions,[21] afforded Evofosfamide (TH-302) in 62% yield, which

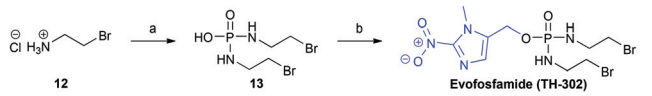

Scheme 4 Synthesis of Evofosfamide (TH-302). Reagents and conditions: a $POCl_3$, Et_3N, CH_2Cl_2, −10 °C; b. PPh_3, DIAD, **8**, THF, 0 °C → rt, 3 h, 62%.

compares well with the previously reported synthesis (48% yield).[16]

In conclusion, we have developed a high yielding, rapid and reliable synthesis of the 2-aminoimidazole ester **4**, which is a key intermediate in the synthesis of many bioreductive prodrugs. We have optimised the nitration conditions for this compound, and demonstrated that the 2-nitroimidazole-based ester **7** can be transformed into a range of synthetically useful derivatives. This work represents a comprehensive and optimised set of synthetic procedures for the synthesis of 2-nitroimidazole derivatives, which are essential components for developing bioreductive prodrugs and dyes. We have demonstrated the utility of our new methodology by applying it in the efficient synthesis of the bioreductive prodrug clinical candidate Evofosfamide (TH-302).

SJC, EMH and LJOC thank MRC for the award of a studentship to LJOC. SJC, EMH and CC-K thank Cancer Research UK for the award of a studentship to CC-K. SJC, EMH and CNGE thank Cancer Research UK and EPSRC for the award of a studentship to CNGE, through the CR-UK and EPSRC Cancer Imaging Centre in Oxford. SJC and JS thank the European Commission for the award of a Marie Curie Fellowship to JS (PIIF-GA-2012-331327, HYPOXPROBE). EMH thanks Cancer Research UK for research funding. SJC thanks St Hugh's College, Oxford, for research funding.

Notes and references

1 T. Rossignol, C. Ding, A. Guida, C. d'Enfert, D. G. Higgins and G. Butler, *Eukaryotic Cell*, 2009, **8**, 550–559.
2 B. A. Smit, D. S. Neuman and M. L. Stachowiak, *Plant Physiol.*, 1990, **92**, 1021–1028.
3 M. C. Drew, *Annu. Rev. Plant Physiol. Plant Mol. Biol.*, 1997, **48**, 223–250.
4 G. L. Semenza, F. Agani, D. Feldser, N. Iyer, L. Kotch, E. Laughner and A. Yu, *Adv. Exp. Med. Biol.*, 2000, **475**, 123–130.
5 M. Höckel and P. Vaupel, *J. Natl. Cancer Inst.*, 2001, **93**, 266–276.
6 J. M. Brown and W. R. Wilson, *Nat. Rev. Cancer*, 2004, **4**, 437–447.
7 W. R. Wilson and M. P. Hay, *Nat. Rev. Cancer*, 2011, **11**, 393–410.
8 E. A. Blanche, L. Maskell, M. A. Colucci, J. L. Whatmore and C. J. Moody, *Tetrahedron*, 2009, **65**, 4894–4903.

Published on 10 July 2015. Downloaded on 06/04/2016 16:58:48.

 This journal is © the Partner Organisations 2015

9 M. A. Colucci, C. J. Moody and G. D. Couch, *Org. Biomol. Chem.*, 2008, **6**, 637–656.
10 T. Fryatt, H. I. Pettersson, W. T. Gardipee, K. C. Bray, S. J. Green, A. Slawin, H. D. Beall and C. J. Moody, *Bioorg. Med. Chem.*, 2004, **12**, 1667–1687.
11 T. Fryatt, D. T. Goroski, Z. D. Nilson, C. J. Moody and H. D. Beall, *Bioorg. Med. Chem. Lett.*, 1999, **9**, 2195–2198.
12 C. Cazares-Korner, I. M. Pires, I. D. Swallow, S. C. Grayer, L. J. O'Connor, M. M. Olcina, M. Christlieb, S. J. Conway and E. M. Hammond, *ACS Chem. Biol.*, 2013, **8**, 1451–1459.
13 G. Asato and B. G, *J. Med. Chem.*, 1972, **15**, 1086–1088.
14 F. P. Tally, V. L. Sutter and S. M. Finegold, *Antimicrob. Agents Chemother.*, 1975, **7**, 672–675.
15 W. J. Ross and W. B. Jamieson, *J. Med. Chem.*, 1975, **18**, 158–161.
16 J.-X. Duan, H. Jiao, J. Kaizerman, T. Stanton, J. W. Evans, L. Lan, G. Lorente, M. Banica, D. Jung, J. Wang, H. Ma, X. Li, Z. Yang, R. M. Hoffman, W. S. Ammons, C. P. Hart and M. Matteucci, *J. Med. Chem.*, 2008, **51**, 2412–2420.
17 M. Matteucci, J.-X. Duan, H. Jiao, J. Kaizerman, S. Ammons and M. H. Hopkins, *US Patent Office*, WO 2007/002931 A2, 2007.
18 B. Cavalleri, R. Ballotta and G. Lancini, *J. Heterocycl. Chem.*, 1972, **9**, 979–984.
19 M. Matteucci, P. Rao and J.-X. Duan, *US Patent Office*, WO 2004/087075 A2, 2004.
20 B. Cavalleri, R. Ballotta, V. Arioli and G. Lancini, *J. Med. Chem.*, 1973, **16**, 557–560.
21 O. Mitsunobu, *Synthesis*, 1981, 1–28.

Published on 10 July 2015. Downloaded on 06/04/2016 16:58:48.

Design, synthesis and evaluation of molecularly targeted hypoxia-activated prodrugs

Liam J O'Connor[1,2], Cindy Cazares-Körner[1–3], Jaideep Saha[1,3], Charles N G Evans[1,2], Michael R L Stratford[2], Ester M Hammond[2] & Stuart J Conway[1]

[1]Department of Chemistry, Chemistry Research Laboratory, University of Oxford, Oxford, UK. [2]Department of Oncology, Cancer Research UK (CRUK)/Medical Research Council (MRC) Institute for Radiation Oncology, University of Oxford, Oxford, UK. [3]These authors contributed equally to this work. Correspondence should be addressed to E.M.H. (ester.hammond@oncology.ox.ac.uk) or S.J.C. (stuart.conway@chem.ox.ac.uk).

Published online 24 March 2016; doi:10.1038/nprot.2016.034

Regions of insufficient oxygen supply—hypoxia—occur in diverse contexts across biology in both healthy and diseased organisms. The difference in the chemical environment between a hypoxic biological system and one with normal oxygen levels provides an opportunity for targeting compound delivery to hypoxic regions by using bioreductive prodrugs. Here we detail a protocol for the efficient synthesis of (1-methyl-2-nitro-1*H*-imidazol-5-yl)methanol, which is a key intermediate that can be converted into a range of 1-methyl-2-nitro-1*H*-imidazole–based precursors of bioreductive prodrugs. We outline methods for attaching the bioreductive group to a range of functionalities, and we discuss the strategy for positioning of the group on the biologically active parent compound. We have used two parent checkpoint kinase 1 (Chk1) inhibitors to exemplify the protocol. The PROCEDURE also describes a suite of reduction assays, of increasing biological relevance, to validate the bioreductive prodrug. These assays are applied to an exemplar compound, CH-01, which is a bioreductive Chk1 inhibitor. This protocol has broad applications to the development of hypoxia-targeted compounds.

© 2016 Macmillan Publishers Limited. All rights reserved.

INTRODUCTION

Background

Regions of low oxygen (hypoxia) occur in a diverse range of biological contexts, including in disease states, bacterial infections and some healthy organs[1,2]. Notably, during tumor development, oxygen supply quickly becomes a growth-limiting factor, because of the high number of metabolically active tumor cells. In response to the problem of inadequate oxygen supply, the process of angiogenesis is initiated to create a tumor vasculature. However, this vasculature has many aberrant features, and although it manages to sustain the tumor it also results in regions of hypoxia, in which only the most aggressive fraction of the tumor cells can survive[3]. These hypoxic regions occur at distances >100 μm from a functional vessel, and they can be both chronic and acute[4]. The oxygen concentration within a tumor is, therefore, extremely heterogeneous and fluctuates substantially[5,6]. Hypoxic cells are resistant to radiotherapy, as the DNA damage induced by radiation, which is required for cell killing, occurs in an oxygen-dependent manner[7]. Therefore, hypoxic cells comprise the most aggressive tumor fraction, and they are the most important to treat in order to improve patient prognosis[8]. Bioreductive prodrugs are biologically inactive molecules, which are converted to an active drug by enzymatic reduction[3]. These drugs harness the substantial differences in chemical environment between hypoxia and normoxia to target drug compounds to these therapeutically challenging tumor regions. This technology is also applicable to targeting compounds to regions of hypoxia in a wide range of other biological settings.

Development of the protocol

We have developed a protocol in which a bioreductive group precursor is synthesized and then coupled to a biologically active molecule so as to abrogate, or substantially reduce, the primary biological activity of the compound. As part of the protocol, we have established a sequence of assays to confirm that the bioreductive group is reduced, that the molecule subsequently fragments, and that the desired active inhibitor is released.

To demonstrate the principle of the concept described above, we attached the bioreductive 4-nitrobenzyl group to a known Chk1 and Aurora A kinase inhibitor, with the aim of targeting this therapeutically relevant compound to areas of hypoxia[9]. We chose compound **6** (**Fig. 1**) as the Chk1 inhibitor to study, as it had a clear structure-activity relationship (SAR) profile that indicated that alkylation of the primary hydroxyl group would result in a substantial loss of activity, and furthermore because such a modification would be synthetically simple. Compound **1** was synthesized and subjected to the reduction assays to determine whether fragmentation occurs, and whether the intact, active kinase inhibitor was consequently released. First, exposure to zinc and ammonium chloride in dimethylformamide (DMF) resulted in the formation of the nitroso- (**4**) and amine-derived (**5**) reduction products. Stirring these products in phosphate buffer at pH 7.4 resulted in fragmentation to give the active kinase inhibitor (**6**). Compound **1** was then treated with bactosomal human NADPH–cytochrome P450 (CYP) reductases in potassium phosphate buffer under hypoxic conditions. Again, reduction and fragmentation to release the active kinase inhibitor (**6**) was observed, whereas under normoxic conditions the prodrug (**1**) was stable. Having shown that compound **1** acted as a bioreductive prodrug, we demonstrated that treatment of RKO, A549, H1299 or H1975 cells resulted in increased DNA damage, consistent with the release of a Chk1 inhibitor, in an oxygen-dependent manner[9].

The work described above used the 4-nitrobenzyl bioreductive group. However, many hypoxia-activated compounds use the 1-methyl-2-nitroimidazole group as the bioreductive functionality (*vide infra*). Despite this common use, synthesis of 1-methyl-2-nitroimidazoles following literature procedures has proven to be challenging. Therefore, to address this problem, we have recently

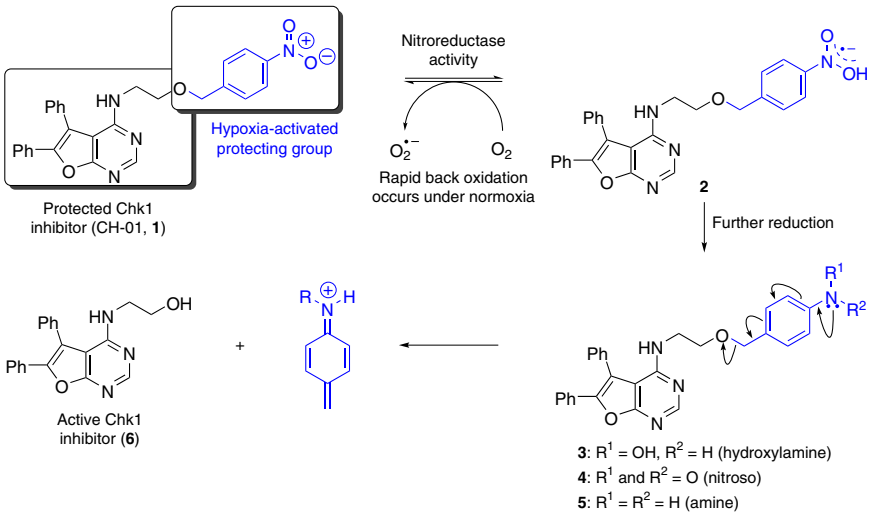

Figure 1 | Attachment of the 4-nitrobenzyl group to the terminal hydroxyl group of the Chk1 inhibitor 6 affords the inactive compound **1**. Under hypoxic conditions, the nitro group is reduced to form an electron-donating substituent, which induces fragmentation and ejects the active Chk1 inhibitor **6** (ref. 9). Reprinted with permission from Cazares-Korner *et al.*[9].

reported a high-yielding, rapid and reliable route to a key intermediate in the synthesis of 1-methyl-2-nitroimidazole-based bioreductive prodrugs[10]. The intermediate can be transformed into 1-methyl-2-nitroimidazole derivatives **14**–**18** (**Fig. 2**) that contain useful synthetic handles for attachment of the bioreductive group to a range of functional groups. Our synthesis builds on the work published by Cavalleri *et al.*[11] and a patent disclosed by Matteucci *et al.*[12].

Applications of the method

To date, we have applied our methodology to demonstrate the oxygen-dependent release of a biologically active compound in tumor cell lines. The next phase of our work will be to demonstrate the targeting of the compounds to the hypoxic fraction of tumors. However, in addition to solid tumors, the occurrence of hypoxia is more widespread throughout biology. For example, areas of the kidney have a much lower oxygen tension than most other parts of the body, and biofilms can also become substantially hypoxic. Consequently, this protocol could potentially be adapted to enable the selective delivery of compounds in these settings.

Comparison with other methods

Most of the previous work in the bioreductive field has focused on the use of bioreductive groups that selectively activate alkylating agents or similar compounds, which cause direct DNA damage and/or other nonspecific cytotoxicity[3]. Examples of such compounds include E09, RH1 and AQ4N, the activation of which is based on a quinone moiety; PR-104 and NLCQ-1, which contain nitroaromatic groups; and SN30000, TPZ and CEN-209, which contain a nitroxide moiety. A number of these agents have been tested clinically, although none are in widespread use. TH-302 is the most advanced agent clinically, and it is currently in phase 2 clinical trials for a variety of cancers (ClinicalTrials.gov identifiers: NCT02093962, NCT01403610, NCT02402062 and NCT00742963). It has also recently entered phase 3 trials, in combination with other therapeutics, for the treatment of metastatic pancreatic cancer and metastatic soft-tissue sarcoma (ClinicalTrials.gov identifiers: NCT01746979 and NCT01440088).

The approach taken in our work is distinct from that described above, as the bioreductive component is appended to the active molecule and functions as the removable component of the prodrug. Therefore, bioreduction only affects the bioreductive protecting-group component of the prodrug, leading to the fragmentation and release of the desired active drug component. Despite not being that widely used to date, there are some examples of the synthesis of biologically active compounds protected by bioreductive groups. An early example of this approach was a prodrug of a poly(ADP-ribose)polymerase (PARP) inhibitor that was protected with a 1-methyl-2-nitroimidazole or a nitrofuran group reported by Parveen *et al.*[13]. In this case, only the chemical reduction of the prodrug was reported. No data on the compound's propensity for bioreduction, or the activity of the protected compound, were included. Damen *et al.*[14] developed a range of paclitaxel-based bioreductive prodrugs with a range of protecting groups attached to the taxol side chain. In most cases, these compounds underwent chemical reduction, and a number of the compounds demonstrated reduced cytotoxicity under normoxic conditions. However, bioreduction of the compounds under hypoxic conditions was not evaluated[14]. A less common 4,7-dioxindole-3-methyl-based prodrug was used by Ferrer *et al.*[15] to release prednisolone with the aim of targeting hypoxic regions in rheumatoid arthritis. Again, reduction was chemically demonstrated using $SnCl_2$, but no bioreduction was reported[15]. Subsequently, 20(*S*)-camptothecin (a DNA topoisomerase I inhibitor)[16], doxorubicin[17], 6-thioguanine[18], lysyl oxidase inhibitors[19], O^6-benzylguanine (O^6-BG, an inhibitor for O^6-alkylguanine-DNA alkyltransferase)[20] and IC86621 (an inhibitor of DNA-dependent protein kinase)[21] have been converted to prodrugs using nitroaryl protecting groups. Fluorescent compounds have been released from a nitroquinoline group[22] or a 4-nitrobenzyl group[23], and inhibitors of vascular endothelial growth factor (VEGF)-induced angiogenesis have been released from 4-nitrobenzyl– or quinone-based prodrugs[24]. An interesting branch of this field is self-inactivating bioreductive groups that quench the inherent electrophilicity of the bioreduction product[25]. In our work, we released a Chk1 and Aurora A kinase inhibitor from a 4-nitrobenzyl-based prodrug and demonstrated an oxygen-dependent effect of the released compound in four cancer cell lines (RKO, A549, H1299 and H1975)[9].

Experimental design

Choice of bioreductive protecting group. Five distinct chemical moieties, nitro groups, quinones, aromatic *N*-oxides, aliphatic *N*-oxides and transition metals, have been identified as being sensitive to bioreduction[3]. The *N*-oxides have been used as bioreductive groups only when the functionality is embedded

© 2016 Macmillan Publishers Limited. All rights reserved.

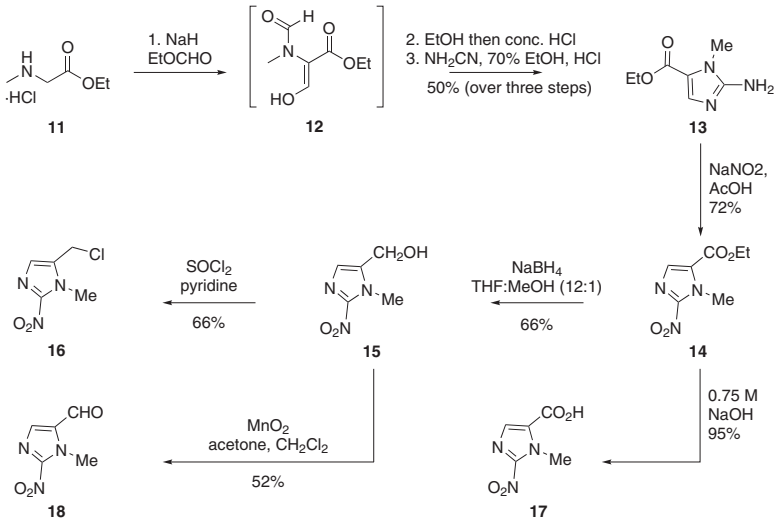

Figure 2 | Synthetic scheme for the preparation of the ester (**14**), hydroxyl (**15**) chloromethyl (**16**), carboxylic acid (**17**) and aldehyde-based (**18**) nitroimidazole derivatives[10].

within the core structure of a molecule. Nitroaryl-based compounds have been used both as bioreductive components embedded in molecules and as groups to trigger fragmentation. For example, the nitrobenzyl moiety is used in the structure of PR-104A, whereas in the case of TH-302 the DNA cross-linking component is released by bioreduction of a nitroimidazole group. Given their widespread use, the nitroaryl-based compounds are among the most amenable for use in the development of a bioreductive prodrug. In addition to the 4-nitrobenzyl and 1-methyl-2-nitroimidazole groups, nitrofuran- and nitrothiophene-based groups have also been used as the basis of bioreductive compounds (*vide supra*). Of these groups, the 4-nitrobenzyl group and the 1-methyl-2-nitroimidazole group have been most extensively used.

In principle, the most important considerations when choosing which bioreductive group to use are its propensity to undergo bioreduction and the oxygen concentration at which this process occurs. However, as oxygen-dependent bioreduction in mammals is thought to occur predominantly via a one-electron mechanism, the propensity of a particular group to undergo bioreduction does not correlate directly with a compound's electrochemical reduction potential. In addition, the instability of the $ArNO_2^-$ radical in water makes measuring these values difficult. The reduction potentials $E(ArNO_2/ArNO_2^-)$ versus the normal hydrogen electrode (NHE) in water at pH 7 for commonly used nitroaryl bioreductive groups have been estimated and are shown in **Figure 3** (ref. 26); a smaller negative value indicates that the group undergoes more facile reduction. As can be seen, the 1-methyl-2-nitroimidazole group (**9**) and the nitrothiophene-based group (**8**) have the same reduction potential, whereas the 4-nitrobenzyl group (**10**) has a more negative reduction potential, indicating that it undergoes less facile reduction. These observations can potentially be used to tune the sensitivity of the prodrug to the particular hypoxic environment to which it is to be targeted. Although values determined from the NHE are suitable guidelines, the reduction rate of the compound is also dependent on a number of other factors, including the local pH (ref. 26). In addition, the propensity of the drug component to be a good leaving group has a role in the rate of its release. It is therefore possible that under certain circumstances reduction of the protecting group might not lead to fragmentation of the prodrug.

The reagents required to attach the 4-nitrobenzyl, nitrofuran- and nitrothiophene-based groups to biologically active compounds are readily available from commercial sources. The precursors for attaching the 1-methyl-2-nitroimidazole group are less readily available, and hence we have developed an optimized protocol for the synthesis of a range of derivatives with useful synthetic handles for attachment to biologically active compounds (**Fig. 2**). Of the various conditions that were previously reported for this transformation, we found the optimal method to be treatment of sarcosine ethyl ester with ethyl formate and sodium hydride in a formylation step[10]. Removal of the unwanted *N*-formyl under acidic conditions and then treatment with cyanamide in acidified ethanol afforded aminoimidazole **13**. Diazotization with sodium nitrite afforded the nitroimidazole **14**, which can be viewed as the first useful product of this synthesis when developing bioreductive prodrugs. The ester can be hydrolyzed to acid **17**, or it can be reduced directly to alcohol **15**. Alcohol **15** was transformed to chloride **16** by treatment with thionyl chloride and pyridine; the procedures that were used to obtain the corresponding bromide typically resulted in lower yields. Oxidation of **15** using MnO_2 gave the aldehyde **18** (ref. 10).

The synthetic availability of the ester **14**, alcohol **15**, chloride **16** and acid **17** derivatives affords some flexibility to the process of attaching the bioreductive group to the biologically active entity. Some useful methods for coupling the two components are shown in **Figure 4**. The hydroxyl group can be coupled directly to an acid chloride, or it can be coupled to a carboxylic acid using standard ester coupling conditions. The hydroxyl group can also be converted into a good leaving group, which enables a hydroxyl group in the biologically active compound to act as a nucleophile to achieve alkylation. The carboxylic acid can be coupled to a hydroxyl group using standard coupling conditions, or the ester could be directly coupled. Oxidation of the hydroxyl group to yield the aldehyde allows attachment of the bioreductive group to an amine in the biologically active compound. However, consideration must be given to the generally poor leaving-group ability of amines. An alternative option is coupling of the amine with a chloroformate, to yield the carbamate. Fragmentation of amines

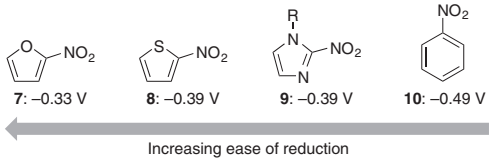

Figure 3 | Estimated values of reduction potentials $E(ArNO_2/ArNO_2^-)$ versus NHE in water at pH 7 for commonly used nitroaryl bioreductive systems (**7**–**10**)[26]. R = alkyl or hydroxyalkyl.

© 2016 Macmillan Publishers Limited. All rights reserved.

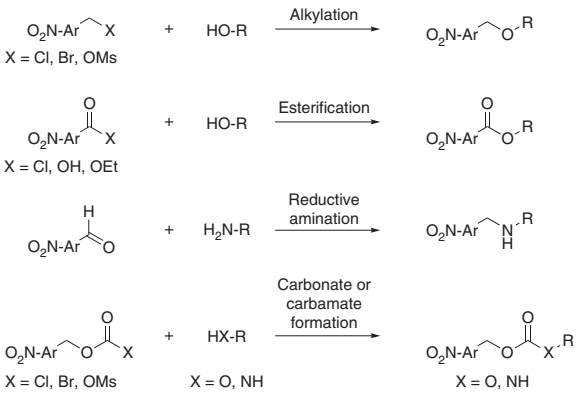

Figure 4 | Possible methods of attaching the bioreductive group (O_2N-Ar) to the biologically active compound (R).

via a carbamate intermediate might improve the fragmentation of the prodrug.

Position of protecting-group attachment. For the bioreductive prodrug to be effective, the unreduced, protected form of the compound must be inactive at its primary cellular target, or it should at least show substantially reduced activity as compared to that of the compound released upon fragmentation. To achieve the required difference in activity, the bioreductive group must be attached to a functional group that is important for the biological activity of the released compound. In the case of CH-01, the kinase inhibitor **6** was selected to form the basis of the molecule, as a very clear SAR had been established in the initial publication, indicating that modification of the hydroxyl group resulted in a marked loss of activity (**Fig. 5**)[27]. Substitution of the hydroxyl is thought to reduce activity by disrupting an intramolecular hydrogen bond, but also because the 4-nitrobenzyl group is too large to reside in the ATP-binding pocket of Chk1, as based on X-ray crystal structure analysis.

Subsequent work focused on another Chk1 inhibitor (**19**), which afforded greater choice in positions to attach the bioreductive group than that of compound **6**. On the basis of the analysis of an X-ray crystal structure of **19** bound to Chk1, it was decided that the bioreductive group should be attached to the 1-position of the 1*H*-pyrazolo[3,4-*b*]pyridine ring, as this nitrogen atom donated a key hydrogen bond to the kinase hinge region; this interaction is essential for compound binding (**Fig. 5**). Using a ^{32}P-ATP filter–binding assay, it was observed that substitution with a bioreductive group at the hydroxyl position of **6**, and at the 1-position of the pyridine ring of **19**, led to a large reduction in Chk1 affinity as compared with the unsubstituted analogs.

In general, once the prodrug has been synthesized, comparison of the biological activity of the parent compound in the same assay, at the same time, is essential before the work progresses. In addition, it is useful to assess the general cytotoxicity of the prodrug at this stage to ensure that the compound is suitable for use in cells.

Assessment of the reduction and bioreduction of a prodrug. To demonstrate the application of our protocol, the assays described have been used to assess the reduction behavior of compound **1**, as a representative bioreductive prodrug. Users of this protocol may apply the assays described directly to any other bioreductive prodrug compound, making necessary changes where applicable to molecular weight and concentration calculations.

To determine whether the prodrug fragments as expected to give the desired product, we have developed a sequence of reduction and bioreduction assays that assess the behavior of a hypoxia-activated prodrug. In the first instance, the prodrug is treated with Zn powder and NH_4Cl in DMF for a given time (typically between 0.5 and 24 h), followed by stirring in potassium phosphate buffer at pH 7.4 for 24 h (see Steps 2 and 3). The fragmentation of the prodrug is analyzed using HPLC. As most of the nitroaryl groups are reduced under these conditions, this experiment determines whether the prodrug will fragment upon reduction. In addition, as the HPLC retention time of the desired active compound will be predetermined, the experiment also confirms that the expected fragmentation product is obtained. This aspect of the protocol is only suitable when the prodrug does not contain other functionalities that are reduced under the conditions described (e.g., aryl halides).

The second experiment is used to assess the propensity of the prodrug to undergo bioreduction when treated with bactosomal human NADPH-CYP reductases[9]. Compound **1** is again used as a representative compound for this assay (see protocol Step 4). As there are many mechanisms by which a nitroaryl-based prodrug can be reduced *in vivo*, and the pathways will likely vary between cell lines and types, it is not feasible to definitively assess all possible modes of enzymatic reduction *in vitro*. However, NADPH-CYP reductases are known to reduce nitroaryl groups *in vivo* in an oxygen-dependent manner, and hence they provide a useful model system to predict the likelihood of the prodrug undergoing bioreduction *in vivo*. LC-MS analysis of the reductase reaction mixture at given time points (0.5–48 h) enables confirmation of the reduction. In addition, it is sometimes possible to identify intermediates in the reduction pathway, including the hydroxylamine, nitroso and amine derivatives, which are produced before fragmentation to give the final product. An absence of reduction in a normoxia control experiment will provide evidence for the reduction being oxygen-dependent and enzyme-mediated.

The final analysis of the prodrug assesses its bioreduction in a representative cell line. Here we describe the procedure using cultured RKO (colorectal) cells; however, we have found that HCT116, OE21, A549, HepG2 and H1299 cells are also suitable

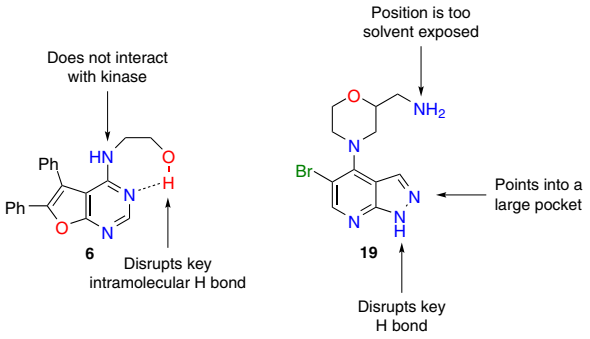

Figure 5 | Analysis of possible positions to which a bioreductive group may be attached on compounds **6** and **19**.

© 2016 Macmillan Publishers Limited. All rights reserved.

for these experiments (see protocol Step 5). The chosen cells are treated with the compound under either normoxic or hypoxic conditions, the cells are lysed, and the parent compound and its metabolites are analyzed by HPLC and/or LC-MS. For initial testing, we have found the use of almost anoxic conditions (<0.1% O_2) to be ideal, but this approach can then be extended to studies at milder levels of hypoxia (e.g., 0.5–2% O_2).

Limitations

A number of potential limitations exist for this protocol that should be highlighted. (i) It might not be possible to attach the bioreductive group to the bioactive compound in a manner that sufficiently disrupts the biological activity of the parent molecule. (ii) The leaving-group ability (pKa) of the atom to which the bioreductive group is attached has an important role in the overall fragmentation process. Attachment of the bioreductive group to a poor leaving group will result in the stalling of the fragmentation process once the nitro group has been reduced. This limitation can be potentially overcome by attaching the bioreductive group to the parent molecule via a linker (e.g., a carbonate group) that itself is a good leaving group and will enhance the overall fragmentation process. (iii) The zinc reduction assay is not compatible with compounds that contain functional groups that are unstable under the reaction conditions. Under these circumstances, alternative chemical conditions for the reduction of the nitroaryl group can be used[28].

MATERIALS

REAGENTS

! CAUTION Most of the reagents and solvents used in the protocol should be handled with care, and they require the use of protective goggles, gloves and lab coats. All manipulations must be performed in well-ventilated laboratory fume hoods.

Chemical synthesis

- Tetrahydrofuran (THF; Sigma-Aldrich, cat. no. 34865)
- Methanol (MeOH; Sigma-Aldrich, cat. no. 34860)
- Dichloromethane (CH_2Cl_2; Sigma-Aldrich, cat. no. 34856)
- Acetic acid (AcOH; Sigma-Aldrich, cat. no. 320099)
- Acetone (Sigma-Aldrich, cat. no. 34850)
- Ethanol (EtOH; Sigma-Aldrich, cat. no. 32221)
- Hexane (Sigma-Aldrich, cat. no. 34859)
- Ethyl acetate (EtOAc; Sigma-Aldrich, cat. no. 34858)
- Petroleum ether (PE, 40–60 °C boiling point; Sigma-Aldrich, cat. no. 34491)
- *N*,*N*-Dimethylformamide (DMF; Sigma-Aldrich, cat. no. D4551)
- Pyridine, anhydrous (Sigma-Aldrich, cat. no. 270970)
- Acetonitrile (CH_3CN; Sigma-Aldrich, cat. no. 34851)
- Sarcosine ethyl ester hydrochloride (Sigma-Aldrich, cat. no. 255084)
- Ethyl formate (Sigma-Aldrich, cat. no. 112682)
- Sodium hydride (NaH, 60% dispersion in mineral oil; Sigma-Aldrich, cat. no. 452912) **! CAUTION** NaH is pyrophoric, and it can cause severe burns on skin contact. It reacts violently with alcohols and water and liberates hydrogen gas. Excess NaH can be quenched with 2-propanol.
- Cyanamide (Sigma-Aldrich, cat. no. 187364)
- Sodium nitrite ($NaNO_2$; Sigma-Aldrich, cat. no. 237213)
- Sodium borohydride ($NaBH_4$; Fisher Scientific, cat. no. 10409190)
- Trifluoroacetic acid (TFA; Sigma-Aldrich, cat. no. 302031)
- Trichloroacetic acid (TCA; Sigma-Aldrich, cat. no. T6399)
- Formic acid (FA; Sigma-Aldrich, cat. no. 56302)
- Concentrated hydrochloric acid (conc. HCl; Fisher Scientific, cat. no. 10251183) **! CAUTION** conc. HCl is corrosive and it can cause severe burns on skin contact.
- Sodium sulfite (Na_2SO_3; Sigma-Aldrich, cat. no. 239231)
- Magnesium sulfate ($MgSO_4$; Fisher Scientific, cat. no. 10224680)
- Potassium carbonate (K_2CO_3; Fisher Scientific, cat. no. 10121440)
- Sodium hydrogen carbonate ($NaHCO_3$; Fisher Scientific, cat. no. 10020510)
- Sodium hydroxide (NaOH; Fisher Scientific, cat. no. 10306200) **! CAUTION** NaOH is corrosive and can cause severe burns on skin contact.
- Sodium chloride (NaCl; Fisher Scientific, cat. no. 10112640)
- Thionyl chloride ($SOCl_2$; Sigma-Aldrich, cat. no. 88952) **! CAUTION** $SOCl_2$ is corrosive and can cause severe burns on skin contact.
- Manganese(IV) dioxide (MnO_2; Sigma-Aldrich, cat. no. 243442)
- Argon gas (BOC, cat. no. 2936780)

Chemical reduction (see Steps 2 and 3)

- Zinc dust (Sigma-Aldrich, cat. no. 209988)
- Ammonium chloride (Fisher Scientific, cat. no. 10060030)
- *N*,*N*-Dimethylformamide (DMF; Sigma-Aldrich, cat. no. D4551)
- DMSO (Sigma-Aldrich cat. no. D8418)
- K_2HPO_4 buffer, 0.5 M, pH 7.4 (BD Gentest, cat. no. 451201)

Bioreductive assays (see Steps 4 and 5)

- DMSO (Sigma-Aldrich, cat. no. D8418)
- Solution A (comprises $MgCl_2$, $NADP^+$ and glucose-6-phosphate; Corning, cat. no. 451220)
- Solution B (comprises glucose-6-phosphate dehydrogenase; Corning, cat. no. 451200)
- K_2HPO_4 buffer, 0.5 M, pH 7.4 (BD Gentest, cat. no. 451201)
- Bactosomal human NADPH-CYP reductases (Cypex, cat. no. CYP004)
- Acetonitrile (CH_3CN; Sigma-Aldrich, cat. no. 34851)
- RKO cells (Colorectal; American Type Culture Collection (ATCC), cat. no. ATCC CRL-2577) **▲ CRITICAL** This protocol uses, but is not limited to, RKO (colorectal) cells as a representative cell line for use in bioreductive experiments. We have found that HCT116, OE21, A549, HepG2 and H1299 cells are also suitable for these experiments. Purchase and culture details can be found at http://lgcstandards-atcc.org/ **! CAUTION** Regularly check that the cell lines used in your research match their recognized cell line identity criteria and are not infected with mycoplasma.
- DMEM (Sigma-Aldrich, cat. no. D6046)
- FBS (Autogen Bioscience, cat. no. S0615)
- Penicillin-streptomycin (Life Technologies, cat. no. 15140-122)
- PBS, 1× (Fisher Scientific, cat. no. 10173433)

EQUIPMENT

General

- Refrigerators (−80, −20 and 4 °C)
- Access to analytical facilities (HPLC, LC-MS, NMR and high-resolution MS (HRMS))

Chemistry

- Analytical weighing balance
- Spatulas
- Round-bottom flasks
- Teflon-coated magnetic stir bars
- Rubber septa
- Disposable syringes and needles
- Balloons (for creating inert atmospheres in flasks)
- Hotplate stirrers
- Oil bath (equipped with silicone oil)
- Silica thin-layer chromatography (TLC) plates (Silica gel 60 F254, Merck)
- Capillary spotters
- TLC developing chamber
- Methods for visualizing TLC (UV-lamp or dips ($KMnO_4$, 4-anisaldehyde, phosphomolybdic acid stains))
- Universal indicator paper
- Rotary evaporator with water bath
- Sintered funnel
- Conical flasks
- Separating funnels (50, 100 and 250 ml)
- Glass columns for column chromatography (diameters: 30, 20 and 10 mm)
- Celite 545 (Sigma-Aldrich, cat. no. 419931)
- Silica gel for column chromatography (Geduran Si 60; Merck-Millipore, cat. no. 111567)
- Plastic funnel

© 2016 Macmillan Publishers Limited. All rights reserved.

- Test tubes
- Measuring cylinders
- Vacuum gas manifold (Schlenk line)
- Heavy-duty rubber tubing (for manifold)
- Vacuum pump
- Desiccator (for drying samples under high vacuum)
- Solvent purifier (MBraun SPS-800)
- Distillation apparatus
- Filter tips (Supelco, Iso-Disc filters, polytetrafluoroethylene (PTFE)-4-4, size × porosity: 4 mm × 0.45 µm)

Biology

- Bactron II anaerobic chamber (Shell Labs) or similar hypoxia chamber
- Whitley H35 Hypoxystation (Don Whitley) or similar controlled oxygen chamber
- Aerobic incubator (37 °C)
- Standard incubator for mammalian tissue culture, maintained at 37 °C, 21% O_2 and 5% CO_2
- Sterile distilled water
- HPLC vials
- Screw-cap vials
- Cell culture hood
- Bench-top light microscope
- Cell culture flasks
- Falcon conical centrifuge tubes
- Pipetboy pipette controller
- Pipettes
- Neubauer chamber (basic hemocytometer)
- Microcentrifuge tubes
- Centrifuge
- Cell scrapers
- Glass Petri dishes, 6 cm

EQUIPMENT SETUP

Analytical HPLC to identify reaction products In this protocol, HPLC analysis was carried out on a PerkinElmer Flexar system with a binary LC pump and UV-visible LC detector and a Dionex Acclaim 120 column (5 µm, 150 × 4.6 mm), although other similar systems may be used. Use a 10-min gradient as shown below, in which solvent A is 95% H_2O, 5% (vol/vol) MeCN + 0.1% (vol/vol) TFA and solvent B is 5% (vol/vol) H_2O, 95% (vol/vol) MeCN + 0.1% (vol/vol) TFA. The flow rate is 1 ml/min, and data are collected at 254 nm or 360 nm unless otherwise stated.

Time (min)	% A	% B
0–2	60	40
2–12	60–0	40–100
12–14	0	100
14–15	0–60	100–40
15–20	60	40

Analytical HPLC to determine compound purity Carry out HPLC analysis on a Waters 2695 system using a Hichrom RPB column (100 × 3.2 mm, 35 °C) or a Gemini-NX column (150 × 3.0 mm, 35 °C). Other similar HPLC systems may be used. Separation is achieved at a flow rate of 0.5 ml/min with a gradient of MeCN in 10 mM aqueous formic acid over 6 min when using the RPB column. For compound detection, use a photodiode array spectrophotometer (Waters 2996) and a mass spectrometer (Waters Micromass ZQ mass spectrometer). Injections of approximately 10 µl are made. Inject samples dissolved in DMSO, MeCN, H_2O or a mixture thereof.

PROCEDURE

Synthesis of compound 13 ● TIMING 8–10 h

▲ CRITICAL The drug of interest will be functionalized with a group that is reduced under hypoxic conditions (**Fig. 1**). Once it is reduced, the active drug is released. A number of hypoxia-activated protecting groups may be selected, including those listed in **Figures 2** and **3**. Some of the hypoxia-activated protecting-group precursors are commercially available. We include a procedure for the preparation of the nitroimidazole derivatives shown in **Figure 2**. These derivatives are not commercially available and are excellent candidates for derivatization. If you are using a commercially available compound to derivatize your drug, skip to Step 26A to begin reduction studies. The bioreductive properties of the hypoxia-activated drug need to be determined, as described in Step 26A–D. For these steps, we have used the example CH-01. Should the reader desire to use CH-01 as a control compound, details concerning synthesis and analytical data for this molecule can be found in Cazares-Korner *et al.*[9].

1| Add 2.00 g of sarcosine ethyl ester hydrochloride, **11** (0.013 mol), to a 500-ml round-bottom flask equipped with a Teflon-coated magnetic stir bar.

▲ CRITICAL STEP If the commercial sarcosine hydrochloride is not in a powder form, we recommend grinding it in a mortar and pestle before addition.

2| Add 45 ml of ethyl formate and 45 ml of THF to the reaction flask to form a suspension. Stir the suspension vigorously. Add 5 g of NaH (60% dispersion in mineral oil, 0.13 mol) slowly at ambient temperature (typically 18–21 °C in our laboratory) under an atmosphere of nitrogen or argon, and stir it for 3 h. A pale-yellow suspension should form.

! CAUTION NaH is pyrophoric and can cause severe burns on skin contact. It reacts violently with alcohols and water and liberates hydrogen gas. This step should be performed carefully with portion-wise addition, and it should be done in a well-ventilated fume hood. For reaction scales over 5 g, cool the reaction mixture to 0 °C and vent the flask with a needle outlet. Necessary precautions against any fire and explosion should be taken.

? TROUBLESHOOTING

3| Concentrate the reaction mixture on a rotary evaporator at 40 °C for ~20 min, or until it is dry. Triturate the resulting yellow solid with 75 ml of hexane to remove the mineral oil, and then decant the hexane off from the solid. Repeat the trituration with 75 ml of hexane.

© 2016 Macmillan Publishers Limited. All rights reserved.

4| Dry the pale-yellow solid under reduced pressure on a rotary evaporator at 40 °C for ~10 min.

5| Re-equip the flask containing the yellow solid with a Teflon-coated magnetic stir bar.

6| Add 40 ml of absolute EtOH and 8 ml of concentrated aqueous HCl solution. Reflux the reaction mixture under reflux for 2 h. A colorless solid should form, and the supernatant reaction solution should be pale yellow.
! CAUTION Add concentrated HCl slowly, in an open flask in a well-ventilated area, as liberation of HCl gas can occur.

7| Remove the colorless solid by filtration while hot, through a sintered funnel into a clean 500-ml round-bottom flask. Wash the colorless solid in the sintered funnel with 30 ml of boiling absolute EtOH, twice. Combine the filtrates, and remove the EtOH under reduced pressure on a rotary evaporator at 40 °C for ~30 min.

8| Dilute the remaining aqueous solution that results from concentration *in vacuo* (Step 7) with 70 ml of absolute EtOH and 30 ml of distilled H_2O. Adjust the pH of the solution to 3, as determined by universal indicator paper, using a 2 M aqueous solution of NaOH.

9| Add 1.09 g of cyanamide (0.026 mol) to the solution and heat it under reflux for 1.5 h. Allow the reaction solution to cool to ambient temperature, and concentrate the reaction solution to ~1/8 of the original volume under reduced pressure on a rotary evaporator at 50 °C for ~20 min.

10| Adjust the pH of the solution to 8–9, using solid K_2CO_3, as determined by universal indicator paper.
▲ CRITICAL STEP Upon approaching pH 8–9, a pale-yellow solid will begin to precipitate, which is the desired product coming out of solution. Stir or swirl the aqueous solution when adding solid K_2CO_3 to avoid localized effervescence.

11| Remove the solid from the mixture by filtration using a sintered funnel. Wash the solid with 20 ml of 1 M aqueous K_2CO_3 solution. Wash the solid with 10 ml of distilled H_2O, twice.

12| Dry the solid, compound **13**, under high vacuum for 24 h. The expected yield for intermediate **13** is 50% (1.10 g over three steps, $n = 5$).

13| Characterize and check the purity of the compound by NMR (^1H and ^{13}C), MS and HPLC analysis. The R_f value of the product is 0.42 in 1:9 (vol/vol) MeOH:CH_2Cl_2. Methods for compound characterization and analytical data can be found in the **Supplementary Data**.
■ PAUSE POINT Compound **13** can be stored at ambient temperature for 6 months.

Synthesis of compound 14 ● TIMING 4–6 h
14| Add 0.97 g of compound **13** (0.0057 mol) and 10 ml of glacial acetic acid to a 100-ml round-bottom flask equipped with a Teflon-coated magnetic stir bar.

15| Dissolve 3.95 g of $NaNO_2$ (0.057 mol) in 5 ml of H_2O. Add this solution to the flask from Step 14 dropwise via a syringe, and then stir the reaction at ambient temperature for 4 h.
▲ CRITICAL STEP In our hands, conducting the reaction in an overall lower proportion of aqueous AcOH led to reduced yield of the desired product. We suggest a final reaction solution of ~66% (vol/vol) aqueous AcOH for the reaction, which in our hands resulted in a yield of 72%.

16| Check the progress of the reaction by TLC analysis. The R_f value of the desired product **14** is 0.85 in a 1:9 (vol/vol) mixture of MeOH and CH_2Cl_2.

17| After completion of the reaction, transfer the reaction mixture into a 50-ml separating funnel and extract the product with 20 ml of CH_2Cl_2. Wash the organic layer with 20 ml of brine, followed by 20 ml of saturated aqueous Na_2SO_3 solution. Dry the organic layer over anhydrous $MgSO_4$ (10 g) to remove the residual water. Remove the $MgSO_4$ by filtration, and then concentrate the filtrate under reduced pressure on a rotary evaporator at 40 °C for ~10 min.

18| Dissolve the residue from Step 17 in 3 ml of CH_2Cl_2, and adsorb onto Celite under reduced pressure on a rotary evaporator at 40 °C for ~5 min, or until it is dry.

© 2016 Macmillan Publishers Limited. All rights reserved.

19| Load the Celite onto a silica gel (Geduran Si 60) column (30 mm in diameter), and elute the column with CH_2Cl_2 (typically 2–3 column volumes) under nitrogen pressure (flash chromatography), collecting 10-ml fractions.

20| Run TLC analysis of the fractions to identify compound **14**, and then combine the desired fractions. The R_f value of the desired product is 0.85 in a 1:9 (vol/vol) mixture of MeOH and CH_2Cl_2. Remove the CH_2Cl_2 under reduced pressure on a rotary evaporator at 40 °C for ~20 min or until dry.

21| Dry the resulting solid, compound **14**, under high vacuum for 1 h.

22| The expected yield for compound **14** is 72% (0.83 g, $n = 3$) as a pale-yellow solid.

23| Characterize and check the purity of the compound by NMR (^1H and ^{13}C), MS and HPLC analysis. Methods for compound characterization and analytical data can be found in the **Supplementary Data**.
■ **PAUSE POINT** Compound **14** can be stored at ambient temperature for 3 months.

24| Compound **14** is the first useful product of this synthetic procedure, and it could be attached to a biologically active compound via an ester coupling reaction (Step 25; **Fig. 4**). Refer to **Figure 2** in order to proceed with the synthetic route applicable to the functional group required. Compound **15** is prepared by following the steps in option A. Compound **16** is prepared by following the steps in options A and B. Compound **17** is prepared by following the steps in option C. Compound **18** is prepared by following the steps in options C and D.

(A) Synthesis of compound 15 ● **TIMING 3–5 h**

(i) Add 0.23 g of compound **14** (0.0012 mol) to a 50-ml oven-dried round-bottom flask equipped with a Teflon-coated magnetic stir bar and a rubber septum. Flush the flask with argon by inserting a needle attached with a balloon filled with argon gas.

(ii) Dissolve the compound by adding 6 ml of anhydrous THF and 0.5 ml of MeOH. Cool the solution to 0 °C using an ice bath.

(iii) Add to the reaction mixture at 0 °C 0.13 g of $NaBH_4$ (0.0035 mol) portion-wise and stir for 45 min and then at ambient temperature for 1 h.

(iv) Cool the reaction mixture to 0 °C using an ice bath. Quench the reaction by adding ice (10 g) to the reaction mixture.

(v) Allow the reaction mixture to warm to ambient temperature, and adjust the pH of the solution to 7, as determined by universal indicator paper, using 1 M aqueous HCl solution.

(vi) Saturate the aqueous solution with solid NaCl, and then transfer the resulting mixture to a 50-ml separating funnel.
▲ **CRITICAL STEP** The aqueous layer must be saturated to drive the desired organic components into the organic solvent used in the next step.

(vii) Extract the organic components with EtOAc (5 × 15 ml). Combine the organic layers and transfer them to a 250-ml separating funnel, and then wash them with 60 ml of a saturated aqueous $NaHCO_3$ solution. Dry the organic layers over anhydrous $MgSO_4$ (20 g) to remove the residual water. Remove the $MgSO_4$ by filtration, and then concentrate the filtrate under reduced pressure on a rotary evaporator at 40 °C for ~20 min or until dry.

(viii) Dissolve the residue from Step 24A(vii) in 3 ml of CH_2Cl_2 and adsorb onto Celite under reduced pressure on a rotary evaporator at 40 °C for ~5 min or until dry.

(ix) Load the Celite onto a silica gel (Geduran Si 60) column (20 mm diameter), and elute the column with PE and EtOAc (gradient, 50–100% (vol/vol) EtOAc, typically 6–7 column volumes) under nitrogen pressure (flash chromatography), collecting 5-ml fractions.

(x) Run TLC analysis of the fractions to identify **15**, and then combine the desired fractions. The R_f value of the product is 0.5 in 9:1 (vol/vol) mixture of CH_2Cl_2 and MeOH. Remove the EtOAc under reduced pressure on a rotary evaporator at 40 °C for ~20 min or until dry.

(xi) Further dry the resulting solid, compound **15**, under high vacuum for 1 h.

(xii) The expected yield for compound **15** is 66% (0.11 g, $n = 3$) as a pale yellow solid.

(xiii) Characterize and check the purity of the compound by NMR (^1H and ^{13}C), MS and HPLC analysis. Methods for compound characterization and analytical data can be found in the **Supplementary Data**.
■ **PAUSE POINT** Compound **15** can be stored at ambient temperature for 12 months.

(B) Synthesis of compound 16 ● **TIMING 4–6 h**

(i) Add 0.20 g of compound **15** (0.0013 mol) to an oven-dried 50-ml round-bottom flask equipped with a Teflon-coated magnetic stir bar and a rubber septum.

(ii) Flush the flask with argon by inserting a needle attached with a balloon filled with argon gas.

(iii) Dissolve the compound by adding 8 ml of CH_2Cl_2 to the flask. Add 0.3 ml of distilled pyridine (0.0036 mol, 2.9 equivalents (eq.)) via a syringe and needle, and then cool the reaction mixture to 0 °C using an ice bath.

© 2016 Macmillan Publishers Limited. All rights reserved.

(iv) Prepare a separate solution of thionyl chloride (0.28 ml, 0.0039 3 eq.) in CH_2Cl_2 (2 ml), and add it to the reaction solution, dropwise at 0 °C, via a syringe and a needle. Stir the resulting solution at 0 °C for 1 h, followed by a further 1 h at ambient temperature.

(v) Check the progress of the reaction by TLC analysis. The R_f value of the product is 0.4 in 1:1 (vol/vol) mixture of EtOAc and PE.

(vi) Quench the reaction by the addition of ice (5 g) to it, followed by 5 ml of saturated aqueous $NaHCO_3$ solution. Transfer the solution to a 100-ml separating funnel and add H_2O (10 ml).
! CAUTION Addition of concentrated saturated aqueous $NaHCO_3$ should be done slowly with vigorous stirring in an open flask, as effervescence can occur.

(vii) Extract the organic components with CH_2Cl_2 (2 × 15 ml). Combine the organic layers, and then wash them with 30 ml of brine. Dry the organic layers over anhydrous $MgSO_4$ (10 g) to remove the residual water. Remove the $MgSO_4$ by filtration, and concentrate the filtrate under reduced pressure on a rotary evaporator at 40 °C for ~10 min or until dry.

(viii) Dissolve the residue from Step 24B(vii) in 1 ml of EtOAc and adsorb onto Celite under reduced pressure on a rotary evaporator at 40 °C for ~5 min or until dry.

(ix) Load the Celite onto a silica gel (Geduran Si 60) column (20 mm in diameter), and elute the column with PE and EtOAc (gradient, 50–100% (vol/vol) EtOAc, (typically 7–8 column volumes) under nitrogen pressure (flash chromatography), collecting 5-ml fractions.

(x) Analyze the fractions by TLC to identify compound **16**, and combine the desired fractions. The R_f value of the product is 0.4 in 1:1 (vol/vol) mixture of EtOAc and PE. Remove the EtOAc under reduced pressure on a rotary evaporator at 40 °C for ~20 min or until dry.

(xi) Dry the resulting solid, compound **16**, under high vacuum for 1 h.

(xii) The expected yield for compound **16** is 66% (0.11 g, $n = 2$) as a pale-yellow solid.

(xiii) Characterize and check the purity of the compound by NMR (^1H and ^{13}C), MS and HPLC analysis. Methods for compound characterization and analytical data can be found in the **Supplementary Data**.
■ PAUSE POINT Compound **16** can be stored at 0 °C for 2 months.

(C) Synthesis of compound 17 ● TIMING 2–3 h

(i) Add 0.10 g of compound **14** (0.0005 mol) to a 10-ml round-bottom flask equipped with a Teflon-coated magnetic stir bar and rubber septum.

(ii) Add to the round-bottom flask 2 ml of aqueous 0.75 M NaOH solution, and stir the resulting suspension at ambient temperature for 2 h. After this time, a homogeneous solution will form.

(iii) Adjust the pH of the reaction mixture to 1, as determined by universal indicator paper, using concentrated aqueous HCl solution. Upon approaching a pH value of 1, an off-white precipitate forms. Add 15 ml of EtOAc to the reaction mixture, and transfer it to a 100-ml separating funnel.

(iv) Extract the organic components with EtOAc (4 × 15 ml). Combine the organic layers and dry them over anhydrous $MgSO_4$ (20 g) to remove the residual water. Remove the $MgSO_4$ by filtration, and then concentrate the filtrate under reduced pressure on a rotary evaporator at 40 °C for ~20 min or until dry.

(v) Further dry the resulting solid under high vacuum for 2 h.

(vi) The expected yield for compound **17** is 95% (0.082 g, $n = 2$) as an off-white solid.

(vii) Characterize and check the purity of the compound by NMR (^1H and ^{13}C), MS and HPLC analysis. Methods for compound characterization and analytical data can be found in the **Supplementary Data**.
■ PAUSE POINT Compound **17** can be stored at ambient temperature for 6 months.

(D) Synthesis of compound 18 ● TIMING 3 d

(i) Add 0.05 g of compound **15** (0.00031 mol) and 0.16 g of MnO_2 (0.0018 mol) to a 10-ml round-bottom flask equipped with a Teflon-coated magnetic stir bar and a rubber septum.

(ii) Flush the flask with argon by inserting a needle attached with a balloon filled with argon gas.

(iii) Dissolve the compound by adding 2.7 ml of CH_2Cl_2 and 0.7 ml of acetone to the round-bottom flask via a syringe and a needle. Stir the reaction mixture at ambient temperature for 3 d.

(iv) Filter the reaction mixture through a bed of Celite to remove the MnO_2, and then wash the Celite with CH_2Cl_2 (10 ml). Combine the filtrates, and then concentrate them under reduced pressure on a rotary evaporator at 40 °C for ~10 min or until dry.

(v) Dissolve the residue in 2 ml of acetone, and then adsorb it onto Celite under reduced pressure on a rotary evaporator at 40 °C for ~5 min or until dry.

(vi) Load the Celite onto a silica gel (Geduran Si 60) column (10 mm in diameter), and elute the column with PE and acetone (1:1 (vol/vol), typically 4–5 column volumes) under nitrogen pressure (flash chromatography), collecting 5-ml fractions.

© 2016 Macmillan Publishers Limited. All rights reserved.

(vii) Analyze the fractions by TLC to identify compound **18**, and then combine the desired fractions. The R_f value of the product is 0.7 in a 1:1 (vol/vol) mixture of acetone and PE. Remove the volatile components under reduced pressure on a rotary evaporator at 40 °C for ~20 min or until dry.

(viii) Dry the resulting solid, compound **18**, under high vacuum for 1 h.

(ix) The expected yield for compound **18** is 52% (0.025 g, $n = 2$) as a colorless solid.

(x) Characterize and check the purity of the compound by NMR (^{1}H and ^{13}C), MS and HPLC analysis. Methods for compound characterization and analytical data can be found in the **Supplementary Data**.

■ **PAUSE POINT** Compound **18** can be stored at 20 °C for 12 months.

25| Functionalize a biologically active molecule using your chosen protecting group. Methods for doing this are summarized in **Figure 4**. Any prodrug resulting from this functionalization can be applied to the following steps.

Testing oxygen-dependent release of the drug

26| Perform the following experiments to determine what compound is produced on chemical reduction of the functionalized compound (typical procedures for the zinc reduction method; options A and B), and to find out what is produced upon enzymatic reduction (option C). Option D is a quick, efficient, representative method for indicating whether a cell line of interest is capable of O_2-dependent reduction of a bioreductive candidate compound. This protocol uses, but is not limited to, RKO (colorectal) cells as a representative cell line for use in bioreductive experiments. We have found that HCT116, OE21, A549, HepG2 and H1299 cells are also suitable for these experiments. Purchase and culture details can obtained from ATCC.

(A) Chemical reduction of compound 1 (CH-01) ● **TIMING 16 h plus analysis**

(i) Add 1.0 mg of subject compound (0.0021 mol for CH-01, which is used here as a representative compound) to a 5-ml round-bottom flask equipped with a Teflon-coated magnetic stir bar and a rubber septum.

(ii) Add 2 ml of DMF to the reaction flask.

(iii) Add 20 µl of 10% (wt/vol) aqueous ammonium chloride to the reaction solution.

(iv) Take a 100-µl aliquot from the reaction solution. This will serve as $T = 0$ (where T = time) for the HPLC analysis.
▲ **CRITICAL STEP** The $T = 0$ aliquot must be taken before the addition of zinc in the next step, as the reduction reaction will occur rapidly.

(v) Add 5 mg of zinc dust (0.0765 mol, 36 eq. for CH-01) to the reaction mixture and stir it at ambient temperature for 16 h.

(vi) Collect aliquots of the reaction mixture at $T = 1$ h and $T = 16$ h. Analyze the aliquots by HPLC (see Equipment Setup). Please note that the HPLC method may require adjustment for other compounds. Please further note that we found reduction from nitro to amine ($R_1 = R_2 = H$ in **Fig. 1**) to be complete by 16 h, as determined by HPLC analysis of the solution. Should monitoring of reduction be desired by this method, we recommend collecting 100-µl aliquots at the desired time points (0.5, 1, 2 h and so on).
▲ **CRITICAL STEP** Allow the reaction mixture to settle before collecting aliquots. Zinc particles may block the flow in the HPLC system. Alternatively, allow aliquots to settle, and be sure to remove the supernatant from excess zinc metal. The use of filtered tips (Supelco, Iso-Disc filters, PTFE-4-4, size × porosity: 4 mm × 0.45 µm) when using a syringe helps to avoid this problem.
? TROUBLESHOOTING

(B) Determination of compound 1 (CH-01) fragmentation ● **TIMING 24 h plus analysis**

(i) Add 95 µl of 0.1 M K_2HPO_4 (pH 7.4) buffer to a 2-ml microcentrifuge tube.

(ii) Collect 5 µl of the $T = 16$ h aliquot collected in Step 26A(vi) and add it to the buffer solution.

(iii) Incubate the resulting solution at 37 °C for 24 h.

(iv) Analyze the solution by HPLC (see Equipment Setup), and the determine the ratio of the remaining prodrug to its reduced metabolite and active inhibitor. Please note that the reduced prodrug of representative compound CH-01 was found to be stable in DMF, the reaction solvent used in Step 26A(vi). The reduced amine species ($R^1 = R^2 = H$ in **Figure 1**) fragmented when incubated in buffer solution as in Step 3. Depending on the propensity of the reduced intermediate of your chosen prodrug to fragment, some fragmentation may already occur in Step 2. This can again be determined by HPLC analysis.
? TROUBLESHOOTING

(C) *In vitro* reduction of compound 1 (CH-01) ● **TIMING 1–24 h plus analysis**

(i) Prepare a stock solution of compound **1** in DMSO such that the volume of DMSO added is <1% of the total assay volume.
▲ **CRITICAL STEP** A typical DMSO stock concentration for use in the assay should be in the range of 0.25–10 mM.

(ii) Take two 5-ml vials, each equipped with a screw-on cap.

© 2016 Macmillan Publishers Limited. All rights reserved.

(iii) To each vial, add the following: 50 µl of solution A; 10 µl of solution B; 729.3 µl of deionized H_2O; 200 µl of 0.5 M $KHPO_4$ (pH 7.4) buffer; and 1 µl of DMSO stock solution.
▲ **CRITICAL STEP** Solutions A and B represent an NADPH regeneration system, supplied by Corning.
▲ **CRITICAL STEP** The final concentration of the substrate prodrug may be adjusted. We recommend HPLC analysis of the compound's UV absorbance at various concentrations. The final compound concentration in the assay may then be adjusted, such that the compound may be visualized in the assay aliquots by HPLC. For CH-01, our representative compound, the DMSO stock solution concentration used was 10 mM, and the final CH-01 concentration in the reaction mixture was 10 µM.
(iv) Cool each vial containing the assay solution to 0–4 °C with ice.
(v) Add 9.7 µl of bactosomal human NADPH-CYP reductases (enzyme concentration in the purchased solution: 10.3 nmol/ml) to each vial. The final enzyme concentration in the reaction solution is 92 pmol/ml.
▲ **CRITICAL STEP** Enzyme concentration between batches may vary. We recommend maintaining a final enzyme concentration of 92 pmol/ml. Volume adjustments to change the enzyme concentration should be compensated for by modifying the volume of deionized H_2O appropriately.
▲ **CRITICAL STEP** Bactosomal human NADPH-CYP reductase enzymes should be kept at –80 °C, and they should be thawed on ice thoroughly before use, to avoid denaturation of the enzyme.
(vi) Label one vial 'Hypoxia' and the other 'Normoxia'.
(vii) Take two 200-µl microcentrifuge tubes, and to each add 50 µl of MeCN.
(viii) Take a 50-µl aliquot from vial 'Hypoxia'. Add it to the 50 µl of MeCN in one of the microcentrifuge tubes. Label this microcentrifuge tube 'Hypoxia, T = 0'. Store it at –20 °C.
■ **PAUSE POINT** Aliquots may be stored at –20 °C for up to 2 weeks before HPLC analysis.
(ix) Repeat the procedure outlined in Step 26C(viii) for the 'Normoxia' vial.
(x) Place the 'Hypoxia' vial inside a Bactron II anaerobic chamber (Shell Labs) at <0.1% O_2 set to incubate at 37 °C. Place the 'Normoxia' vial inside an incubation chamber at 37.0 °C under aerobic (21% O_2) conditions.
(xi) Repeat the procedure outlined in Step 26C(vii–ix) for T = 2, 4, 24 h or for other desired time points.
▲ **CRITICAL STEP** Do not remove the vials from their respective incubation chambers. The 1-ml assay volume will take time to equilibrate with anaerobic conditions (~20–30 min). Place the screw-on caps on top of each vial to minimize evaporation. Do not seal them, as this will limit exposure to the chamber's atmosphere.
▲ **CRITICAL STEP** The suggested time points are those of an example assay, which is used here to determine the bioreduction of compound **1**. When reduced concentrations of the substrate prodrug are used, time points may be shortened.
(xii) Remove aliquot samples from the –20 °C freezer and defrost them at ambient temperature.
(xiii) Centrifuge the thawed samples at 13,000*g* for 10 min at 4 °C. Remove the supernatant from each sample.
(xiv) Analyze each sample (both the 'Hypoxia' and 'Normoxia' vials at T = 0, 2, 4 and 24 h) by HPLC (see Equipment Setup).
? TROUBLESHOOTING
(xv) Determine the ratio of the remaining prodrug to its reduced metabolite and active inhibitor for each sample.

(D) *In vitro* evaluation of the bioreductive prodrug ● TIMING 3–5 d

(i) Culture RKO cells in a cell culture flask (e.g., a 75 cm^3 Corning flask) in the appropriate medium (DMEM containing 10% (vol/vol) FBS, 100 U/ml of penicillin and 100 µg/ml of streptomycin). Culture the cells in a standard humidified incubator at 37 °C and 5% CO_2 until they reach ~70% confluence. Please note that cells should be growing exponentially.
! CAUTION Regularly check that the cell lines used in your research match their recognized cell line identity criteria and are not infected with mycoplasma.
(ii) Seed 250,000 cells into a 6-cm glass dish. Four dishes are required.
▲ **CRITICAL STEP** Glass dishes are required to ensure that oxygen levels decrease as rapidly as possible. Plastic dishes, which retain oxygen, can also be used, but longer incubation times may be needed.
(iii) Incubate the dishes in a standard humidified incubator at 37 °C and 5% CO_2 for 15 h.
(iv) Treat two of the dishes with a 25 µM solution of the compound of interest in 5 ml of fresh DMEM (10% (vol/vol) FBS, 100 U/ml penicillin and 100 µg/ml streptomycin). The two other dishes should be used as negative controls (no bioreductive prodrug present) for hypoxic and normoxic conditions.
▲ **CRITICAL STEP** Note that this is a representative concentration used for experiments with compound **1**. Optimization of dose might be required to avoid issues associated with nonspecific cytotoxicity.
(v) Incubate one dish dosed with the compound of interest, and one negative control dish in a Bactron II anaerobic chamber (Shell Labs) for 6 h at 37 °C and <0.1% O_2. Incubate one dish dosed with the compound of interest and one negative control dish in a standard humidified incubator at 37 °C and 5% CO_2 for 6 h.
(vi) Remove the medium from each dish, and then wash the cells twice with 3 ml of PBS.

© 2016 Macmillan Publishers Limited. All rights reserved.

(vii) Add 1 ml of PBS to each dish and use a cell scraper to gently detach the cells from the glass surface. Transfer each 1-ml cell suspension to a 2.5-ml microcentrifuge tube.
▲ CRITICAL STEP Scrape the cells gently to avoid damaging them in the process. Damage to cells will lead to potential loss of endogenous metabolites, and it will decrease the overall cell number for analysis.
(viii) Centrifuge the cell suspensions at a speed of 250–350*g* for 10 min at 4 °C. Remove and discard the supernatant to leave the cell pellet.
(ix) Lyse the cells with 100 µl of MeCN or 3% (vol/vol) TCA in PBS. Centrifuge the cells at 13,000*g* for 15 min at 4 °C. Remove and keep the supernatant.
(x) Analyze the supernatant by HPLC (see Equipment Setup) to determine the intracellular presence of metabolites of the compound of interest.
? TROUBLESHOOTING

? TROUBLESHOOTING

Troubleshooting advice can be found in **Table 1**.

TABLE 1 | Troubleshooting table.

Step	Problem	Possible reason	Solution
2	The yellow suspension has not formed	NaH is inactive	Purchase fresh NaH
12	Low yield of the product	EtOH remains in the reaction solution after rotary evaporation	Ensure that all of the EtOH is removed through rotary evaporation and that the reaction mixture is adequately concentrated
26A(vi)	Prodrug is not visualized by HPLC	Visualization at inappropriate wavelength	Look for a maximum in the UV trace and collect data at this wavelength
	Zinc reduction yields multiple peaks by HPLC analysis	Compound functionalities other than the nitro group are sensitive to zinc reduction	Proceed to evaluate the compound in NADPH-CYP reductase assay
26B(iv)	The prodrug fragments before buffer treatment	Propensity for fragmentation upon reduction is good	Proceed to evaluate the compound in NADPH-CYP reductase assay
	Bioreductive group (nitro) gets reduced but does not fragment	Reduced metabolites (amino or nitroso) are stable and have poor fragmentation propensity	Allow longer incubation in potassium phosphate buffer. If the problem persists, use a different bioreductive group or use a linker (such as carbamate or carbonate) to improve fragmentation
	Cannot visualize the parent compound or its metabolites by HPLC	Compound concentration is too low	Increase the concentration of the compound in the assay. Please note that this approach requires either an increased duration/number of time points or a corresponding increase in enzyme concentration from the recommended 92 pmol/ml
	No metabolites are detected by HPLC	The enzyme has been denatured	Ensure that the enzyme is stored in aliquots at –80 °C. Avoid freezing and thawing the whole batch between experiments
		The prodrug is not a substrate for the enzyme	Consider using alternative bioreductive groups
		The concentration of the parent compound is too high	Reduce the concentration of the parent compound
		The chosen cell line lacks appropriate reductase enzymes	Choose an alternative cell line or determine the presence of the reductase of interest by western blot analysis
	Neither the parent compound nor metabolites are detected by HPLC	Concentration of the compound is too low or too few cells are used in the assay	Repeat the assay with an increased dose of the compound of interest, or with a greater number of cells
		The compound is metabolically unstable	Select an alternative cell line with reduced metabolic activity
	The reduced compound is detected by HPLC, but not the fragmentation product	The propensity for *in vitro* fragmentation of the reduced metabolite is poor	Consider the use of bioreductive linker groups, such as carbamates, to enhance leaving-group ability

© 2016 Macmillan Publishers Limited. All rights reserved.

● TIMING

Steps 1–13, synthesis of compound **13**: 8–10 h
Steps 14–23, synthesis of compound **14**: 4–6 h
Step 24A, synthesis of compound **15**: 3–5 h
Step 24B, synthesis of compound **16**: 4–6 h
Step 24C, synthesis of compound **17**: 2–3 h
Step 24D, synthesis of compound **18**: 3 d
Step 25, functionalization of the compound with the protecting group: 12 h–2 d
Step 26A, typical procedure for zinc reduction method: reduction of compound **1** (CH-01): 16 h plus analysis
Step 26B, typical procedure for zinc reduction method: determination of compound **1** (CH-01) fragmentation: 24 h plus analysis
Step 26C, typical procedure for NADPH-CYP reductases assay: *in vitro* reduction of compound **1** (CH-01): 1–24 h plus analysis
Step 26D, typical procedure for *in vitro* evaluation of the bioreductive prodrug: 3–5 d

ANTICIPATED RESULTS

The **Supplementary Data** file provides characterization data for compounds **13**–**18**.

Step 2

Analysis of aliquots by HPLC should reveal reduction of the nitro functionality to hydroxylamine, nitroso intermediates or amino product. Identity of the metabolites observed can be confirmed via LC-MS analysis.

Step 3

Incubation in buffer should induce fragmentation of the reduced prodrug species.

Step 4

Aliquot evaluation by HPLC of the hypoxia-activated prodrug incubated with bactosomal human NADPH-CYP reductases under hypoxic conditions should reveal an increase in the concentration of fragmentation product with time. Under normoxic conditions, the prodrug should remain stable.

Step 5

Hypoxia-activated prodrug should not show activation under normoxic conditions. Under hypoxic conditions, the reduction step occurs and the fragmentation product is detectable.

© 2016 Macmillan Publishers Limited. All rights reserved.

npg

Note: Any Supplementary Information and Source Data files are available in the online version of the paper.

ACKNOWLEDGMENTS S.J.C., E.M.H. and L.J.O.C. thank the UK Medical Research Council (MRC) for the award of a studentship to L.J.O.C. S.J.C., E.M.H. and C.C.-K. thank Cancer Research UK (CRUK) for the award of a studentship to C.C.-K. S.J.C., E.M.H. and C.N.G.E. thank CRUK and the UK Engineering and Physical Sciences Research Council (EPSRC) for the award of a studentship to C.N.G.E., through the CRUK and EPSRC Cancer Imaging Centre in Oxford (OCIC). S.J.C. and J.S. thank the European Commission for the award of a Marie Curie Fellowship to J.S. (PIIF-GA-2012-331327, Hypoxprobe). E.M.H. thanks CRUK for research funding. S.J.C. thanks St. Hugh's College, Oxford, for research funding.

AUTHOR CONTRIBUTIONS The study was conceived and planned by S.J.C. and E.M.H., and they also supervised the *in vitro* bioreduction studies. The chemical synthesis was conducted by L.J.O.C., C.C.-K., J.S. and C.N.G.E. The chemical synthesis was supervised by S.J.C. The *in vitro* bioreduction studies and the cellular bioreduction studies were performed by L.J.O.C., C.C.-K. and M.R.L.S. The cellular bioreduction studies were supervised by E.M.H. All authors interpreted the data. The manuscript was written by L.J.O.C., J.S., E.M.H. and S.J.C. All authors commented on the manuscript.

COMPETING FINANCIAL INTERESTS The authors declare no competing financial interests.

Reprints and permissions information is available online at http://www.nature.com/reprints/index.html.

1. Hammond, E.M. *et al.* The meaning, measurement and modification of hypoxia in the laboratory and the clinic. *Clin. Oncol. (R. Coll. Radiol.)* **26**, 277–288 (2014).
2. McKeown, S.R. Defining normoxia, physoxia and hypoxia in tumours—implications for treatment response. *Br. J. Radiol.* **87**, 20130676 (2014).
3. Wilson, W.R. & Hay, M.P. Targeting hypoxia in cancer therapy. *Nat. Rev. Cancer* **11**, 393–410 (2011).
4. Thomlinson, R.H. & Gray, L.H. The histological structure of some human lung cancers and the possible implications for radiotherapy. *Br. J. Cancer* **9**, 539–549 (1955).
5. Vaupel, P. The role of hypoxia-induced factors in tumor progression. *Oncologist* **9**, 10–17 (2004).
6. Yasui, H. *et al.* Low-field magnetic resonance imaging to visualize chronic and cycling hypoxia in tumor-bearing mice **70**, 6427–6436 (2010).
7. Nordsmark, M. *et al.* Prognostic value of tumor oxygenation in 397 head and neck tumors after primary radiation therapy. An international multi-center study. *Radiother. Oncol.* **77**, 18–24 (2005).
8. Begg, A.C., Stewart, F.A. & Vens, C. Strategies to improve radiotherapy with targeted drugs. *Nat. Rev. Cancer* **11**, 239–253 (2011).
9. Cazares-Korner, C. *et al.* CH-01 is a hypoxia-activated prodrug that sensitizes cells to hypoxia/reoxygenation through inhibition of Chk1 and Aurora A. *ACS Chem. Biol.* **8**, 1451–1459 (2013).
10. O'Connor, L.J. *et al.* Efficient synthesis of 2-nitroimidazole derivatives and the bioreductive clinical candidate evofosfamide (TH-302). *Org. Chem. Front.* **2**, 1026–1029 (2015).
11. Cavalleri, B., Ballotta, R. & Lancini, G. Synthesis of 1-alkyl-2-nitroimidazole-5-carboxaldehydes. *J. Heterocycl. Chem.* **9**, 979–984 (1972).
12. Matteucci, M. *et al.* Phosphoramidate alkylator prodrugs. Patent no. WO 2007/002931 A2 (2007).

13. Parveen, I., Naughton, D.P., Whish, W. & Threadgill, M.D. 2-Nitroimidazol-5-ylmethyl as a potential bioreductively activated prodrug system: reductively triggered release of the PARP inhibitor 5-bromoisoquinolinone. *Bioorg. Med. Chem. Lett.* **9**, 2031–2036 (1999).
14. Damen, E.W.P., Nevalainen, T.J., van den Bergh, T.J.M., de Groot, F.M.H. & Scheeren, H.W. Synthesis of novel paclitaxel prodrugs designed for bioreductive activation in hypoxic tumour tissue. *Bioorg. Med. Chem.* **10**, 71–77 (2002).
15. Ferrer, S., Naughton, D.P. & Threadgill, M.D. H-1 NMR studies on the reductively triggered release of heterocyclic and steroid drugs from 4,7-dioxoindole-3-methyl prodrugs. *Tetrahedron* **59**, 3445–3454 (2003).
16. Zhang, Z., Tanabe, K., Hatta, H. & Nishimoto, S.-I. Bioreduction activated prodrugs of camptothecin: molecular design, synthesis, activation mechanism and hypoxia selective cytotoxicity. *Org. Biomol. Chem.* **3**, 1905–1910 (2005).
17. Hay, M.P., Wilson, W.R. & Denny, W.A. Nitroarylmethylcarbamate prodrugs of doxorubicin for use with nitroreductase gene-directed enzyme prodrug therapy. *Bioorg. Med. Chem.* **13**, 4043–4055 (2005).
18. Thomson, P. *et al.* Hypoxia-driven elimination of thiopurines from their nitrobenzyl prodrugs. *Bioorg. Med. Chem. Lett.* **17**, 4320–4322 (2007).
19. Granchi, C. *et al.* Bioreductively activated lysyl oxidase inhibitors against hypoxic tumours. *ChemMedChem* **4**, 1590–1594 (2009).
20. Zhu, R. *et al.* 4-Nitrobenzyloxycarbonyl derivatives of *O*(6)-benzylguanine as hypoxia-activated prodrug inhibitors of *O*(6)-alkylguanine-DNA alkyltransferase (AGT), which produces resistance to agents targeting the *O*-6 position of DNA guanine. *J. Med. Chem.* **54**, 7720–7728 (2011).
21. Lindquist, K.E. *et al.* Selective radiosensitization of hypoxic cells using BCCA621C: a novel hypoxia activated prodrug targeting DNA-dependent protein kinase. *Tumor Microenviron. Ther.* **1**, 46–55 (2013).
22. Couch, G.D., Burke, P.J., Knox, R.J. & Moody, C.J. Synthesis of 2-aryl-6-methyl-5-nitroquinoline derivatives as potential prodrug systems for reductive activation. *Tetrahedron* **64**, 2816–2823 (2008).
23. Cui, L. *et al.* A new prodrug-derived ratiometric fluorescent probe for hypoxia: high selectivity of nitroreductase and imaging in tumor cell. *Org. Lett.* **13**, 928–931 (2011).
24. Blanche, E.A., Maskell, L., Colucci, M.A., Whatmore, J.L. & Moody, C.J. Synthesis of potential prodrug systems for reductive activation. Prodrugs for anti-angiogenic isoflavones and VEGF receptor tyrosine kinase inhibitory oxindoles. *Tetrahedron* **65**, 4894–4903 (2009).
25. Naughton, D.P. Drug targeting to hypoxic tissue using self-inactivating bioreductive delivery systems. *Adv. Drug Deliv. Rev.* **53**, 229–233 (2001).
26. Wardman, P. Some reactions and properties of nitro radical-anions important in biology and medicine. *Environ. Health Perspect.* **64**, 309–320 (1985).
27. Foloppe, N. *et al.* Structure-based design of novel Chk1 inhibitors: insights into hydrogen bonding and protein-ligand affinity. *J. Med. Chem.* **48**, 4332–4345 (2005).
28. Larock, R.C. *Comprehensive Organic Transformations* (Wiley-VCH, 1999).

© 2016 Macmillan Publishers Limited. All rights reserved.

2.16. 5-(Bromomethyl)-6-nitroquinoline

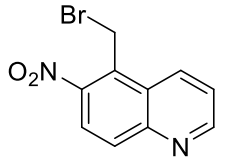


```
Current Data Parameters
NAME      5-(bromomethyl)-6-nitroquinoline
EXPNO                   1
PROCNO                  1

F2 - Acquisition Parameters
Date_           20130430
Time              19.24
INSTRUM          avc500
PROBHD   5 mm CPDUL 13C
PULPROG             zg30
TD                 65536
SOLVENT            CDCl3
NS                    16
DS                     4
SWH           10330.578 Hz
FIDRES         0.157632 Hz
AQ            3.1719425 sec
RG                   2.8
DW                48.400 usec
DE                 6.00 usec
TE                298.0 K
D1           1.00000000 sec
TD0                    1

======== CHANNEL f1 ========
NUC1                  1H
P1                10.60 usec
PL1                6.00 dB
PL1W         0.95905519 W
SFO1        500.3030896 MHz

F2 - Processing parameters
SI                 32768
SF          500.3000284 MHz
WDW                   EM
SSB      0
LB                0.30 Hz
GB       0
PC                1.00
```

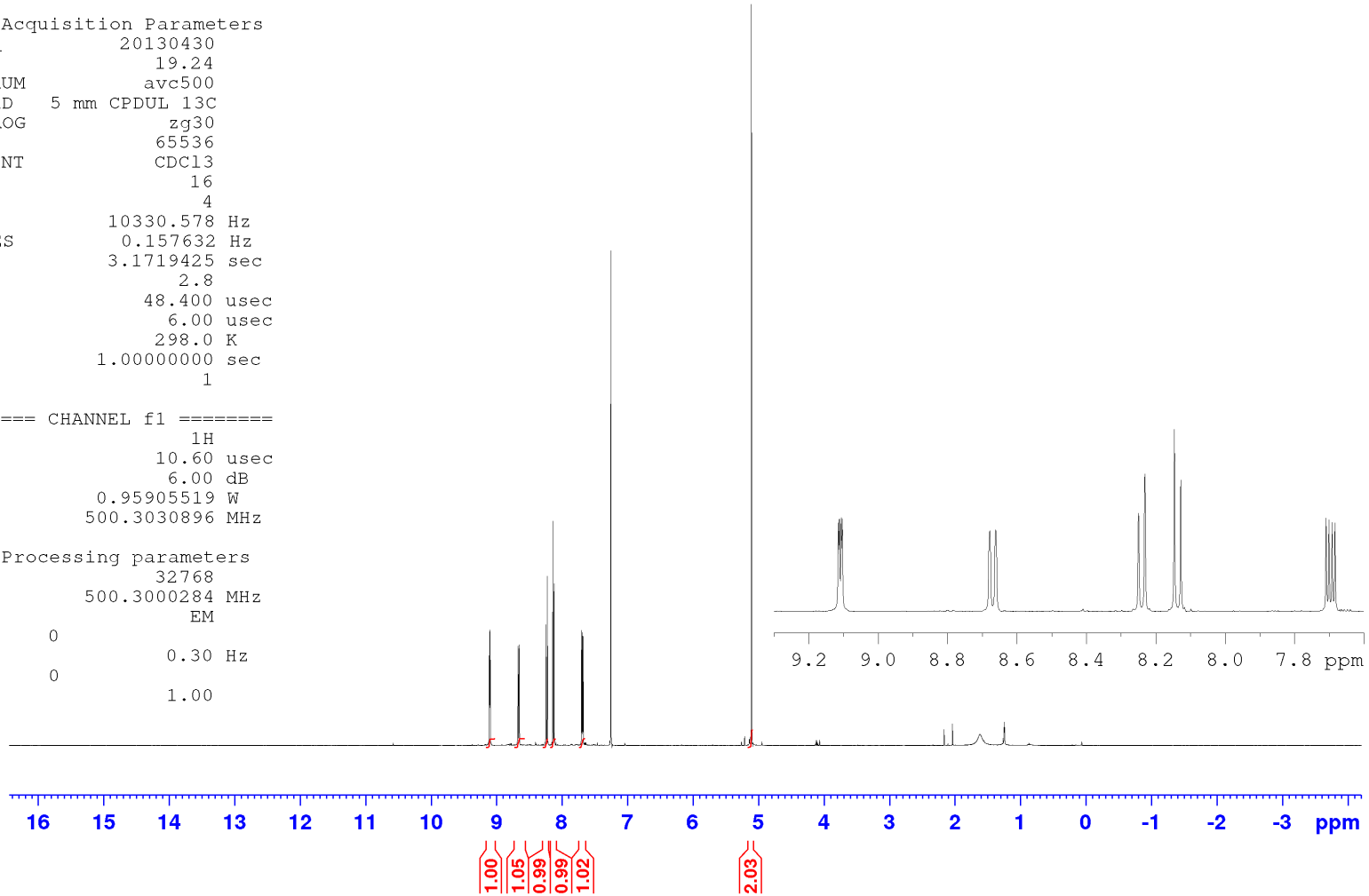

2.16. 5-(Bromomethyl)-6-nitroquinoline

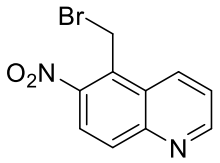


```
Current Data Parameters
NAME      5-(bromomethyl)-6-nitroquinoline
EXPNO                   4
PROCNO                  1

F2 - Acquisition Parameters
Date_           20130430
Time              20.39
INSTRUM          avc500
PROBHD   5 mm CPDUL 13C
PULPROG          zgpg30
TD                65536
SOLVENT           CDCl3
NS                 1024
DS                    2
SWH           31250.000 Hz
FIDRES         0.476837 Hz
AQ            1.0485760 sec
RG                  912
DW               16.000 usec
DE               20.00 usec
TE               298.0 K
D1           2.00000000 sec
D11          0.03000000 sec
TD0                   1

======== CHANNEL f1 ========
NUC1                13C
P1                10.25 usec
PL1                8.00 dB
PL1W         1.62029624 W
SFO1        125.8131151 MHz

======== CHANNEL f2 ========
CPDPRG[2         waltz16
NUC2                1H
PCPD2             80.00 usec
PL2                6.00 dB
PL12              23.56 dB
PL13              29.56 dB
PL2W         0.95905519 W
PL12W        0.01682068 W
PL13W        0.00422516 W
SFO2        500.3020012 MHz

F2 - Processing parameters
SI                32768
SF          125.8005220 MHz
WDW                  EM
SSB       0
LB                1.00 Hz
GB        0
PC                1.40
```

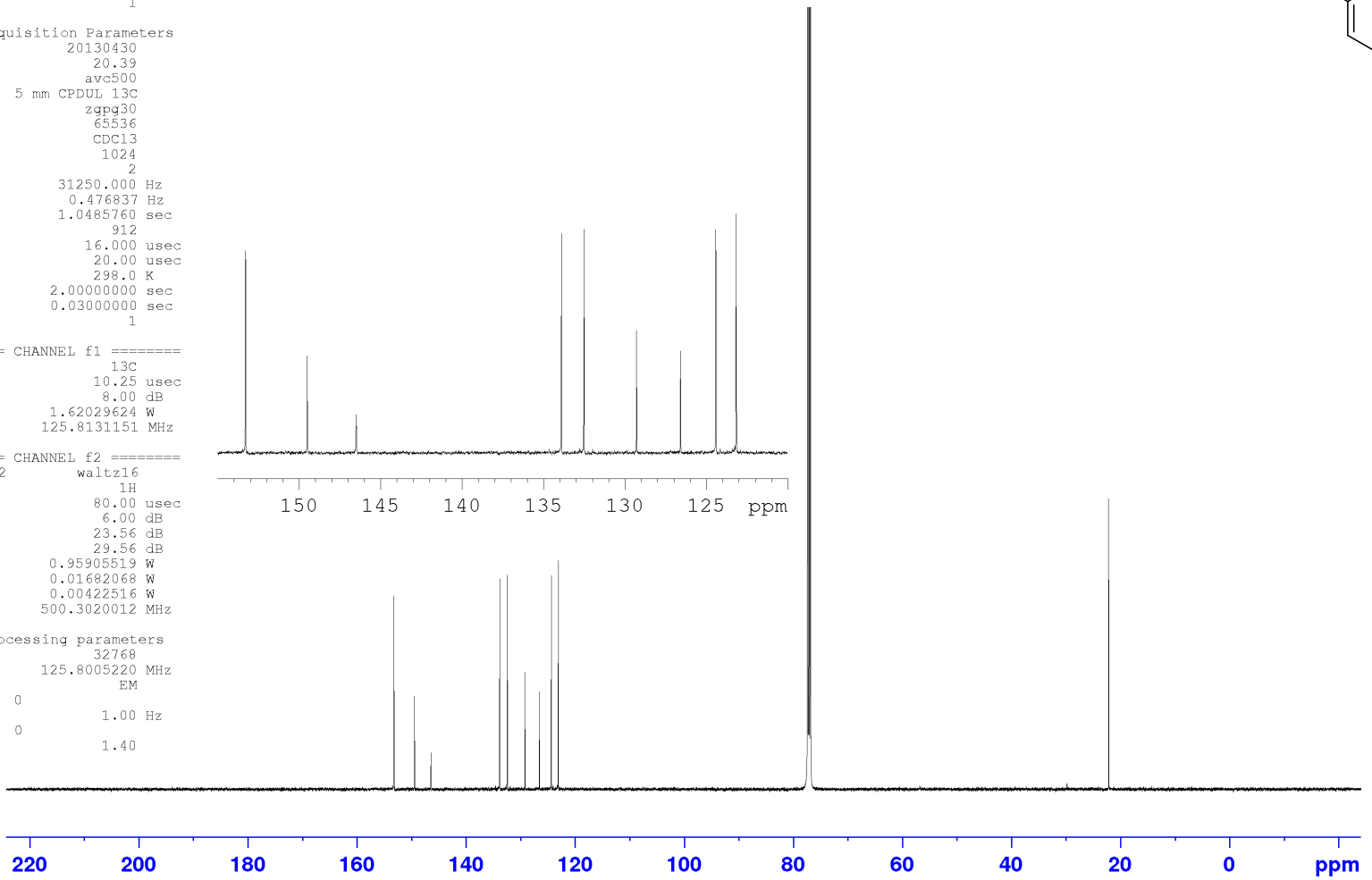

2.17. (6-Nitroquinolin-5-yl)methanol

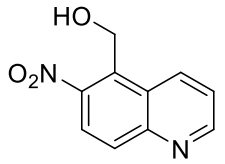

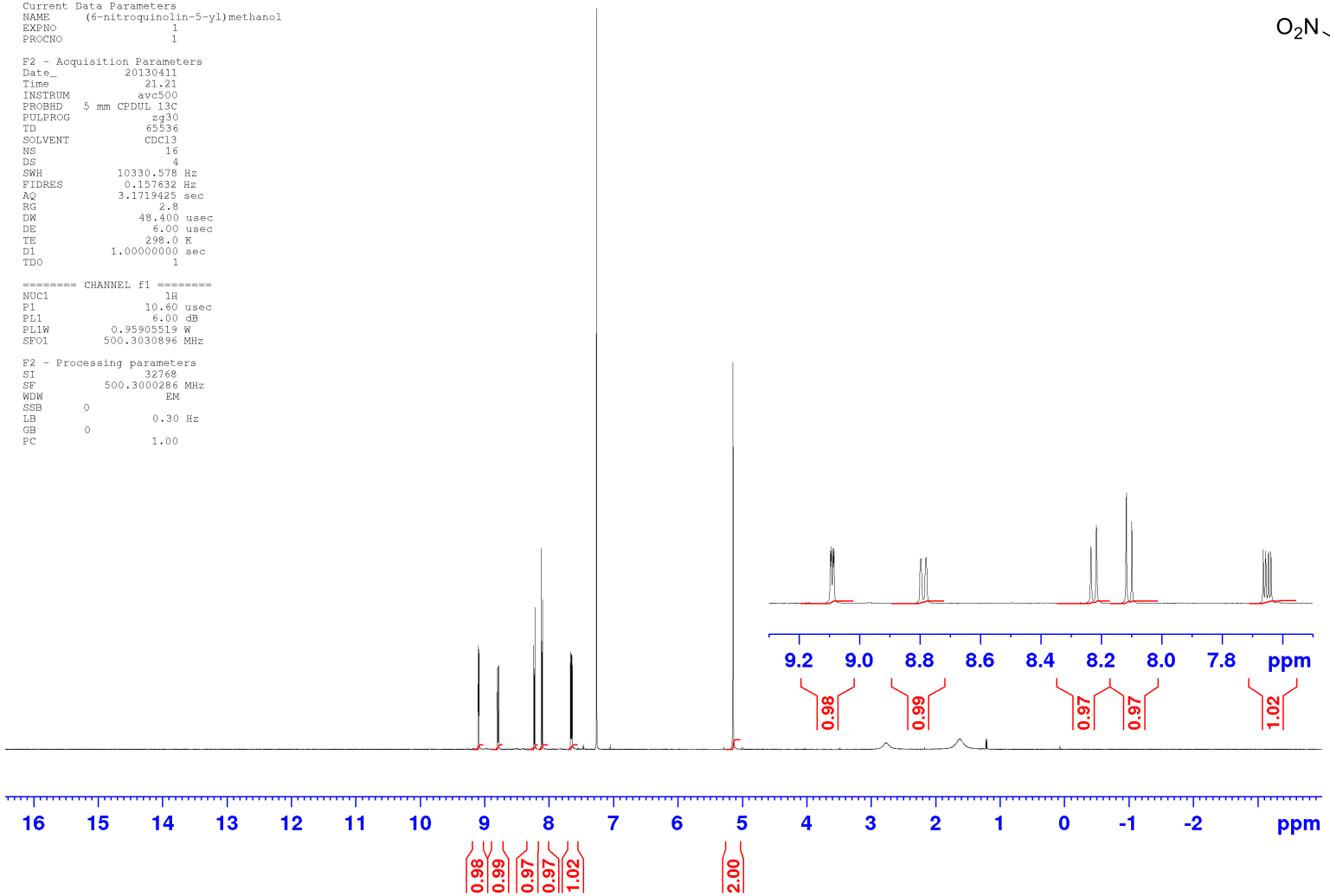

2.17. (6-Nitroquinolin-5-yl)methanol

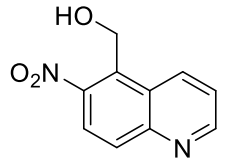

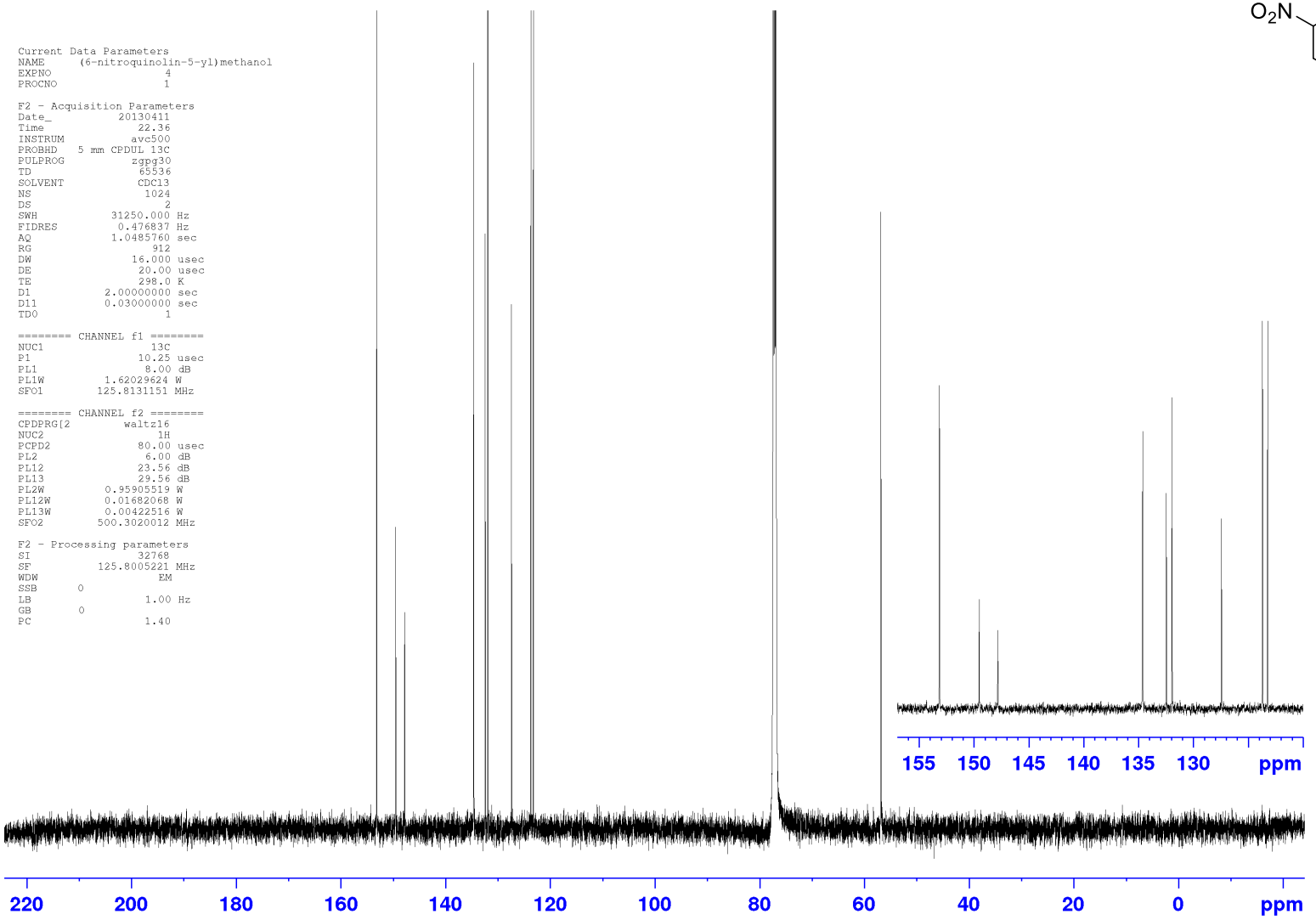

2.18. (6-Chloroquinolin-5-yl)methanol

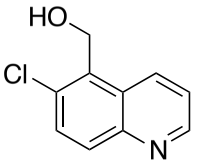


```
Current Data Parameters
NAME      (6-chloroquinolin-5-yl)methanol
EXPNO                  1
PROCNO                 1

F2 - Acquisition Parameters
Date_           20121123
Time                3.55
INSTRUM          avc500
PROBHD   5 mm CPTXI 1H-
PULPROG             zg30
TD                 65536
SOLVENT            CDCl3
NS                    16
DS                     2
SWH            10330.578 Hz
FIDRES          0.157632 Hz
AQ             3.1719425 sec
RG                  50.8
DW                48.400 usec
DE                 6.00 usec
TE                298.0 K
D1           1.00000000 sec
TD0                    1

======== CHANNEL f1 ========
NUC1                  1H
P1                  9.50 usec
PL1       0 dB
PL1W         3.81806731 W
SFO1        500.3030896 MHz

F2 - Processing parameters
SI                 32768
SF           500.3000248 MHz
WDW                   EM
SSB       0
LB                 0.30 Hz
GB        0
PC                 1.00
```

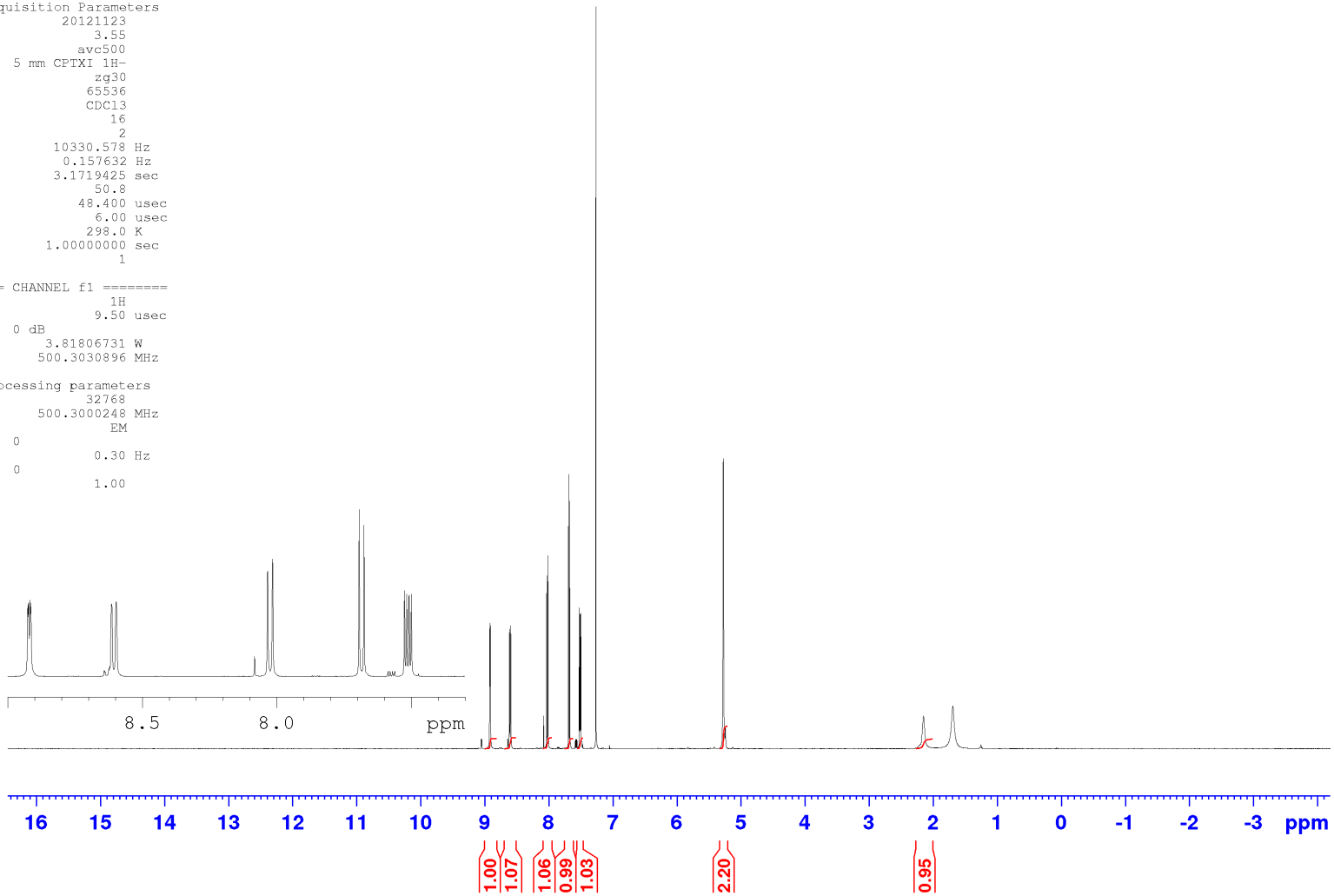

2.18. (6-Chloroquinolin-5-yl)methanol

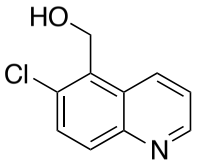

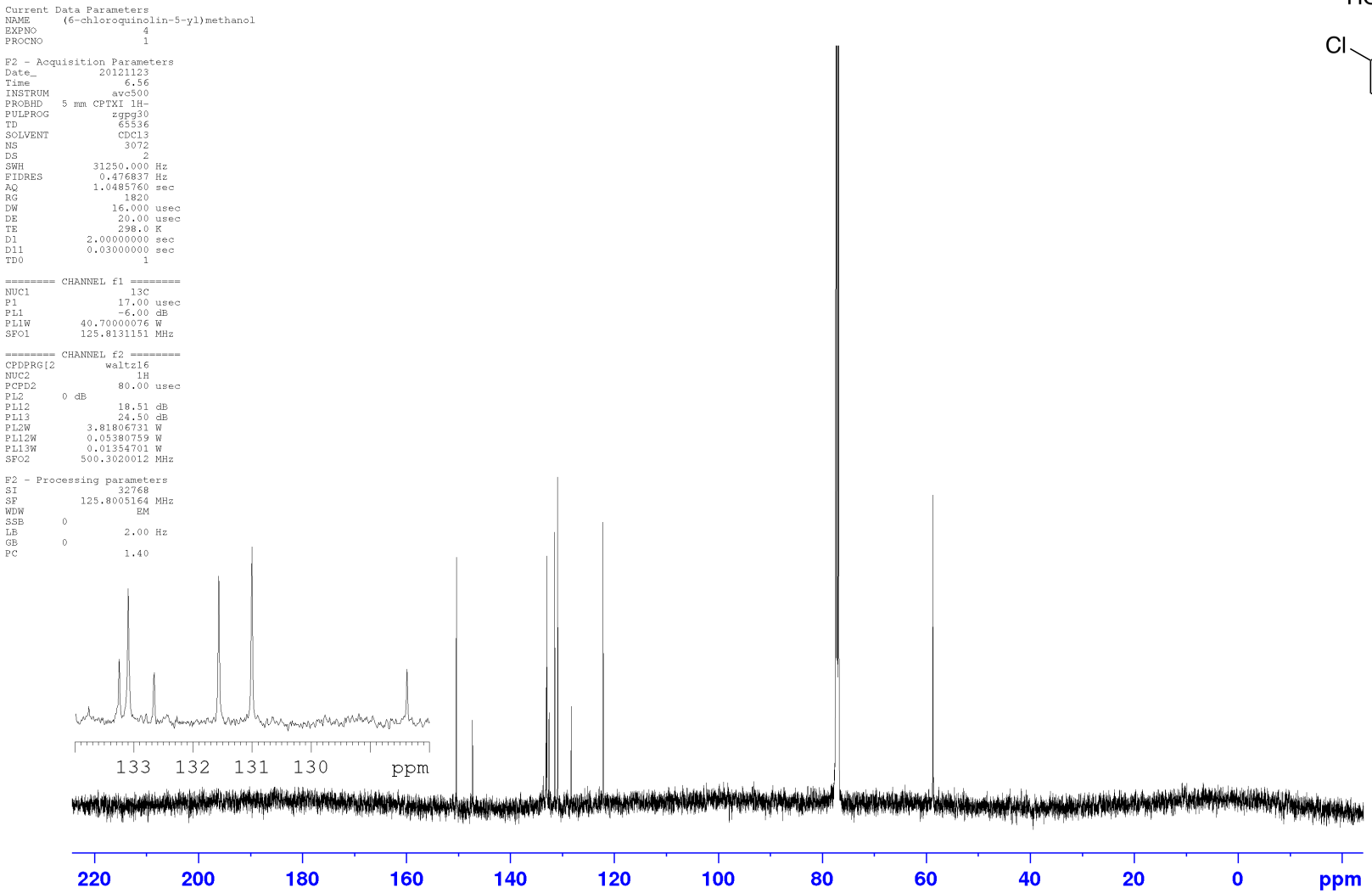

2.19. 6-Chloroquinoline-5-carbaldehyde

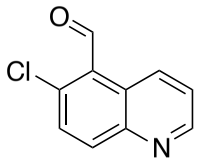


```
Current Data Parameters
NAME      6-chloroquinoline-5-carbaldehyde
EXPNO                  1
PROCNO                 1

F2 - Acquisition Parameters
Date_           20130123
Time              23.06
INSTRUM          avc500
PROBHD   5 mm CPDUL 13C
PULPROG             zg30
TD                 65536
SOLVENT            CDCl3
NS                    16
DS                     2
SWH           10330.578 Hz
FIDRES         0.157632 Hz
AQ            3.1719425 sec
RG                   3.2
DW                48.400 usec
DE                 6.00 usec
TE                300.0 K
D1           1.00000000 sec
TD0                    1

======== CHANNEL f1 ========
NUC1                  1H
P1                 10.60 usec
PL1                 6.00 dB
PL1W          0.95905519 W
SFO1        500.3030896 MHz

F2 - Processing parameters
SI                 32768
SF          500.3000279 MHz
WDW                   EM
SSB       0
LB                 0.30 Hz
GB        0
PC                 1.00
```

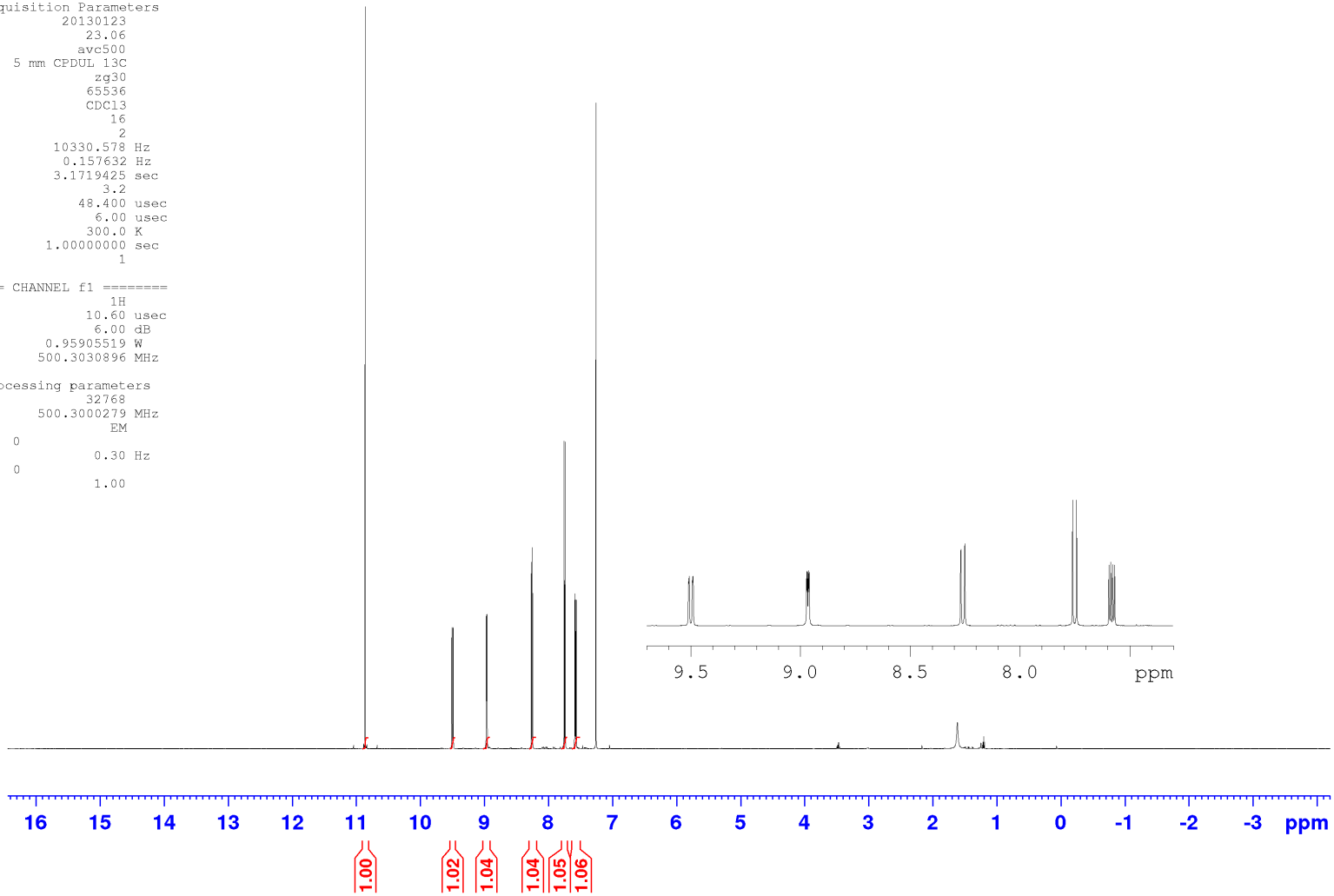

2.19. 6-Chloroquinoline-5-carbaldehyde

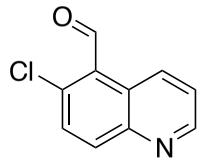

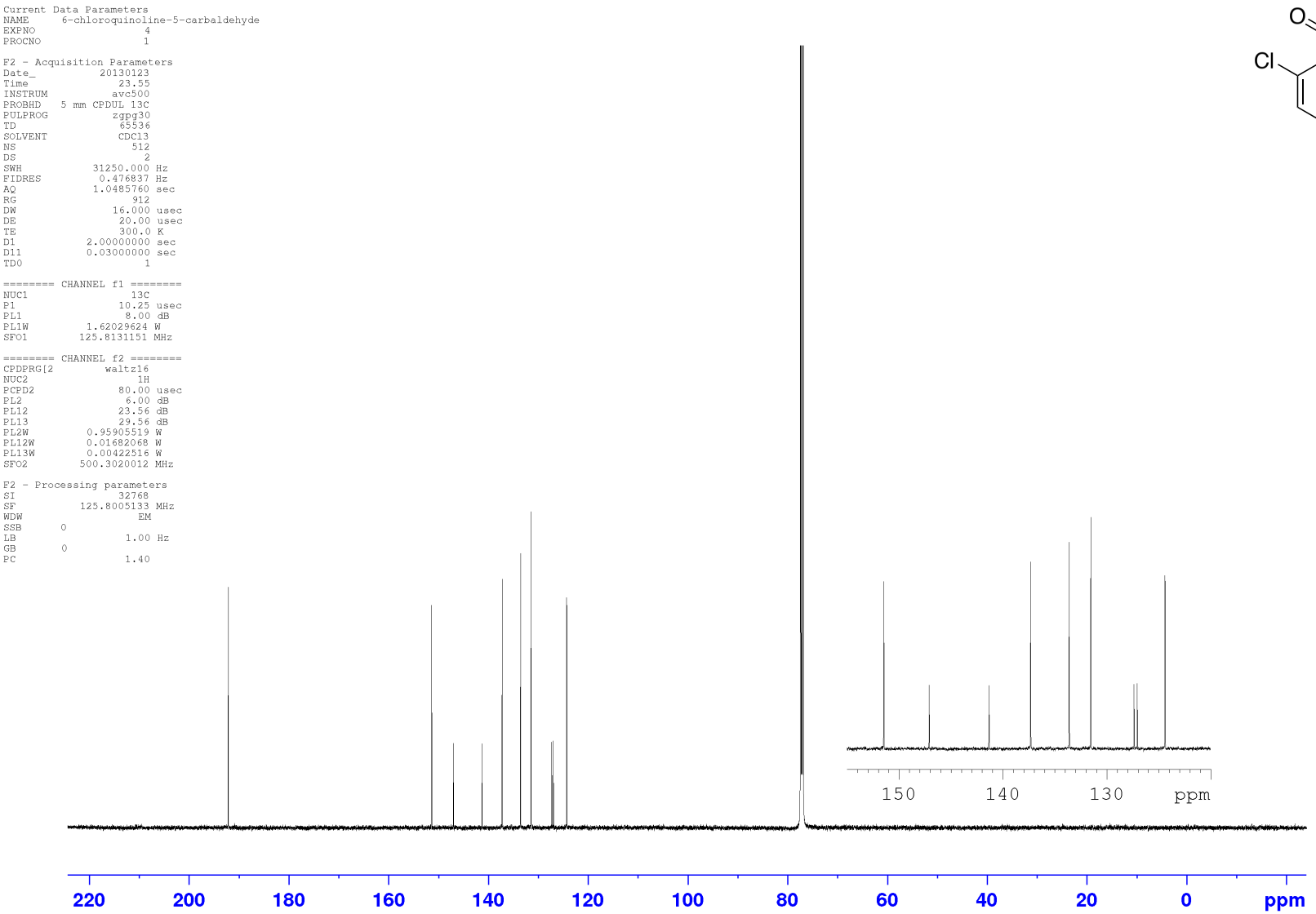

2.23. 5,8-Dibromo-6-chloroquinoline

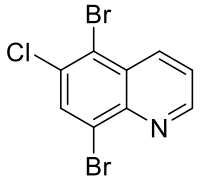


```
Current Data Parameters
NAME      5,8-dibromo-6-chloroquinoline
EXPNO                 1
PROCNO                1

F2 - Acquisition Parameters
Date_          20130110
Time               9.50
INSTRUM          avc500
PROBHD   5 mm CPDUL 13C
PULPROG            zg30
TD                65536
SOLVENT           CDCl3
NS                   16
DS                    2
SWH           10330.578 Hz
FIDRES         0.157632 Hz
AQ            3.1719425 sec
RG                  3.2
DW                48.400 usec
DE                 6.00 usec
TE                298.0 K
D1           1.00000000 sec
TD0                   1

======== CHANNEL f1 ========
NUC1                 1H
P1                10.60 usec
PL1                6.00 dB
PL1W         0.95905519 W
SFO1        500.3030896 MHz

F2 - Processing parameters
SI                32768
SF          500.3000292 MHz
WDW                  EM
SSB       0
LB                0.30 Hz
GB        0
PC                1.00
```

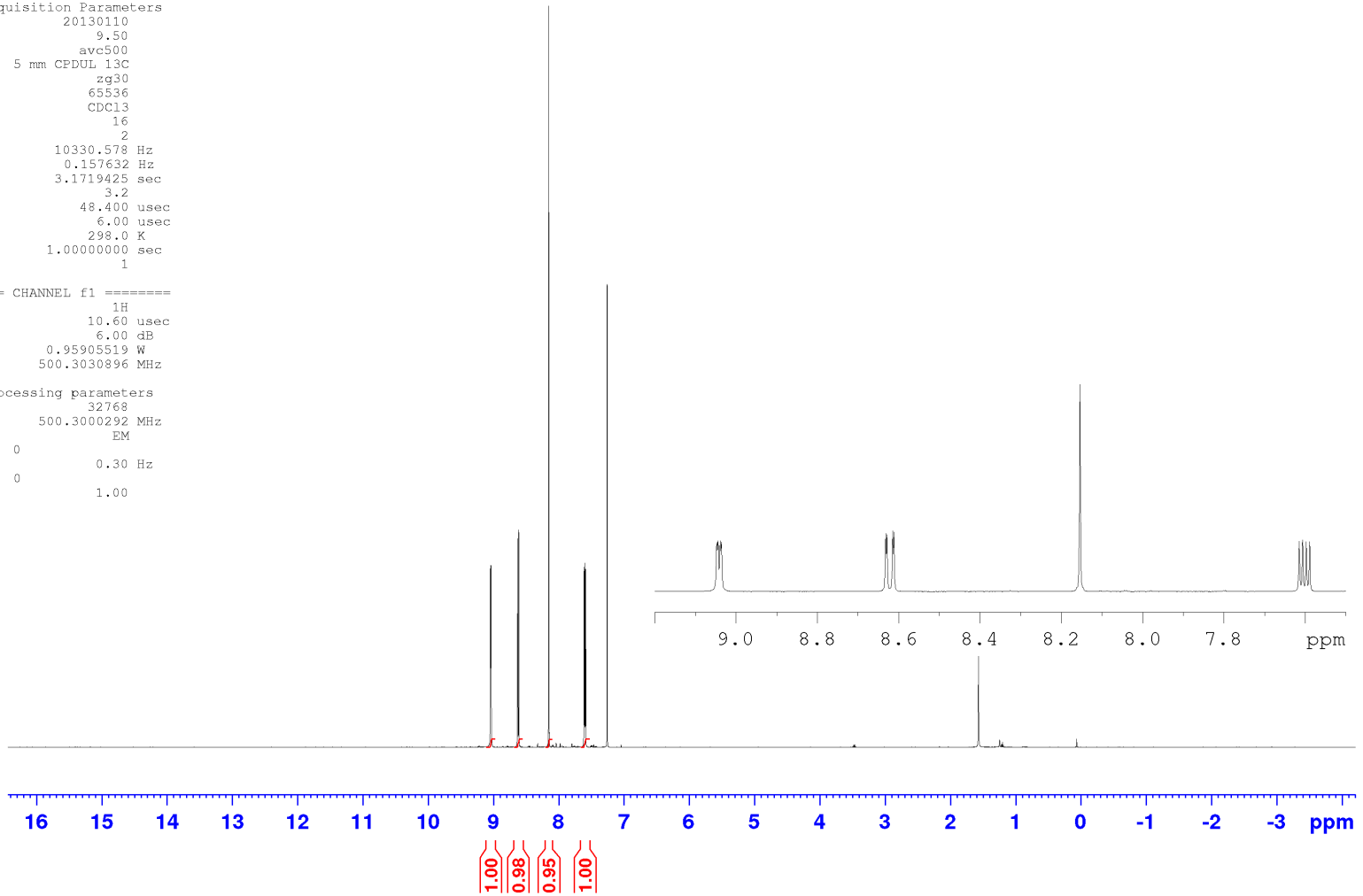

2.23. 5,8-Dibromo-6-chloroquinoline

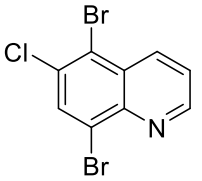


```
Current Data Parameters
NAME      5,8-dibromo-6-chloroquinoline
EXPNO                 4
PROCNO                1

F2 - Acquisition Parameters
Date_           20130110
Time              11.05
INSTRUM           avc500
PROBHD    5 mm CPDUL 13C
PULPROG           zgpg30
TD                65536
SOLVENT           CDCl3
NS                 1024
DS                    2
SWH           31250.000 Hz
FIDRES        0.476837 Hz
AQ            1.0485760 sec
RG                  912
DW               16.000 usec
DE               20.00 usec
TE               298.0 K
D1           2.00000000 sec
D11          0.03000000 sec
TD0                   1

======== CHANNEL f1 ========
NUC1                 13C
P1                 10.25 usec
PL1                 8.00 dB
PL1W         1.62029624 W
SFO1        125.8131151 MHz

======== CHANNEL f2 ========
CPDPRG[2          waltz16
NUC2                 1H
PCPD2              80.00 usec
PL2                 6.00 dB
PL12               23.56 dB
PL13               29.56 dB
PL2W         0.95905519 W
PL12W        0.01682068 W
PL13W        0.00422516 W
SFO2        500.3020012 MHz

F2 - Processing parameters
SI                 32768
SF          125.8005219 MHz
WDW                   EM
SSB       0
LB                 1.00 Hz
GB        0
PC                 1.40
```

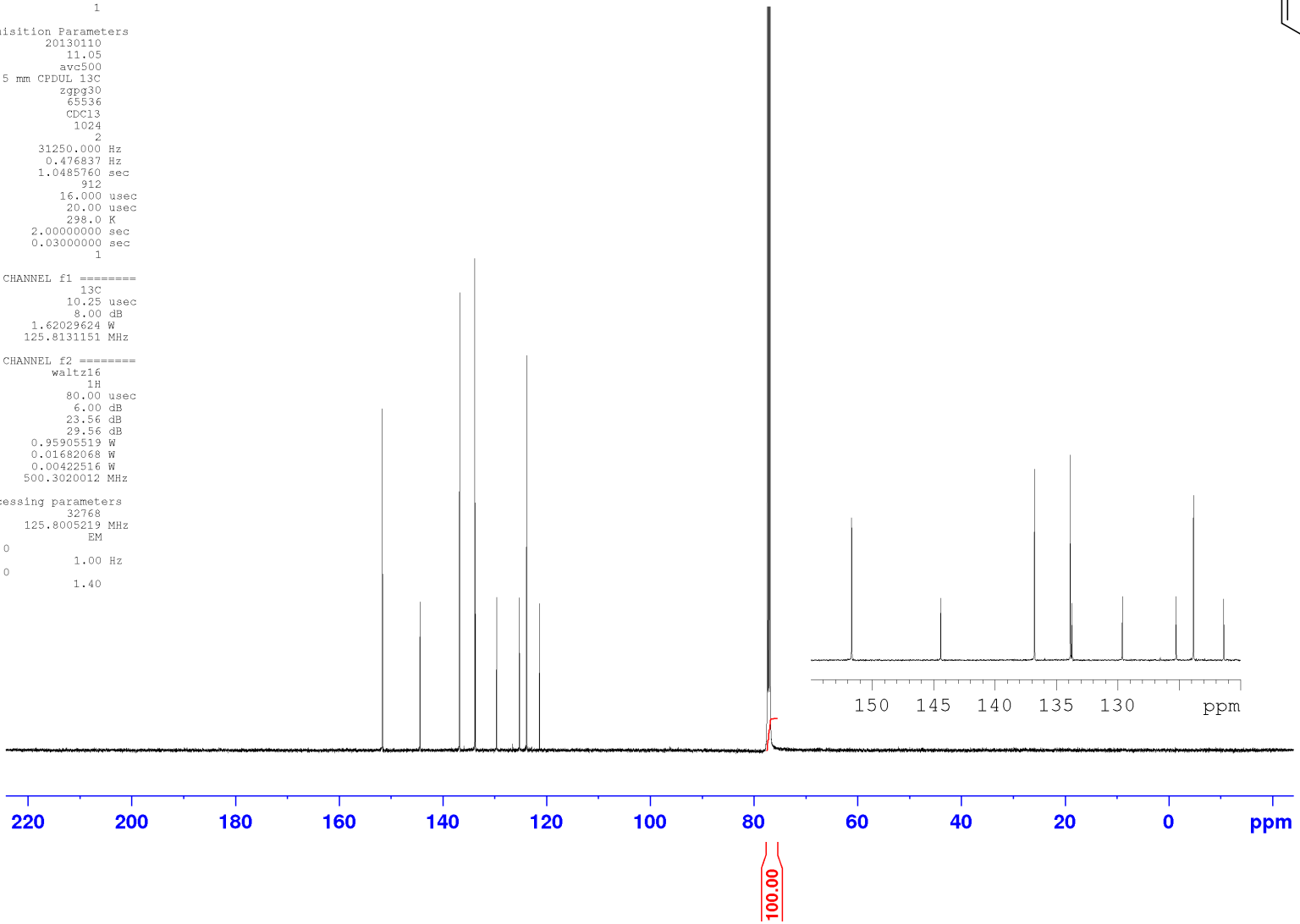

2.25. 5-Bromo-6-chloro-2-isopropylquinoline

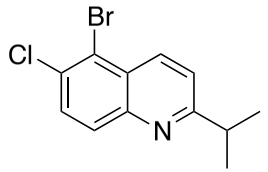


```
Current Data Parameters
NAME      2-isopropyl-5-bromo-6-chloroquinoline
EXPNO                   1
PROCNO                  1

F2 - Acquisition Parameters
Date_           20130123
Time              14.43
INSTRUM          avc500
PROBHD   5 mm CPDUL 13C
PULPROG             zg30
TD                65536
SOLVENT           CDCl3
NS                   16
DS                    2
SWH           10330.578 Hz
FIDRES         0.157632 Hz
AQ            3.1719425 sec
RG                  2.8
DW                48.400 usec
DE                 6.00 usec
TE                300.0 K
D1           1.00000000 sec
TD0                   1

======== CHANNEL f1 ========
NUC1                 1H
P1                10.60 usec
PL1                6.00 dB
PL1W         0.95905519 W
SFO1        500.3030896 MHz

F2 - Processing parameters
SI                32768
SF          500.3000284 MHz
WDW                  EM
SSB       0
LB                0.30 Hz
GB        0
PC                1.00
```

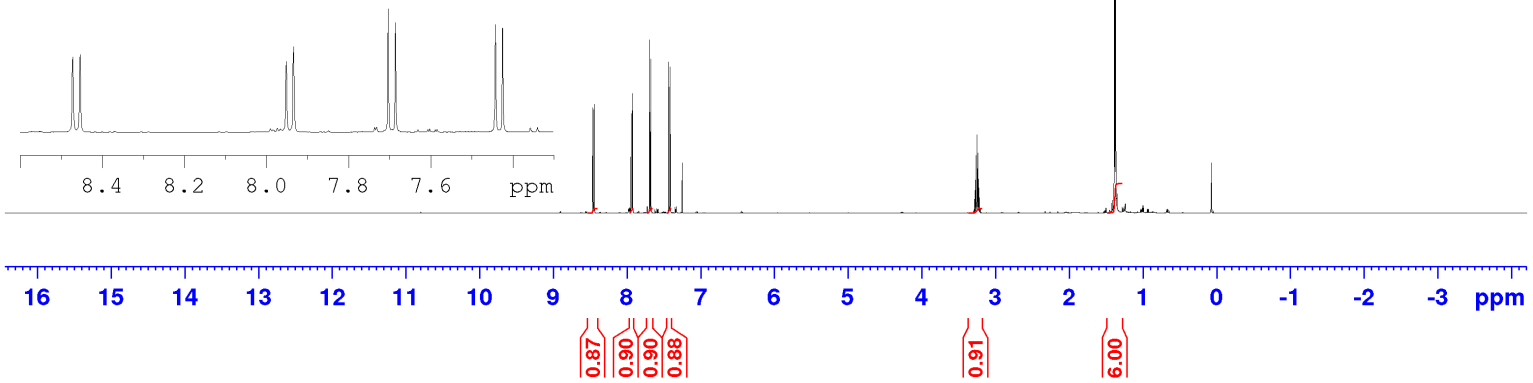

2.25. 5-Bromo-6-chloro-2-isopropylquinoline

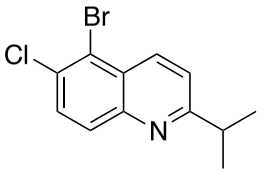

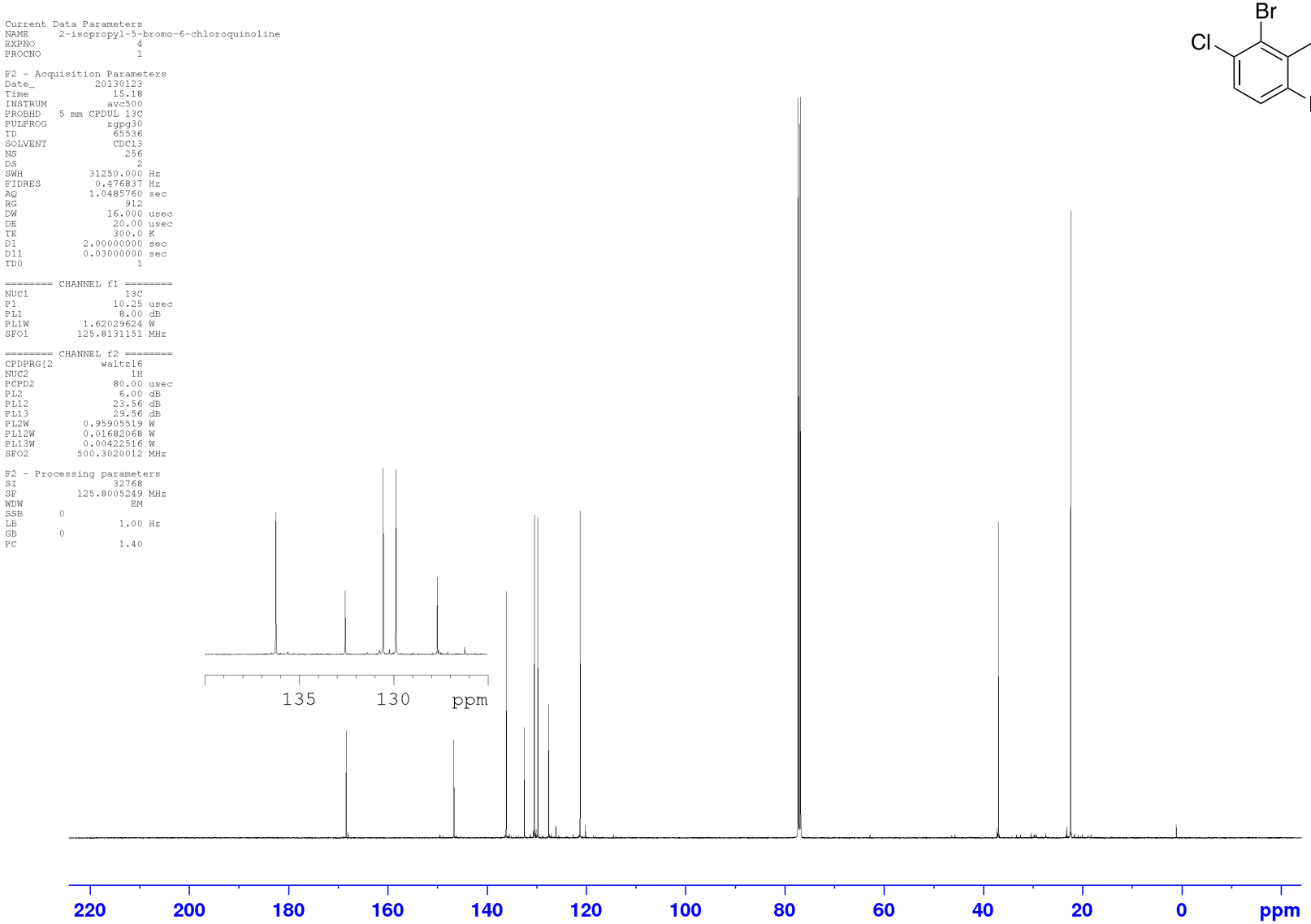

2.28. 6-Chloro-5-(((2-fluorobenzyl)oxy)methyl)quinoline

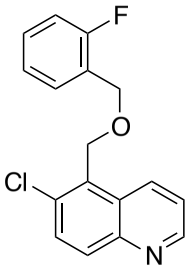


```
Current Data Parameters
NAME      5-(((2-fluorobenzyl)oxy)methyl)-6-nitroquinoline
EXPNO                  1
PROCNO                 1

F2 - Acquisition Parameters
Date_           20130227
Time                4.52
INSTRUM          avc500
PROBHD   5 mm CPDUL 13C
PULPROG             zg30
TD                 65536
SOLVENT            CDCl3
NS                    16
DS                     4
SWH            10330.578 Hz
FIDRES          0.157632 Hz
AQ             3.1719425 sec
RG                   3.2
DW                48.400 usec
DE                 6.00 usec
TE                298.0 K
D1           1.00000000 sec
TD0                    1

======== CHANNEL f1 ========
NUC1                  1H
P1                 10.60 usec
PL1                 6.00 dB
PL1W          0.95905519 W
SFO1         500.3030896 MHz

F2 - Processing parameters
SI                 32768
SF           500.3000302 MHz
WDW                   EM
SSB       0
LB                 0.30 Hz
GB        0
PC                 1.00
```

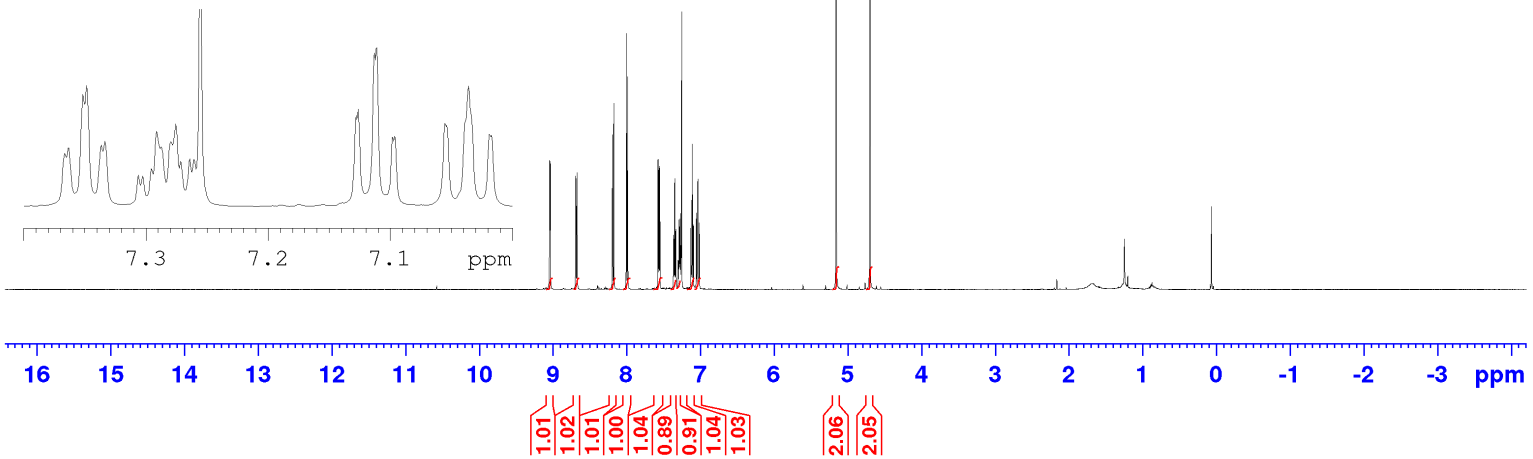

2.28. 6-Chloro-5-(((2-fluorobenzyl)oxy)methyl)quinoline

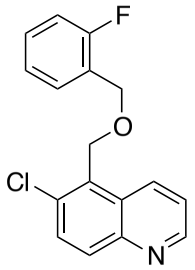

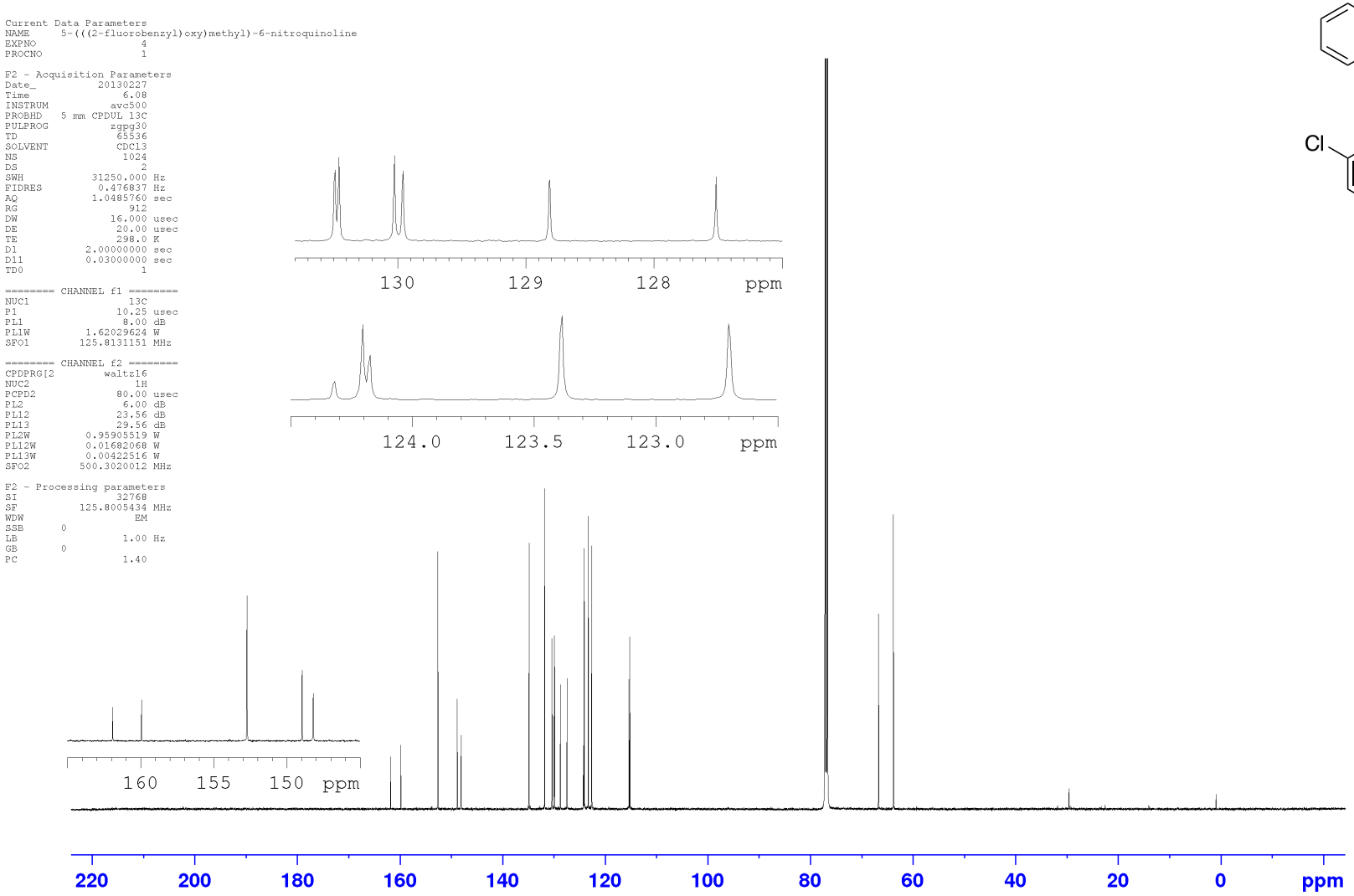

2.28. 6-Chloro-5-(((2-fluorobenzyl)oxy)methyl)quinoline

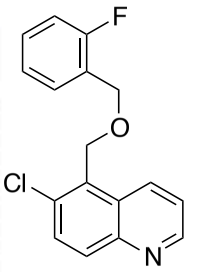


```
NAME          1c27770402
EXPNO                  1
PROCNO                 1
Date_           20130205
Time              10.20
INSTRUM           avb500
PROBHD   5 mm PATXI 1H/
PULPROG         zgfhigqn
TD                131072
SOLVENT             CDCl3
NS                    16
DS                     4
SWH          113636.367 Hz
FIDRES         0.866977 Hz
AQ             0.5767668 sec
RG                  1030
DW                 4.400 usec
DE                 6.50 usec
TE                298.0 K
D1            1.00000000 sec
D11           0.03000000 sec
D12           0.00002000 sec
TD0                    1

======== CHANNEL f1 ========
NUC1                  19F
P1                 10.00 usec
PL1                 0.90 dB
SFO1         470.4041911 MHz

======== CHANNEL f2 ========
CPDPRG2           waltz16
NUC2                  1H
PCPD2              80.00 usec
PL2                 1.00 dB
PL12               22.00 dB
PL2W         13.20863628 W
PL12W         0.10491993 W
SFO2         499.9819999 MHz
SI                 65536
SF           470.4512360 MHz
WDW                   EM
SSB                    0
LB                  0.30 Hz
GB                     0
PC                  1.00
```

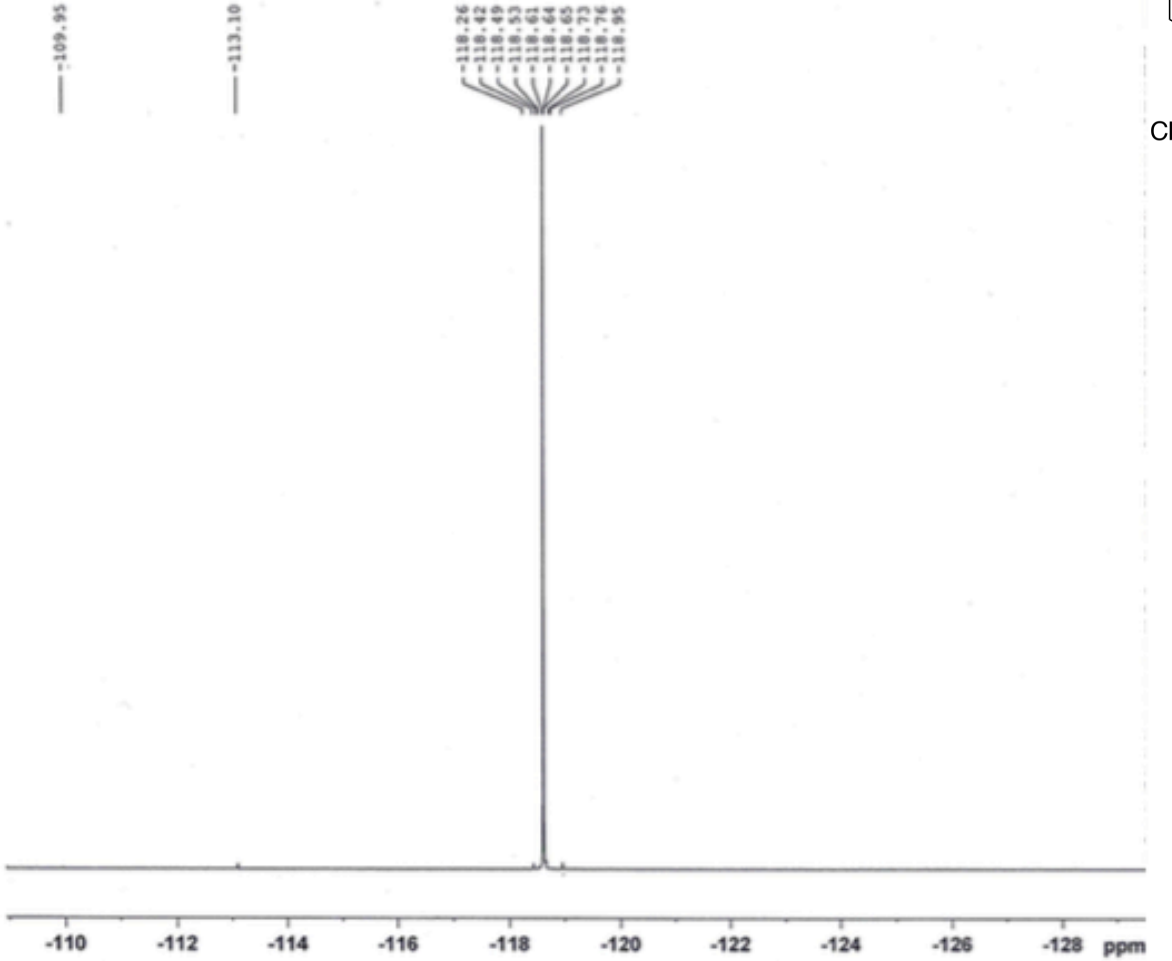

2.29. 6-Chloro-5-(((4-fluorobenzyl)oxy)methyl)quinoline

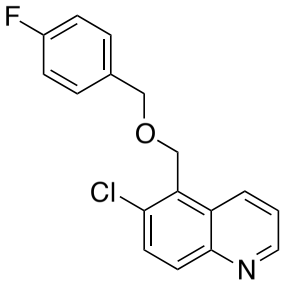


```
Current Data Parameters
NAME      6-chloro-5-(((4-fluorobenzyl)oxy)methyl)quinoline
EXPNO                  1
PROCNO                 1

F2 - Acquisition Parameters
Date_           20121201
Time              10.06
INSTRUM          avc500
PROBHD   5 mm CPDUL 13C
PULPROG             zg30
TD                 65536
SOLVENT            CDCl3
NS                    16
DS                     2
SWH           10330.578 Hz
FIDRES         0.157632 Hz
AQ            3.1719425 sec
RG                   2.8
DW                48.400 usec
DE                 6.00 usec
TE                298.0 K
D1           1.00000000 sec
TD0                    1

======== CHANNEL f1 ========
NUC1                  1H
P1                 10.60 usec
PL1                 6.00 dB
PL1W          0.95905519 W
SFO1        500.3030896 MHz

F2 - Processing parameters
SI                 32768
SF          500.3000279 MHz
WDW                   EM
SSB       0
LB                 0.30 Hz
GB        0
PC                 1.00
```

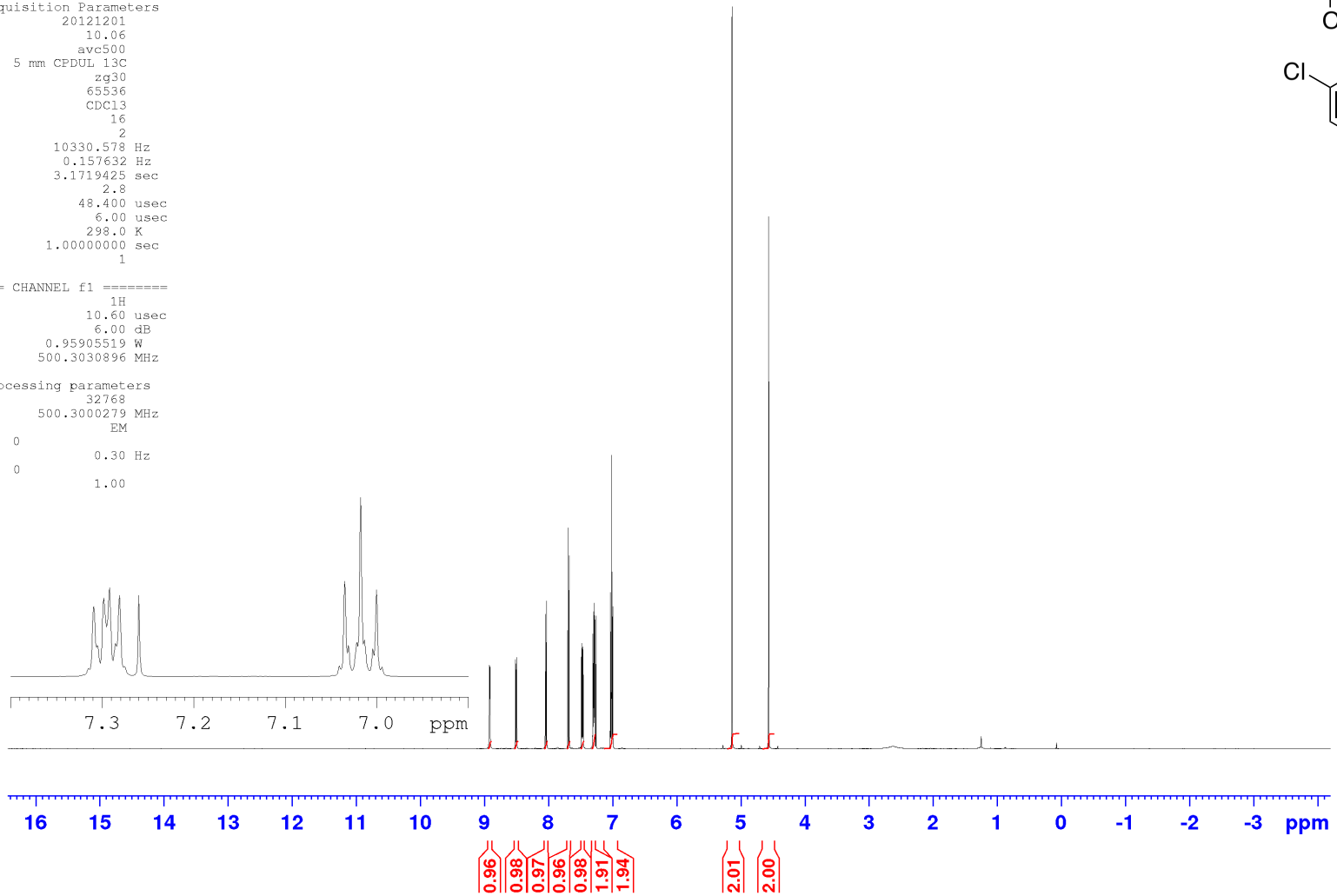

2.29. 6-Chloro-5-(((4-fluorobenzyl)oxy)methyl)quinoline

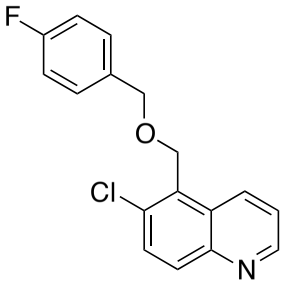


```
Current Data Parameters
NAME      6-chloro-5-(((4-fluorobenzyl)oxy)methyl)quinoline
EXPNO                 4
PROCNO                1

F2 - Acquisition Parameters
Date_           20121201
Time              10.58
INSTRUM          avc500
PROBHD   5 mm CPDUL 13C
PULPROG          zgpg30
TD                65536
SOLVENT           CDCl3
NS                  512
DS                    2
SWH           31250.000 Hz
FIDRES        0.476837 Hz
AQ            1.0485760 sec
RG                 1820
DW               16.000 usec
DE                20.00 usec
TE                298.0 K
D1           2.00000000 sec
D11          0.03000000 sec
TD0                   1

======== CHANNEL f1 ========
NUC1                 13C
P1                 10.25 usec
PL1                 8.00 dB
PL1W         1.62029624 W
SFO1        125.8131151 MHz

======== CHANNEL f2 ========
CPDPRG[2           waltz16
NUC2                 1H
PCPD2              80.00 usec
PL2                 6.00 dB
PL12               23.56 dB
PL13               29.56 dB
PL2W         0.95905519 W
PL12W        0.01682068 W
PL13W        0.00422516 W
SFO2        500.3020012 MHz

F2 - Processing parameters
SI                 32768
SF          125.8005493 MHz
WDW                  EM
SSB       0
LB                 1.00 Hz
GB        0
PC                 1.40
```

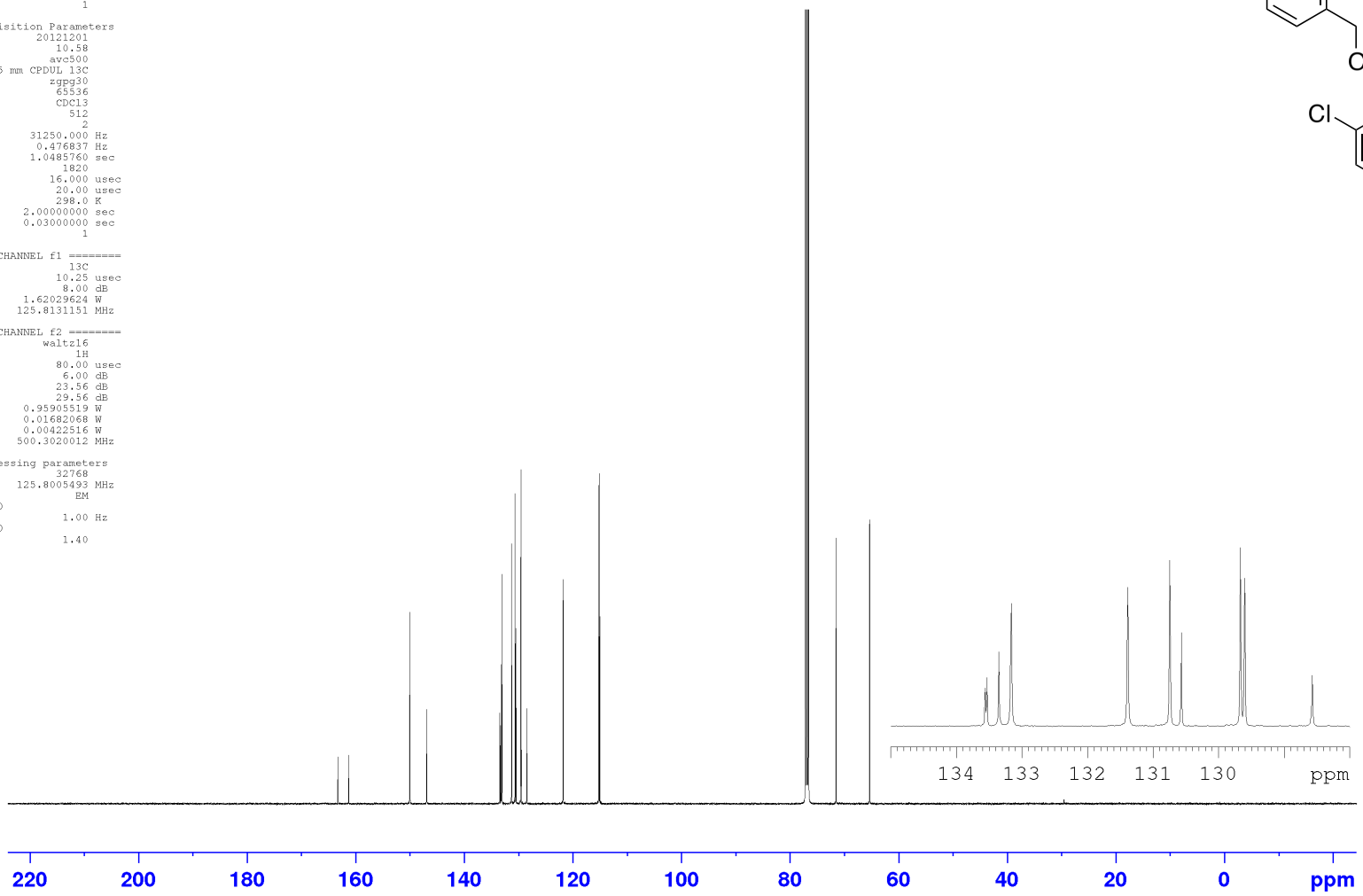

2.29. 6-Chloro-5-(((4-fluorobenzyl)oxy)methyl)quinoline

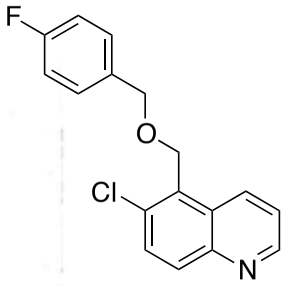

NAME	1c20972811	
EXPNO	1	
PROCNO	1	
Date_	20121128	
Time	10.03	
INSTRUM	avb500	
PROBHD	5 mm PATXI 1H/	
PULPROG	zgfhigqn	
TD	131072	
SOLVENT	CDCl3	
NS	16	
DS	4	
SWH	113636.367	Hz
FIDRES	0.866977	Hz
AQ	0.5767668	sec
RG	1290	
DW	4.400	use
DE	6.50	use
TE	298.0	K
D1	1.00000000	sec
D11	0.03000000	sec
D12	0.00002000	sec
TD0	1	
======== CHANNEL f1 ========		
NUC1	19F	
P1	10.00	use
PL1	0.90	dB
SFO1	470.4041911	MHz
======== CHANNEL f2 ========		
CPDPRG2	waltz16	
NUC2	1H	
PCPD2	80.00	use
PL2	1.00	dB
PL12	22.00	dB
PL2W	13.20863628	W
PL12W	0.10491993	W
SFO2	499.9819999	MHz
SI	65536	
SF	470.4512360	MHz
WDW	EM	
SSB	0	
LB	0.30	Hz
GB	0	
PC	10.00	

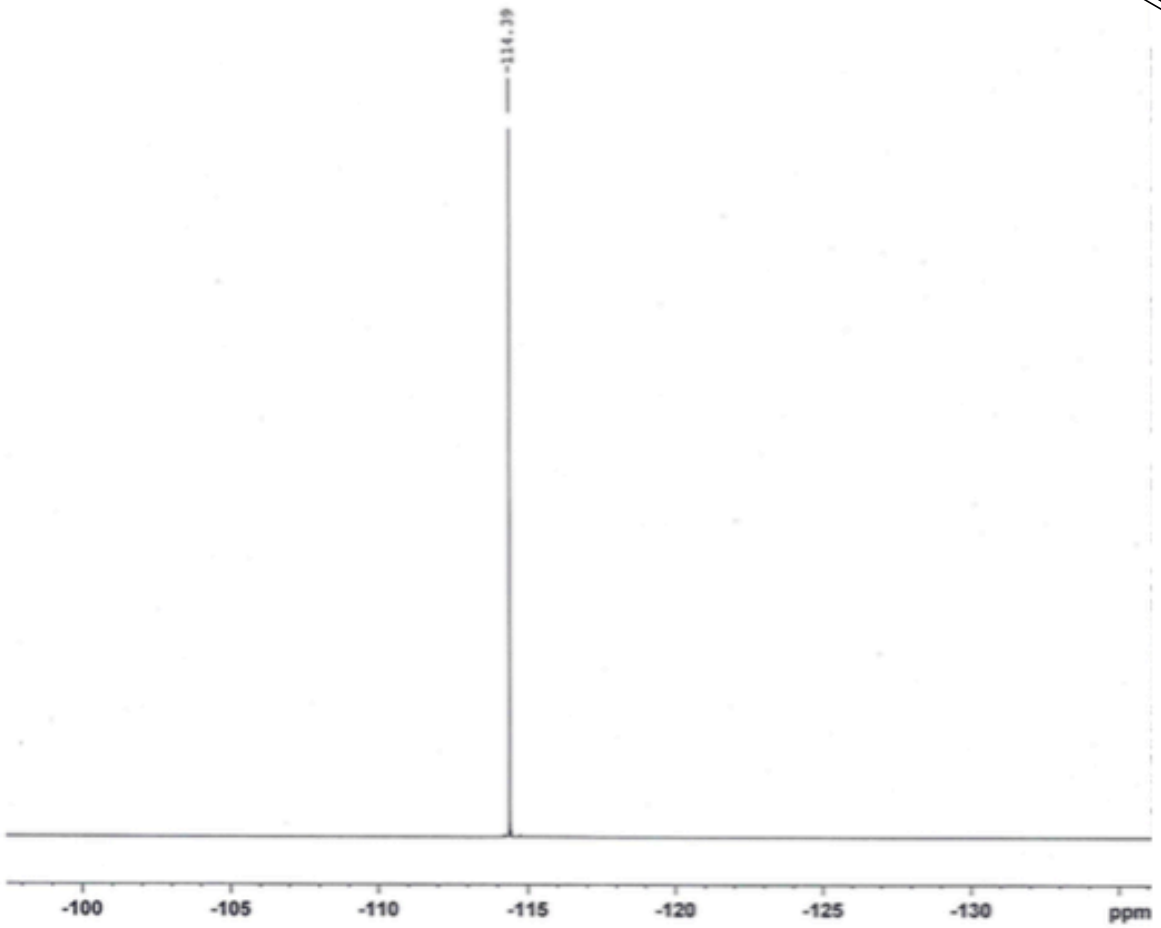

2.30. 5-((Benzyloxy)methyl)-6-chloroquinoline

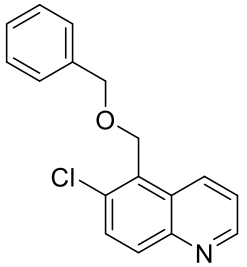


```
Current Data Parameters
NAME      5-((benzyloxy)methyl)-6-chloroquinoline
EXPNO                  1
PROCNO                 1

F2 - Acquisition Parameters
Date_           20130310
Time               7.02
INSTRUM          avc500
PROBHD   5 mm CPDUL 13C
PULPROG            zg30
TD                65536
SOLVENT           CDCl3
NS                   16
DS                    4
SWH           10330.578 Hz
FIDRES         0.157632 Hz
AQ            3.1719425 sec
RG                  2.8
DW               48.400 usec
DE                6.00 usec
TE               298.0 K
D1           1.00000000 sec
TD0                    1

======== CHANNEL f1 ========
NUC1                  1H
P1                10.60 usec
PL1                6.00 dB
PL1W         0.95905519 W
SFO1        500.3030896 MHz

F2 - Processing parameters
SI                 32768
SF          500.3000285 MHz
WDW                   EM
SSB       0
LB                 0.30 Hz
GB        0
PC                 1.00
```

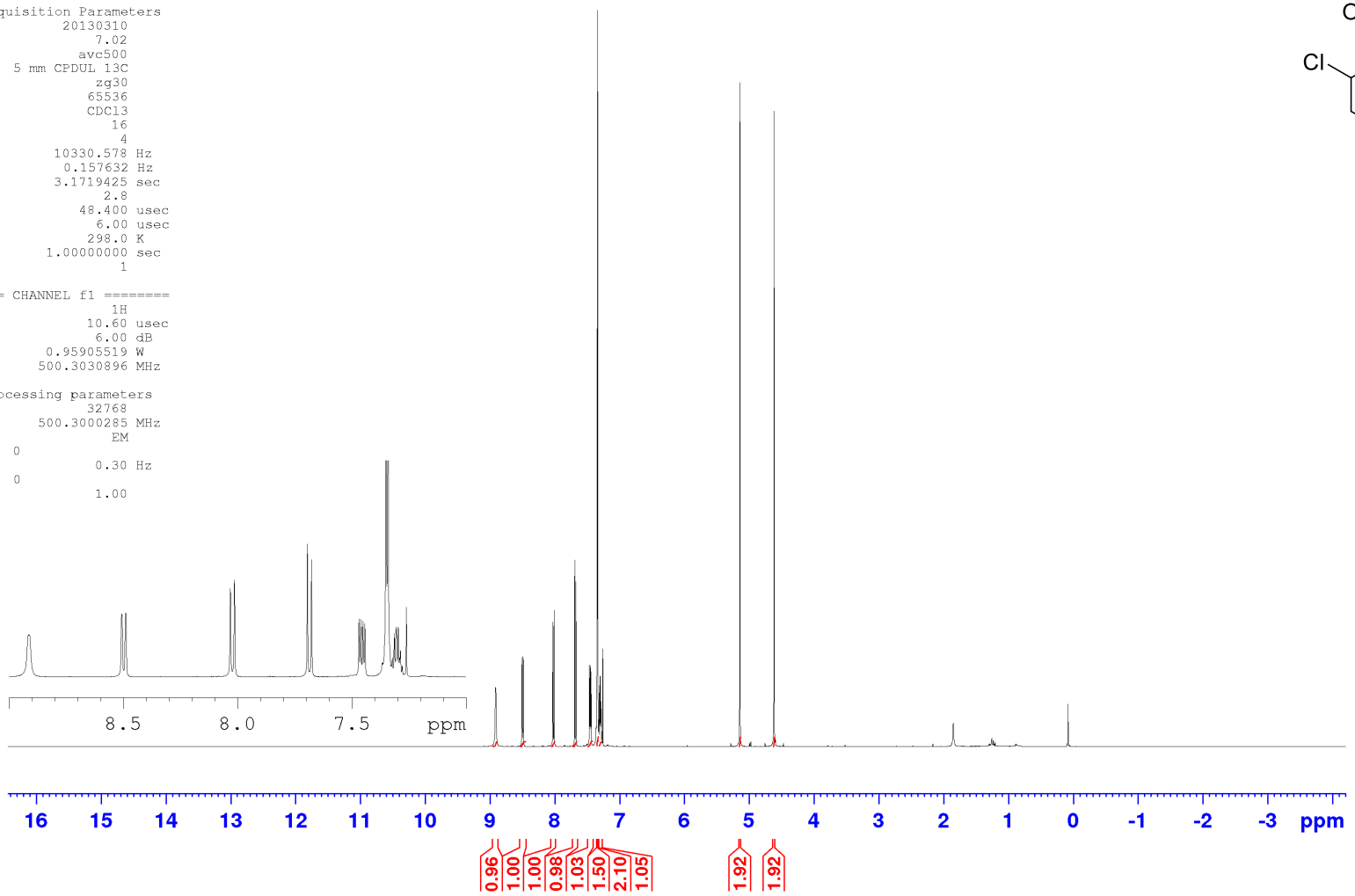

2.30. 5-((Benzyloxy)methyl)-6-chloroquinoline

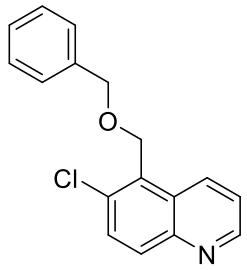


```
Current Data Parameters
NAME      5-((benzyloxy)methyl)-6-chloroquinoline
EXPNO                 4
PROCNO                1

F2 - Acquisition Parameters
Date_          20130310
Time               9.11
INSTRUM          avc500
PROBHD   5 mm CPDUL 13C
PULPROG          zgpg30
TD                65536
SOLVENT           CDCl3
NS                 2048
DS                    2
SWH           31250.000 Hz
FIDRES         0.476837 Hz
AQ            1.0485760 sec
RG                  912
DW               16.000 usec
DE               20.00 usec
TE               298.0 K
D1           2.00000000 sec
D11          0.03000000 sec
TD0                   1

======== CHANNEL f1 ========
NUC1                 13C
P1                10.25 usec
PL1                8.00 dB
PL1W         1.62029624 W
SFO1        125.8131151 MHz

======== CHANNEL f2 ========
CPDPRG[2         waltz16
NUC2                 1H
PCPD2             80.00 usec
PL2                6.00 dB
PL12              23.56 dB
PL13              29.56 dB
PL2W         0.95905519 W
PL12W        0.01682068 W
PL13W        0.00422516 W
SFO2        500.3020012 MHz

F2 - Processing parameters
SI                32768
SF          125.8005258 MHz
WDW                  EM
SSB       0
LB                1.00 Hz
GB        0
PC                1.40
```

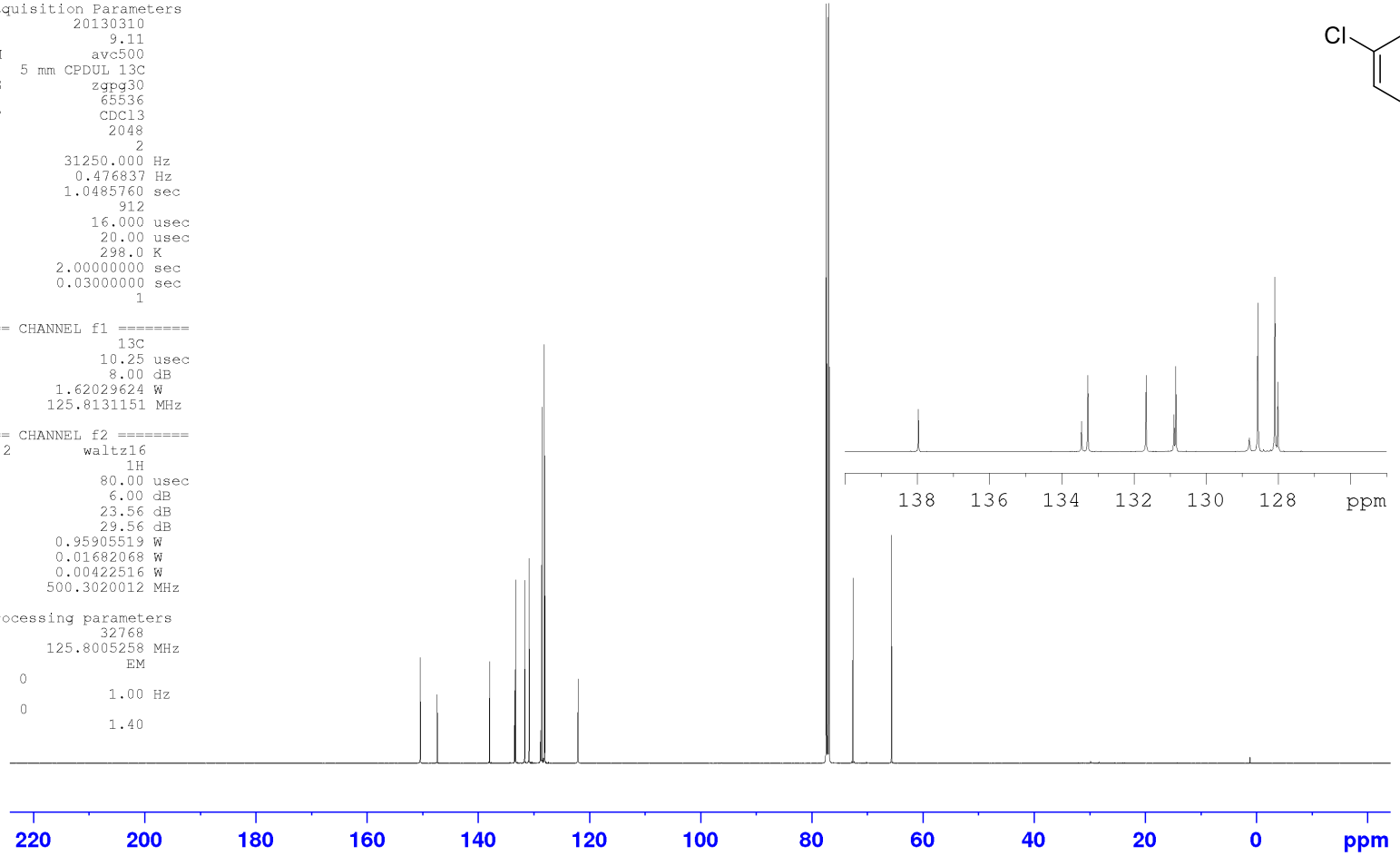

2.31. (6-Chloroquinolin-5-yl)methyl acetate

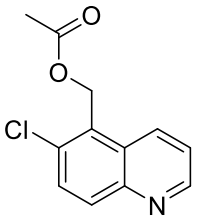


```
Current Data Parameters
NAME      (6-chloroquinolin-5-yl)methyl acetate
EXPNO                  1
PROCNO                 1

F2 - Acquisition Parameters
Date_           20130215
Time              10.04
INSTRUM          avc500
PROBHD   5 mm CPDUL 13C
PULPROG            zg30
TD                65536
SOLVENT           CDCl3
NS                   16
DS                    4
SWH           10330.578 Hz
FIDRES         0.157632 Hz
AQ            3.1719425 sec
RG                    2
DW               48.400 usec
DE                6.00 usec
TE               298.0 K
D1           1.00000000 sec
TD0                   1

======== CHANNEL f1 ========
NUC1                 1H
P1                10.60 usec
PL1                6.00 dB
PL1W         0.95905519 W
SFO1        500.3030896 MHz

F2 - Processing parameters
SI                32768
SF          500.3000281 MHz
WDW                  EM
SSB       0
LB                0.30 Hz
GB        0
PC                1.00
```

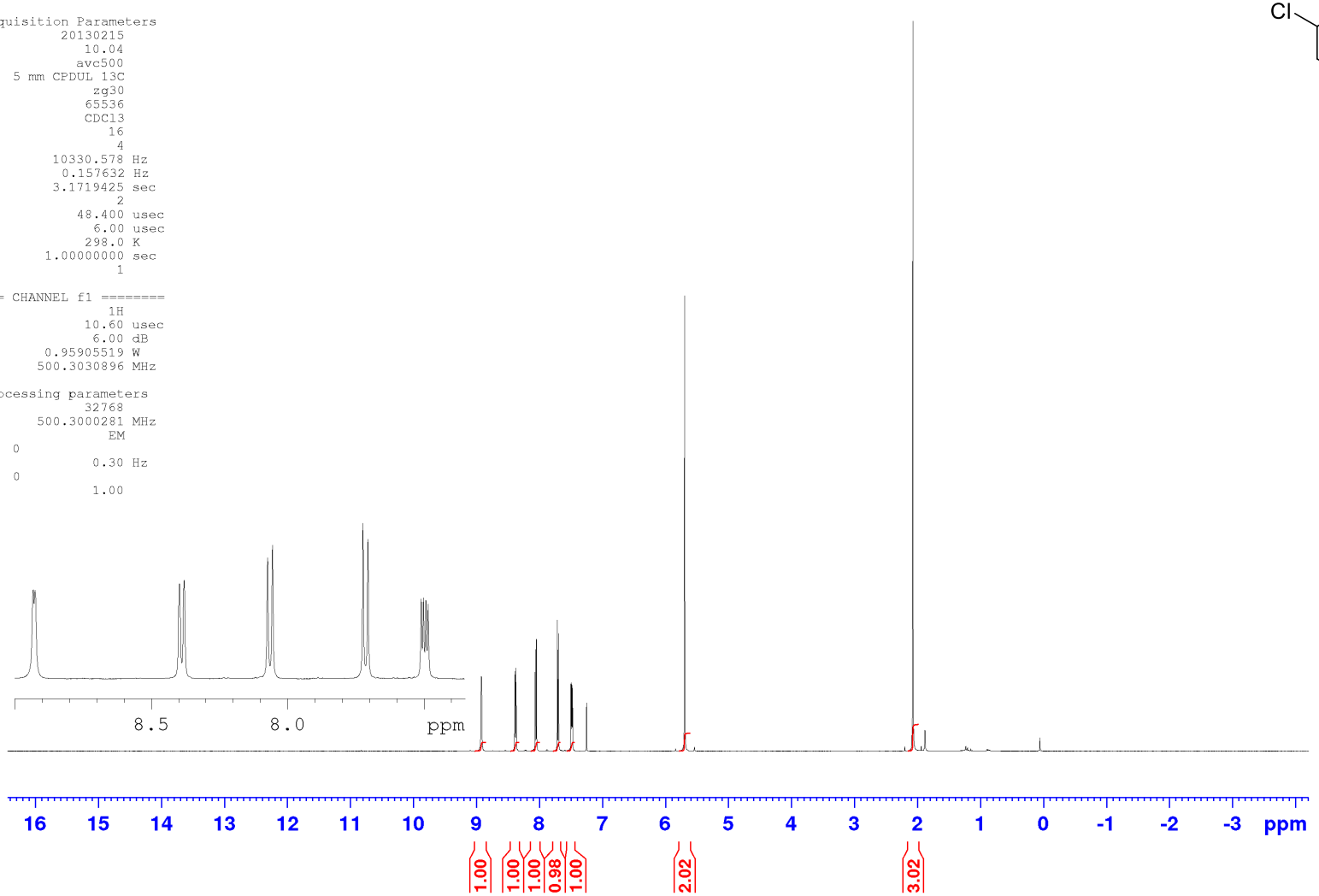

2.31. (6-Chloroquinolin-5-yl)methyl acetate

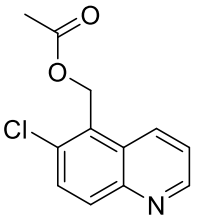


```
Current Data Parameters
NAME      (6-chloroquinolin-5-yl)methyl acetate
EXPNO                 4
PROCNO                1

F2 - Acquisition Parameters
Date_           20130215
Time              10.39
INSTRUM          avc500
PROBHD   5 mm CPDUL 13C
PULPROG          zgpg30
TD                65536
SOLVENT           CDCl3
NS                  256
DS                    2
SWH           31250.000 Hz
FIDRES        0.476837 Hz
AQ            1.0485760 sec
RG                  912
DW               16.000 usec
DE               20.00 usec
TE               298.0 K
D1           2.00000000 sec
D11          0.03000000 sec
TD0                   1

======== CHANNEL f1 ========
NUC1                 13C
P1                 10.25 usec
PL1                 8.00 dB
PL1W         1.62029624 W
SFO1        125.8131151 MHz

======== CHANNEL f2 ========
CPDPRG[2          waltz16
NUC2                 1H
PCPD2              80.00 usec
PL2                 6.00 dB
PL12               23.56 dB
PL13               29.56 dB
PL2W         0.95905519 W
PL12W        0.01682068 W
PL13W        0.00422516 W
SFO2        500.3020012 MHz

F2 - Processing parameters
SI                 32768
SF          125.8005248 MHz
WDW                  EM
SSB       0
LB                 1.00 Hz
GB        0
PC                 1.40
```


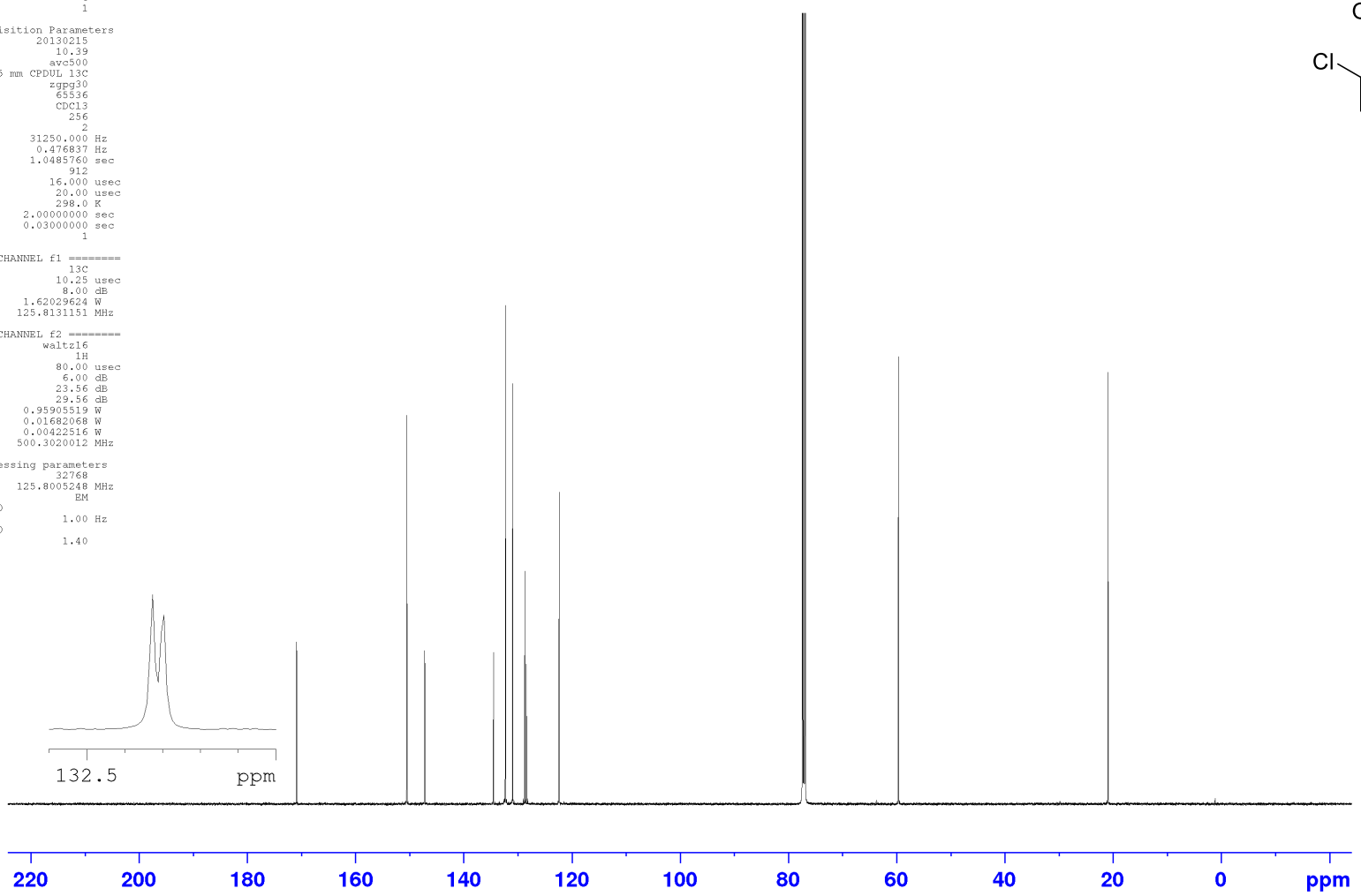

2.32. 5-(((2-Fluorobenzyl)oxy)methyl)-6-nitroquinoline

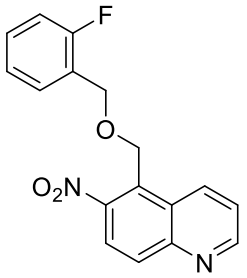


```
Current Data Parameters
NAME      5-(((2-fluorobenzyl)oxy)methyl)-6-nitroquinoline
EXPNO                  1
PROCNO                 1

F2 - Acquisition Parameters
Date_           20130227
Time                4.52
INSTRUM          avc500
PROBHD    5 mm CPDUL 13C
PULPROG             zg30
TD                 65536
SOLVENT            CDCl3
NS                    16
DS                     4
SWH            10330.578 Hz
FIDRES          0.157632 Hz
AQ             3.1719425 sec
RG                   3.2
DW                48.400 usec
DE                 6.00 usec
TE                298.0 K
D1           1.00000000 sec
TD0                    1

======== CHANNEL f1 ========
NUC1                  1H
P1                 10.60 usec
PL1                 6.00 dB
PL1W          0.95905519 W
SFO1         500.3030896 MHz

F2 - Processing parameters
SI                 32768
SF           500.3000302 MHz
WDW                   EM
SSB       0
LB                 0.30 Hz
GB        0
PC                 1.00
```

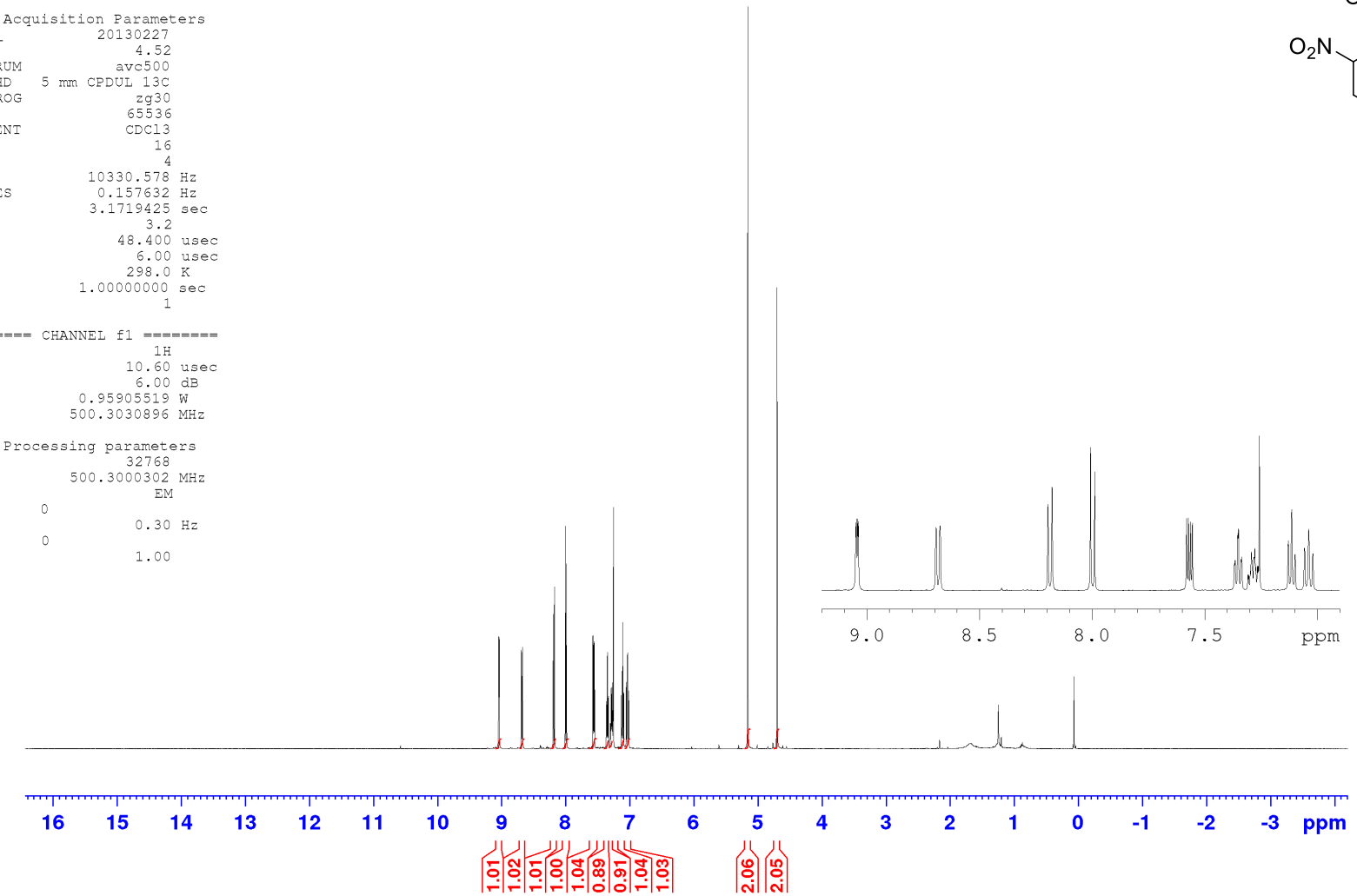

2.32. 5-(((2-Fluorobenzyl)oxy)methyl)-6-nitroquinoline

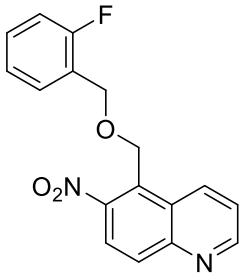

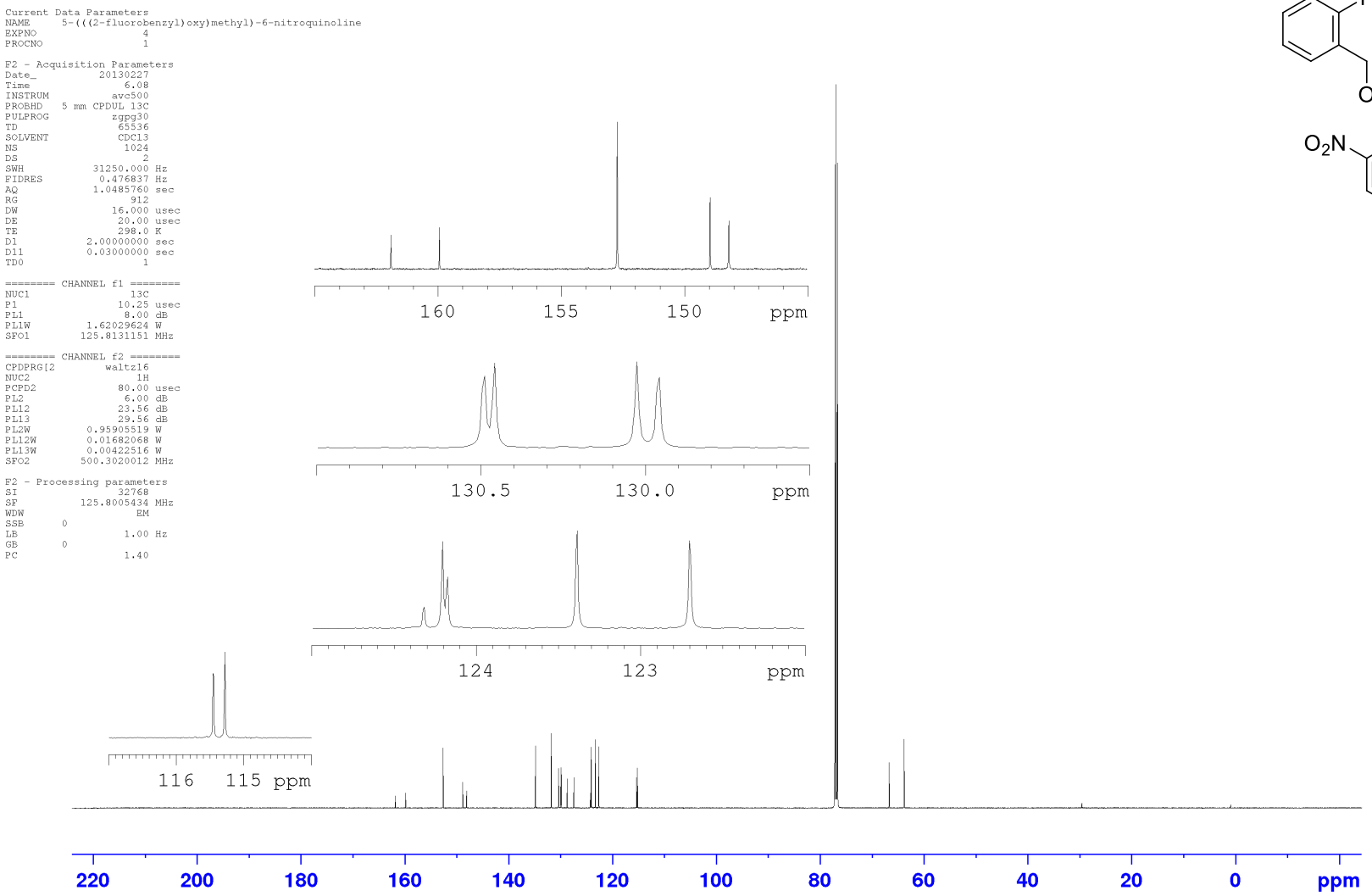

2.32. 5-(((2-Fluorobenzyl)oxy)methyl)-6-nitroquinoline

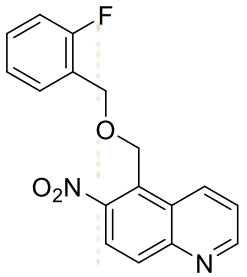

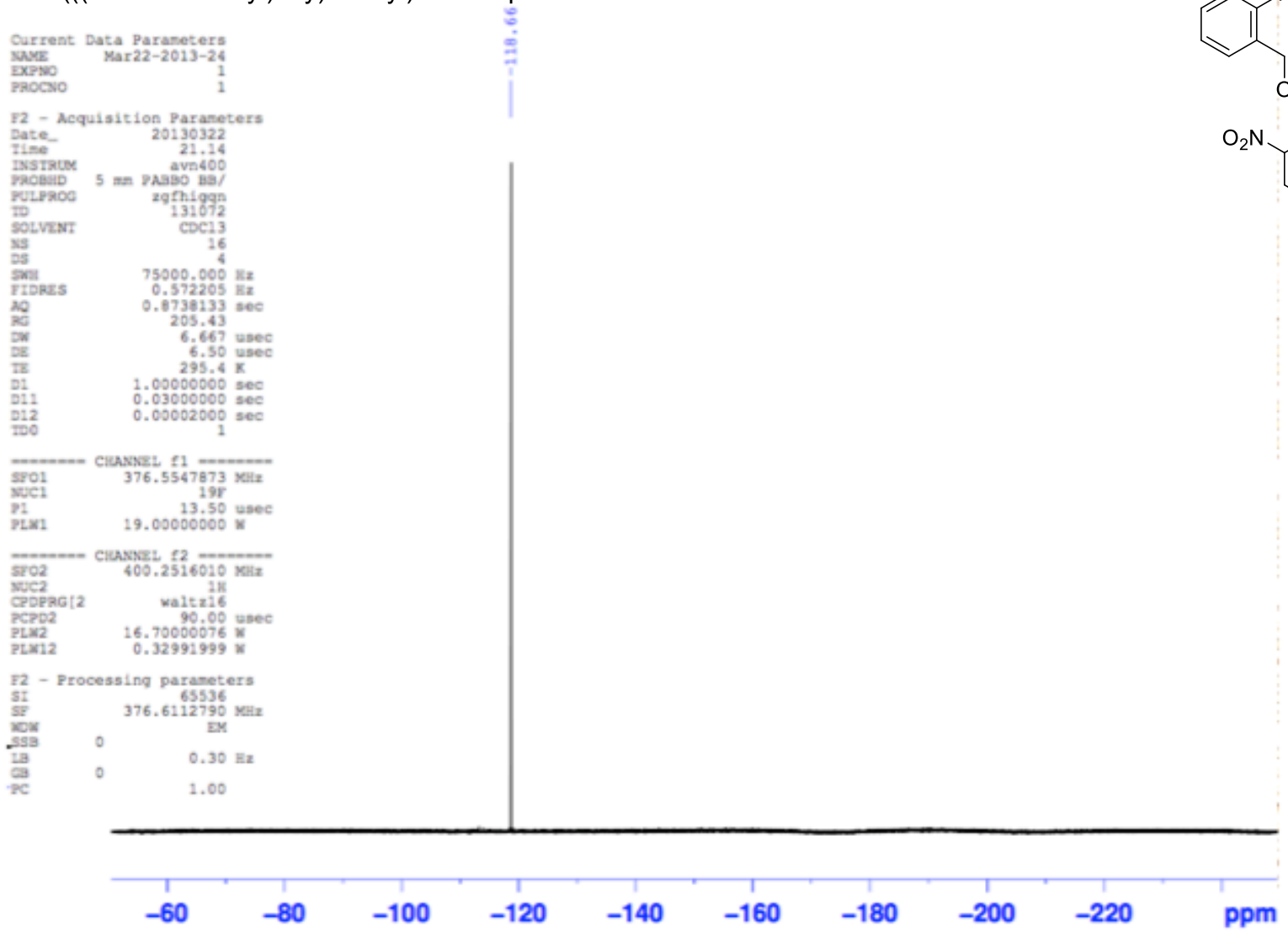

2.33. 5-(((4-Fluorobenzyl)oxy)methyl)-6-nitroquinoline

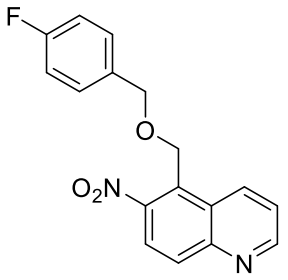


```
Current Data Parameters
NAME      5-(((4-fluorobenzyl)oxy)methyl)-6-nitroquinoline
EXPNO                  1
PROCNO                 1

F2 - Acquisition Parameters
Date_           20130410
Time                8.08
INSTRUM          avc500
PROBHD   5 mm CPDUL 13C
PULPROG             zg30
TD                 65536
SOLVENT            CDCl3
NS                    16
DS                     4
SWH            10330.578 Hz
FIDRES          0.157632 Hz
AQ             3.1719425 sec
RG                  1.78
DW                48.400 usec
DE                 6.00 usec
TE                298.0 K
D1           1.00000000 sec
TD0                    1

======== CHANNEL f1 ========
NUC1                  1H
P1                 10.60 usec
PL1                 6.00 dB
PL1W          0.95905519 W
SFO1         500.3030896 MHz

F2 - Processing parameters
SI                 32768
SF           500.3000281 MHz
WDW                   EM
SSB       0
LB                 0.30 Hz
GB        0
PC                 1.00
```

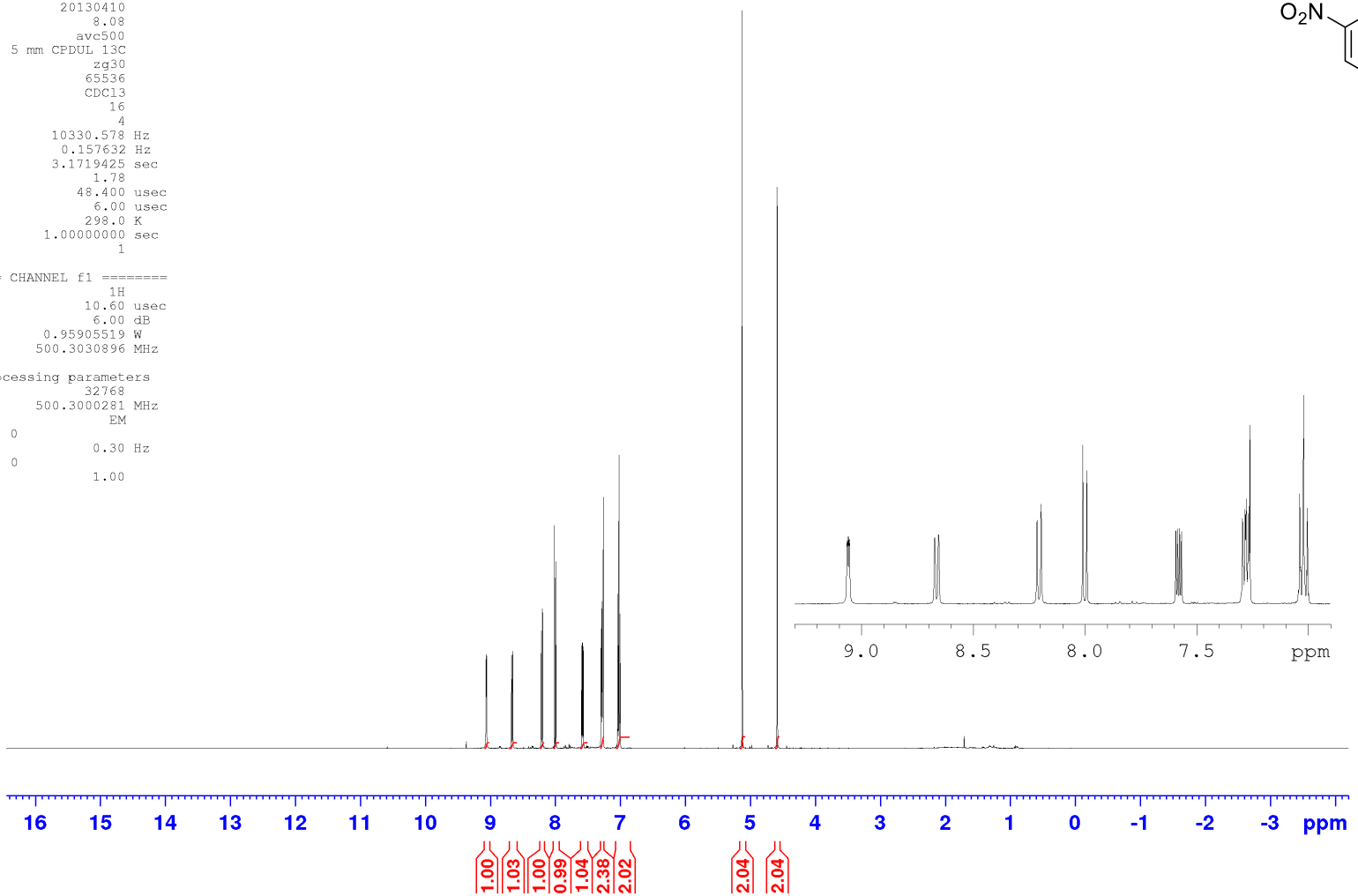

2.33. 5-(((4-Fluorobenzyl)oxy)methyl)-6-nitroquinoline

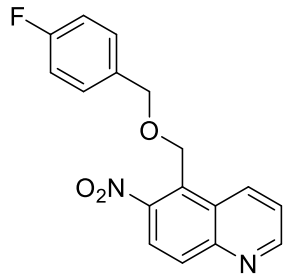


```
Current Data Parameters
NAME      5-(((4-fluorobenzyl)oxy)methyl)-6-nitroquinoline
EXPNO                  4
PROCNO                 1

F2 - Acquisition Parameters
Date_           20130410
Time               9.24
INSTRUM          avc500
PROBHD   5 mm CPDUL 13C
PULPROG          zgpg30
TD                65536
SOLVENT           CDCl3
NS                 1024
DS                    2
SWH           31250.000 Hz
FIDRES         0.476837 Hz
AQ            1.0485760 sec
RG                  912
DW               16.000 usec
DE               20.00 usec
TE               298.0 K
D1           2.00000000 sec
D11          0.03000000 sec
TD0                   1

======== CHANNEL f1 ========
NUC1                13C
P1                10.25 usec
PL1                8.00 dB
PL1W         1.62029624 W
SFO1        125.8131151 MHz

======== CHANNEL f2 ========
CPDPRG[2         waltz16
NUC2                1H
PCPD2             80.00 usec
PL2                6.00 dB
PL12              23.56 dB
PL13              29.56 dB
PL2W         0.95905519 W
PL12W        0.01682068 W
PL13W        0.00422516 W
SFO2        500.3020012 MHz

F2 - Processing parameters
SI                 32768
SF          125.8005231 MHz
WDW                   EM
SSB       0
LB                 1.00 Hz
GB        0
PC                 1.40
```

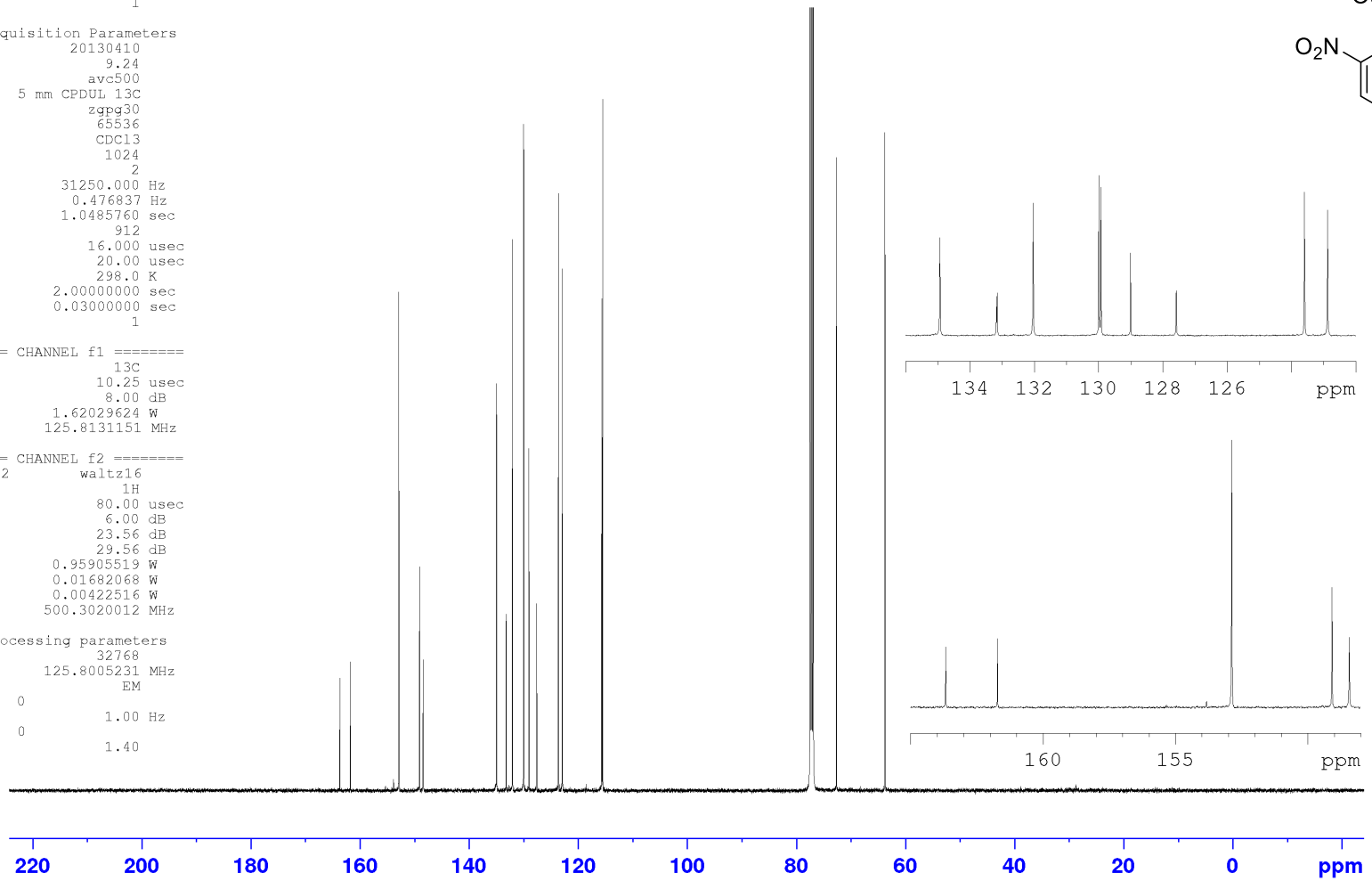

2.33. 5-(((4-Fluorobenzyl)oxy)methyl)-6-nitroquinoline

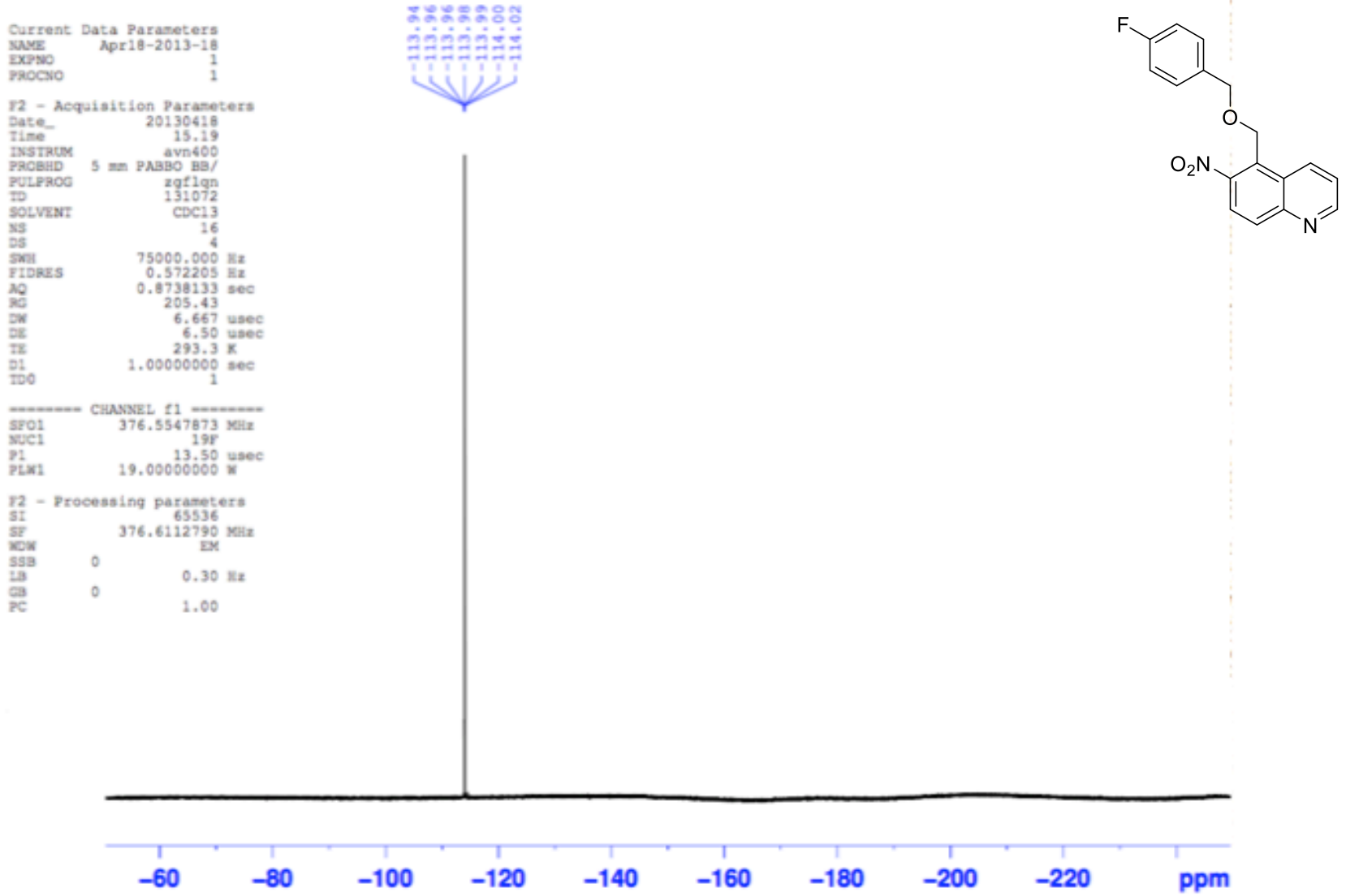

2.36. 6-Nitroquinoline-5-carbaldehyde

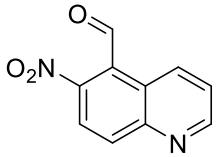


```
Current Data Parameters
NAME      6-nitroquinoline-5-carbaldehyde
EXPNO                   1
PROCNO                  1

F2 - Acquisition Parameters
Date_           20130405
Time                1.08
INSTRUM          avc500
PROBHD   5 mm CPDUL 13C
PULPROG             zg30
TD                 65536
SOLVENT            CDCl3
NS                    16
DS                     4
SWH            10330.578 Hz
FIDRES          0.157632 Hz
AQ             3.1719425 sec
RG                   3.2
DW                48.400 usec
DE                 6.00 usec
TE                298.0 K
D1           1.00000000 sec
TD0                    1

======== CHANNEL f1 ========
NUC1                  1H
P1                 10.60 usec
PL1                 6.00 dB
PL1W          0.95905519 W
SFO1         500.3030896 MHz

F2 - Processing parameters
SI                 32768
SF           500.3000277 MHz
WDW                   EM
SSB       0
LB                 0.30 Hz
GB        0
PC                 1.00
```

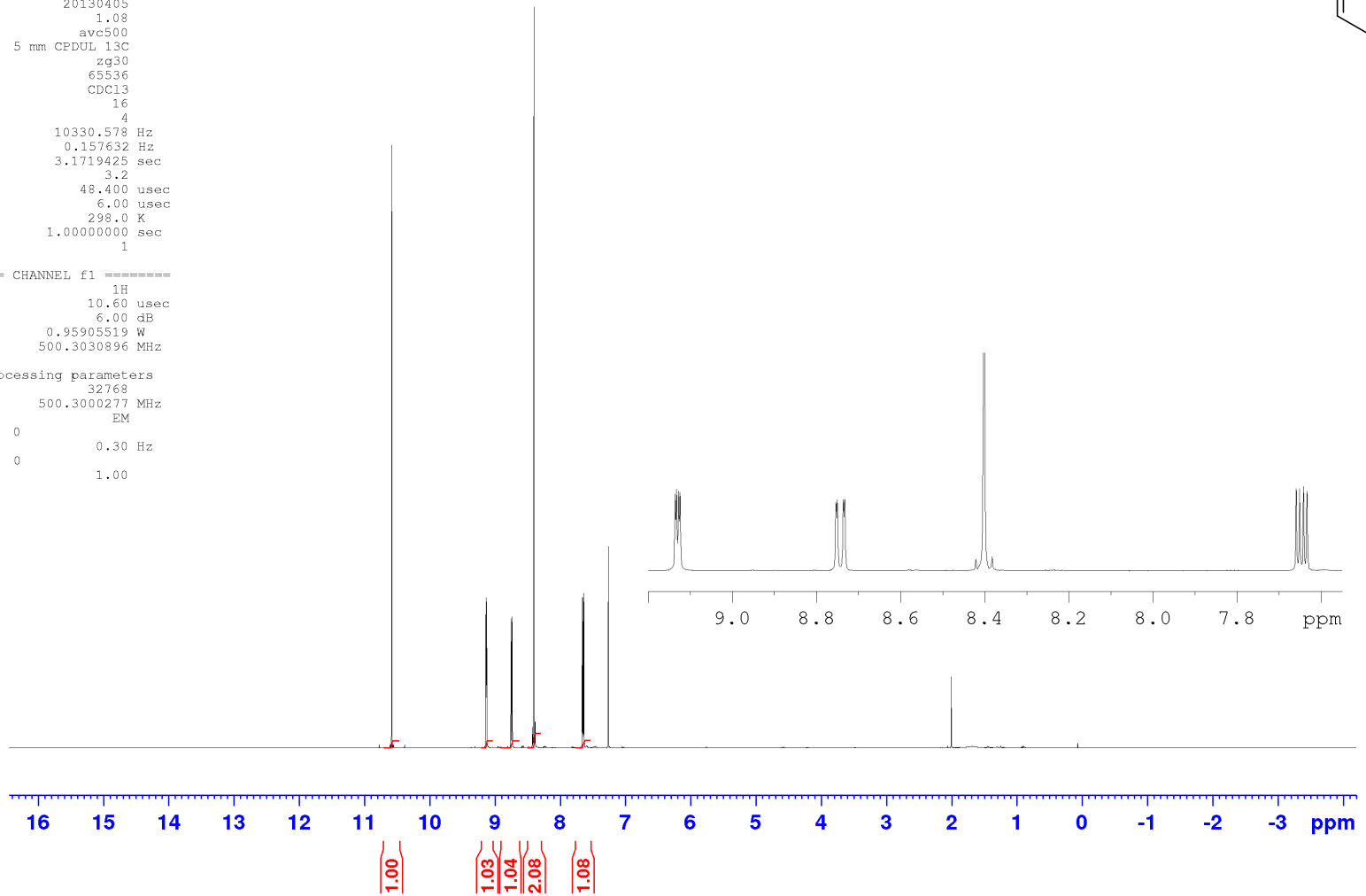

2.36. 6-Nitroquinoline-5-carbaldehyde

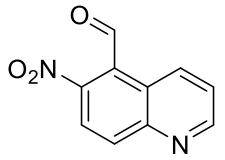


```
Current Data Parameters
NAME      6-nitroquinoline-5-carbaldehyde
EXPNO                   4
PROCNO                  1

F2 - Acquisition Parameters
Date_           20130405
Time                1.57
INSTRUM          avc500
PROBHD   5 mm CPDUL 13C
PULPROG          zgpg30
TD                65536
SOLVENT           CDCl3
NS                  512
DS                    2
SWH           31250.000 Hz
FIDRES         0.476837 Hz
AQ            1.0485760 sec
RG                  912
DW               16.000 usec
DE               20.00 usec
TE               298.0 K
D1            2.00000000 sec
D11           0.03000000 sec
TD0                   1

======== CHANNEL f1 ========
NUC1                 13C
P1                10.25 usec
PL1                8.00 dB
PL1W         1.62029624 W
SFO1        125.8131151 MHz

======== CHANNEL f2 ========
CPDPRG[2         waltz16
NUC2                 1H
PCPD2             80.00 usec
PL2                6.00 dB
PL12              23.56 dB
PL13              29.56 dB
PL2W         0.95905519 W
PL12W        0.01682068 W
PL13W        0.00422516 W
SFO2        500.3020012 MHz

F2 - Processing parameters
SI                32768
SF          125.8005242 MHz
WDW                  EM
SSB       0
LB                1.00 Hz
GB        0
PC                1.40
```

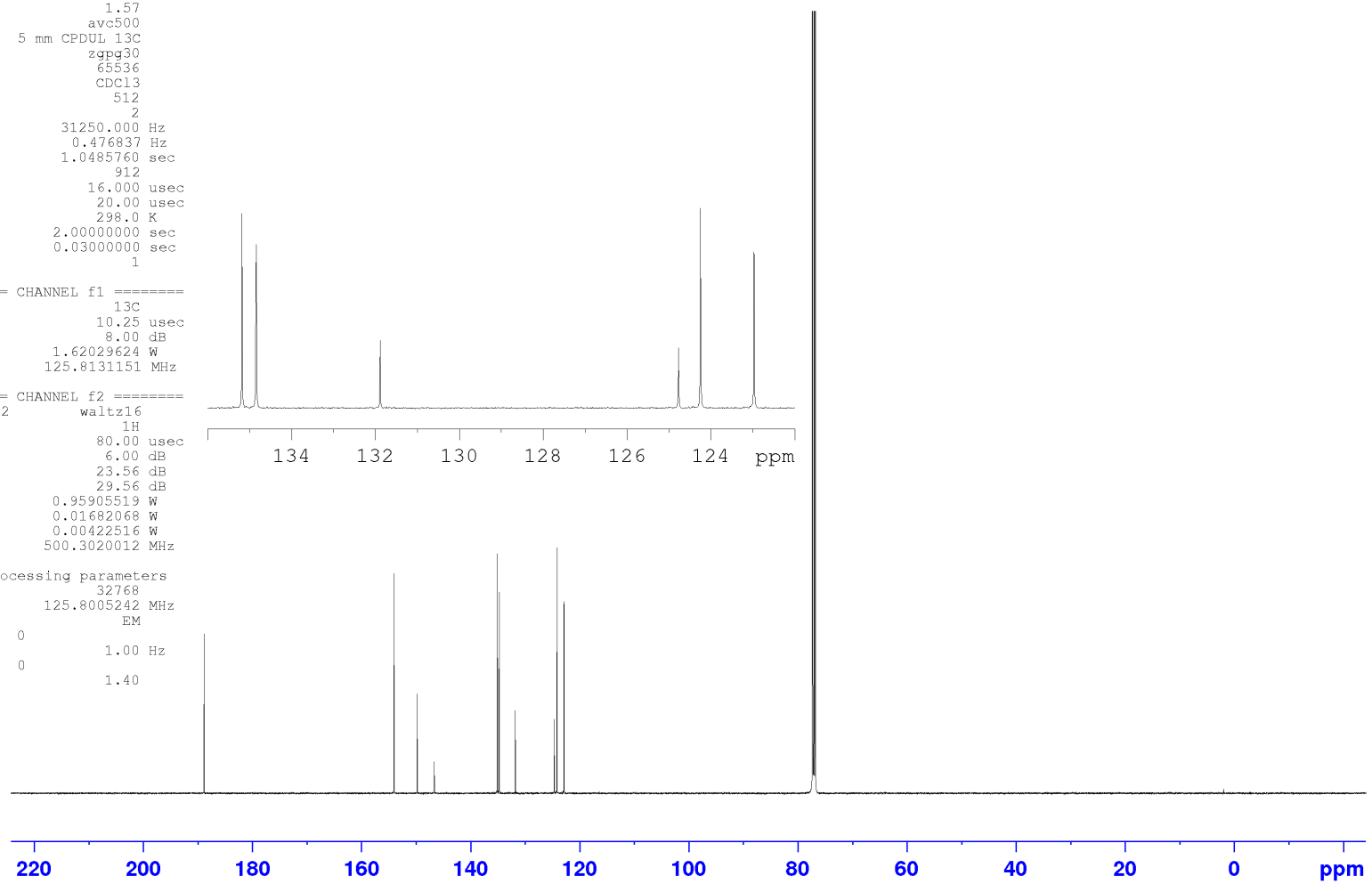

2.37. 5-Bromo-6-nitroquinoline

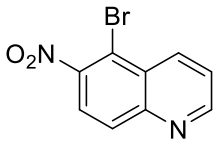


```
Current Data Parameters
NAME      5-bromo-6-nitroquinoline
EXPNO                  1
PROCNO                 1

F2 - Acquisition Parameters
Date_           20130223
Time              12.16
INSTRUM          avc500
PROBHD   5 mm CPDUL 13C
PULPROG            zg30
TD                65536
SOLVENT           CDCl3
NS                   16
DS                    4
SWH           10330.578 Hz
FIDRES         0.157632 Hz
AQ            3.1719425 sec
RG                  2.8
DW                48.400 usec
DE                 6.00 usec
TE                298.0 K
D1           1.00000000 sec
TD0                   1

======== CHANNEL f1 ========
NUC1                  1H
P1                10.60 usec
PL1                6.00 dB
PL1W         0.95905519 W
SFO1        500.3030896 MHz

F2 - Processing parameters
SI                32768
SF          500.3000240 MHz
WDW                  EM
SSB       0
LB                0.30 Hz
GB        0
PC                1.00
```

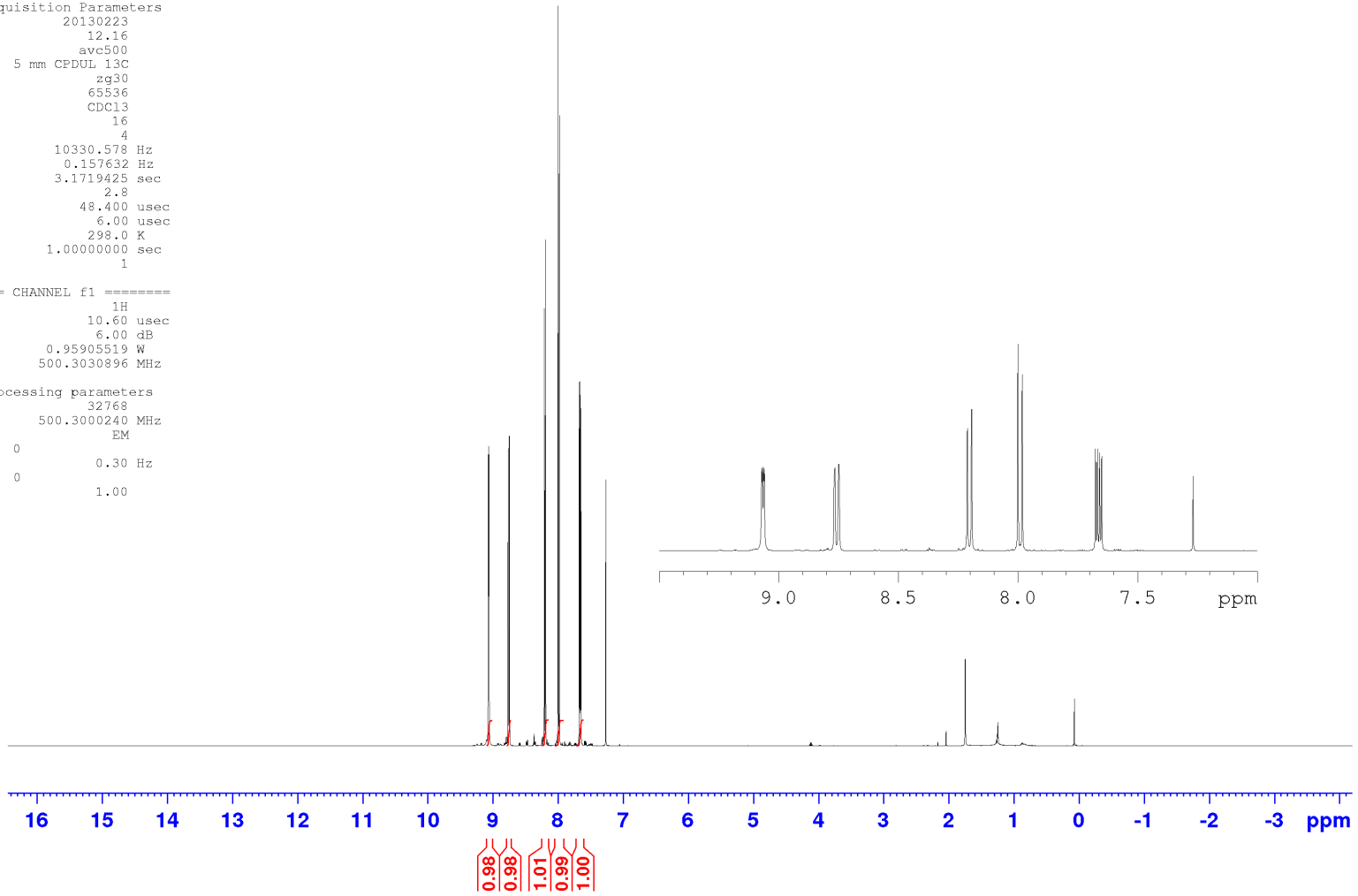

2.37. 5-Bromo-6-nitroquinoline

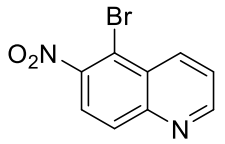


```
Current Data Parameters
NAME      5-bromo-6-nitroquinoline
EXPNO                  4
PROCNO                 1

F2 - Acquisition Parameters
Date_           20130223
Time              12.52
INSTRUM          avc500
PROBHD   5 mm CPDUL 13C
PULPROG          zgpg30
TD                65536
SOLVENT           CDCl3
NS                  256
DS                    2
SWH           31250.000 Hz
FIDRES         0.476837 Hz
AQ            1.0485760 sec
RG                  912
DW               16.000 usec
DE               20.00 usec
TE               298.0 K
D1            2.00000000 sec
D11           0.03000000 sec
TD0                   1

======== CHANNEL f1 ========
NUC1                 13C
P1                10.25 usec
PL1                8.00 dB
PL1W         1.62029624 W
SFO1        125.8131151 MHz

======== CHANNEL f2 ========
CPDPRG[2         waltz16
NUC2                 1H
PCPD2             80.00 usec
PL2                6.00 dB
PL12              23.56 dB
PL13              29.56 dB
PL2W         0.95905519 W
PL12W        0.01682068 W
PL13W        0.00422516 W
SFO2        500.3020012 MHz

F2 - Processing parameters
SI                32768
SF          125.8005249 MHz
WDW                  EM
SSB       0
LB                1.00 Hz
GB        0
PC                1.40
```

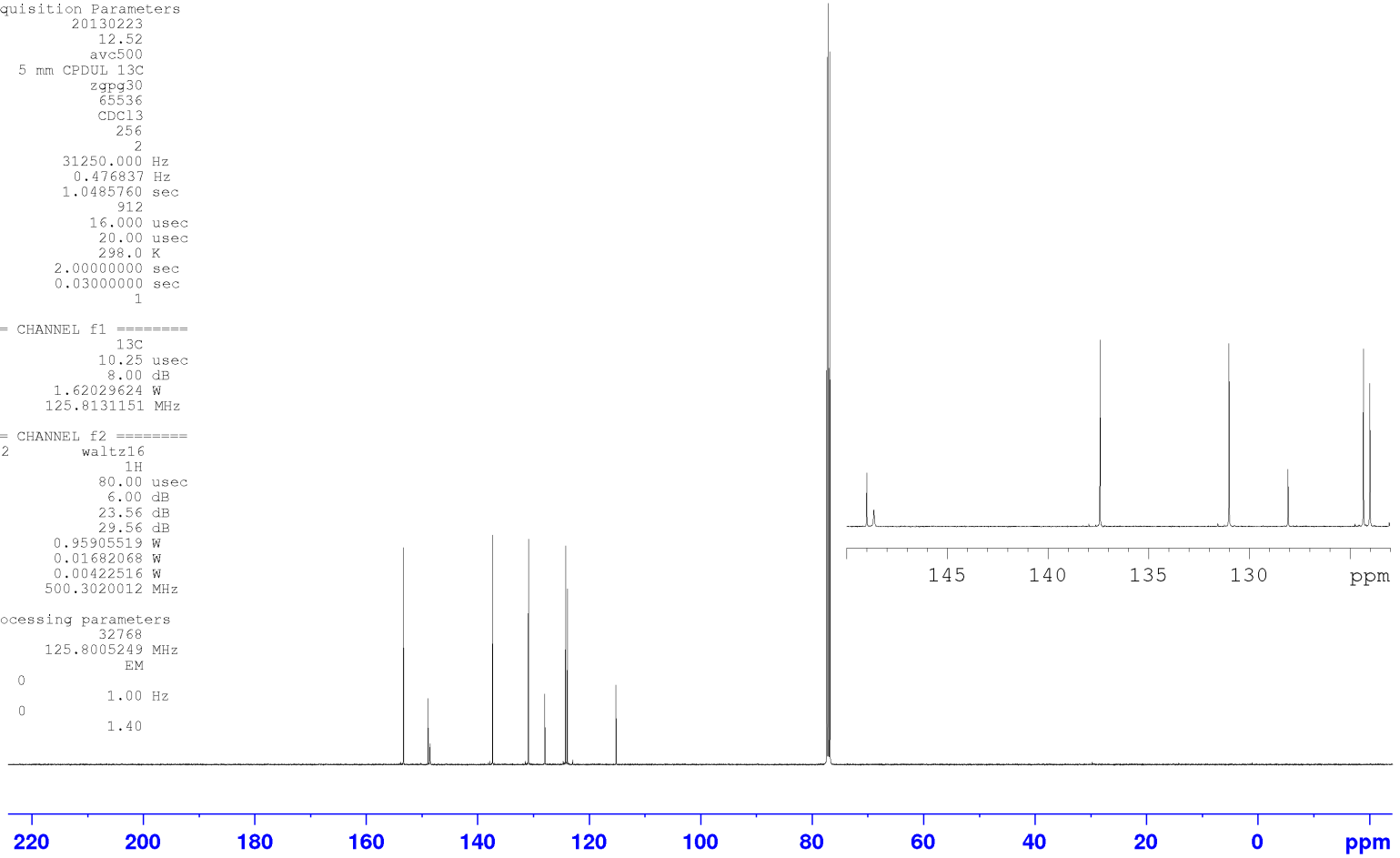

2.40. 5-Amino-8-bromo-6-nitroquinoline

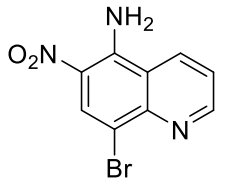


```
Current Data Parameters
NAME      8-bromo-6-nitroquinolin-5-amine
EXPNO                   1
PROCNO                  1

F2 - Acquisition Parameters
Date_           20130305
Time                6.10
INSTRUM          avc500
PROBHD   5 mm CPDUL 13C
PULPROG             zg30
TD                 65536
SOLVENT             DMSO
NS                    16
DS                     4
SWH           10330.578 Hz
FIDRES         0.157632 Hz
AQ            3.1719425 sec
RG                   3.2
DW                48.400 usec
DE                 6.00 usec
TE                298.0 K
D1           1.00000000 sec
TD0                    1

======== CHANNEL f1 ========
NUC1                  1H
P1                 10.60 usec
PL1                 6.00 dB
PL1W          0.95905519 W
SFO1        500.3030896 MHz

F2 - Processing parameters
SI                 32768
SF          500.3000000 MHz
WDW                   EM
SSB       0
LB                 0.30 Hz
GB        0
PC                 1.00
```

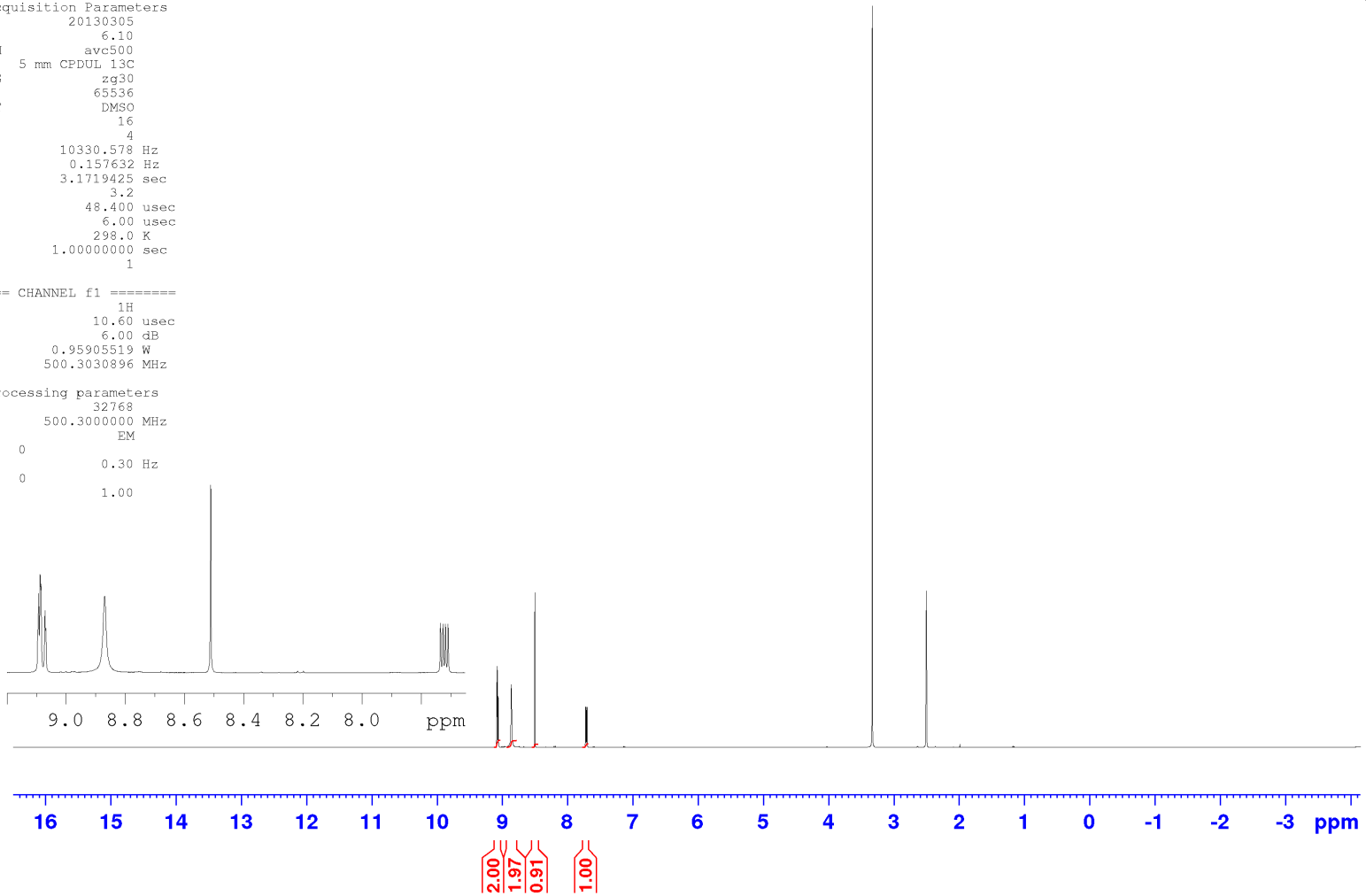

2.40. 5-Amino-8-bromo-6-nitroquinoline

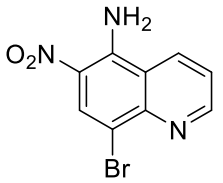


```
Current Data Parameters
NAME      8-bromo-6-nitroquinolin-5-amine
EXPNO                   4
PROCNO                  1

F2 - Acquisition Parameters
Date_            20130305
Time                6.59
INSTRUM           avc500
PROBHD   5 mm CPDUL 13C
PULPROG           zgpg30
TD                 65536
SOLVENT              DMSO
NS                    512
DS                      2
SWH             31250.000 Hz
FIDRES          0.476837 Hz
AQ              1.0485760 sec
RG                    912
DW                16.000 usec
DE                 20.00 usec
TE                 298.0 K
D1             2.00000000 sec
D11            0.03000000 sec
TD0                     1

======== CHANNEL f1 ========
NUC1                  13C
P1                 10.25 usec
PL1                 8.00 dB
PL1W          1.62029624 W
SFO1        125.8131151 MHz

======== CHANNEL f2 ========
CPDPRG[2          waltz16
NUC2                  1H
PCPD2              80.00 usec
PL2                 6.00 dB
PL12               23.56 dB
PL13               29.56 dB
PL2W          0.95905519 W
PL12W         0.01682068 W
PL13W         0.00422516 W
SFO2        500.3020012 MHz

F2 - Processing parameters
SI                 32768
SF           125.8005938 MHz
WDW                   EM
SSB       0
LB                 1.00 Hz
GB        0
PC                 1.40
```

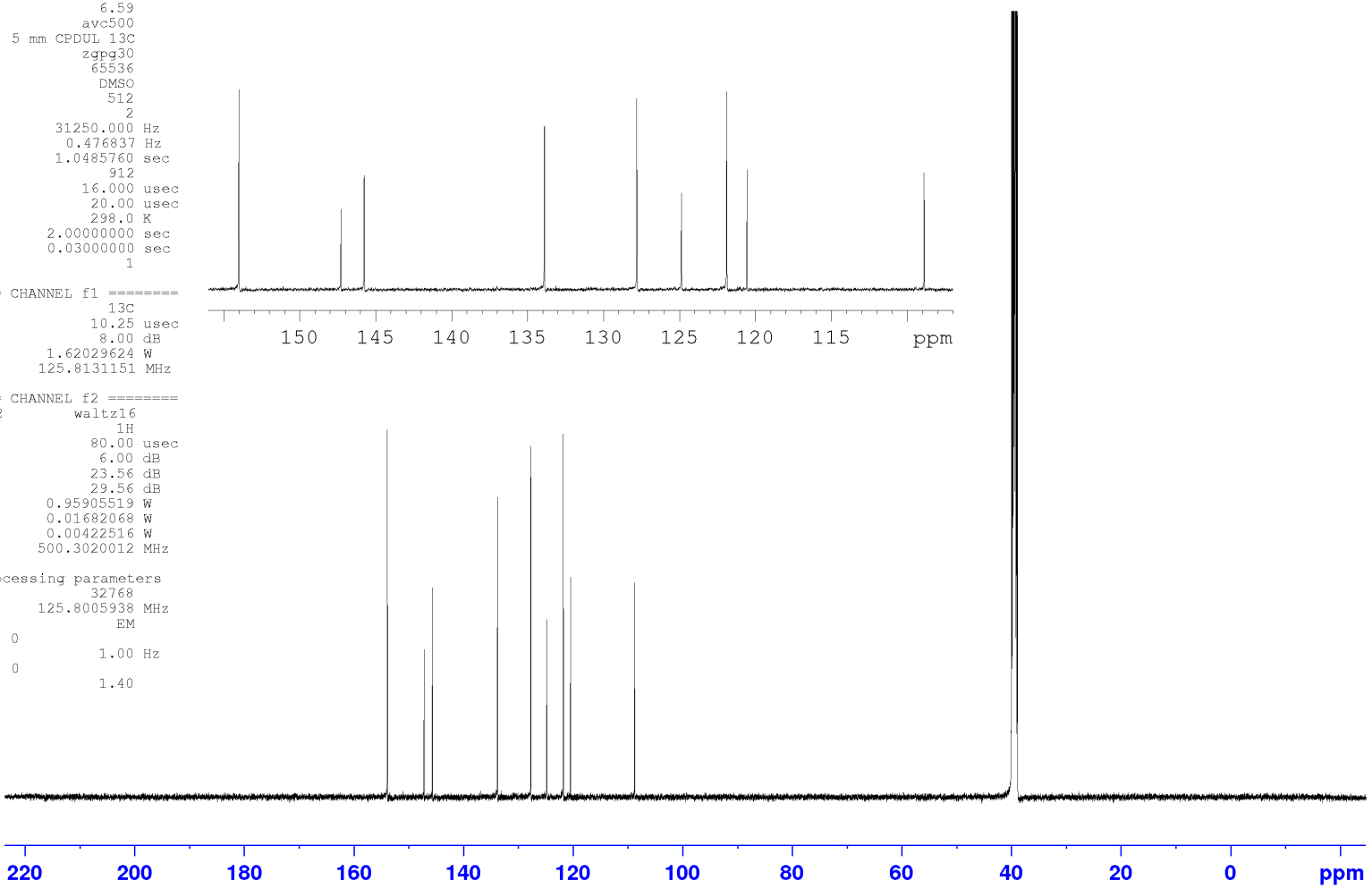

2.47. 6,6'-Dinitro-5,5'-biquinoline

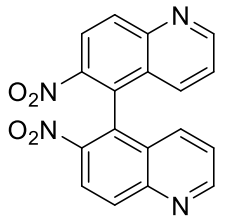


```
Current Data Parameters
NAME         Biquinoline
EXPNO                  1
PROCNO                 1

F2 - Acquisition Parameters
Date_           20130512
Time                3.30
INSTRUM          avc500
PROBHD   5 mm CPDUL 13C
PULPROG             zg30
TD                 65536
SOLVENT            CDCl3
NS                    16
DS                     4
SWH           10330.578 Hz
FIDRES         0.157632 Hz
AQ            3.1719425 sec
RG                   2.8
DW                48.400 usec
DE                 6.00 usec
TE                298.0 K
D1           1.00000000 sec
TD0                    1

======== CHANNEL f1 ========
NUC1                  1H
P1                 10.60 usec
PL1                 6.00 dB
PL1W          0.95905519 W
SFO1        500.3030896 MHz

F2 - Processing parameters
SI                 32768
SF          500.3000279 MHz
WDW                   EM
SSB       0
LB                 0.30 Hz
GB        0
PC                 1.00
```

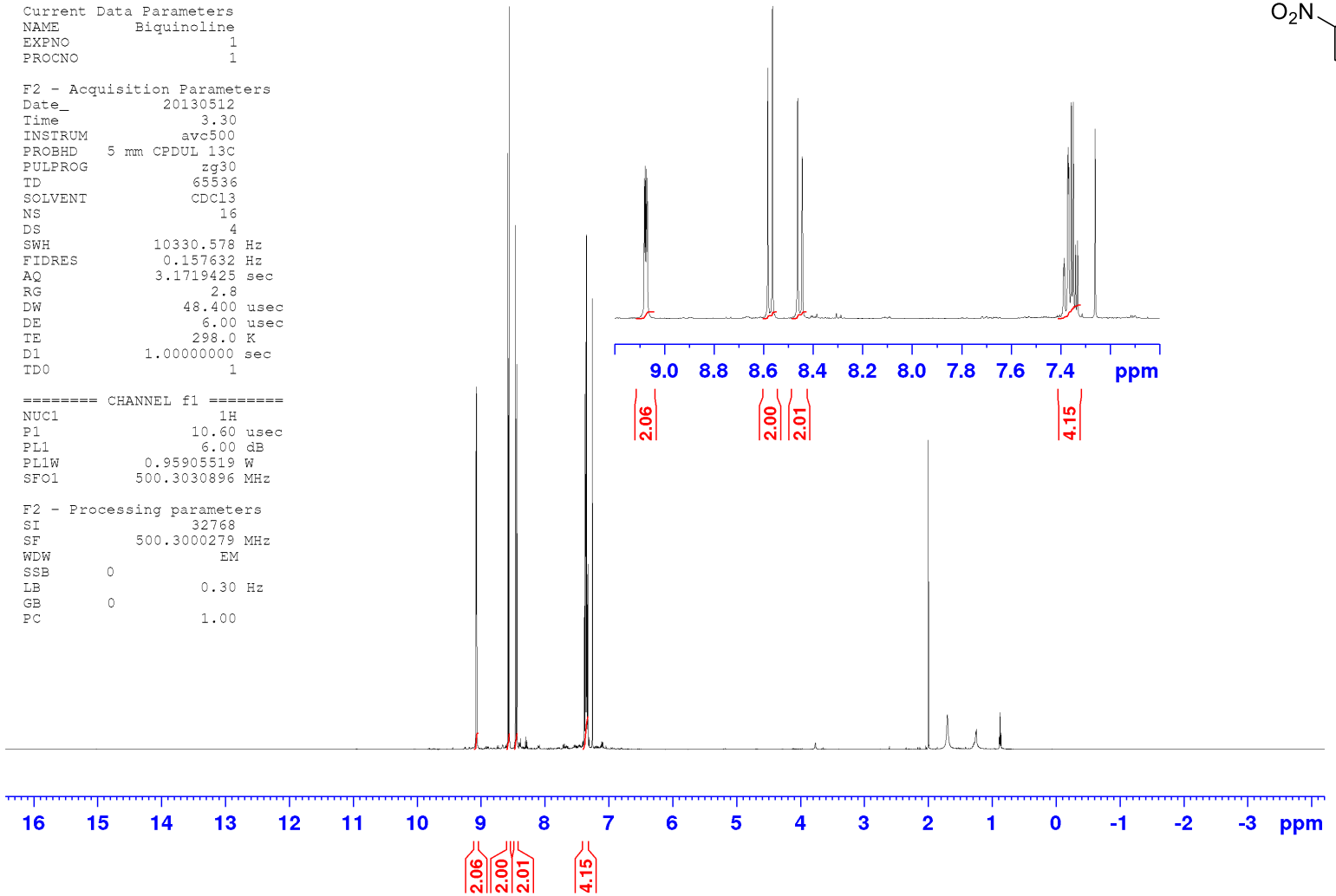

2.47. 6,6'-Dinitro-5,5'-biquinoline

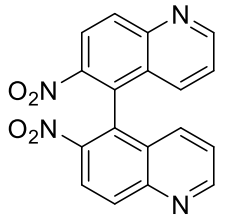

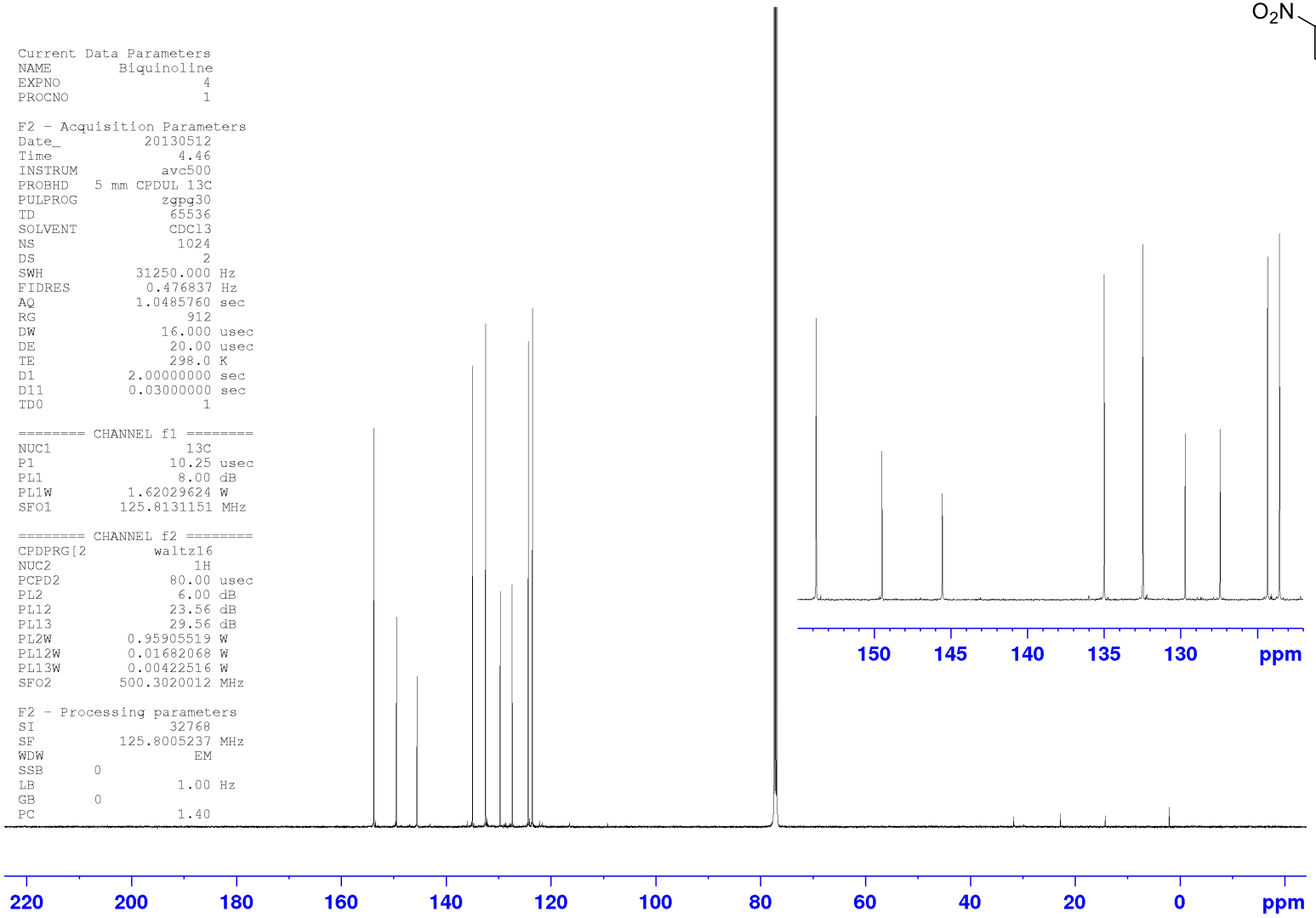

2.49. (3-(3,5-Dimethylisoxazol-4-yl)-5-((6-nitroquinolin-5-yl)methoxy)phenyl)(phenyl)methanol

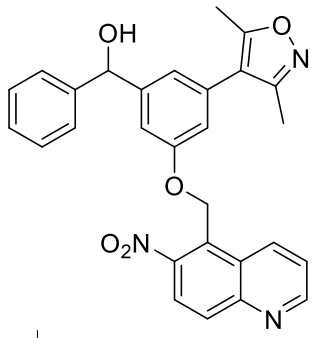


```
Current Data Parameters
NAME      Caged product
EXPNO                 1
PROCNO                1

F2 - Acquisition Parameters
Date_           20130518
Time              13.04
INSTRUM          avc500
PROBHD   5 mm CPDUL 13C
PULPROG             zg30
TD                 65536
SOLVENT            CDCl3
NS                    16
DS                     4
SWH           10330.578 Hz
FIDRES         0.157632 Hz
AQ            3.1719425 sec
RG                   2.8
DW                48.400 usec
DE                 6.00 usec
TE                298.0 K
D1           1.00000000 sec
TD0                   1

======== CHANNEL f1 ========
NUC1                 1H
P1                10.60 usec
PL1                6.00 dB
PL1W         0.95905519 W
SFO1        500.3030896 MHz

F2 - Processing parameters
SI                 32768
SF          500.3000299 MHz
WDW                   EM
SSB      0
LB                0.30 Hz
GB       0
PC                1.00
```

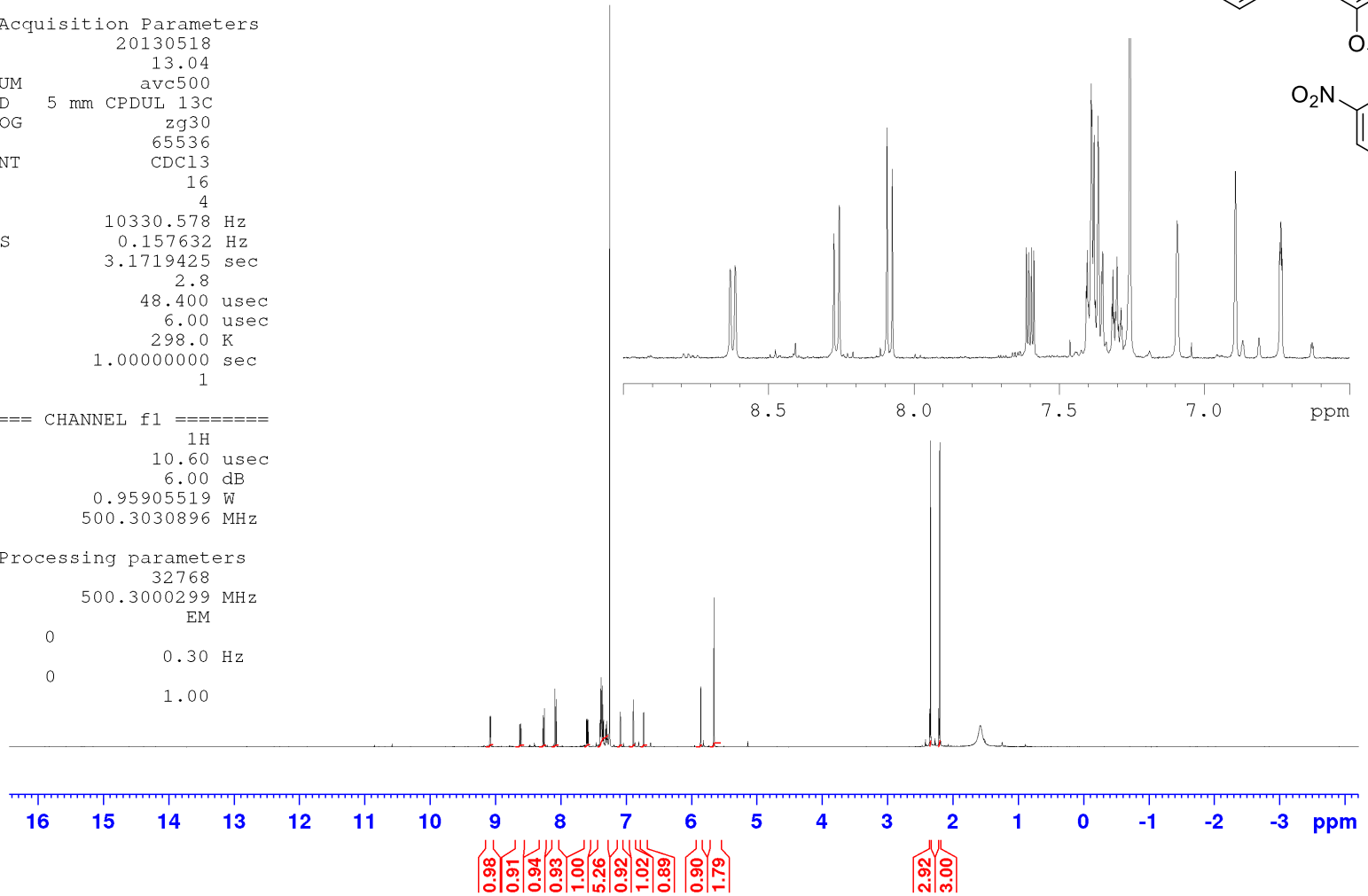

2.49. (3-(3,5-Dimethylisoxazol-4-yl)-5-((6-nitroquinolin-5-yl)methoxy)phenyl)(phenyl)methanol

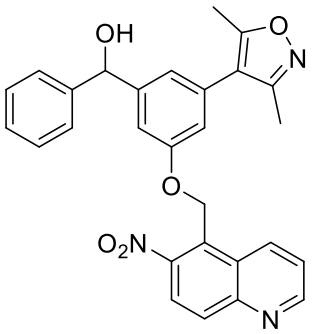


```
Current Data Parameters
NAME       Caged product
EXPNO                  4
PROCNO                 1

F2 - Acquisition Parameters
Date_           20130518
Time              14.20
INSTRUM          avc500
PROBHD   5 mm CPDUL 13C
PULPROG          zgpg30
TD                65536
SOLVENT           CDCl3
NS                 1024
DS                    2
SWH           31250.000 Hz
FIDRES         0.476837 Hz
AQ            1.0485760 sec
RG                  912
DW               16.000 usec
DE               20.00 usec
TE               298.0 K
D1           2.00000000 sec
D11          0.03000000 sec
TD0                   1

======== CHANNEL f1 ========
NUC1                 13C
P1                10.25 usec
PL1                8.00 dB
PL1W         1.62029624 W
SFO1        125.8131151 MHz

======== CHANNEL f2 ========
CPDPRG[2         waltz16
NUC2                 1H
PCPD2             80.00 usec
PL2                6.00 dB
PL12               23.56 dB
PL13               29.56 dB
PL2W         0.95905519 W
PL12W        0.01682068 W
PL13W        0.00422516 W
SFO2        500.3020012 MHz

F2 - Processing parameters
SI                32768
SF          125.8005220 MHz
WDW                  EM
SSB       0
LB                1.00 Hz
GB        0
PC                1.40
```

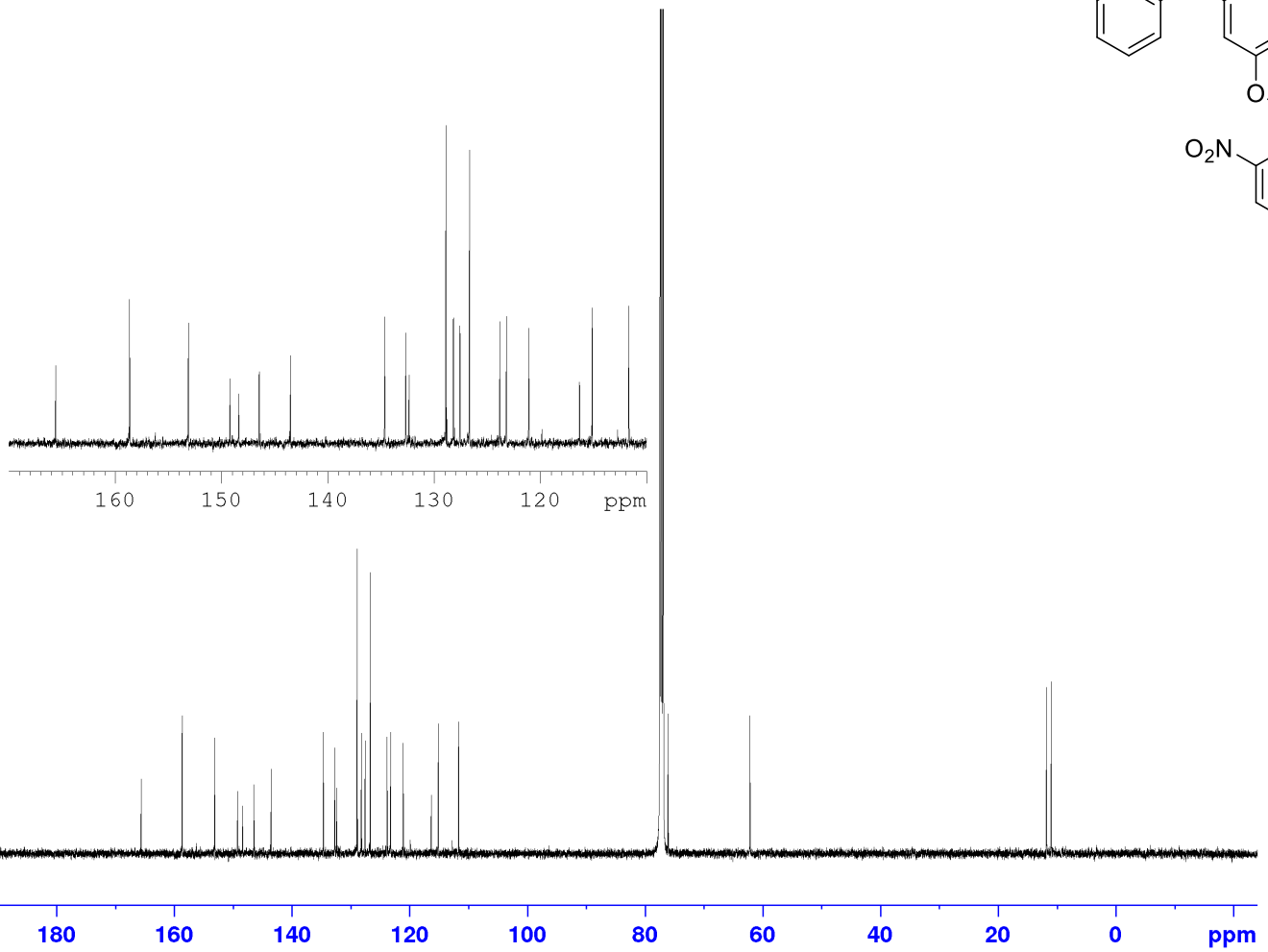

2.56. (6-Aminoquinolin-5-yl)methanol

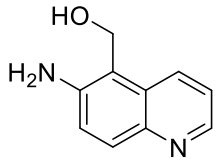


```
Current Data Parameters
NAME      (6-aminoquinolin-5-yl)methanol
EXPNO                  1
PROCNO                 1

F2 - Acquisition Parameters
Date_           20130805
Time              10.09
INSTRUM          avc500
PROBHD   5 mm CPDUL 13C
PULPROG            zg30
TD                65536
SOLVENT            MeOD
NS                   16
DS                    4
SWH           10330.578 Hz
FIDRES         0.157632 Hz
AQ            3.1719425 sec
RG                 1.78
DW               48.400 usec
DE                6.00 usec
TE               298.0 K
D1           1.00000000 sec
TD0                   1

======== CHANNEL f1 ========
NUC1                  1H
P1                10.60 usec
PL1                6.00 dB
PL1W         0.95905519 W
SFO1        500.3030896 MHz

F2 - Processing parameters
SI                32768
SF          500.3000122 MHz
WDW                  EM
SSB       0
LB                0.30 Hz
GB        0
PC                1.00
```

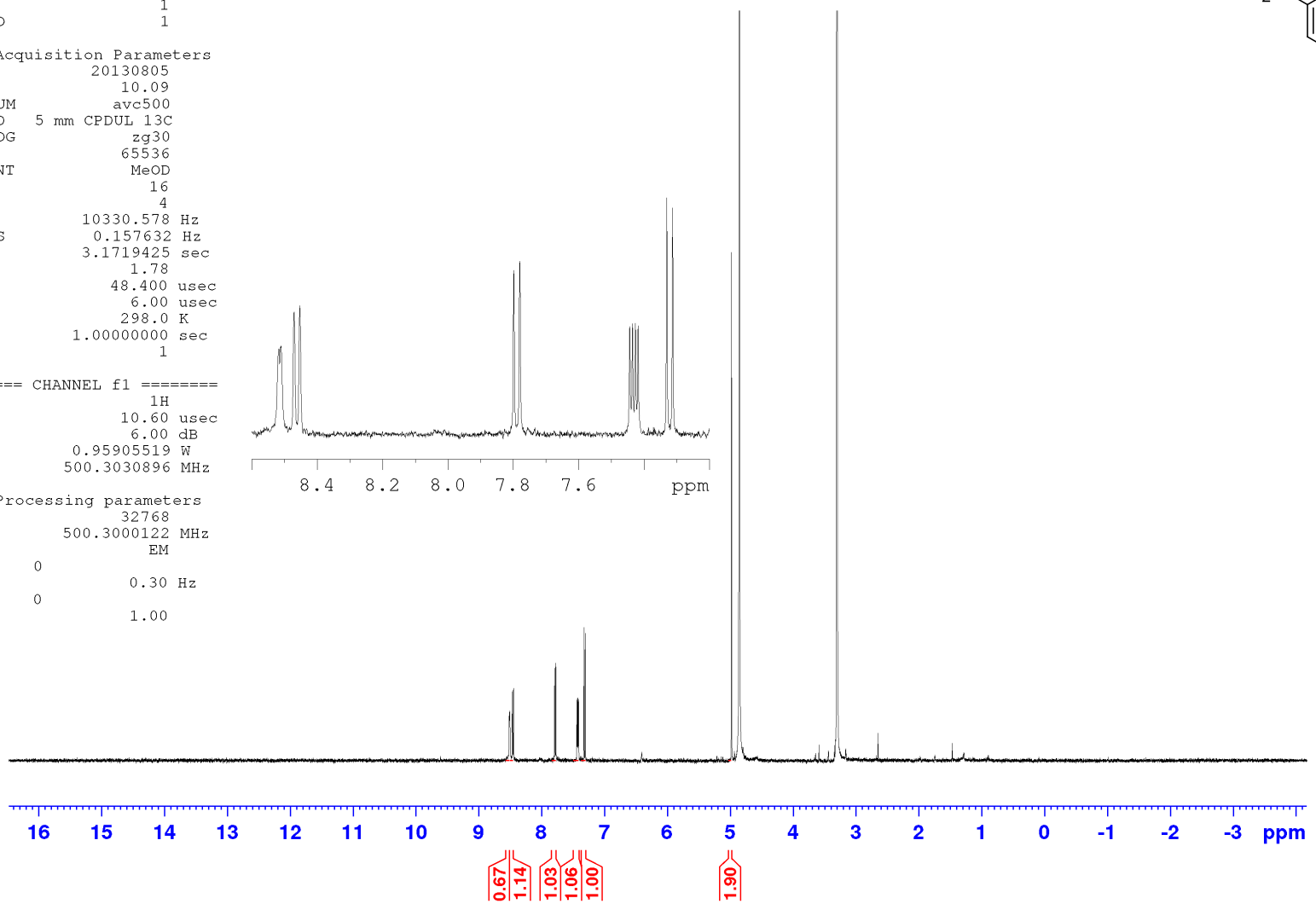

2.56. (6-Aminoquinolin-5-yl)methanol

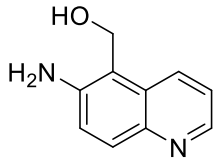


```
Current Data Parameters
NAME      (6-aminoquinolin-5-yl)methanol
EXPNO                   4
PROCNO                  1

F2 - Acquisition Parameters
Date_           20130805
Time              11.27
INSTRUM          avc500
PROBHD   5 mm CPDUL 13C
PULPROG          zgpg30
TD                65536
SOLVENT             MeOD
NS                 3072
DS                    2
SWH           31250.000 Hz
FIDRES         0.476837 Hz
AQ            1.0485760 sec
RG                  912
DW               16.000 usec
DE               20.00 usec
TE               298.0 K
D1           2.00000000 sec
D11          0.03000000 sec
TD0                   1

======== CHANNEL f1 ========
NUC1                 13C
P1                 10.25 usec
PL1                 8.00 dB
PL1W         1.62029624 W
SFO1        125.8131151 MHz

======== CHANNEL f2 ========
CPDPRG[2         waltz16
NUC2                 1H
PCPD2              80.00 usec
PL2                 6.00 dB
PL12               23.56 dB
PL13               29.56 dB
PL2W         0.95905519 W
PL12W        0.01682068 W
PL13W        0.00422516 W
SFO2        500.3020012 MHz

F2 - Processing parameters
SI                 32768
SF          125.8003564 MHz
WDW                   EM
SSB       0
LB                 1.00 Hz
GB        0
PC                 1.40
```

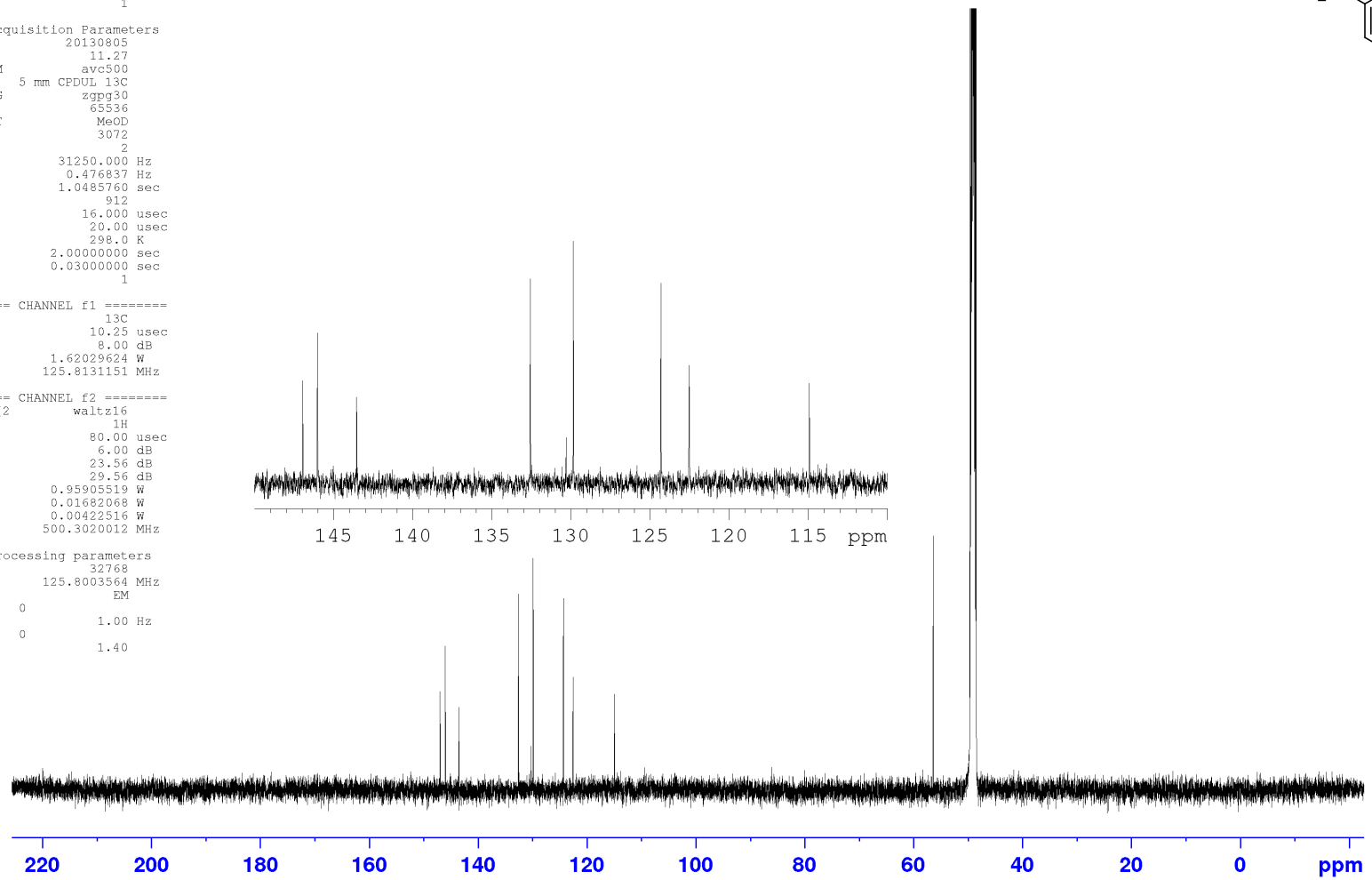

3.1. (*E*)-2-(2-(4-Aminostyryl)-4*H*-chromen-4-ylidene)malononitrile

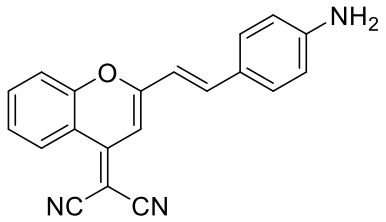

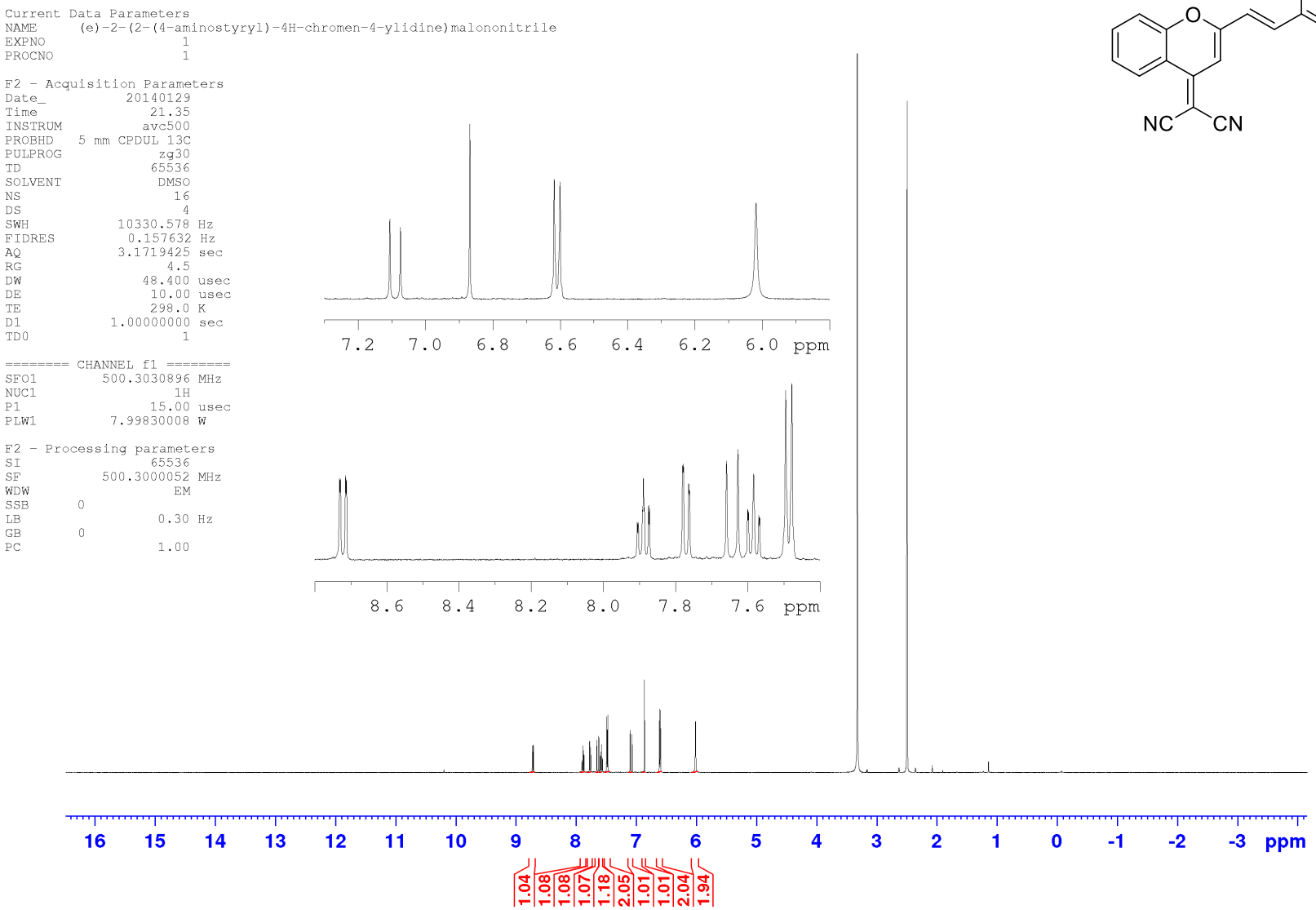

3.1. (*E*)-2-(2-(4-Aminostyryl)-4*H*-chromen-4-ylidene)malononitrile

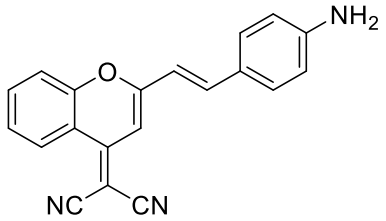

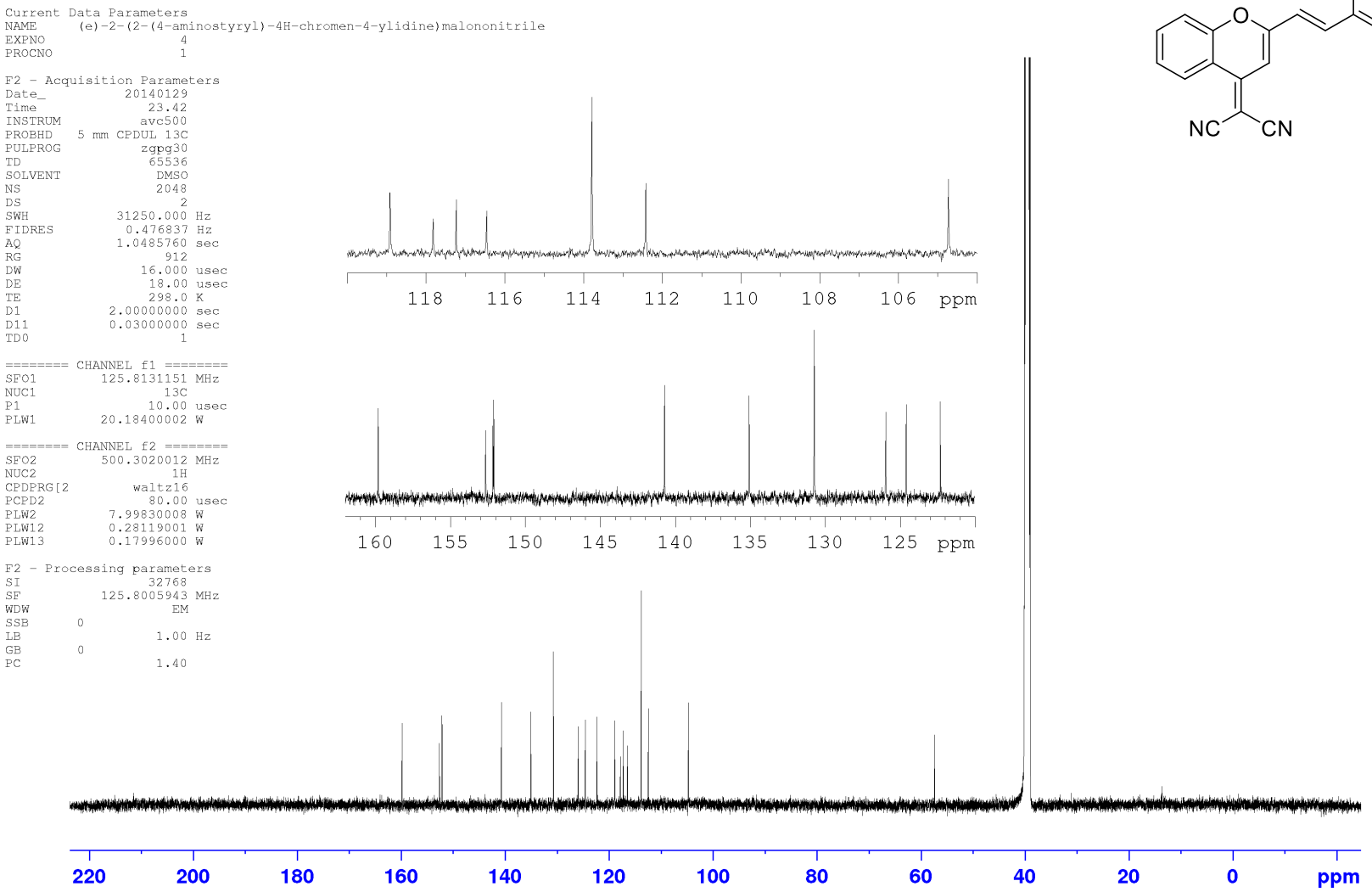

3.2. (*E*)-2-(2-(4-Nitrostyryl)-4*H*-chromen-4-ylidene)malononitrile

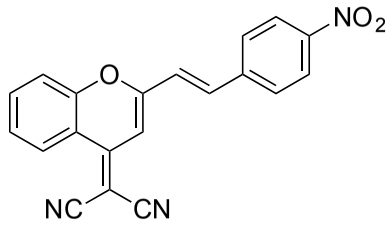


```
Current Data Parameters
NAME      LOC200 Service
EXPNO                 1
PROCNO                1

F2 - Acquisition Parameters
Date_          20140424
Time               7.26
INSTRUM          avc500
PROBHD   5 mm CPDUL 13C
PULPROG            zg30
TD                65536
SOLVENT            DMSO
NS                   64
DS                    4
SWH           10330.578 Hz
FIDRES         0.157632 Hz
AQ            3.1719425 sec
RG                    4
DW               48.400 usec
DE               10.00 usec
TE               298.0 K
D1           1.00000000 sec
TD0                   1

======== CHANNEL f1 ========
SFO1        500.3030896 MHz
NUC1                1H
P1                15.00 usec
PLW1         7.99830008 W

F2 - Processing parameters
SI                65536
SF          500.3000051 MHz
WDW                  EM
SSB      0
LB                0.30 Hz
GB       0
PC                1.00
```

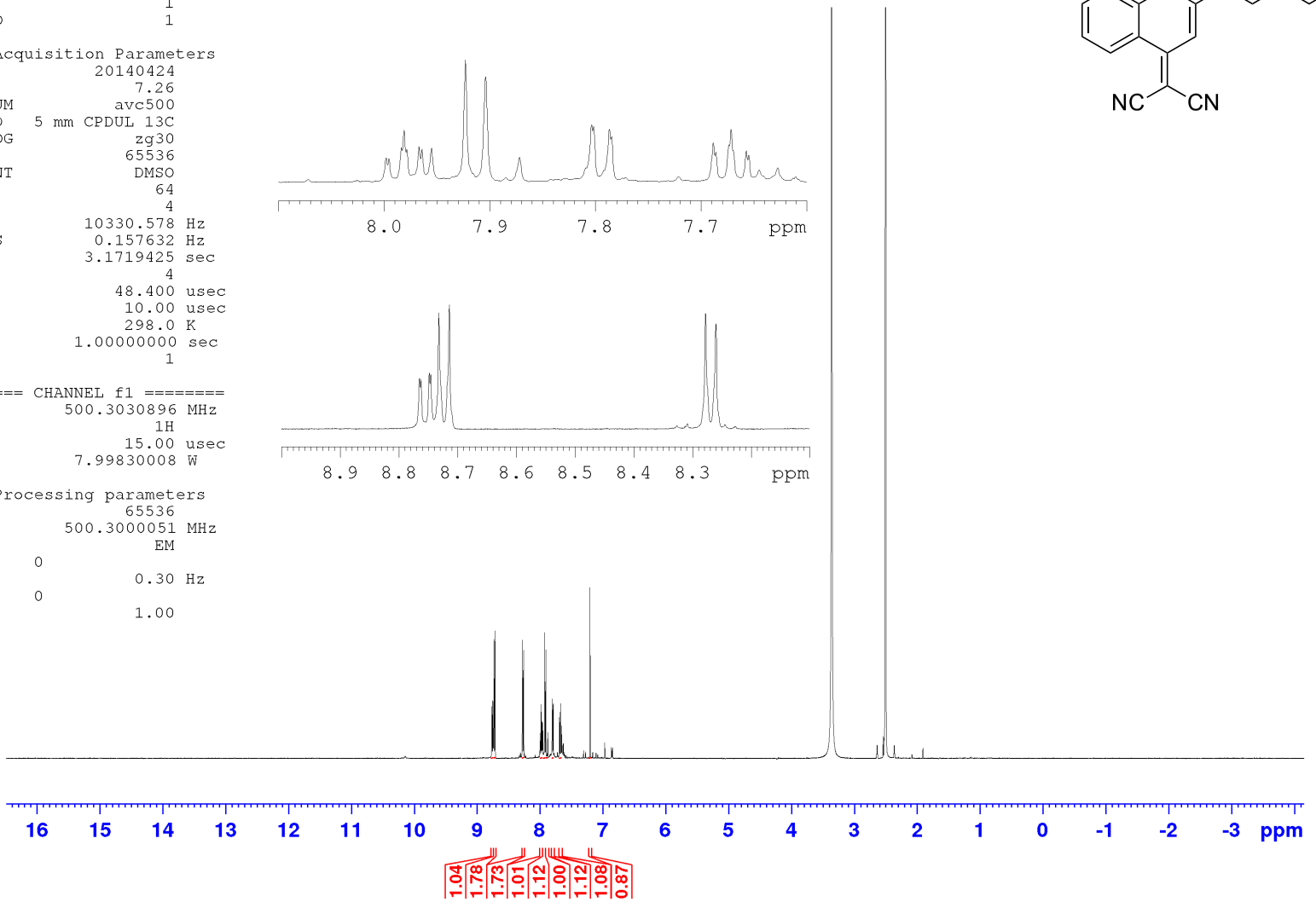

3.2. (*E*)-2-(2-(4-Nitrostyryl)-4*H*-chromen-4-ylidene)malononitrile

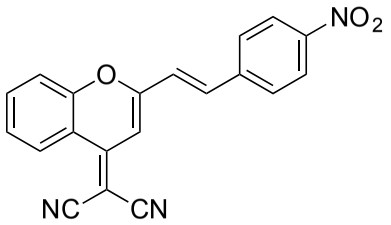


```
Current Data Parameters
NAME      LOC200 Service
EXPNO                  4
PROCNO                 1

F2 - Acquisition Parameters
Date_           20140424
Time              15.01
INSTRUM          avc500
PROBHD    5 mm CPDUL 13C
PULPROG          zgpg30
TD                65536
SOLVENT             DMSO
NS                  3072
DS                     2
SWH            31250.000 Hz
FIDRES             0.476837 Hz
AQ             1.0485760 sec
RG                   912
DW                16.000 usec
DE                18.00 usec
TE                298.0 K
D1            2.00000000 sec
D11           0.03000000 sec
TD0                    1

======== CHANNEL f1 ========
SFO1         125.8131152 MHz
NUC1                  13C
P1                 10.00 usec
PLW1         20.18400002 W

======== CHANNEL f2 ========
SFO2         500.3020012 MHz
NUC2                  1H
CPDPRG[2          waltz16
PCPD2              80.00 usec
PLW2          7.99830008 W
PLW12         0.28119001 W
PLW13         0.17996000 W

F2 - Processing parameters
SI                 32768
SF           125.8005945 MHz
WDW                   EM
SSB       0
LB                 1.00 Hz
GB        0
PC                 1.40
```

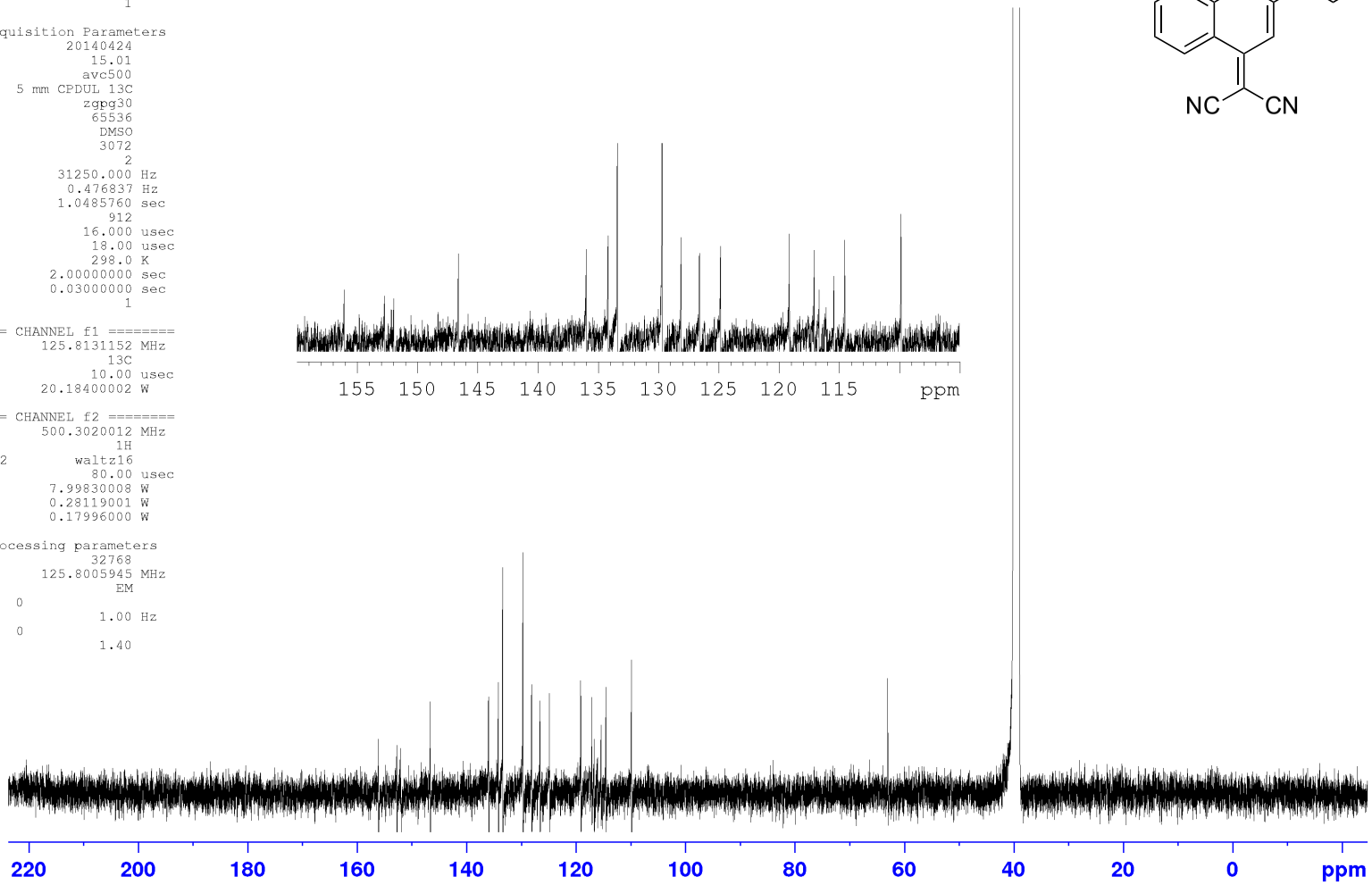

3.16. (*E/Z*)-2-(2-Methyl-4*H*-chromen-4-ylidene)-3-oxo-3-(piperidin-1-yl)propanenitrile

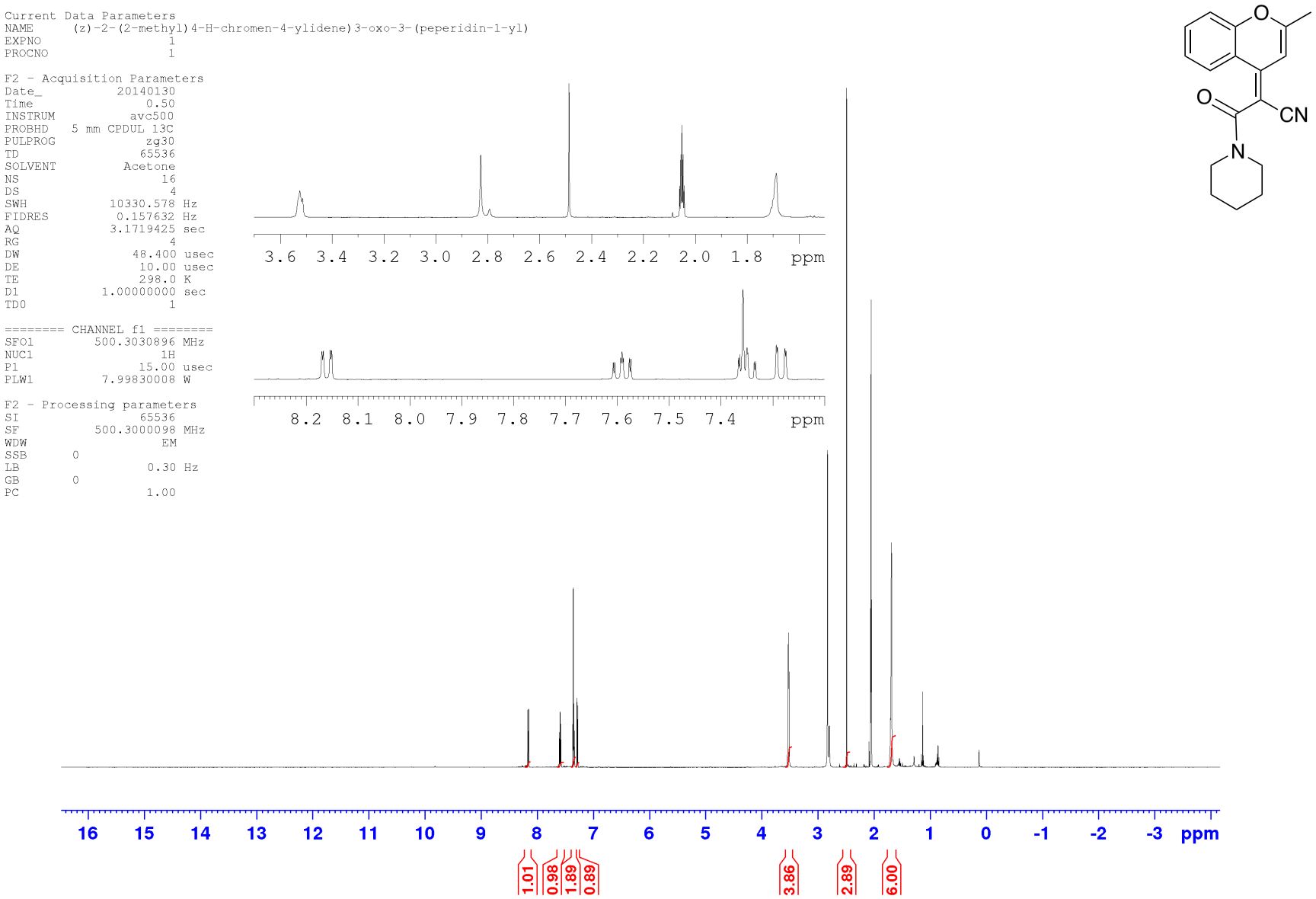

3.16. (*E/Z*)-2-(2-Methyl-4*H*-chromen-4-ylidene)-3-oxo-3-(piperidin-1-yl)propanenitrile

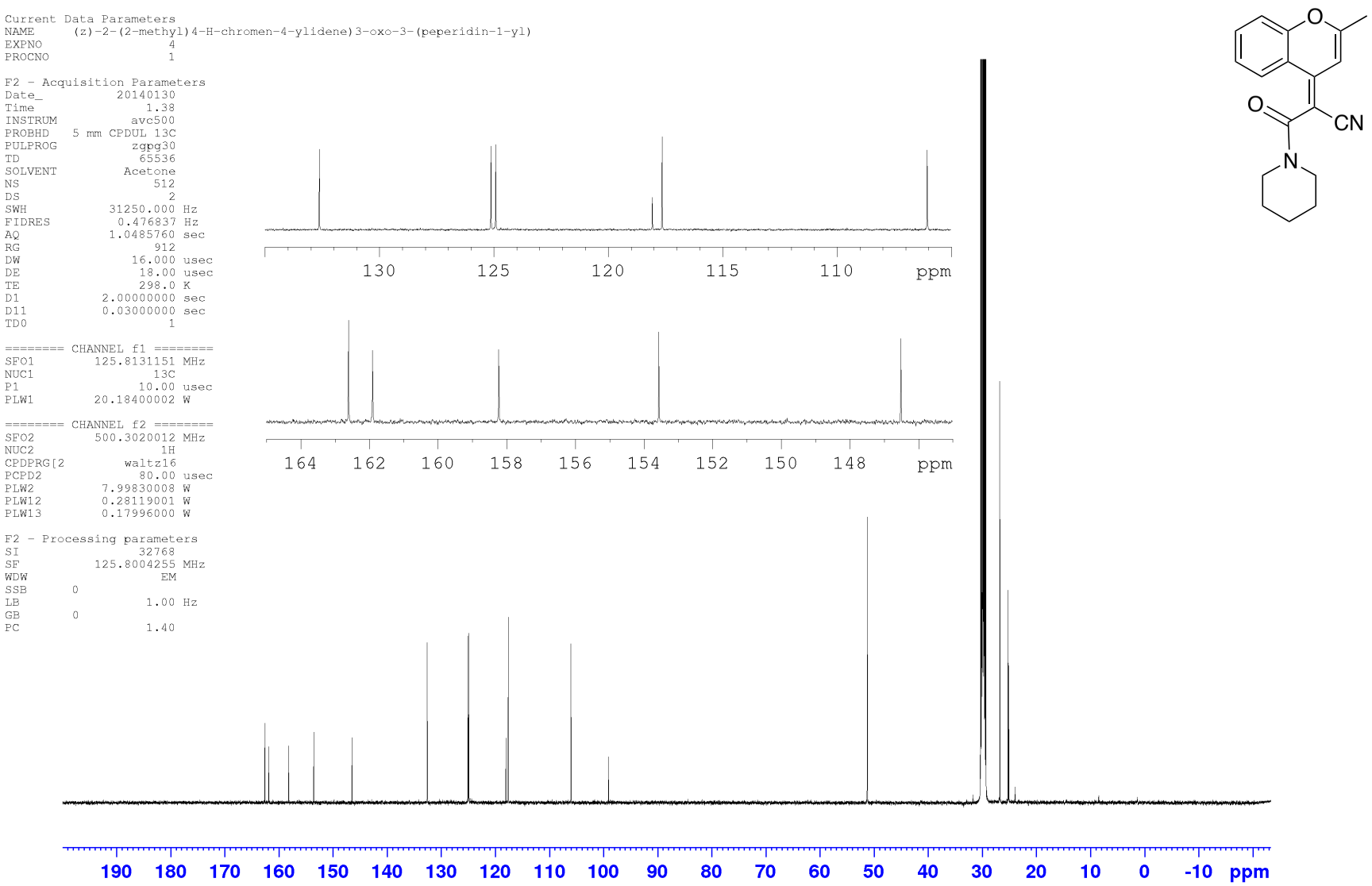

3.21. (*E*)-2-(2-(4-Hydroxystyryl)-4*H*-chromen-4-ylidene)malononitrile

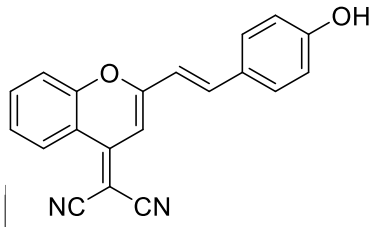


```
Current Data Parameters
NAME      (E)-2-(2-(4-hydroxystyryl)-4H-chromen-4-ylidene)malononitrile
EXPNO                  1
PROCNO                 1

F2 - Acquisition Parameters
Date_           20140121
Time               13.07
INSTRUM            av700
PROBHD   5 mm CPTCI 1H-
PULPROG            zg30
TD                65536
SOLVENT         Acetone
NS                   16
DS                    2
SWH            14097.744 Hz
FIDRES          0.215115 Hz
AQ             2.3243434 sec
RG                    8
DW                35.467 usec
DE                10.00 usec
TE                298.0 K
D1            1.00000000 sec
TD0                   1

======== CHANNEL f1 ========
SFO1         699.9943227 MHz
NUC1                 1H
P1                 8.00 usec
PLW1          5.48680019 W

F2 - Processing parameters
SI                 65536
SF           699.9900121 MHz
WDW                   EM
SSB       0
LB                 0.30 Hz
GB        0
PC                 1.00
```

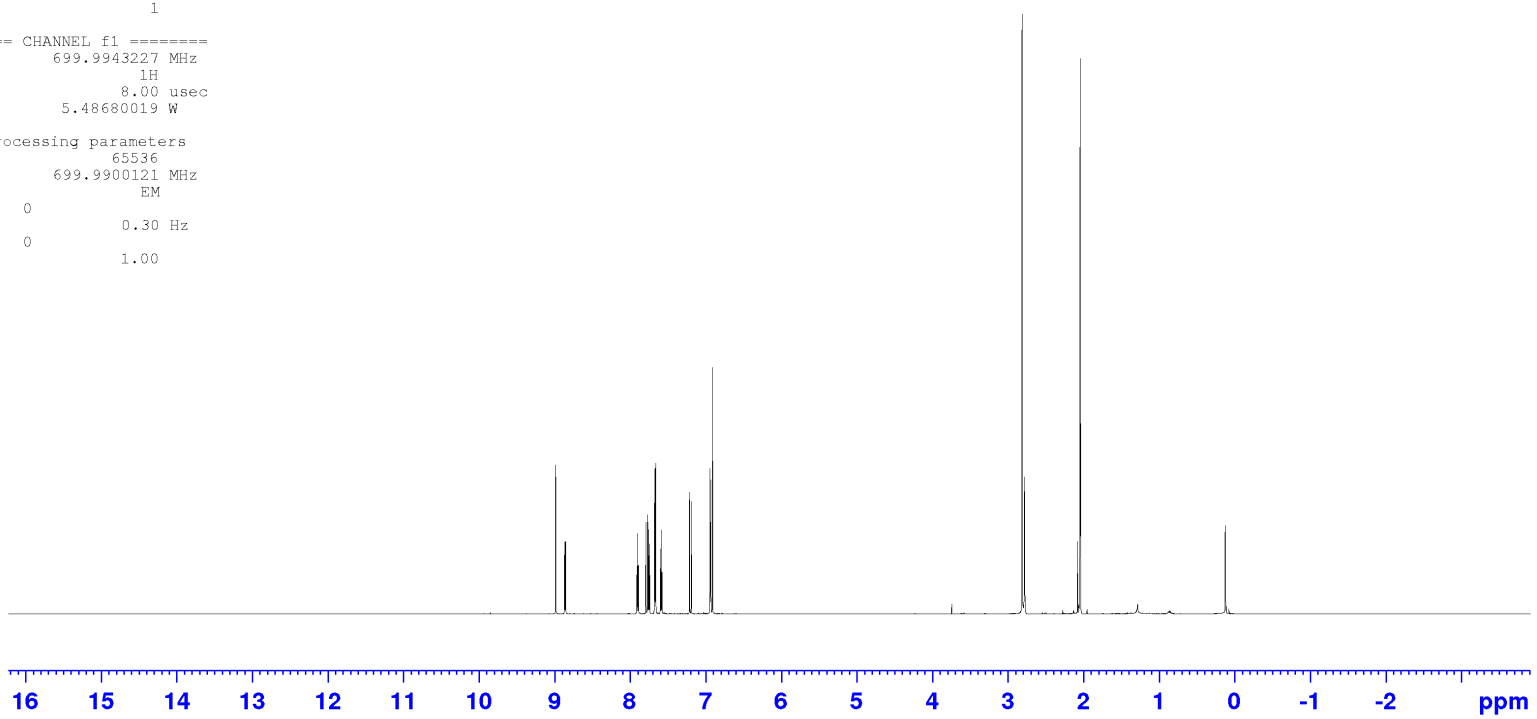

3.21. (*E*)-2-(2-(4-Hydroxystyryl)-4*H*-chromen-4-ylidene)malononitrile

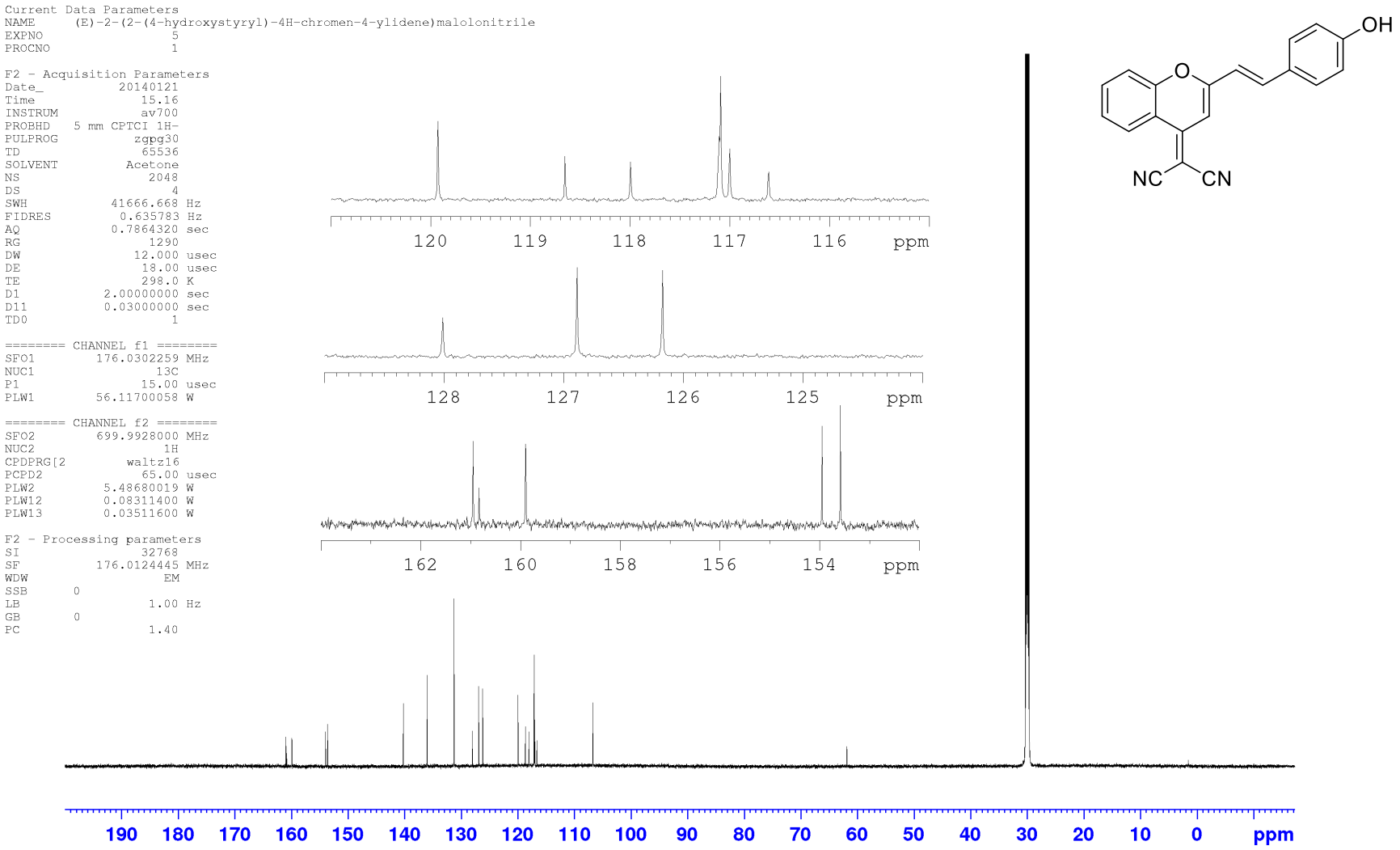

3.24. (*E*)-2-(4-Nitrostyryl)-4*H*-chromen-4-one

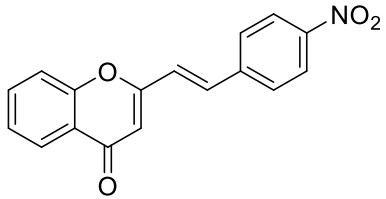


```
Current Data Parameters
NAME      (E)-2-(4-nitrostyryl)-4H-chromen-4-one
EXPNO                  1
PROCNO                 1

F2 - Acquisition Parameters
Date_           20140130
Time               5.33
INSTRUM          avc500
PROBHD   5 mm CPDUL 13C
PULPROG             zg30
TD                 65536
SOLVENT             DMSO
NS                    16
DS                     4
SWH            10330.578 Hz
FIDRES          0.157632 Hz
AQ             3.1719425 sec
RG                   4.5
DW                48.400 usec
DE                10.00 usec
TE                298.0 K
D1            1.00000000 sec
TD0                    1

======== CHANNEL f1 ========
SFO1         500.3030896 MHz
NUC1                   1H
P1                 15.00 usec
PLW1          7.99830008 W

F2 - Processing parameters
SI                 65536
SF           500.3000051 MHz
WDW                   EM
SSB       0
LB                 0.30 Hz
GB        0
PC                 1.00
```

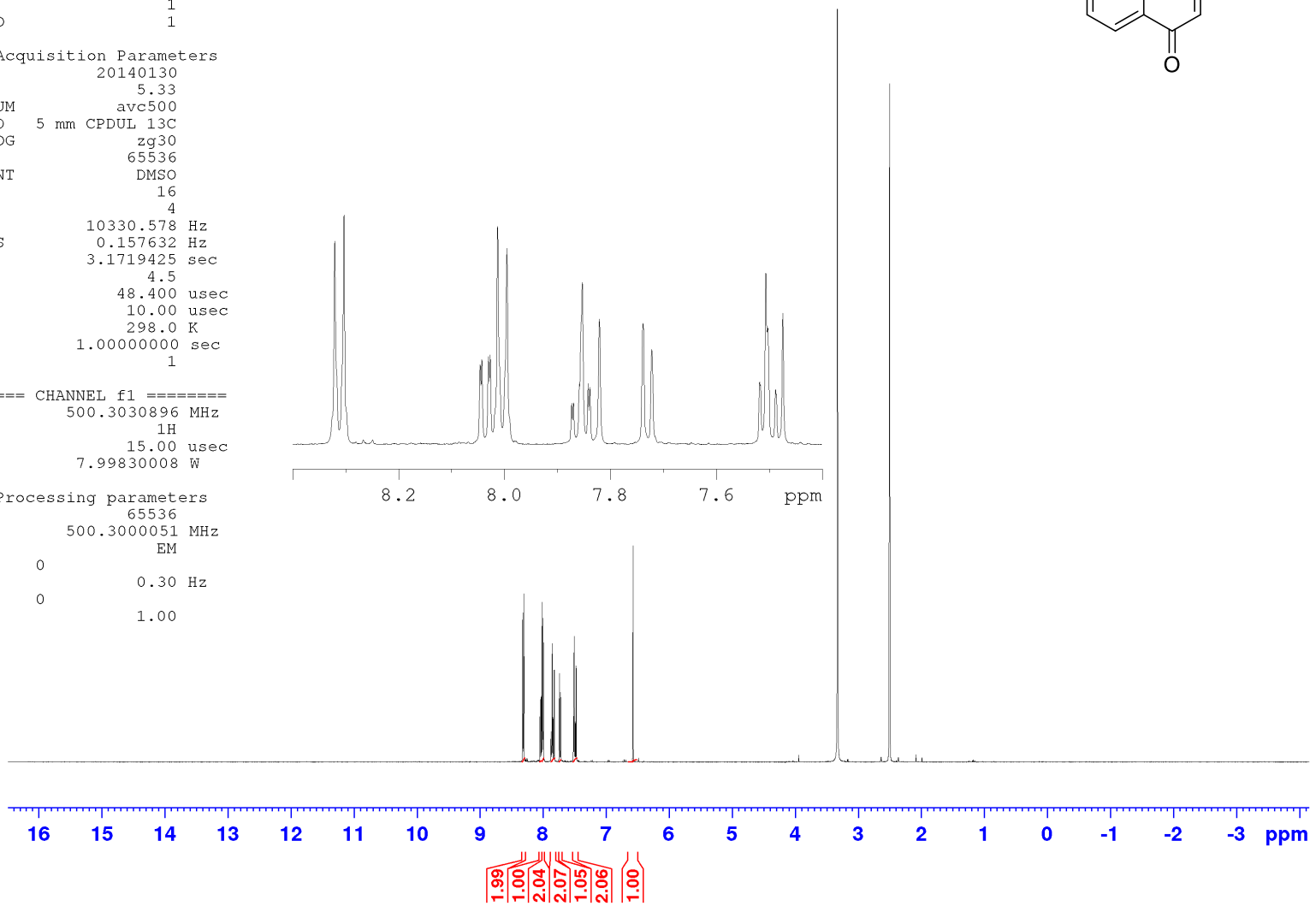

3.24. (*E*)-2-(4-Nitrostyryl)-4*H*-chromen-4-one

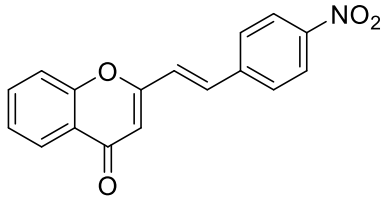

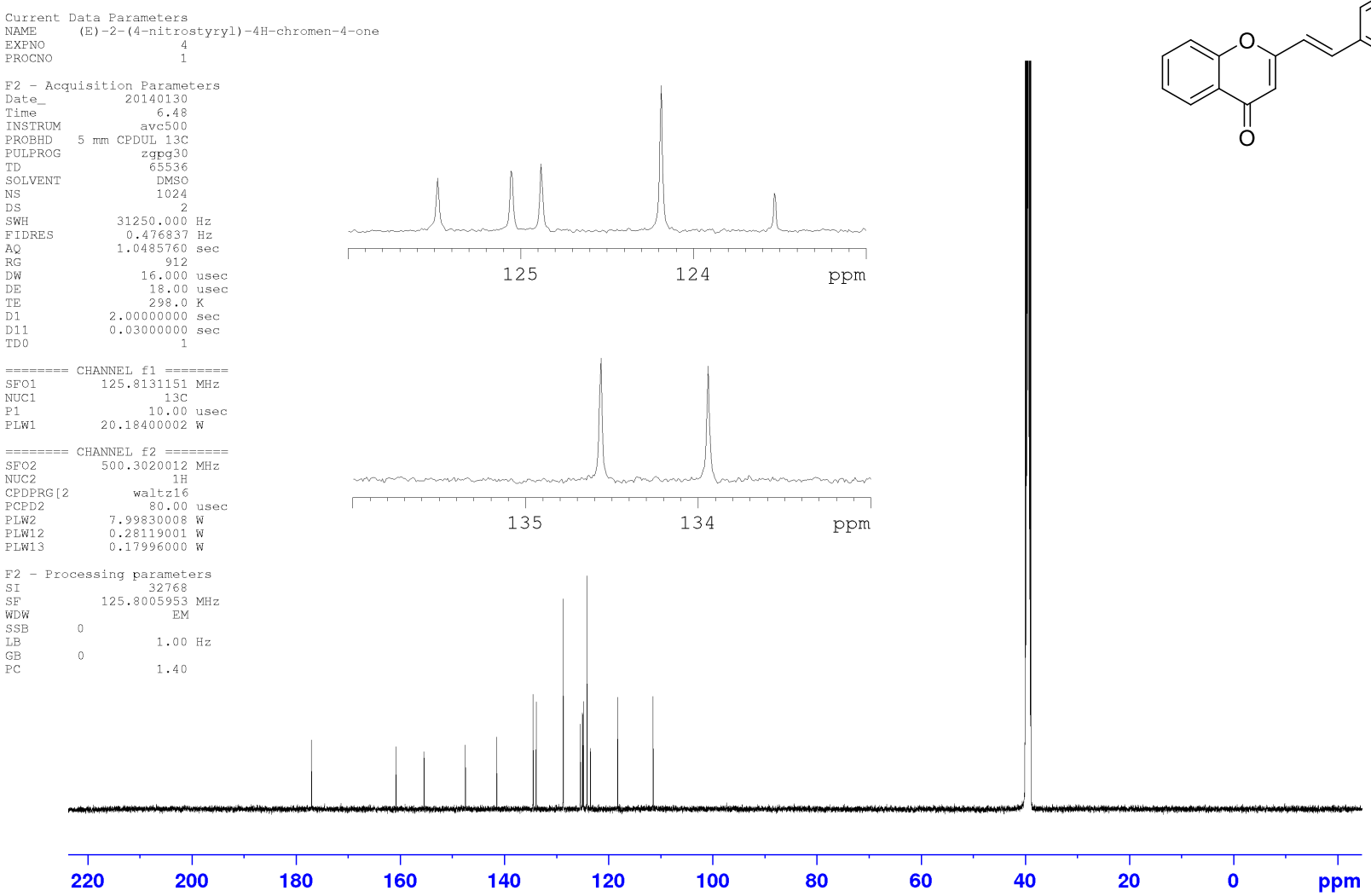

3.25. 2-(1-(4-Nitrophenyl)-2-(4-oxo-4*H*-chromen-2-yl)ethyl)malononitrile

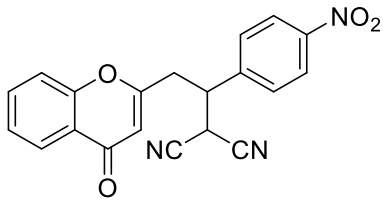


```
Current Data Parameters
NAME      2-(1-(4-nitrophenyl)-2-(4-oxo-4H-
EXPNO                   1
PROCNO                  1

F2 - Acquisition Parameters
Date_            20131211
Time                10.28
INSTRUM           avc500
PROBHD    5 mm CPDUL 13C
PULPROG             zg30
TD                 65536
SOLVENT             DMSO
NS                    16
DS                     4
SWH           10330.578 Hz
FIDRES         0.157632 Hz
AQ            3.1719425 sec
RG                   4.5
DW                48.400 usec
DE                10.00 usec
TE                298.0 K
D1           1.00000000 sec
TD0                    1

======== CHANNEL f1 ========
SFO1         500.3030896 MHz
NUC1                   1H
P1                 15.00 usec
PLW1          7.99830008 W

F2 - Processing parameters
SI                 65536
SF           500.3000052 MHz
WDW                   EM
SSB       0
LB                 0.30 Hz
GB        0
PC                 1.00
```

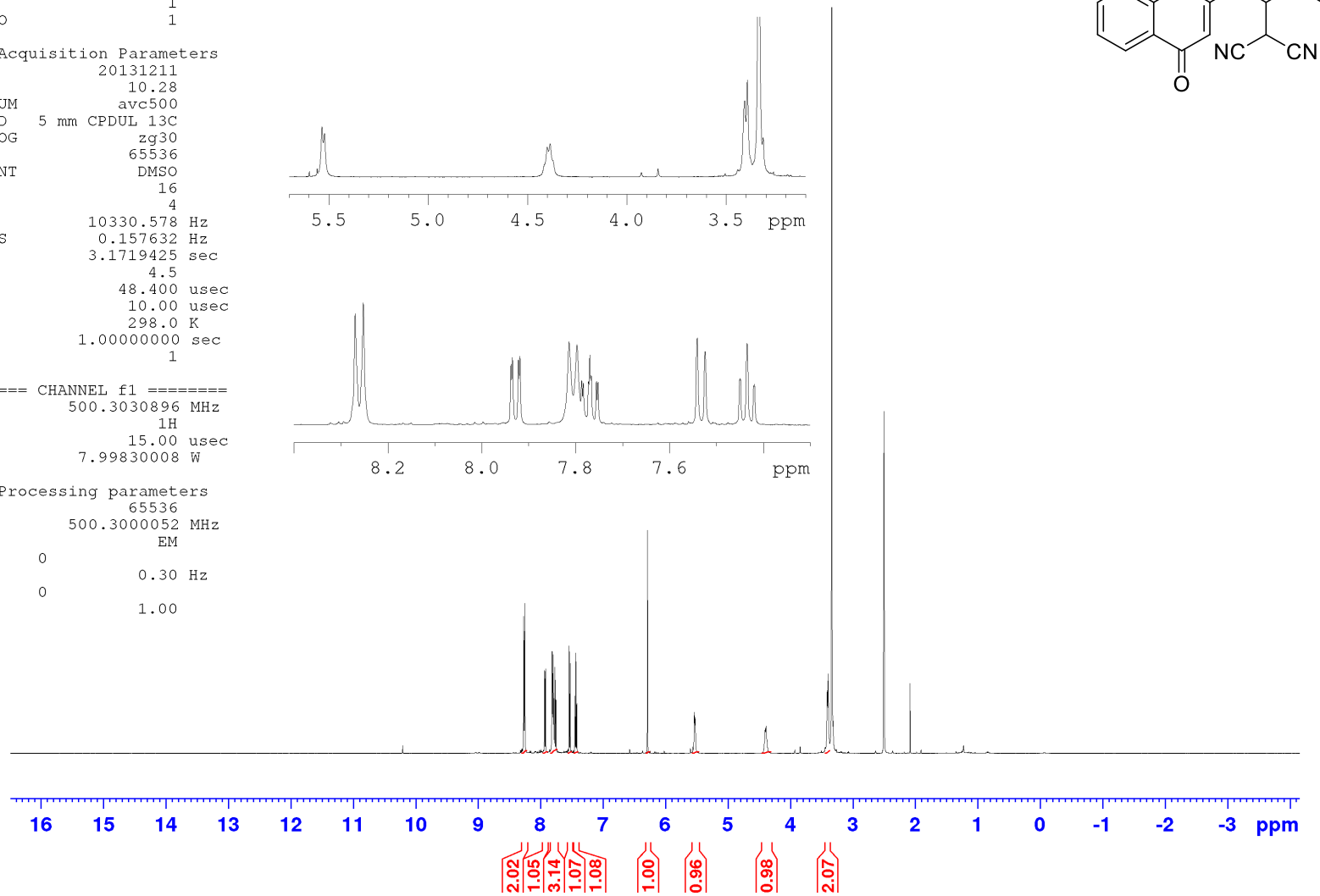

3.25. 2-(1-(4-Nitrophenyl)-2-(4-oxo-4*H*-chromen-2-yl)ethyl)malononitrile

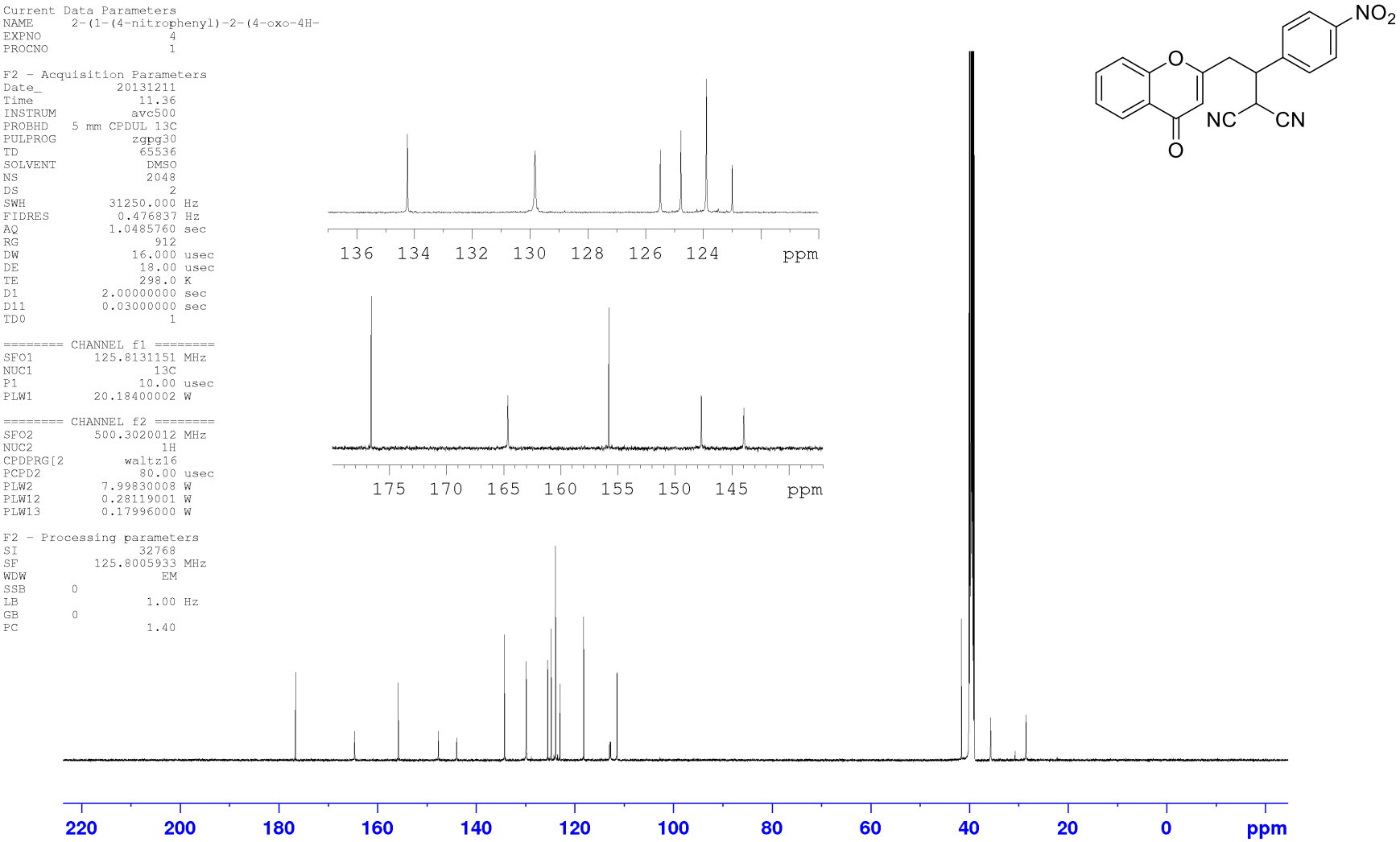

3.27. (*E*)-4-(2-(4-(Dicyanomethylene)-4*H*-chromen-2-yl)vinyl)phenyl trifluoromethanesulfonate

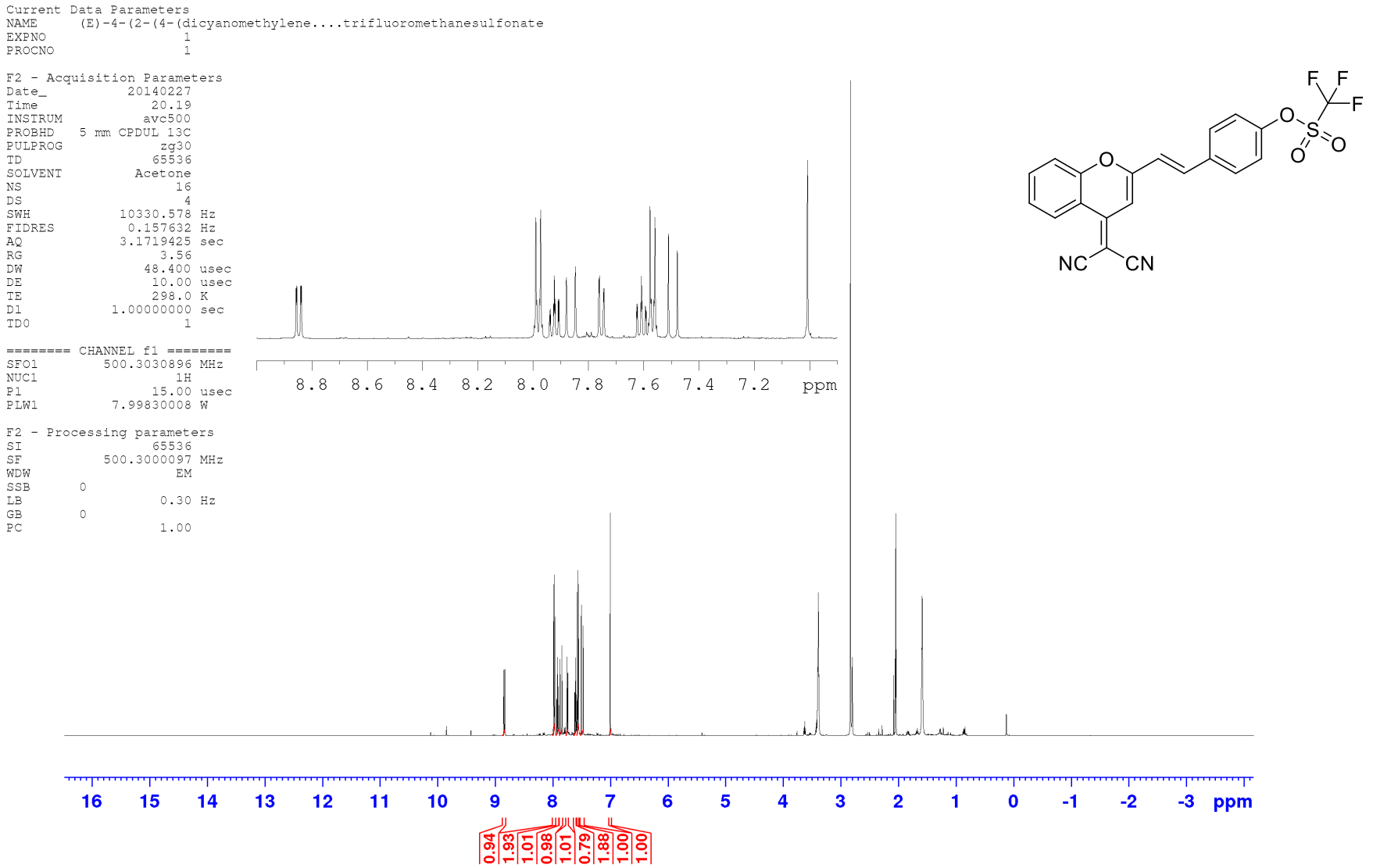

3.27. (*E*)-4-(2-(4-(Dicyanomethylene)-4*H*-chromen-2-yl)vinyl)phenyl trifluoromethanesulfonate

```
Current Data Parameters
NAME      (E)-4-(2-(4-(dicyanomethylene....trifluoromethanesulfonate
EXPNO                  4
PROCNO                 1

F2 - Acquisition Parameters
Date_           20140227
Time              22.26
INSTRUM          avc500
PROBHD   5 mm CPDUL 13C
PULPROG          zgpg30
TD                65536
SOLVENT         Acetone
NS                 2048
DS                    2
SWH           31250.000 Hz
FIDRES         0.476837 Hz
AQ             1.0485760 sec
RG                  912
DW                16.000 usec
DE                18.00 usec
TE                298.0 K
D1            2.00000000 sec
D11           0.03000000 sec
TD0                   1

======== CHANNEL f1 ========
SFO1         125.8131151 MHz
NUC1                13C
P1                10.00 usec
PLW1         20.18400002 W

======== CHANNEL f2 ========
SFO2         500.3020012 MHz
NUC2                 1H
CPDPRG[2          waltz16
PCPD2              80.00 usec
PLW2          7.99830008 W
PLW12         0.28119001 W
PLW13         0.17996000 W

F2 - Processing parameters
SI                 32768
SF           125.8004244 MHz
WDW                  EM
SSB       0
LB                1.00 Hz
GB        0
PC                1.40
```


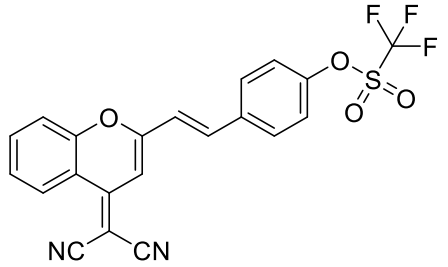

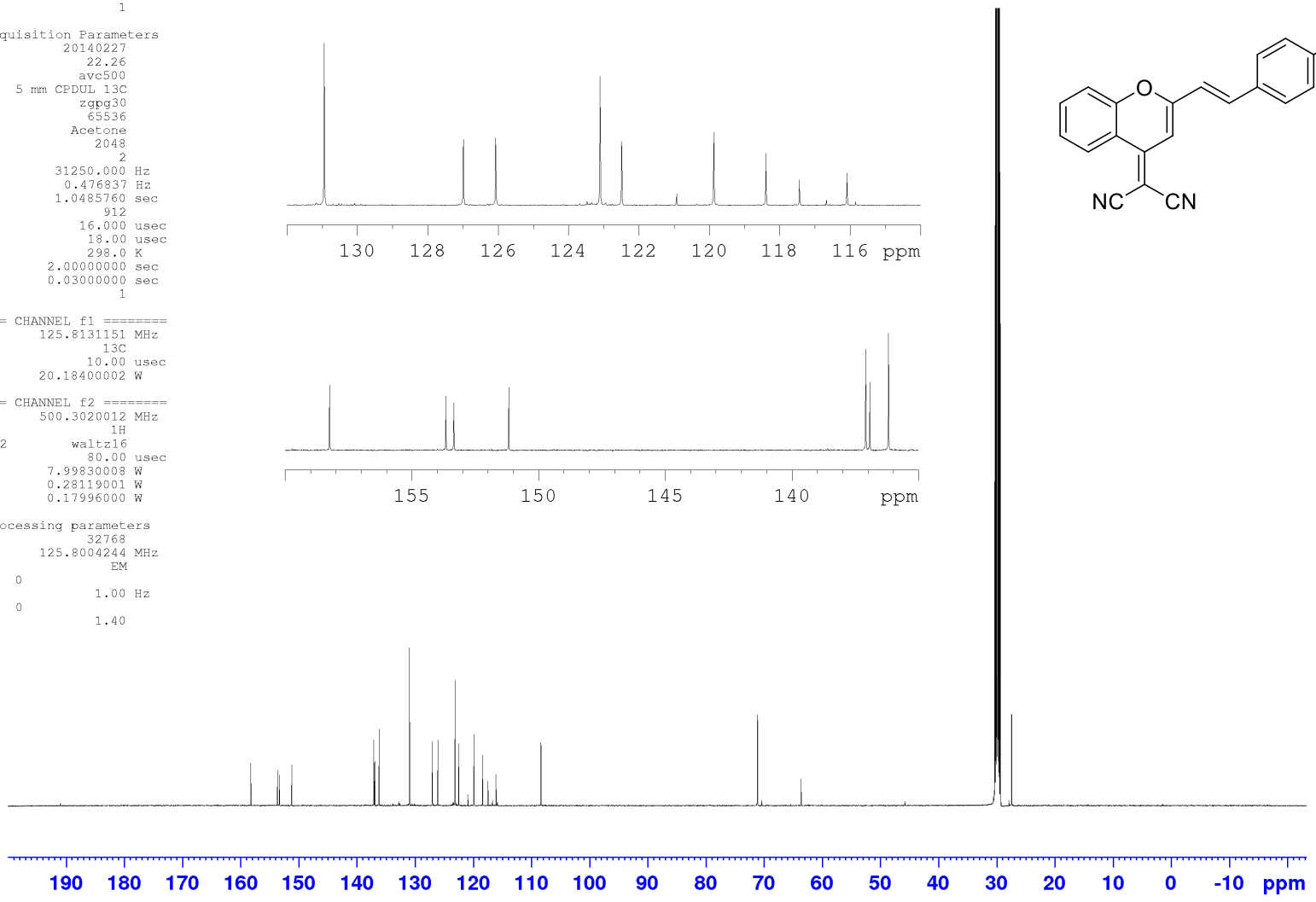

3.27. (*E*)-4-(2-(4-(Dicyanomethylene)-4*H*-chromen-2-yl)vinyl)phenyl trifluoromethanesulfonate

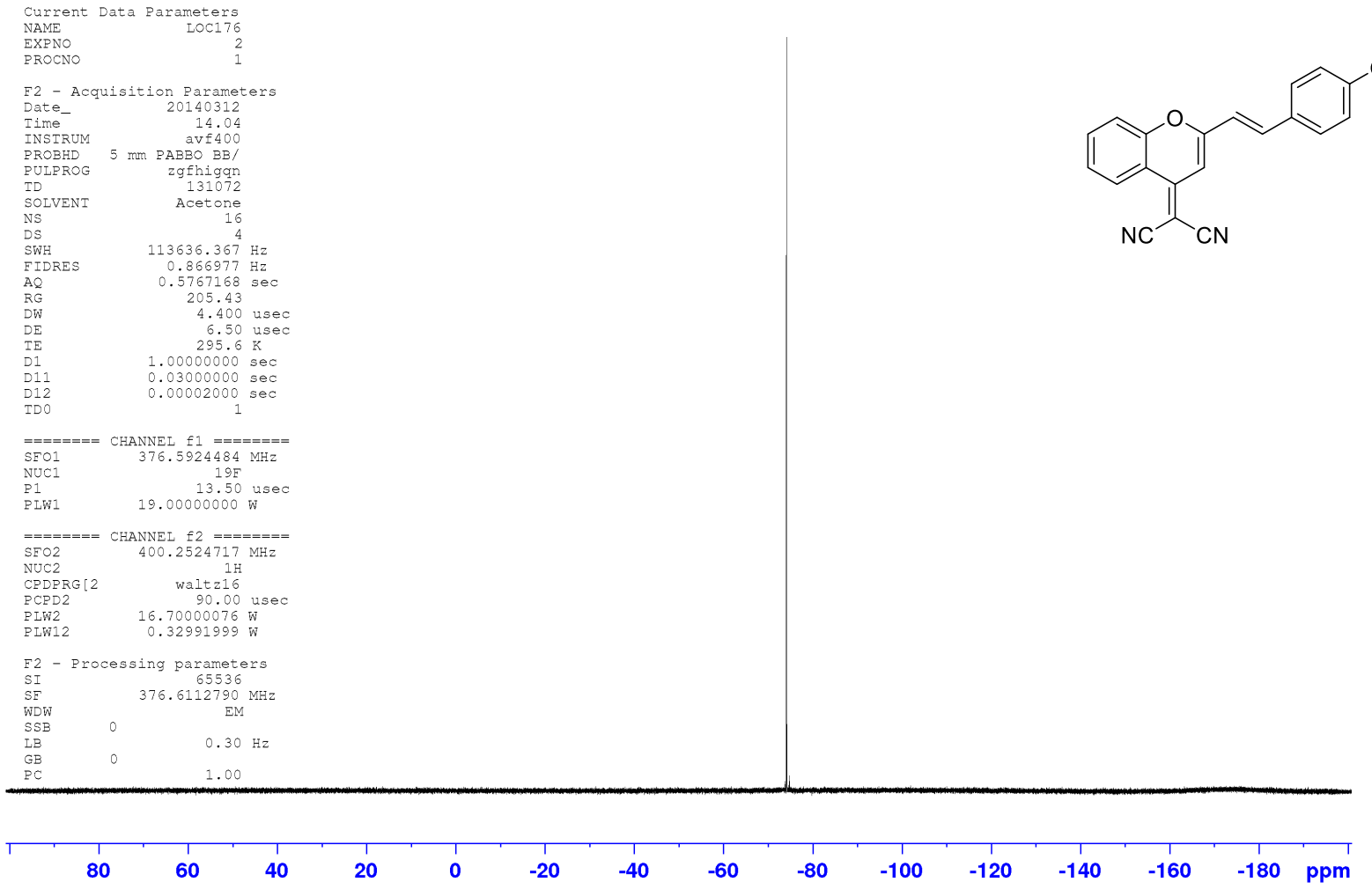

3.29. (*E*)-2-(2-(4-Azidostyryl)-4*H*-chromen-4-ylidene)malononitrile

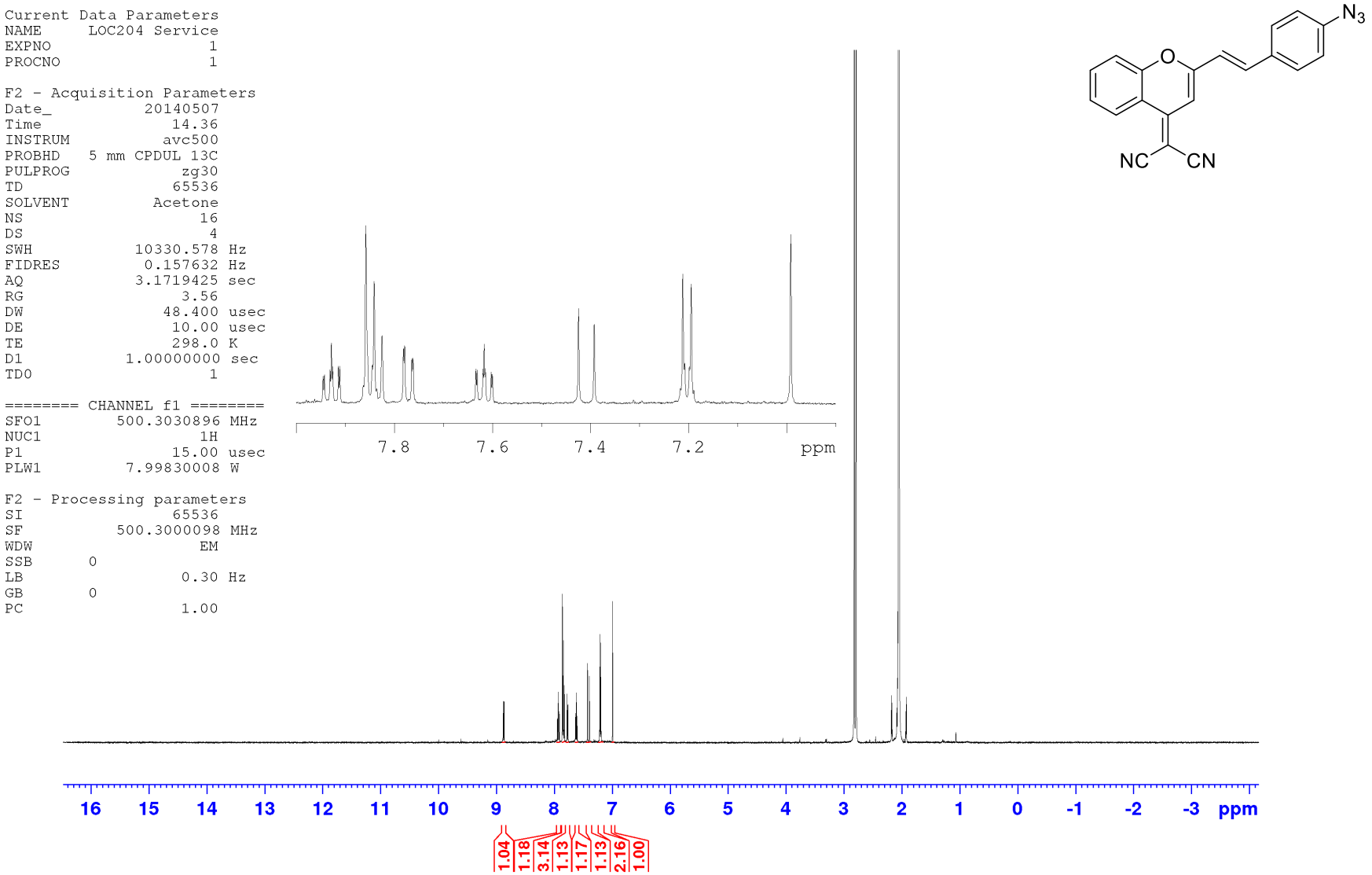

3.29. (*E*)-2-(2-(4-Azidostyryl)-4*H*-chromen-4-ylidene)malononitrile

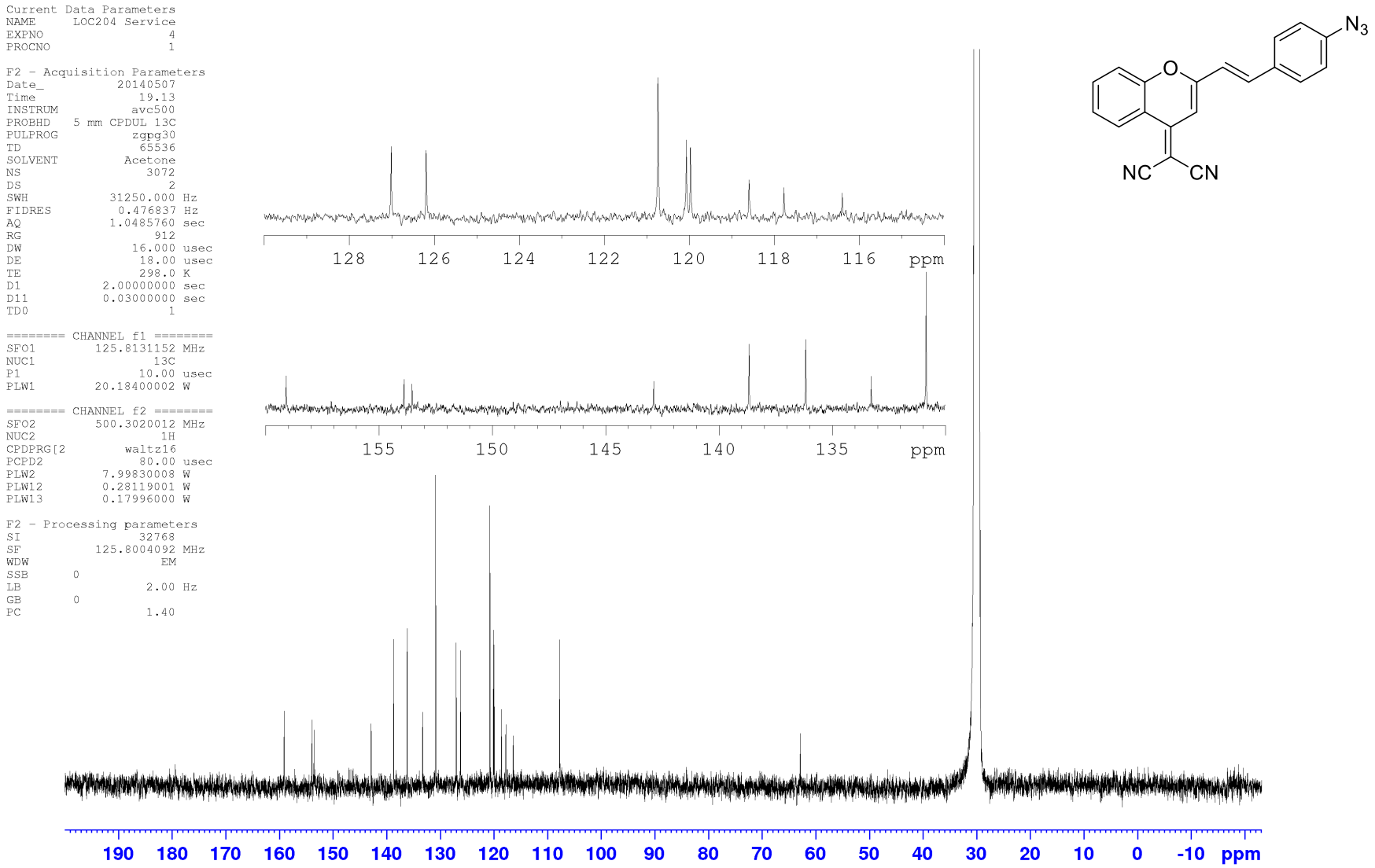

3.34. Methyl-3-(bromomethyl)-4-nitrobenzoate

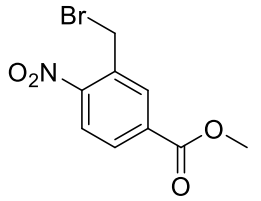


```
Current Data Parameters
NAME      LOC299 Service lo10592304
EXPNO                 1
PROCNO                1

F2 - Acquisition Parameters
Date_           20150425
Time               3.24
INSTRUM          avc500
PROBHD   5 mm CPDUL 13C
PULPROG            zg30
TD                65536
SOLVENT           CDCl3
NS                   16
DS                    4
SWH           10330.578 Hz
FIDRES         0.157632 Hz
AQ            3.1719425 sec
RG                 3.56
DW               48.400 usec
DE               10.00 usec
TE               298.0 K
D1           1.00000000 sec
TD0                   1

======== CHANNEL f1 ========
SFO1         500.3030896 MHz
NUC1                 1H
P1                15.00 usec
PLW1          7.99830008 W

F2 - Processing parameters
SI                65536
SF           500.3000136 MHz
WDW                  EM
SSB       0
LB                0.30 Hz
GB        0
PC                1.00
```

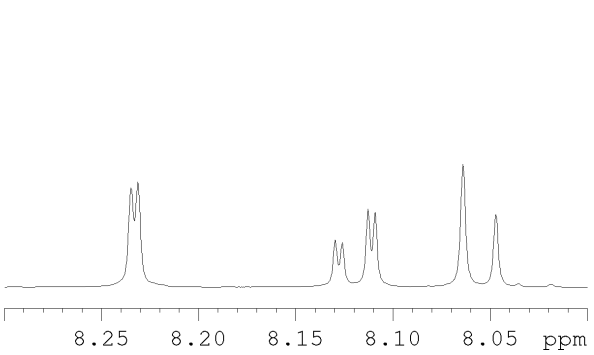

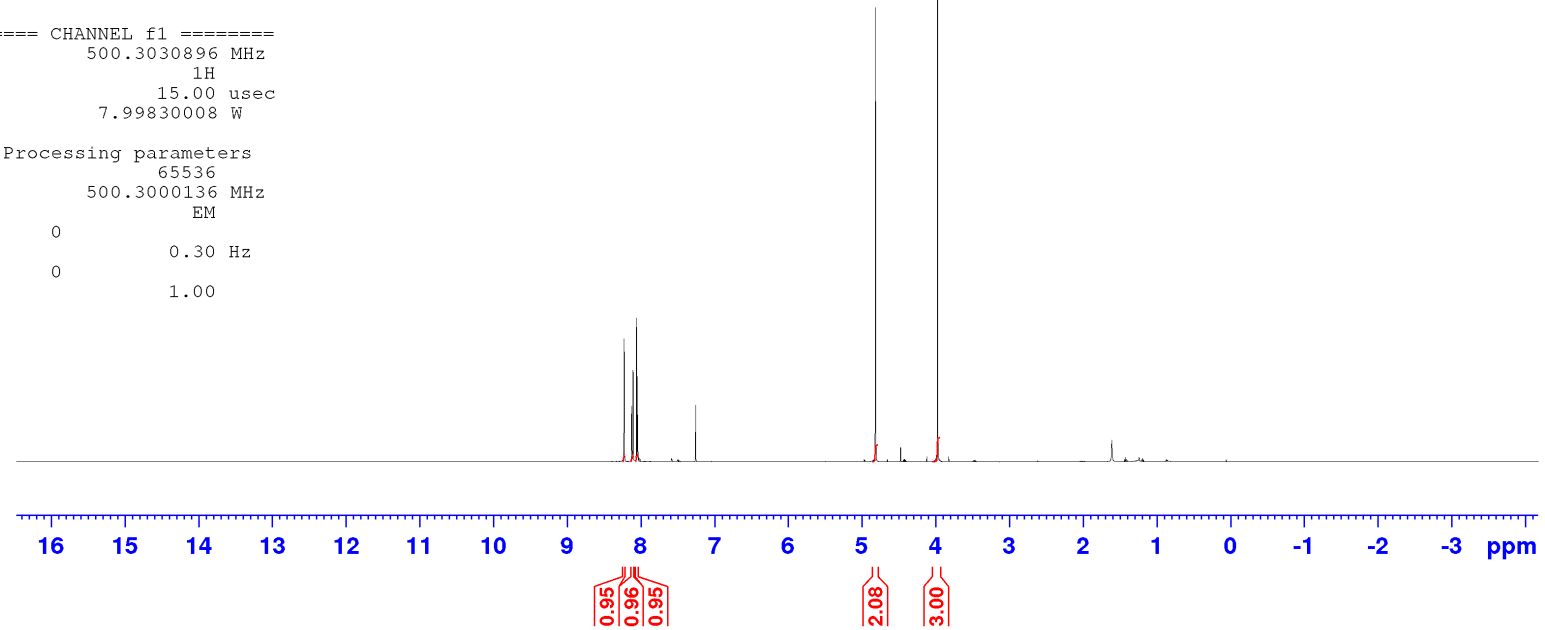

3.34. Methyl-3-(bromomethyl)-4-nitrobenzoate

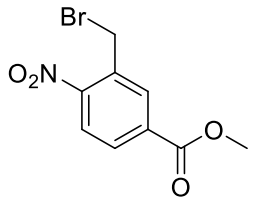


```
Current Data Parameters
NAME      LOC299 Service lo10592304
EXPNO                 4
PROCNO                1

F2 - Acquisition Parameters
Date_          20150425
Time               4.39
INSTRUM          avc500
PROBHD   5 mm CPDUL 13C
PULPROG          zgpg30
TD                65536
SOLVENT           CDCl3
NS                 1024
DS                    2
SWH           31250.000 Hz
FIDRES         0.476837 Hz
AQ            1.0485760 sec
RG                  912
DW               16.000 usec
DE                18.00 usec
TE                298.0 K
D1           2.00000000 sec
D11          0.03000000 sec
TD0                   1

======== CHANNEL f1 ========
SFO1        125.8131152 MHz
NUC1                13C
P1                10.00 usec
PLW1        20.18400002 W

======== CHANNEL f2 ========
SFO2        500.3020012 MHz
NUC2                1H
CPDPRG[2         waltz16
PCPD2             80.00 usec
PLW2         7.99830008 W
PLW12        0.28119001 W
PLW13        0.17996000 W

F2 - Processing parameters
SI                32768
SF          125.8005217 MHz
WDW                  EM
SSB       0
LB                1.00 Hz
GB        0
PC                1.40
```

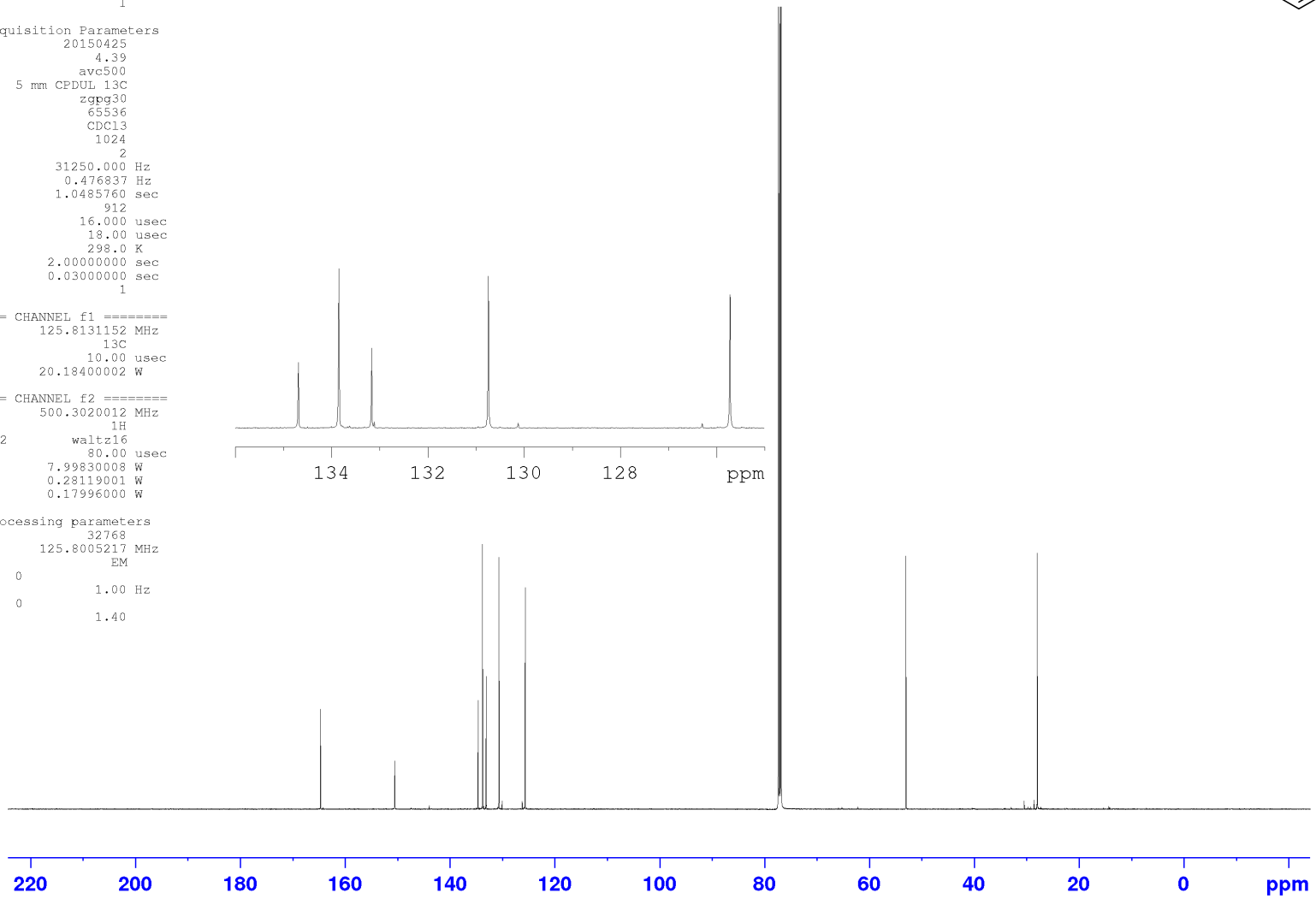

3.35. Methyl-3-(hydroxymethyl)-4-nitrobenzoate

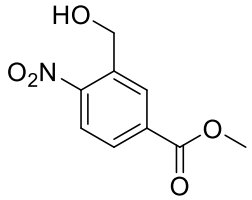


```
Current Data Parameters
NAME      LOC294 Service lo10142004
EXPNO                 1
PROCNO                1

F2 - Acquisition Parameters
Date_           20150421
Time              23.37
INSTRUM          avc500
PROBHD   5 mm CPDUL 13C
PULPROG            zg30
TD                65536
SOLVENT           CDCl3
NS                   16
DS                    4
SWH           10330.578 Hz
FIDRES         0.157632 Hz
AQ            3.1719425 sec
RG                 3.56
DW               48.400 usec
DE               10.00 usec
TE               298.0 K
D1           1.00000000 sec
TD0                   1

======== CHANNEL f1 ========
SFO1        500.3030896 MHz
NUC1                1H
P1                15.00 usec
PLW1         7.99830008 W

F2 - Processing parameters
SI                65536
SF          500.3000136 MHz
WDW                 EM
SSB       0
LB                0.30 Hz
GB        0
PC                1.00
```

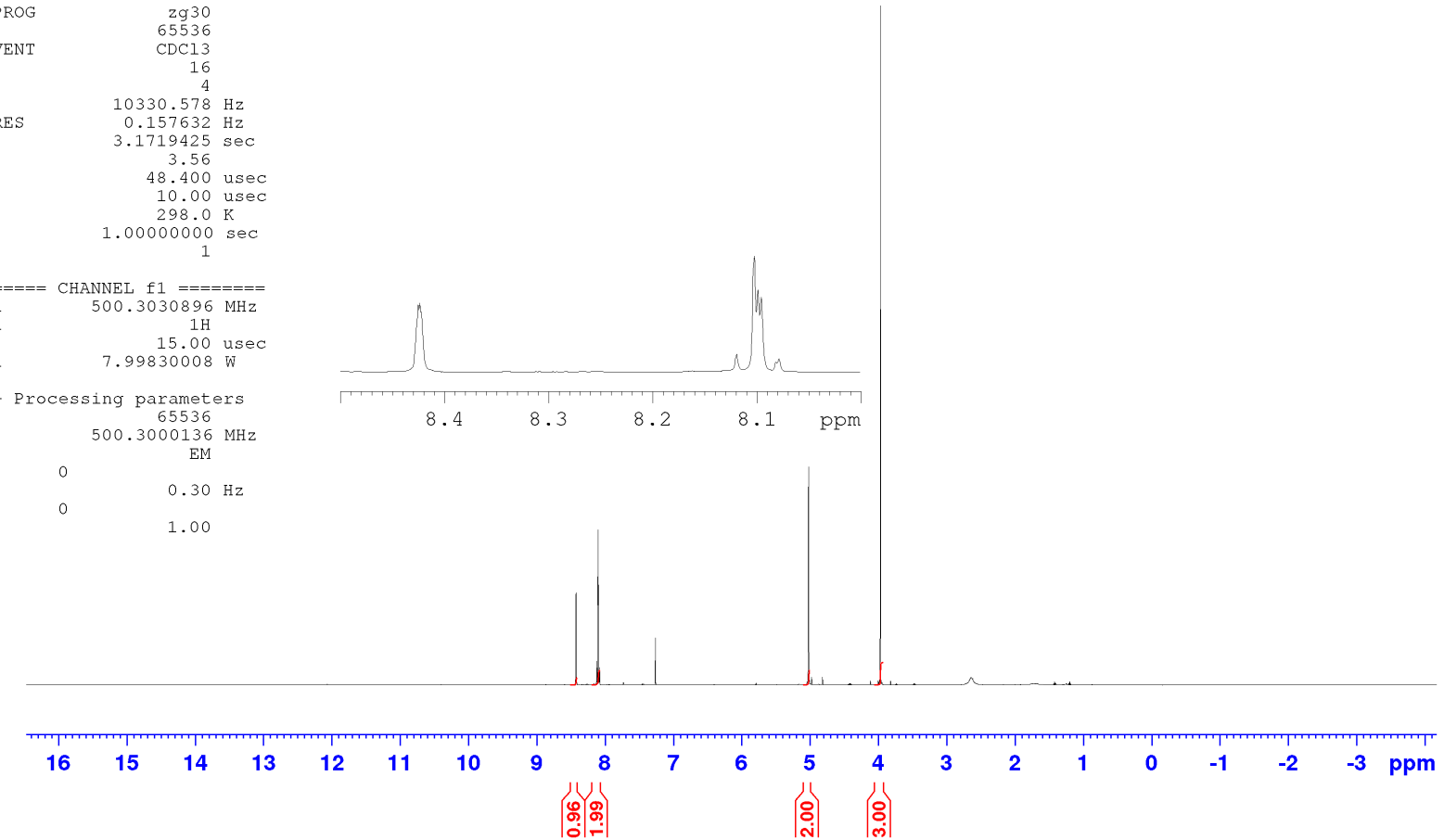

3.35. Methyl-3-(hydroxymethyl)-4-nitrobenzoate

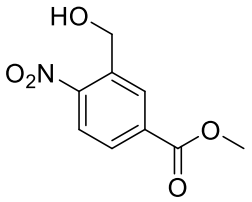


```
Current Data Parameters
NAME      LOC294 Service lo10142004
EXPNO                 4
PROCNO                1

F2 - Acquisition Parameters
Date_           20150422
Time                0.46
INSTRUM          avc500
PROBHD   5 mm CPDUL 13C
PULPROG          zgpg30
TD                65536
SOLVENT           CDCl3
NS                  512
DS                    2
SWH           31250.000 Hz
FIDRES         0.476837 Hz
AQ             1.0485760 sec
RG                  912
DW               16.000 usec
DE               18.00 usec
TE               298.0 K
D1            2.00000000 sec
D11           0.03000000 sec
TD0                   1

======== CHANNEL f1 ========
SFO1        125.8131152 MHz
NUC1                13C
P1                10.00 usec
PLW1        20.18400002 W

======== CHANNEL f2 ========
SFO2        500.3020012 MHz
NUC2                1H
CPDPRG[2         waltz16
PCPD2             80.00 usec
PLW2          7.99830008 W
PLW12         0.28119001 W
PLW13         0.17996000 W

F2 - Processing parameters
SI                32768
SF          125.8005218 MHz
WDW                 EM
SSB       0
LB                1.00 Hz
GB        0
PC                1.40
```

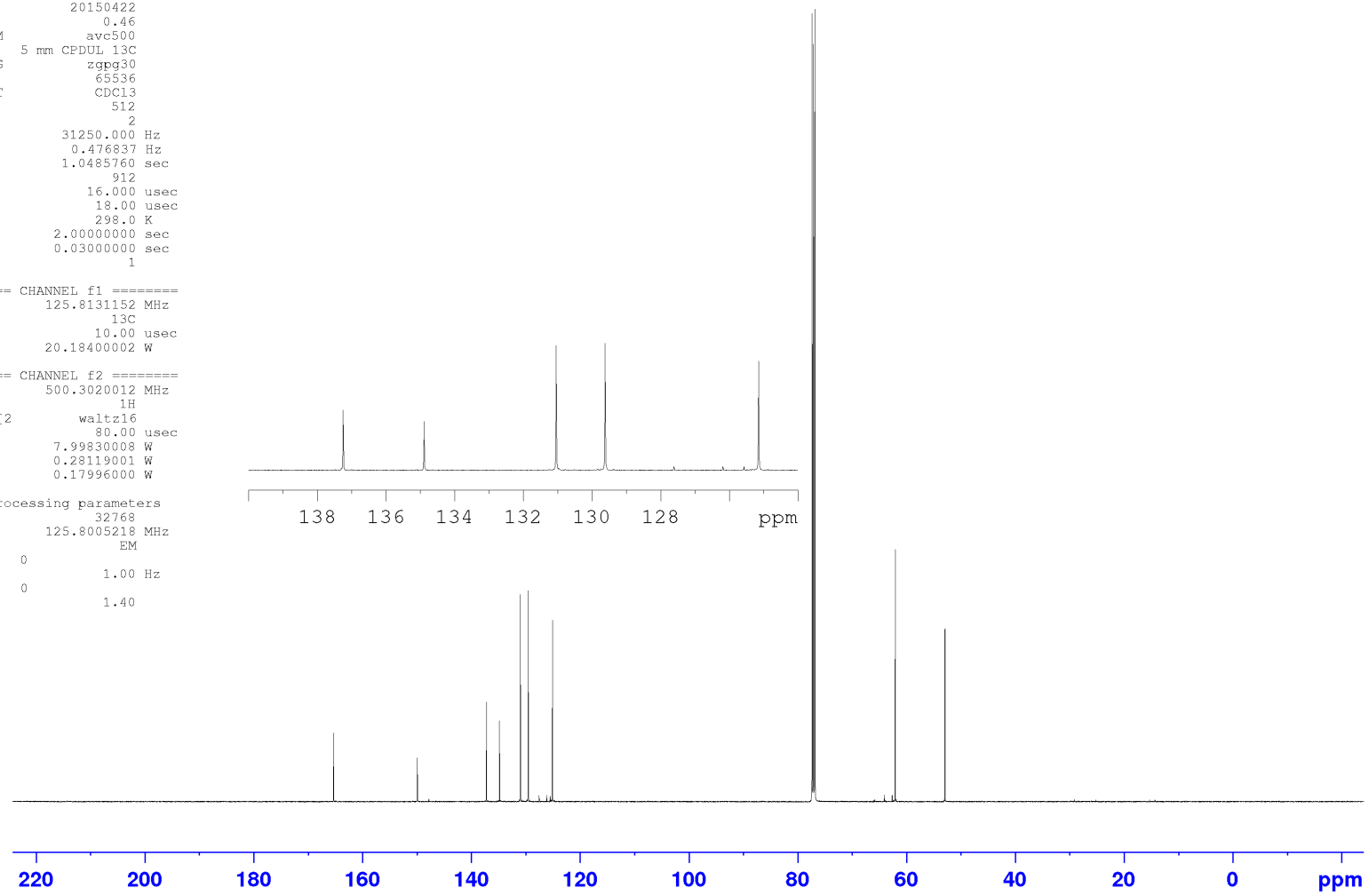

3.37. Methyl-3-(((*tert*-butyldimethylsilyl)oxy)methyl)-4-nitrobenzoate

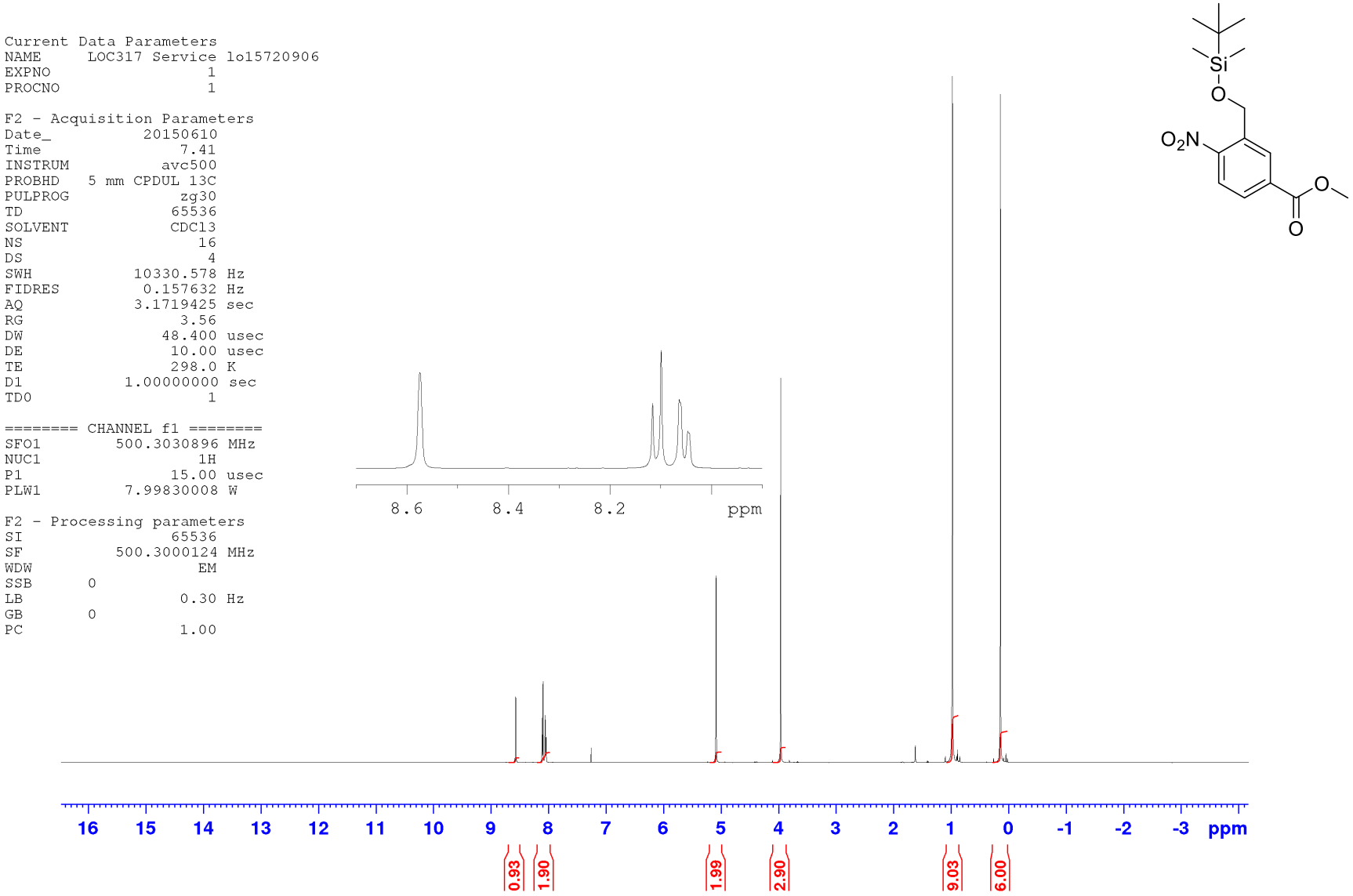

3.37. Methyl-3-(((*tert*-butyldimethylsilyl)oxy)methyl)-4-nitrobenzoate

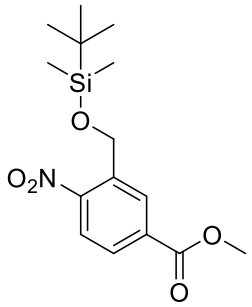


```
Current Data Parameters
NAME      LOC317 Service lo15720906
EXPNO                 4
PROCNO                1

F2 - Acquisition Parameters
Date_          20150610
Time               8.36
INSTRUM          avc500
PROBHD   5 mm CPDUL 13C
PULPROG          zgpg30
TD                65536
SOLVENT           CDCl3
NS                  256
DS                    2
SWH           31250.000 Hz
FIDRES         0.476837 Hz
AQ            1.0485760 sec
RG                  912
DW               16.000 usec
DE               18.00 usec
TE               298.0 K
D1           2.00000000 sec
D11          0.03000000 sec
TD0                   1

======== CHANNEL f1 ========
SFO1        125.8131152 MHz
NUC1                13C
P1                10.00 usec
PLW1        20.18400002 W

======== CHANNEL f2 ========
SFO2        500.3020012 MHz
NUC2                1H
CPDPRG[2         waltz16
PCPD2             80.00 usec
PLW2           7.99830008 W
PLW12          0.28119001 W
PLW13          0.17996000 W

F2 - Processing parameters
SI                 32768
SF          125.8005553 MHz
WDW                   EM
SSB       0
LB                 1.00 Hz
GB        0
PC                 1.40
```

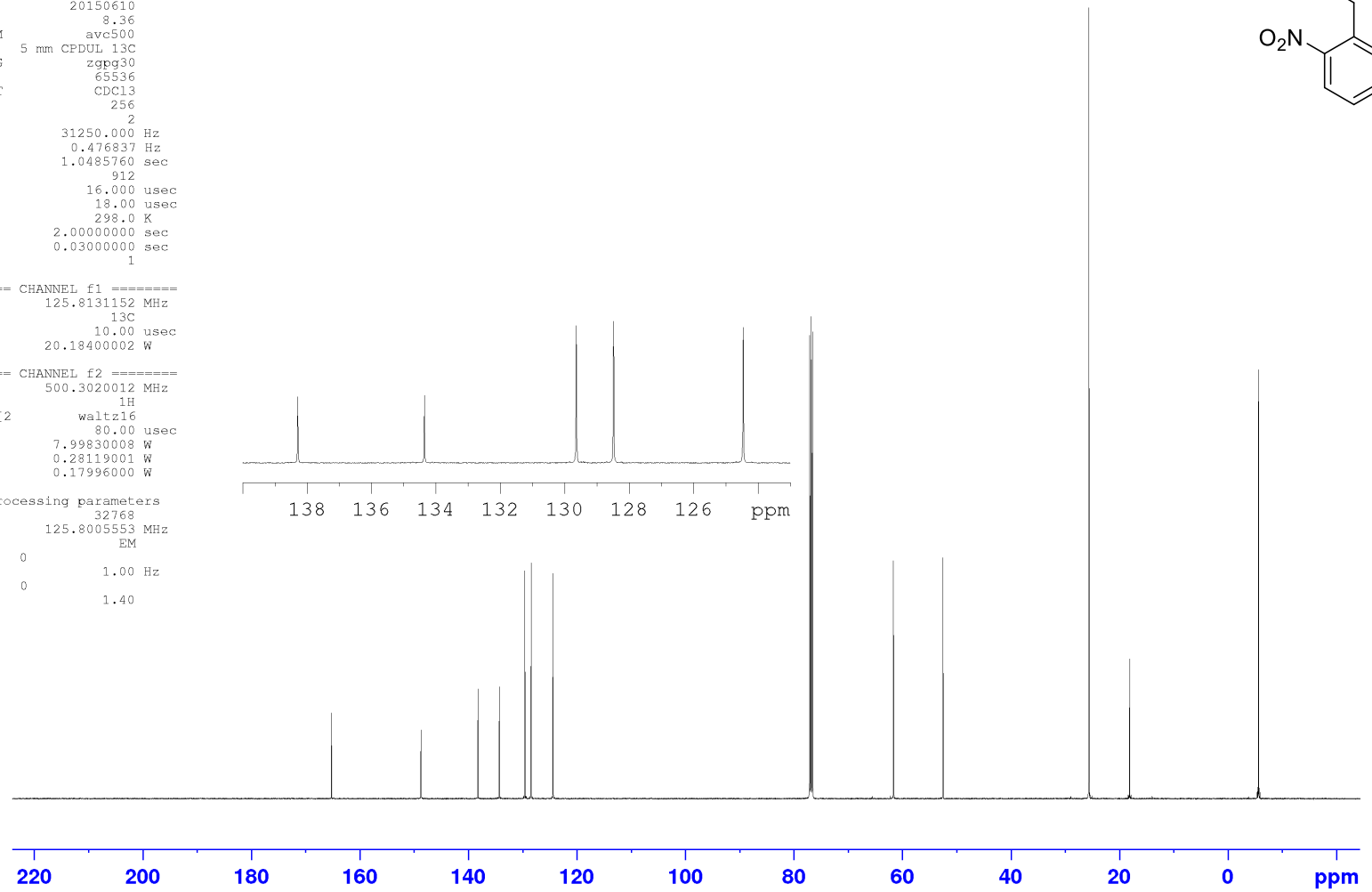

3.38. (3-(((*tert*-Butyldimethylsilyl)oxy)methyl)-4-nitrophenyl)methanol

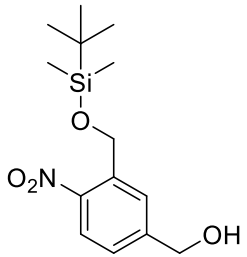


```
Current Data Parameters
NAME      LOC318 Service lo16121106
EXPNO                 1
PROCNO                1

F2 - Acquisition Parameters
Date_           20150613
Time              10.16
INSTRUM          avc500
PROBHD   5 mm CPDUL 13C
PULPROG            zg30
TD                65536
SOLVENT           CDCl3
NS                   16
DS                    4
SWH           10330.578 Hz
FIDRES         0.157632 Hz
AQ             3.1719425 sec
RG                 3.56
DW                48.400 usec
DE                10.00 usec
TE                298.0 K
D1            1.00000000 sec
TD0                   1

======== CHANNEL f1 ========
SFO1        500.3030896 MHz
NUC1                1H
P1                15.00 usec
PLW1         7.99830008 W

F2 - Processing parameters
SI                65536
SF           500.3000141 MHz
WDW                  EM
SSB      0
LB                0.30 Hz
GB       0
PC                1.00
```

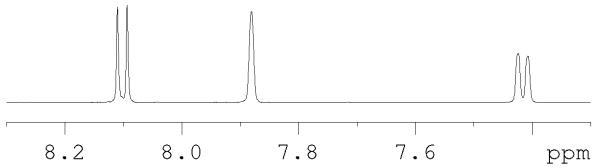

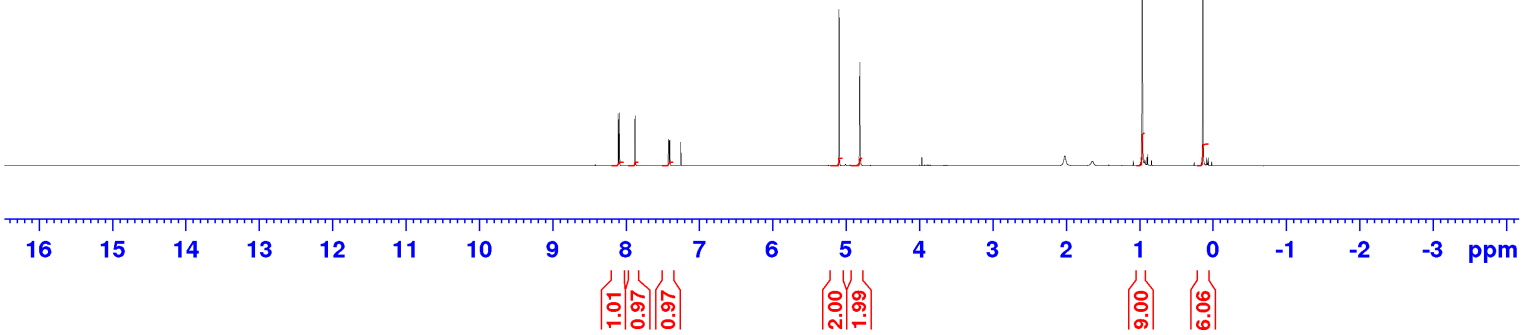

3.38. (3-(((*tert*-Butyldimethylsilyl)oxy)methyl)-4-nitrophenyl)methanol

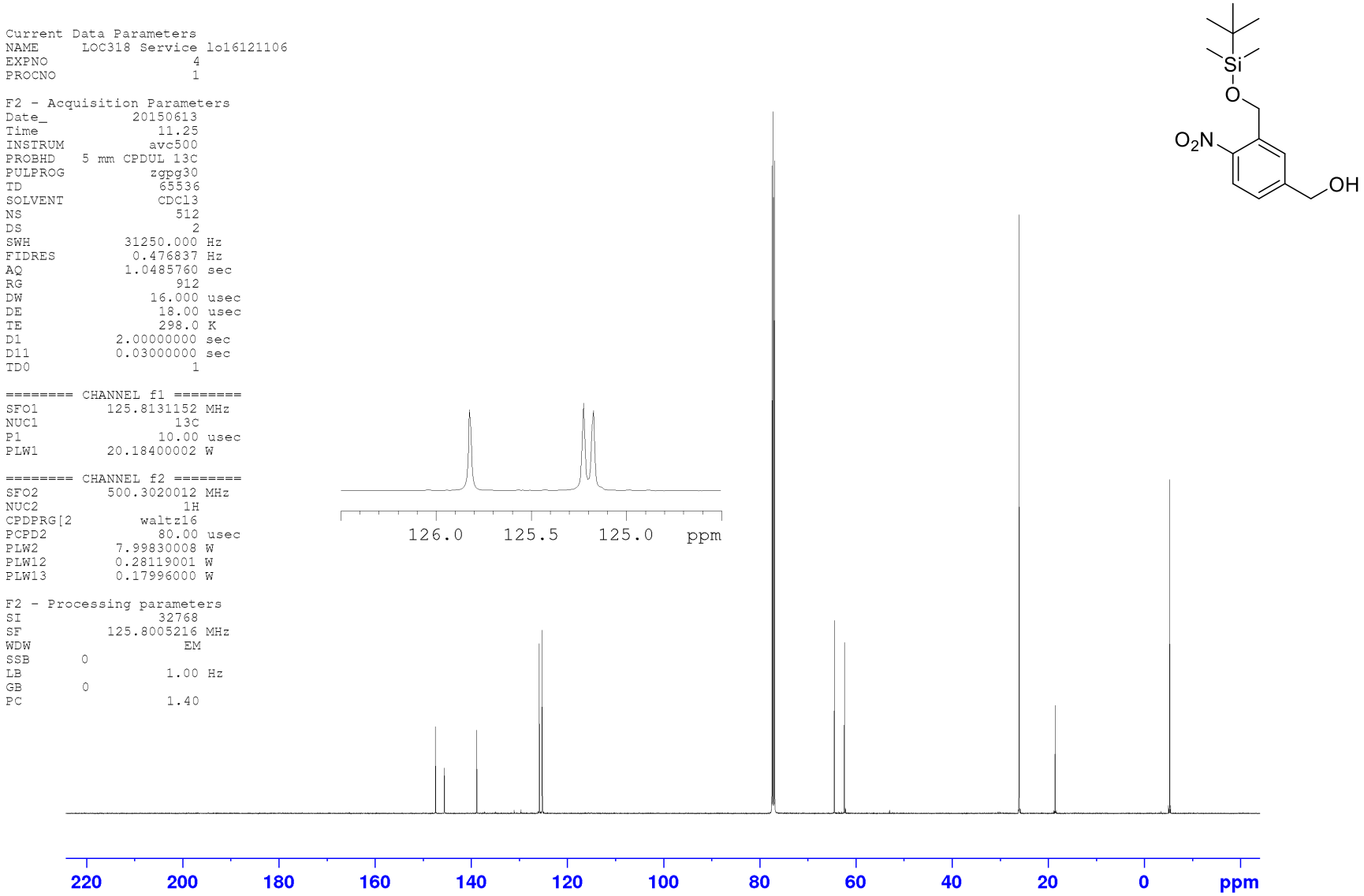


```
Current Data Parameters
NAME      LOC318 Service lo16121106
EXPNO                 4
PROCNO                1

F2 - Acquisition Parameters
Date_           20150613
Time              11.25
INSTRUM          avc500
PROBHD   5 mm CPDUL 13C
PULPROG          zgpg30
TD                65536
SOLVENT           CDCl3
NS                  512
DS                    2
SWH           31250.000 Hz
FIDRES         0.476837 Hz
AQ            1.0485760 sec
RG                  912
DW               16.000 usec
DE               18.00 usec
TE                298.0 K
D1           2.00000000 sec
D11          0.03000000 sec
TD0                   1

======== CHANNEL f1 ========
SFO1         125.8131152 MHz
NUC1                13C
P1                10.00 usec
PLW1         20.18400002 W

======== CHANNEL f2 ========
SFO2         500.3020012 MHz
NUC2                 1H
CPDPRG[2         waltz16
PCPD2              80.00 usec
PLW2          7.99830008 W
PLW12         0.28119001 W
PLW13         0.17996000 W

F2 - Processing parameters
SI                  32768
SF           125.8005216 MHz
WDW                  EM
SSB       0
LB                1.00 Hz
GB        0
PC                1.40
```

3.39. 3-(((*tert*-Butyldimethylsilyl)oxy)methyl)-4-nitrobenzaldehyde

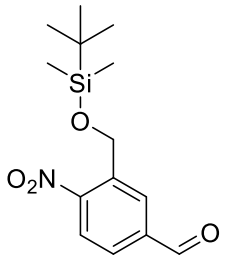


```
Current Data Parameters
NAME      LOC320 Service lc16441606
EXPNO                 1
PROCNO                1

F2 - Acquisition Parameters
Date_           20150617
Time              13.51
INSTRUM          avc500
PROBHD   5 mm CPDUL 13C
PULPROG            zg30
TD                65536
SOLVENT           CDCl3
NS                   16
DS                    4
SWH           10330.578 Hz
FIDRES         0.157632 Hz
AQ             3.1719425 sec
RG                 3.56
DW                48.400 usec
DE                10.00 usec
TE                298.0 K
D1            1.00000000 sec
TD0                   1

======== CHANNEL f1 ========
SFO1        500.3030896 MHz
NUC1                1H
P1                15.00 usec
PLW1          7.99830008 W

F2 - Processing parameters
SI                 65536
SF          500.3000159 MHz
WDW                   EM
SSB       0
LB                0.30 Hz
GB        0
PC                1.00
```

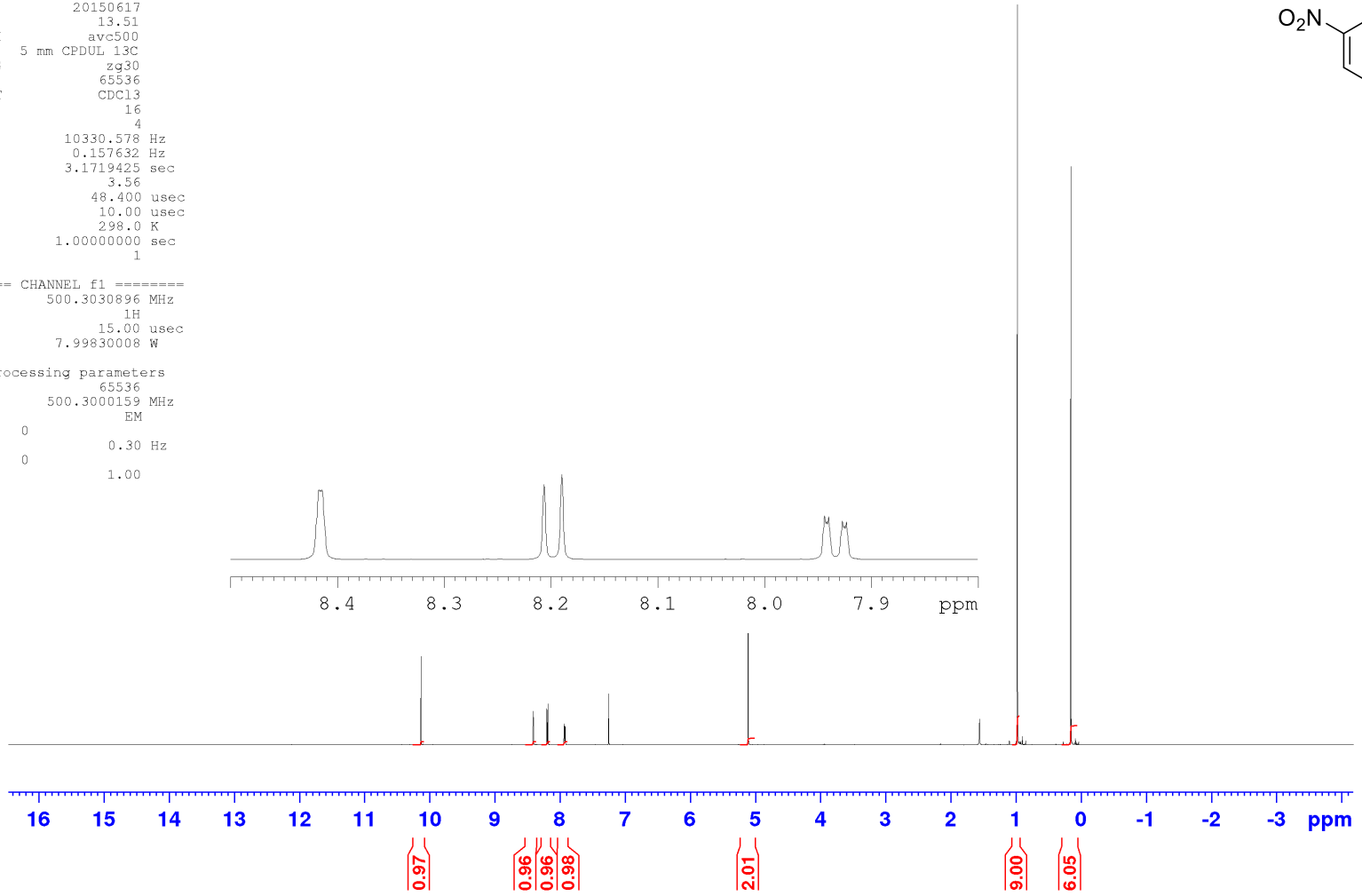

3.39. 3-(((*tert*-Butyldimethylsilyl)oxy)methyl)-4-nitrobenzaldehyde

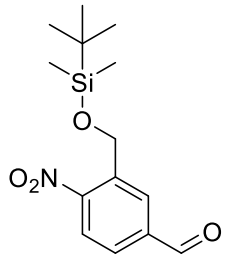


```
Current Data Parameters
NAME      LOC320 Service lc16441606
EXPNO                  4
PROCNO                 1

F2 - Acquisition Parameters
Date_           20150617
Time              15.05
INSTRUM          avc500
PROBHD   5 mm CPDUL 13C
PULPROG          zgpg30
TD                65536
SOLVENT           CDCl3
NS                 1024
DS                    2
SWH           31250.000 Hz
FIDRES         0.476837 Hz
AQ            1.0485760 sec
RG                  912
DW               16.000 usec
DE               18.00 usec
TE               298.0 K
D1           2.00000000 sec
D11          0.03000000 sec
TD0                   1

======== CHANNEL f1 ========
SFO1         125.8131152 MHz
NUC1                13C
P1                10.00 usec
PLW1         20.18400002 W

======== CHANNEL f2 ========
SFO2         500.3020012 MHz
NUC2                1H
CPDPRG[2         waltz16
PCPD2             80.00 usec
PLW2          7.99830008 W
PLW12         0.28119001 W
PLW13         0.17996000 W

F2 - Processing parameters
SI                 32768
SF           125.8005203 MHz
WDW                  EM
SSB       0
LB                1.00 Hz
GB        0
PC                1.40
```


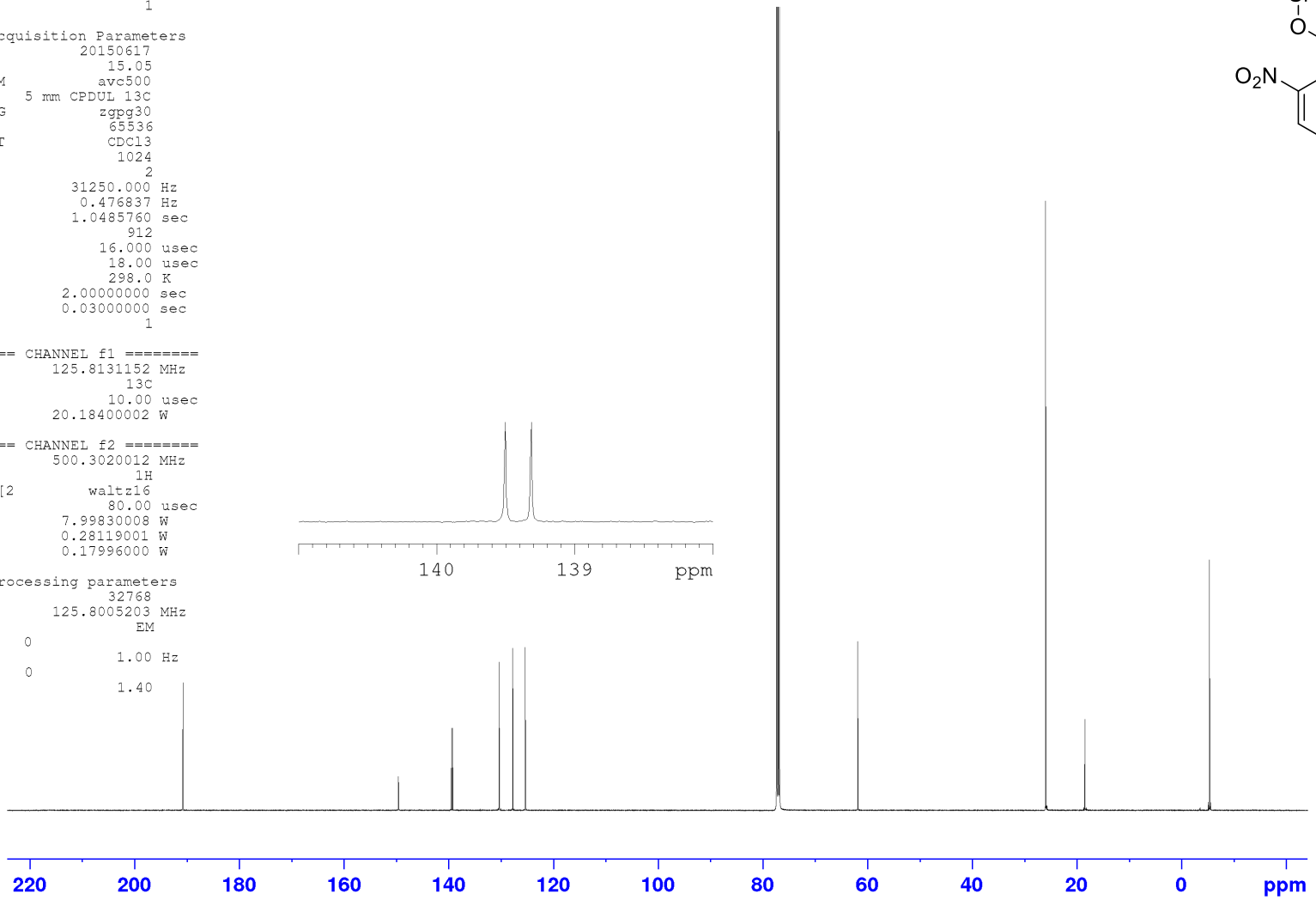

5.1. (*E*)-1-Ethyl-2-(2-(6-hydroxy-2,3-dihydro-1*H*-xanthen-4-yl)vinyl)-3,3-dimethyl-3*H*-indol-1-ium iodide

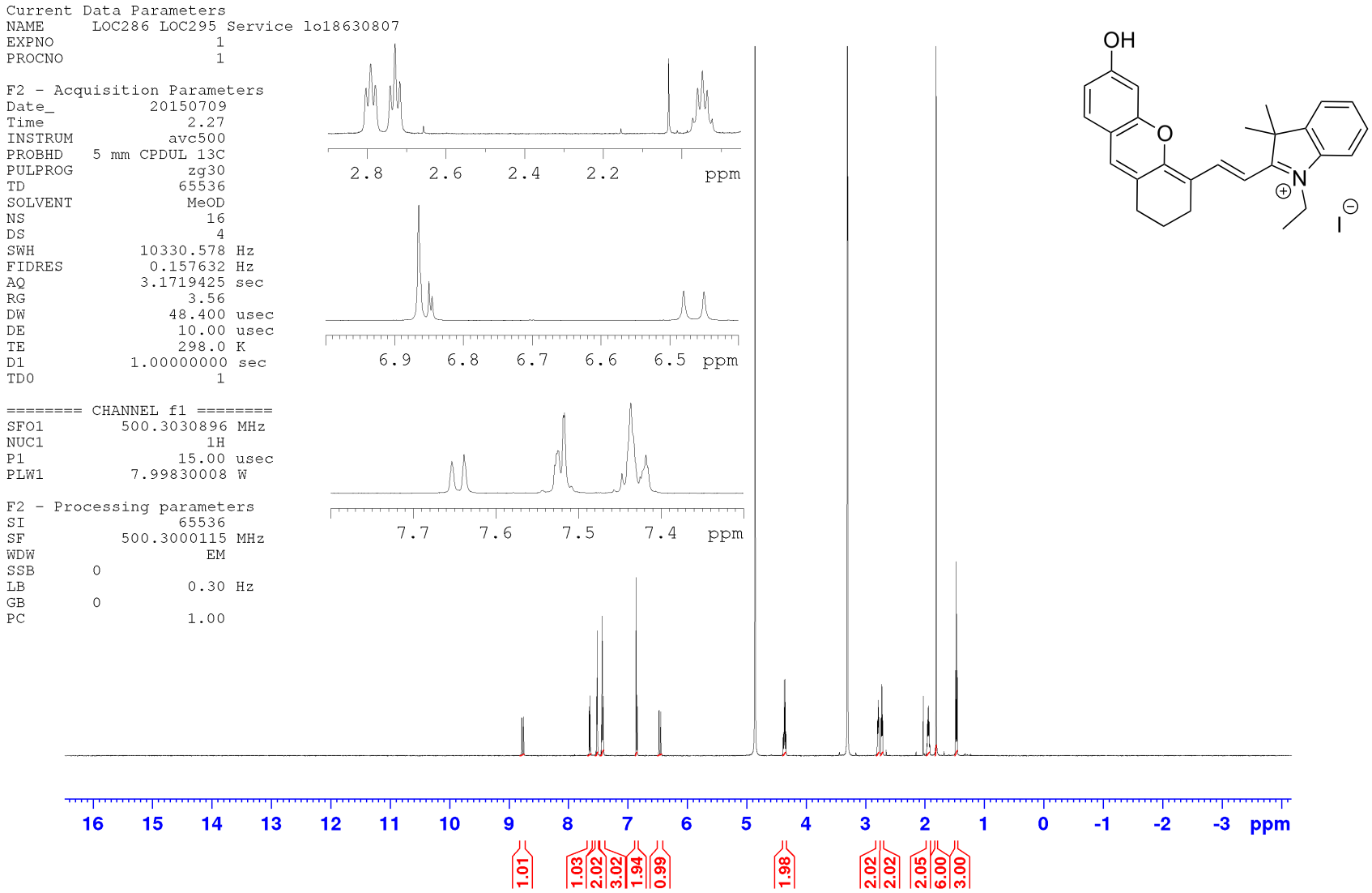

5.1. (*E*)-1-Ethyl-2-(2-(6-hydroxy-2,3-dihydro-1*H*-xanthen-4-yl)vinyl)-3,3-dimethyl-3*H*-indol-1-ium iodide

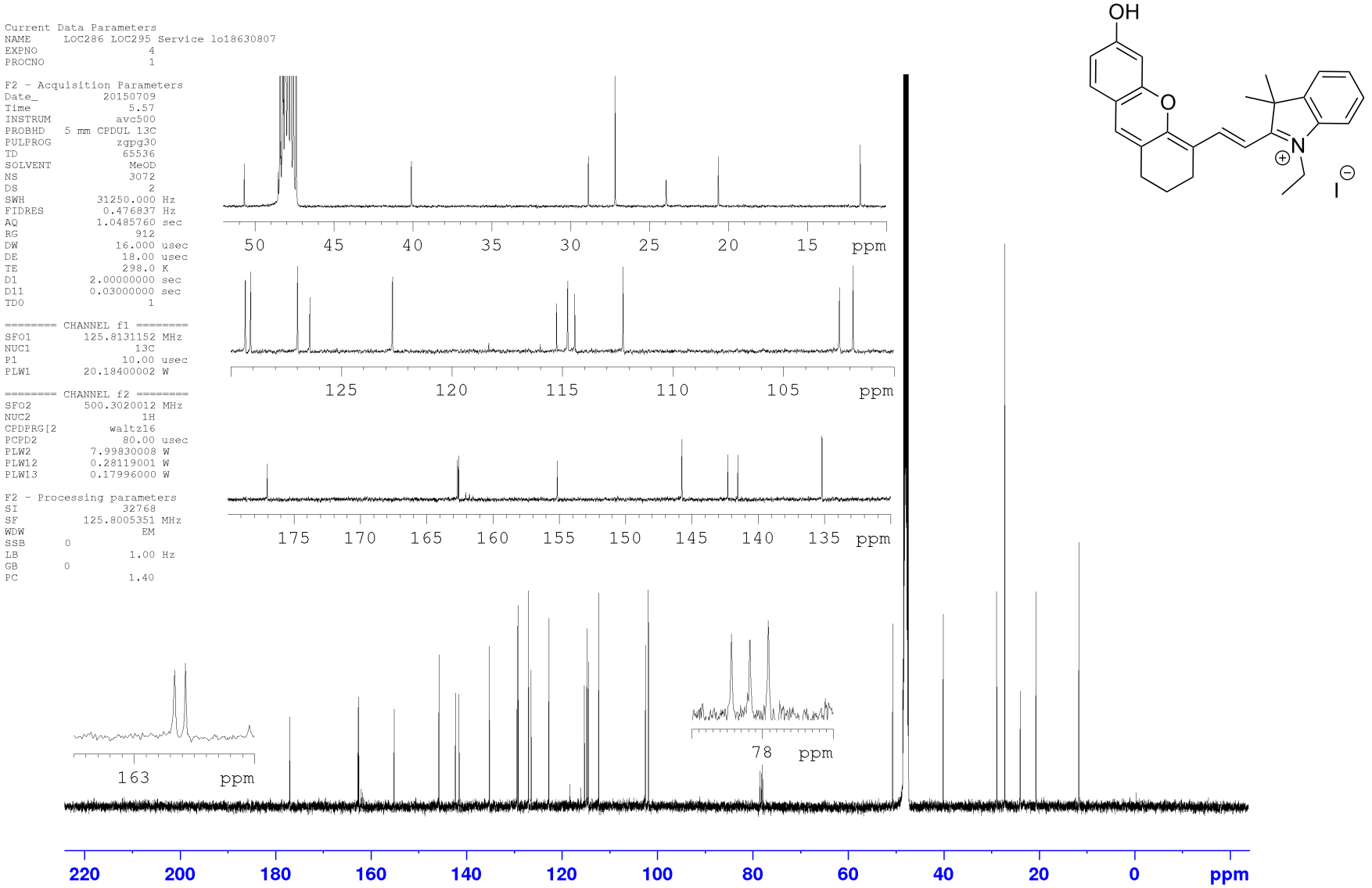

5.8. (*E*)-(3-(3,5-Dimethylisoxazol-4-yl)-5-((5-(((4-(2-(1-ethyl-3,3-dimethyl-3*H*-1λ^4-indol-2-yl)vinyl)-2,3-dihydro-1*H*-xanthen-6-yl)oxy)methyl)-2-nitrobenzyl)oxy)phenyl)(4-fluorophenyl)methanol

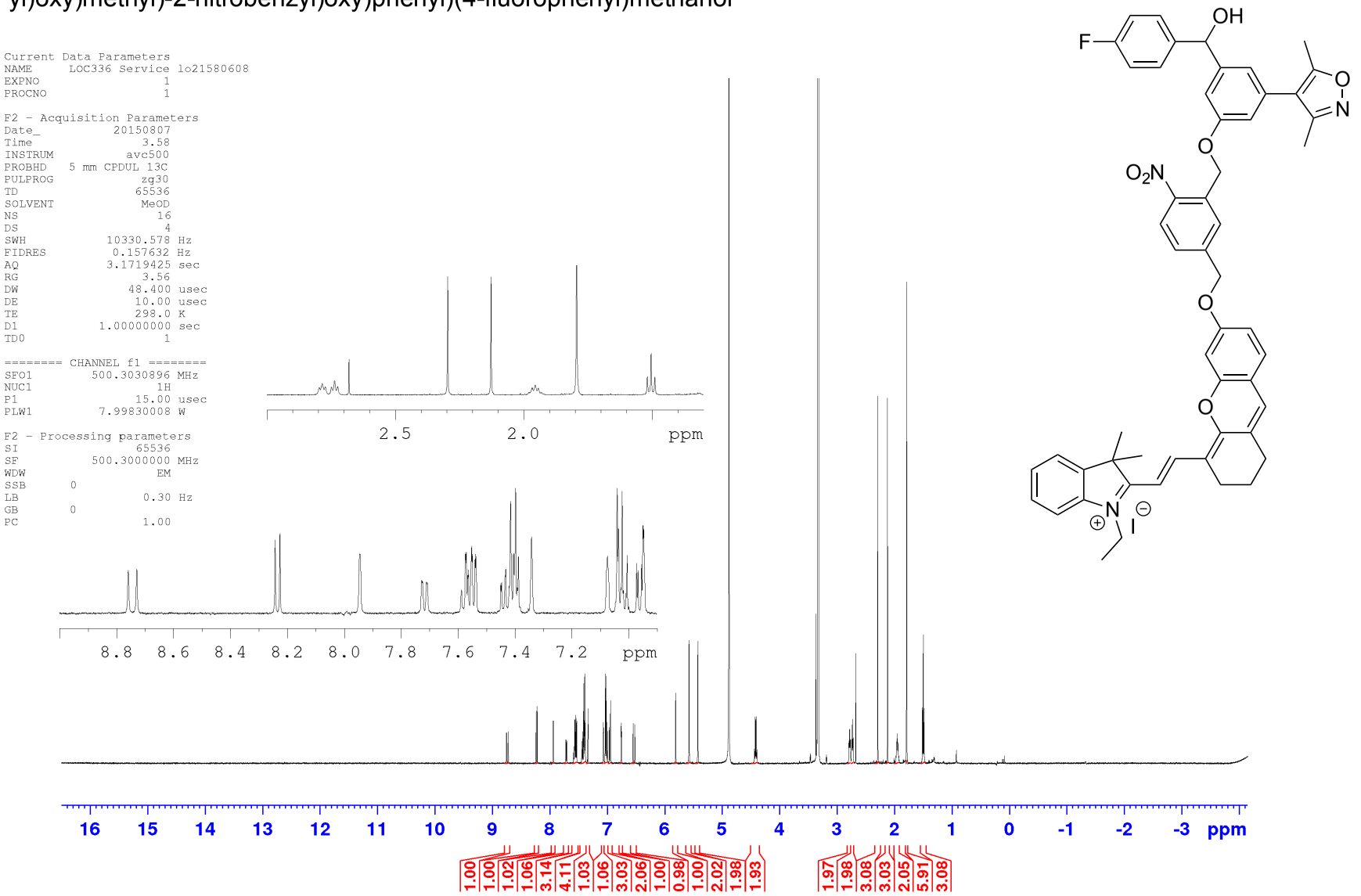

5.8. (*E*)-(3-(3,5-Dimethylisoxazol-4-yl)-5-((5-(((4-(2-(1-ethyl-3,3-dimethyl-3*H*-1λ^4-indol-2-yl)vinyl)-2,3-dihydro-1*H*-xanthen-6-yl)oxy)methyl)-2-nitrobenzyl)oxy)phenyl)(4-fluorophenyl)methanol

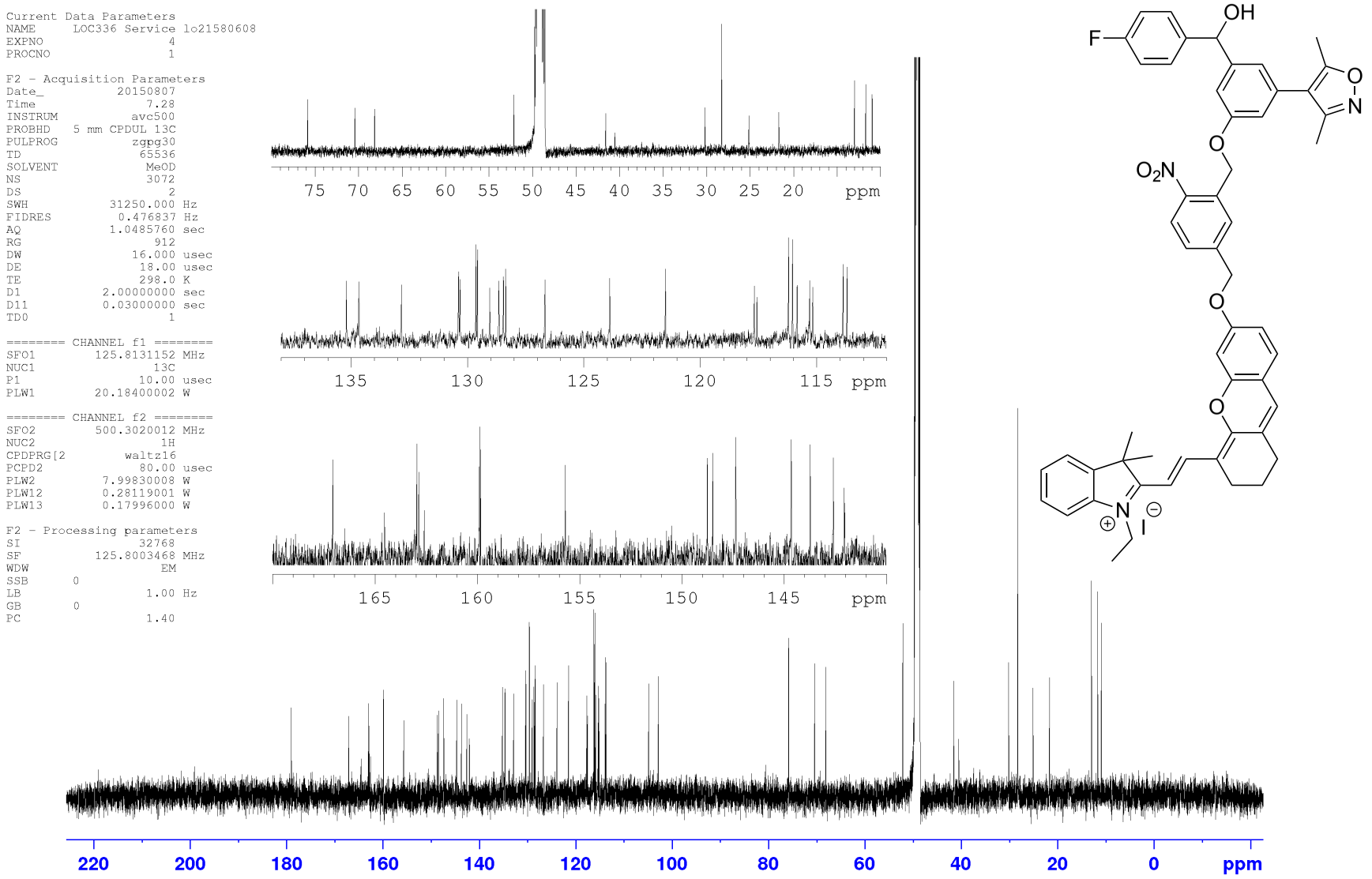

5.8. (*E*)-(3-(3,5-Dimethylisoxazol-4-yl)-5-((5-(((4-(2-(1-ethyl-3,3-dimethyl-3*H*-1λ^4-indol-2-yl)vinyl)-2,3-dihydro-1*H*-xanthen-6-yl)oxy)methyl)-2-nitrobenzyl)oxy)phenyl)(4-fluorophenyl)methanol

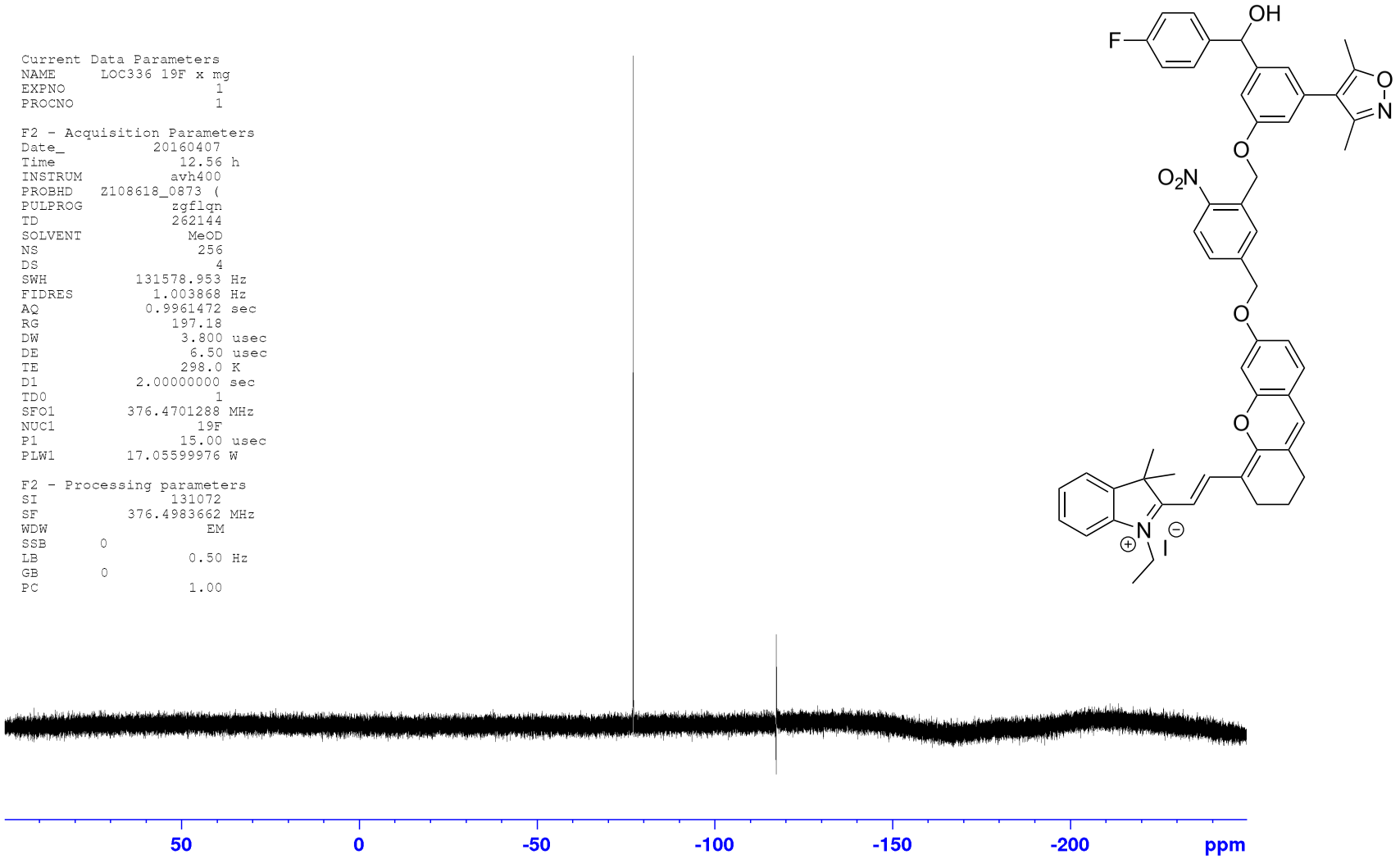

5.15. (3-((5-(Bromomethyl)-2-nitrobenzyl)oxy)-5-(3,5-dimethylisoxazol-4-yl)phenyl)(4-fluorophenyl)methanol

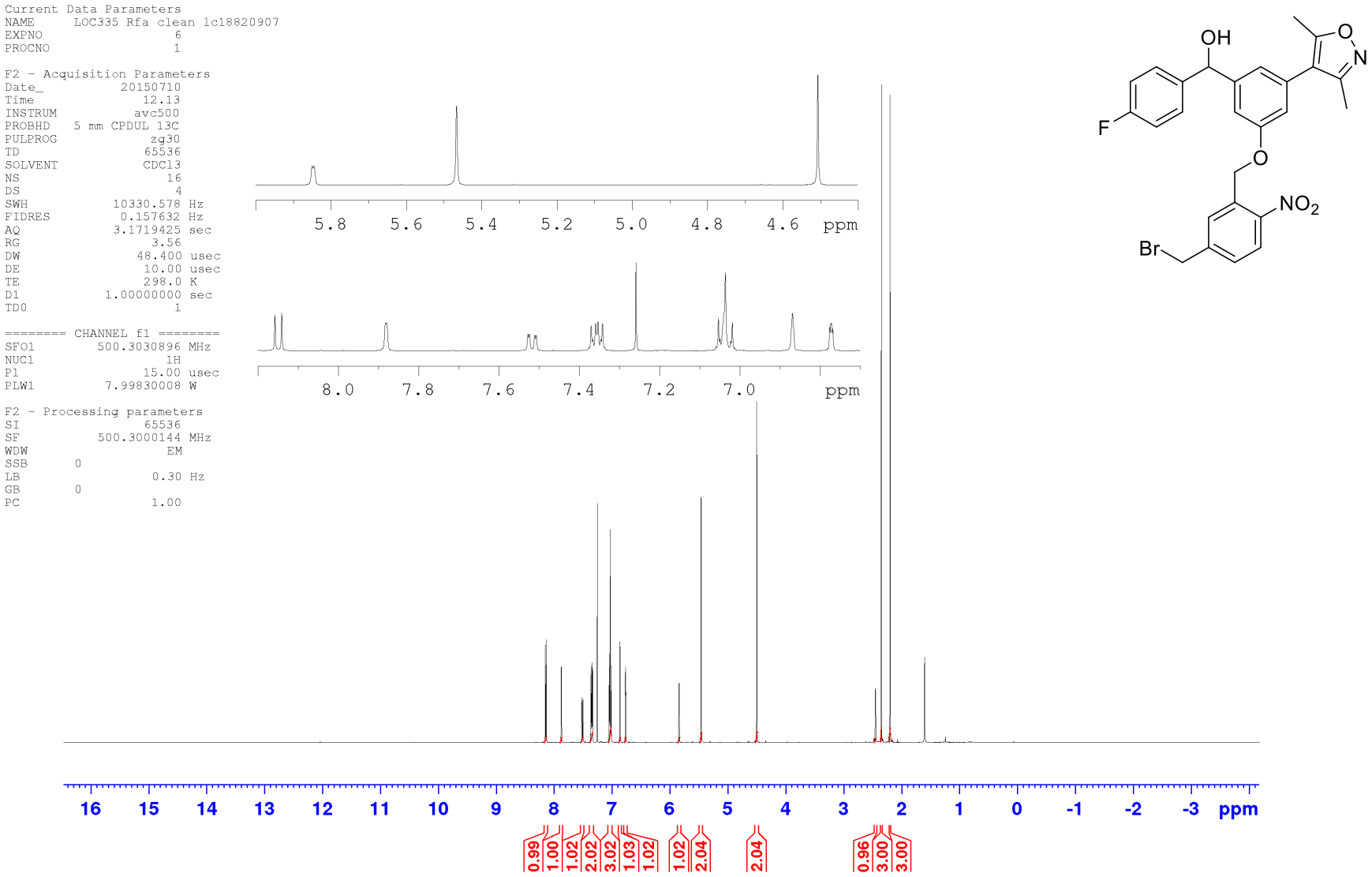

5.15. (3-((5-(Bromomethyl)-2-nitrobenzyl)oxy)-5-(3,5-dimethylisoxazol-4-yl)phenyl)(4-fluorophenyl)methanol

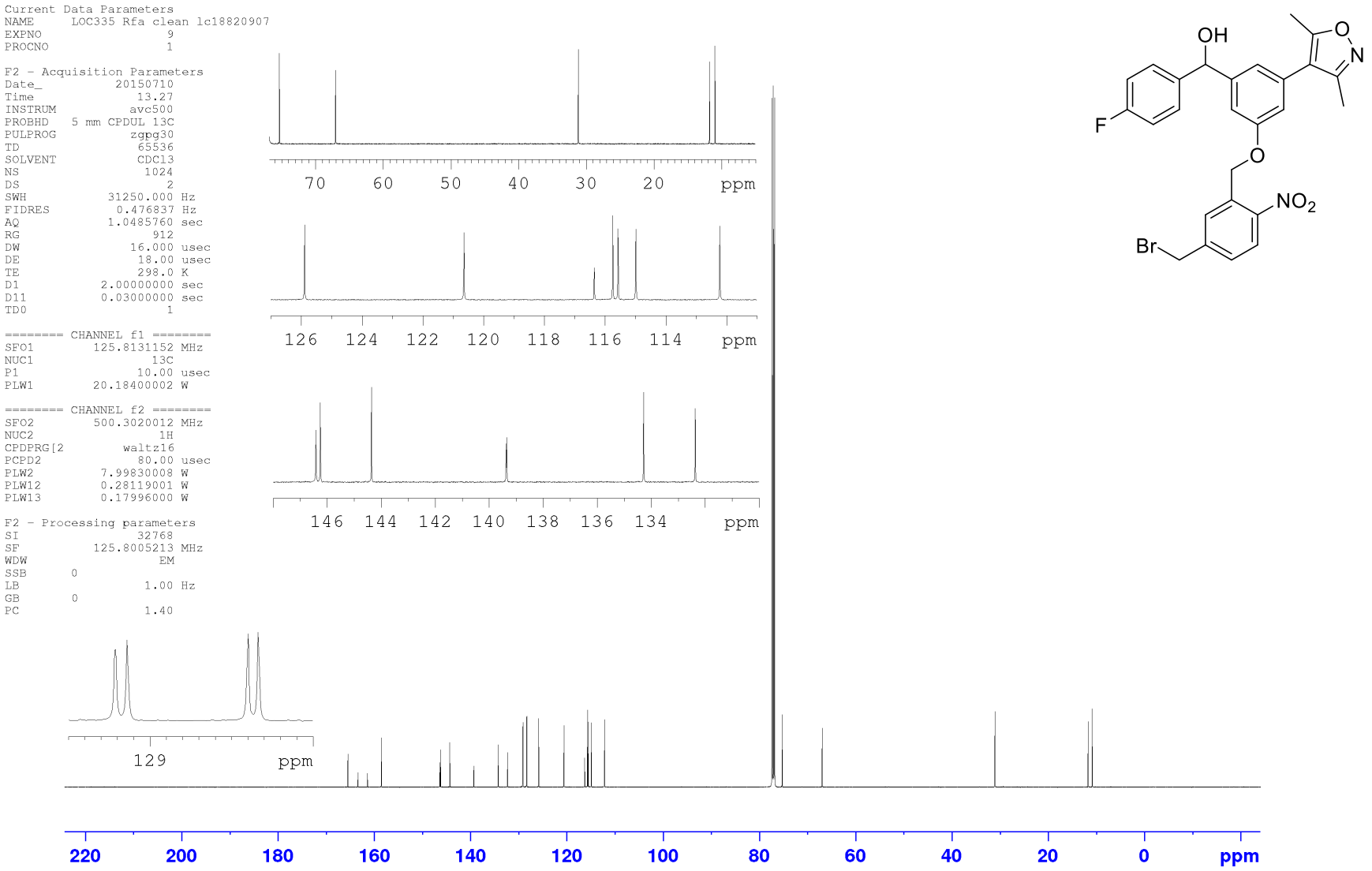

5.15. (3-((5-(Bromomethyl)-2-nitrobenzyl)oxy)-5-(3,5-dimethylisoxazol-4-yl)phenyl)(4-fluorophenyl)methanol

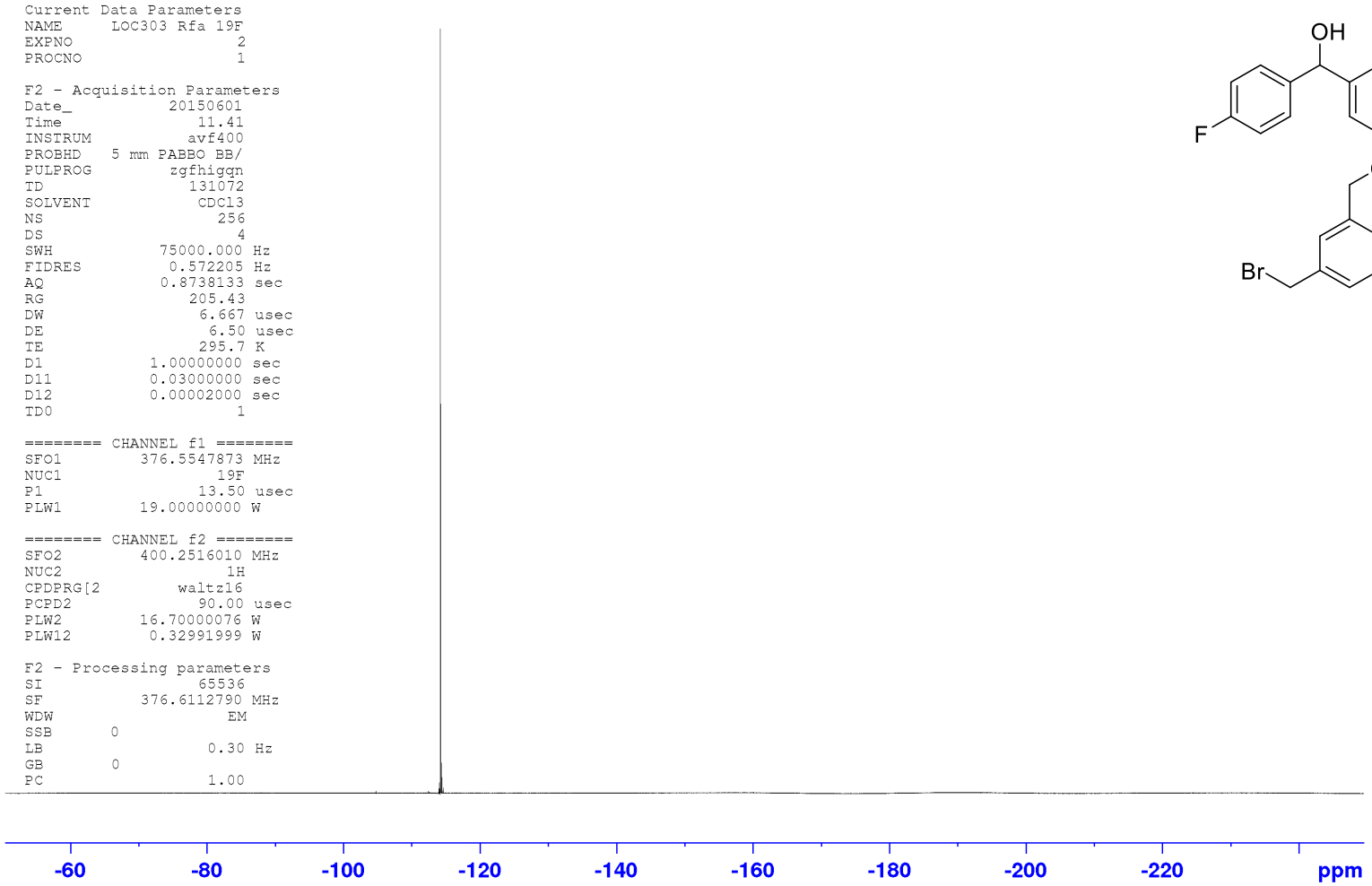

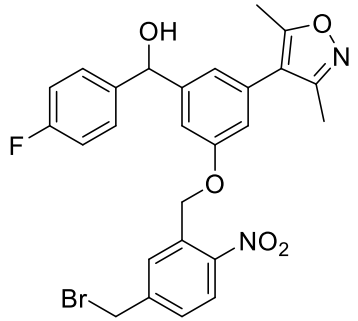

5.16. 2,4-Bis(bromomethyl)-1-nitrobenzene

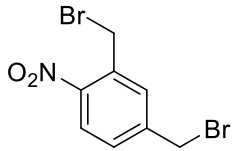


```
Current Data Parameters
NAME      LOC293b Service lo09761604
EXPNO                 1
PROCNO                1

F2 - Acquisition Parameters
Date_           20150416
Time              16.56
INSTRUM          avc500
PROBHD    5 mm CPDUL 13C
PULPROG            zg30
TD                65536
SOLVENT           CDCl3
NS                   16
DS                    4
SWH           10330.578 Hz
FIDRES         0.157632 Hz
AQ            3.1719425 sec
RG                 3.56
DW               48.400 usec
DE               10.00 usec
TE               298.0 K
D1           1.00000000 sec
TD0                   1

======== CHANNEL f1 ========
SFO1         500.3030896 MHz
NUC1                 1H
P1                15.00 usec
PLW1          7.99830008 W

F2 - Processing parameters
SI                65536
SF           500.3000119 MHz
WDW                  EM
SSB       0
LB                0.30 Hz
GB        0
PC                1.00
```

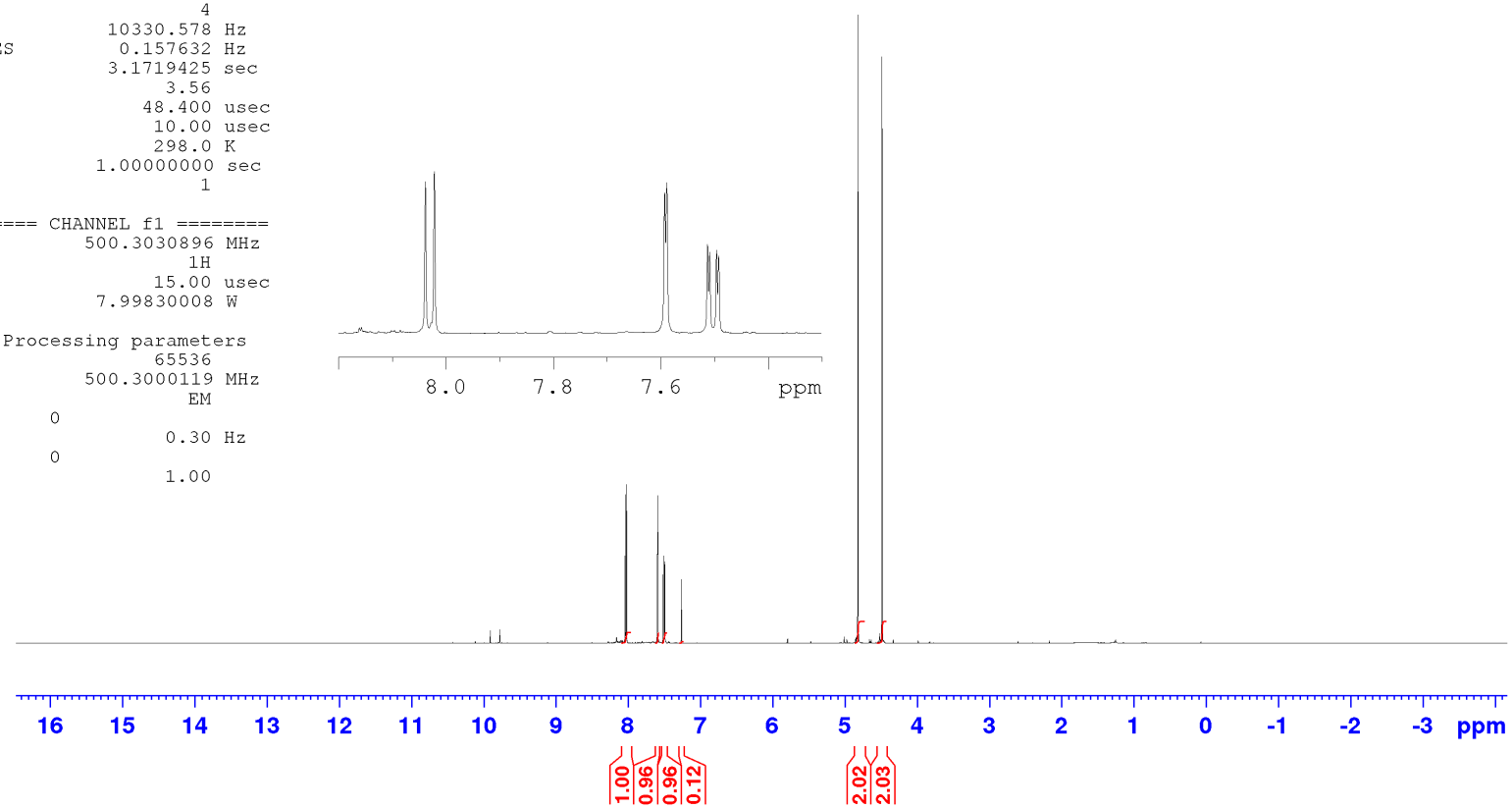

5.16. 2,4-Bis(bromomethyl)-1-nitrobenzene

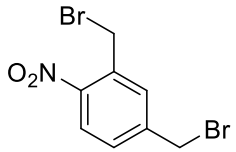


```
Current Data Parameters
NAME     LOC293b Service lc09761604
EXPNO                 4
PROCNO                1

F2 - Acquisition Parameters
Date_          20150416
Time              17.51
INSTRUM          avc500
PROBHD   5 mm CPDUL 13C
PULPROG          zgpg30
TD                65536
SOLVENT           CDCl3
NS                  256
DS                    2
SWH           31250.000 Hz
FIDRES         0.476837 Hz
AQ            1.0485760 sec
RG                  912
DW               16.000 usec
DE               18.00 usec
TE               298.0 K
D1           2.00000000 sec
D11          0.03000000 sec
TD0                   1

======== CHANNEL f1 ========
SFO1        125.8131152 MHz
NUC1                13C
P1                10.00 usec
PLW1        20.18400002 W

======== CHANNEL f2 ========
SFO2        500.3020012 MHz
NUC2                1H
CPDPRG[2         waltz16
PCPD2             80.00 usec
PLW2           7.99830008 W
PLW12          0.28119001 W
PLW13          0.17996000 W

F2 - Processing parameters
SI                32768
SF          125.8005225 MHz
WDW                  EM
SSB       0
LB                1.00 Hz
GB        0
PC                1.40
```

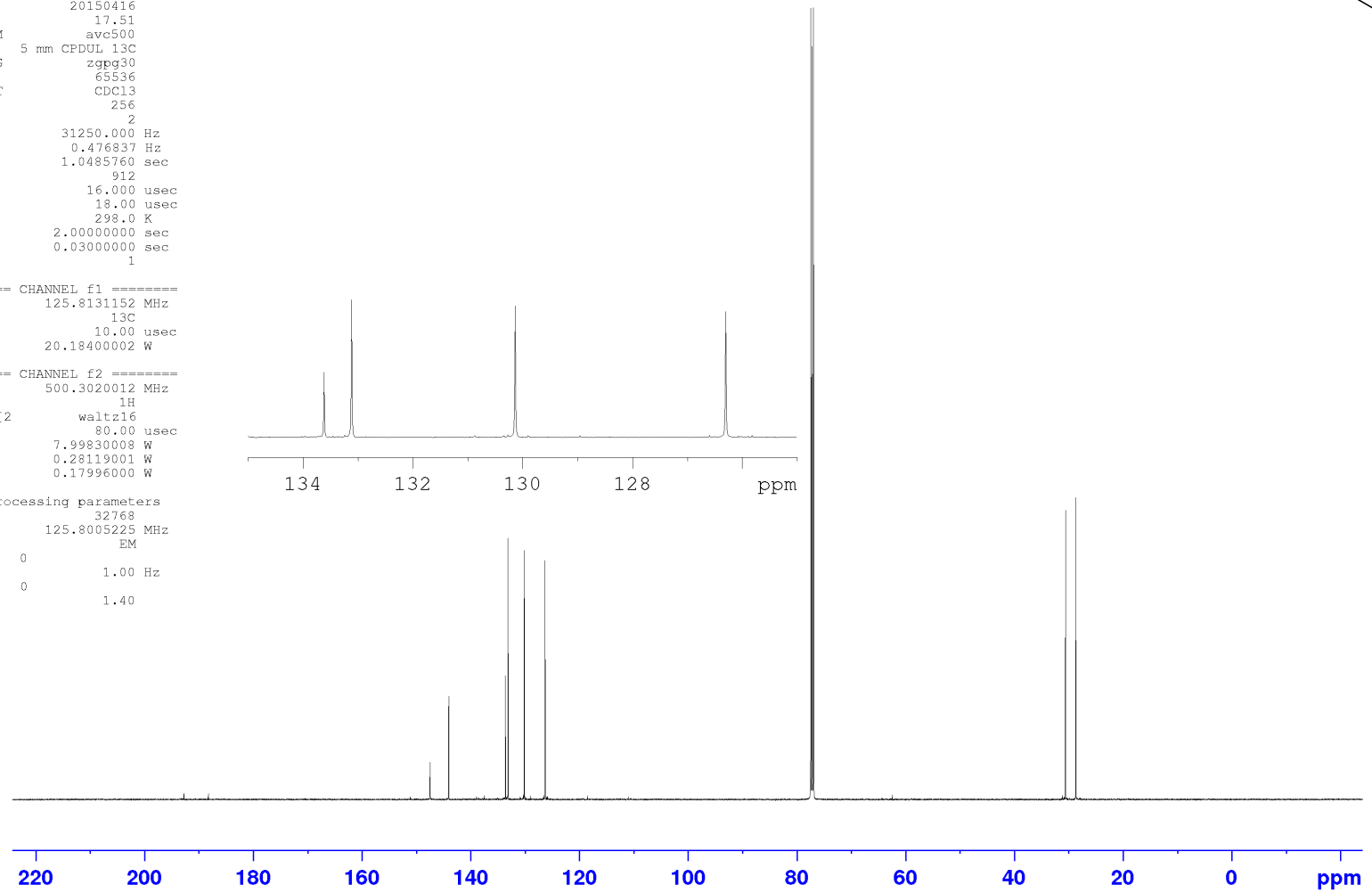

5.17. (4-Nitro-1,3-phenylene)dimethanol

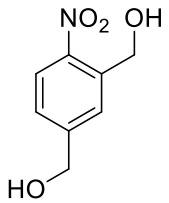


```
Current Data Parameters
NAME      LOC235 Service
EXPNO                 1
PROCNO                1

F2 - Acquisition Parameters
Date_          20150120
Time               1.41
INSTRUM          avc500
PROBHD   5 mm CPDUL 13C
PULPROG            zg30
TD                65536
SOLVENT           CDCl3
NS                   16
DS                    4
SWH           10330.578 Hz
FIDRES         0.157632 Hz
AQ            3.1719425 sec
RG                    4
DW               48.400 usec
DE               10.00 usec
TE               298.0 K
D1           1.00000000 sec
TD0                   1

======== CHANNEL f1 ========
SFO1        500.3030896 MHz
NUC1                1H
P1                15.00 usec
PLW1         7.99830008 W

F2 - Processing parameters
SI                65536
SF           500.3000137 MHz
WDW                  EM
SSB      0
LB                0.30 Hz
GB       0
PC                1.00
```

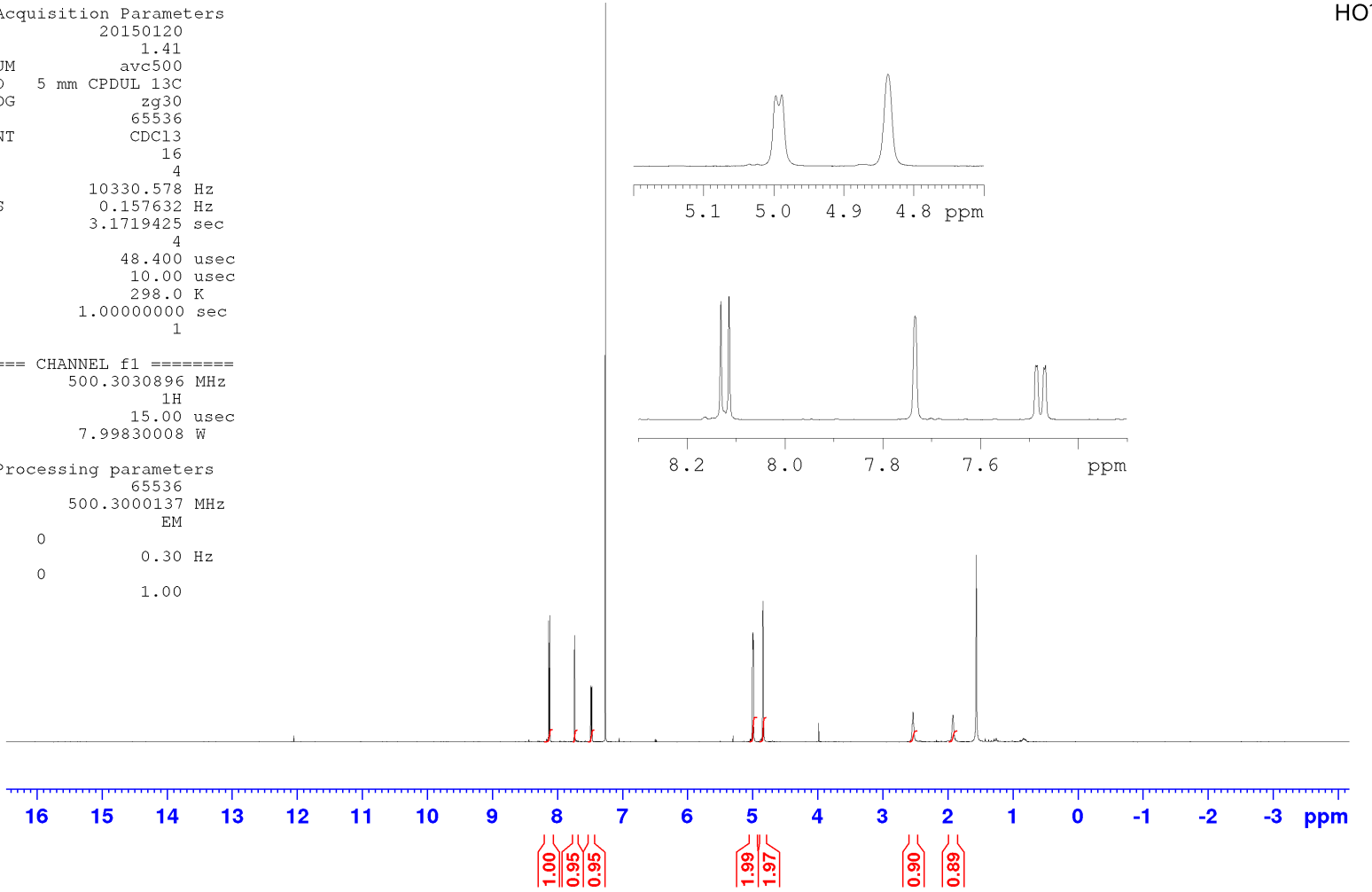

5.17. (4-Nitro-1,3-phenylene)dimethanol

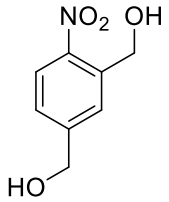


```
Current Data Parameters
NAME      LOC235 Service
EXPNO                 4
PROCNO                1

F2 - Acquisition Parameters
Date_          20150120
Time               5.10
INSTRUM          avc500
PROBHD   5 mm CPDUL 13C
PULPROG          zgpg30
TD                65536
SOLVENT           CDCl3
NS                 3072
DS                    2
SWH           31250.000 Hz
FIDRES         0.476837 Hz
AQ            1.0485760 sec
RG                  912
DW               16.000 usec
DE                18.00 usec
TE                298.0 K
D1           2.00000000 sec
D11          0.03000000 sec
TD0                   1

======== CHANNEL f1 ========
SFO1         125.8131152 MHz
NUC1                 13C
P1                 10.00 usec
PLW1        20.18400002 W

======== CHANNEL f2 ========
SFO2         500.3020012 MHz
NUC2                 1H
CPDPRG[2         waltz16
PCPD2              80.00 usec
PLW2          7.99830008 W
PLW12         0.28119001 W
PLW13         0.17996000 W

F2 - Processing parameters
SI                32768
SF           125.8005190 MHz
WDW                  EM
SSB       0
LB                 1.00 Hz
GB        0
PC                 1.40
```


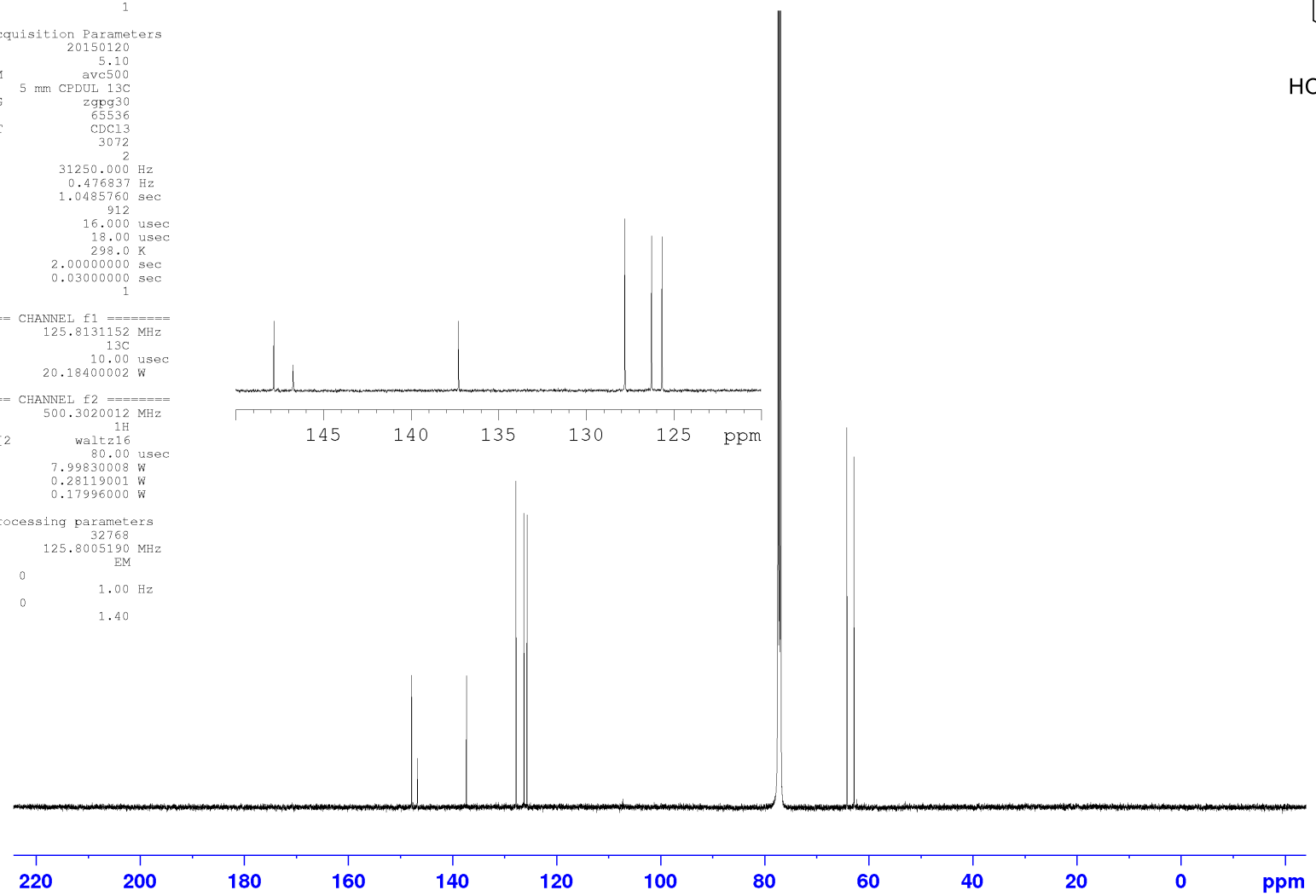

5.18. (3-((3-(Bromomethyl)-4-nitrobenzyl)oxy)-5-(3,5-dimethylisoxazol-4-yl)phenyl)(4-fluorophenyl)methanol

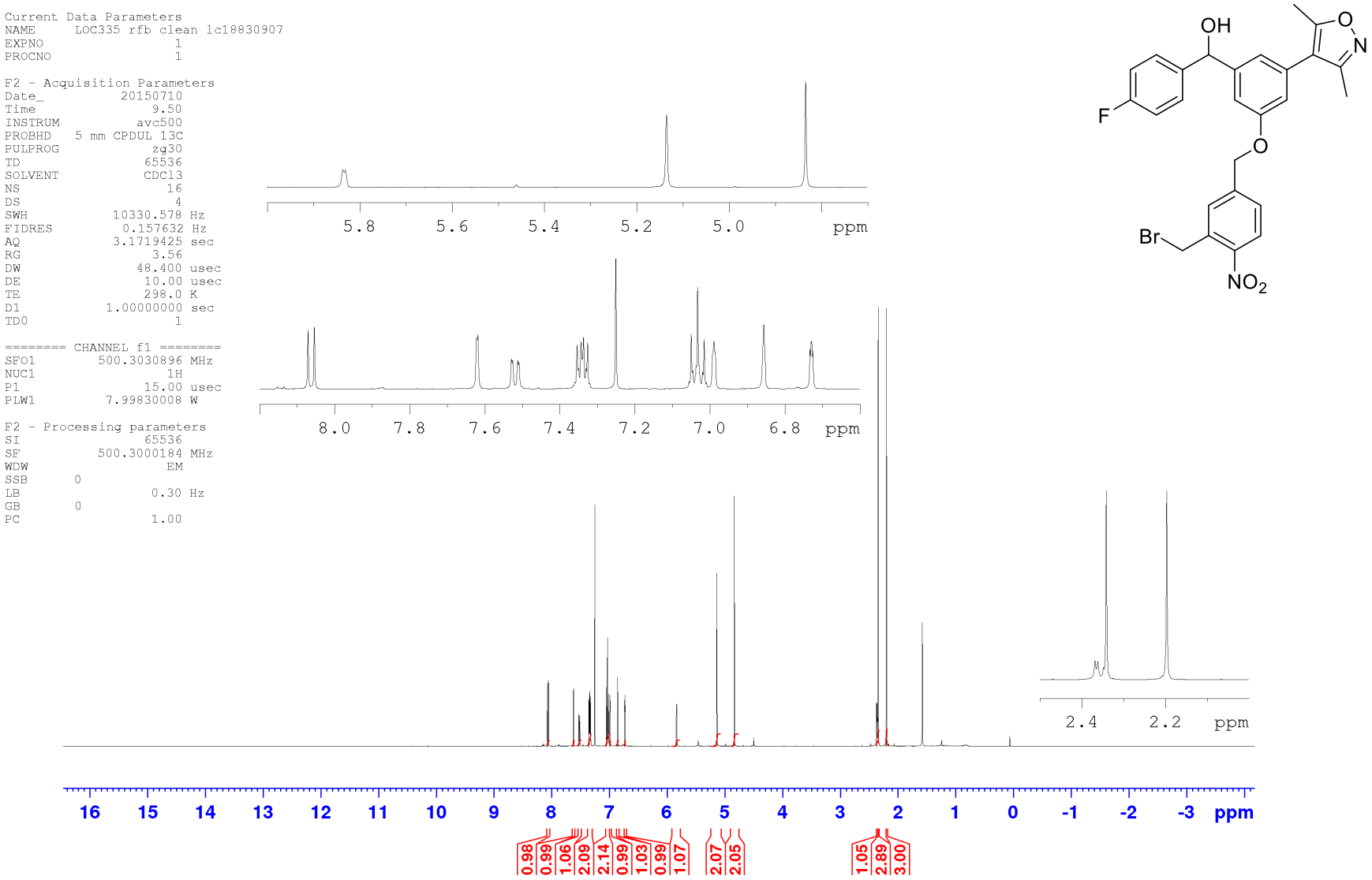

5.18. (3-((3-(Bromomethyl)-4-nitrobenzyl)oxy)-5-(3,5-dimethylisoxazol-4-yl)phenyl)(4-fluorophenyl)methanol

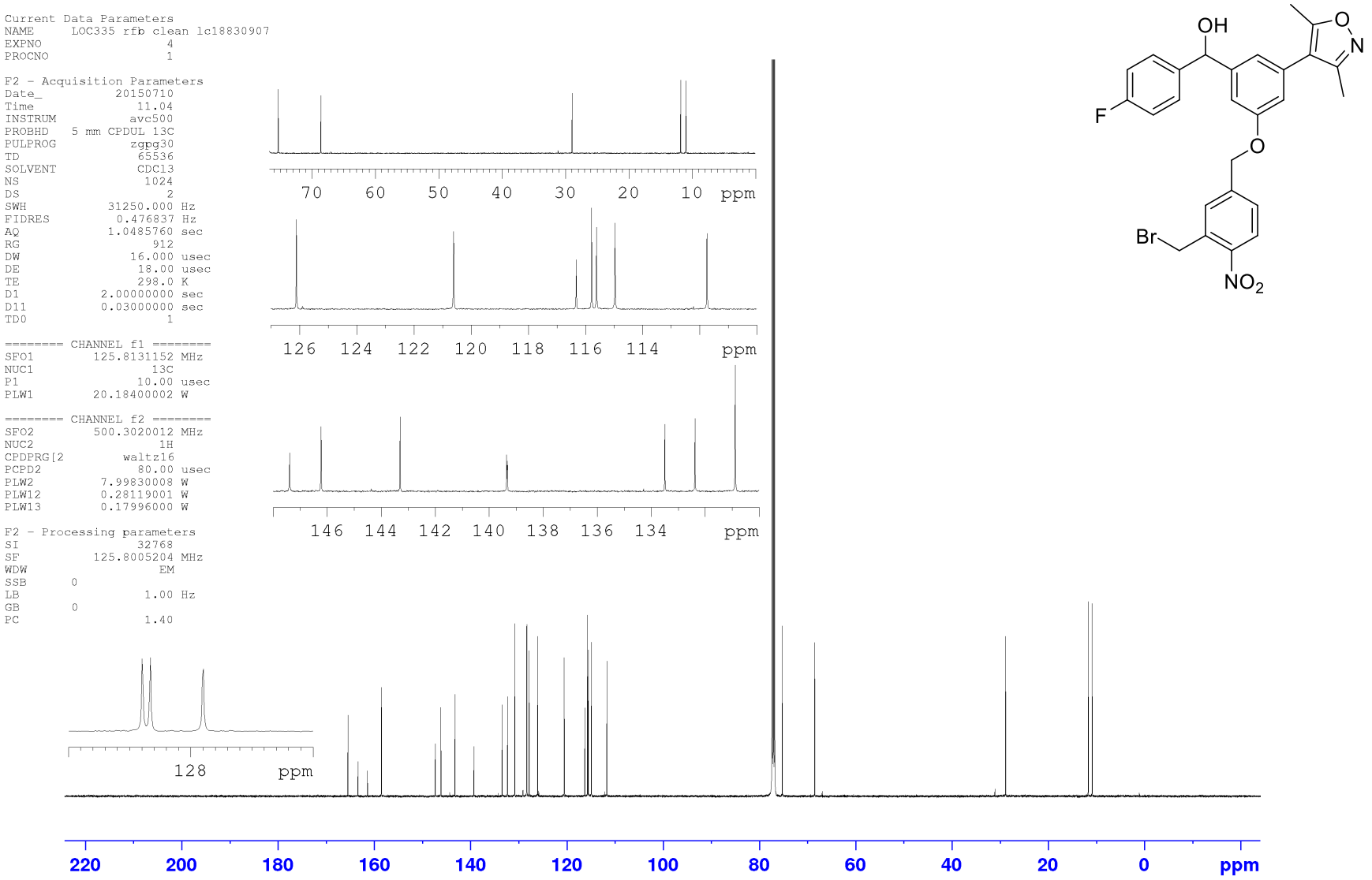

5.18. (3-((3-(Bromomethyl)-4-nitrobenzyl)oxy)-5-(3,5-dimethylisoxazol-4-yl)phenyl)(4-fluorophenyl)methanol

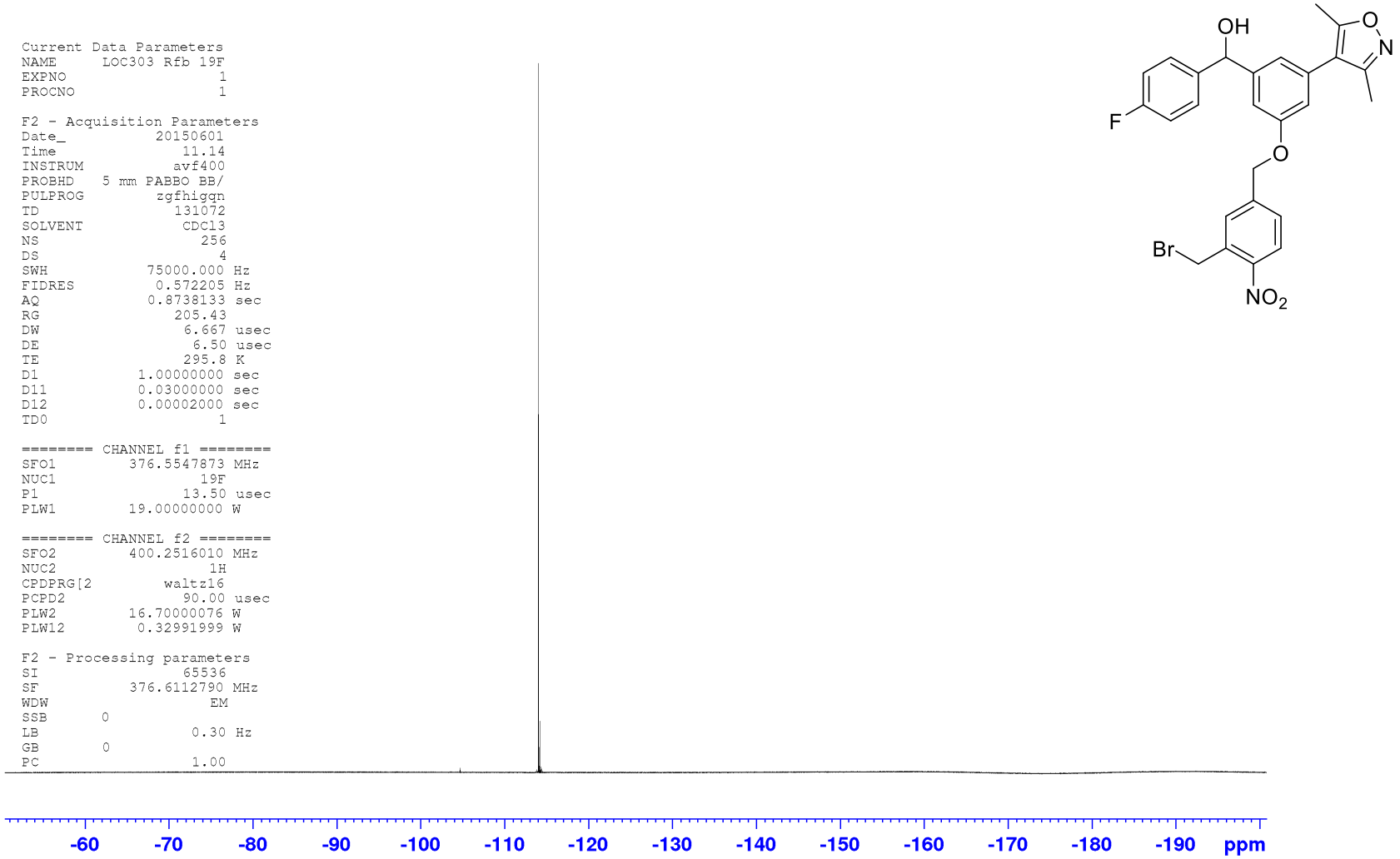

5.26. 1-Ethyl-2-((*E*)-2-((*E*)-3-(2-((*E*)-1-ethyl-3,3-dimethylindolin-2-ylidene)ethylidene)-2-((4-nitrophenethyl)amino)cyclohex-1-en-1-yl)vinyl)-3,3-dimethyl-3*H*-indol-1-ium iodide

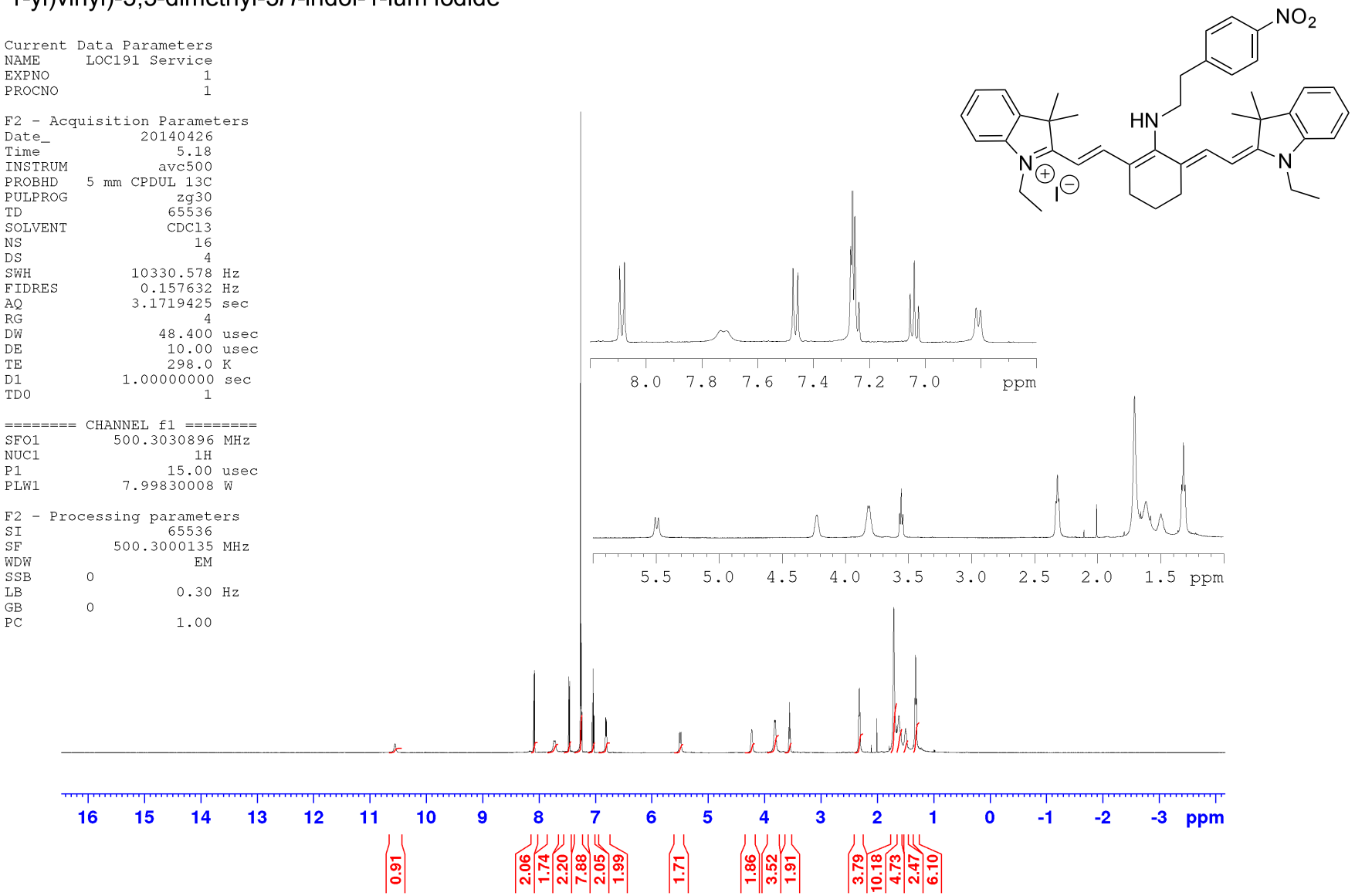

5.26. 1-Ethyl-2-((*E*)-2-((*E*)-3-(2-((*E*)-1-ethyl-3,3-dimethylindolin-2-ylidene)ethylidene)-2-((4-nitrophenethyl)amino)cyclohex-1-en-1-yl)vinyl)-3,3-dimethyl-3*H*-indol-1-ium iodide

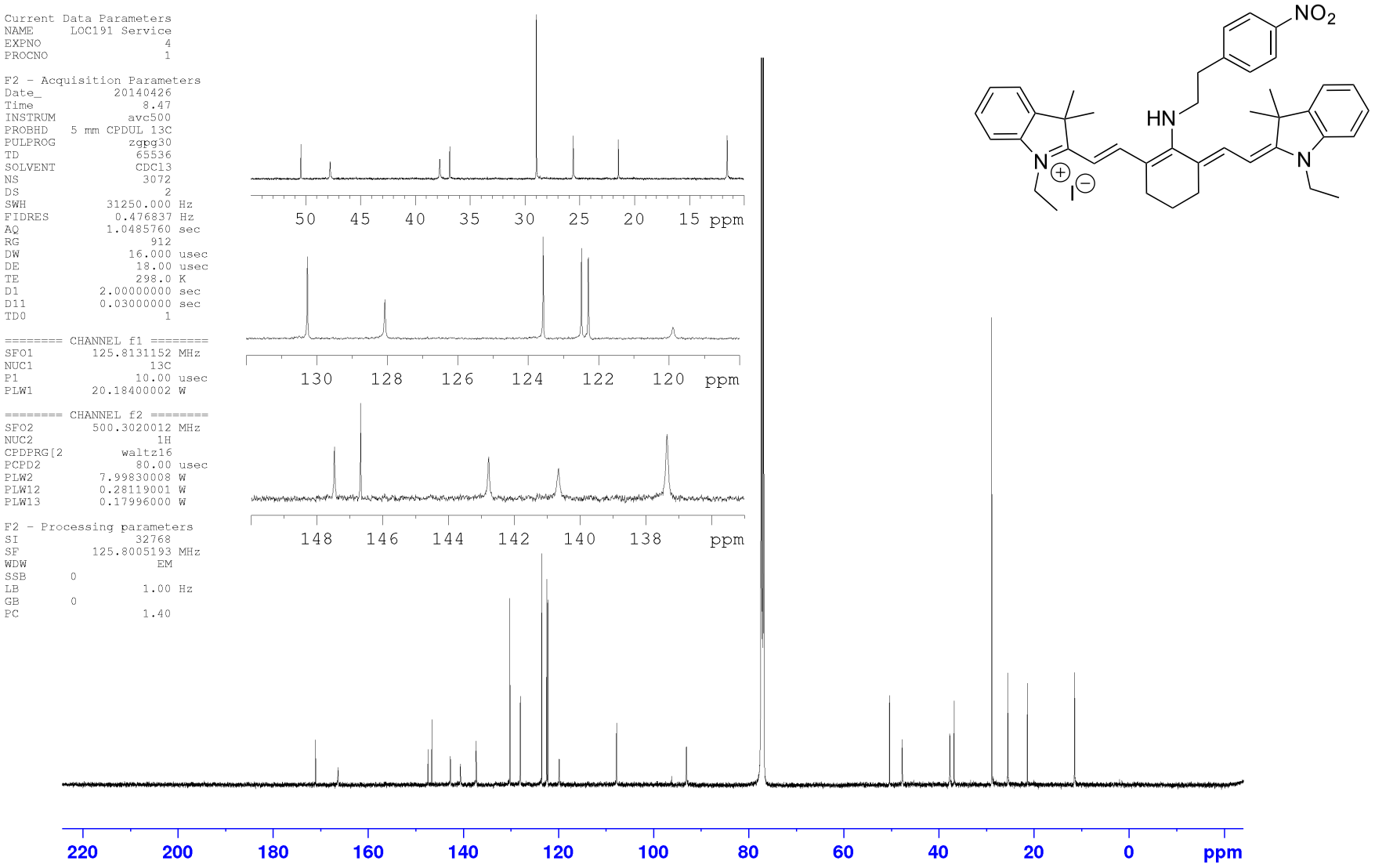

5.33. (*E*)-1-Ethyl-3,3-dimethyl-2-(2-(6-((4-nitrobenzyl)oxy)-2,3-dihydro-1*H*-xanthen-4-yl)vinyl)-3*H*-indol-1-ium iodide

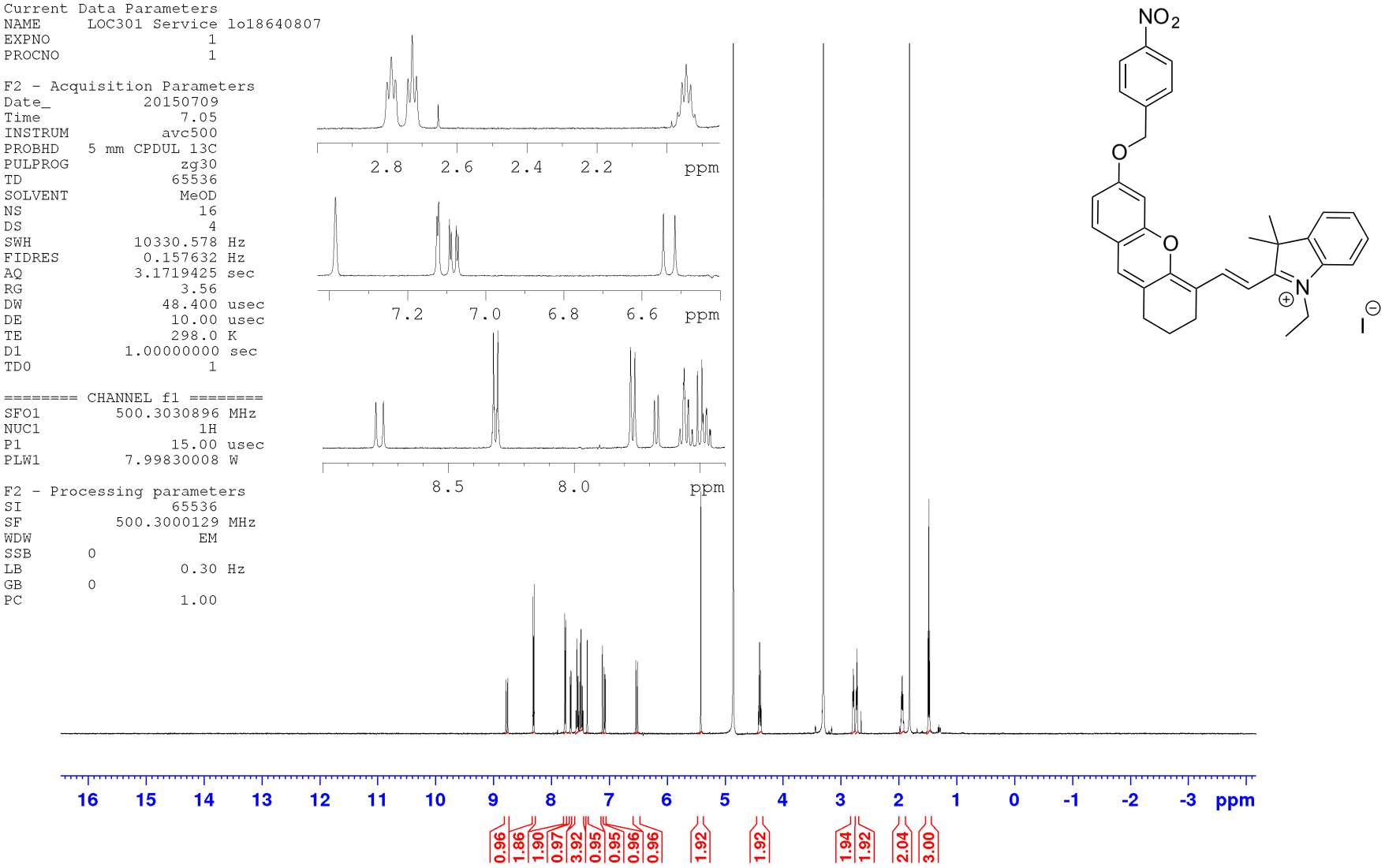

5.33. (*E*)-1-Ethyl-3,3-dimethyl-2-(2-(6-((4-nitrobenzyl)oxy)-2,3-dihydro-1*H*-xanthen-4-yl)vinyl)-3*H*-indol-1-ium iodide

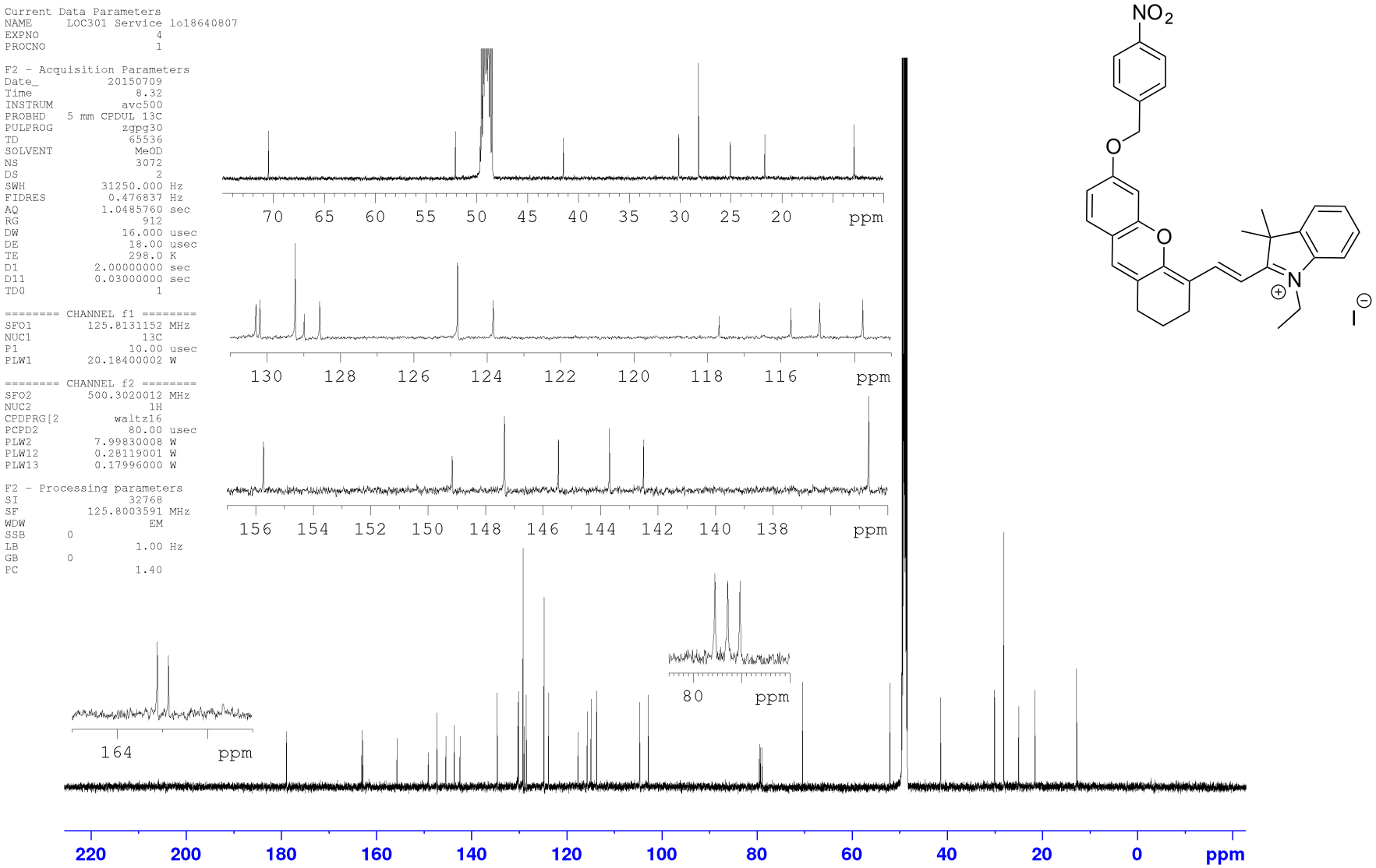

Developmental Therapeutics Program

One Dose Mean Graph

NSC: 772561 / 1	**Conc:** 1.00E-5 Molar	**Test Date:** Feb 19, 2013
Experiment ID: 1302OS27		**Report Date:** Apr 02, 2013

Panel/Cell Line	Growth Percent
Leukemia	
CCRF-CEM	46.69
HL-60(TB)	10.03
K-562	42.10
MOLT-4	58.75
RPMI-8226	14.86
SR	27.08
Non-Small Cell Lung Cancer	
A549/ATCC	55.40
HOP-62	47.23
HOP-92	25.58
NCI-H226	65.50
NCI-H23	68.13
NCI-H322M	47.65
NCI-H460	67.19
NCI-H522	22.13
Colon Cancer	
COLO 205	37.11
HCC-2998	62.25
HCT-116	58.05
HCT-15	36.70
HT29	34.60
KM12	53.11
SW-620	72.08
CNS Cancer	
SF-268	71.46
SF-295	42.47
SF-539	62.49
SNB-19	52.68
SNB-75	-13.15
Melanoma	
LOX IMVI	27.34
MALME-3M	60.05
M14	55.98
MDA-MB-435	43.93
SK-MEL-2	60.41
SK-MEL-28	61.17
SK-MEL-5	54.17
UACC-257	40.41
UACC-62	31.55
Ovarian Cancer	
IGROV1	46.02
OVCAR-3	46.70
OVCAR-4	32.49
OVCAR-5	73.34
OVCAR-8	38.62
NCI/ADR-RES	59.24
SK-OV-3	43.68
Renal Cancer	
786-0	54.79
A498	-3.34
ACHN	60.58
CAKI-1	23.81
SN12C	74.48
TK-10	12.58
UO-31	16.92
Prostate Cancer	
PC-3	48.45
DU-145	87.55
Breast Cancer	
MCF7	20.88
MDA-MB-231/ATCC	62.42
HS 578T	33.68
BT-549	64.67
T-47D	47.15
MDA-MB-468	24.93
Mean	45.14
Delta	58.29
Range	100.70

Mean Growth Percent - Growth Percent